State of Oregon
Oregon Department of Geology and Mineral Industries
Ian P. Madin, Interim State Geologist

OPEN-FILE REPORT O-15-06

COASTAL FLOOD HAZARD STUDY, LINCOLN COUNTY, OREGON

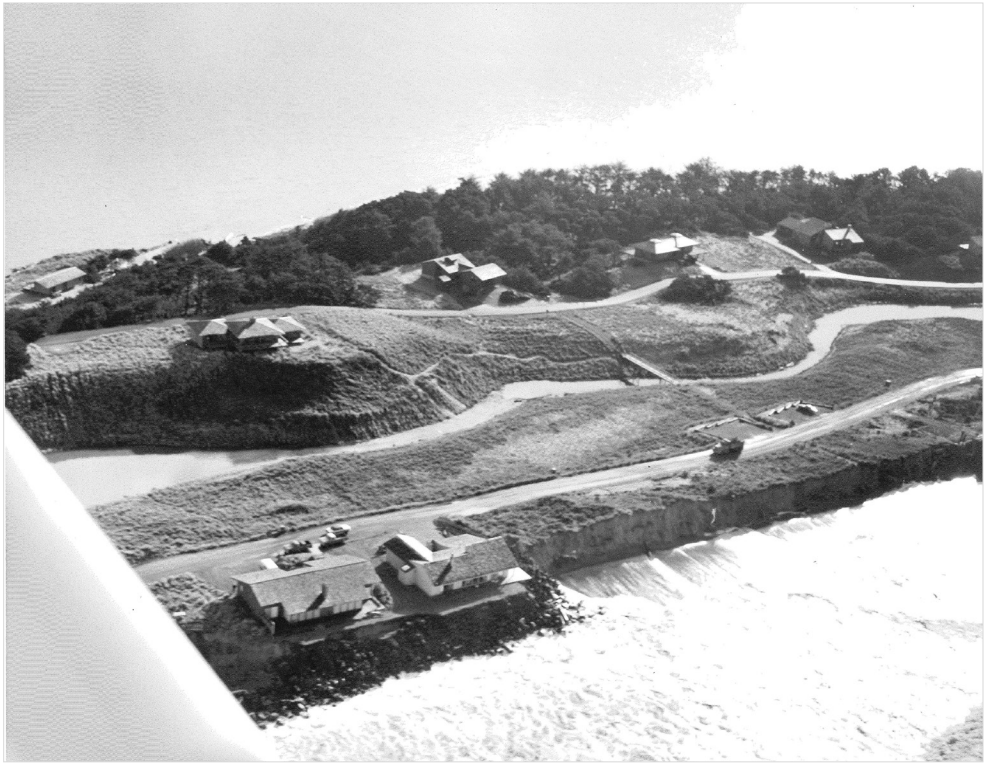

By Jonathan C. Allan[1], Peter Ruggiero[2], Nick Cohn[2], Gabriel Garcia[2], Fletcher E. O'Brien[3], Katherine Serafin[2], Laura L. Stimely[1], and Jed T. Roberts[3]

2015

[1] Oregon Department of Geology and Mineral Industries, Coastal Field Office, P.O. Box 1033, Newport, OR 97365
[2] College of Earth, Ocean and Atmospheric Sciences, Oregon State University, Corvallis, OR 97331
[3] Oregon Department of Geology and Mineral Industries, 800 NE Oregon St., Ste. 965, Portland, OR 97232

DISCLAIMER

This product is for informational purposes and may not have been prepared for or be suitable for legal, engineering, or surveying purposes. Users of this information should review or consult the primary data and information sources to ascertain the usability of the information. This publication cannot substitute for site-specific investigations by qualified practitioners. Site-specific data may give results that differ from the results shown in the publication.

Cover photograph: The erosion of Siletz Spit. The erosion of the beach and dune came close to reaching the road backing the beach. Shore protection structures were rapidly built to protect those homes built on the spit, while undeveloped lots were left to erode. Photo taken by Oregon Highway Department, January 26, 1972.

Oregon Department of Geology and Mineral Industries Open-File Report O-15-06
Published in conformance with ORS 516.030

For additional information:
Administrative Offices
800 NE Oregon Street #28, Suite 965
Portland, OR 97232
Telephone (971) 673-1555
Fax (971) 673-1562
http://www.oregongeology.org
http://www.oregon.gov/DOGAMI/

TABLE OF CONTENTS

List of Figures ..... *v*

List of Tables ..... *ix*

1.0 INTRODUCTION **1**

2.0 COASTAL GEOLOGY AND GEOMORPHOLOGY OF LINCOLN COUNTY **5**

2.1 Local Geology 5
2.2 Tsunami Hazards Associated with the Cascadia Subduction Zone and from Distant Earthquake Sources 10
2.3 Coastal Geomorphology 13
2.4 Coastal Erosion and Flood History 22
2.4.1 Lincoln County historical shoreline positions 22

3.0 BEACH AND BLUFF MORPHOLOGY ASSESSMENTS **36**

3.1 Survey Methodology 41
3.1.1 Lincoln County survey control procedures 42
3.2 Beach Characterization 47
3.3 Recent Coastal Changes in Lincoln County 58
3.4 Bathymetry 65

4.0 TIDES **71**

4.1 Tide Characteristics on the Central to Northern Oregon Coast 72
4.2 Seasonal Changes 75
4.3 Oregon Storm Surges 76
4.4 Non-Tidal Residual Analyses 76
4.5 Lincoln County Tides 80
4.6 Still Water Level (SWL) 82

5.0 PACIFIC NORTHWEST WAVE CLIMATE **86**

5.1 Development of a Synthesized Wave Climate for Input into SWAN 89
5.2 Comparison of GROW Versus Measured Waves 95
5.3 SWAN model development and parameter settings 99
5.3.1 Wind effects 100
5.3.2 Frictional and whitecapping dissipation of the wave energies 104
5.3.3 Look up table development 104
5.4 Summary of SWAN results 110

6.0 WAVE RUNUP AND OVERTOPPING **113**

6.1 Runup Models for Beaches 114
6.1.1 Stockdon runup model 114
6.1.2 Direct Integration method—beaches 114
6.1.3 Comparison between the Stockdon and DIM runup calculations 115
6.2 “Barrier” Runup Calculations 118
6.2.1 Introduction 118
6.2.2 Specific procedure for calculation “barrier” runup 120
6.2.3 “Barrier” runup reduction factors 122
6.3 Lincoln County Wave Runup and Total Water Level Calculations 132
6.4 Overtopping Calculations 140
6.4.1 Mean overtopping rate at the “barrier” crest 141
6.4.2 Overtopping limits and flood hazard zones landward of the “barrier” crest 143
6.4.3 Initial testing of the landward limit of wave overtopping 145
6.4.4 Wave overtopping and hazard zone limits calculated for Lincoln County 146

7.0 COASTAL EROSION CAUSED BY INDIVIDUAL STORMS 151
7.1 Models of Foredune Erosion 151
7.1.1 The Komar and others (1999) model 151
7.1.2 The Kriebel and Dean (1993) model 153
7.2 Erosion Modeling on Lincoln County beaches 155
8.0 FLOOD MAPPING 165
8.1 Detailed Coastal Zone VE Flood Zone Mapping 165
8.1.1 Bluff-backed beaches 165
8.1.2 Dune-backed beaches 167
8.1.3 Mapping of estuarine flooding 174
9.0 ACKNOWLEDGMENTS 176
10.0 REFERENCES 176
11.0 APPENDICES 181
11.1 Appendix A: Ground Survey Accuracy Assessment Protocols 181
11.2 Appendix B: Tillamook County Beach and Bluff Profiles 182
11.2.1 Cape Perpetua 182
11.2.2 Yachats 185
11.2.3 Waldport 190
11.2.4 Alsea Spit 217
11.2.5 South Beach 228
11.2.6 Newport 249
11.2.7 Yaquina Head 258
11.2.8 Beverly Beach 259
11.2.9 Otter Rock 270
11.2.10 Cape Foulweather 273
11.2.11 Miroco 274
11.2.12 Rocky Creek 276
11.2.13 Whale Cove 277
11.2.14 Depoe Bay 280
11.2.15 Fogarty Creek 287
11.2.16 Siletz Spit 291
11.2.17 Lincoln City 308
11.2.18 Salmon River 337
11.2.19 Cascade Head 340
11.2.20 Supplemental Transects 343

LIST OF FIGURES

Figure 1-1. Location map of Lincoln County coastline ... 3
Figure 1-2. Three representative examples of the steps that may be taken to derive coastal flood hazard maps on the Pacific Northwest coast ... 4
Figure 2-1. Looking south along Siletz spit toward Fishing Rock and Government Point in the far distance ... 7
Figure 2-2. Looking east at Cascade Head (left) and the Salmon River estuary with its barrier spit ... 8
Figure 2-3. Looking south toward Yaquina Head in the distance ... 8
Figure 2-4. Oblique aerial photo of homes perched along the cliff top at Roads End, Lincoln City, Oregon ... 9
Figure 2-5. Sea cliff erosion at Gleneden Beach, Lincoln County ... 9
Figure 2-6. Variations in the percent abundances of various heavy minerals observed on the central to northern Oregon coast ... 10
Figure 2-7. Geomorphic classification of northern Lincoln City beach, Salmon River estuary, and Cascade Head ... 14
Figure 2-8. Geomorphic classification of Gleneden Beach, Siletz Spit, and southern Lincoln City Beach ... 15
Figure 2-9. Geomorphic classification of the Fogarty Creek, Depoe Bay, Cape Foulweather, Otter Rock, and northern Beverly Beach areas ... 16
Figure 2-10. Geomorphic classification of the southern Beverly Beach littoral cell, Yaquina Head, Newport cell, and South Beach areas ... 17
Figure 2-11. Geomorphic classification of the southern end of the South Beach cell, Ona Beach, Seal Rock, and Alsea Spit areas ... 18
Figure 2-12. Geomorphic classification of the Waldport cell, Yachats, and Cape Perpetua areas ... 19
Figure 2-13. Lincoln County dune crest elevations ... 20
Figure 2-14. Lincoln County beach slopes ... 20
Figure 2-15. Basalt dominates the local geology between Cape Foulweather and Depoe Bay ... 21
Figure 2-16. Shoreline variability in the north Yachats area ... 24
Figure 2-17. Shoreline variability along southern Alsea Spit ... 25
Figure 2-18. A 1983 aerial photo taken of the southern end of Alsea Spit at the height of the 1982-83 El Niño ... 26
Figure 2-19. An erosion scarp caused by the northward shift of the Alsea Bay inlet during the 1982-83 El Niño ... 27
Figure 2-20. Remediation during and immediately following the 1982-83 El Niño event ... 27
Figure 2-21. Shoreline changes at the mouth of Yaquina Bay ... 29
Figure 2-22. Shoreline variability in the north Newport (Agate Beach) area ... 30
Figure 2-23. The erosion of Siletz Spit following a major storm on January 26, 1973 ... 31
Figure 2-24. Responses to the Siletz erosion consisted of dumping riprap in front of the homes, while adjacent empty lots were left unprotected and continued to erode ... 32
Figure 2-25. Shoreline variability along Siletz Spit ... 33
Figure 2-26. Aerial photo taken in January 1974 showing the extent of the 1972-73 winter erosion ... 34
Figure 2-27. Erosion of bluffs adjacent to the Inn at Spanish Head (mid photo) during a series of storms in the 1977-78 winter ... 35
Figure 3-1. Location map of beach profiles measured in the vicinity of Cape Perpetua (transects 1–4), Yachats (5–14), the Waldport subcell (transects 15–67), and Alsea Spit (transects 68–86) ... 37
Figure 3-2. Location map of beach profiles measured near Seal Rock ... 38
Figure 3-3. Location map of beach profiles measured in the Beverly Beach cell ... 39
Figure 3-4. Location map of beach profiles measured along Siletz Spit ... 40
Figure 3-5. The Trimble R7 base station antenna in operation on the Tillamook Plains ... 42
Figure 3-6. A 180-epoch calibration check is performed on a survey monument (DRIFTWOOD) established in the Alsea Spit littoral cell ... 46
Figure 3-7. Surveying the morphology of the beach at Bandon using a Trimble 5800 “rover” GPS ... 46
Figure 3-8. Residuals of GPS survey points relative to zero (transect) line ... 47
Figure 3-9. Plot showing various beach cross-sections at the LINC 69 (aka Alsea 2) profile site ... 48

Figure 3-10. Alongshore changes in beach slopes (tan β), beach-dune juncture (Ej) elevations, and dune/bluff crest/tops along Lincoln County 50
Figure 3-11. Cobble/boulder beach located on the south side of Yaquina Head and north of Newport 50
Figure 3-12. Measured beach morphological changes carried out between 1997 and 2013 for selected sites between Yachats and Alsea Bay 59
Figure 3-13. Measured beach morphological changes carried out between 1997 and 2013 for selected sites between Alsea Bay and Seal Rock 59
Figure 3-14. Oblique photo looking west across the Alsea spit tip 60
Figure 3-15. Measured beach morphological changes carried out between 1997 and 2013 for selected sites between Yaquina Bay and Yaquina Head. Data include both lidar and GPS surveys of the beaches 61
Figure 3-16. Measured beach morphological changes carried out between 1997 and 2013 for selected sites between Fogarty Creek and Siletz Bay. Data include both lidar and GPS surveys of the beaches. 61
Figure 3-17. Measured beach morphological changes carried out between 1997 and 2013 for selected sites between Siletz Bay and Roads End 62
Figure 3-18. Erosion of bluffs in the Taft area during the winter of 1977-78 63
Figure 3-19. Positional changes in the beach/dune toe (elevation of 5 m [16 ft]) along the Lincoln County coastline between 1997 and 2009 derived from lidar data 64
Figure 3-20. U.S. federal, state, and local agency bathymetric data sets used to compile the central Oregon coast DEM 66
Figure 3-21. Data acquisition boat and onboard equipment 68
Figure 3-22. Collected bathymetry transects measured offshore the coast of the Lincoln City, Siletz Spit, Depoe Bay, Otter Rock, and Beverly Beach littoral cells 68
Figure 3-23. Collected bathymetry transects measured offshore the coast of Newport, South Beach to Alsea Bay, and Waldport to Yachats 69
Figure 3-24. Combined topographic and bathymetric cross-shore transects measured offshore from Beverly Beach and Depoe Bay 70
Figure 4-1. Location map of NDBC (black) and CDIP (yellow) wave buoys, tide gauges (red) and GROW wave hindcast stations (red suns) 72
Figure 4-2. Empirical PDF plots for various tide gauges for overlapping years of data (2005–2013) 73
Figure 4-3. Empirical PDFs for various tide gauges based on all available data 74
Figure 4-4. Seasonal plot of tides along the south-central Oregon coast down into northern California 75
Figure 4-5. Comparison of non-tidal residuals determined for SB versus GB, SB versus CH, and SB versus PO tide gauges 78
Figure 4-6. Comparison of non-tidal residuals (NTRs, top), and their differences (bottom) between the GB, SB, and CH tide gauges for the 2007-08 winter 78
Figure 4-7. (Left) Histogram of surge magnitudes determined for the GB, SB, and CH tide gauge stations 79
Figure 4-8. Daily tidal elevations measured at South Beach, Newport on the central Oregon coast 80
Figure 4-9. Seasonal cycles in monthly-mean water levels based on data from the South Beach tide gauge 81
Figure 4-10. The trends of “winter” (red) and “summer” (blue) mean sea levels measured by the SB tide gauges 82
Figure 4-11. Assessments of changes in RSLs based on tide-gauge records compared with benchmark and GPS measurements of land-elevation changes, with their corresponding RSL rates obtained by adding the 2.28 mm/yr PNW eustatic rise in sea level 83
Figure 4-12. Extreme-value analyses of the still water level (SWL) determined for the combined South Beach/Garibaldi tide gauge time series 85
Figure 5-1. The SWAN model domain developed for the Lincoln County coast 88
Figure 5-2. Map showing the regional divisions from which synthesized wave climates have been developed 89
Figure 5-3. Available wave data sets timeline 90
Figure 5-4. Differences in the empirical probability distribution functions of the on shore and off shore buoys 91
Figure 5-5. Example development of transformation parameters between the Washington buoy (#46005) and the Tillamook (#46089) buoy for period range 10 s to 12 s 91

Figure 5-6. Adjusted probability density functions (corrected using the constant offset approach) for buoy 46005 (green line), buoy 46029 (red line), and WIS station 81048 (blue line) as compared to the raw probability density function for buoy 46089 (black line) 92
Figure 5-7. Synthesized wave climate developed for Lincoln County 93
Figure 5-8. Seasonal variability in the deepwater wave climate offshore from the northern Oregon coast 94
Figure 5-9. (*left*) Predominant wave directions for the summer months (June-August), and (*right*) winter (December-February). Colored scale indicates the significant wave height in meters 94
Figure 5-10. PDFs of significant wave heights plotted on a Top) normal and Bottom) log scale. Plots include all existing data from these stations 96
Figure 5-11. PDFs of peak wave periods from 2004 through 2009 on a Top) normal and Bottom) log plot 97
Figure 5-12. Two examples of storms where measured and modeled waves are compared 98
Figure 5-13. PDFs of calculated 2% extreme runup elevations for NDBC 46005, 46089, and GROW hindcast results 99
Figure 5-14. Left) Map showing the locations of the northern Oregon coast buoys, and transect lines (A and B), and Right) model domain 101
Figure 5-15. Model-model comparison at 500-m depth on transect A for the 2006 simulation 102
Figure 5-16. Model-model comparison at 100-m depth on transect A for the 2006 simulation 102
Figure 5-17. Model data comparison at NDBC buoy #46029 for the 2006 simulations 103
Figure 5-18. Model data comparison at Station Aoff (GROW station location) versus 46089 for the 2010 simulations 103
Figure 5-19. The impact of ignoring bottom frictional dissipation and dissipation due to whitecapping for a 10-m significant wave height with a peak period of 20 s approaching from a direction of 285 degrees. 104
Figure 5-20. The impact of ignoring bottom frictional dissipation and dissipation due to whitecapping for a 14-m significant wave height with a peak period of 14 s approaching from a direction of 270 degrees 105
Figure 5-21. Joint probability of wave height and dominant direction derived from the GROW time series 106
Figure 5-22. SWAN wave modeling and calculated alongshore wave variability using the look-up table approach 106
Figure 5-23. SWAN wave modeling and calculated alongshore wave variability using the look-up table approach for an 11-m and 15-m wave 107
Figure 5-24. SWAN wave modeling and calculated alongshore wave variability using the look-up table approach for a 10-m wave 108
Figure 5-25. Joint probability of wave height and peak period from the GROW time series 108
Figure 5-26. Joint probability of dominant direction and peak period from the GROW time series 109
Figure 5-27. Individual parameter PDFs and bin edges using the combined buoy wave time series 110
Figure 5-28. Example SWAN simulation offshore from Lincoln County 111
Figure 5-29. Comparison of alongshore varying wave height at the 20-m contour extracted from the lookup tables (blue line) and from a direct SWAN computation (black line) with an offshore boundary condition characterized as H_s = 6 m, T_p = 12, D_p = 210, and a water level of 0-m NAVD88 111
Figure 5-30. Comparison of alongshore varying wave period at the 20-m contour extracted from the lookup tables (blue line) and from a direct SWAN computation (black line) with an offshore boundary condition characterized as H_s = 6 m, T_p = 12 s, D_p = 320, and a water level of 0m NAVD88 112
Figure 5-31. Comparison of alongshore varying wave direction at the 20-m contour extracted from the lookup tables (blue line) and from a direct SWAN computation (black line) with an offshore boundary condition characterized as H_s = 6 m, T_p = 12 s, D_p = 320, and a water level of 0m NAVD88 112
Figure 6-1. Conceptual model showing the components of wave runup associated with incident waves 113
Figure 6-2. Calculated setup, swash and runup using the Stockdon and DIM runup equations 116
Figure 6-3. Total water level calculations using the Stockdon (foreshore slope) and DIM runup equations (nearshore slope) 117
Figure 6-4. Wave runup on a beach backed by a structure or bluff 118
Figure 6-5. Example profile (Linc 4) where a broad rock platform fronts a bluff 121
Figure 6-6. Determination of an average slope based on an iterative approach 122
Figure 6-7. Example peak over threshold (POT) extreme value theory results for the Lincoln 6 transect site 132

Figure 6-8. Nomenclature of overtopping parameters available for mapping base flood elevations (BFEs) and flood hazard zones 141
Figure 6-9. Calculations of bore height decay from wave overtopping at Cape Lookout State Park at the peak of the 2-3 March 1999 storm based on a range of alpha (α) values 145
Figure 7-1. (A) The foredune erosion model. (B) The geometric model used to assess the maximum potential beach erosion in response to an extreme storm 152
Figure 7-2. Maximum potential erosion (R_∞) due to a change in water levels 153
Figure 7-3. Example plot of the approach used to define storm duration along the Coos County shoreline 155
Figure 7-4. Example transect from Coos County showing the locations of h_b (red crosses), used to define the cross-shore width (W_b) of the surf zone 156
Figure 7-5. Plot showing the dune erosion parameters (tan β, A, W_b, and h_b) used to calculate the profile responses (T_S), storm durations (T_D), alpha, and the storm-induced dune erosion 157
Figure 7-6. Plot showing the storm duration hours (T_D), the calculated time scale of profile response hours (T_S), alpha, and the storm induced K&D and geometric model erosion adjusted using equation 7.10 for the dune-backed profiles along the Lincoln County shore 157
Figure 7-7. Application of the duration reduced erosion estimate to the most likely winter profile at LINC 70, near the south end of Alsea Spit 161
Figure 7-8. Application of the duration reduced erosion estimate to the most likely winter profile at LINC 238 where overtopping and breaching occurs 163
Figure 7-9. Example profile where a barrier beach is overtopped and eroded 163
Figure 7-10. Overtopping of the barrier beach adjacent to Garrison Lake during a major storm on February 16, 1999 164
Figure 8-1. Example of a bluff-backed beach (LINC 6) where the calculated total water level and defined velocity (VE) zone extend into the bluff 165
Figure 8-2. Example of alongshore zone breaks and their relationship to geomorphic barriers and surveyed transects 166
Figure 8-3. Overtopping along the LINC 24 transect (near Yachats) 168
Figure 8-4. LINC 214 transect at Lincoln Beach with overtopping Splash zone 168
Figure 8-5. Example beach profile (#1609) located near Yaquina Bay State Park 170
Figure 8-6. Example profile from the Clatsop Plains where considerable aggradation and progradation of the dune has occurred 171
Figure 8-7. Example profile (#1929) from Netarts Spit showing the presence of at least two PFD locations 172
Figure 8-8. Plot showing identified PFD locations (yellow dots) along each transect, landward most dune heel (red dots), and derived PFD line (black line) 173
Figure 8-9. Redelineation at the mouth of Alsea Bay (Zone AE and 0.2 Percent Annual Chance Flood Hazard). 174
Figure 8-10. Siletz Bay, showing the effective flood zones incorporated “as is” 175
Figure 8-11. Coastal backwater flooding mapped from SWLs for Yaquina Bay 175

LIST OF TABLES

Table 2-1. Average uncertainties for Pacific Northwest shorelines 22
Table 3-1. Survey benchmarks used to calibrate GPS surveys of the beach along the Lincoln County coastline 44
Table 3-2. Horizontal and vertical coordinates (expressed as a standard deviation) at each of the benchmark locations, compared to the final coordinates referenced in Table 3-1 45
Table 3-3. Identified beach morphological parameters from the most likely winter profile along the Lincoln County shoreline 51
Table 4-1. Pacific Northwest NOAA tide gauges 71
Table 5-1. General statistics of the NDBC buoy and GROW data sets based on the complete time series of data, and truncated time series 95
Table 6-1. Parameters used to define runup (*R*) and total water levels (TWLs) on beaches backed by dunes, structures, and bluffs 123
Table 6-2. 100-year (1%) and 500-year (0.2%) total water levels calculated for the Lincoln County transect sites 133
Table 6-3. Splashdown and hazard zone limits calculated for Lincoln County detailed coastal sites 147
Table 6-4. Depth of flooding at the overtopping zones landward of the structure crest 149
Table 7-1. Calculated storm-induced erosion parameters for dune-backed beaches in Lincoln County 159
Table 8-1. Transect locations where the PFD was not used for mapping due to significant human modification of the dune 173

1.0 INTRODUCTION

The objective of the Lincoln County coastal flood hazard project is to develop a digital flood insurance rate map (DFIRM) and flood insurance study (FIS) report for Lincoln County, Oregon (**Figure 1-1**). A parallel effort is underway to convert the existing Lincoln County Federal Emergency Management Agency (FEMA) flood maps to a new countywide format in the North American Vertical Datum of 1988 (NAVD88); however, the scope of that project is strictly digital conversion and no new studies and/or updated floodplain boundaries are being incorporated. For this effort, the Oregon Department of Geology and Mineral Industries (DOGAMI) will be using available light detection and ranging data (lidar) to redelineate flood hazards within Lincoln County, produce revised DFIRMs and a revised FIS report, and produce other mapping products useable at the local, state, and federal level for mitigation planning, risk analysis, and disaster response.

As part of the redelineation, DOGAMI has been contracted to perform detailed coastal flood hazard studies for the entire length of the Lincoln County shoreline of the Pacific Ocean. These analyses are to include assessments of the 1% annual probability, or 100-year, extreme storm wave event and the associated calculated wave setup, runup, and total water level (i.e., the wave runup superimposed on the tidal level) to help guide the determination of Special Flood Hazard Areas (SFHAs), the most significant being regions subject to high coastal flood risk (Zone VE), characterized with base flood elevations (BFEs) that are used to guide building practices. Additional modeling of the 0.2%, or 500-year, event will also be undertaken.

The detailed analyses have been divided into the following discrete shore sections (**Figure 1-1**):

- Cape Perpetua: encompassing the basalt cliffs at Cape Perpetua, south of Yachats;
- Yachats: extends from Windy Way road to Perch Street;
- Waldport: extends Perch Street to the mouth of Alsea Bay;
- Alsea Spit: From the Alsea Bay mouth to Seal Rock;
- South Beach: From Seal Rock to the Yaquina Bay mouth;
- Newport: From the north Yaquina Bay jetty to the Yaquina Head;
- Yaquina headland:
- Beverly Beach littoral cell: From the north side of Yaquina Head to the south side of Otter Rock;
- Otter Rock: Otter Rock to the Otter Crest State Wayside
- Cape Foulweather: Otter Crest State Wayside to Rocky Creek Avenue in Miroco;
- Miroco: Rocky Creek Avenue to the juncture between the Otter Crest loop and Highway 101;
- Rocky Creek State Park: From the juncture between the Otter Crest loop and Highway 101 to Whale Cove;
- Whale Cove: Whale Cove to Cliff Street;
- Depoe Bay: From Cliff Street to Fogarty Creek;
- Fogarty Creek: Fogarty Creek to Fishing Rock;
- Gleneden Beach/Siletz Spit: From fishing Rock to the mouth of Siletz Bay;
- Lincoln City: From the north side of Siletz Bay mouth to Roads End Point;
- Salmon River Estuary: From Roads End Point to the mouth of the Salmon River estuary; and
- Cascade Head: The Cascade head shoreline.

The development of coastal flood maps is complicated due to its dependence on a myriad of data sources required to perform wave transformation, runup, and overtopping calculations. These challenges are further compounded by an equally wide range of potential settings in which the data and methods can be applied, which range from dune to bluff-backed beaches, sites that may be backed by coastal engineering structures such as sea walls, riprap revetments, or wooden bulkheads, to gravel and hard-rock shorelines. **Figure 1-2** broadly summarizes the steps described in the ensuing sections in order to help

understand conceptually the process that leads ultimately to the completed coastal flood hazard zones.

This report first examines the coastal geology and geomorphology of the Lincoln County shoreline, including a discussion of the erosion history of the coast. The results presented in this section will ultimately form the basis for defining the flood zones along the Lincoln coast. Section 3 presents the results of Real-Time Kinematic Differential Global Positioning Surveys (RTK-DGPS) of the detailed study sites established along the length of the Lincoln County shoreline, undertaken at the peak of the 2012/13 winter. These surveys are also compared with recent historical data derived from lidar data, which are used to help define the most likely winter profile used in the runup calculations described in Section 6. Section 3 also documents various parameters associated with the measured beach profile data, including the beach-dune junction elevation, the beach slope and dune/bluff crest/top elevations.

An examination of the tide data measured by the National Ocean Service (NOS) of the National Oceanographic Atmospheric Administration (NOAA) South Beach, Yaquina Bay tide gauge, is presented in Section 4, including an analysis of the 1% and 0.2% *still water levels* (SWL). Section 5 describes the steps undertaken to develop a synthesized wave climate, critical for developing the input wave statistics used in calculating the wave runup. Section 5 also examines the procedures used to refract the waves from deep water into the nearshore using the SWAN (Simulating Waves Nearshore) wave model. Analyses of the wave runup, including the calculation of the 1% and 0.2% total water levels (TWL), as well as any overtopping calculations, are presented and discussed in Section 6.

Section 7 discusses the steps used to determine the degree of erosion that might occur on the dune-backed beaches, including the approach used to define the duration-reduced erosion factor, important for further establishing the initial conditions on which the runup and overtopping calculations are ultimately performed. Similar discussions are provided describing observations of bluff erosion, characteristic of a few discrete sections of the Lincoln County shoreline. Finally, Section 8 synthesizes all of the information and describes the steps taken to draft new flood maps along the Lincoln County shoreline.

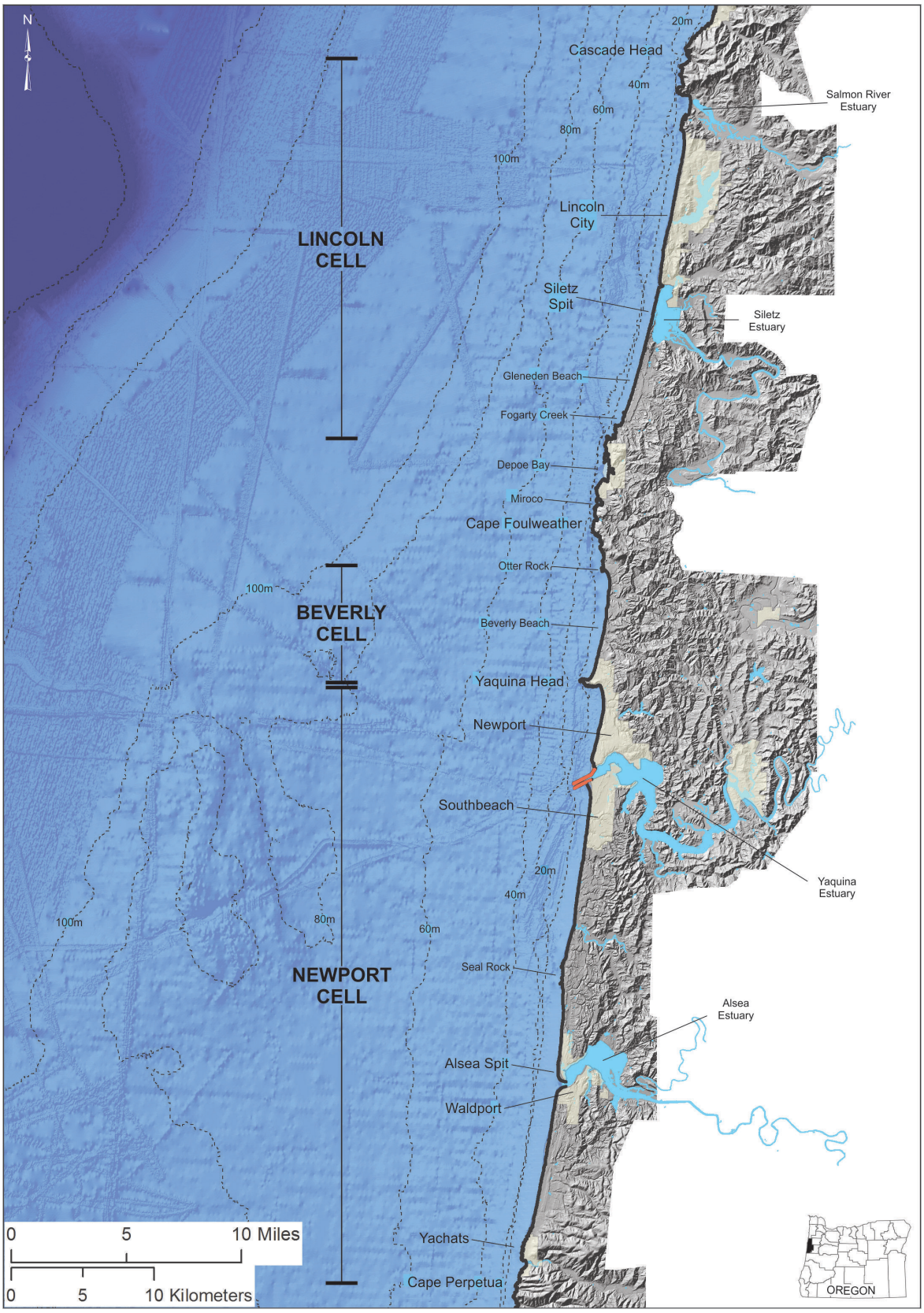

Figure 1-1. Location map of Lincoln County coastline.

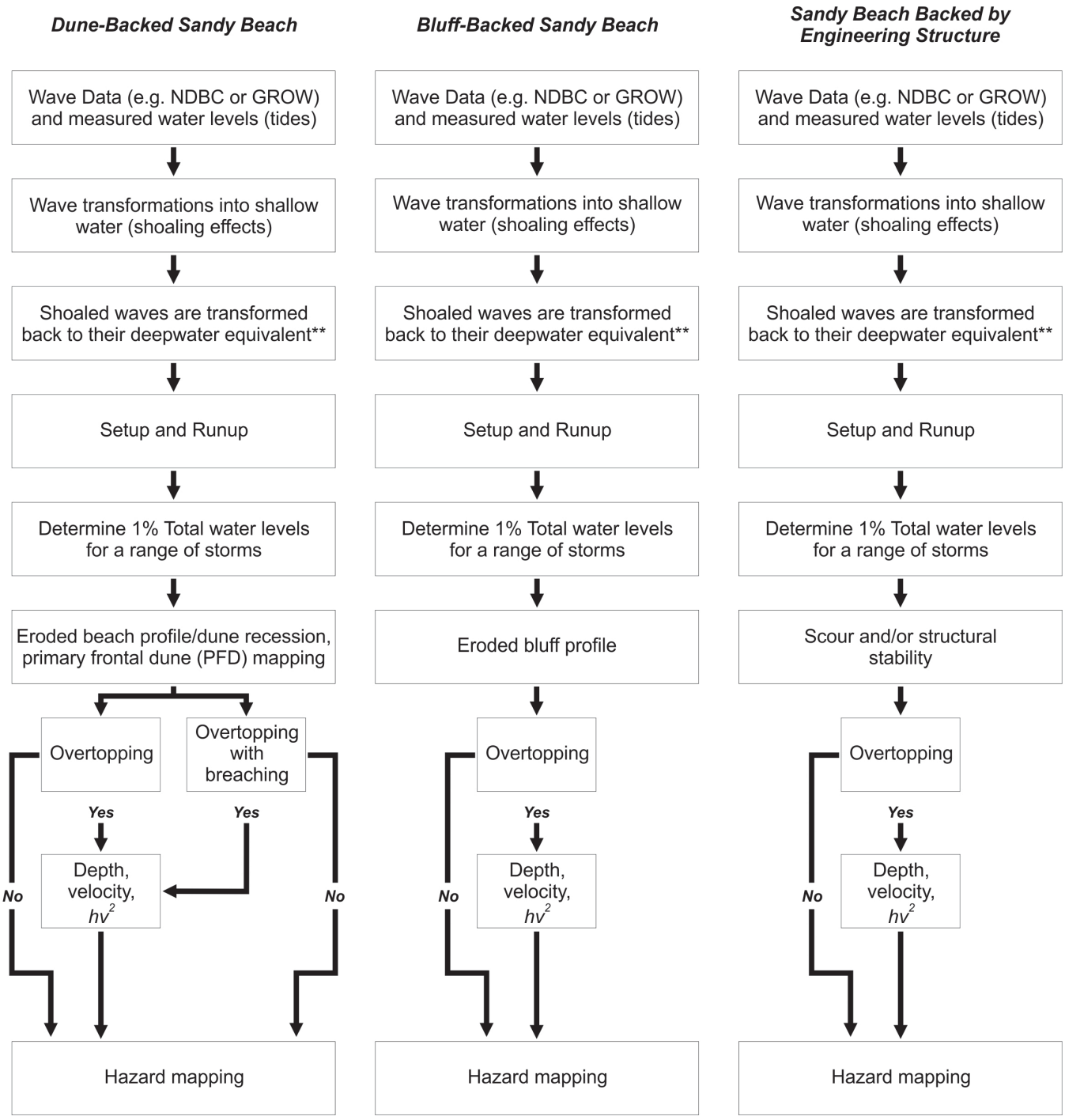

Figure 1-2. Three representative examples of the steps that may be taken to derive coastal flood hazard maps on the Pacific Northwest coast. **Note: The waves are first shoaled using numerical models in order to account for the effect of wave changes (refraction/diffraction) that take place across the shelf and in the nearshore. Because many coastal engineering equations (e.g., wave runup) require deepwater inputs, the "shoaled" waves are then converted back to their deepwater equivalence.

2.0 COASTAL GEOLOGY AND GEOMORPHOLOGY OF LINCOLN COUNTY

Lincoln County is located on the central Oregon coast, between latitudes 45°02′41.83″N (Salmon River estuary) and 44°16′29.98″N (Gwynn Creek, located just south of the Cape Perpetua scenic area), and longitudes 124°6′56.28″W and 123°35′50.26″W. The terrain varies from low elevation sandy beaches and dunes on the coast, to elevations over 1,000 m (3,281 ft, e.g., Saddleback Mountain in northeast Lincoln County reaches 1,036 m [3,359 ft]) farther inland. The coastal strip is approximately 120 km (74.6 mi) in length and varies in its geomorphology from broad, low-sloping sandy beaches backed by dunes, beaches backed by bluffs (of varying heights), beaches backed by engineered structures (riprap and seawalls), cobble and boulder beaches adjacent to the headlands, and cliff shorelines. Prominent headlands formed of resistant basalt (e.g., Cape Perpetua, Yaquina Head, and Cape Foulweather to Fogarty Creek) provide natural barriers to alongshore sediment transport (Komar, 1997), effectively dividing the county coastline into three littoral cells (**Figure 1-1)**. These include:

- The Newport littoral cell (~50.6 km [31.4 mi]), which extends from the north side of Cape Perpetua to Yaquina Head;
- The Beverly Beach cell (~8.2 km [5.1 mi]), which extends from Yaquina Head north to Otter Rock; and
- The Lincoln cell (~25.2 km [15.7]), which extends from Fishing Rock to Cascade Head in the north.

Each of these cells is further broken up into a series of smaller subcells due to the presence of four estuaries (in order from south to north, Salmon River, Siletz, Yaquina, and Alsea), one of which (Yaquina Bay) is bounded by prominent jetties (**Figure 1-1**). The county also is characterized with five major rivers (Salmon, Siletz, Yaquina, Alsea, and Yachats Rivers) that terminate in the estuaries or at the ocean. Due to their generally low flows and the terrain through which they cut, these rivers carry little beach sediment out to the open coast today depositing most of their sediment in the estuaries. Hence, the beaches of Lincoln County receive very little terrestrial sediment along the coast today other than from erosion of the backshore.

2.1 Local Geology

Along the Lincoln County coast the predominant geologic unit consists of latest Holocene beach sand present along the full length of the coastline (**Figure 2-1**) (Cooper, 1958). Interspersed between the sand are intrusive rocks (basalt, of Tertiary age), which characterize discrete areas, such as Cascade Head at the northern end of the county coastline (**Figure 2-2**), and the headlands south of Yachats (Schlicker and others, 1973). Other volcanic rocks (Miocene age) form the prominent Cape Foulweather headland as well as the basalt terrace along the Depoe Bay shoreline (Schlicker and others, 1973). These latter rocks are described as fine-grained. In all cases, rockfalls and landslides in these latter units are actively providing new material to the shoreline, albeit at relatively slow rates. These failures contribute to the formation of cobble and boulder berms (**Figure 2-3**), which accumulate along their base, and on their northern/southern flanks, where beaches have merged up against the headlands. Over time, the gravels and cobbles are redistributed along the beach in response to longshore currents. However, in almost all cases the gravels accumulate at the back of the beach where over time, they may become buried by sand.

Much of the shoreline of Lincoln County consists of prominent coastal bluffs formed in Tertiary sediments and fronted by wide, gently sloping, sand beaches composed of predominantly fine-grained beach sediments. The bluffs range in height from a few meters to as much as 40 m (130 ft) high, with the highest bluffs located along the Lincoln City shoreline (south of Roads End and north of Siletz Bay), while the lowest bluffs are located mainly in the southern part of the county (north of Yachats and south of Alsea Bay). The geology of these bluffs is characterized by a combination of siltstone-mudstone units (e.g., Nye

(**Figure 2-3**) and Yamhill (**Figure 2-4**) Formations, both of which are characterized as a clayey siltstone), and sandstones of various formations (e.g., Astoria). In many areas these predominant geologic units are overlaid and may be fronted by a mantling of younger terrace deposits, particularly along the open coast, where coastal processes are presently eroding these sediments exposing both the terrace deposits and the Tertiary sediments (**Figure 2-4**). Formation of the terraces can be attributed to the uplift of the Coast Range due to the subduction of the Juan de Fuca and Gorda plates beneath the North American plate in concert with varying sea level during the Pleistocene (Orr and others, 1992). Thus, a typical sea cliff sequence consists of Tertiary rocks at its base that may be somewhat resistant to wave attack and subaerial processes, capped by a layer of Pleistocene terrace sandstone or recent Holocene dune sands (Komar, 2004). Because of the dramatic ocean vistas gained from the nearly level terraces, many homes and condominiums are now situated along the edge of eroding terraces (**Figure 2-5**). The remainder of the coastline consists of barrier spits that separate estuaries from the open coast. These include the Salmon, Siletz (**Figure 2-1** and **Figure 2-2**), Yaquina and Alsea.

Much of the beach sand present on the Oregon coast consists of grains of quartz and feldspar. The beaches also contain small amounts of heavier minerals (e.g., garnet, hypersthene, augite, and hornblende (**Figure 2-6**), which can be traced to various sediment sources along the Pacific Northwest coast (Clemens and Komar, 1988). For example, garnet and hypersthene is derived from the Klamath Mountains located in southern Oregon and in North California. Because the headlands today extend well out in deep water, they effectively limit sand transport around their ends under the current process regime. This suggests that these heavier minerals were probably transported northward along the coast at a time when sea level was much lower, with few barriers to interrupt their northward movement (Komar, 1997). With distance from their source, the sediments combined with other minerals derived locally from erosion processes in the coast range. As shown in **Figure 2-6**, the concentrations of garnet and hypersthene decrease to the north, while concentrations of augite increase significantly; augite is prevalent in the volcanic rocks present throughout Tillamook County. At Tillamook Head, the concentration of garnet is very small, suggesting that Tillamook Head reflects the most northerly transport of this mineral. North of Tillamook Head, it can be seen that concentrations of hypersthene and hornblende increase again. These latter sediments are derived from the Columbia River, which contributed to the formation of the Clatsop Plains, Long Beach Peninsula, and Grayland Plains. Thus, sediments derived from the Columbia River were transported mainly to the north, supplying the Washington coast and shelf.

With the end of the last glaciations, sea level rose rapidly and the beaches began to migrate landward. New sediments were derived from erosion of the coastal plain that makes up the continental shelf today. At around 5,000–7,000 years ago, the rate of sea level rise slowed as it approached its current level today (Komar, 1997). At this stage the prominent headlands would have begun to interrupt sediment transport. Modern barrier spits and beaches began to form within the headland bounded littoral cells that make up the present coast today.

Along the Tillamook and northern Lincoln County coast, the beaches contain increased concentrations of augite, indicative of their having been derived locally (**Figure 2-6**). Increased concentrations of hornblende are also apparent along much of the Lincoln County shoreline, particularly south of Cape Foulweather and north of Heceta Head. Such characteristics imply that at the time, rivers and streams were carrying these sediments out to the coast where they mixed with other sediments. These concentrations likely increased during the past 150 years as human settlement accelerated leading to increased deforestation (Peterson and others, 1984; Komar and others, 2004). This correspondingly contributed to increased sediment loads in the various rivers. However, analyses of the sediment characteristics in Tillamook Bay, the largest estuary in the county, indicated that while fine sediments pass through the estuary, the bulk of the coarser sediments remain behind where

they accumulate as bars and shoals in Tillamook Bay. Furthermore, sediments within Tillamook Bay are predominantly of a marine origin (60%), while river sediments make up 40% of the sediment in the estuary. This finding is consistent with the work of Peterson and others (1984) and Clemens and Komar (1988) who observed that because of the combination of low river discharge and high tidal regime in Oregon estuaries, the majority of the estuaries are in fact natural "sinks" for the sediment. Thus, the beaches of Oregon receive very little sediment input from rivers and streams today. Accordingly, sediment supply is essentially confined to those areas backed by coastal bluffs, particularly those areas overlain by more erosive Pleistocene marine terrace sandstones (raised ancient beach and dune sands) and more recent Holocene dune sands that drape the landscape.

Prior to the 1940s, many of the barrier spits were devoid of significant vegetation. With the introduction European beach grass (*Ammophila arenaria*) in the early 1900s and its subsequent proliferation along the Oregon coast, the grass essentially resulted in the stabilization of the dunes and barrier spits. The product today is an extensive foredune system, which consist of large "stable" dunes containing significant volumes of sand. Accompanying the stabilization of the dunes, humans have settled on them, building in the most desirable locations, typically on the most seaward foredune. As will be shown throughout this report, construction of these homes and facilities in such areas poses a significant risk as periodically storms erode into the dunes. This has resulted in many cases where the foundations of the homes are undermined, eventually requiring riprap coastal engineering structures to mitigate the erosion problem.

Figure 2-1. Looking south along Siletz spit toward Fishing Rock and Government Point in the far distance (photo: E. Harris, DOGAMI, 2011).

Figure 2-2. Looking east at Cascade Head (left) and the Salmon River estuary with its barrier spit (photo: E. Harris, DOGAMI, 2011).

Figure 2-3. Looking south toward Yaquina Head in the distance. Coastal bluffs of the Nye formation characterize much of the shore within the Beverly Beach littoral cell. Note the presence of a relatively extensive cobble berm, which serve to protect the bluff toe from coastal erosion (photo: J. Allan, DOGAMI, 2004).

Figure 2-4. Oblique aerial photo of homes perched along the cliff top at Roads End, Lincoln City, Oregon. Dark banding in the upper terrace face reflects ground water seepage down through the terrace sediments, where it comes into contact with the less permeable Tertiary siltstones of the Yamhill Formation. Note the recent slump failure in mid photo (photo: E. Harris, DOGAMI, 2011).

Figure 2-5. Sea cliff erosion at Gleneden Beach, Lincoln County. Image shows the presence of terrace sands that are rapidly eroding in response to cliff toe erosion. An emergency riprap structure is being constructed to mitigate the problem (photo: L. Stimely, DOGAMI, 2013).

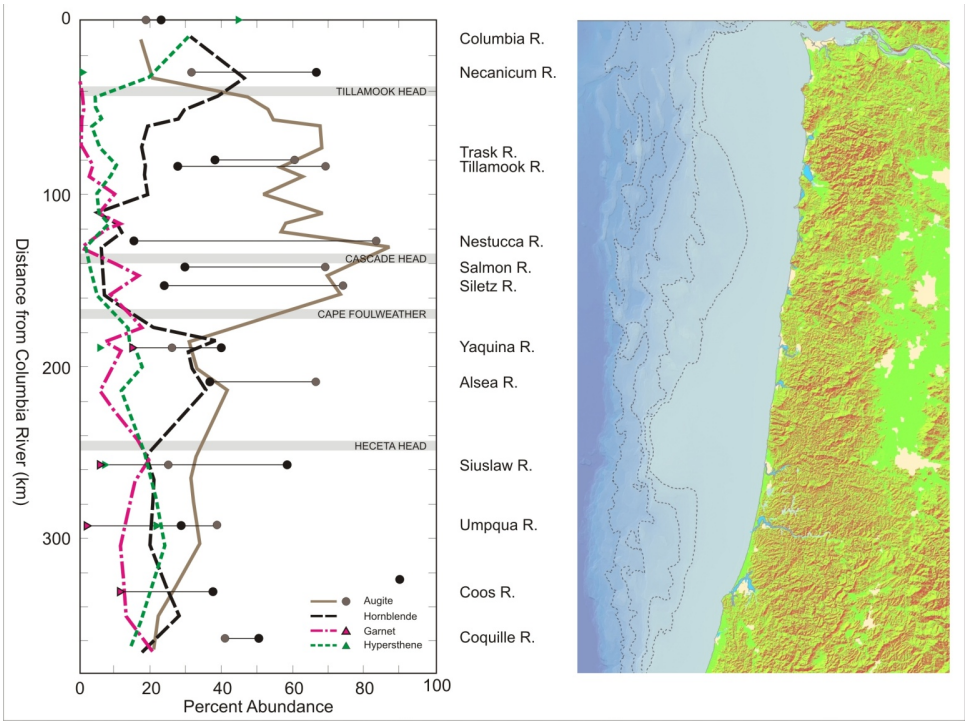

Figure 2-6. Variations in the percent abundances of various heavy minerals observed on the central to northern Oregon coast (after Clemens and Komar, 1988).

2.2 Tsunami Hazards Associated with the Cascadia Subduction Zone and from Distant Earthquake Sources

There is considerable geologic evidence from estuaries and coastal lakes along the Cascadia subduction zone of episodic occurrences of abrupt coastal subsidence immediately followed by significant ocean flooding associated with major tsunamis that swept across the ocean beaches and also traveled well inland through the bays and estuaries. Coastal paleoseismic records document the impacts of as many as 13 major subduction zone earthquakes and associated tsunamis over the past ~7,000 years (Witter and others, 2003; Kelsey and others, 2005; Witter and others, 2010), while recent studies of turbidite records within sediment cores collected in deep water at the heads of Cascadia submarine canyons provide evidence for at least 41 distinct tsunami events over the past ~10,000 years (Goldfinger and others, 2003; Goldfinger, 2009; Goldfinger and others, 2012). The length of time between these events varies from as short as a century to as long as 1,200 years, with the average recurrence interval for major Cascadia earthquakes (magnitude [M_W] > 9) estimated to be ~530 years (Witter and others, 2010).

The most recent Cascadia subduction zone earthquake occurred on January 26, 1700 (Satake and others, 1996; Atwater and others, 2005) and is estimated to have been a magnitude (M_W) 9 or greater based on the size of the tsunami documented along the coast of Japan. This event probably ruptured the full length (~1,200 km) of the subduction zone, based on correlations between tsunami deposits identified at multiple sites along the length of the PNW coast.

There is now increasing recognition that great earthquakes do not necessarily result in a complete rupture of the Cascadia subduction zone (i.e., rupture along the full 1,200-km fault zone), such that partial ruptures of the plate boundary have occurred in the paleo-records due to smaller earthquakes with magnitudes (M_W) < 9 (Witter and others, 2003; Kelsey and others, 2005). These

partial segment ruptures appear to occur more frequently on the southern Oregon coast, determined from paleotsunami studies (stratigraphic coring, radiocarbon dating and marine diatom analyses) undertaken at several locations on the southern Oregon coast, including Bradley Lake located just south of Bandon, the Sixes River and the Coquille estuary. According to Kelsey and others (2005), initial estimates of the recurrence intervals of Bradley Lake tsunami incursion is typically shorter (~380–400 years) than the average recurrence intervals inferred for great earthquakes (~530 years). Furthermore, they have documented from those records that local tsunamis from Cascadia earthquakes recur in clusters (~250–400 years) followed by gaps of 700–1,300 years, with the highest tsunamis associated with earthquakes occurring at the beginning and end of a cluster.

Recent analyses of the turbidite records (Goldfinger, 2009; Goldfinger and others, 2012) suggest that of the 41 events in the geologic past:

- 20 events were probably associated with a rupture of the full Cascadia subduction zone, characterized by a magnitude (M_W) ~9 or greater earthquake;
- 2-3 events reflected a partial rupture (~75%) of the length of the subduction zone, characterized by an estimated earthquake magnitude (M_W) of ~8.5-8.8 earthquake;
- 10-11 events were associated with a partial rupture (~50%), characterized by an estimated earthquake magnitude (M_W) of ~8.3-8.5 earthquake; and
- 8 events reflected a partial rupture (~25%), with an estimated earthquake magnitude (M_W) of ~7.6-8.4.

These last 19 shorter ruptures are concentrated in the southern part of the margin and have estimated recurrence intervals of ~240–320 years. Goldfinger (2009) estimated that time-independent probabilities for segmented ruptures range from 7–9% for full margin ruptures to ~18% in 50 years for a southern segment rupture; time dependent rupture analyses indicate that the probability increases to ~25% in 50 years for the northern zone.

Aside from local tsunamis associated with the Cascadia Subduction Zone, the Oregon coast is also susceptible from tsunamis generated by distant events, particularly along the coast of Japan, along the Aleutian Island chain, and from the Gulf of Alaska. The most recent distant tsunami event occurred on March 11, 2011, when a magnitude (M_W) 9.0 earthquake occurred 129 km (80 miles) offshore from the coast of Sendai, northeast Honshu, Japan (Allan and others, 2012a). This earthquake triggered a catastrophic tsunami that within minutes inundated the northeast coast of Japan, sweeping far inland; most recent reports indicate 15,854 dead and another 3,155 missing. Measurements derived from a tide gauge on the impacted shore (Ayukawa, Ishinomaki, Miyagi Prefecture) recorded a tsunami amplitude of 7.6 m, before the gauge was destroyed by the initial tsunami wave (Yamamoto, 2011), while post-tsunami surveys indicate that the tsunami water levels within the inundation zone reached as high as 19.5 m (Mori and others, 2011). The tsunami also propagated eastward across the Pacific Ocean, impacting coastal communities in Hawaii and along the west coast of the continental United States — Washington, Oregon, and California.

Damage in Oregon, Washington, and northern California from the tsunami was almost entirely confined to harbors, including Depoe Bay, Coos Bay, Brookings in Oregon, and in Crescent City, California, having been moderated by the arrival of the tsunami's highest waves during a relatively low tide (Allan and others, 2012a). At Crescent City, an open-coast breakwater, the to-and-fro surge of the water associated with the tsunami waves overturned and sank 15 vessels and damaged 47, while several boats were swept offshore. Flood damage also occurred during the early hours of March 12; for example, an RV park near the mouth of Elk Creek was flooded when a 1.05 m (3.4 ft) tsunami wave arrived, coinciding with high tide. The total damage to the Crescent City harbor and from the effects of the flooding has been placed at $12.5 million. At

Brookings on the southern Oregon coast, 12 fishing vessels put to sea at about 6 am, prior to the arrival of the tsunami waves. However, the *Hilda*, a 220-ton fishing boat and the largest in the harbor, broke loose under the forces of the wave-induced currents, washing around the harbor and smashing into and sinking several other boats. Much of the commercial part of the harbor and about one third of the sports basin were destroyed; the total damage has been estimated at about $10 million.

Prior to the Tōhoku tsunami, the previous most significant distant tsunami occurred on March 27th 1964, when a magnitude (M_W) 9.2 earthquake occurred near Prince William Sound in Alaska, which generated a catastrophic local tsunami in Alaska, while the effects of the tsunami was also felt around the Pacific Basin. The tsunami caused significant damage to infrastructure in the coastal communities of Seaside and Cannon Beach and killed four people camping along Beverly Beach in Lincoln County.

In 2009, the Oregon Department of Geology and Mineral Industries (DOGAMI) initiated a multi-year study to accelerate remapping of the Oregon coast for tsunami inundation using state of the art computer modeling and laser based terrain mapping (lidar). The outcome of this effort was the creation of new and more accurate tsunami evacuation maps for the entire length of the coast. DOGAMI, in collaboration with researchers (Zhang and Baptista) at the Oregon Health and Science University (OHSU), Oregon State University (Goldfinger), and the Geological Survey of Canada (Wang), developed a new approach to produce a suite of next-generation tsunami hazard maps for Oregon (Priest and others, 2010; Witter and others, 2010). Modeling tsunami inundation on the southern Oregon coast was initiated late in 2009 and consisted of a range of scenarios, including 15 Cascadia events and two distant earthquake source events (e.g., 1964 Prince William Sound earthquake magnitude [M_W] 9.2 earthquake (Witter, 2008)). The last of the suite of new evacuation maps (TIM series) was released in 2013; the maps are also available in an online tsunami hazard portal (http://nvs.nanoos.org/TsunamiEvac).

Associated with great Cascadia earthquakes is a near instantaneous lowering (subsidence) of the coast by ~0.4 m (1.3 ft) to as much as 3 m (9.8 ft) (Witter and others, 2003). This process equates to raising sea level by the same amount along the entire Pacific Northwest coastline. Following the earthquake, coastal erosion is expected to accelerate everywhere as the beaches and shorelines adjusted to a new equilibrium condition that, over time, would likely decrease asymptotically (Komar and others, 1991). On the southern Oregon coast, Komar and others have suggested that the extensive development of sea stacks offshore from Bandon may be evidence for that erosion response following the last major subduction zone earthquake in 1700. Over the past century, the erosion appears to have stabilized as there is little evidence for any progressive erosion trend. This suggests that the south coast is now being uplifted (estimated to be ~0.6 to 1.1 m) due to the Cascadia subduction zone having become locked again, such that strain is now building toward the next major earthquake. With the release of that energy and land subsidence, cliff erosion along the Bandon shore (and elsewhere on the Oregon coast) would be expected to begin again.

2.3 Coastal Geomorphology

On the basis of geology and geomorphology, the Lincoln County shoreline can be broadly divided into four morphological beach types. These are depicted in **Figure 2-7** to **Figure 2-12** and include:

1. ***Dune-backed beaches:*** Dune-backed beaches make up approximately 16.1% of the Lincoln County shoreline, much of which is associated with the barrier spits (e.g., Salmon, Siletz, and Alsea Spits, **Figure 2-7**, Figure 2-8, and **Figure 2-11**). The geomorphology of the beaches can be generalized as having wide, dissipative surf zones with low sloping foreshores that are backed by high dunes containing significant sand volume (**Figure 2-1**). Dune crest elevations reach their highest peak immediately south of the Yaquina Bay south jetty (15.3 m [50.2 ft]), and along the southern one-third of Alsea Spit (17.2 m [56 ft]) (**Figure 2-13**). In both areas, the dunes are actively gaining sand and are experiencing significant dune building. Along the remainder of the county, mean dune crest elevations are 10.7 m (35.1 ft), with most dunes being in the range of 9 to 12.6 m (29.5–41.3 ft). The average beach slope (tan β) for dune-backed beaches is summarized in **Figure 2-14** where it is apparent that slopes vary significantly along the Lincoln County coast, with the lowest mean slopes occurring in the vicinity of Newport (mean = 0.022), and are steepest along Gleneden Beach/Siletz Spit in the Lincoln littoral cell (mean = 0.078). In the Beverly Beach littoral cell, the beach slopes appear to be bi-modal and is likely due to the fact that parts of this shore is backed by gravel (**Figure 2-3**), or may be influenced by antecedent conditions associated with the local geologic rock units, which are close to the surface throughout this cell.
2. ***Cliffed/Rocky shore:*** Cliffed shores make up the second largest (35.3%) geomorphic "type" in the county (**Figure 2-2**). Examples of this type of shore exist around each of the major headlands, and are particularly prevalent between Cape Foulweather and Fogarty Creek. This particular shore type invariably consists of near-vertical cliffs that plunge into the ocean, or steep-sloping basalt ramps that slope steeply down into the ocean (**Figure 2-15**). In some cases, the cliffs may be fronted by rock platforms and/or talus.
3. ***Bluff-backed beaches:*** Bluff-backed beaches fronted by a wide, dissipative sand beach make up the bulk (~48.6%) of the Lincoln County coastline (**Figure 2-4** and **Figure 2-5**). This particular geomorphic type dominates the shoreline between Yachats and Waldport, Seal Rock to Newport, Newport to Otter Rock, Gleneden Beach, and along the Lincoln City shoreline. The bluffs that back the beaches vary in height from ~7 m (23 ft) to greater than 40 m (131 ft). Beach slopes (tan β) seaward of the bluffs are similar to those observed throughout Lincoln County, averaging about 0.037 (σ = 0.014). In several areas (e.g., Beverly Beach littoral cell) the sand beach may be backed by a gravel beach (**Figure 2-3**), making the beach slopes composite characterized by a gently sloping sand beach that is backed by a steep sloping gravel berm.

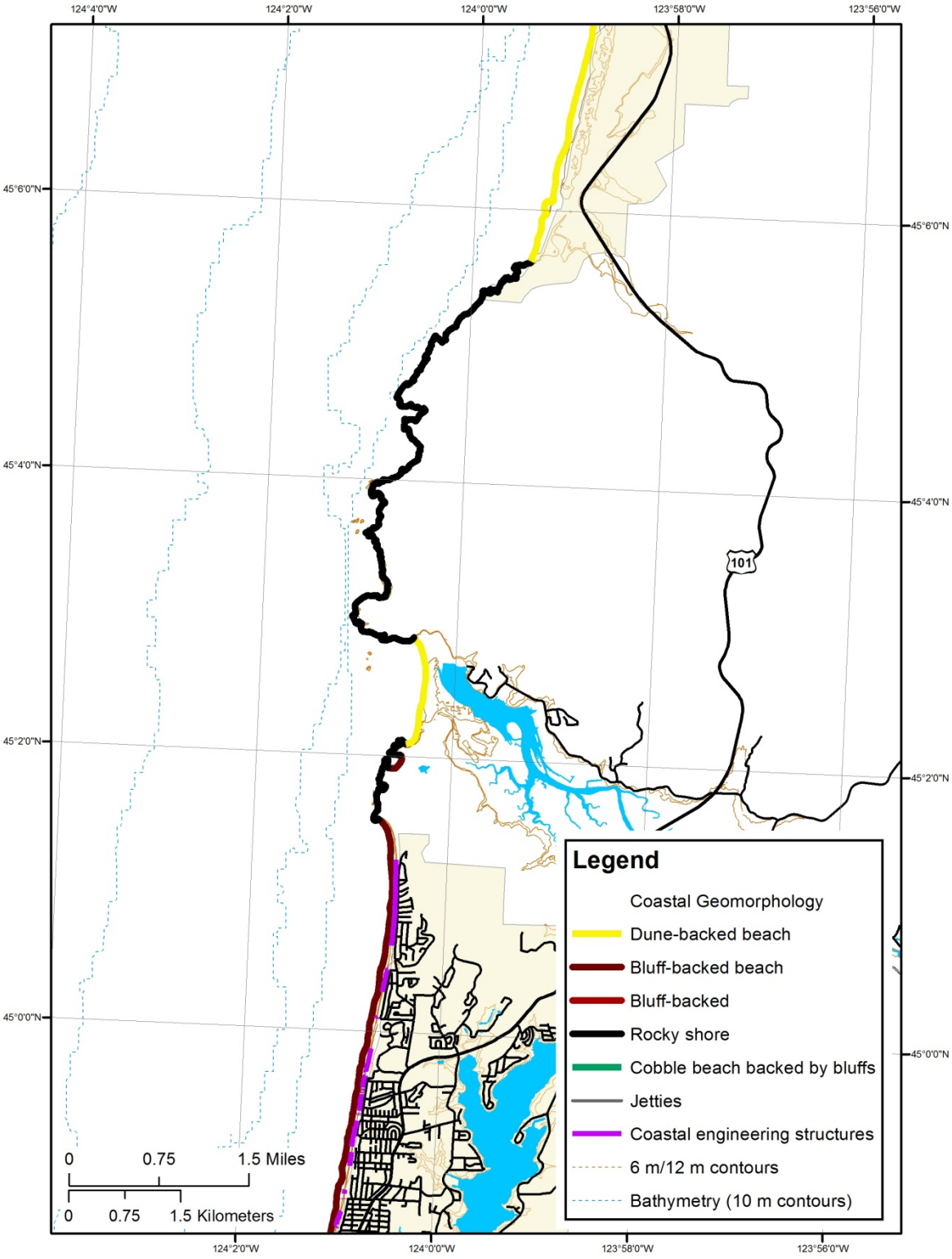

Figure 2-7. Geomorphic classification of northern Lincoln City beach, Salmon River estuary, and Cascade Head.

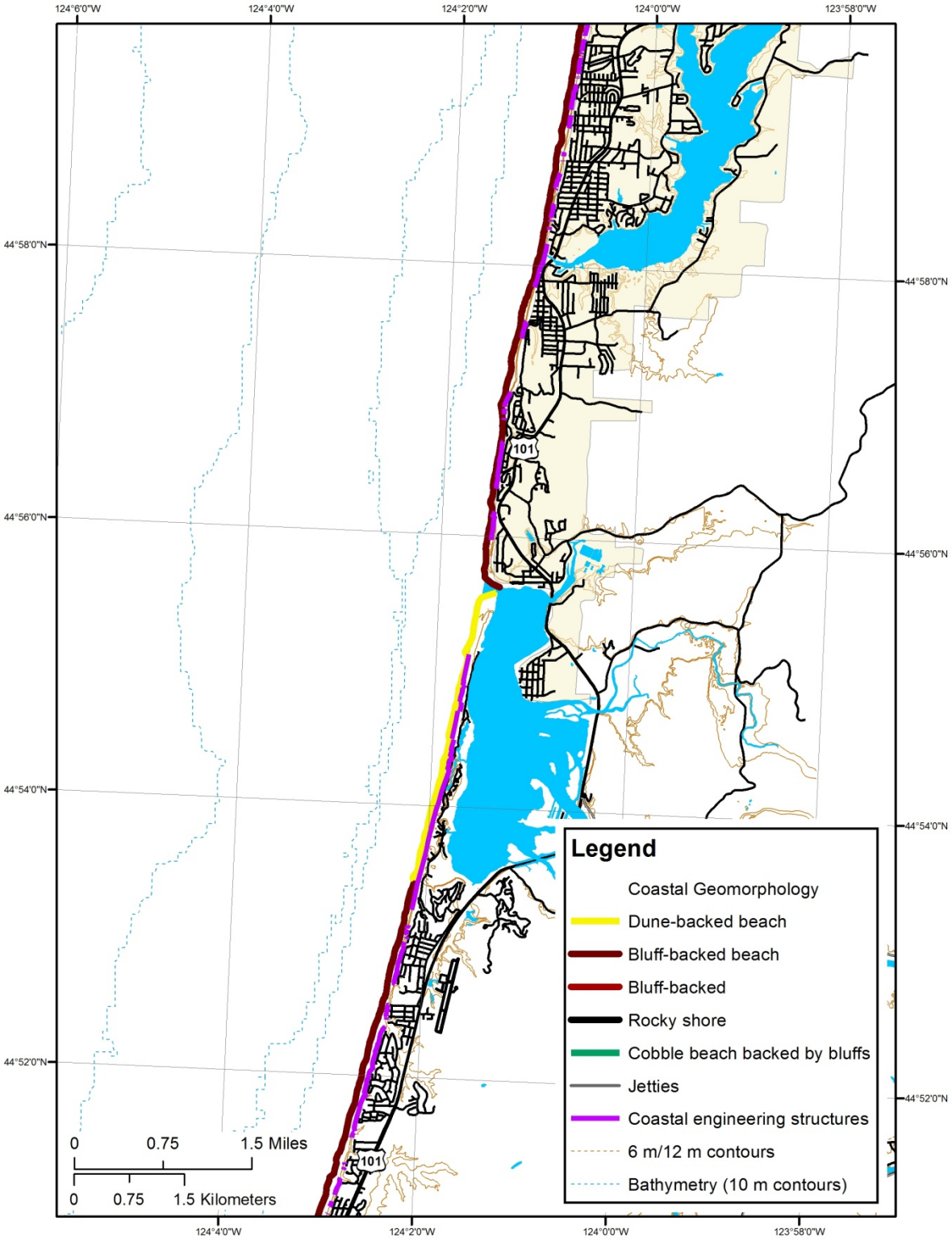

Figure 2-8. Geomorphic classification of Gleneden Beach, Siletz Spit, and southern Lincoln City Beach.

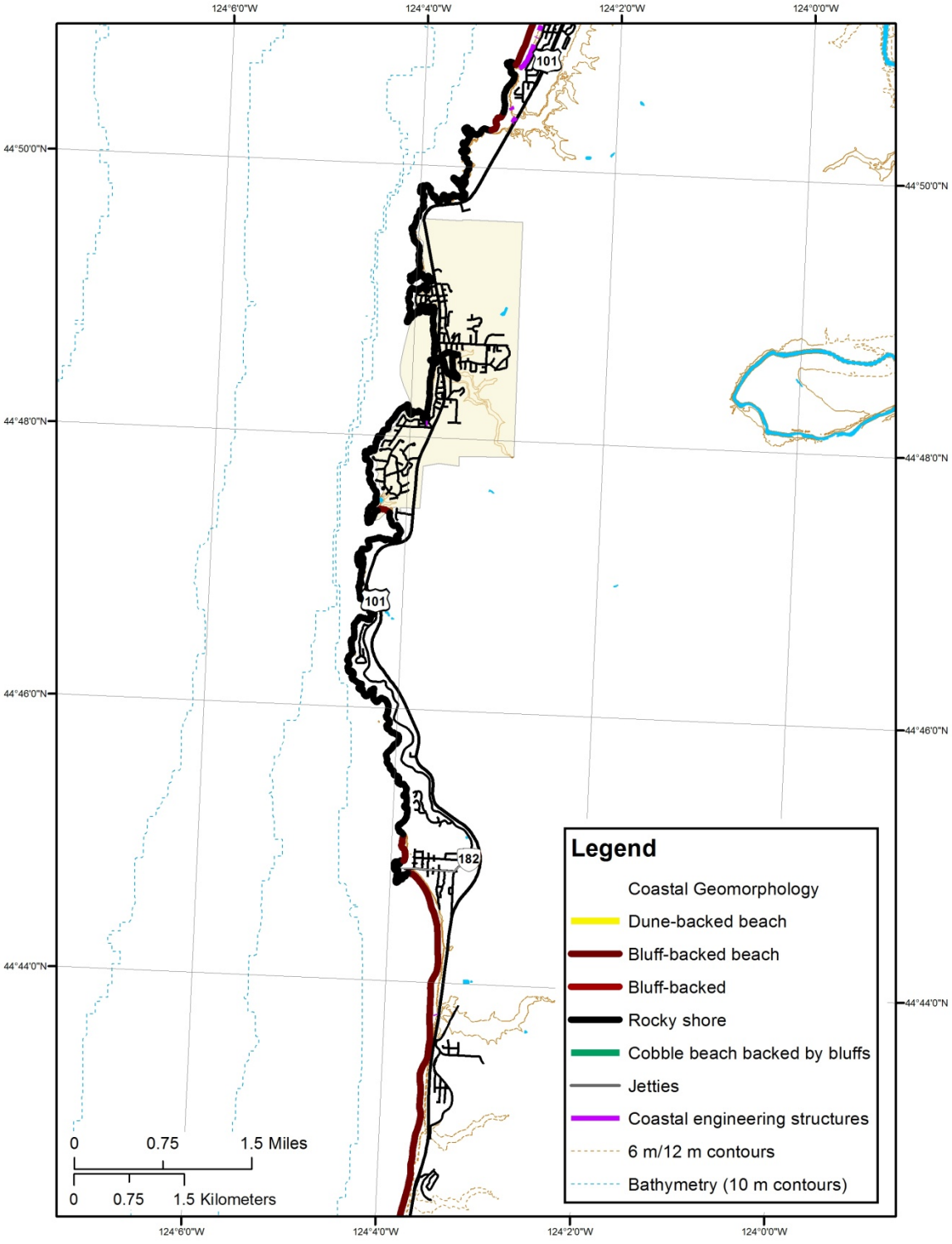

Figure 2-9. Geomorphic classification of the Fogarty Creek, Depoe Bay, Cape Foulweather, Otter Rock, and northern Beverly Beach areas.

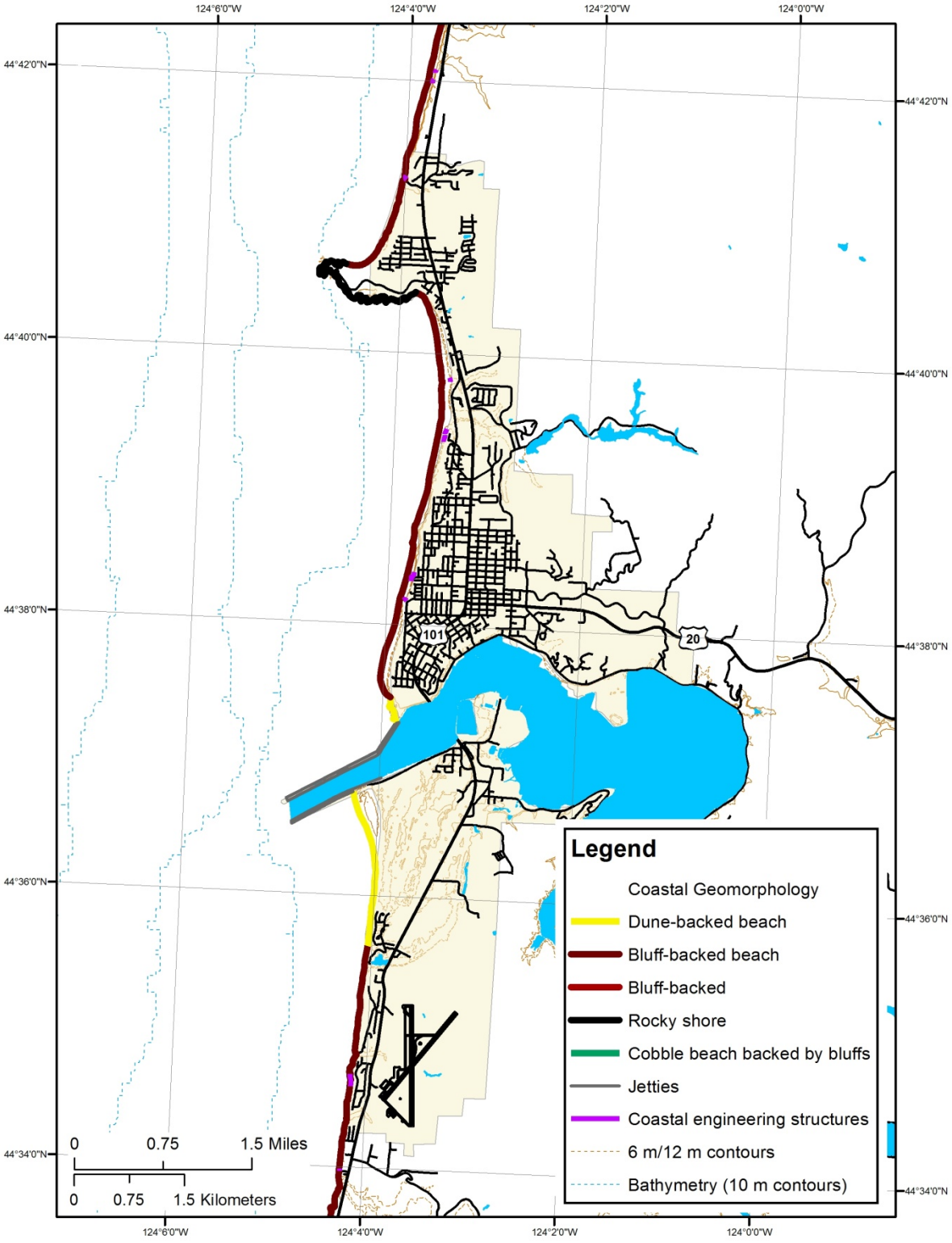

Figure 2-10. Geomorphic classification of the southern Beverly Beach littoral cell, Yaquina Head, Newport cell, and South Beach areas.

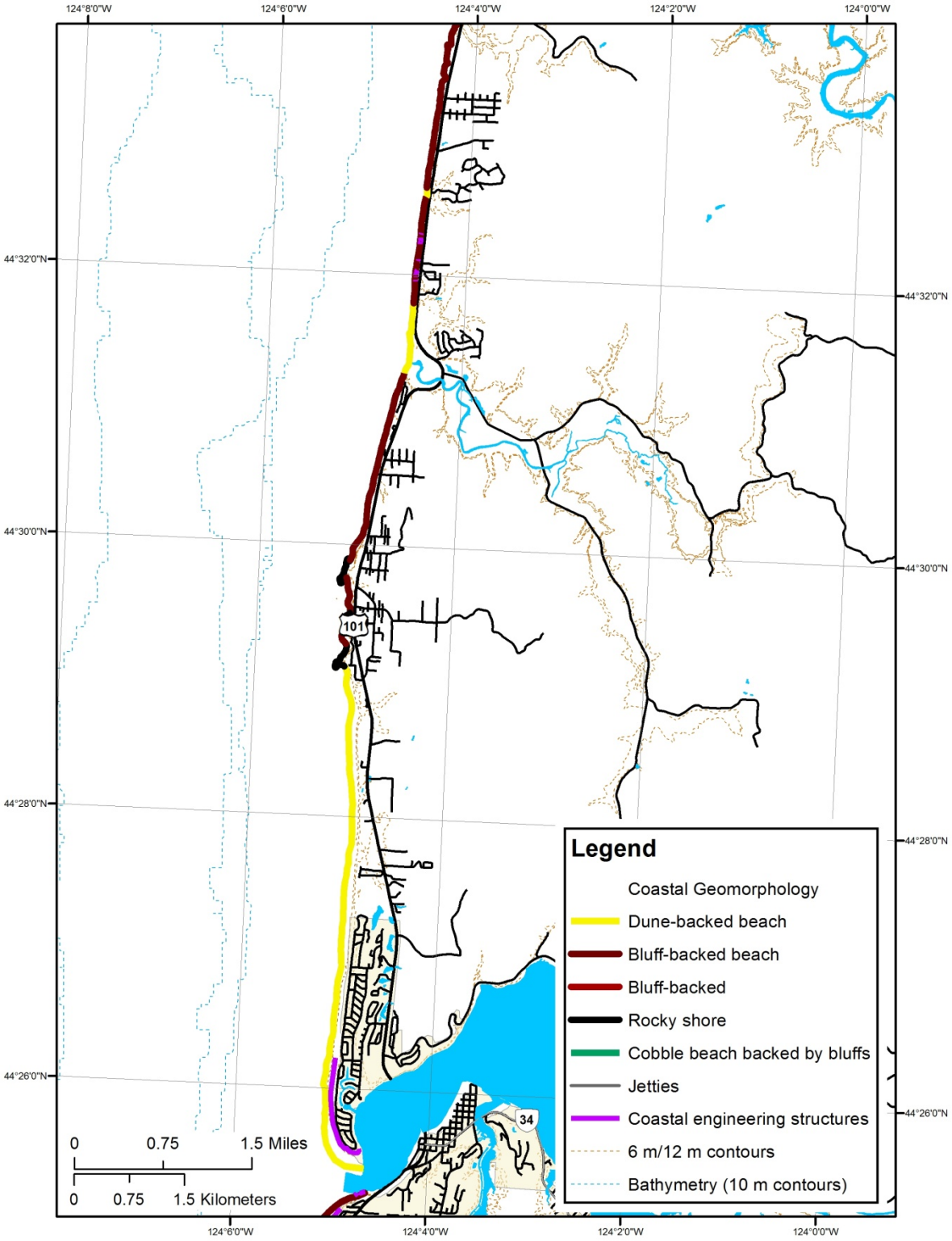

Figure 2-11. Geomorphic classification of the southern end of the South Beach cell, Ona Beach, Seal Rock, and Alsea Spit areas.

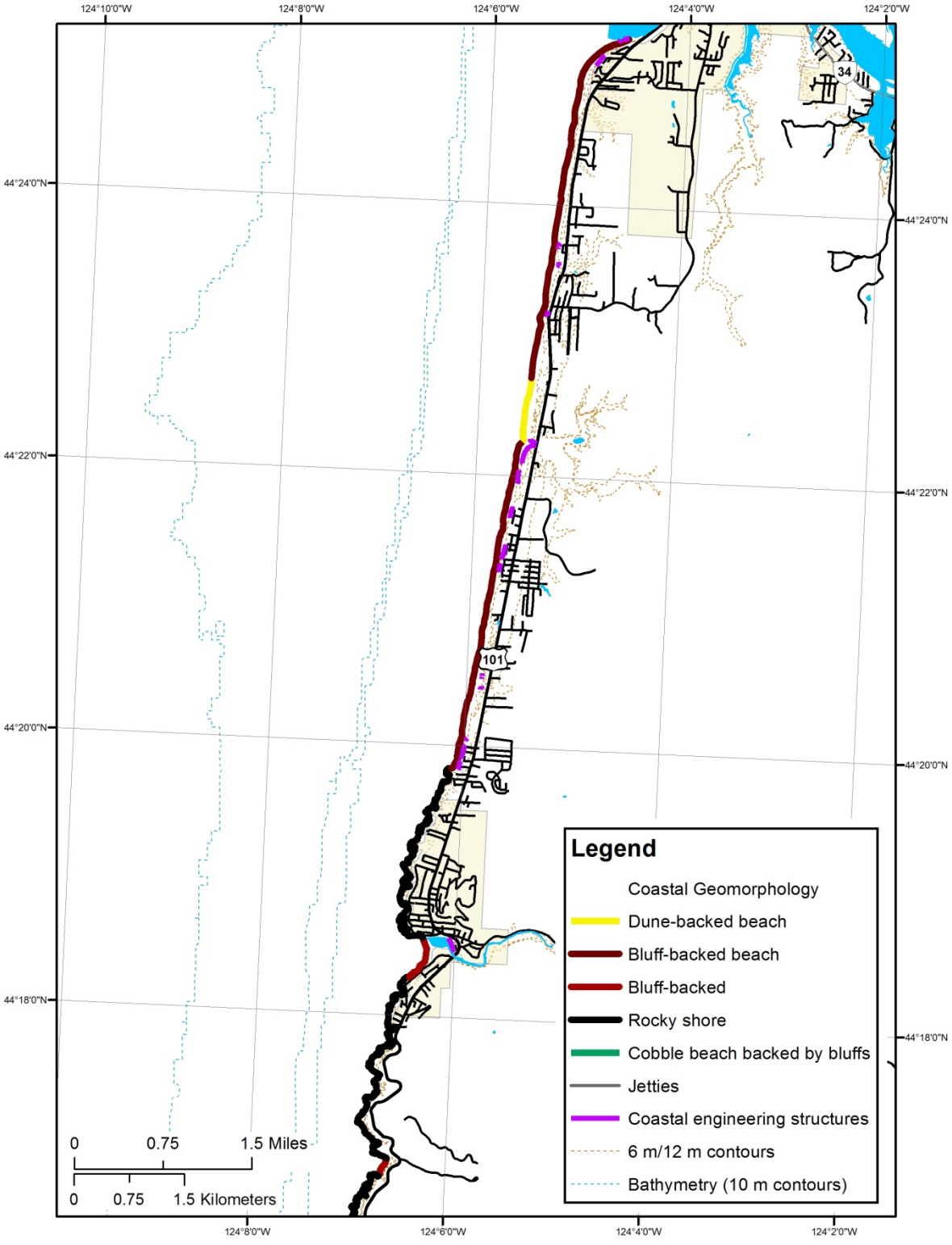

Figure 2-12. Geomorphic classification of the Waldport cell, Yachats, and Cape Perpetua areas.

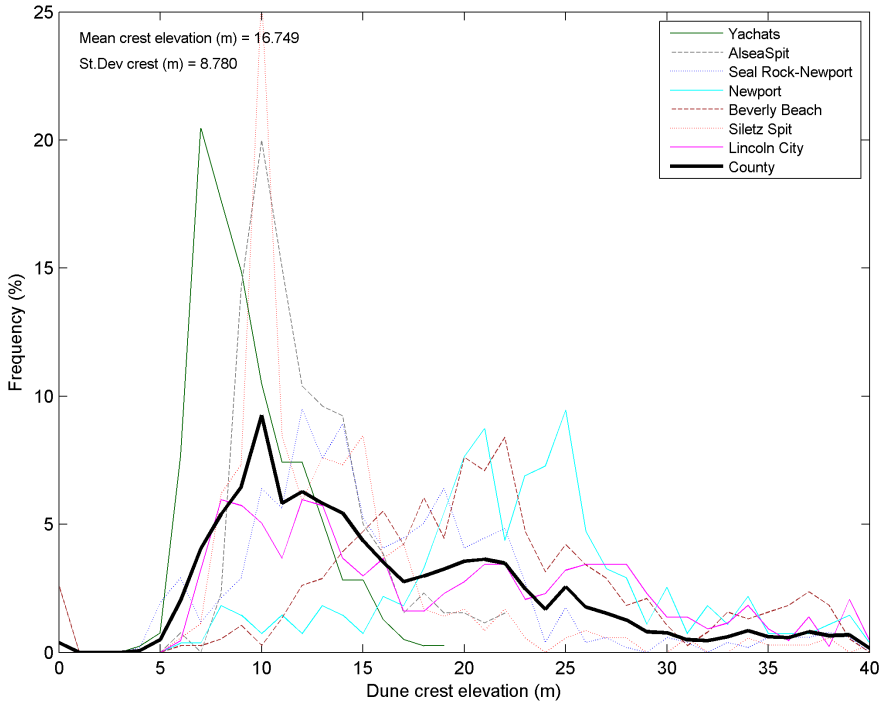

Figure 2-13. Lincoln County dune crest elevations. Note: elevations are relative to NAVD88.

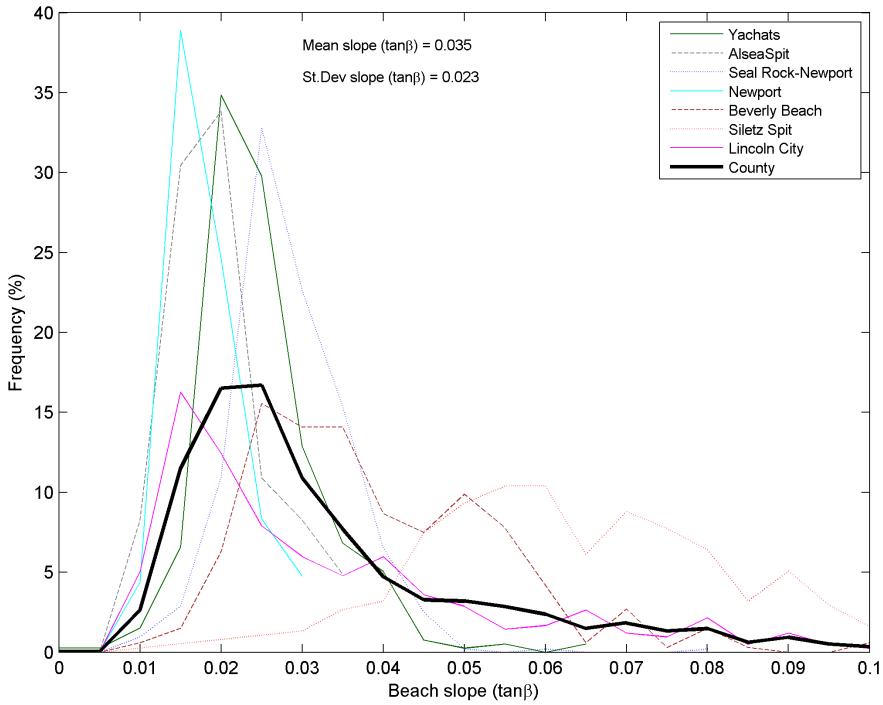

Figure 2-14. Lincoln County beach slopes.

Figure 2-15. Basalt dominates the local geology between Cape Foulweather and Depoe Bay. Much of this coastline consists of either plunging cliffs or steeply sloping rock ramps (photo: J. Allan, DOGAMI, 2012).

2.4 Coastal Erosion and Flood History

2.4.1 Lincoln County historical shoreline positions

This section presents a qualitative discussion of large-scale morphological changes derived from analyses of historical and contemporary shorelines derived for the Lincoln County coastline. This summary stems from work undertaken by researchers at DOGAMI and OSU over the past two decades (Priest and others, 1993; Allan and others, 2003; Allan and Harris, 2012; Allan and Stimely, 2013; Ruggiero and others, 2013).

National Ocean Service (NOS) Topographic (T)-sheet shoreline positions covering the 1920s and 1950s were previously obtained from NOAA. These lines reflect the Mean High Water (MHW) line mapped by early NOS surveyors, on an average tide typically in mid- to late summer. Additional shorelines were derived from a variety of other sources including: 1967 digital orthophotos (Ruggiero and others, 2013), and from 1997, 1998, 2002, 2009, and 2010 lidar data. Pre-lidar historical shorelines use the High Water Line (HWL) as a shoreline proxy. The HWL has been used by researchers for more than 150 years because it could be visually identified in the field or from aerial photographs. In contrast, shorelines derived from lidar data are datum-based and can be extracted objectively using a tidal datum, such as Mean High Water (MHW) or Mean Higher High Water (MHHW). Studies by Moore (2000) and Ruggiero and others (2003) note that HWL-type shoreline proxy are virtually never coincident with datum-based MHW-type shorelines. In fact they are almost universally estimated to be higher (landward) on the beach profile when compared to MHW shorelines (Ruggiero and others, 2013). According to Ruggiero and others the average absolute horizontal offset between the HWL and MHW range from ~6 m (~19 ft) to as much as 50 m (164 ft), while the average is typically less than 20 m (65 ft). Offsets are typically greatest on flat, dissipative beaches where the wave runup may be large and smallest where beaches are steep (e.g., gravel beaches).

Estimates of the uncertainty of HWL shoreline measurements have been assessed in a number of studies (e.g., Moore, 2000; Ruggiero and others, 2013). These uncertainties reflect the following errors: 1) mapping methods and materials for historical shorelines (including the offset between the HWL and MHW shoreline), 2) the registration of shoreline positions relative to Cartesian coordinates, and 3) shoreline digitizing, and have been summarized in **Table 2-1**.

Table 2-1. Average uncertainties for Pacific Northwest shorelines (Ruggiero and others, 2013).

	NOS T-Sheets (1800s to 1950s)		DRGs (1940s to 1990s)		Aerial Photography (1960s to 1990s)		Lidar	
Total shoreline position uncertainty	18.3 m	60 ft	21.4 m	70 ft	15.1 m	50 ft	4.1 m	14 ft

Shorelines measured by DOGAMI staff using Real-Time Kinematic Differential Global Positioning System (RTK-DGPS) surveys of the beach are also available for selected areas in Lincoln County (Allan and Hart, 2008; Allan and Stimely, 2013). These latter data sets provide additional insights into the spatial and temporal variability of shoreline changes taking place along the Lincoln coastline and have been collected since 2008 in order to document the seasonal to interannual variability in shoreline positions along the County. In all cases, the GPS shorelines reflect measurements of the Mean Higher High Water (MHHW) line located at an elevation of 2.3 m (7.5 ft). We have relied on the latter as opposed to the MHW line, because previous studies indicate that MHHW most closely approximates the MHW line surveyed by early NOS surveyors. Errors associated with these various products are described by Moore (2000). GPS shore-

line positioning errors, a function of the orientation of the GPS receiver relative to the slope of the beach are estimated to be ~±0.1 to ±0.2 m (±0.3 to ±0.6 ft).

The approach adopted here is to describe the broad morphological changes identified along the coast, beginning in the south at Yachats, and progressing northward toward the Salmon River estuary.

2.4.1.1 Yachats to Waldport

Much of the shoreline between Yachats and the mouth of Alsea Bay is backed by relatively low (7–9 m [23–30 ft]), near vertical bluffs. Coastal engineering is prevalent along much of the cell, where localized erosion has presented problems to properties. This is especially the case in the southern half of the subcell. Based on the available shoreline data to date (**Figure 2-16**), it can be seen that the shorelines have varied in position by some 40 to 90 m (131 to 295 ft). In general, the 1967 shoreline tends to track seaward (i.e., more sand) of the more recent shorelines, while the 2010 shoreline reflects the most landward (erosional) extent. Farther north, near the Alsea Bay mouth, the pattern reverses slightly with the 1920s era shoreline tracking close to the bluff line (i.e., most landward), while the 2010 shoreline is located furthest seaward. Variability near the mouth increases significantly, such that the shorelines are now separated by as much as 127 m (417 ft). These latter data highlight the greater instability seen in shorelines adjacent to the mouths of estuaries.

2.4.1.2 Alsea Spit (Bayshore)

Shoreline variability along Alsea Spit is presented in **Figure 2-17**. As can be seen from the Figure the 1920s era shoreline highlights the most eroded state, while surveys undertaken in 2007 (GPS) and 2009 (lidar) indicate the beach in an accreted state. In general, the shoreline positions vary significantly, ranging from 120 m (394 ft) to as much as 230 m (755 ft). (Stembridge, 1975) noted that up until the mid 1970s the spit had been actively accreting at an estimated rate of 3 m/yr (10 ft/yr), as the extreme high tide line shifted seaward by as much as 91 m (300 ft) since 1939. As is typical of all spits, by far the greatest shoreline changes are observed at the spit tip.

Without doubt, the most significant event to impact the community of Bayshore on Alsea Spit was the major 1982-83 El Niño climate event (**Figure 2-18** to **Figure 2-20**). El Niños and La Niñas represent opposite extremes in an otherwise continuum of global climate events, with “average” conditions generally prevailing between those extremes. In the past three decades there have been a number of El Niño events, with the 1982-83 and 1997-98 events having been the strongest on record, while the period between 1990 and 1995 was characterized by persistent EL Niño conditions, the longest on record (Trenberth, 1999). During an El Niño, important to coastal erosion are occurrences of elevated mean water levels that cause the measured tides to be much higher than normal, produced by warmer offshore water temperatures, the geostrophic effects of northward flowing currents, and sea-level "waves" emanating from the tropics. During "average" or La Niña years, these processes are not as strong, so that mean water levels along the coast are closer to normal. Also important along the U.S. West Coast are the changing wave conditions between El Niño and La Niña events. During an El Niño there is a southerly shift of the jet stream, which results in a higher incidence of storms that cross the coast of California (Komar, 1986; Peterson and others, 1990; Storlazzi and Griggs, 2000), and a general increase in the significant waves heights offshore the Oregon coast (Allan and Komar, 2006).

The erosion of Alsea Spit was due in large part to the northward migration of beach sand, which deflected the tidal inlet to the north. This enabled waves to break much closer to shore than would otherwise normally have occurred, eroding the primary dune located at the back of the beach. Although the erosion originated during the 1982-83 El Niño, the problem persisted for several years after the event as a result of the disrupted inlet dynamics. According to (Stembridge, 1975), the spit appeared to have been relatively stable over the preceding years and there was little noticeable change to its morphology before the 1982-83 El Niño. **Figure 2-18** shows the magnitude of the erosion at the peak of the 1982-83 event. The dashed black line indicates the location

of a riprap structure built during and after the event, highlighting the magnitude of the erosion. A red crossed line at mid photo indicates the location of an erosion scarp that formed at the peak of the 1982-83 El Niño, prior to emergency riprap having been installed. Hence, it can be seen that at this particular location part of the primary dune came very close to having been breached, which in all likelihood could have exacerbated the erosion problem even further.

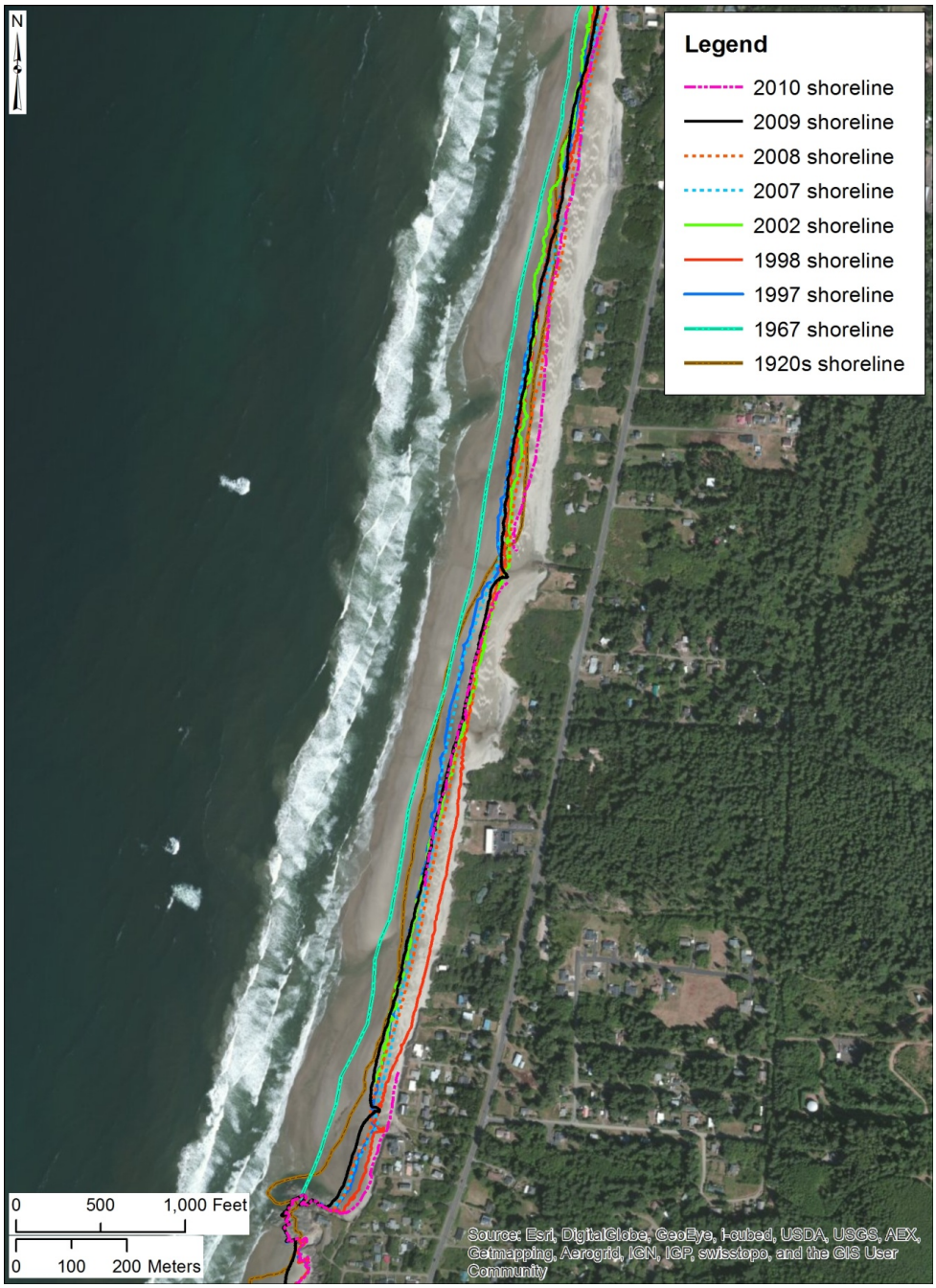

Figure 2-16. Shoreline variability in the north Yachats area. Note: The 1920s (1927/28) shoreline is derived from NOS T-sheets, 1967 is from orthorectified aerial photographs, and 1997–2009 are derived from lidar.

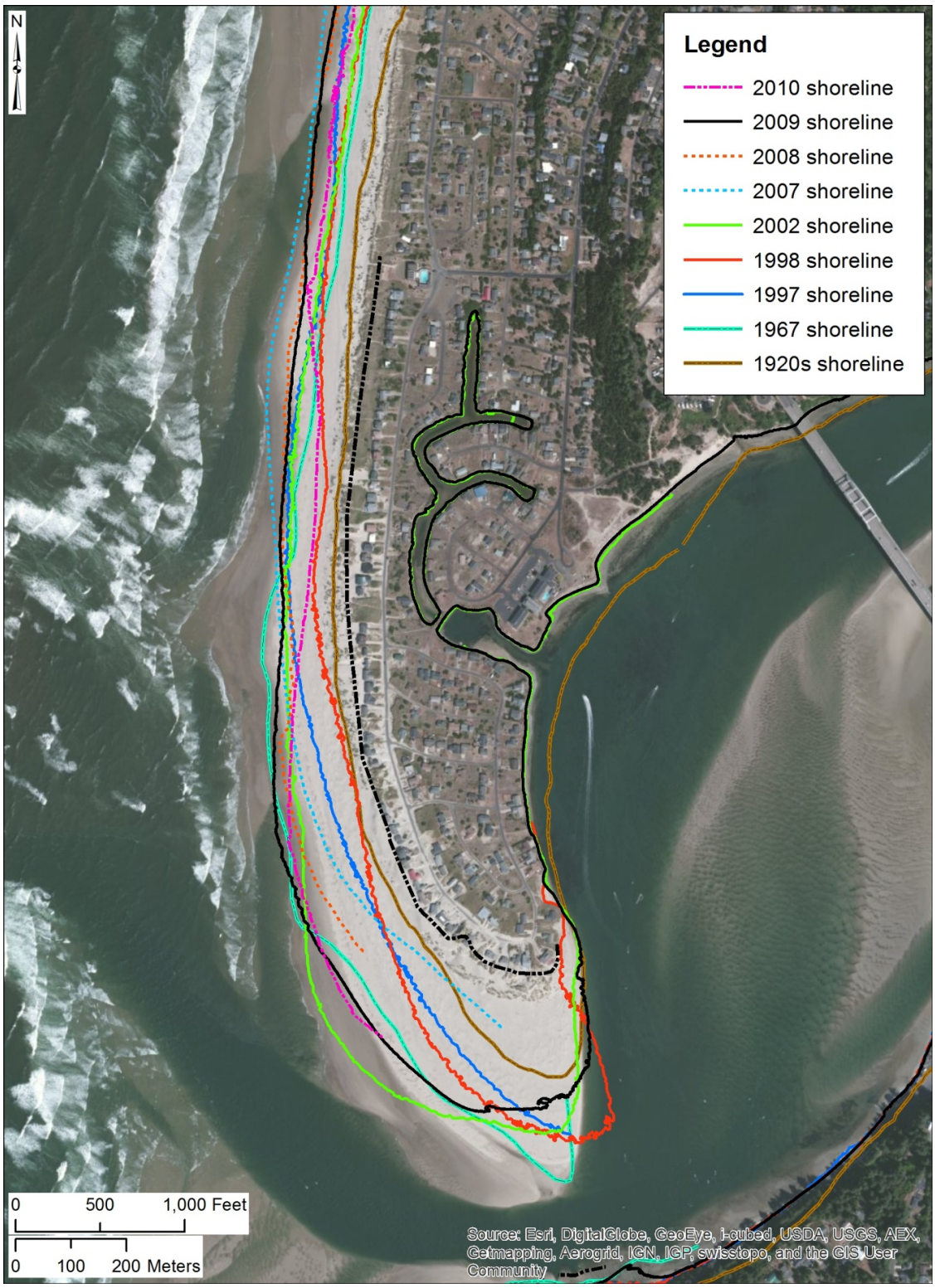

Figure 2-17. Shoreline variability along southern Alsea Spit. Note: The 1920s (1927/28) shoreline is derived from NOS T-sheets, 1967 is from orthorectified aerial photographs, and 1997–2009 are derived from lidar. The dashed black line indicates the approximate location of riprap buried beneath the dune sand.

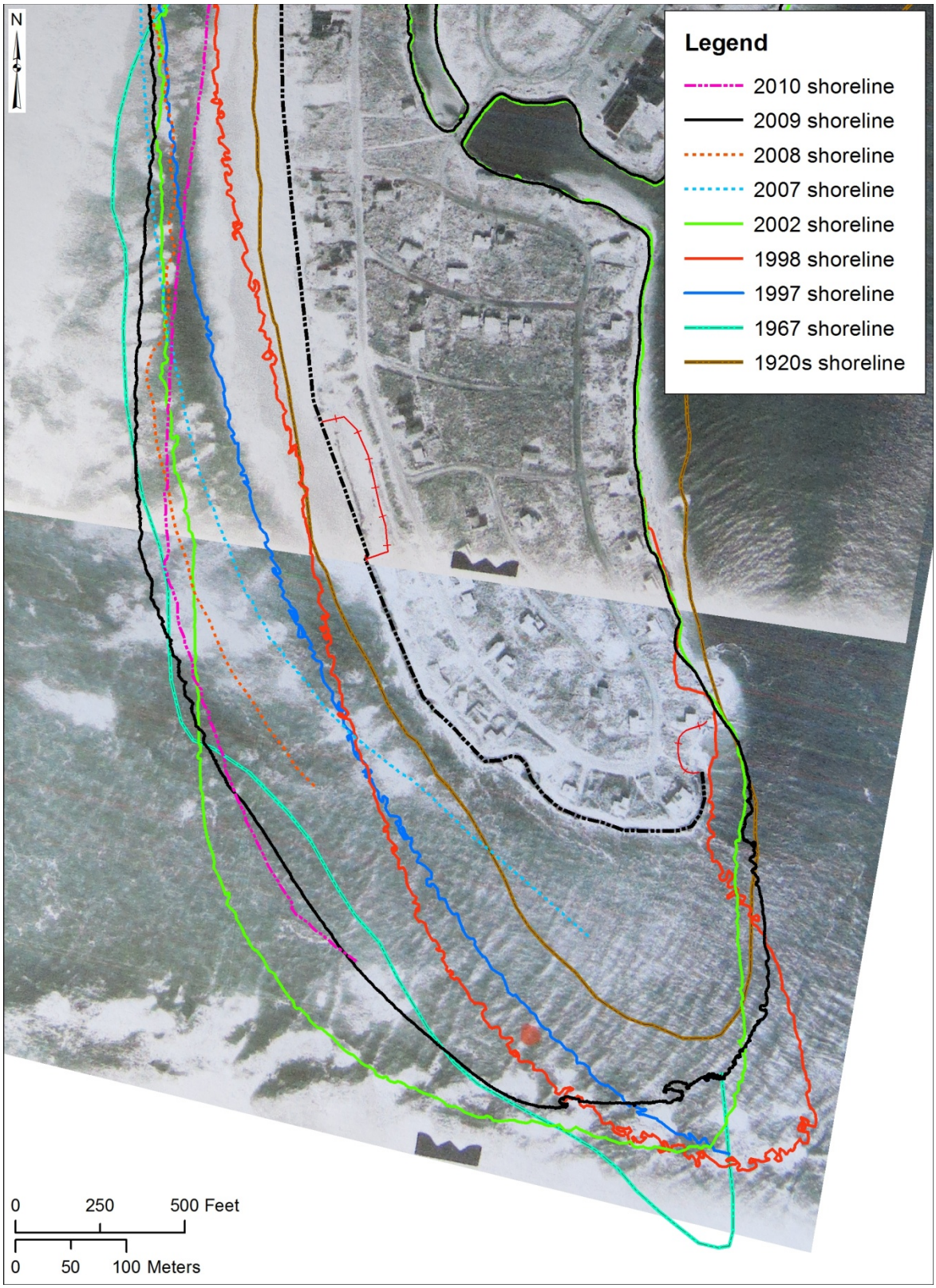

Figure 2-18. A 1983 aerial photo taken of the southern end of Alsea Spit at the height of the 1982-83 El Niño.

Figure 2-19. An erosion scarp caused by the northward shift of the Alsea Bay inlet during the 1982-83 El Niño enabled large waves to break closer to the shore, eroding backshore properties (photo: P.D. Komar, 1983).

Figure 2-20. Remediation during and immediately following the 1982-83 El Niño event included placement of emergency riprap seaward of the erosion scarp (photo: P.D. Komar, 1983).

Following the 1982-83 El Niño, the beach and primary dune grew significantly in 1986 and by 1987 the inlet had returned to its original position (Komar, 1997). Since then, it is apparent from an examination of **Figure 2-17** and **Figure 2-18**, that new homes have been constructed either on top of or just seaward of the riprap structure and erosion scarp, bringing those newer homes potentially into harms way from future coastal erosion events.

In the winter of 1997-98, a second major El Niño occurred. However, aside from a few localized erosion effects the spit did not experience any major erosion. The effect of the erosion can be seen from an examination of the 1998 (and to a lesser extent 2007) shoreline, which tend to track much closer to the line of houses located on top of the primary dune, and especially in the vicinity of the spot where the dune almost breached during the 1982-83 El Niño. The curvilinear nature to the 1998 shoreline suggests the localized effects were possibly caused by the presence of rip current embayments, which formed near the end of the 1997-98 winter.

2.4.1.3 Seal Rock to Newport

From Seal Rock to Newport, the shoreline responses are broadly similar to those seen in the Yachats to Waldport section. In general, the 1967 shoreline tracks the furthest seaward, while the 1920s, 1998, and 2010 shorelines reflect the most eroded state. However, localized hotspot erosion effects are apparent at a few discrete locations such as just north of Ona Beach. The latter reflected a landward shift in the position of the 1998 shoreline, placing it approximately 18 m from the primary dune and likely contributing to an erosion scarp that remains apparent in the area to this day.

Shoreline changes due to jetty construction are evident at the mouth of Yaquina bay in Newport (**Figure 2-21**). The Yaquina bay jetties are one of the oldest navigation projects on the Oregon coast. Construction of the jetties commenced in 1889 and was completed by 1896; the north jetty was extended in 1966. South of the south jetty, it can be seen that the shoreline prograded seaward between 1830 and 1899. Between 1899 and the 1920s (**Figure 2-21**), the shoreline advanced seaward by approximately 300 to 450 m (984 to 1476 ft). Adjacent to the jetty, the shoreline advanced an additional 270 m (886 ft) between 1940 and 1967. North of the north jetty, the overall shoreline response was much less. This latter response is entirely due to the orientation of the jetties and its blocking effect on sand transported around the end of the jetties. In general, during the summer sand north of the north jetty is able to be transported to the south due to the prevalence of northwesterly wind and waves, where it accumulates up against the north jetty. In the winter, the reverse applies with waves arriving out of the southwest, effectively shifting the sand back to the north. In contrast, the transport of sand south of the south jetty is limited due to a weakening of the waves as they refract around the jetties, while allowing northerly sand transport to occur unrestricted in the winter allowing the sand to pile up against the south jetty.

Farther north in the Newport Cell, **Figure 2-22** indicates that the beach and shoreline have been gaining sand since at least the 1920s, enabling the beach to accrete and prograde seaward. In general, the beach has advanced seaward by about 200 to 250 m (656 to 820 ft). This response is consistent with observations by Haxell and Holman (2004), who argued that the accumulation of sand in this region can be attributed to a long-term increase in wave heights and a general shift in the wave approach angles to the south enabling a stronger northward directed sand transport regime to dominate. While the results of Haxel and Holman describe the dominant processes contributing to the recent beach growth, the exact source of where the sediments are being derived from remain somewhat unclear.

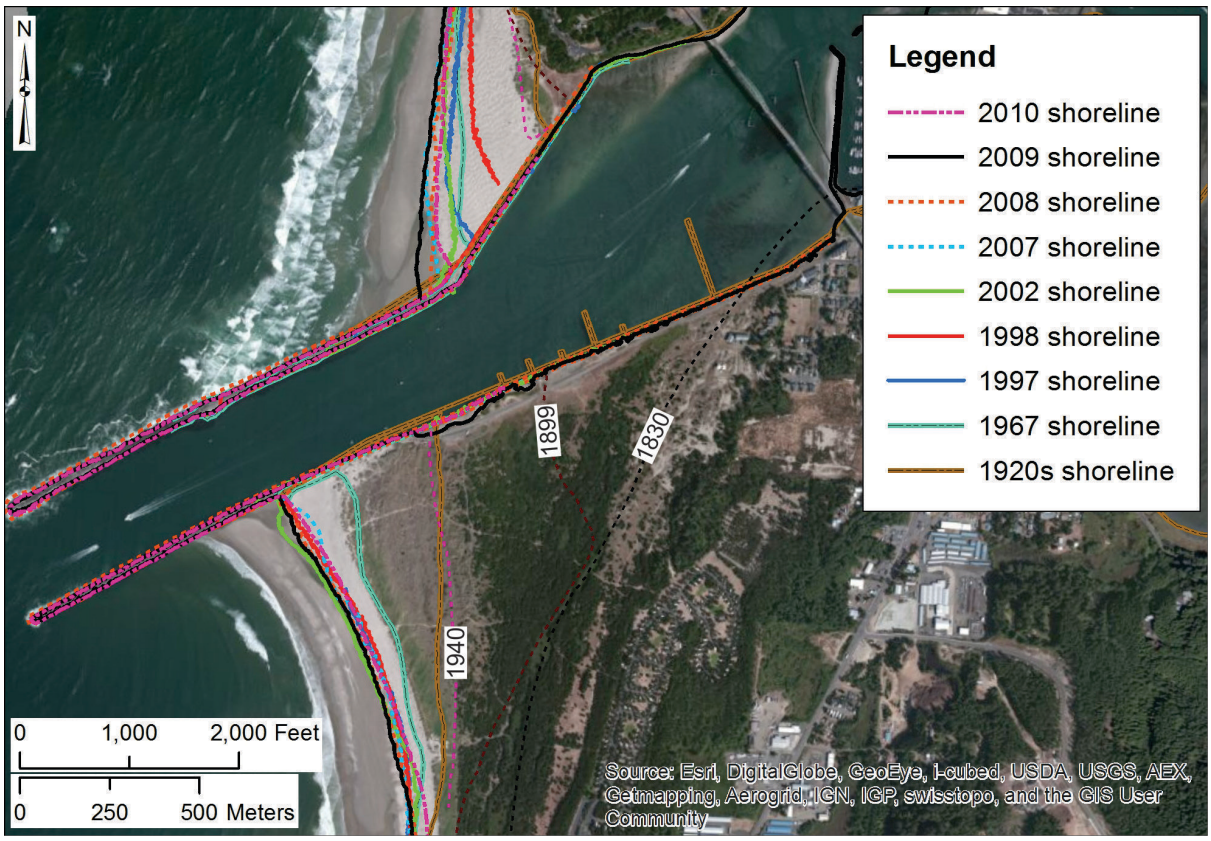

Figure 2-21. Shoreline changes at the mouth of Yaquina Bay. Note: The 1920s (1927/28) shoreline is derived from NOS T-sheets, 1967 is from orthorectified aerial photographs, and 1997–2009 are derived from lidar. The dashed black line indicates the approximate location of riprap buried beneath the dune sand.

2.4.1.4 Beverly Beach cell

The Beverly Beach littoral cell is one of the smallest cells on the Oregon coast at approximately 8 km (5 mi) long. The cell is considered to be essentially sand starved, with limited sand inputs. For the most part the 2010 shoreline reflects the most eroded state, while the 2002 and 2009 shorelines reflect the more accreted conditions. Erosion is evident everywhere in the cell, but is particularly acute in the southern half of the littoral cell. The range of shoreline responses vary from about 20 to 50 m (66 to 164 ft) in the south, increasing to as much as 70 m (230 ft) at the north end of the cell.

2.4.1.5 Depoe Bay to Fishing Rock

The shoreline from Otter Rock northward to Fogarty Creek is almost entirely made of basalt cliffs or basalt ramps that plunge into the ocean. Shoreline responses in this area are generally negligible.

2.4.1.6 Gleneden Beach and Siletz Spit

The Lincoln City littoral cell is divided into two subcells: Gleneden Beach/Siletz Spit in the south and Lincoln in the north. The Gleneden Beach/Siletz Spit subcell is approximately 9.2 km (5.7 mi) in length. Due to the coarseness of the beach sediments in this cell, the beaches are characteristically steep and the shoreline response tend to be more dynamic. Coastal engineering riprap structures are prevalent along the length of the shoreline, a testament to the erosional history of this area.

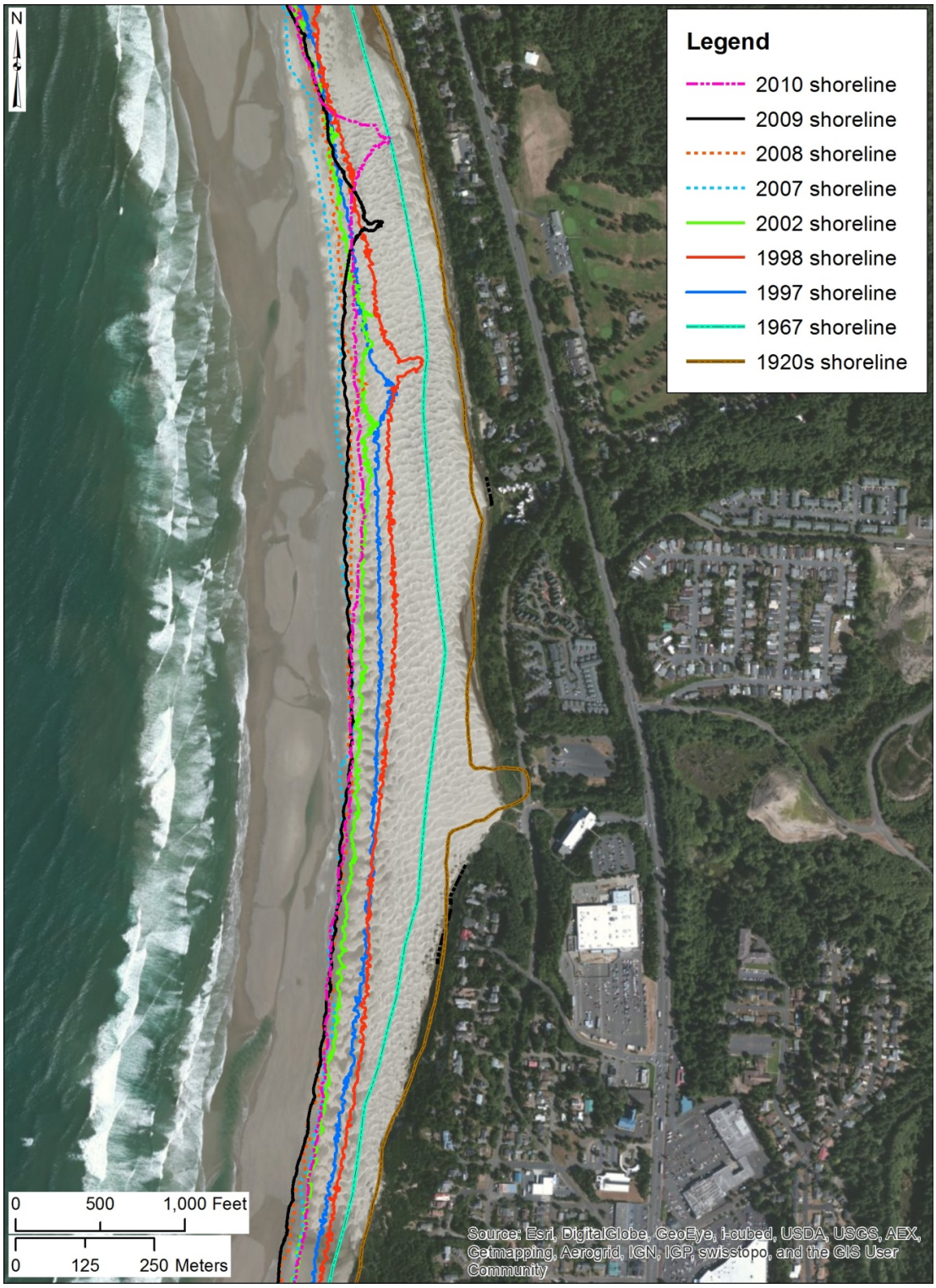

Figure 2-22. Shoreline variability in the north Newport (Agate Beach) area. Note: The 1920s (1927/28) shoreline is derived from NOS T-sheets, 1967 is from orthorectified aerial photographs, and 1997–2009 are derived from lidar. The dashed black line indicates the approximate location of riprap buried beneath the dune sand.

Probably the most extreme example of shoreline erosion hazards in Lincoln County occurred along Siletz Spit in the early 1970s. Development of the spit began in the 1960s, with a few homes being constructed out on the primary dune. Storm induced erosion did not become an issue until the winter of 1970-71, when a series of major storms cut into the dune and threatened several of the homes built closest to the beach (Komar, 1997). The erosion was not particularly severe such that homeowners were able to respond by dumping riprap in the area of concentrated wave attack, effectively stopping the erosion.

In the winter of 1972-73, a major storm occurred just prior to Christmas. The large waves immediately began cutting into the foredunes of Siletz Spit, threatening several homes located midway along the spit (*Cover photo*), and forming a prominent erosion scarp. (From the scale of the erosion scarp and the homes captured in the cover photo, we estimate that the erosion scarp was probably on the order of 4.9 to 6 m (16 to 20 ft) high making it one of the largest observed on the Oregon coast.) One home, under construction at the time, was eventually lost as the erosion scarp retreated rapidly, eventually overtaking the home (**Figure 2-23**). Additional storms in January further exacerbated the problem. Riprap was dumped en mass to protect the various homes (**Figure 2-24**), while adjacent empty lots were essentially left unprotected as developers and homeowners argued over who should pay for the rock. However, as the erosion progressed additional riprap was required to protect the flanks of the existing homes. The erosion persisted throughout the month and came very close to reaching the road (**Figure 2-24**). The erosion was eventually halted when the developer stepped in to protect the empty lots, which fronted the road (Komar, 1997).

Figure 2-23. The erosion of Siletz Spit following a major storm on January 26, 1973, which eventually claimed one home (photo courtesy of Oregon Highway Department, January 26, 1973).

Figure 2-24. Responses to the Siletz erosion consisted of dumping riprap in front of the homes, while adjacent empty lots were left unprotected and continued to erode (photo courtesy of Oregon Highway Department, January 26, 1973).

Figure 2-25 presents the shoreline variability for Siletz Spit. In most cases the 1967 and 1920s shorelines reflect the more eroded state, while the 2009 and 2010 lidar shorelines reflect the more accreted condition. In general, the shorelines range over a distance of 30 to 70 m (98 to 230 ft). **Figure 2-26** is a close-up of the spit area that was directly impacted by the 1972-73 winter erosion, compared with a modern photo of the same area. The photo reflects the same area as shown in the cover photo of this report. Evident from **Figure 2-26** is the scale of the event, which highlights the complete removal of the sand beach fronting the homes. Further examination of the aerial photos highlights the effect of rip embayments during the storm, which contributed to highly localized hotspots of erosion, such as shown in the top photo of **Figure 2-26**. Also evident from the figure is the extent of the erosion (dashed red line) attributed to the 1972-73 winter storms. When viewed on a modern photo of the spit, the number of new homes built seaward of the erosion line becomes clearly evident.

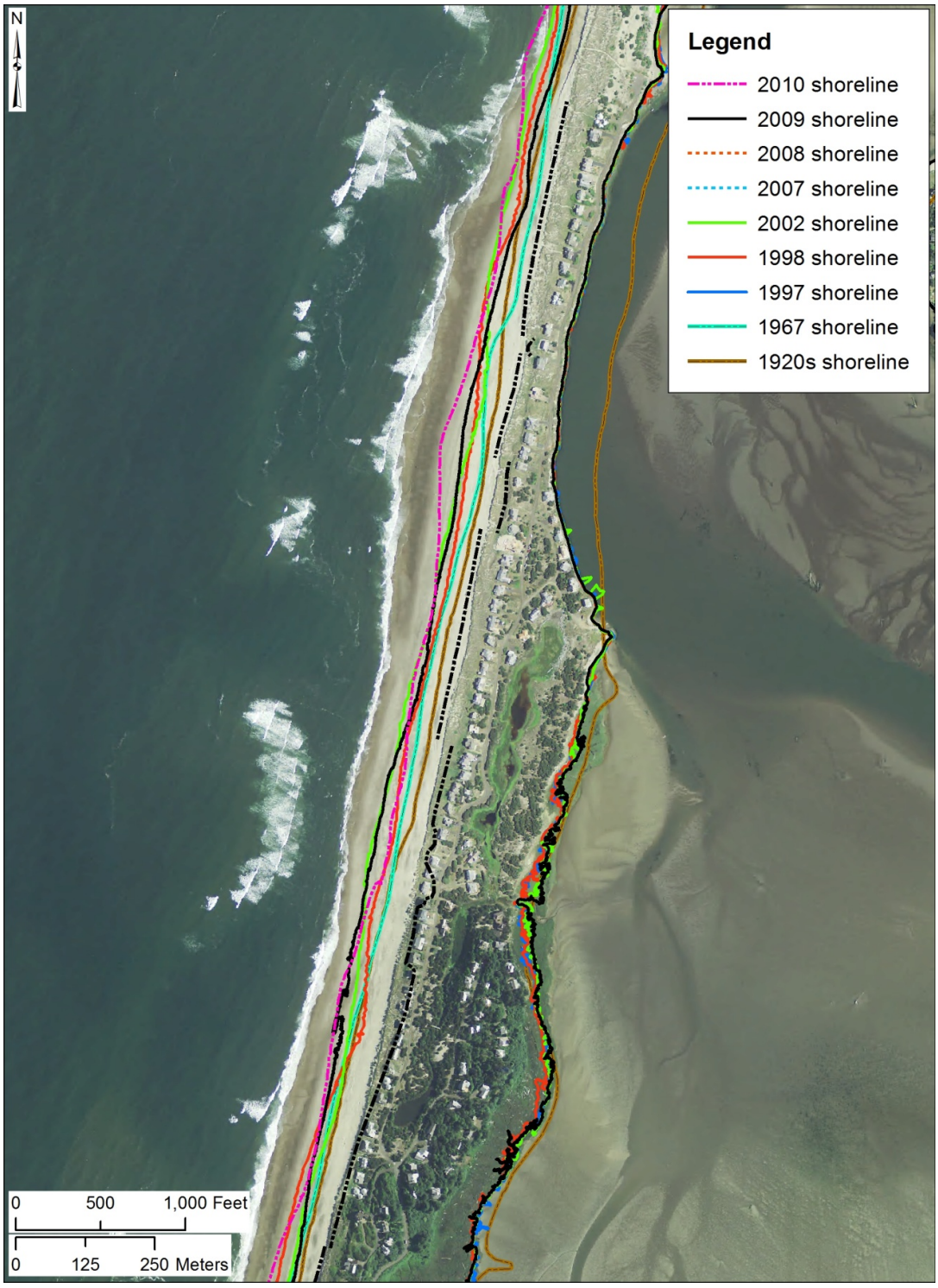

Figure 2-25. Shoreline variability along Siletz Spit. Note: The 1920s (1927/28) shoreline is derived from NOS T-sheets, 1967 is from orthorectified aerial photographs, and 1997–2009 are derived from lidar. The dashed black line indicates the approximate location of riprap buried beneath the dune sand. Lines of riprap located out on the beach (e.g., mid to upper photo) reflect areas, where the riprap is known to be buried immediately in front of the homes but the exact location could not be determined.

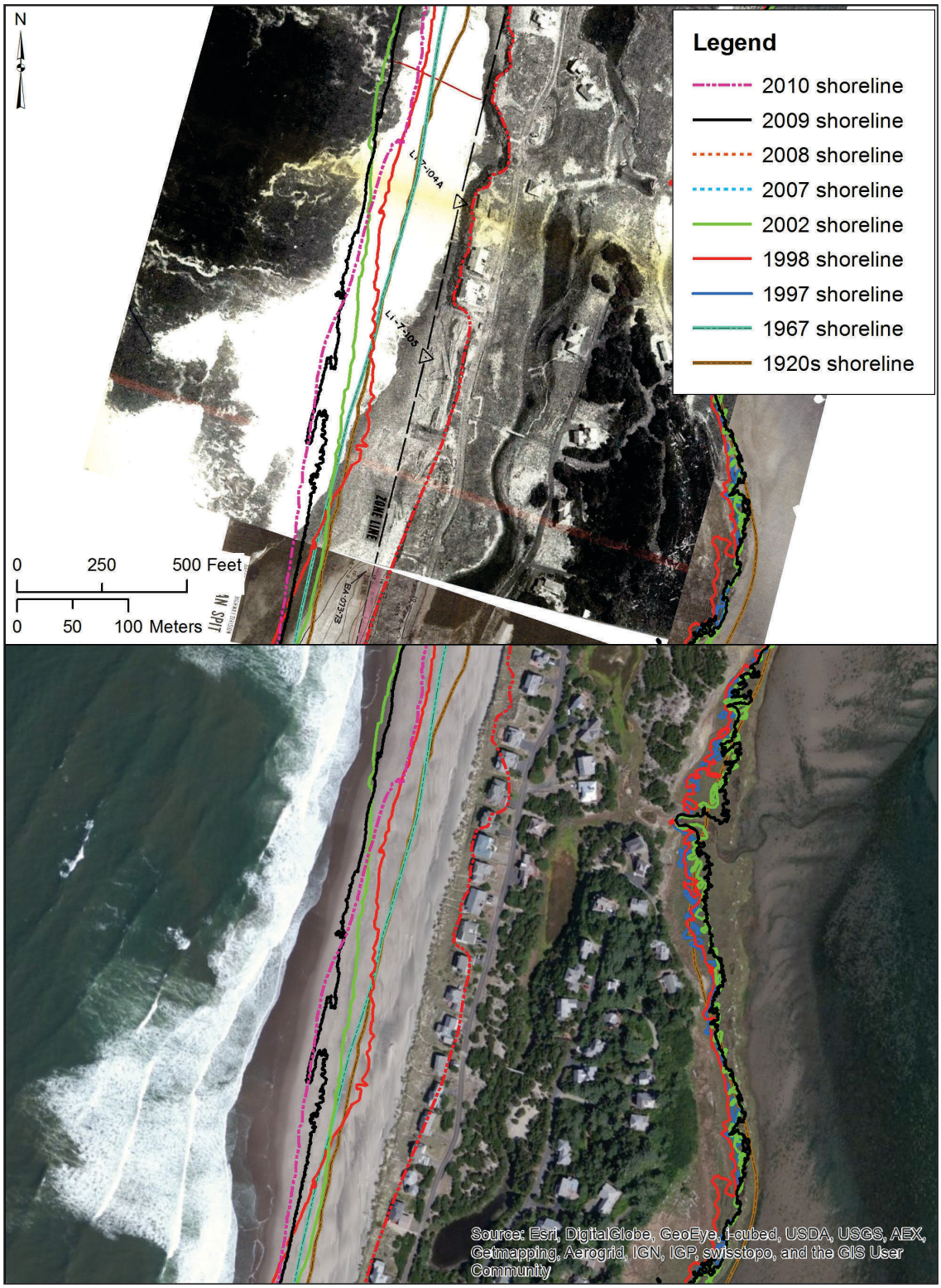

Figure 2-26. Aerial photo taken in January 1974 showing the extent of the 1972-73 winter erosion and the location of riprap used to mitigate the erosion (*top*), and the same information overlaid on a modern aerial image of the area (*bottom*).

2.4.1.7 Lincoln City

The Lincoln City subcell extends from the mouth of Siletz Bay to Cascade Head. With the exception of the beach immediately south of the Salmon River estuary that is backed by dunes, virtually the entire Lincoln subcell is backed by bluffs that average ~20.5 m (67.3 ft) in height (σ = ±10.6 m [34.8 ft]). As a result, risk from coastal flooding is considered to be generally low along much of the Lincoln shore, with the exception of a few discrete sections where the backshore elevations tend to be much lower (e.g., D-River), and/or construction of buildings has been built too close to the beach. As with the Siletz subcell, much of the shoreline along Lincoln Beach has been protected by a combination of riprap structures and to a lesser extent, vertical seawalls. The presence of these structures is a testament to the erosional history that has plagued this area. For example, Komar (1997) describes a major storm that occurred during the winter of 1977-78, which resulted in significant toe erosion along the bluffs adjacent to the Inn at Spanish Head (located just north of the Siletz Bay mouth) (**Figure 2-27**).

Shoreline variability within this cell is consistent with observations described above for locations elsewhere in Lincoln County. By far the greatest variations are observed adjacent to the mouth of Siletz Bay. Farther north, the beaches vary from 25 to as much as 80 m (82 to 263 ft). In general, the 2002 and 2009 shorelines reflect the most accreted state, while the 1967 and 1998 shorelines reflect the more eroded conditions.

Figure 2-27. Erosion of bluffs adjacent to the Inn at Spanish Head (mid photo) during a series of storms in the 1977-78 winter (photo: P. D. Komar, 1978).

3.0 BEACH AND BLUFF MORPHOLOGY ASSESSMENTS

Field surveys were undertaken throughout Lincoln County in the summer of 2011, and again during the 2012 winter in order to better define the seasonal variability. These surveys serve two important objectives:

1. To establish beach profile transects along discrete but representative sections of the shoreline's geomorphology/geology, including sections of coast where coastal engineering structures have been constructed, for the purposes of coastal hydraulic analyses.
2. To provide representative measurements of the beach in its winter state, whether it be derived from lidar or GPS data, in order to define the morphology, elevations, and slope of the beach face for use in subsequent wave runup and over-toping computations.

Surveying along the Lincoln County coast was initially carried out in August and September 2011, and again in February/March 2012. The surveys were completed late in the winter season when Oregon beaches are typically in their most eroded state (Aguilar-Tunon and Komar, 1978; Komar, 1997; Allan and Komar, 2002; Allan and Hart, 2008). A total of 313 primary beach profile transects were established along the length of Lincoln County (**Figure 3-1** to **Figure 3-4**). These can be subdivided according to the following study reaches:

- Cape Perpetua: 4 sites;
- Yachats: 10 sites;
- Waldport littoral cell: 53 sites;
- Alsea Spit: 21 sites;
- South Beach: 42 sites;
- Newport cell: 17 sites;
- Yaquina headland: 2 sites
- Beverly Beach littoral cell: 22 sites;
- Otter Rock: 5 sites;
- Cape Foulweather: 2 sites;
- Miroco: 3 sites;
- Rocky Creek State Park: 2 sites;
- Whale Cove: 6 sites;
- Depoe Bay: 13 sites;
- Fogarty Creek: 8 sites;
- Gleneden Beach/Siletz Spit: 34 sites;
- Lincoln City: 58 sites;
- Salmon River Estuary: 6 sites; and
- Cascade Head: 5 sites.

Eighteen new transects were later added in order to better define the 1% TWL and overtopping in areas subject to more complicated backshore topography, while an additional 24 transects were established to better define the extent of overtopping in certain reaches in order to better constrain the overtopping. For the latter cases, the 1% TWL was fixed to the primary transect, and the overtopping was recalculated based on the local beach geomorphology.

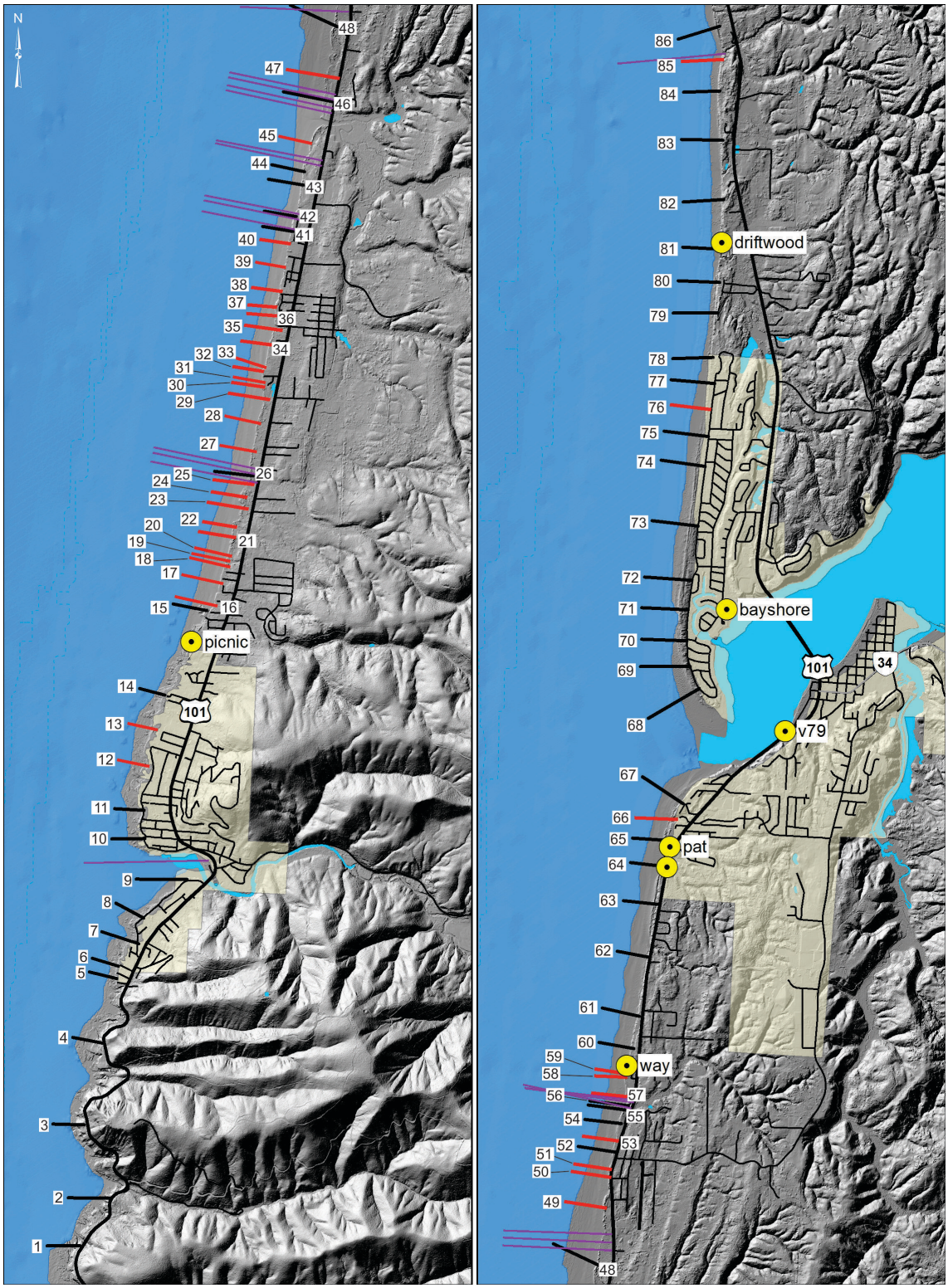

Figure 3-1. Location map of beach profiles measured in the vicinity of Cape Perpetua (transects 1–4), Yachats (5–14), the Waldport subcell (transects 15–67), and Alsea Spit (transects 68–86) in Lincoln County. Red lines denote transects where overtopping has been identified. Yellow circles denote the locations of benchmarks used in local site calibrations, while the solid purple lines denote supplemental transect locations.

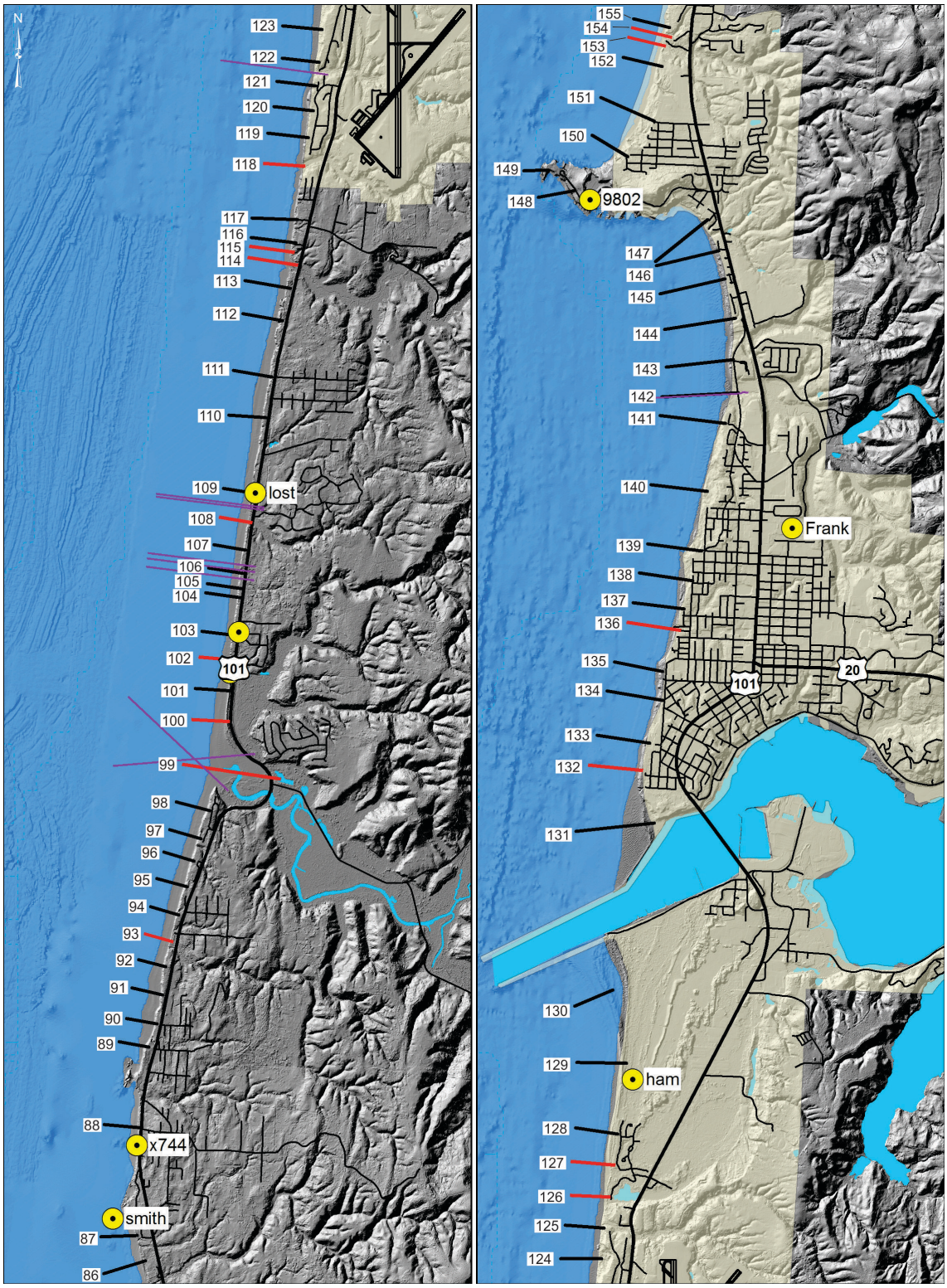

Figure 3-2. Location map of beach profiles measured near Seal Rock (transects 86–88), South Beach area (transects 89–130), in the Newport subcell (transects 131–147), Yaquina Head (transects 148–149), and in the southern Beverly Beach cell (transects 150–155). Red lines denote transects where overtopping has been identified. Yellow circles denote the locations of benchmarks used in local site calibrations, while the solid purple lines denote supplemental transect locations.

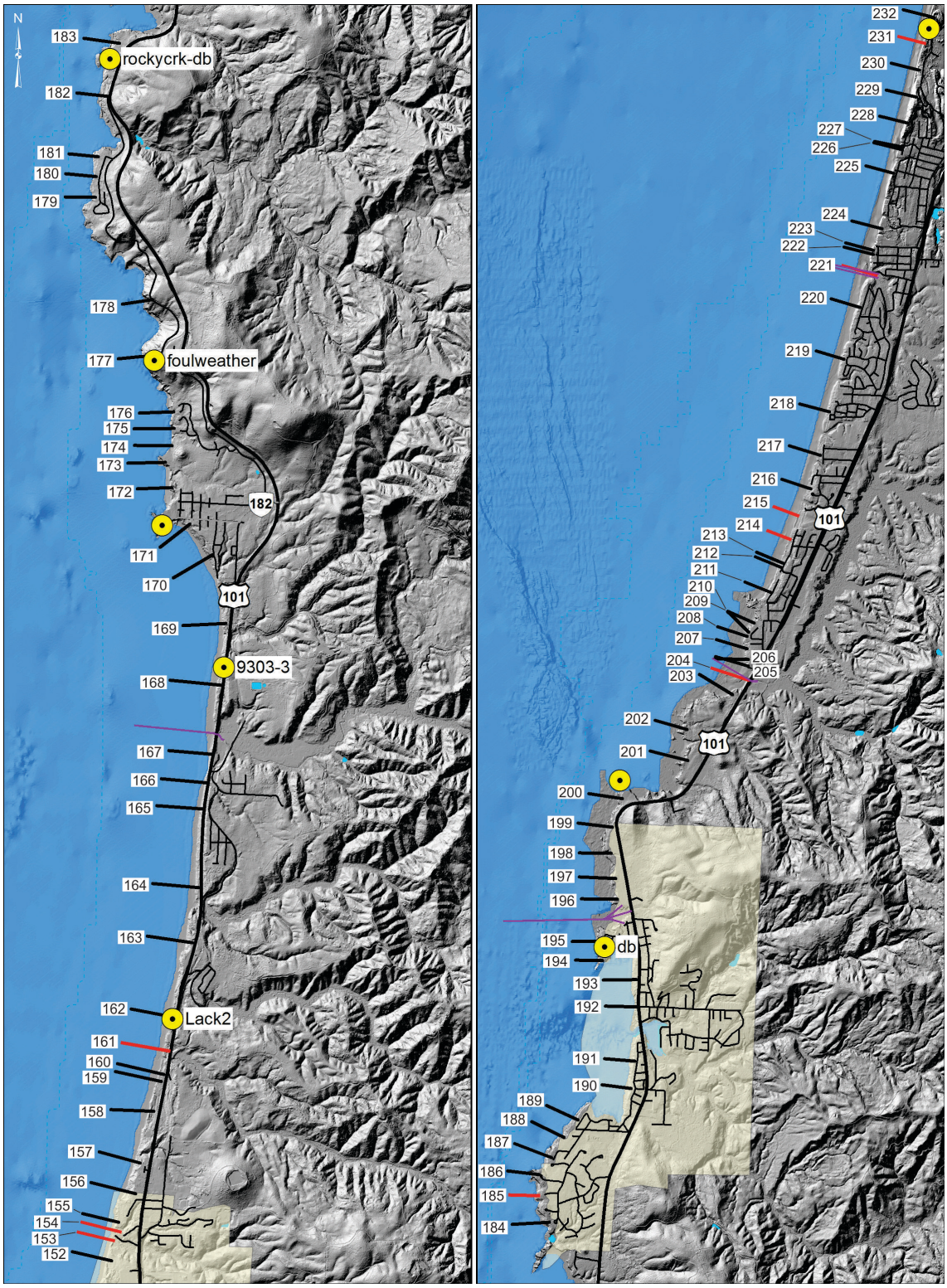

Figure 3-3. Location map of beach profiles measured in the Beverly Beach cell (transects 152–171), Otter Rock to Miroco (transects 172–183), Whale Cove to Fogarty Creek (transects 184–210), and along Gleneden Beach/Siletz Spit (transects 211–232). Red lines denote transects where overtopping has been identified. Yellow circles denote the locations of benchmarks used in local site calibrations, while the solid purple lines denote supplemental transect locations.

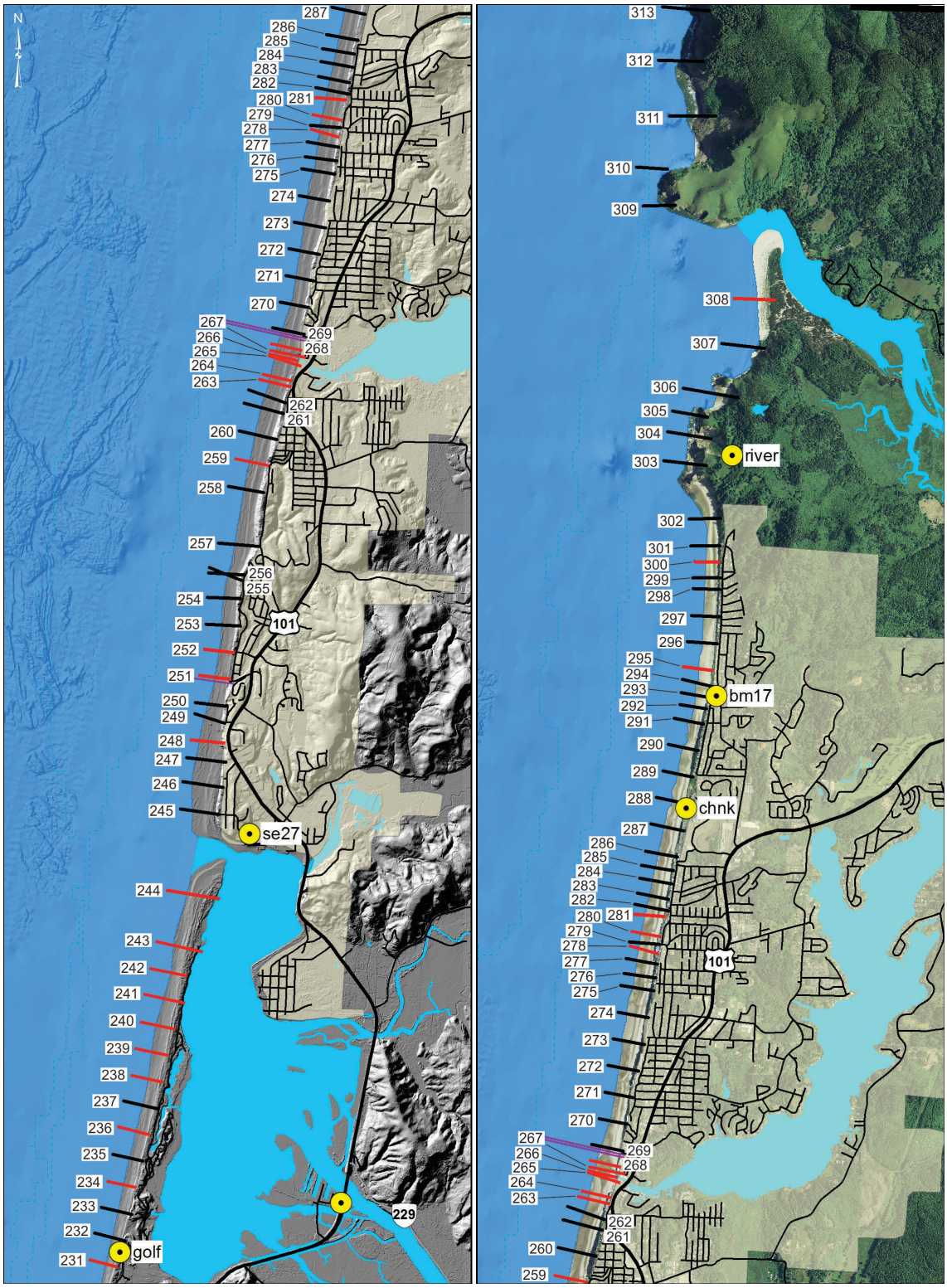

Figure 3-4. Location map of beach profiles measured along Siletz Spit (transects 231–244), Lincoln City subcell (transects 245–302), Salmon River estuary (transects 303–308), and on Cascade Head (transects 309–313). Red lines denote transects where overtopping has been identified. Yellow circles denote the locations of benchmarks used in local site calibrations, while the solid purple lines denote supplemental transect locations.

3.1 Survey Methodology

Beach profiles that are orientated perpendicular to the shoreline can be surveyed using a variety of approaches, including a simple graduated rod and chain, surveying level and staff, Total Station theodolite and reflective prism, light detection and ranging (lidar) airborne altimetry, and Real-Time Kinematic Differential Global Positioning System (RTK-DGPS) technology. Traditional techniques such as leveling instruments and Total Stations are capable of providing accurate representations of the morphology of a beach, but are demanding in terms of time and effort. At the other end of the spectrum, high-resolution topographic surveys of the beach derived from lidar are ideal for capturing the three-dimensional state of the beach, over an extended length of coast within a matter of hours; other forms of lidar technology are now being used to measure nearshore bathymetry out to moderate depths, but are dependent on water clarity. However, the lidar technology remains expensive and is impractical along small segments of shore, and more importantly, the high costs effectively limits the temporal resolution of the surveys and hence the ability of the end-user to understand short-term changes in the beach morphology (Bernstein and others, 2003).

Within this range of technologies, the application of RTK-DGPS for surveying the morphology of both the subaerial and subaqueous portions of the beach has effectively become the accepted standard (Morton and others, 1993; Ruggiero and Voigt, 2000; Bernstein and others, 2003; Ruggiero and others, 2005), and has been the surveying technique used in this study. The global Positioning System (GPS) is a worldwide radio-navigation system formed from a constellation of 24 satellites and their ground stations, originally developed by the U.S. Department of Defense; in 2007 the Russian Government made their GLONASS satellite network available increasing the number of satellites to ~46 (as of February 2011). In its simplest form, GPS can be thought of as triangulation with the GPS satellites acting as reference points, enabling users to calculate their position to within several meters (e.g., using inexpensive off the shelf hand-held units), while survey grade GPS units are capable of providing positional and elevation measurements that are accurate to a centimeter. At least four satellites are needed mathematically to determine an exact position, although more satellites are generally available. The process is complicated because all GPS receivers are subject to error, which can significantly degrade the accuracy of the derived position. These errors include the GPS satellite orbit and clock drift plus signal delays caused by the atmosphere and ionosphere and multipath effects (where the signals bounce off features and create a poor signal). For example, hand-held autonomous receivers have positional accuracies that are typically less than about 10 m (<~30 ft), but can be improved to less than 5 m (<~15 ft) using the Wide Area Augmentation System (WAAS). This latter system is essentially a form of differential correction that accounts for the above errors, which is then broadcast through one of two geostationary satellites to WAAS enabled GPS receivers.

Greater survey accuracies are achieved with differential GPS (DGPS) using two or more GPS receivers to simultaneously track the same satellites enabling comparisons to be made between two sets of observations. One receiver is typically located over a known reference point and the position of an unknown point is determined relative to that reference point. With the more sophisticated 24-channel dual-frequency RTK-DGPS receivers, positional accuracies can be improved to the sub-centimeter level when operating in static mode and to within a few centimeters when in RTK mode (i.e., as the rover GPS is moved about). In this study we used Trimble® 24-channel dual-frequency R7/R8 and 5700/5800 GPS receivers. This system consists of a GPS base station (R7 and/or 5700 unit), Zephyr Geodetic™ antenna (model 2), HPB450 radio modem, and R8 (and/or 5800) "rover" GPS (**Figure 3-5**). Trimble reports that both the R7/R8 and 5700/5800 GPS systems have horizontal errors of approximately ±1 cm + 1 ppm (parts per million * the baseline length) and ±2 cm in the vertical (Trimble, 2005).

To convert a space-based positioning system to a ground-based local grid coordinate system, a precise mathematical transformation is necessary. While some of these adjustments are accomplished by specifying the map projection, datum, and geoid model prior to commencing a field survey, an additional transformation is necessary whereby the GPS measurements are tied to known ground control points (**Figure 3-6**). This latter step is called a GPS site calibration, such that the GPS measurements are calibrated to ground control points with known vertical and horizontal coordinates using a rigorous least-squares adjustments procedure. Performing the calibration is initially undertaken in the field using the Trimble TSC2 GPS controller and then re-evaluated in the office using Trimble Business Office software (v2.5).

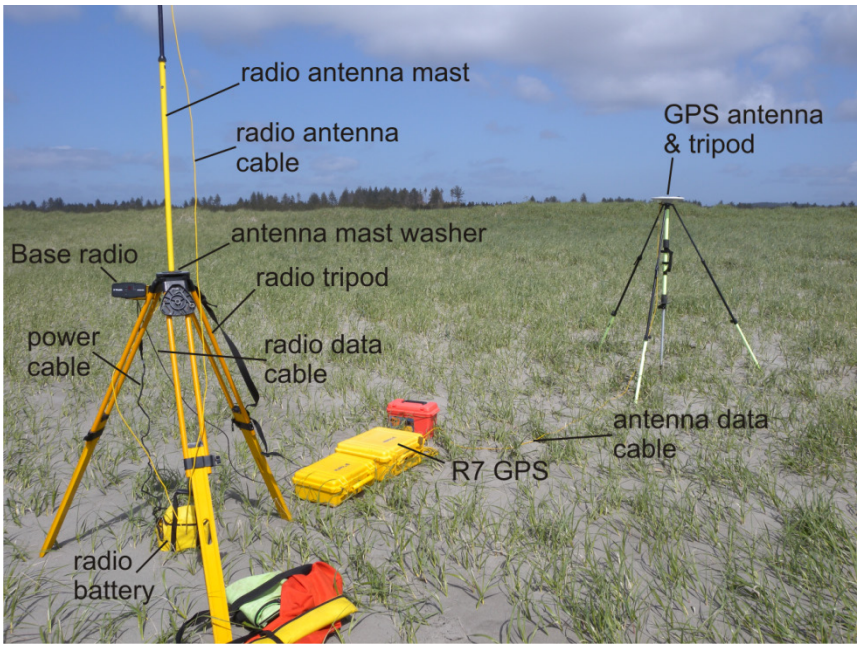

Figure 3-5. The Trimble R7 base station antenna in operation on the Tillamook Plains. Corrected GPS position and elevation information is then transmitted by an HPB450 Pacific Crest radio to the R8 GPS rover unit.

3.1.1 Lincoln County survey control procedures

Survey control (**Table 3-1**) the Lincoln County shore was provided by occupying multiple benchmarks established by the Coastal Field Office of DOGAMI. The approaches used to established the benchmarks are fully described in the reports by Allan and Hart (2007, 2008).

Coordinates assigned to the benchmarks (Table 3-1), were derived by occupying a Trimble R8 GPS receiver over the established benchmark, which then receives real-time kinematic corrections via the Oregon Real Time GPS Network (ORGN, http://www.theorgn.net/). The ORGN is a network of permanently installed, continuously operating GPS reference stations established and maintained by ODOT and partners (essentially a CORS network similar to those operated and maintained by the National Geodetic Survey [NGS]) that provide real-time kinematic (RTK) correctors to field GPS users over the internet via cellular phone networks. As a result, GPS users that are properly equipped to take advantage of these correctors, such as the Trimble system used in this study, can survey in the field to the one centimeter horizontal accuracy level in real time.

Each benchmark was observed on at least two occasions, at different times of the day or on alternate days, and the derived values were QC'd and if reasonable, were averaged. Furthermore, additional checking was undertaken for each of the GPS base station sites (**Table 3-1**), by comparing the multi-hour GPS measurements to coordinates and elevations derived using the Online Positioning User Service (OPUS) maintained by the NGS (http://www.ngs.noaa.gov/OPUS/ [Soler and others, 2011]). OPUS provides a simplified way to access high-accuracy National Spatial Reference System (NSRS) coordinates using a network of continuously operating GPS reference stations (CORS, http://www.ngs.noaa.gov/CORS/). In order to use OPUS, static GPS measurements are typically made using a fixed height tripod for periods of 2 hours or greater. OPUS returns a solution report with positional accuracy confidence intervals for adjusted coordinates and elevations for the observed point. In all cases we used the Oregon State Plane coordinate system, northern zone (meters), while the vertical datum is relative to the North American Vertical Datum of 1988 (NAVD88).

For each of the discrete shore reaches, the R7 GPS base station was located on the prescribed base station monument (e.g., CHNK, GOLF, ROCKYCRK, LACK, ONA, DRIFTWOOD, WAY (**Table 3-1**), using a 2.0-m fixed-height tripod. Survey control was provided by undertaking 180 GPS epoch measurements (~3 minutes of measurement per calibration site) using the calibration sites indicated in **Table 3-1**, enabling us to perform a GPS site calibration which brought the survey into a local coordinate system. This step is critical in order to eliminate various survey errors that may be compounded by factors such as poor satellite geometry, multipath, and poor atmospheric conditions, combining to increase the total error to several centimeters. **Table 3-2** shows the relative variability identified when comparing the mean derived benchmark coordinate and the original ORGN/OPUS derivations. As can be seen from **Table 3-2**, differences in the horizontal and vertical values at the various benchmarks were typically less than 2 cm (i.e., within one standard deviation [σ]).

Having completed a local site calibration (**Figure 3-6**), cross-shore beach profiles were surveyed with the R8 GPS rover unit mounted on a backpack, worn by a surveyor (**Figure 3-7**). This was undertaken during periods of low tide, enabling more of the beach to be surveyed. The approach was to generally walk from the landward edge of the primary dune or bluff edge, down the beach face and out into the ocean to approximately wading depth. A straight line, perpendicular to the shore was achieved by navigating along a pre-determined line displayed on a hand-held Trimble TSC2 computer controller, connected to the R8 receiver. The computer shows the position of the operator relative to the survey line and indicates the deviation of the GPS operator from the line. The horizontal variability during the survey is generally minor, being typically less than about ±0.25 m either side of the line (**Figure 3-8**), which results in negligible vertical uncertainties due to the relatively uniform nature of beaches characteristic of much of the Oregon coast (Ruggiero and others, 2005). Based on our previous research at numerous sites along the Oregon coast , this method of surveying can reliably detect elevation changes on the order of 4-5 cm, that is well below normal seasonal changes in beach elevation, which typically varies by 1-2 m (3-6 ft) (Ruggiero and others, 2005; Allan and Hart, 2007, 2008).

Analysis of the beach survey data involved a number of stages. The data were first imported into MathWorks® MATLAB® environment (a suite of computer programming languages)using a customized script. A least-squares linear regression was then fit to the profile data. The purpose of this script is to examine the reduced data and eliminate those data point residuals (e.g., **Figure 3-8**) that exceed a ±0.75-m threshold (i.e., the outliers) either side of the predetermined profile line. The data are then exported into an Microsoft® Excel® database for archiving purposes. A second MATLAB script takes the Excel profile database and plots the survey data (relative to the earlier surveys) and outputs the generated figure as a Portable Network Graphics (PNG) file. Appendix B shows the reduced beach profile plots for the Lincoln County transects.

Table 3-1. Survey benchmarks used to calibrate GPS surveys of the beach along the Lincoln County coastline. Asterisk signifies the location of the GPS base station during each respective survey. NGS denotes National Geodetic survey monument, OPRD denotes Oregon Parks and Recreation Department, LCSO denotes Lincoln County Surveyor's Office, ORGN signifies ORGN derivation solution.

Study Area	Primary Identification (PID) Name[1]	Northing (m)	Easting (m)	Elevation (m)
Lincoln City	RIVER–NGS/ORGN	2223683.583	157280.301	157.331
	BM17–OPRD/ORGN	2223540.028	155068.688	15.102
	CHNK–DOGAMI/ORGN*	2223262.413	154037.219	15.507
	SE27–LCSD/ORGN	2222180.879	146288.557	3.830
Siletz Spit	SE27–LCSO/ORGN	2222180.880	146288.558	3.823
	GOLF–NGS/ORGN*	2220990.260	142440.212	9.749
	S45–NGS/ORGN	2221245.744	140662.756	16.321
	BALD2–NGS/ORGN	2218150.018	135528.360	17.122
Depoe Bay	BALD2–NGS/ORGN	2218150.018	135528.360	17.122
	DB–DOGAMI/ORGN	2218006.887	133996.049	23.718
	ROCKYCRK–DOGAMI/ORGN*	2217337.174	130513.062	23.127
	FOUL–DOGAMI/ORGN	2217745.957	127738.331	140.251
Beverly Beach	9303-4–LCSO/ORGN	2217818.258	126223.765	28.395
	9303-3–LCSO/ORGN	2218387.072	124915.694	22.222
	LACK–NGS/ORGN*	2217913.212	121683.519	19.203
	9802–LCSO/ORGN	2216687.812	118228.302	43.074
Newport	LACK–NGS/ORGN*	2217913.212	121683.519	19.203
	9802–LCSO/ORGN	2216687.812	118228.302	43.074
	FRANKW–DOGAMI/ORGN	2218548.409	115204.692	50.395
	HAM–NGS/ORGN	2217080.408	110137.435	6.399
South Beach	HAM–NGS/ORGN	2217080.408	110137.435	6.399
	LOSTCRK–LCSO/ORGN	2216147.759	103932.219	12.982
	ONA–DOGAMI/ORGN*	2215916.240	102277.468	6.901
	144TH–LCSO/ORGN	2215993.879	102651.669	14.268
	X744–NGS/ORGN	2215056.571	97933.169	15.972
Alsea Spit	144TH–LCSO/ORGN	2215993.879	102651.669	14.268
	SMITH–NGS/ORGN	2214834.631	97258.674	5.180
	DRIFTWOOD–DOGAMI/ORGN*	2215152.091	94880.430	16.528
	BAYSHORE–DOGAMI/ORGN	2215199.068	91508.083	4.171
	V79–NGS/ORGN	2215737.774	90388.750	4.551
Yachats	V79–NGS/ORGN	2215737.774	90388.750	4.551
	PAT–DOGAMI/ORGN	2214678.503	89328.402	12.441
	09271–LCSO/ORGN	2214650.674	89141.148	10.012
	WAY–NGS/ORGN*	2214281.515	87315.754	8.684
	PICNIC–LCSO/ORGN	2212695.951	79822.401	9.418

Notes: Coordinates are expressed in the Oregon State Plane Coordinate System, northern zone (meters) and the vertical datum is NAVD'88.

[1]Control provided using both horizontal and vertical values derived by averaging multiple separate GPS occupations with survey control provide by the Oregon Reference Geodetic Network (ORGN).

Table 3-2. Horizontal and vertical coordinates (expressed as a standard deviation) at each of the benchmark locations, compared to the final coordinates referenced in Table 3-1. Asterisk signifies the location of the GPS base station during each respective survey.

Study Area	Primary Identification (PID) Name[1]	Northing (m) σ	Easting (m) σ	Elevation (m) σ
Lincoln City	RIVER	0.003	0.009	0.009
	BM17	0.007	0.007	0.030
	CHNK*	0.001	0.000	0.023
	SE27	0.006	0.020	0.023
Siletz Spit	SE27	0.006	0.020	0.023
	GOLF*	0.008	0.016	0.011
	S45	0.005	0.011	0.014
	BALD2	0.019	0.006	0.023
Depoe Bay	BALD2	0.019	0.006	0.023
	DB	0.011	0.016	0.018
	ROCKYCRK*	0.004	0.014	0.003
	FOUL	0.006	0.015	0.008
Beverly Beach	9303-4	0.006	0.014	0.016
	9303-3	0.007	0.020	0.008
	LACK*	0.009	0.003	0.008
	9802	0.004	0.027	0.017
Newport	LACK*	0.009	0.003	0.008
	9802	0.004	0.027	0.017
	FRANKW	0.046	0.011	0.008
	HAM	0.012	0.015	0.009
South Beach	HAM	0.012	0.015	0.009
	LOSTCRK	0.035	0.013	0.001
	ONA*	0.004	0.006	0.002
	144th	0.002	0.019	0.002
	X744	0.014	0.023	0.005
Alsea Spit	144th	0.002	0.019	0.002
	SMITH	0.000	0.021	0.002
	DRIFTWOOD	0.010	0.003	0.006
	BAYSHORE	0.015	0.010	0.012
	V79	0.017	0.018	0.016
Yachats	V79	0.017	0.018	0.016
	PAT	0.018	0.019	0.003
	09271	0.007	0.008	0.014
	WAY*	0.001	0.014	0.014
	PICNIC	0.011	0.007	0.008

Figure 3-6. A 180-epoch calibration check is performed on a survey monument (DRIFTWOOD) established in the Alsea Spit littoral cell in Lincoln County. This procedure is important for bringing the survey into a local coordinate system and for reducing errors associated with the GPS survey (photo: J. C. Allan, DOGAMI).

Figure 3-7. Surveying the morphology of the beach at Bandon using a Trimble 5800 "rover" GPS.

To supplement the GPS beach and bluff data, high-resolution lidar data measured by Watershed Sciences, Inc. (WSI) in 2009 for DOGAMI were also analyzed and integrated into the beach profile data set. This was especially important for backshore areas where it was not possible to easily survey with the GPS gear. In addition, lidar data flown by the USGS/NASA/NOAA in 1997, 1998, and 2002 were also used to extend the time series of the beach and bluff profile data. In particular, the 1998 lidar data measured at the end of the major 1997-98 El Niño was analyzed, providing additional measurements of the beach in an eroded state that can be compared with more recent winter surveys of the beach. The 1997, 1998, and 2002 lidar data were downloaded from NOAA's Coastal Service Center (http://coast.noaa.gov/dataregistry/search/collection/info/coastallidar), gridded in Esri® ArcGIS® using a triangulated irregular network (TIN) algorithm, and distance and elevation data were extracted from the grid lidar digital elevation models (DEMs).

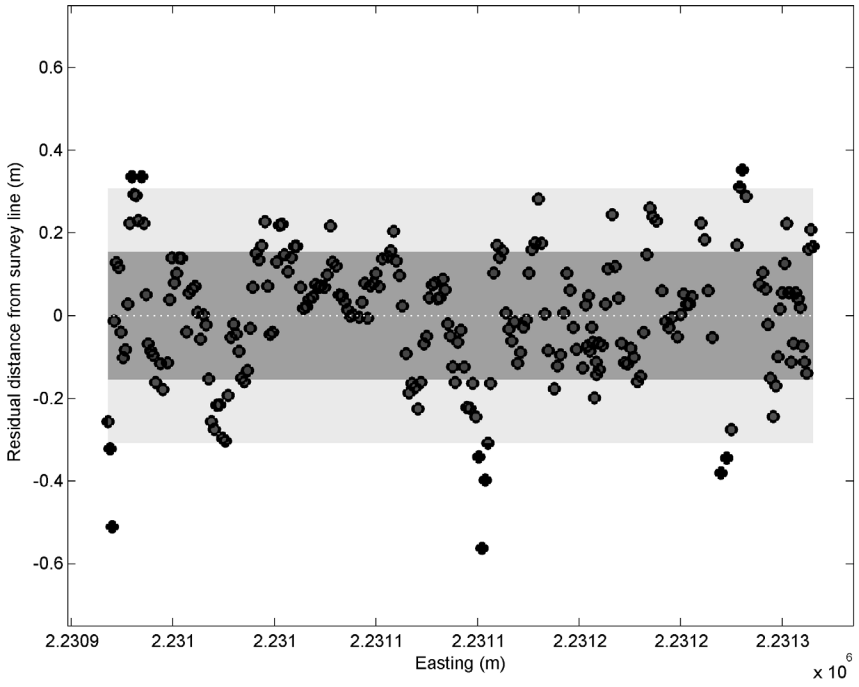

Figure 3-8. Residuals of GPS survey points relative to zero (transect) line. Example reflects the Cannon Beach 10 profile line. Dark grey shading indicates 68.3% of measurements located ±0.15 m (1σ) from the transect line, while 95.5% (2σ) of the measurements are located within ±0.30 m of the profile line (grey shading).

3.2 Beach Characterization

Analyses of the beach profile data were undertaken using additional scripts developed in MATLAB. These scripts require the user to interactively locate the positions of the seaward edge and crest of the Primary Frontal Dune (PFD) backing the beach, and then evaluate the beach-dune juncture (E_j) elevations and beach slopes (tan β) for the 1997, 1998, 2002, 2008/2009, 2011 and 2012 surveys along each of the profile sites. Beach slope was determined by fitting a linear regression through the measured profile data. In all cases, the slope of the beach face was determined to be the region of the beach located between Mean Sea Level (~1.4 m, MLLW) and the highest observed tide (~3.8 m, MLLW), an approach that is

consistent with methodologies adopted by Ruggiero and others (2005) and Stockdon and others (2006). Determination of the location of the beach-dune junctures (E_j) was accomplished interactively using the MATLAB scripts and from local knowledge of the area. In general, the beach-dune juncture (E_j) reflects a major break in slope between the active part of the beach face and the toe location of the primary dune or bluff. For most sites along the Oregon coast, the beach-dune junctures (E_j) typically occurs at elevations between about 4-6 m (NAVD88). **Figure 3-9** provides an example of the identified beach-dune juncture (E_j) for one site, LINC 69, after it has been eroded (described in Section 7), and is located at the south end of Alsea Spit (**Figure 3-1**). In this example, it is apparent that a smaller secondary dune was developing seaward of the primary dune in 1997, but was subsequently wiped out in the 1997-98 El Niño. Furthermore, the primary dune has aggraded significantly (almost 4 m [~13 ft] vertically) since the late 1990s. Examination of the profile data indicates that the beach-dune juncture (E_j) has varied in elevation, a function of repeated phases of both erosion and accretion events. As of winter 2013, the beach-dune juncture was close in elevation to the eroded position depicted by the magenta circle in **Figure 3-9**, located at an elevation of 6.8 m (22.3 ft). Although not shown in **Figure 3-9**, the beach face slope was determined to be steep, $\tan\beta$ = 0.098; **Figure 3-9** also depicts the location of the dune crest, which was determined to be 17.2 m (56.4 ft) and the landward location of the *primary frontal dune* (PFD). These latter data are used later to develop new VE flood zones along the Lincoln County coast.

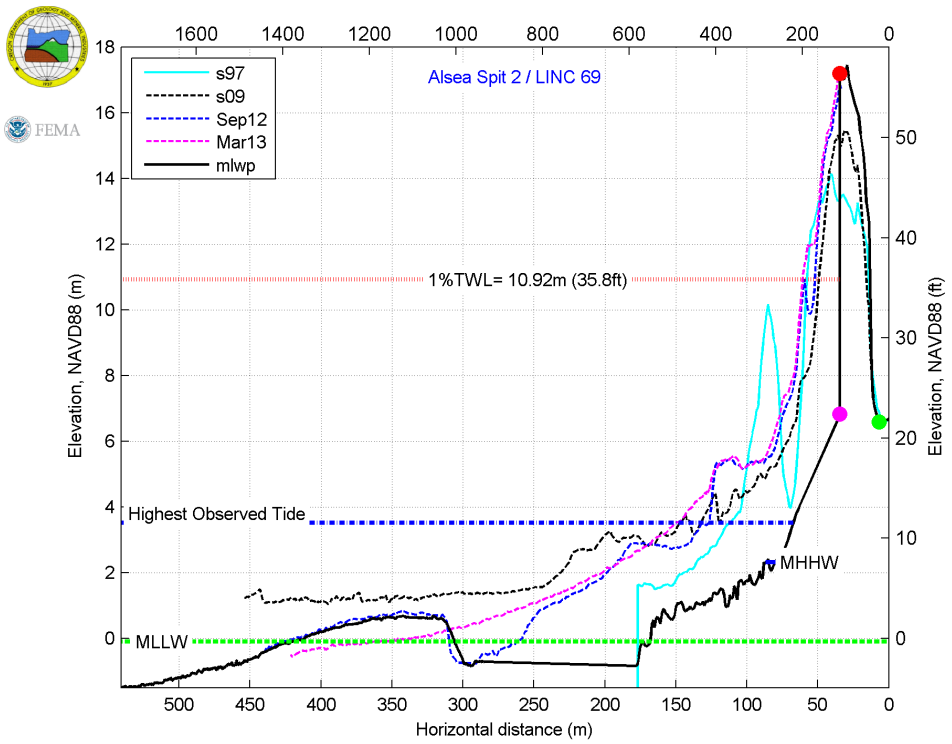

Figure 3-9. Plot showing various beach cross-sections at the LINC 69 (aka Alsea 2) profile site. In this example, the most likely winter profile (MLWP) is depicted as the solid heavy black line, the *eroded* beach-dune juncture location, dune crest and primary frontal dune location (PFD) is characterized respectively by the magenta, red, and green circles. The plot also provides a dramatic example of the degree of aggradation that has taken place on the foredune.

To estimate beach erosion and profile changes for a specific coastal setting that occurs during a particular storm, it is essential to first define the initial conditions of the morphology of the beach prior to the actual event of interest (Northwest Hydraulic Consultants, 2005). This initial beach profile is referred to as the most likely winter profile (*MLWP*) condition for that particular coastal setting and is depicted in **Figure 3-9** as the heavy black line. The *MLWP* was assessed based on an examination of the combined surveyed profiles and lidar data. In the **Figure 3-9** example, a combination of our 2012 summer survey and the 2009 lidar survey of the primary dune and backshore were found to best characterizes the landward component of the *MLWP*, while the 1997 survey best captured the state of the active beach and seaward edge of the foredune. Landward of the dune crest, information on the backshore topography was derived by incorporating the actual measured GPS data because those data provided the best representation of the actual ground surface. Where GPS survey data were not available, we used topographic data derived from the 2009 lidar flown for DOGAMI.

Table 3-3 summarizes the various morphological parameters identified for each transect site along the Lincoln County coastline, including their geomorphic classification. **Figure 3-10** provides a plot of the alongshore changes in beach slopes (tan β), mean sediment grain sizes (M_z), beach-dune juncture (E_j) elevations, and the dune/bluff/structure crest heights. In general, the steepest slopes are confined to those beaches with coarse sediments on the foreshore (e.g., Gleneden Beach/Siletz Spit), while sites containing finer sediments are characterized by generally lower beach slopes (e.g., Newport cell). Mean grain sizes along Gleneden Beach/Siletz Spit are characterized as coarse sand (M_z = 0.3Ø (0.8 mm (Peterson and others, 1994)) and decrease to M_z = 3.0Ø (0.12 mm, or very fine sand) in the Newport/South Beach portion of the Lincoln County coastline. The steepest beach slopes are typically identified adjacent to the headlands, where the composition of the beach is comprised predominantly of gravels and boulders and the sediment is locally sourced from the headlands as a result of landslides (**Figure 3-11**).

Figure 3-10 also plots the beach/dune and beach/bluff juncture elevations (Ej) for the various study sites. Values for Ej vary significantly along the length of the Lincoln County coast. The lowest Ej values tend to occur along the toe of coastal cliffs (e.g., along the headlands, between Cape Foulweather and Depoe Bay, and along Cascade Head, **Figure 3-10**). In general, the highest beach-dune juncture elevations are found along Siletz Spit, and immediately south of the south Newport jetties; the latter reflects an area that is actively aggrading, while the former reflects a steep reflective beach system. In addition, **Figure 3-10** (bottom) indicates the dune/bluff/structure crest elevations. Because these heights are indicative of the potential for flooding, with higher crests generally limiting flood overtopping, it can be seen that the risk from coastal flooding and inundation is likely to be highest along much of the shores north of Yachats (and south of Alsea Bay) and along the north end of Siletz Spit and the south end of the Lincoln City cell. Along the remainder of the shore, the beaches are protected by prominent bluffs (e.g., between Seal Rock and South Beach, much of the Beverly Beach cell, Otter Rock to Depoe Bay, and along much of the Lincoln City cell) and/or dunes (e.g., Alsea Spit) with crest elevations that range from 10 to 30 m (33–98 ft) that effectively preclude wave overtopping and hence inundation in those areas. Nevertheless, some of these sites are subject to erosion hazards that likely will influence the extent of the flood zones in those areas, after factoring the potential for erosion from storms.

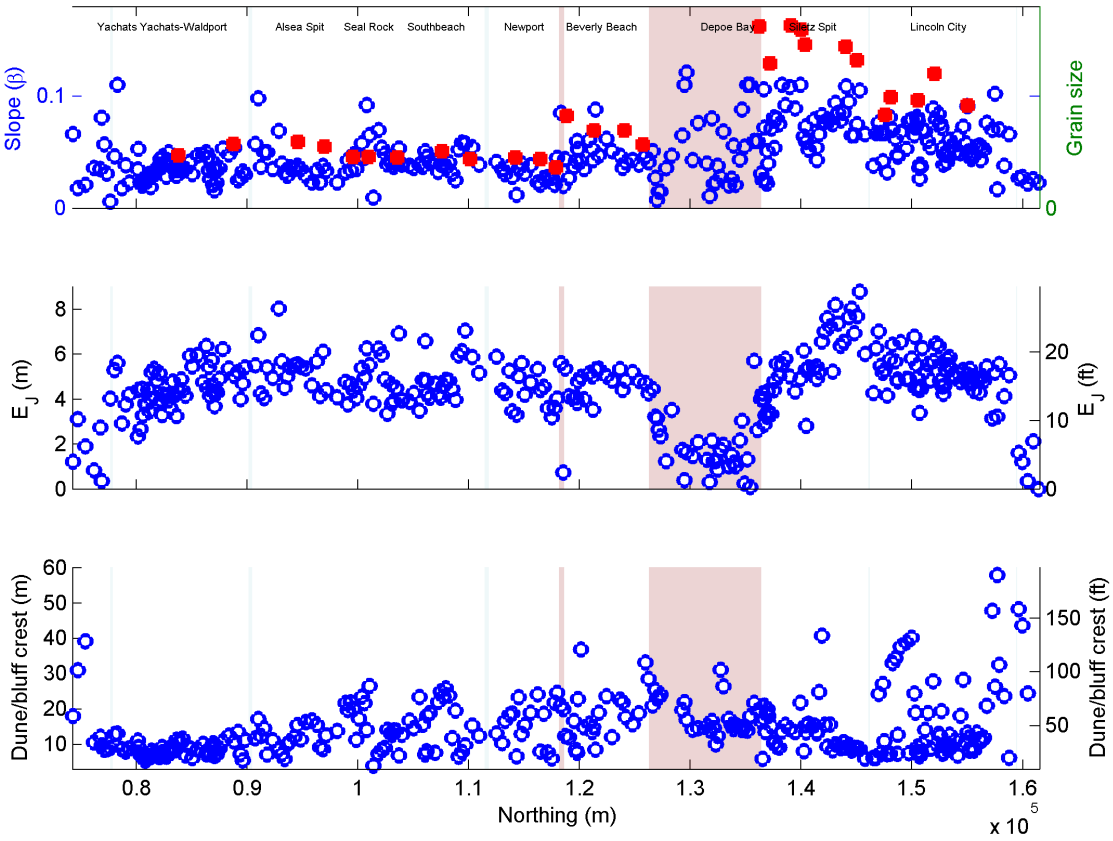

Figure 3-10. Alongshore changes in beach slopes (tan β), beach-dune juncture (Ej) elevations, and dune/bluff crest/tops along Lincoln County. Red squares indicate mean sediment grain-sizes measured by Peterson and others (1994). Vertical blue shading denotes the location of estuary mouths, while the red shading denotes the location of major headlands.

Figure 3-11. Cobble/boulder beach located on the south side of Yaquina Head and north of Newport (photo by P.D. Komar).

Table 3-3. Identified beach morphological parameters from the most likely winter profile along the Lincoln County shoreline. Parameters include the beach-dune junction elevation (E_{i}_MLWP), beach slope (tan β), and a site description.

Reach	Transect	D_{HIGH} (m)	D_{LOW} (m)	Beach Slope (tan β)	Description
Cape Perpetua	LINC1	18.025	1.217	0.066	narrow rock platform backed by high cliffs
	LINC2	30.946	3.107	0.018	dissipative sand beach backed by high cliffs
	LINC3	39.090	1.902	0.021	broad rock platform backed by high cliffs
	LINC4	10.580	0.836	0.036	broad rock platform backed by high cliffs
Yachats	LINC5	12.193	2.735	0.035	rock platform backed by moderately high bluff
	LINC6	9.761	0.360	0.081	rock platform backed by moderately low bluff
	LINC7	8.538	-0.574	0.057	rock platform backed by moderately low bluff
	LINC8	8.660	-0.821	0.031	sand beach fronts rock platform and backshore
	LINC9	9.057	4.019	0.006	sandy beach backed by bluff
	LINC10	12.935	5.284	0.046	rock platform and sandy beach backed by bluff
	LINC11	13.090	5.605	0.110	sand beach backed by riprap
	LINC12	8.697	2.916	0.018	narrow rock platform backed by low bluff
	LINC13	8.012	3.761	0.038	broad rock platform backed by low bluff
	LINC14	8.944	4.202	0.023	sand beach fronts rock platform backed by low bluff
Waldport	LINC15	11.154	2.339	0.035	sand beach fronts rock platform backed by low bluff
	LINC16	9.271	4.411	0.053	sand beach fronts low vertical bluff
	LINC17	7.115	2.673	0.023	sand beach fronts riprap structure
	LINC18	6.575	4.450	0.020	sand beach fronts low vertical bluff
	LINC19	7.084	3.275	0.024	sand beach fronts riprap structure
	LINC20	6.414	3.270	0.026	sand beach fronts low vertical bluff
	LINC21	5.475	3.797	0.024	sand beach fronts low vertical bluff
	LINC22	6.243	3.750	0.026	sand beach fronts low vertical bluff
	LINC23	6.844	4.406	0.025	sand beach fronts low vertical bluff
	LINC24	6.347	3.458	0.031	sand beach fronts low vertical bluff
	LINC25	6.488	4.003	0.019	sand beach fronts riprap structure
	LINC26	8.247	5.181	0.028	sand beach fronts low vertical bluff
	LINC27	7.369	5.345	0.033	sand beach fronts low vertical bluff
	LINC28	6.870	4.816	0.034	sand beach fronts low vertical bluff
	LINC29	6.481	5.146	0.038	sand beach fronts low vertical bluff
	LINC30	7.542	3.905	0.044	sand beach fronts low vertical bluff
	LINC31	6.742	3.941	0.044	sand beach fronts low vertical bluff
	LINC32	9.283	3.288	0.037	sand beach fronts low vertical bluff
	LINC33	7.880	4.211	0.046	sand beach fronts low vertical bluff
	LINC34	6.987	4.117	0.042	sand beach fronts low vertical bluff
	LINC35	6.581	4.164	0.028	sand beach fronts riprap structure
	LINC36	7.938	4.172	0.042	sand beach fronts low vertical bluff
	LINC37	7.807	3.938	0.050	sand beach fronts riprap structure
	LINC38	9.099	3.606	0.042	sand beach fronts riprap structure
	LINC39	8.511	4.777	0.041	sand beach fronts moderately low bluff
	LINC40	8.408	4.185	0.034	sand beach fronts moderately low bluff
	LINC41	11.324	3.246	0.029	sand beach fronts riprap structure
	LINC42	10.700	4.363	0.034	sand beach fronts riprap structure
	LINC43	10.635	4.878	0.034	sand beach fronts moderately high vertical bluff
	LINC44	11.648	4.390	0.034	sand beach fronts riprap structure
	LINC45	6.933	4.142	0.035	sand beach fronts riprap structure
	LINC46	8.937	5.919	0.042	dune-backed beach
	LINC47	6.181	5.441	0.031	dune-backed beach
	LINC48	8.599	5.958	0.047	dune-backed beach
	LINC49	10.191	4.743	0.048	sand beach fronts moderately high vertical bluff
	LINC50	7.258	6.361	0.050	dune-backed beach
	LINC51	8.129	4.496	0.045	sand beach fronts riprap structure

Reach	Transect	D_{HIGH} (m)	D_{LOW} (m)	Beach Slope (tan β)	Description
	LINC52	7.937	5.417	0.034	dune-backed beach
	LINC53	7.271	4.136	0.026	sand beach fronts riprap structure
	LINC54	9.015	5.728	0.042	dune-backed beach
	LINC55	10.356	4.290	0.021	sand beach fronts moderately high vertical bluff
	LINC56	9.322	4.620	0.036	dune-backed beach
	LINC57	6.811	3.678	0.016	sand beach fronts riprap structure
	LINC58	7.091	4.326	0.023	sand beach fronts low vertical bluff
	LINC59	7.480	4.272	0.034	sand beach fronts riprap structure
	LINC60	8.898	4.906	0.036	sand beach fronts moderately high vertical bluff
	LINC61	10.859	6.219	0.053	sand dune fronts moderately high vertical bluff
	LINC62	12.513	5.358	0.048	sand dune fronts moderately high vertical bluff
	LINC63	10.828	5.021	0.054	sand dune fronts moderately high vertical bluff
	LINC64	13.583	5.199	0.025	sand beach fronts moderately high vertical bluff
	LINC65	7.290	3.992	0.027	sand dune fronts moderately high vertical bluff
	LINC66	5.528	4.690	0.033	dune-backed beach
	LINC67	11.260	5.405	0.030	sand beach fronts moderately high vertical bluff
Alsea Spit	LINC68	11.754	5.501	0.057	dune-backed beach
	LINC69	17.199	6.833	0.098	dune-backed beach
	LINC70	12.411	4.253	0.037	dune-backed beach
	LINC71	14.596	4.038	0.050	dune-backed beach
	LINC72	7.173	5.397	0.050	dune-backed beach
	LINC73	11.202	4.940	0.035	dune-backed beach
	LINC74	8.746	8.015	0.069	dune-backed beach
	LINC75	7.264	5.675	0.040	dune-backed beach
	LINC76	5.936	4.498	0.032	sand beach fronts low vertical bluff
	LINC77	10.139	4.995	0.029	sand beach fronts low vertical bluff
	LINC78	10.670	5.427	0.037	sand beach fronts low vertical bluff
	LINC79	12.084	5.488	0.035	sand dune fronts moderately high vertical bluff
	LINC80	15.499	5.539	0.038	sand dune fronts moderately high vertical bluff
	LINC81	11.427	5.430	0.035	sand dune fronts moderately high vertical bluff
	LINC82	16.323	5.360	0.029	sand beach fronts moderately high vertical bluff
	LINC83	16.819	4.606	0.023	sand beach fronts moderately high vertical bluff
	LINC84	15.558	5.676	0.034	sand beach fronts moderately high vertical bluff
	LINC85	9.209	4.129	0.023	sand beach fronts moderately high vertical bluff
	LINC86	8.697	6.101	0.038	dune-backed beach, backed further by bluffs
	LINC87	12.566	4.395	0.033	sand beach fronts high vertical bluff
	LINC88	13.829	4.077	0.023	sand beach fronts high vertical bluff
South Beach	LINC89	21.717	4.764	0.032	sand beach fronts high vertical bluff
	LINC90	19.753	3.760	0.043	sand beach fronts high vertical bluff
	LINC91	21.883	4.663	0.045	sand beach fronts high vertical bluff
	LINC92	20.049	4.386	0.048	sand beach fronts high vertical bluff
	LINC93	11.324	4.036	0.035	sand beach fronts high vertical bluff
	LINC94	17.328	4.572	0.046	sand beach fronts high vertical bluff
	LINC95	23.471	5.384	0.058	sand beach fronts high vertical bluff
	LINC96	21.673	4.943	0.045	sand beach fronts high vertical bluff
	LINC97	14.112	6.249	0.092	sand beach fronts high vertical bluff
	LINC98	26.503	5.508	0.065	sand beach fronts high vertical bluff
	LINC99	4.038	3.789	0.010	dune-backed beach
	LINC100	7.415	6.243	0.070	dune-backed beach
	LINC101	8.522	5.974	0.054	dune-backed beach
	LINC102	9.045	4.878	0.049	sand beach fronts low vertical bluff
	LINC103	14.179	3.348	0.039	sand beach fronts riprap structure
	LINC104	13.334	4.655	0.041	sand beach fronts moderately high vertical bluff
	LINC105	12.719	3.805	0.046	sand beach fronts riprap structure
	LINC106	13.949	3.912	0.037	sand beach fronts moderately high vertical bluff

Reach	Transect	D_{HIGH} (m)	D_{LOW} (m)	Beach Slope (tan β)	Description
	LINC107	13.931	4.477	0.040	sand beach fronts moderately high vertical bluff
	LINC108	6.915	6.915	0.053	sand beach backed by cobbles
	LINC109	12.735	3.943	0.039	sand beach fronts high vertical bluff
	LINC110	16.781	3.881	0.038	sand beach fronts high vertical bluff
	LINC111	14.614	4.267	0.036	sand beach fronts high vertical bluff
	LINC112	23.387	3.480	0.039	sand beach fronts high vertical bluff
	LINC113	15.564	4.846	0.037	sand beach fronts high vertical bluff
	LINC114	7.175	6.571	0.051	dune-backed beach
	LINC115	8.087	4.814	0.046	sand beach fronts high vertical bluff
	LINC116	18.160	4.228	0.046	sand beach fronts riprap structure
	LINC117	18.878	4.050	0.041	sand beach fronts high vertical bluff
	LINC118	7.696	4.679	0.042	sand beach fronts low vertical bluff
	LINC119	22.033	4.185	0.033	sand beach fronts high vertical bluff
	LINC120	24.971	4.060	0.039	sand beach fronts riprap structure
	LINC121	23.486	4.583	0.040	sand beach fronts high vertical bluff
	LINC122	25.845	4.857	0.036	sand beach fronts high vertical bluff
	LINC123	23.811	4.813	0.041	sand beach fronts high vertical bluff
	LINC124	11.830	4.445	0.031	sand beach fronts high vertical bluff
	LINC125	19.537	3.964	0.025	sand beach fronts high vertical bluff
	LINC126	6.579	5.934	0.053	dune-backed beach
	LINC127	7.909	6.129	0.059	dune-backed beach
	LINC128	9.796	7.038	0.058	dune-backed beach
	LINC129	15.373	5.863	0.055	dune-backed beach
	LINC130	12.478	5.151	0.039	dune-backed beach
Newport	LINC131	13.140	5.881	0.041	dune-backed beach
	LINC132	10.388	4.379	0.035	sand beach fronts high vertical bluff
	LINC133	16.665	4.258	0.030	sand beach fronts high vertical bluff
	LINC134	18.413	5.257	0.037	sand beach fronts high vertical bluff
	LINC135	18.755	3.455	0.028	sand beach fronts high vertical bluff
	LINC136	6.669	3.303	0.012	sand beach fronts seawall
	LINC137	23.345	5.020	0.035	sand beach fronts high vertical bluff
	LINC138	12.967	5.597	0.040	sand dune fronts high bluff
	LINC139	15.506	4.190	0.031	sand dune fronts high bluff
	LINC140	18.965	4.738	0.038	sand beach fronts high vertical bluff
	LINC141	24.141	5.329	0.023	sand dune fronts high bluff
	LINC142	8.015	4.395	0.021	dune-backed beach, backed further by bluffs
	LINC143	18.671	4.548	0.027	dune-backed beach, backed further by bluffs
	LINC144	7.781	3.596	0.028	dune-backed beach, backed further by bluffs
	LINC145	6.064	3.189	0.027	sand dune fronts high bluff
	LINC146	21.800	3.604	0.021	sand dune fronts high bluff
	LINC147	24.604	4.021	0.045	sand dune fronts high bluff
Yaquina	LINC148	21.012	5.592	0.085	narrow rock platform backed by high cliffs
Head	LINC149	19.945	0.739	0.020	narrow rock platform backed by high cliffs
Beverly	LINC150	12.395	5.351	0.044	sand beach and platform fronts high vertical bluff
Beach	LINC151	12.037	4.125	0.027	sand beach and platform fronts high vertical bluff
	LINC152	16.648	4.071	0.037	sand beach fronts moderately high vertical bluff
	LINC153	8.459	4.074	0.042	sand beach fronts moderately high vertical bluff
	LINC154	7.662	3.824	0.060	sand beach backed by cobble berm/riprap
	LINC155	22.818	4.776	0.053	sand beach fronts high vertical bluff
	LINC156	36.791	4.980	0.042	sand beach fronts high vertical bluff
	LINC157	14.831	3.994	0.035	sand beach fronts high vertical bluff
	LINC158	15.853	5.141	0.061	sand beach fronts high vertical bluff
	LINC159	13.518	5.000	0.053	sand beach fronts high vertical bluff
	LINC160	14.915	3.525	0.043	sand beach fronts riprap structure
	LINC161	8.559	5.320	0.088	sand beach backed by cobble berm

Reach	Transect	D_{HIGH} (m)	D_{LOW} (m)	Beach Slope (tan β)	Description
	LINC162	18.977	5.346	0.047	sand beach fronts high vertical bluff
	LINC163	23.622	5.016	0.062	sand beach fronts high vertical bluff
	LINC164	12.086	4.816	0.051	sand beach fronts high vertical bluff
	LINC165	22.688	5.331	0.047	sand beach fronts high vertical bluff
	LINC166	21.825	4.401	0.036	sand beach fronts high vertical bluff
	LINC167	17.714	4.820	0.041	sand beach fronts high vertical bluff
	LINC168	15.690	5.194	0.043	sand beach fronts high vertical bluff
	LINC169	18.825	4.807	0.039	sand beach fronts high vertical bluff
	LINC170	33.129	4.713	0.046	sand beach fronts high vertical bluff
	LINC171	28.516	4.251	0.041	sand beach fronts high vertical bluff
Otter Rock	LINC172	21.009	4.444	0.051	rock platform and sandy beach backed by bluff
	LINC173	25.393	3.221	0.027	rock platform backed by bluff
	LINC174	23.010	3.156	0.008	rock platform backed by bluff
	LINC175	23.244	2.644	0.015	rock platform backed by bluff
	LINC176	24.099	2.344	0.015	rock platform backed by bluff
Cape	LINC177	116.753	1.237	0.036	narrow rock platform backed by high cliffs
Foulweather	LINC178	103.606	3.516	0.047	narrow rock platform backed by high cliffs
Miroco	LINC179	19.740	1.743	0.065	basalt ramp with low tide cliff
	LINC180	21.948	0.397	0.110	basalt ramp with low tide cliff
	LINC181	16.989	1.637	0.121	basalt ramp with low tide cliff
Rocky Creek	LINC182	14.183	1.467	0.043	basalt ramp with low tide cliff
	LINC183	14.596	2.088	0.076	basalt ramp with low tide cliff
Whale Cove	LINC184	15.310	1.302	0.040	basalt ramp with low tide cliff
	LINC185	13.989	0.314	0.011	basalt ramp with low tide cliff
	LINC186	16.676	2.155	0.080	basalt ramp with low tide cliff
	LINC187	14.648	1.253	0.022	basalt ramp with low tide cliff
	LINC188	10.068	1.250	0.023	basalt ramp with low tide cliff
	LINC189	12.439	0.868	0.038	basalt ramp with low tide cliff
Depoe Bay	LINC190	31.062	1.745	0.028	narrow rock platform backed by basalt ramp
	LINC191	26.414	1.966	0.069	narrow rock platform backed by basalt cliff
	LINC192	17.251	1.018	0.020	moderately wide rock platform backed by basalt cliff
	LINC193	15.543	1.512	0.027	moderately wide rock platform backed by basalt cliff
	LINC194	14.360	1.173	0.056	basalt cliff
	LINC195	15.519	1.013	0.021	basalt cliff
	LINC196	14.959	2.163	0.043	moderately wide rock platform backed by basalt cliff
	LINC197	14.091	3.035	0.088	narrow rock platform backed by basalt cliff
	LINC198	15.074	0.249	0.055	moderately wide rock platform backed by basalt cliff
	LINC199	13.910	1.321	0.110	basalt cliff
	LINC200	18.001	0.092	0.110	basalt cliff
	LINC201	21.750	5.697	0.060	moderately wide rock platform backed by basalt cliff
	LINC202	19.540	2.624	0.060	moderately wide rock platform backed by basalt cliff
Fogarty	LINC203	16.484	3.988	0.031	bluff fronted by sand and gravel beach and shore platform
Creek	LINC204	5.960	4.247	0.025	riprap fronted by sand and gravel beach and shore platform
	LINC205	17.253	3.999	0.106	bluff fronted by sand and gravel beach and shore platform
	LINC206	20.951	2.861	0.072	riprap fronted by sand and gravel beach and shore platform
	LINC207	13.485	3.282	0.025	bluff fronted by sand and gravel beach and shore platform
	LINC208	18.792	3.215	0.022	bluff fronted by sand and gravel beach and shore platform
	LINC209	20.005	4.334	0.051	bluff fronted by sand and gravel beach and shore platform

Reach	Transect	D_{HIGH} (m)	D_{LOW} (m)	Beach Slope (tan β)	Description
	LINC210	18.034	3.436	0.040	bluff fronted by sand and gravel beach and shore platform
Gleneden Beach/Siletz Spit	LINC211	15.137	3.330	0.071	mixed sand and gravel beach fronts riprap structure
	LINC212	10.448	4.393	0.081	mixed sand and gravel beach fronts riprap structure
	LINC213	10.398	4.798	0.054	mixed sand and gravel beach fronts bluff
	LINC214	9.392	5.565	0.080	mixed sand and gravel beach fronts riprap structure
	LINC215	9.145	5.009	0.075	mixed sand and gravel beach fronts riprap structure
	LINC216	13.620	5.545	0.110	mixed sand and gravel beach fronts riprap structure
	LINC217	15.570	5.785	0.092	mixed sand and gravel beach fronts bluff
	LINC218	14.340	4.998	0.108	mixed sand and gravel beach fronts riprap structure
	LINC219	13.497	4.328	0.089	mixed sand and gravel beach fronts riprap structure
	LINC220	21.776	4.896	0.110	mixed sand and gravel beach fronts riprap structure
	LINC221	8.111	6.149	0.064	mixed sand and gravel beach fronts dune
	LINC222	15.448	5.300	0.073	mixed sand and gravel beach fronts bluff
	LINC223	13.416	2.809	0.059	mixed sand and gravel beach fronts riprap structure
	LINC224	15.850	5.409	0.052	mixed sand and gravel beach fronts bluff
	LINC225	15.390	5.384	0.079	mixed sand and gravel beach fronts riprap structure
	LINC226	13.513	5.449	0.054	mixed sand and gravel beach fronts bluff
	LINC227	13.125	4.887	0.043	mixed sand and gravel beach fronts seawall
	LINC228	24.807	5.201	0.066	mixed sand and gravel beach fronts bluff
	LINC229	40.682	6.543	0.083	mixed sand and gravel beach fronts riprap structure
	LINC230	15.605	7.001	0.077	dune-backed beach overlying riprap structure
	LINC231	9.419	7.592	0.079	dune-backed beach overlying riprap structure
	LINC232	15.636	7.219	0.079	dune-backed beach overlying riprap structure
	LINC233	8.342	5.217	0.075	dune-backed beach overlying riprap structure
	LINC234	10.097	8.183	0.094	dune-backed beach overlying riprap structure
	LINC235	9.877	7.347	0.085	dune-backed beach overlying riprap structure
	LINC236	8.964	6.356	0.078	dune-backed beach overlying riprap structure
	LINC237	10.662	6.537	0.085	dune-backed beach overlying riprap structure
	LINC238	9.091	9.091	0.109	dune-backed beach overlying riprap structure
	LINC239	9.962	7.637	0.095	dune-backed beach overlying riprap structure
	LINC240	8.306	8.017	0.065	dune-backed beach overlying riprap structure
	LINC241	9.086	6.925	0.065	dune-backed beach overlying riprap structure
	LINC242	9.039	7.673	0.075	dune-backed beach overlying riprap structure
	LINC243	8.765	8.765	0.105	dune-backed beach
	LINC244	6.000	6.000	0.066	dune-backed beach
Lincoln City	LINC245	6.231	4.263	0.038	dissipative sand beach fronts high bluffs
	LINC246	6.254	6.254	0.067	dissipative sand beach fronts high bluffs
	LINC247	24.270	7.000	0.076	dissipative sand beach fronts high bluffs
	LINC248	7.621	5.472	0.067	dissipative sand beach fronts seawall
	LINC249	27.100	5.166	0.042	dissipative sand beach fronts high bluffs
	LINC250	10.979	5.279	0.067	dissipative sand beach fronts riprap
	LINC251	7.300	4.153	0.032	dissipative sand beach fronts seawall
	LINC252	7.415	5.758	0.081	dissipative sand beach fronts seawall
	LINC253	32.943	6.413	0.070	dissipative sand beach fronts high bluffs
	LINC254	34.319	5.667	0.062	dissipative sand beach fronts high bluffs
	LINC255	7.410	4.866	0.048	dissipative sand beach fronts seawall and high bluffs
	LINC256	12.766	4.785	0.046	dissipative sand beach fronts seawall and high bluffs
	LINC257	37.604	6.525	0.068	dissipative sand beach fronts high bluffs
	LINC258	38.806	4.899	0.053	dissipative sand beach fronts high bluffs
	LINC259	7.575	4.883	0.078	dissipative sand beach fronts seawall
	LINC260	40.100	5.800	0.079	dissipative sand beach fronts moderately high bluffs
	LINC261	24.403	6.770	0.065	dissipative sand beach fronts moderately high bluffs
	LINC262	18.974	4.487	0.072	dissipative sand beach fronts riprap
	LINC263	7.835	5.492	0.081	dissipative sand beach fronts seawall

Reach	Transect	D_{HIGH} (m)	D_{LOW} (m)	Beach Slope (tan β)	Description
	LINC264	9.440	4.957	0.078	dissipative sand beach fronts riprap
	LINC265	6.798	4.406	0.036	dissipative sand beach fronts seawall
	LINC266	6.700	3.383	0.026	dissipative sand beach fronts riprap
	LINC267	7.069	4.537	0.039	dissipative sand beach fronts riprap
	LINC268	7.897	4.423	0.037	dissipative sand beach fronts seawall
	LINC269	10.260	6.259	0.070	dune-backed beach
	LINC270	14.128	5.222	0.069	dissipative sand beach fronts riprap and bluffs
	LINC271	18.857	5.554	0.060	dissipative sand beach fronts moderately high bluffs
	LINC272	8.800	4.829	0.054	dissipative sand beach fronts riprap and bluffs
	LINC273	27.820	5.684	0.089	dissipative sand beach fronts riprap and bluffs
	LINC274	10.235	6.466	0.079	dissipative sand beach fronts riprap and bluffs
	LINC275	13.002	6.350	0.084	dissipative sand beach fronts riprap and bluffs
	LINC276	12.510	4.815	0.076	dissipative sand beach fronts riprap and bluffs
	LINC277	19.421	5.586	0.072	dissipative sand beach fronts moderately high bluffs
	LINC278	7.419	4.556	0.054	dissipative sand beach fronts seawall
	LINC279	9.806	4.226	0.039	dissipative sand beach fronts riprap and bluffs
	LINC280	7.671	4.584	0.048	dissipative sand beach fronts seawall
	LINC281	8.843	5.283	0.048	dissipative sand beach fronts low bluff
	LINC282	10.062	5.779	0.041	dissipative sand beach fronts moderately high bluffs
	LINC283	9.471	5.500	0.051	dissipative sand beach fronts riprap/low seawall and bluffs
	LINC284	12.776	5.865	0.061	dissipative sand beach fronts moderately high bluffs
	LINC285	9.284	5.358	0.055	dissipative sand beach fronts seawall and bluffs
	LINC286	9.531	5.057	0.054	dissipative sand beach fronts riprap and bluffs
	LINC287	11.137	4.982	0.050	dissipative sand beach fronts riprap and bluffs
	LINC288	6.865	5.143	0.064	dissipative sand beach fronts moderately high bluffs
	LINC289	18.092	4.752	0.049	dissipative sand beach fronts moderately high bluffs
	LINC290	28.243	5.285	0.073	dissipative sand beach fronts moderately high bluffs
	LINC291	10.575	4.853	0.058	dissipative sand beach fronts riprap and bluffs
	LINC292	13.387	5.078	0.091	dissipative sand beach fronts riprap and bluffs
	LINC293	11.936	4.686	0.051	dissipative sand beach fronts low bluff
	LINC294	8.286	5.341	0.047	dissipative sand beach fronts dune and low bluff
	LINC295	9.221	5.021	0.044	dissipative sand beach fronts low bluff
	LINC296	8.311	4.358	0.047	dissipative sand beach fronts riprap and bluffs
	LINC297	13.363	4.891	0.055	dissipative sand beach fronts collapsed riprap and bluff
	LINC298	11.517	4.279	0.056	dissipative sand beach fronts riprap and bluffs
	LINC299	10.933	4.898	0.043	dissipative sand beach fronts seawall and bluffs
	LINC300	11.270	5.022	0.054	dissipative sand beach fronts seawall and bluffs
	LINC301	11.929	4.800	0.052	dissipative sand beach fronts riprap and bluffs
	LINC302	20.930	5.449	0.076	dissipative sand beach fronts high bluffs
Salmon River	LINC303	47.701	3.136	0.070	dune-backed beach backed by bluff
	LINC304	26.308	5.173	0.102	dune-backed beach backed by bluff
	LINC305	57.755	3.220	0.017	Inter-tidal rocky area backed by bluffs
	LINC306	32.488	5.553	0.070	dune-backed beach backed by bluff
	LINC307	23.641	4.128	0.038	dune-backed beach backed by bluff
	LINC308	6.251	5.058	0.066	dune-backed beach
Cascade Head	LINC309	48.172	1.609	0.027	plunging cliff
	LINC310	43.560	1.207	0.028	plunging cliff
	LINC311	24.427	0.358	0.022	boulder beach backed by bluffs
	LINC312	93.240	2.125	0.026	plunging cliff
	LINC313	139.103	0.000	0.023	plunging cliff

Reach	Transect	D_{HIGH} (m)	D_{LOW} (m)	Beach Slope (tan β)	Description
Supplemental	LINC_9_290	5.986	3.518	0.025	sandy beach backed by bluff
Transects	LINC_26_457	7.145	4.451	0.032	sand beach fronts low vertical bluff
	LINC_26_459	6.682	4.453	0.053	sand beach fronts low vertical bluff
	LINC_43_554	8.895	3.653	0.028	sand beach fronts moderately high vertical bluff
	LINC_44_573	8.826	3.259	0.043	sand beach fronts riprap structure
	LINC_44_575	8.786	4.080	0.039	sand beach fronts riprap structure
	LINC_99_1257	4.984	4.196	0.030	Ona Beach - dune-backed beach
	LINC_99_1274	4.300	3.583	0.028	Ona Beach - dune-backed beach
	LINC_106_1340	12.480	4.428	0.069	sand beach fronts moderately high vertical bluff
	LINC_106_1343	8.969	4.267	0.048	sand beach fronts moderately high vertical bluff
	LINC_106_1345	11.830	3.936	0.042	sand beach fronts moderately high vertical bluff
	LINC_109_1366	7.444	4.984	0.056	sand beach fronts high vertical bluff
	LINC_109_1367	8.862	4.690	0.053	sand beach fronts high vertical bluff
	LINC_121_1528	8.926	5.145	0.083	creek (South Beach)
	LINC_167_2257	4.221	4.221	0.050	Spencer Creek, Beverly Beach
	LINC_195_2790	13.245	2.217	0.063	plunging cliff, north of Depoe Bay
	LINC_204_2928	3.239	3.239	0.085	Fogarty Creek
	LINC_250_3385	7.779	5.140	0.085	dissipative sand beach fronts riprap

3.3 Recent Coastal Changes in Lincoln County

This section briefly reviews beach profile changes that have occurred during the past decade, having been documented by lidar and recent GPS surveys of the shore.

The overall approach used to define the morphology of the beach and dune system, including the location of the PFD along the length of county shoreline, and shoreline changes over the past decade, was based on detailed analyses of lidar data measured by the USGS/NASA/NOAA in 1997, 1998 and 2002 and by DOGAMI in 2009. However, because lidar data flown by the USGS/NASA/NOAA are of relatively poor resolution (~1 point/m^2) and reflect a single return (i.e., include vegetation where present), while the lidar data flown by DOGAMI have a higher resolution (8 points/m^2) and are characterized by multiple returns — enabling the development of a bare-earth digital elevation model (DEM) — determination of the most critical beach/dune morphological features was based entirely on analysis of the 2009 lidar data. These data have been supplemented with RTK-DGPS surveys at a number of locations along the Lincoln County coastline, providing the most up-to-date information on recent coastal changes.

Lidar data flown in 1997, 1998, and 2002 were downloaded from NOAA's Coastal Service Center and gridded in ArcGIS using a TIN algorithm; a similar approach was undertaken with the 2009 lidar data. Transects spaced 25 m apart were cast for the full length of the county coastline using the Digital Shoreline Analysis System (DSAS) developed by the USGS (Thieler and others, 2009). For each transect, xyz values for the 1997, 1998, 2002, and 2009 lidar data were extracted at 1-m intervals along each transect line and saved as a text file using a customized ArcGIS script.

Processing of the lidar and GPS data was undertaken in MATLAB using a custom beach profile analysis script developed by DOGAMI. This script requires the user to interactively define various morphological features including the dune/bluff crest/top, bluff slope (where applicable), landward edge of the PFD, beach-dune juncture elevations for each year, and the slope of the beach foreshore.

Figure 3-12 to **Figure 3-17** shows the changes in beach and bluff/dune morphologies at five representative shore sections located respectively between Yachats and Alsea Bay, Alsea Spit to Seal Rock, Newport, Siletz Spit, and along Lincoln Beach.

As noted previously, much of the shoreline between Yachats and Alsea Bay is backed by low bluffs that are eroding into two predominant lithological units: fine-grained marine terrace deposits (Quaternary dune sands), and Tertiary deposits that consists of mostly siltstone to fine-grained sandstone. **Figure 3-12** suggests that bluff erosion is occurring at a relatively slow pace with the transect data showing little change over the past 15 years. Beach elevations typically vary by about 1-2 m (3–6 ft) vertically between summer (accreted) and winter (eroded state), while the beach slopes are predominantly gently sloping. In the north (~transects 61–67), a primary dune has developed seaward of the bluffs (**Figure 3-12**, bottom right). These dunes are periodically eroded during major storms, although the transect data suggests that they are currently building vertically.

Figure 3-13 highlights two contrasting conditions that can be seen along Alsea Spit. In the far south (transects 68–76), it can be seen that the primary dune is undergoing significant aggradation, with the dunes having increased in height by ~2-3 m (6–10 ft) since 1997. The largest dune building has occurred near the spit tip (between the mouth and transect 71), where homes are being inundated with sand (**Figure 3-14**). Farther north, the primary dune gives way to low bluffs that progressively increase in height to the north. As can be seen in **Figure 3-13**, in the far north (transect 86), a primary dune has developed since 1997 and is located immediately seaward of the bluffs. The dune extends ~300 m (984 ft) long along the shore and is ~25 m (82 ft) wide. Despite these dimensions, the dune could easily be removed in a major storm.

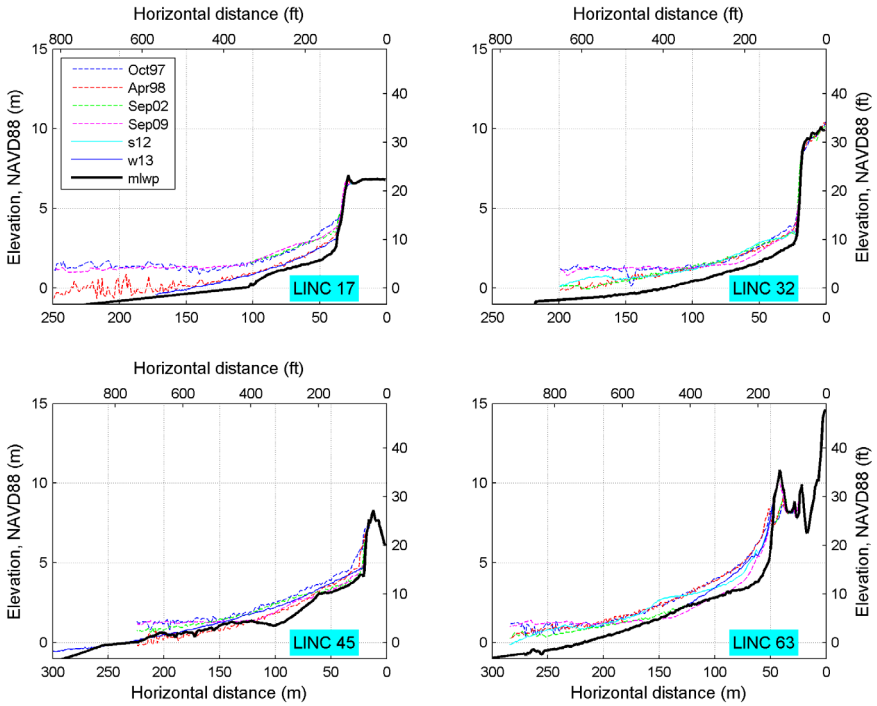

Figure 3-12. Measured beach morphological changes carried out between 1997 and 2013 for selected sites between Yachats and Alsea Bay. Data include both lidar and GPS surveys of the beaches.

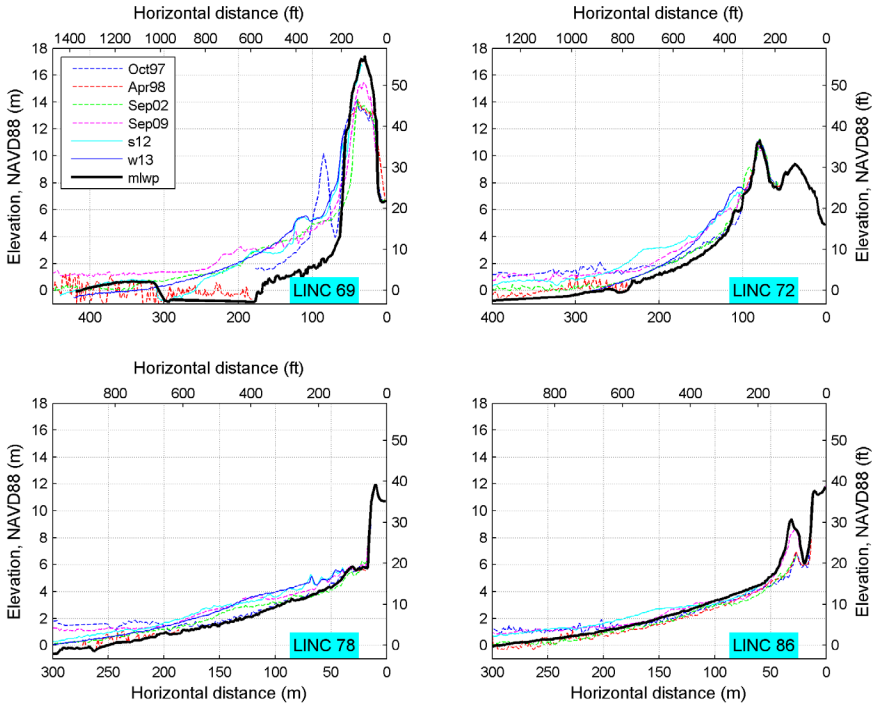

Figure 3-13. Measured beach morphological changes carried out between 1997 and 2013 for selected sites between Alsea Bay and Seal Rock. Data include both lidar and GPS surveys of the beaches.

Figure 3-14. Oblique photo looking west across the Alsea spit tip. Note the build-up of dune sand that has taken place between the homes. Sand is also actively transported across the primary dune, where it accumulates on Oceania Drive requiring periodic maintenance by Lincoln County road crews to remove the sand. The seaward edge of the homes marks the approximate landward extent of dune erosion that occurred as a result of the 1982-83 El Niño erosion (photo: Don Best, spring 2011).

Figure 3-15 highlights two contrasting conditions that can be seen in the Newport area. As described previously, the bulk of this shoreline is backed by high, coastal bluffs, which are eroding into sandstone/siltstone units of the Astoria Formation. Farther south and adjacent to Yaquina Bay, a small dune field has developed immediately north of the north Yaquina jetty (transect 131 in **Figure 3-15**); as noted in Section 2.4.1.3 the accumulation of sand in this region is directly related to the construction of jetties. As can be seen from the figure, the primary dune is actively building vertically, having increased its height from about 11 m (36 ft) in 1997 to over 13 m (43 ft) in 2013. Beach slopes are consistently low along the length of this cell, while the vertical range of beach responses appears to be generally lower than is observed elsewhere in the county.

Beaches in the Siletz subcell (Fishing Rock to the mouth of Siletz Bay) exhibit the steepest slopes in Lincoln County (**Figure 3-10**), due entirely to the coarse nature of the sediments that characterize the beach system. The geomorphology of this section of the coast is broadly similar to those observed elsewhere in the county, with essentially two contrasting beach states: those that are backed by moderate to high bluffs and beaches backed by dunes. Bluffs dominate the southern two thirds of the shoreline, while dunes are confined to the northern one-third (i.e., along the spit). **Figure 3-16** presents the beach profile responses for selected transects along the cell. As can be seen from these data, it is not uncommon for the beaches to experience vertical changes that are on the order of 2-3 m (6–10 ft), which leads to large shoreline excursions as the beach erodes landward during storms and rebuilds seaward during the summer, when sand is returned to the subaerial beach. Transects 212 and 224 located at the south end of the cell, provides the best examples of recent bluff erosion responses, which have cut back in those areas by about 2–4 m (6–13 ft) since 1997. As described previously (Section 2.4.1.6), a large portion of the Siletz cell is now protected with coastal engineering structures.

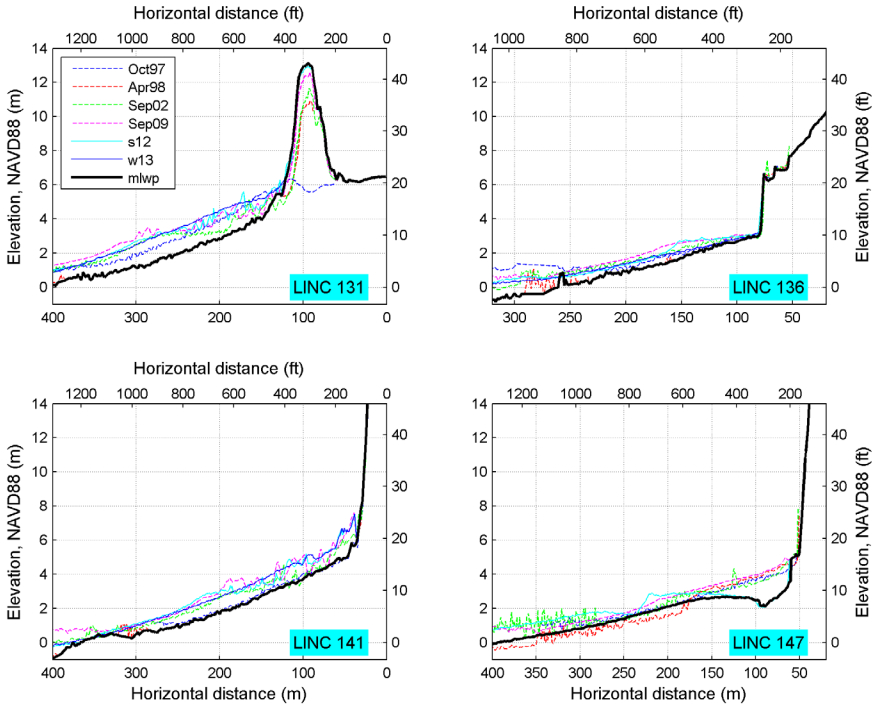

Figure 3-15. Measured beach morphological changes carried out between 1997 and 2013 for selected sites between Yaquina Bay and Yaquina Head. Data include both lidar and GPS surveys of the beaches.

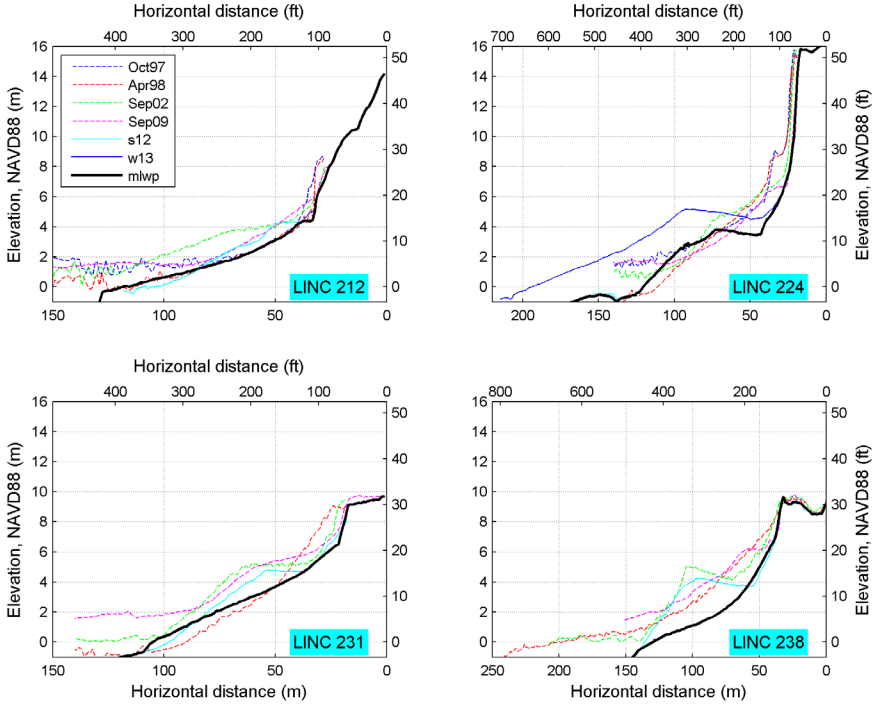

Figure 3-16. Measured beach morphological changes carried out between 1997 and 2013 for selected sites between Fogarty Creek and Siletz Bay. Data include both lidar and GPS surveys of the beaches.

The Lincoln cell is made up almost entirely of high coastal bluffs, much of which is eroding into Quaternary dune deposits, overlying much older Tertiary sediments. The bluffs along this shore are some of the highest in the county, reaching heights of 20 to 40 m (65 to 131 ft). In the south (transect 247, **Figure 3-17**), adjacent to Siletz Bay, a broad beach has built seaward of the bluffs. However, as noted in Section 2.4.1.7, during major storms it is possible for the entire fronting beach to be removed and the bluff toe to come under sustained wave attack (**Figure 3-18**). Nevertheless, as can be seen from the LINC 247 transect, erosion of the bluffs appears to have been generally negligible over the past 15 years implying that at least over this period the beach system has remained broad, providing protection to the bluffs.

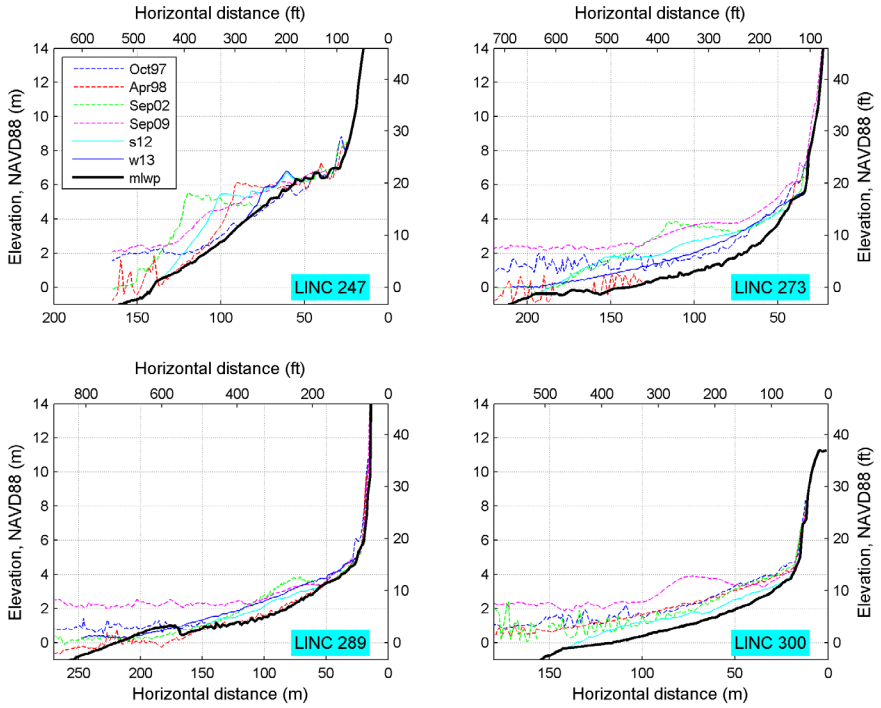

Figure 3-17. Measured beach morphological changes carried out between 1997 and 2013 for selected sites between Siletz Bay and Roads End. Data include both lidar and GPS surveys of the beaches.

Figure 3-19 presents the alongshore varying shoreline responses derived from lidar measurements collected since 1997. Data shown in **Figure 3-19** correspond to the approximate horizontal position of the beach/dune or bluff toe, which typically occurs at an elevation of ~5 to 6 m (16 to 20 ft). Baseline data from which the comparisons have been made is the position of the beach in 1997 prior to the 1997–1998 El Niño. **Figure 3-19** shows the derived change measurements for both the 1997-98 El Niño, and the net change that has taken place between 1997 and 2009. Here we have divided the county into the seven main subcells: Yachats to Alsea Bay, Alsea Spit, Seal Rock to South Beach (Yaquina Bay), Newport, Beverly beach, Fishing Rock to Siletz Bay, and along Lincoln Beach. In general, it can be seen that the greatest shoreline responses (erosion or accretion) are observed north of Yachats, along the southern half of Alsea Spit, adjacent to Yaquina Head in Newport, and along Siletz Spit. Elsewhere, the derived shoreline responses indicate generally negligible patterns of change (erosion or accretion).

North of Yachats, the measured beach responses suggests a mostly erosional response over the past 15 years, with the amount of erosion greatest in the northern half of that particular subcell. As can be seen in **Figure 3-19**, the erosion averages about −11.2 m (−36.8 ft); 1σ = 13.3 m (43.6 ft). It is of interest that the recent problems with excess sand that is plaguing the southern end of Alsea Spit (**Figure 3-19**), appears to be strongly related to the loss of beach in the northern half of the Yachats subcell. Much of this transformation has taken place since 2002, as sand is re-distributed along the shore, where it eventually by-passes the mouth of Alsea Bay. Furthermore, this alongshore shift in beach sand is consistent with sand transport observations made by Haxel and Holman (2004) for the Newport area.

Finally, large shoreline excursions (both erosion and accretion) are clearly evident in the Siletz subcell. Some of the largest changes can be seen adjacent to the mouth of Siletz Bay (e.g., respectively the north end of Siletz Spit and south end of Lincoln Beach plots).

Figure 3-18. Erosion of bluffs in the Taft area during the winter of 1977-78 resulted in the removal of the fronting beach, exposing the bluff toe to direct wave attack (photo: Oregon Highway Department, 1978).

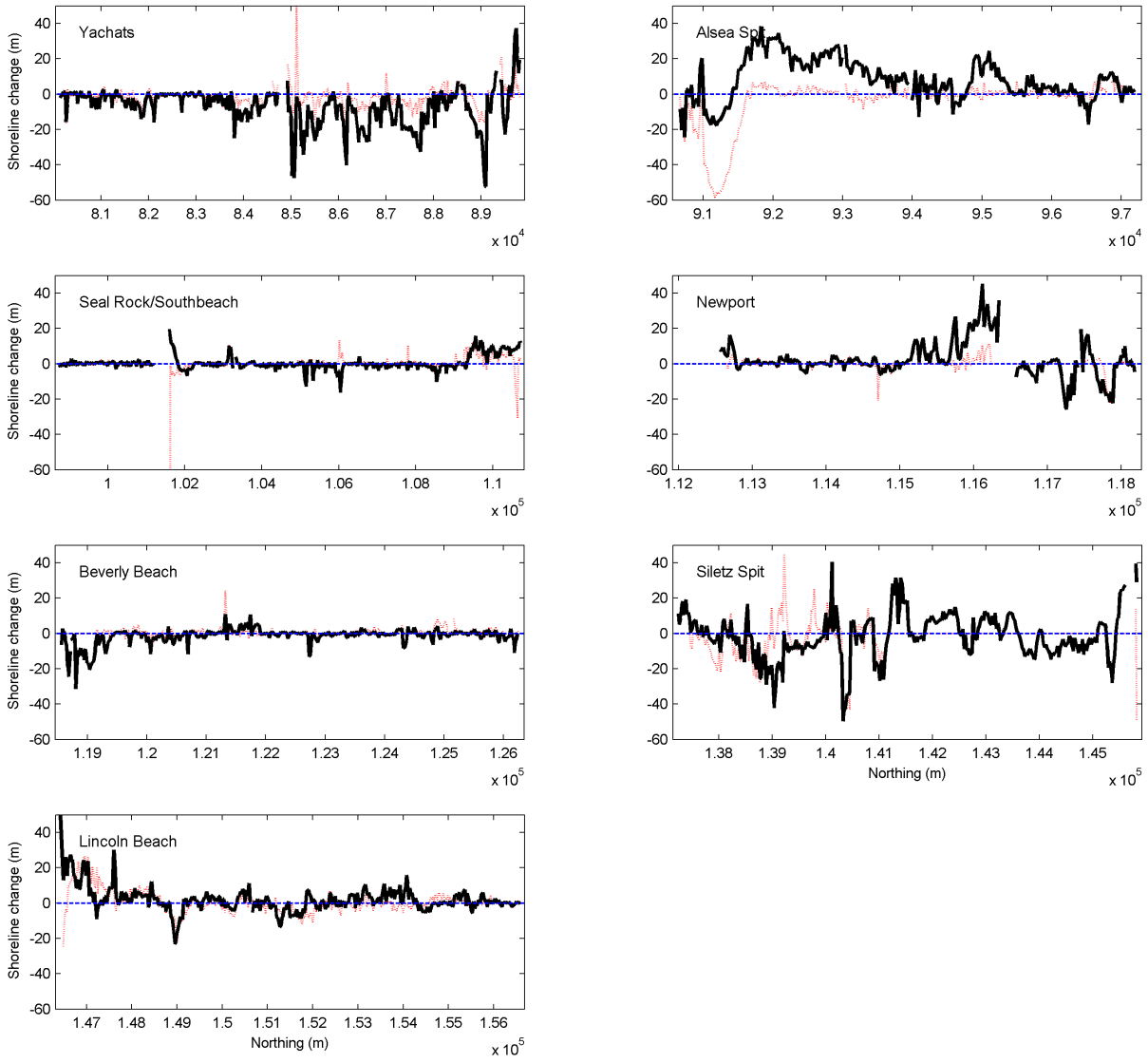

Figure 3-19. Positional changes in the beach/dune toe (elevation of 5 m [16 ft]) along the Lincoln County coastline between 1997 and 2009 derived from lidar data. Baseline data are the position of the dune toe in 1997. Note: dashed red line is the response following the 1997-98 El Niño, while the solid black line denotes the net change between 1997 and 2009.

3.4 Bathymetry

Important for calculating wave transformations and determining nearshore beach slopes is information on the local bathymetry offshore from the Lincoln County coast. For the purposes of this study we have adopted two approaches:

1) For the purposes of SWAN numerical wave modeling, we used bathymetric data compiled by the National Geophysical Data Center (NGDC), an office of the National Oceanic and Atmospheric Administration (NOAA) for the purposes of developing an integrated bathymetric-topographic digital elevation model (DEM) for tsunami inundation modeling.
2) For erosion assessments and wave runup calculations, we used bathymetric data collected in late summer 2010 with the aid of personal watercrafts (Ozkan-Haller and others, 2009).

For the purposes of developing an integrated bathymetric-topographic digital elevation model (DEM) that can be used for tsunami inundation modeling, the National Geophysical Data Center (NGDC), an office of the National Oceanic and Atmospheric Administration (NOAA) has compiled detailed bathymetric data across the continental shelf from multiple agencies. The synthesized bathymetric-topographic DEM (Central Oregon Coast; http://www.ngdc.noaa.gov/¬dem/squareCellGrid/download/320) is a 1/3 arc-second (approximately 10 m [~33 ft]) DEM of the central Oregon coast that spans all of Lincoln County, and includes the offshore rocks, small islands, and reefs that would affect wave shoaling. The DEM was generated from a diverse suite of digital data sets that span the region (Carignan and others, 2009). A summary of the data sources and methods used to synthesize the data to develop the Astoria and Garibaldi DEMs is described in the reports by Carignan and others (2009a). In general, the best available data were obtained by the NGDC and shifted to common horizontal and vertical datums: North America Datum 1983 (NAD 83) and Mean High Water (MHW).

NGDC used shoreline, bathymetric, and topographic digital data sets (**Figure 3-20**) from several U.S. federal, state and local agencies (e.g., NOAA's National Ocean Service (NOS), Office of Coast Survey (OCS) and Coastal Services Center (CSC); the U.S. Geological Survey (USGS); the U.S. Army Corps of Engineers (USACE); and the Oregon Department of Fish and Wildlife/Marine Resource Program (ODFW). Having converted all the data to a common coordinate system and vertical datum, the grid data were checked for anomalous data and corrected accordingly. Because the data sets, particularly in deep water and near to the coast, were relatively sparse, further manipulation and smoothing was required to create a uniform grid. These products were then compared with the original surveys to ensure grid accuracy. According to Carignan and others (2009a) the final DEM is estimated to have an accuracy of up to 10 m (~33 ft), while some portions of the grid are more accurate (e.g., the coastal strip where high-resolution lidar data were available). The bathymetric portion of the data set is estimated to have an accuracy of between 0.1 m (0.33 ft) and 5% of the water depth, again depending on the type of survey data that was used to calibrate the final grid development.

Finally, despite all these efforts it is important to note that a limitation of the DEMs being developed by NGDC is the virtual absence of suitable bathymetric data in the nearshore (effectively landward of the 10 m [33 ft] bathymetry contour), because few survey boats are able to venture into this highly turbulent and dangerous portion of the surf zone. The exception to this is where surveys have been undertaken by the USACE in the entrance channels to estuaries where navigable water depths need to be maintained. Thus, there is some uncertainty about estimating nearshore slopes for the surf zone due to the absence of sufficient data for this region, with the user having to make some assumptions based on the best available data that is present outside the surf zone and information at the shoreface. This is a recognized problem with all coastal flood analyses. To resolve this problem, we used a Coastal Profiling System (CPS) that has been developed for nearshore bathymetric surveys by Dr. Peter Ruggiero (Department of Geosciences, Oregon State University (Ruggiero and others, 2005)). The CPS consists of a highly maneuverable personal

watercraft that is equipped with a survey grade GPS receiver and antenna, an echo sounder and an on board computer. Repeatability tests undertaken by Ruggiero and colleagues indicate sub-decimeter accuracy on the order of 0.15 m (0.5 ft) (Ozkan-Haller and others, 2009). **Figure 3-21** provides an example of the CPS system, while **Figure 3-22** and **Figure 3-23** presents the mapped coverage of our bathymetric surveys undertaken in the 2012 summer. An example of two of the bathymetric transects undertaken in Lincoln County is presented in **Figure 3-24**.

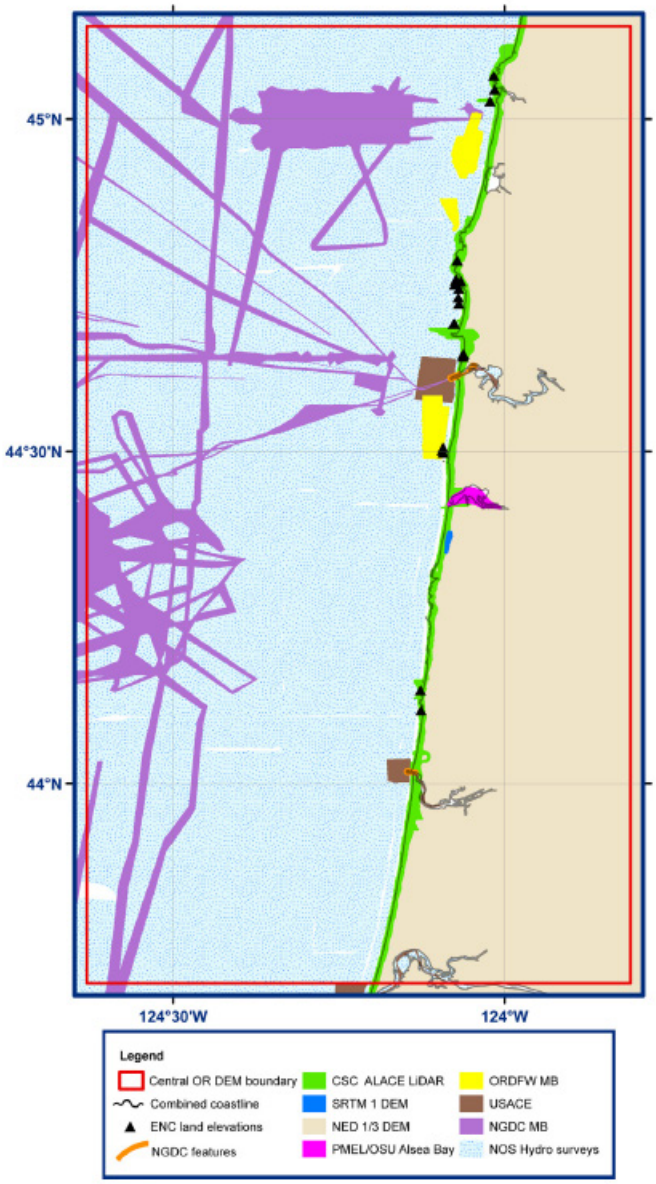

Figure 3-20. U.S. federal, state, and local agency bathymetric data sets used to compile the central Oregon coast DEM (Carignan and others, 2009a).

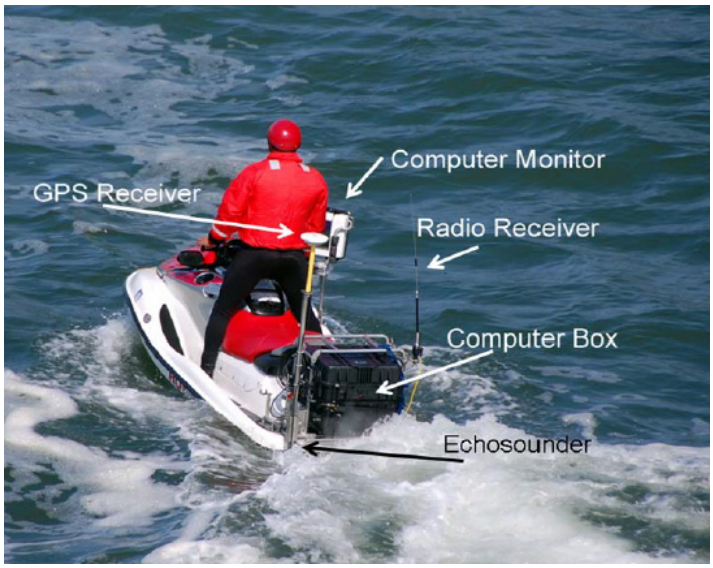
GPS Receiver
Computer Monitor
Radio Receiver
Computer Box
Echosounder

Figure 3-21. Data acquisition boat and onboard equipment (photo: P. Ruggiero, OSU).

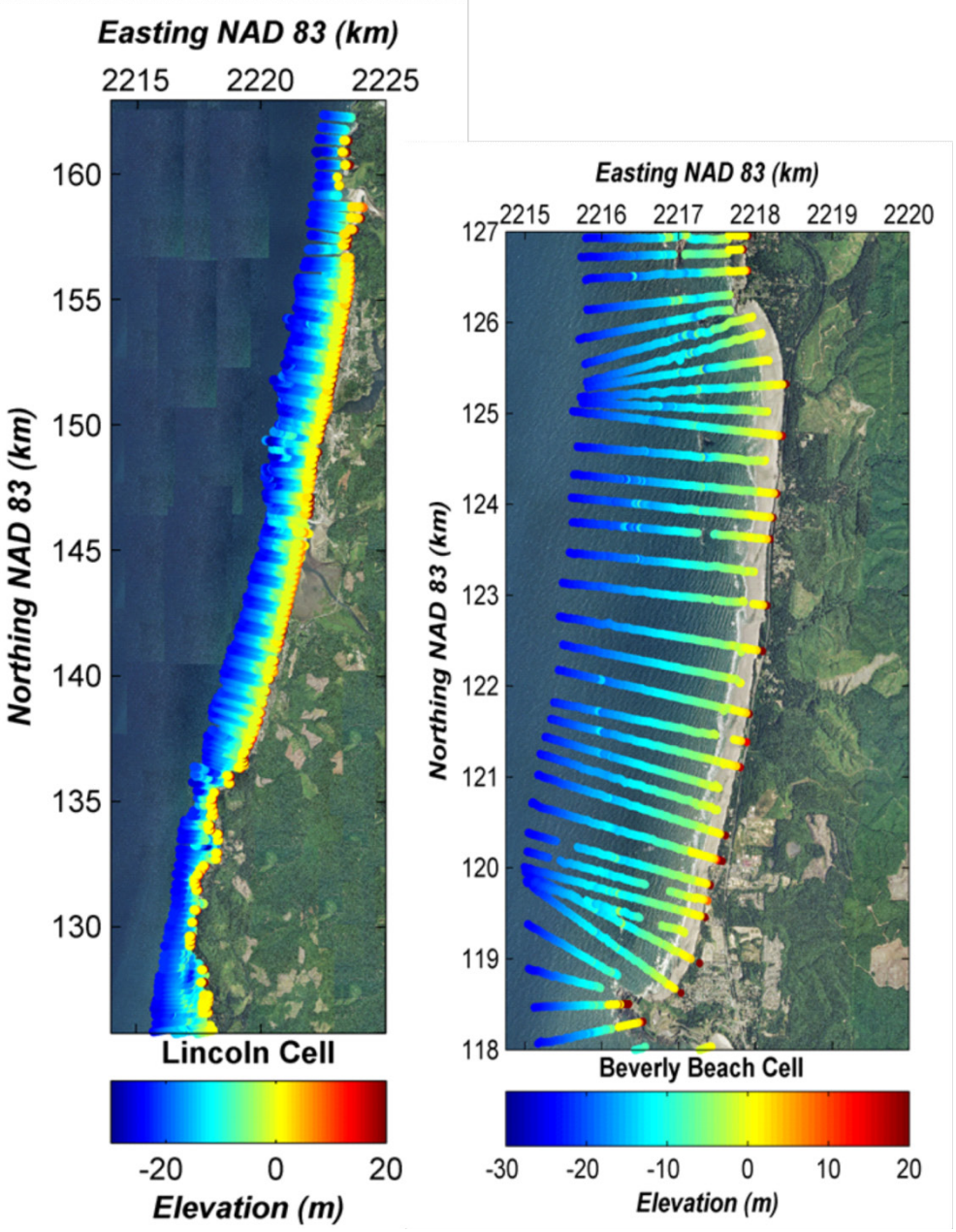

Figure 3-22. Collected bathymetry transects measured offshore the coast of the Lincoln City, Siletz Spit, Depoe Bay, Otter Rock, and Beverly Beach littoral cells, Lincoln County, Oregon.

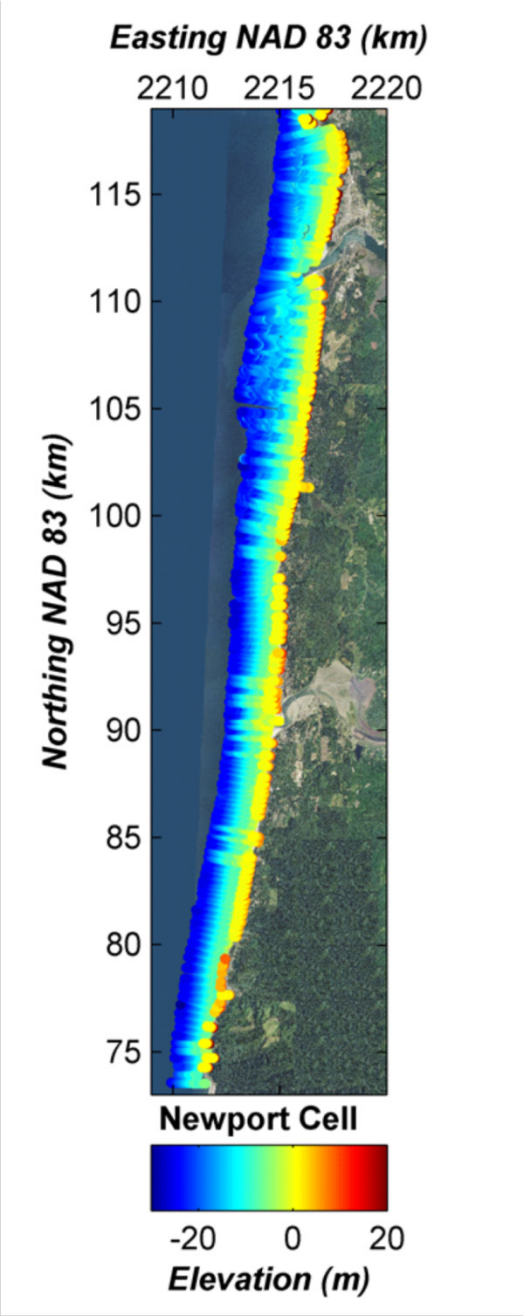

Figure 3-23. Collected bathymetry transects measured offshore the coast of Newport, South Beach to Alsea Bay, and Waldport to Yachats, Lincoln County, Oregon.

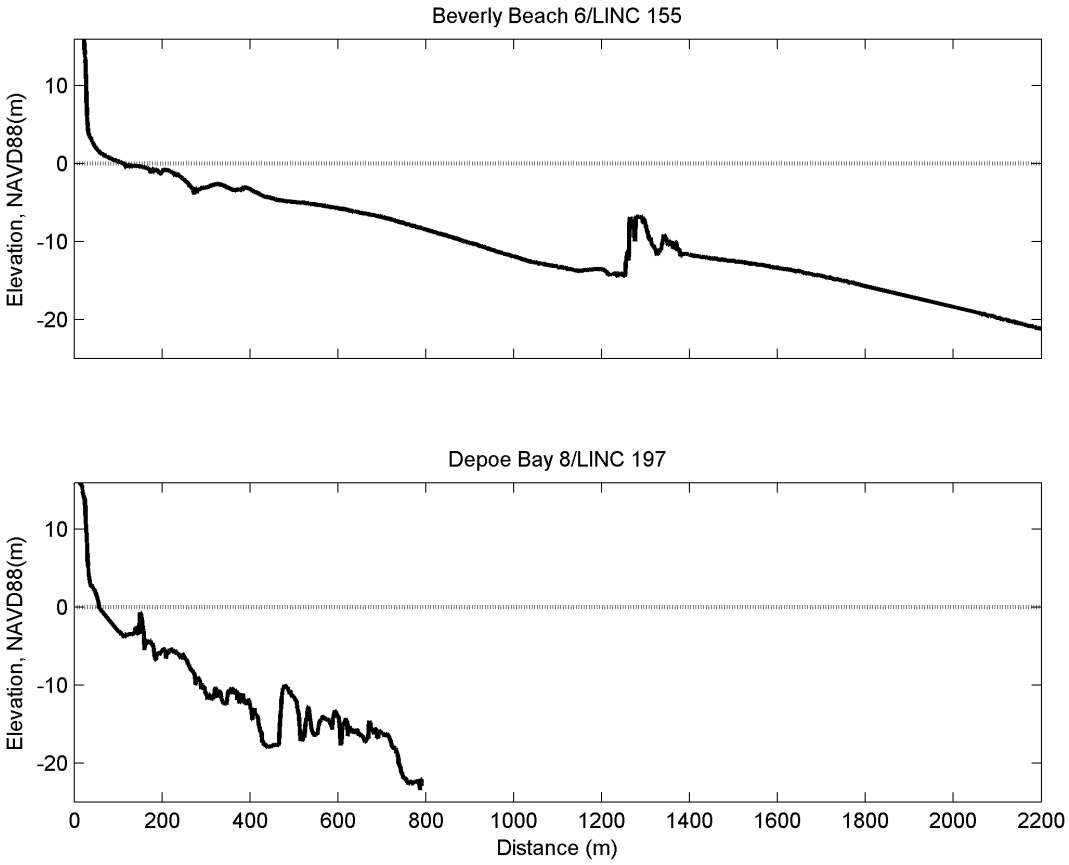

Figure 3-24. Combined topographic and bathymetric cross-shore transects measured offshore from Beverly Beach and Depoe Bay (central Lincoln County coastline) showing the presence of sand bars and an offshore reef (top plot) and significant reef offshore from Depoe Bay. Note the contrasting nearshore slopes between the two sites, with steeper topography observed at Depoe Bay and wider shallower topography offshore from Beverly Beach.

4.0 TIDES

Measurements of tides on the Oregon coast are available from various tide gauges operated by NOS (http://www.tidesandcurrents.noaa.gov/map/index.shtml?type=PreliminaryData&region=Oregon). Hourly tidal records are available from the following coastal sites (**Table 4-1**): the Columbia River (Astoria, #9439040), Tillamook Bay (Garibaldi, #9437540), Newport (South Beach, #9435380), Coos Bay (Charleston, #9432780) and at Port Orford (#9431647) on the southern Oregon coast. Long-term tidal records are also available from the Crescent City tide gauge (#9419750), located in northern California. The objective of this section is to establish which tide gauge would be most appropriate in applications directed toward FEMA wave and total water level analyses for the Lincoln County coastline.

Information relating to the Astoria (AST), Garibaldi (GB), South Beach (SB), Charleston (CH), Port Orford (PO) and Crescent City (CC) tide gauges in this region are listed in **Table 4-1**, including their available records. **Figure 4-1** maps the locations of the most pertinent tide gauges present on the Oregon coast, along with the locations of various wave buoys operated by the National Data Buoy Center (NDBC) and the Coastal Data Information Program (CDIP), and Global Reanalysis of Ocean Waves (GROW) Fine Northeast Pacific wave hindcast data. These latter stations are pertinent to discussions of the wave climate and modeling described in Section 5, and ultimately in calculations of wave runup and overtopping.

Table 4-1. Pacific Northwest NOAA tide gauges.

Gauge Site	Gauge Location	Record Interval	Years
Oregon			
Astoria (AST)	Astoria	Feb.1925 – 2013	87.8
Garibaldi (GB)	Tillamook Bay, near the inlet mouth	Jul. 2005 – 2013	7.4
South Beach (SB)	Yaquina Bay, near the inlet mouth	Feb.1967 – 2013	45.8
Charleston (CH)	Coos Bay, near the inlet mouth	Apr. 1970 – 2013	42.7
Port Orford (PO)	Port Orford, open coast harbor	Oct. 1978 –2013	34.2
California			
Crescent City (CC)	Crescent City, open coast harbor	Sep. 1933 – 2013	79.3

As can be seen in **Table 4-1**, a number of the gauges have long records (30+ years) suitable for coastal flood analyses. The longest tide-gauge record (88 and 80 years, respectively) is from Astoria, located 23.5 km up-channel from the mouth of the Columbia River and at Crescent City in northern California. The South Beach gauge has a moderately long record on the order of 45 years (**Table 4-1**); the SB gauge is located within Yaquina Bay, ~2 km from the open coast. The shortest record (~7 years), are those for Garibaldi located near the mouth of Tillamook Bay, including only 7.4 years. For the purposes of this study, we have ignored the Astoria tide gauge station data due to its location well north of Lincoln County and because of its greater distance from the open coast.

All hourly tide data were purchased from NOS and were processed using various scripts developed in MATLAB. In addition to the measured tides, hourly tide predictions were calculated for all years using NOS tide prediction program, NTP4.

4.1 Tide Characteristics on the Central to Northern Oregon Coast

Tides along the Oregon coast are classified as moderate, with a maximum range of up to 4.3 m (14 ft) and an average range of about 1.8 m (6 ft) (Komar, 1997). There are two highs and two lows each day, with successive highs (or lows) usually having markedly different levels. Tidal elevations are given in reference to the mean of the lower low water levels (MLLW) and can be easily adjusted to the NAVD88 vertical datum. (MLLW to NAVD88 conversions may be performed using values provided for a specific tide gauge by NOS or by using the VDATUM [http://vdatum.noaa.gov/] tool developed by NOAA. For example, the adjustment from NAVD88 to MLLW at the SB tide gauge is +0.225 m [0.74 ft] as determined by NOS [http://www.co-ops.nos.noaa.gov/benchmarks.¬html?id=9435380].) As a result, most tidal elevations are positive numbers with only the most extreme lower lows having negative values.

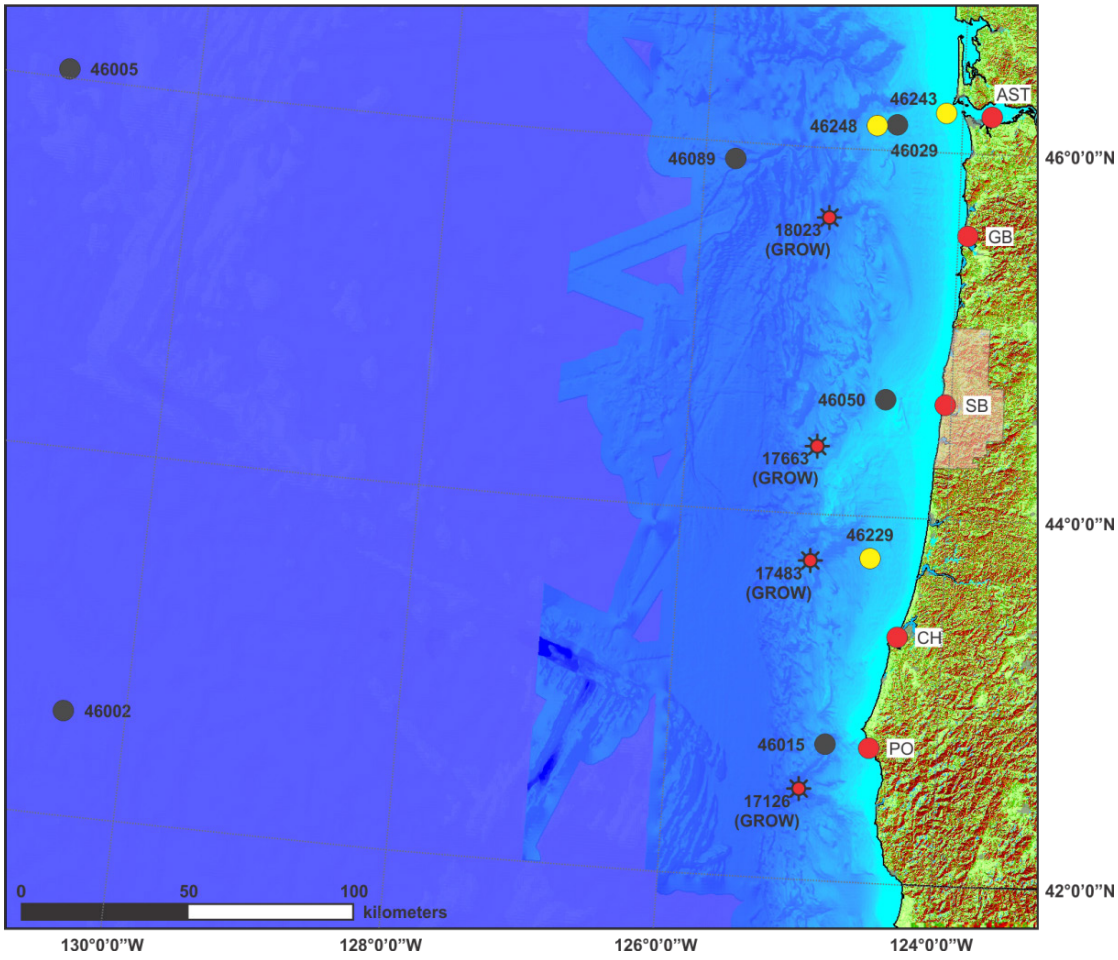

Figure 4-1. Location map of NDBC (black) and CDIP (yellow) wave buoys, tide gauges (red) and GROW wave hindcast stations (red suns).

Initial analyses of the measured tides focused on developing empirical probability density function (PDF) plots of the measured tidal elevations for each of the tide gauges located along the Oregon coast. The objective here is to assess the measured tides in order to identify any significant characteristics (including

differences) between the gauges. **Figure 4-2** presents a series of PDF plots from each of the gauges. Because the gauges are characterized by varying record lengths, we have initially truncated the analyzed data to the period 2006 to 2011, when measurements were available from all four gauges.

As seen in the top plot of **Figure 4-2**, the gauges can be broadly characterized into two distinct regions. Those along the central Oregon coast (SB and GB) indicate a higher incidence of water levels > 2 m (> 6.5 ft, i.e., > MHW). In contrast, there is a systematic decrease in the elevation of the higher tides with progress south along the Oregon coast, with the lowest tides experienced at CC in northern California. These differences are probably related to a combination of effects associated with the regional oceanography (upwelling, shelf currents, and Coriolis effects that deflect the currents toward the coast) (Legaard and Thomas, 2006). The lower plot in **Figure 4-2** shows the same PDF, but now truncated to span tidal elevations between 2 and 4 m (6.5–13 ft). Based on this latter plot, it is evident that the GB and SB gauge are characterized by much higher water levels, when compared with the rest of the coast. In terms of determining ultimately which tide gauge to base the still water level time series on, these initial results suggest strongly that we can effectively rule out the PO and CC gauges as potential candidate sites as they consistently yield much lower water levels. At the high water level end of the plot, differences between the three remaining gauges (GB, SB, and CH) are relatively minor.

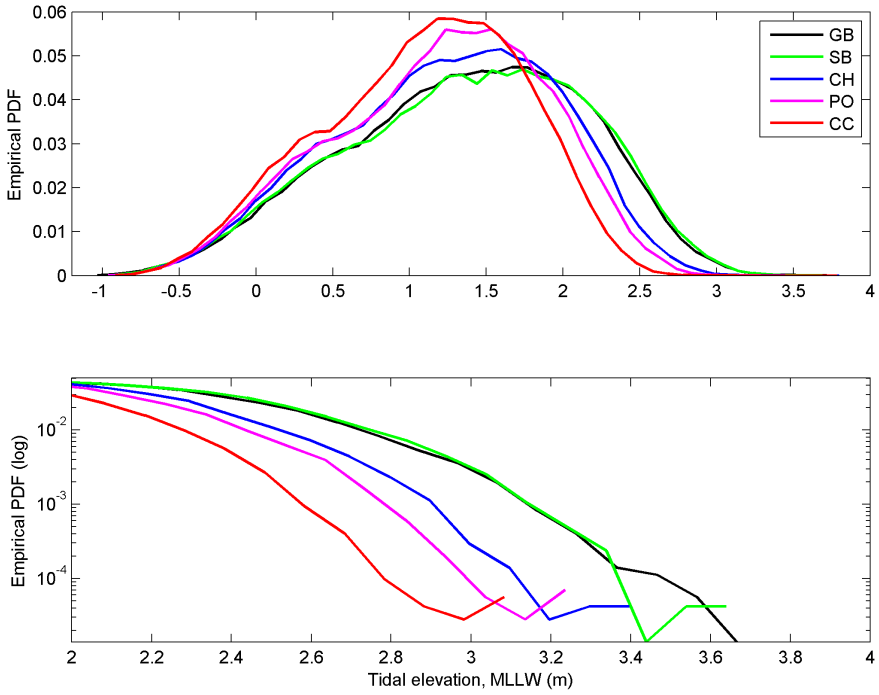

Figure 4-2. Empirical PDF plots for various tide gauges for overlapping years of data (2005–2013). Top) PDF plots showing the complete range of tidal elevations; Bottom) truncated to higher water levels.

Figure 4-3 is broadly similar to **Figure 4-2**, with the exception that the PDFs now include the complete time series of data measured by the respective tide gauges. In general, the CC gauge is characterized by a higher incidence of water levels between about −0.18 and 1.5 m (−0.6–4.9 ft), and a lower incidence of water

levels between 1.8 and 3 m (5.9–9.8 ft). This patter is broadly similar for the PO and CH gauges. In contrast, the PDF plots for both the GB and SB tide gauges are essentially the same, with the SB gauge characterized by marginally higher tides. This last feature of the SB gauge is almost certainly a function of its much longer record (46 years versus 7), such that the highest water level on record occurred in December 1969. Detailed examination of the hourly tides indicate that the higher incidence of SB water levels in the wings of the PDF reflect the fact that both the Higher Highs and Lower Highs are greatest at SB when compared with the other gauges, while the Lower Lows and Higher Lows are generally lower at SB compared with the gauges south of CH.

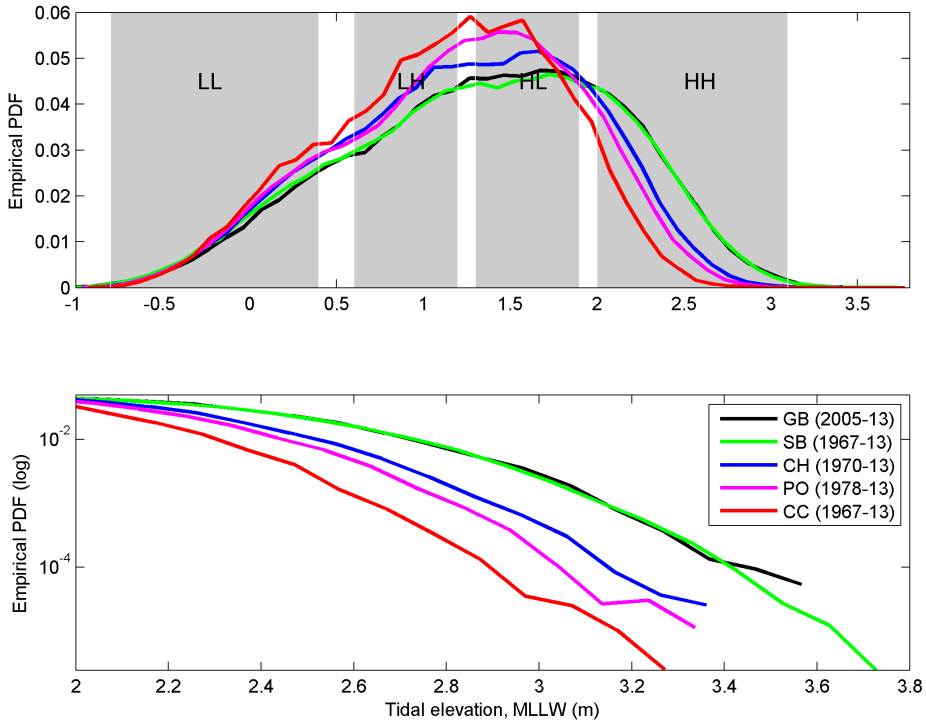

Figure 4-3. Empirical PDFs for various tide gauges based on all available data. Top) PDF plot showing the complete range of tidal elevations. LL, LH, HL, and HH denote the Lower Lows, Lower Highs, Higher Lows, and Higher Highs in the tide data. Bottom) PDF truncated to higher water levels.

At the extreme high end of the complete PDF plots (**Figure 4-3**), the highest water levels measured at GB, SB and CH gauges are respectively 3.63, 3.71, and 3.39 m (11.9, 12.2, 11.1 ft). These results equate to a difference of 0.08 m (0.26 ft) between GB and SB and 0.32 m (1.05 ft) between SB and CH. Evident from the plot is the fact that the extreme water levels progressively decrease to the south, indicating a latitudinal dependence on the water levels. Furthermore, differences between these values and those reported by NOS for the respective stations differ by no more than a few centimeters. Overall, the relative consistency in the PDF plots generated for each gauge, particularly at the more extreme end of the measured water levels, is indicative of the areal impact of major North Pacific extratropical storms, which can affect stretches of coast up to 1500 km (932 miles, i.e., 3 times the length of the Oregon coast) in length (Davis and Dolan, 1993; Allan and Komar, 2002).

4.2 Seasonal Changes

Figure 4-4 presents a plot of the characteristic seasonal cycles determined for the five gauges, enabling further examination of their characteristics. All five gauges depict the typical seasonal cycle that reflects the combination of ocean upwelling effects along the coast, and seasonal reversals in the California current system. In general, water levels tend to be highest during the months of December, through March, decreasing to their minimum in the period between May and July. **Figure 4-4** also depicts a pattern whereby the winter peaks progressively increase toward the north, from CC to GB. In contrast, **Figure 4-4** indicates that there is a southward increase in the water levels during late summer/early fall period, reaching its peak down in CC; in fact, the latter pattern continues south along the U.S. West Coast such that as far south as Los Angeles, the peak in the seasonal cycle has been shifted from its winter peak on the PNW coast to a late summer (September) peak on the southern California coast.

Finally, although not shown in **Figure 4-4**, all the tide gauges are strongly influenced by the El Niño Southern Oscillation phenomena, which periodically causes mean sea levels along the U.S. West Coast to increase (Komar and others, 2011). This response is due to an intensification of the processes, especially enhanced ocean sea surface temperatures offshore from the Oregon coast. This occurred particularly during the unusually strong 1982-83 and 1997-98 El Niños, whereby mean sea levels increased by approximately 20–25 cm (~0.8 ft) above the normal seasonal cycle in mean sea level depicted in **Figure 4-4** (i.e., for a total mean sea level rise of up to 50 cm (1.6 ft) relative to the preceding summer). As a result, under these latter conditions wave swash processes are able to reach to much higher elevations on the beach, potentially eroding dunes and bluffs.

As a result of differences in the tidal regime observed at Crescent City in northern California relative to the tide gauges on the Oregon coast, the Crescent City tide gauge was ruled out for further consideration.

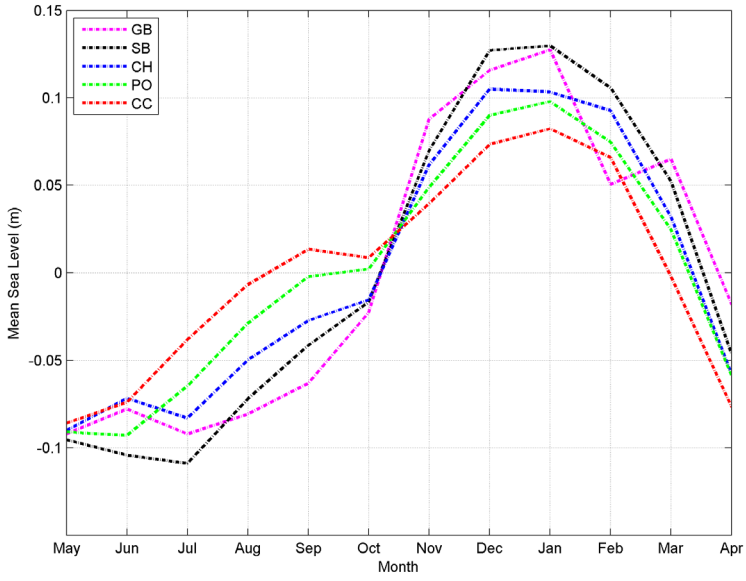

Figure 4-4. Seasonal plot of tides along the south-central Oregon coast down into northern California.

4.3 Oregon Storm Surges

The actual level of the measured tide can be considerably higher than the predicted tides provided in standard Tide Tables, and is a function of a variety of atmospheric and oceanographic forces, which ultimately combine to raise the mean elevation of the sea. These latter processes also vary over a wide range of timescales, and may have quite different effects on the coastal environment. For example, strong onshore winds coupled with the extreme low atmospheric pressures associated with a major storm can cause the water surface to be locally raised along the shore as a storm surge, and have been found in tide-gauge measurements to be as much as 1.5 m (4.9 ft) along the Pacific Northwest coast (Allan and Komar, 2002). However, during the summer months these processes can be essentially ignored due to the absence of major storms systems.

Analyses have been undertaken to examine the non-tidal residuals and ultimately the storm surges identified at the various tide gauges on the northern Oregon coast. The objective of this analysis is to provide a better understanding of the spatial and temporal variability of storms as they track across the North Pacific, the magnitudes (and frequency) of the surges, and the potential differences in the non-tidal residuals between the gauges due to variations in the storms tracks, barometric pressures and winds. This last point is particularly important in terms of finalizing the tide gauge time series to be used in the Lincoln total water level analyses.

For the PNW, the measured water level (h_t) at a particular tide gauge is given by the following relationship:

$$h_t(t) = z_o + X_{at}(t) + X_{oc}(t) + S(t) \qquad \text{(Eq. 4-1)}$$

where z_o is the mean water level, X_{at} is the predicted astronomical tide, X_{oc} is the altered mean water level due to ocean processes (water temperatures, currents and El Niño "sea-level" waves), and with S being the contribution by the storm surge at time t. The predicted astronomical tide for the specific tide gauge is calculated using its harmonic constituents:

$$X_{at} = \sum_{i=1}^{M} H_i \cos(\sigma_i t + \varphi_i) \qquad \text{(Eq. 4-2)}$$

where H_i is the amplitude of the constituent i, σ_i is its frequency, and φ_i the phase of the constituent, M being the number of tidal constituents included in the analysis.

4.4 Non-Tidal Residual Analyses

The procedures used to analyze the non-tidal residuals and storm surge incidence follow those developed by Allan and others (2011), which utilized a harmonic analysis method of least squares (HAMELS) approach developed in MATLAB to estimate the amplitude and phase for any set of tidal constituents at each of the tide gauge sites (Boon, 2004). The purpose here is to develop a predicted time series of the water levels produced entirely by astronomic forces that excludes the seasonal component produced by oceanographic processes on the West Coast; the seasonal component can be integrated into tide predictions through the solar annual (Sa) and solar semiannual (Ssa) tide and is integrated as an *average term* in the predicted tides provide by NOS.

HAMELS analyses of tide gauge data have previously been completed for the SB and TP tide gauges (Allan and others, 2011). Thus, similar analyses were undertaken using the AST and GB tide gauges. The specific steps included the following:

- HAMELS was used to derive an estimate of the amplitude and phase for the tidal constituents. This was initially done using just a spring/summer data set for testing purposes and then expanded to the full year of data;
- Having determined the tidal constituents, HAMELS was used to derive the astronomic tide predictions for the entire record on a year-by-year basis (eliminates any long-term trend). The non-tidal residuals (NTRs) were

calculated by subtracting the astronomic tide from the measured tides;

- The NTR time series were then filtered using a moving average filter (averaged over +/- 30 days) with zero phase shift, and the seasonal cycle was removed from the NTRs;
- The winter standard deviation was calculated and those events exceeding 2*σ were used to define individual surge events (Zhang and others, 2001).

Figure 4-5 presents a plot of the derived NTRs for the South Beach (SB), Garibaldi (GB), Charleston (CH) and Port Orford (PO) tide gauges. These data reflect the corresponding NTRs associated with the Higher Highs and Higher Lows of the diurnal tidal cycle, which were determined using a peak detection algorithm in MATLAB. Analyses here span the period of record for the respective tide gauges. Correlation (R^2) values calculated for the three plots are 0.91, 0.91, and 0.81 respectively, with the strongest correlation found between the SB and GB tide gauges on the open coast, while the weakest correlation was between the SB and the PO tide gauges. Because there is a noticeable change in the tidal forcing with progress south along the Oregon coast, the general decrease in correlation between the SB and PO tide gauges is not overly surprising. Because the PO tide gauge differs sufficiently from the tidal regime observed at the CH, SB and GB gauges, the PO gauge was also eliminated from further consideration.

Figure 4-6 presents the actual time series of de-seasoned NTRs derived for the GB, SB, and CH tide gauges for the 2007-08 winter. In this example, the NTRs have been time adjusted to a single station (SB). As can be seen in this example, all three tide gauges tend to track closely to each other, consistently capturing the same peaks and troughs. Of the three gauges, the CH gauge tends to produce slightly lower NTRs and as can be seen from **Figure 4-6**, measures a significantly lower NTR (~0.2 m [0.6 ft]) during the peak of a storm that occurred in December 2007. These differences are further highlighted in the anomaly plot (**Figure 4-6,** bottom), which indicates more subtle differences between SB and GB tide gauges, with both gauges characterized by anomalies that reach as much as 0.1 m (0.33 ft). In contrast, anomalies between the SB and CH tide gauges tend to be a little larger, particularly during the major storm event in December 2007. Much of this reflects differences in the position of the storms relative to the tide-gauges, the storm's barometric pressures, winds, and the associated wave forcing along the coast. Overall, differences between the three tide gauges probably reflect mostly subtle shifts in the timing of the events as they impact the coast, reinforcing our confidence that the effects of North Pacific extratropical storms are indeed widespread, affecting large tracts of the coast at similar times.

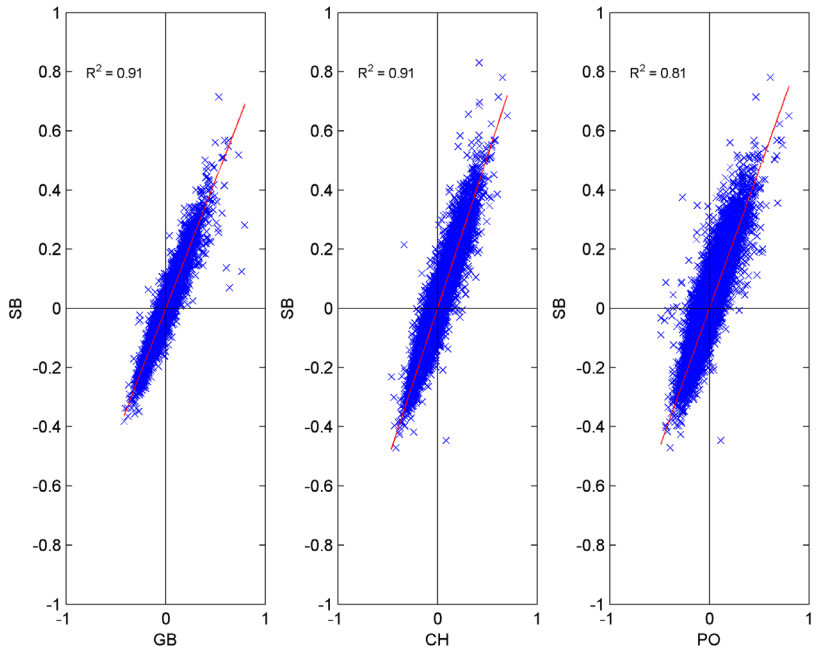

Figure 4-5. Comparison of non-tidal residuals determined for SB versus GB, SB versus CH, and SB versus PO tide gauges. Values plotted here reflect the daily peak values.

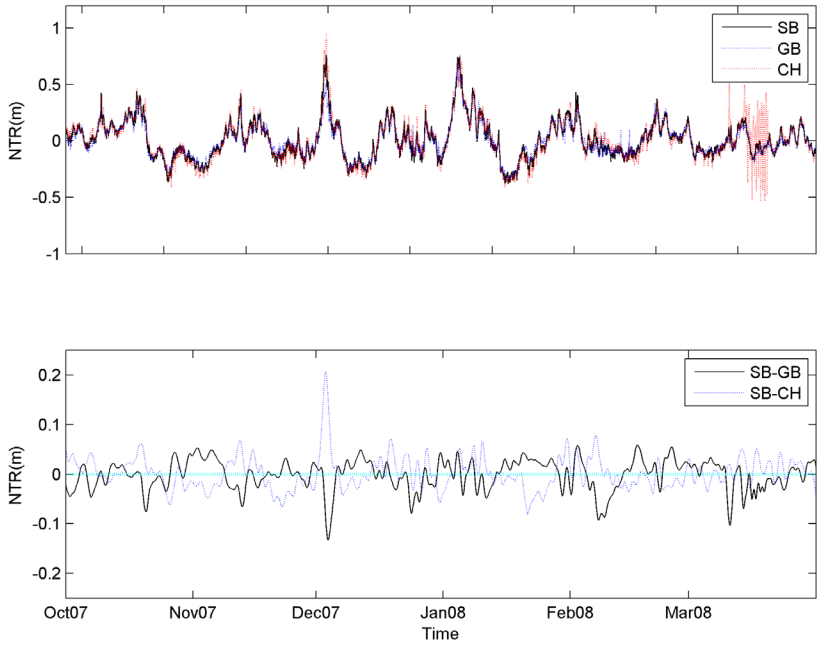

Figure 4-6. Comparison of non-tidal residuals (NTRs, top), and their differences (bottom) between the GB, SB, and CH tide gauges for the 2007-08 winter.

.

Having identified the NTRs for each of the tide gauges, individual storm surge events have been identified following the procedures of Zhang and others (2001) and Allan and others (2011). **Figure 4-7** (left) presents a log number plot of all surge events for the SB, CH, and GB gauges. The plot indicates that for the most part the three gauges are showing relatively similar patterns in terms of the storm surge magnitudes. In general, the mean storm surges increase northward (0.43 m [1.4 ft] at CH to 0.54 m [1.8 ft] at GB), while the highest surges have occurred at SB (1.42 m [4.7 ft]); despite its significantly longer record, the highest surge observed at the Astoria tide gauge (not included in **Figure 4-7**) reached 1.1 m (3.6 ft). **Figure 4-7** (right) presents the empirical CDF calculated for the three gauges, further highlighting the progressive shift in the surge magnitudes to the north. Again, the CH gauge stands out as generally producing the lowest NTRs, further confirming why this site should be excluded for further consideration.

Taken together, these analyses confirm that the two open coast tide gauges located in Newport on the central Oregon coast and at Garibaldi in Tillamook Bay, overall provide the best measure of the open-coast still water levels, important in FEMA total water level and overtopping analyses. The main distinction between these two stations is the length of available measurements, with the Newport site having the longest record (~45 years), and Garibaldi having the shortest.

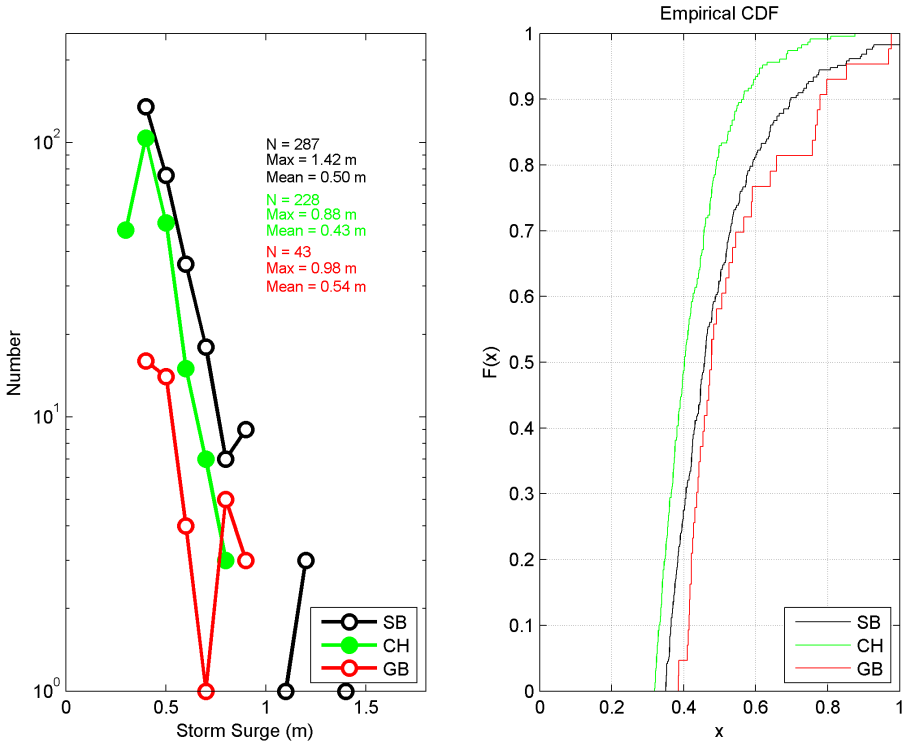

Figure 4-7. (Left) Histogram of surge magnitudes determined for the GB, SB, and CH tide gauge stations. (Right) Cumulative distribution plot of storm surge magnitudes.

4.5 Lincoln County Tides

The previous analyses have highlighted relative similarities between the SB and GB gauges and to a lesser extent between SB and CH. As a result of these analyses, we have based our final still water level (SWL) and wave runup calculations on the measured tides at the South Beach gauge (#9435380) in Yaquina Bay (1967–2013). **Figure 4-8** shows the tidal elevation statistics derived from the South Beach tide gauge (the longest temporal record), with a mean range of 1.91 m (6.3 ft) and a diurnal range of 2.54 m (8.3 ft). The highest tide measured from this record reached 3.73 m (12.2 ft), recorded in December 1969 during a major storm. These values are comparable to those measured at the Garibaldi site (mean = 1.9 m, diurnal = 2.53 m), with the only real difference being the fact that this latter gauge recorded a peak water level of 3.64 m (11.9 ft) in December 2005 due to its shorter record.

As noted previously, tides on the Oregon coast tend to be enhanced during the winter months due to warmer water temperatures and the presence of northward flowing ocean currents that raise water levels along the shore, persisting throughout the winter rather than lasting for only a couple of days as is the case for a storm surge (Komar 1997). This effect can be seen in the monthly averaged water levels derived from the combined time series (**Figure 4-9**), but where the averaging process has removed the water-level variations of the tides, yielding a mean water level for the entire month. Based on 45 years of data, the results in **Figure 4-9** show that on average monthly-mean water levels during the winter are nearly 25 cm (0.8 ft) higher than in the summer. Water levels are most extreme during El Niño events, due to an intensification of the processes, largely enhanced ocean sea surface temperatures offshore from the Oregon coast (Komar 1997, Allan and Komar, 2002; Komar and others, 2011). This occurred particularly during the unusually strong 1982-83 and 1997-98 El Niños. As seen in **Figure 4-9**, water levels during those climate events were approximately 25–30 cm (0.8–1 ft) higher than the seasonal peak and as much as 56 cm (1.8 ft) higher than during the preceding summer, enabling wave swash processes to reach much higher elevations on the beach during the winter months, with storm surges potentially raising the water levels still further.

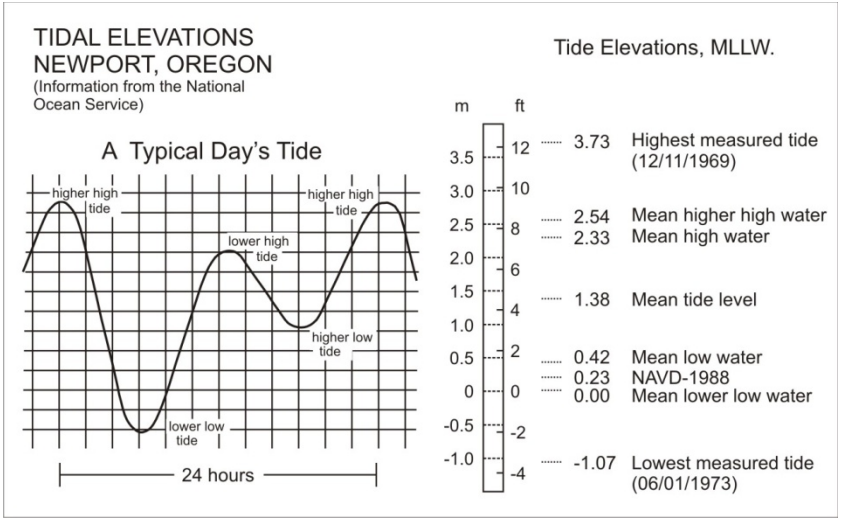

Figure 4-8. Daily tidal elevations measured at South Beach, Newport on the central Oregon coast. Data from NOS (http://www.co-ops.nos.noaa.gov/waterlevels.html?id=9435380).

Aside from seasonal to interannual effects of climate events on ocean water levels, also of interest are the long-term trends associated with relative sea level changes due to climate change along the Lincoln County coastline. **Figure 4-10** presents results from an analysis of the SB time series based on a separate analysis of the summer and winter tide levels. For our purposes "winter" is defined as the combined average tide level measured over a three-month period around the peak of the seasonal maximum in winter water levels, typically the months of December through February. Similarly, "summer" water levels reflect the combined average tide level measured over a three-month period around the seasonal minimum, typically the months between May through July when water levels also tend to be less variable (Komar and others, 2011). As observed previously in **Figure 4-9**, the winter tidal elevations are systematically displaced upward by about 25 cm (0.8 ft) above the summer, with the difference between the regression lines reflecting the seasonal change in ocean water levels from summer to winter. **Figure 4-10** also emphasizes the extremes associated with major El Niños, with the peaks between the 1983 and 1997 major events having been systematically shifted upward over the years due to relative sea level changes along this particular section of the coast. In contrast, the summer regression line is characterized by significantly less scatter in the residuals because it effectively excludes the influence of storms and El Niños that are dominant during the winter. With this approach, it can be seen that the central Oregon coast is slowly being transgressed at a rate of ~2.70 ±0.85 mm.yr^{-1}, and is slightly lower than that reported by NOS (~2.72 ±1.03 mm.yr^{-1}). However, work by Burgette and others (2009) revealed that the SB tide gauge has previously been affected by localized subsidence, particularly in the late 1960s/early 1970s that has continued to decrease over time up until the mid 1990s. Since then, repeat surveys of NGS benchmark indicate that the land appears to be now stable. Accounting for these effects reduces the rate of sea level rise at the SB gauge to ~1.33 ±0.79 mm.yr^{-1}.

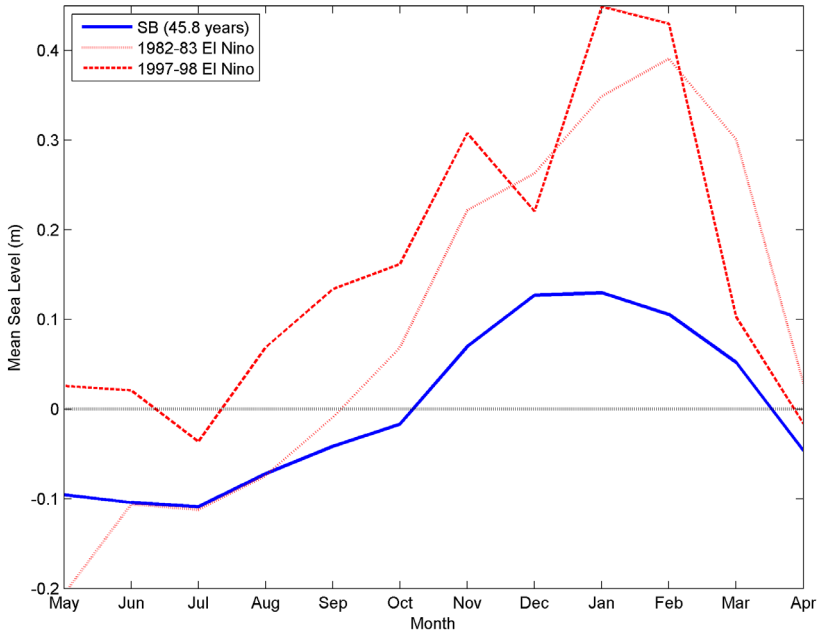

Figure 4-9. Seasonal cycles in monthly-mean water levels based on data from the South Beach tide gauge.

Finally, it is important to appreciate that the trends shown in **Figure 4-10** reflect relative sea level changes due to the fact that the PNW coast of Oregon and Washington is locally influenced by changes in the elevation of the land due to regional tectonics as well as by the global rise in sea level, with the net change being important to both coastal erosion and flood hazards. **Figure 4-11** presents a synthesis of both tectonic land elevation changes and sea level trends derived for multiple stations along the PNW coast (Komar and others, 2011), correlated against differential surveys of first-order NGS benchmarks (e.g., Burgette and others, 2009), and GPS CORS stations. Results here indicate that in general the southern Oregon coast is an emergent coast with tectonic uplift of the land outpacing sea level rise. In contrast the central to northern Oregon coast (i.e., Lincoln County) is slowly being transgressed by sea level, even though it is tectonically rising, though at a slower rate than along the south coast.

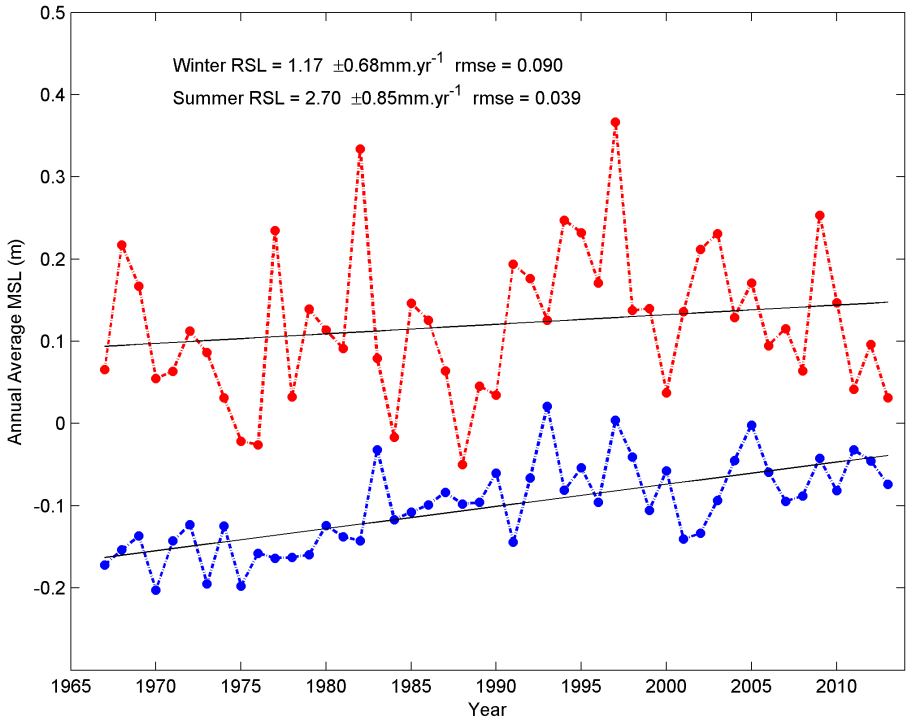

Figure 4-10. The trends of "winter" (red) and "summer" (blue) mean sea levels measured by the SB tide gauges. Results for the summer regression are statistically significant, while the estimated winter rate is not significant at the 95% confidence level.

4.6 Still Water Level (SWL)

The still water level (SWL) is the sum of the predicted astronomical tide listed in Tide Tables, plus the effects of processes such as an El Niño or storm surge that can elevate the measured tide above the predicted tide (Northwest Hydraulic Consultants, 2005). Of importance to erosion and flooding hazards are the extremes of the measured tides. In conventional analyses of extreme values, the general assumption is that the data being analyzed (e.g., the annual maxima) represent independent and identically distributed (stationary) sequences of random variables. The generalized extreme value (GEV) family of distributions is the cornerstone of extreme value theory, in which the cumulative distribution function is given as:

$$G(z, \mu, \sigma, \xi) = \exp\left\{-\left[1 + \xi\left(\frac{z-\mu}{\sigma}\right)\right]^{-1/\xi}\right\} \qquad (4.3)$$

defined on

$$\left\{z: 1 + \frac{\xi(z-\mu)}{\sigma} > 0\right\},$$

where the parameters satisfy $-\infty < \mu < \infty$, $\sigma > 0$, $-\infty < \xi < \infty$ (Coles, 2001). The model has three parameters; μ is a location parameter, σ is a scale parameter, and ξ is a shape parameter. The EV-II (Frechet) and EV-III (Weibull) classes of extreme value distributions correspond respectively to the cases of ξ > 0 and ξ < 0. When ξ = 0, equation 4.3 collapses to the Gumbel or EV-I type extreme value distribution. By inferring the shape parameter ξ (estimated here, along with the other parameters, by maximizing the log-likelihood function), the data themselves determine the most appropriate type of tail behavior and it is not necessary to make an a priori assumption about which individual extreme family to adopt as in a classical Weibull-type extreme wave height analysis (Coles, 2001).

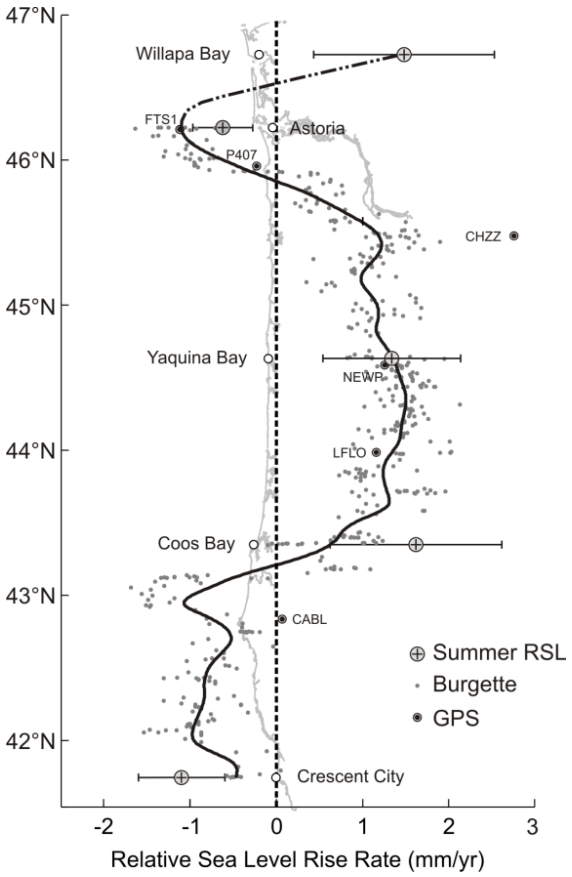

Figure 4-11. Assessments of changes in RSLs based on tide-gauge records compared with benchmark and GPS measurements of land-elevation changes, with their corresponding RSL rates obtained by adding the 2.28 mm/yr PNW eustatic rise in sea level (Komar and others, 2011).

The GEV is often applied to annual maxima data in an approach referred to as the annual maximum method (AMM). However, one of the primary shortcomings of fitting an extreme-value distribution with annual maximum data is that useful information about the extremes is inherently discarded, particularly when data are sampled on either a daily or hourly basis (as in the case of the measured tides and deep-water significant wave heights measured by Oregon tide gauges and NDBC wave buoys). Two well-known approaches exist for characterizing extremes by utilizing data other than simply annual (block) maxima. The first is based on the behavior of the r-largest-order statistics within a block, for low r, and the second is based on exceedances above a high threshold value. For the purposes of this study, we use the peak-over-threshold (POT) approach for determining the extreme SWL and wave heights.

In the peak-over-threshold (POT) method, a high threshold, u, is chosen in which the statistical properties of all exceedances over u and the amounts by which the threshold is exceeded are analyzed. It is assumed that the number of exceedances in a given year follows a Poisson distribution with annual mean νT, where ν is the event rate and T = 1 year, and that the threshold excesses $y > 0$ are modeled using the Generalized Pareto Distribution (GPD) given by:

$$H(y, \sigma, \xi) = 1 - \left(1 + \frac{\xi y}{\sigma}\right)^{-1/\xi} \qquad (4.4)$$

where ξ is the shape parameter of the GEV distribution and σ is a scale parameter related to GEV parameters by $\sigma = \sigma + \xi(u - \mu)$. The event rate can also be expressed in a form compatible with the GEV distribution provided that

$$\nu = \left(1 + \frac{\xi(u-\mu)}{\sigma}\right)^{-1/\xi}.$$

Estimates of extreme quantiles of the distributions are obtained by inverting the distributions in equation 4.3. For GPD-Poisson analyses the N-year return level, y_N, is given as:

$$y_N = \mu + \frac{\sigma}{\xi}\left[(N n_y \zeta_u)^{\xi} - 1\right] \qquad (4.5)$$

where n_y is the number of observations per year and ζ_u is the probability of an individual observation exceeding the threshold u.

Figure 4-12 presents results of the GEV analyses for the SB measured tides. In constructing this plot, we used a threshold of 2.99 m (9.8 ft). Included in the figure are the calculated 1- through 500-year SWLs. As can be seen in **Figure 4-12**, the 1% SWL calculated for the SB time series is 3.52 m (11.55 ft, relative to NAVD88). When adjusted to the MLLW vertical datum, this value becomes 3.73 m (12.2 ft, NAVD88); note the adjustment from NAVD88 to MLLW is calculated to be +0.225 m (0.74 ft) at the SB site. The 500-year SWL is estimated to be 3.60 m (11.8 ft) relative to the NAVD88 vertical datum. As observed previously, the highest tide measured in the combined time series reached 3.49 m (11.4 ft, relative to NAVD88).

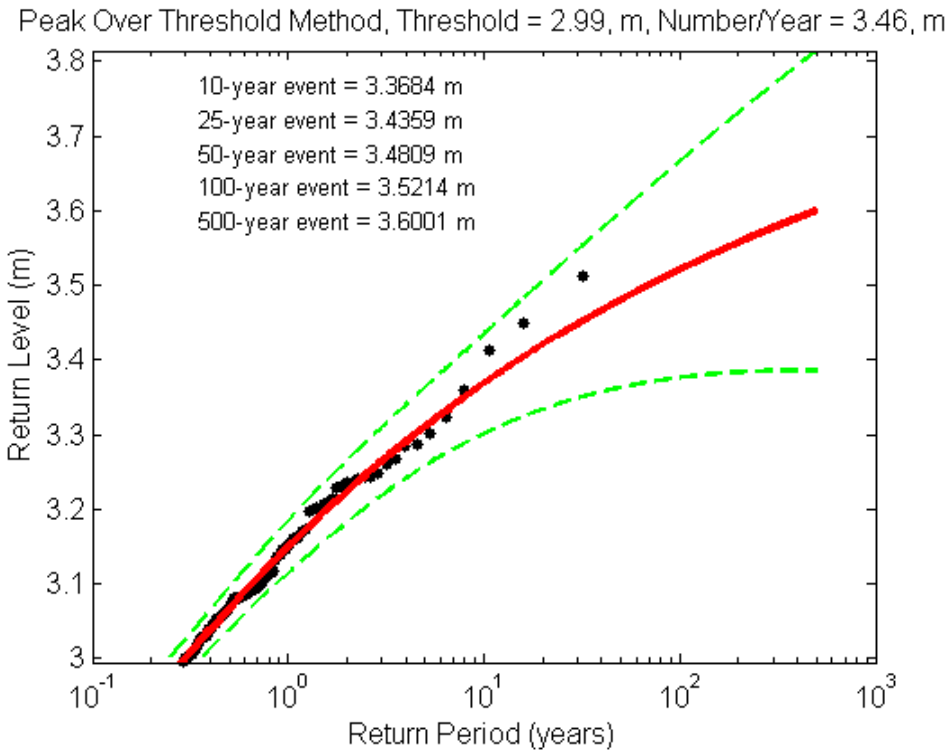

Figure 4-12. Extreme-value analyses of the still water level (SWL) determined for the combined South Beach/Garibaldi tide gauge time series. These data are relative to the NAVD88 vertical datum.

5.0 PACIFIC NORTHWEST WAVE CLIMATE

The wave climate offshore from the Oregon coast is one of the most extreme in the world, with winter storm waves regularly reaching heights in excess of several meters. This is because the storm systems emanating from the North Pacific travel over fetches that are typically a few thousand miles in length and are also characterized by strong winds, the two main factors that account for the development of large wave heights and long wave periods (Tillotson and Komar, 1997). These storm systems originate near Japan or off the Kamchatka Peninsula in Russia, and typically travel in a southeasterly direction across the North Pacific toward the Gulf of Alaska, eventually crossing the coasts of Oregon and Washington or along the shores of British Columbia in Canada (Allan and Komar, 2002).

Wave statistics (heights and periods and more recently wave direction) have been measured in the Eastern North Pacific using wave buoys and sensor arrays since the mid 1970s. These data have been collected by the National Data Buoy Center (NDBC) of NOAA, and by the Coastal Data Information Program (CDIP) of Scripps Institution of Oceanography (**Figure 4-1**). The buoys cover the region between the Gulf of Alaska and Southern California, and are located in both deep and in intermediate to shallow water over the continental shelf. The NDBC operates some 30 stations along the West Coast of North America, while CDIP has at various times carried out wave measurements at 80 stations. Presently there are two CDIP buoys operating offshore from the mouth of the Columbia River (#46243 and #46248), and one offshore from Coos Bay (#46229) on the south central Oregon coast. NDBC currently maintains six buoys offshore the Oregon coast, including: Washington (#46005), Tillamook (#46089), Columbia River Bar (#46029), Stonewall Bank (#46050), Oregon (#46002) and Port Orford (#46015) on the southern Oregon coast. Wave measurements by NDBC are obtained hourly (CDIP provides measurements every 30 minutes), and are transmitted via satellite to the laboratory for analysis of the wave energy spectra, significant wave heights and peak spectral wave periods. These data can be obtained directly from the NDBC through their website (http://www.ndbc.noaa.gov/maps/Northwest.shtml).

An alternate source of wave data appropriate for FEMA flood modeling is hindcast wave data such as the Global Reanalysis of Ocean Waves Fine Northeast Pacific Hindcast (GROW-FINE NEPAC), purchased through Oceanweather Inc., and Wave Information Studies (WIS; http://wis.usace.army.mil/) hindcasts developed by the USACE (Baird, 2005). GROW is a global wave model, while GROW Fine Northeast Pacific extends the original model by incorporating a higher resolution model analysis (4 times as many data nodes), basin-specific wind adjustments based on QUIKSCAT scatterometry, enhancements due to Southern Ocean swells, and inclusion of shallow water physics (Oceanweather Inc., 2010). These data can ultimately be applied to offshore structure design, tow-analysis, operability, and other applications where wind and wave data are required. Standard products from GROW include time series of wind and wave parameters (including sea/swell partitions), extreme criteria, operability statistics, and wave spectra (Oceanweather Inc., 2010). The advantage of GROW as opposed to measured data is that it provides a continuous time series of wave and wind data suitable for FEMA flood modeling. In contrast, measured data obtained from wave buoys may be characterized by significant data gaps due to the instruments having come off their mooring or from instrument failure. The main disadvantage of GROW Fine Northeast Pacific data is that it is modeled based on basin-scale wind models and data, and the data time series is 3 hourly as opposed to hourly as provided by the buoys. For the purposes of this study, we have explored both data sets in order to define the most appropriate time series of wave data. To that end, GROW Fine Northeast Pacific data were purchased for four nodes offshore the Oregon coast. **Figure 4-1** identifies the location of the GROW sites: station #18023 located offshore from southern Clatsop/northern Lincoln County; #17663 offshore from Lincoln County; #17483 offshore from Coos

County; and #17126 offshore from Curry County. Besides the hourly measured wave buoy data, we also obtained wave hindcast information on the deepwater wave climate determined through comparisons with the WIS station located adjacent to NDBC buoy 46005.

Analyses of the wave climate offshore from Lincoln County were undertaken by DOGAMI staff, and as a subcontract to Dr. Peter Ruggiero, College of Earth, Ocean, and Atmospheric Sciences (CEOAS), OSU, and included numerical analyses of the 1% or 100-year extreme total water levels, which reflect the calculated wave runup superimposed on the tidal level (i.e., the still water level [SWL]) to help determine the degree of coastal flood risk along the coast of Lincoln County.

OSU performed a series of tests and analyses including wave transformations, empirical wave runup modeling, and total water level modeling. For the purposes of this study, OSU used the SWAN (Simulating Waves Nearshore) wave model to transform deepwater waves to the nearshore (typically the 20 m [65.6 ft] contour). The transformed waves were then linearly shoaled back into deep water to derive a refracted deepwater equivalent wave parameterization (wave height and peak period) that can be used to calculate runup levels, which combined with tides, are used to estimate the flood risk along the county's shoreline.

In our Coos County FEMA study (Allan and others, 2012b), the approach we developed involved several stages:

1. A time series of deepwater wave heights and periods was first defined for a particular location offshore of the shelf break, which we used to calculate an initial wave runup and total water level time series based on two representative beach slopes characteristic of beaches in the Coos County detailed study areas.
2. Using the above approach, we defined ~135 discrete storm events for the two different slope types. From on these events, we transformed the deepwater wave statistics associated with these events into the nearshore (20 m water depth) to account for wave refraction and shoaling effects. Depth limited breaking, wind growth, quadruplets, and triad interactions were all turned off in the SWAN runs. The derived nearshore wave statistics were then converted back to their adjusted deepwater equivalent wave height in order to perform the wave runup analyses and ultimately compute the 1% total water levels.

The main limitations associated with this approach were:

1. Only a very limited number of model runs were performed, ~135 per representative beach slope.
2. Because we used only two representative beach slopes, we may have missed a particular wave condition (wave height [H_s], period [T_P], direction [D_d]) and beach slope (tan β) combination that resulted in a higher TWL at the shoreline.
3. The structural function approach used to generate the initial extreme TWLs and therefore to pick the offshore wave conditions input in SWAN is fundamentally limited. Nature gave us only one combination of waves and water levels during the 30 years we used to generate input conditions, which is not necessarily a statistically robust sample.

For the purposes of the Lincoln County study, including other detailed FEMA coastal studies already completed for Oregon, we have developed a more refined approach that reflects the following enhancements.

1. Rather than steps 1 and 2 as described for our Coos County study, modeling will be carried out based on analyses of the full range of wave and tide combinations observed over the historical period. This approach will ultimately provide a more robust measure of the 1% (and other desired return periods) total water levels.
2. We have developed a lookup table approach for analyzing thousands of possible storm combinations rather than only a few hundred as performed in Coos County. The general idea

is that a "lookup table" can be developed by transforming all combinations of wave quadruplets (H_S, T_P, D_d, and water levels). We used SWAN to compute the transformed wave characteristics of these waves up to wave breaking.

3. Our approach still suffers from the 3rd limitation listed above for the Coos County study.

The area over which the SWAN grid was set up is shown in **Figure 5-1**. In general, our analyses proceeded in the following order:

1. Develop a long time series of both measured (NDBC) and modeled (WIS) wave conditions (~30 years long) at approximately the shelf edge offshore of the study area;
2. Run the SWAN model with a full range of input conditions, using constant offshore boundary conditions, to compute bathymetric induced wave transformations up to wave breaking.
3. Develop "lookup tables" from the suite of SWAN simulations.
4. Transform the long time series through the "lookup tables" such that we generate alongshore varying long time series at approximately the 20 m depth contour throughout the study area.
5. Use the deepwater equivalent alongshore varying wave conditions and the appropriate measured tides from the South Beach time series to compute time series of TWLs for 313 beach profiles along the Lincoln County coast.
6. Using a Poisson-generalized Pareto distribution, compute the 1-, 10-, 25-, 50-, 100-, and 500-year TWL elevations using a peak-over-threshold (POT) approach.
7. Compare extreme TWLs with topographic elevations of various beach-backing features to determine the potential extent of coastal flooding during extreme events.

The following sections describe in more detail the various procedures used in each of the aforementioned steps in this analysis.

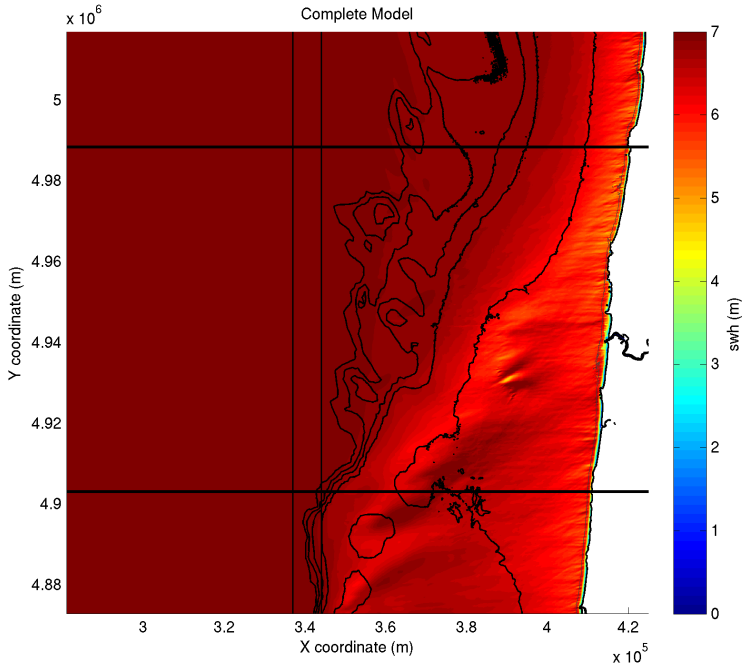

Figure 5-1. The SWAN model domain developed for the Lincoln County coast. The model bathymetry was developed using 1/3 arc-second (~10 m) DEMs downloaded from the NOAA's NGDC. Color scale reflects depth in meters.

5.1 Development of a Synthesized Wave Climate for Input into SWAN

Our primary goal was to use existing measured and hindcast wave time series to generate as long a record of the deep-water wave climate as possible for the offshore boundary of the SWAN model, approximately the edge of the continental shelf break. To this end, we downloaded all available National Data Buoy Center (NDBC; http://www.ndbc.noaa.gov/) and Coastal Data Information Program (CDIP; http://cdip.ucsd.edu/) hourly wave buoy data in the region for several wave buoys. **Figure 5-2** shows the various buoys used to derived a synthesized northern Oregon coast wave data set (data availability shown in **Figure 5-3**). Besides the hourly measured wave buoy data, we also obtained wave hindcast information on the deepwater wave climate determined through the Wave Information Studies (WIS; http://wis.usace.army.mil/) (Baird & Associates, 2005). For the purposes of this study, we used wave hindcast data determined for station 81048 (**Figure 5-2**), which is located adjacent to NDBC buoy #46005. While NDBC #46005 has a high-quality, long record of data (1975–2013), it is located in 2981 m (9,780 ft) of water and is over 400–500 km (250–310 miles) from the shelf edge. Therefore NDBC #46089, a shelf edge, deep water buoy, was selected as the priority buoy to be used in the SWAN analyses. A buoy (Stonewall Bank #46050) located on the shelf was also included in this analysis, reverse shoaled to deep water to account for wave height changes in intermediate depths. Because of the variation in locations and water depths of the buoys, we needed to develop a methodology to transform these "off-shelf" and "on-shelf" waves to the "shelf-edge" offshore boundary condition of the SWAN model. This was necessary as the wave climates observed at 46005 and 46050 are significantly different than the climate observed at the Tillamook and Lincoln offshore buoys (**Figure 5-4**).

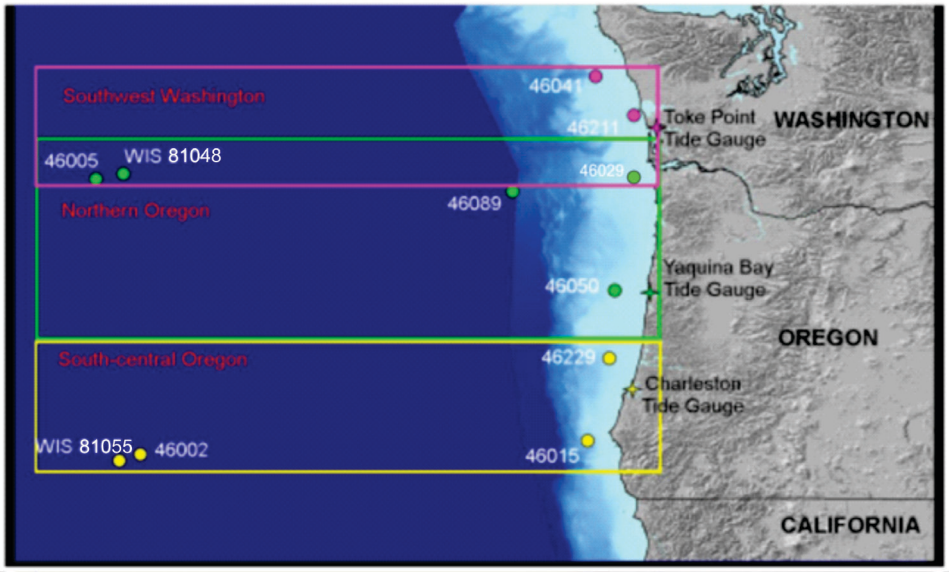

Figure 5-2. Map showing the regional divisions from which synthesized wave climates have been developed.

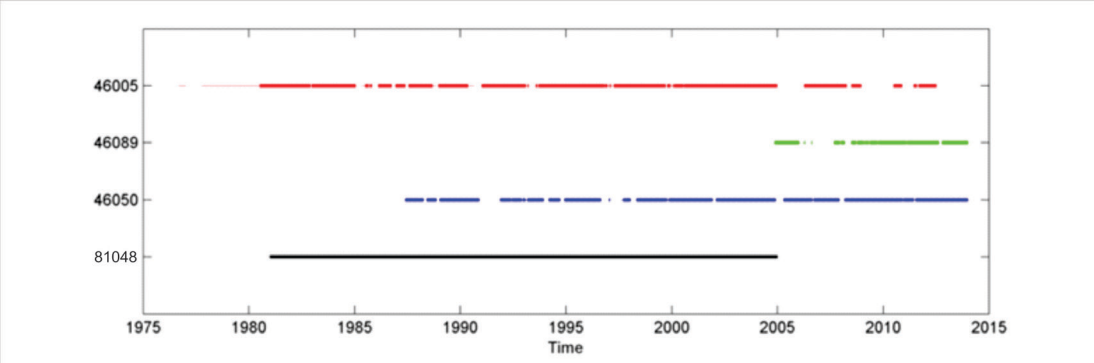

Figure 5-3. Available wave data sets timeline.

To transform the 46005 and 46050 waves to the shelf edge we created wave period bins (0-6, 6-8, 8-10, 10–12, 12–14, 14–16, 16–21, and 21–30 s[1]) to evaluate if there has been a wave period dependent difference in wave heights observed at Washington 46005 and Stonewall Bank 46050 compared with the Tillamook buoy. For our comparisons, the time stamps associated with waves measured at either 46005 or 46050 were adjusted based upon the group celerity (for the appropriate wave period bin) and travel time it takes the wave energy to propagate to the wave gauge locations. For example, for waves in the period range 10–12 s the group celerity is about 8.3 m/s and therefore it takes 13 hours for the energy to propagate from 46005 to the Tillamook buoy (**Figure 5-5**).

After correcting for the time of wave energy propagation, the differences in wave heights between the two buoys, for each wave period bin, were examined in two ways as illustrated in **Figure 5-5**:

1) A best fit linear regression through the wave height differences was computed for each wave period bin; and
2) A constant offset was computed for the wave height differences for each period bin.

Upon examination of the empirical probability density functions (PDF) of the buoys' raw time series (using only the years where overlap between the buoys being compared occurred) and after applying both transformation methods (**Figure 5-6**) it was determined that the constant offset method did a superior job of matching the PDFs, particularly at high wave heights. Therefore, a constant offset adjustment dependent on the wave period was applied to the wave heights of Washington 46005 and Stonewall Bank 46050. Because the WIS hindcast data used in this study was also located well beyond the boundary of the SWAN model (basically at the location of 46005), the same series of steps comparing WIS wave heights to the Tillamook buoy was carried out, with a new set of constant offsets having been calculated and applied.

After applying the wave height offsets to the necessary buoys, gaps in the time series of Tillamook 46089 were filled in respectively with the Stonewall Bank and Washington buoys. Where there were still gaps following this procedure we then filled in the time series with the corrected WIS data. Because wave transformations (particularly refraction) computed by SWAN are significantly dependent on wave direction, when this information was missing in the buoy records it was replaced with WIS data for the same date in the time series (but the wave height and period remained buoy observations where applicable).

[1] The NDBC wave buoys only relatively coarsely resolve long period waves. Between 21 and 30 s, only a wave period of 25 s is populated in the data set. There are no 30-s waves in the time series. Of the waves with periods between 16 s and 20 s, over 80 percent are at approximately 16 s. Only a relatively few waves in the record have recorded periods of 17, 18, and 19 s, respectively. The coarse resolution in the raw data determined our choice of period bin widths.

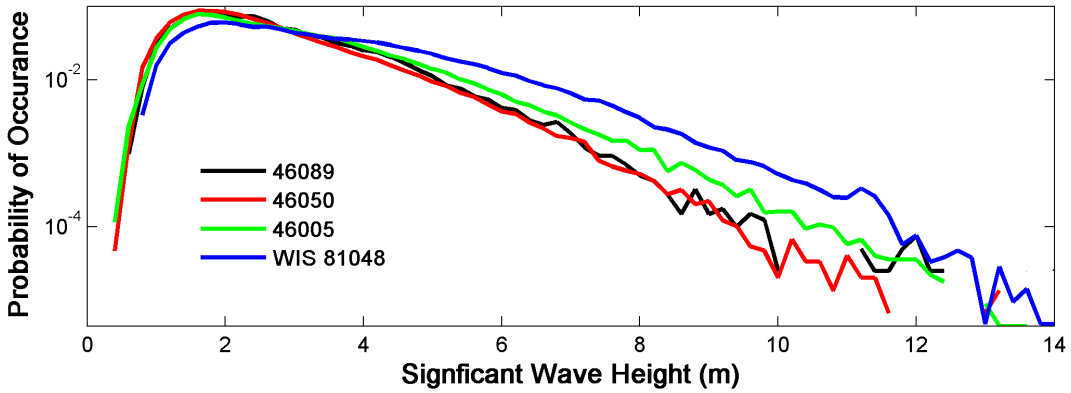

Figure 5-4. Differences in the empirical probability distribution functions of the on shore and off shore buoys.

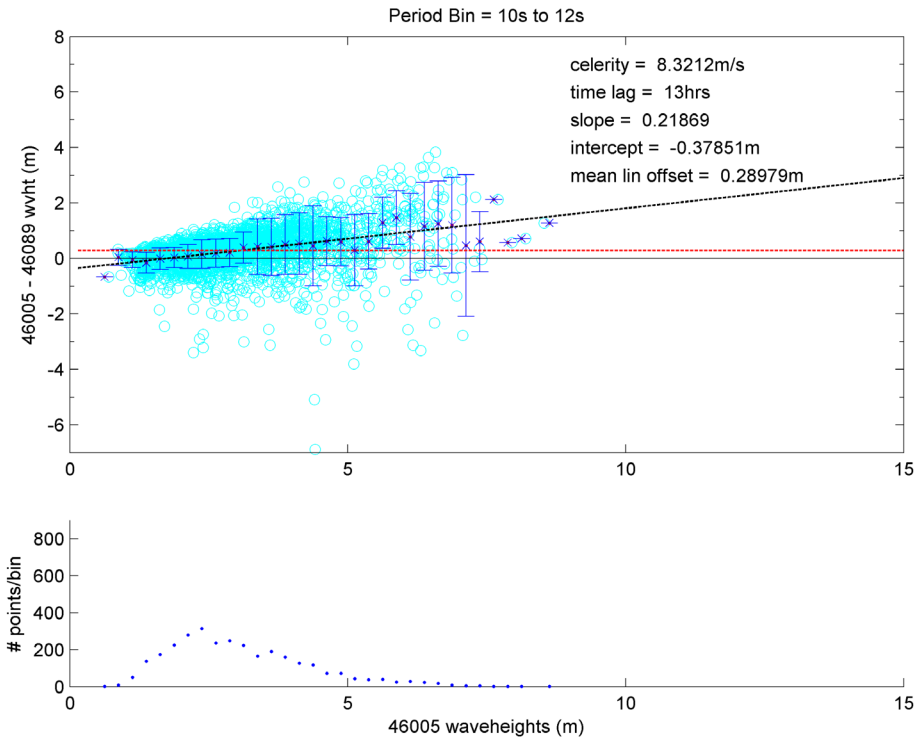

Figure 5-5. Example development of transformation parameters between the Washington buoy (#46005) and the Tillamook (#46089) buoy for period range 10 s to 12 s. In the top panel the dashed black line is the linear regression and the dashed red line is the constant offset. Blue error bars represent the standard deviation of the wave height differences in each period bin (Harris, 2011).

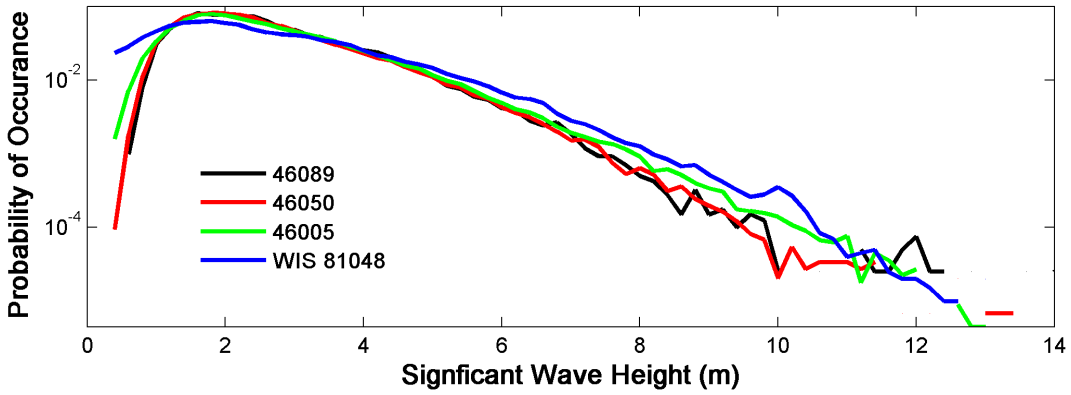

Figure 5-6. Adjusted probability density functions (corrected using the constant offset approach) for buoy 46005 (green line), buoy 46029 (red line), and WIS station 81048 (blue line) as compared to the raw probability density function for buoy 46089 (black line).

The final synthesized wave time series developed for Lincoln County extends from June 1980 through to 31st December, 2011 and consists of approximately ~31 years of data (measurements including at least wave height and periods) (**Figure 5-7**). Forty-two percent of the synthesized wave climate is from NDBC 46050, 36% from NDBC 46005, 15% from NDBC 46089, and ~7% from WIS station 81048. As can be seen from **Figure 5-7A**, the wave climate offshore from the northern Oregon coast is episodically characterized by large wave events (> 8 m (26 ft), with some storms having generated deepwater extreme waves on the order of 14.5 m (48 ft). The average wave height offshore from Lincoln County is 2.6 m (8.5 ft), while the average peak spectral wave period is 10.9 seconds, although periods of 20-25 seconds are not uncommon (**Figure 5-7B**).

The PNW wave climate is characterized by a distinct seasonal cycle that can be seen in **Figure 5-8** by the variability in the wave heights and peak periods between summer and winter. (The groupings evident in the peak periods (**Figure 5-7B**) are directly from the data and are a product of the data processing methods used by the NDBC to establish the wave frequencies and hence periods. It is for this reason that we chose coarse wave period bins for long period waves [i.e., > 16 s].) Monthly mean significant wave heights are typically highest in December and January (**Figure 5-8**), although large wave events (>12 m [39.4 ft]) have occurred in all of the winter months except October. The highest significant wave height observed in the wave climate record is 14.5 m (48 ft). In general, the smallest waves occur during late spring and in the summer, with wave heights typically averaging ~1.5 m during the peak of the summer (July/August). These findings are consistent with other studies that have examined the PNW wave climate (Tillotson and Komar, 1997; Allan and Komar, 2006; Ruggiero and others, 2010b). **Figure 5-7C** shows a probability density function determined for the complete time series, while **Figure 5-7D** is a cumulative frequency curve. The latter indicates that for 50% of the time waves are typically less than 2.2 m (7.2 ft), and less than 4.4 m (14.4 ft) for 90% of the time. Wave heights exceed 6.9 m (22.6 ft) for 1% of the time. However, although rare in occurrence, these large wave events typically produce the most significant erosion and flooding along the Oregon coast.

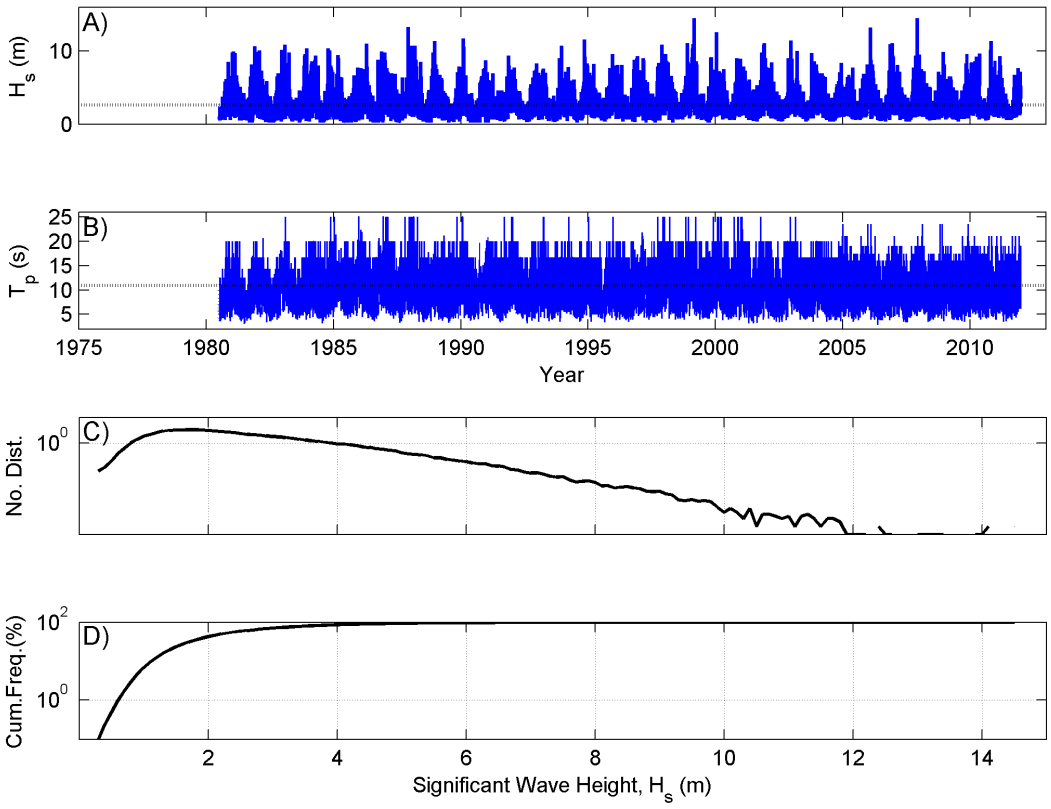

Figure 5-7. Synthesized wave climate developed for Lincoln County. A) Significant wave height with mean wave height denoted (dashed line), B) Peak spectral wave period with mean period denoted (dashed line), C) Probability distribution of wave heights plotted on a semi-log scale, and D) Significant wave height cumulative frequency curve plotted on a semi-log scale.

Finally, **Figure 5-9** provides a wave rose of the significant wave height versus direction developed for the northern Oregon coast. In general, the summer is characterized by waves arriving from the northwest, while winter waves typically arrive from the west or southwest (Komar, 1997). This pattern is shown in **Figure 5-9**, which is based on separate analyses of the summer and winter directional data developed from the synthesized time series. As can be seen in **Figure 5-9**, summer months are characterized by waves arriving from mainly the west-northwest (~48%) to northwesterly quadrant (~42%), with few waves out of the southwest. The bulk of these reflect waves with amplitudes that are predominantly less than 3 m (9.8 ft). In contrast, the winter months are dominated by much larger wave heights out of the west (~23%), and to a lesser extent the northwest (~5.8%), while waves from the southwest account for ~21% of the waves.

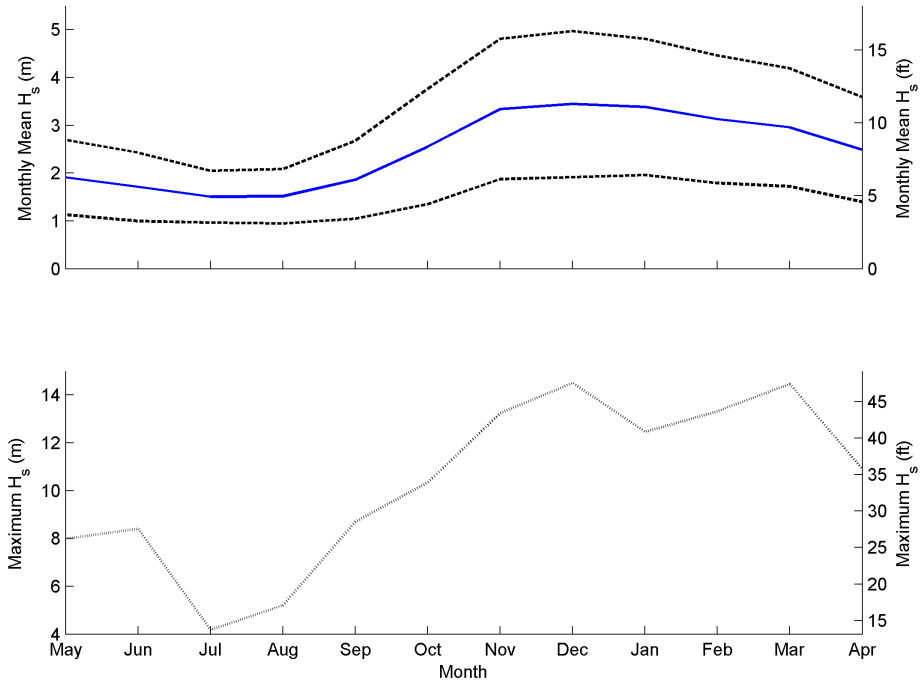

Figure 5-8. Seasonal variability in the deepwater wave climate offshore from the northern Oregon coast. (*top*) The monthly average wave height (blue line) and standard deviation (dashed line); (*bottom*) The maximum monthly significant wave height.

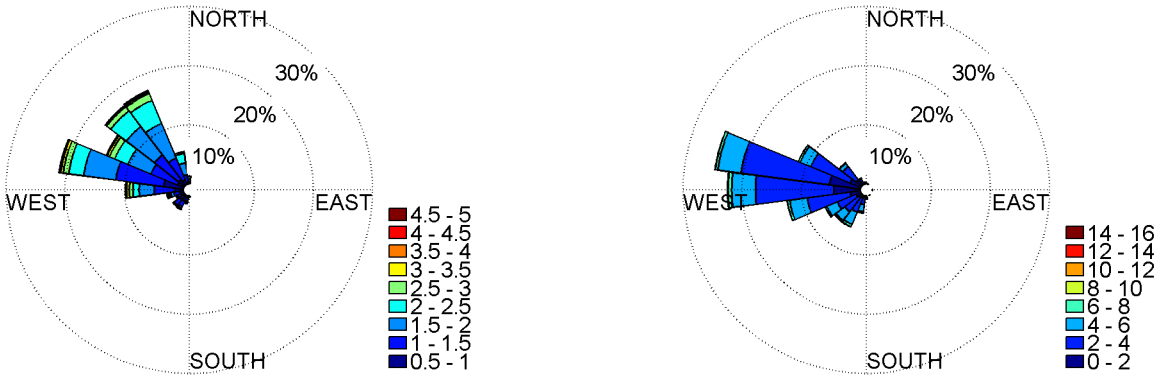

Figure 5-9. (*left*) Predominant wave directions for the summer months (June-August), and (*right*) winter (December-February). Colored scale indicates the significant wave height in meters.

5.2 Comparison of GROW Versus Measured Waves

This section presents a more detailed analysis of GROW Fine Northeast Pacific wave hindcast data compared with measured waves obtained from selected wave buoys offshore from the Oregon coast. The objective here is to better define the degree of congruence between these two contrasting data sets in order to assess their relative strengths and weaknesses. The approach used here is similar to the tide analyses presented in Section 4, using empirical probability density functions (PDF) to assess the shapes of the distributions. For the purposes of this analysis, PDF plots were derived for GROW station (#18023), and NDBC wave buoy 46089 (located 66 km northwest of 18023) and 46005 located 500 km west of 46029 (**Figure 4-1**).

The first plot (**Figure 5-10**) presents a series of significant wave height empirical PDFs for all measured data from NDBC buoys 46005 and 46089 as well as the GROW hindcast data from site 18023. Data from the stations span the following time frames: NDBC 46005 from 1976 through 2010; NDBC 46089 from 2004 through 2010; GROW 18023 from 1980 through 2009. From these PDFs it is immediately apparent that the GROW data contains a larger number of smaller wave heights (in the 2-3 m range) than those measured by the buoys. Additionally, examination of the log-scale plot (bottom of **Figure 5-10**) indicates that the GROW hindcast at 18023 tends to underestimate the more extreme wave heights (waves >7m), which are the most important for inundation and erosion vulnerability studies. **Table 5-1** lists general statistics of the various data sets where the maximum wave height modeled by GROW is shown to be nearly 3 meters lower than that measured by the 46089 buoy. In contrast, GROW indicates on average slightly higher peak periods when compared with the NDBC stations. While differences between NDBC 46005 and NDBC 46089 may simply reflect buoy locations relative to the tracks of the storms, differences between 46089 and GROW 18023 are almost certainly entirely due to the ability of the numerical model to hindcast the waves. Because NDBC station 46089 spans a much shorter measurement period compared with 46005 and the GROW site, the results from the full PDFs may be construed to be misleading. To better assess this potential bias, we again performed analyses of the truncated time series, which revealed near identical results to those presented in **Figure 5-10**. Summary statistics for the truncated time series are included in **Table 5-1**. **Figure 5-11** shows a PDF of the peak periods for 46005, 46089, and GROW for the time period 2004–2009. This last plot clearly indicates that GROW is tending to overestimate the higher peak periods when compared with the measured data.

Table 5-1. General statistics of the NDBC buoy and GROW data sets based on the complete time series of data, and truncated time series. Note: *H* denotes the significant wave height, and *T* is the wave period.

	46005	46089	GROW
Data Availability	1976–present	2004–present	1980–2009
Mean *H*	2.8 m	2. m	2.6 m
Max *H*	13. 6 m	14.5 m	11.7 m
Min *H*	0.2 m	0.4 m	0.72 m
H Standard Dev.	1.4 m	1.3 m	1.1 m
Mean *T*	10.8 s	11.1 s	12.6 s
Data Availability	2004–2009	2004–2009	2004–2009
Mean *H*	2.8 m	2.6 m	2.6 m
Max *H*	12.7 m	14.5 m	11.7 m
Min *H*	0.5 m	0.4 m	0.9 m
H Standard Dev.	1.4 m	1.3 m	1.1 m
Mean *T*	10.6 s	11.1 s	12.7 s

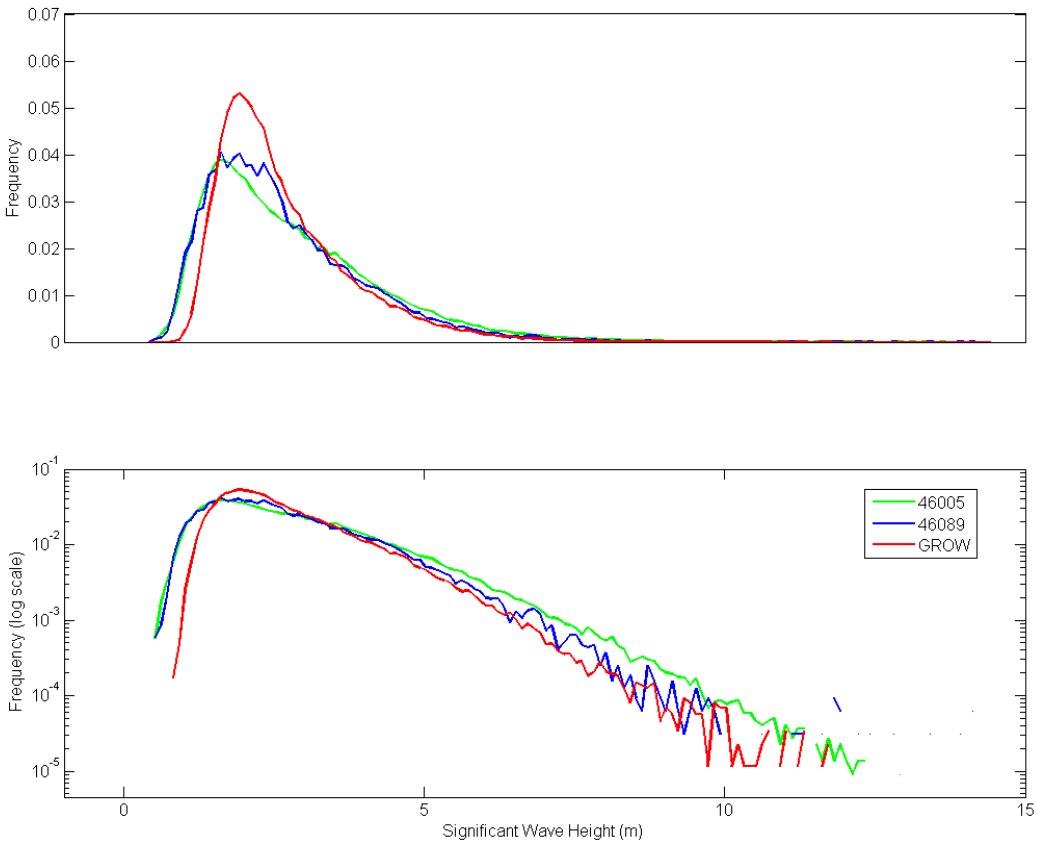

Figure 5-10. PDFs of significant wave heights plotted on a Top) normal and Bottom) log scale. Plots include all existing data from these stations.

Having examined PDFs of the various data sets, additional analyses were carried out for selected individual storms in order to better assess how well GROW is performing. The approach adopted was to select the five largest storms measured by the NDBC 46089. The storm events were selected by using a 3 day filter to ensure the selection of independent storm events. Once the peak of the storm was identified, the data (±2 days) were plotted with the GROW data. **Figure 5-12** presents results from two of the five selected storms. In general, our results indicate that while the timing of the events seems to be accurately determined by the GROW model, the magnitude is often lower than that measured by the wave gauges. This result may be due to the GROW approach of only estimating model results every 3 hours, as opposed to NDBC's hourly buoy measurements. As a result, sampling at 3 hourly intervals has the potential to miss the peak of the storms. In fairness to GROW, the 3 hourly sampling probably reflects the fact that modeling waves on an hourly basis is dependent on having temporally and spatially suitable meteorological information, which remains a challenge for large-scale regional models.

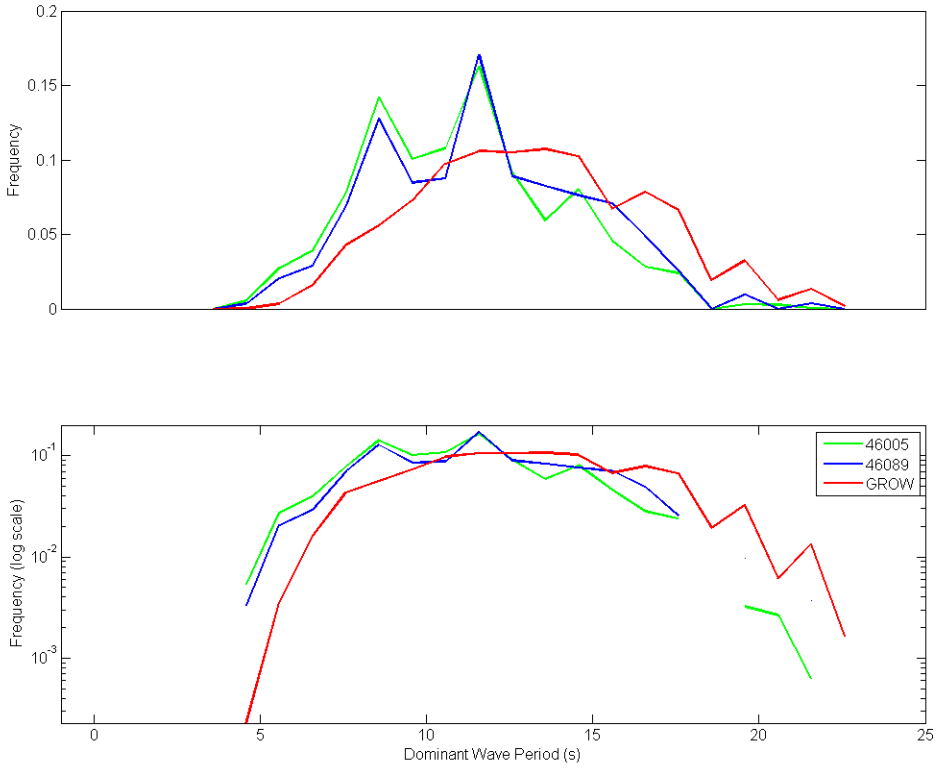

Figure 5-11. PDFs of peak wave periods from 2004 through 2009 on a Top) normal and Bottom) log plot.

Finally, we also compared 2% exceedance extreme runup values estimated using the Stockdon and others, (2006) approach and waves from the buoys and the GROW station. These results are presented in **Figure 5-13** and were calculated using a representative beach slope (tan β) of 0.04, which is typical for Oregon beaches. Only data from 2004 through 2009 were included in these calculations to provide a standard time frame for the comparison. Results indicate that, just as with the significant wave height PDFs, the extreme runup levels (>2.5 m) are underestimated by the GROW model, while the highest calculated runup differs by about 0.4 m (1.3 ft). Although the difference in the calculated runup between GROW and our measured time series is not as large as expected, the shape of the PDF plot would potentially reduce the number of storms available for defining the 100-year wave runup and total water level, as well as in overtopping, inundation, and erosion analyses as required for FEMA detailed coastal studies. From these findings we have concluded that all subsequent modeling of waves for Lincoln County should be based as much as possible on the measured wave time series, as opposed to using GROW hindcast data.

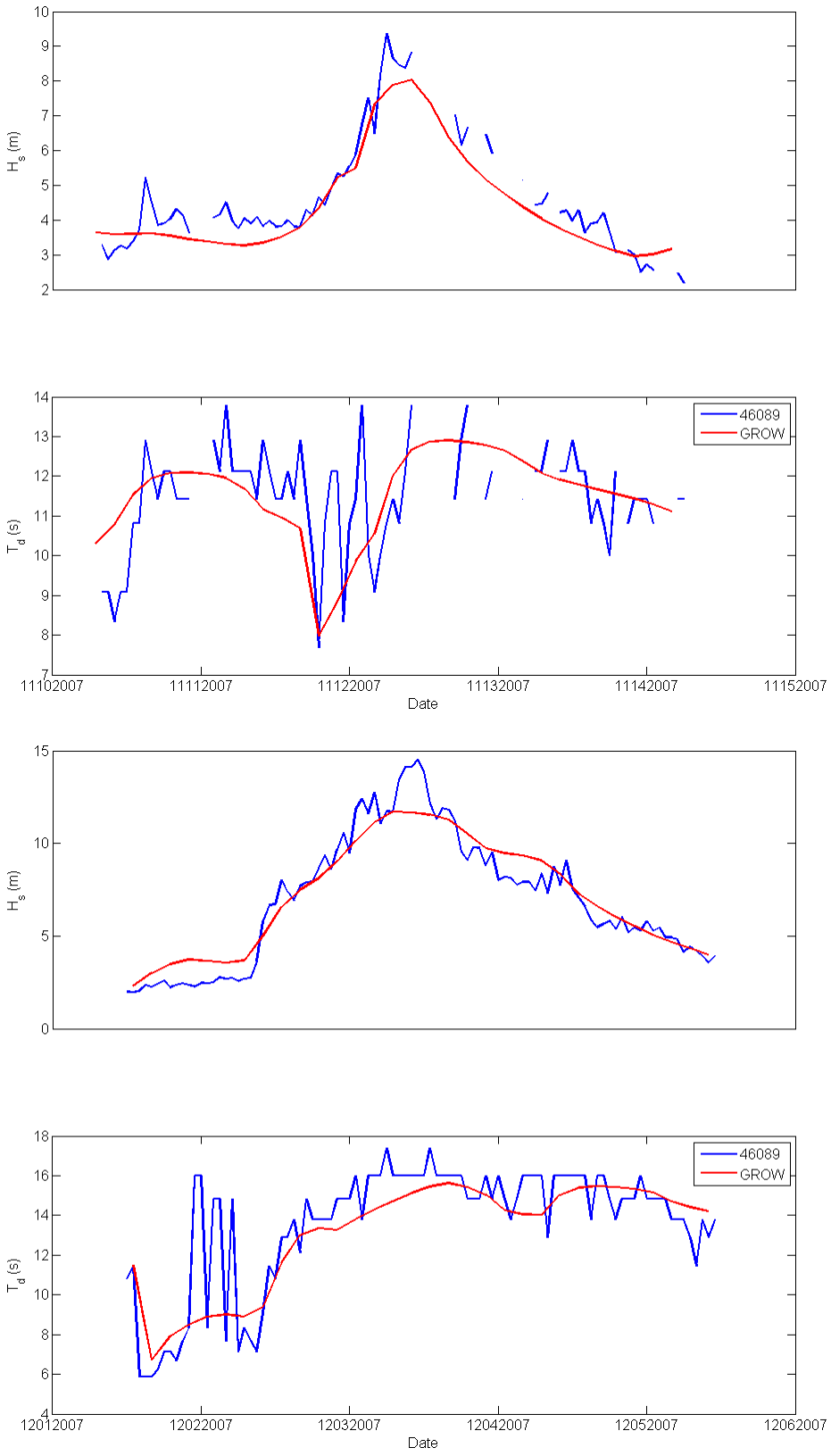

Figure 5-12. Two examples of storms where measured and modeled waves are compared. Top) Storm on November 12, 2007, and Bottom) major storm event on December 3, 2007.

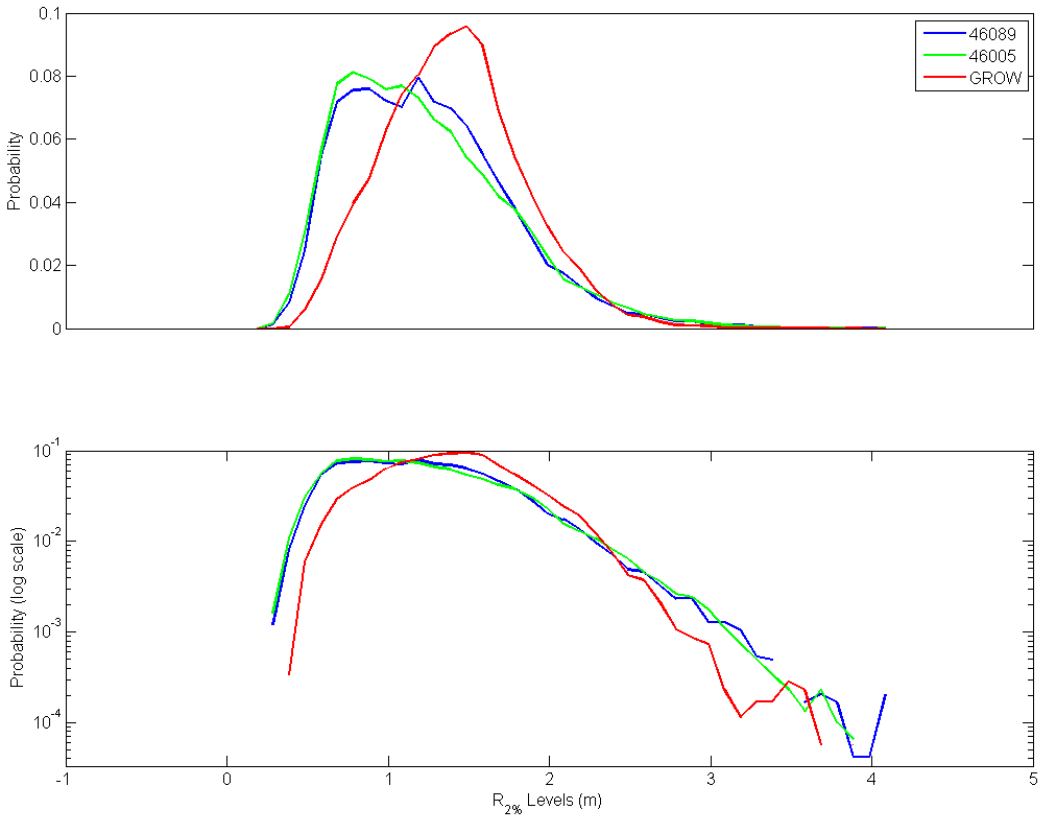

Figure 5-13. PDFs of calculated 2% extreme runup elevations for NDBC 46005, 46089, and GROW hindcast results. An average beach slope of 0.04 was used for runup calculations.

5.3 SWAN model development and parameter settings

We utilized the historical bathymetry assembled by the National Geological Data Center (NGDC) (described in Section 3.4) and created a model grid that covers a large portion of the central Oregon coast (**Figure 5-1**).

SWAN (Simulating WAves Nearshore) version number 40.81, a third-generation wave model developed at the Technical University of Delft in the Netherlands (Booij and others, 1999; Ris and others, 1999), was used in this study. The model solves the spectral action balance equation using finite differences for a spectral or parametric input (as in our case) specified along the boundaries. For the Lincoln County study, the cross-shore and alongshore resolution of the model grid used is 100 × 100 m. The total grid area is 81 km × 144 km in length, which yields 811 × 1,441 computational nodes. The SWAN runs were executed in stationary mode and included physics that account for shoaling, refraction, and breaking, while model settings varying from the default values are discussed in more detail below.

The north, south and west boundaries of the model were specified using grid coordinates and forced using a parameterized JONSWAP spectrum. The functions for spectral peakedness parameters γ and nn in the JONSWAP directional spectra are given as:

$$\gamma = \begin{cases} 3.3 & if\ Tp < 11s \\ 0.5Tp - 1.5\ if\ Tp \geq 11s \end{cases}$$
$$nn = \begin{cases} 4 & if\ Tp < 11s \\ 2.5Tp - 20\ if\ Tp \geq 11s \end{cases} \quad (5.1)$$

Thus, the directional distribution is generated by multiplying the standard JONSWAP frequency spectrum by

$$\cos^{nn}(\theta - \theta_{peak})$$

(Smith and others, 2001). Wind wave spectra are broad (low γ and nn values) while swell typically have narrow distributions (high γ and nn values). The values used in the SWAN wave modeling were based on the input peak periods which ranged $4.055 \leq \gamma \leq 11.03$ and $7.775 \leq nn \leq 42.65$. To ensure that the wave directional spread is sufficiently resolved by the model, we specified directional bins giving a 4 degree directional resolution. The spectrum was discretized in frequency space with 29 bins from 0.032 to 1Hz. Wind was not included in the SWAN simulations and therefore no energy growth due to wind, or quadruplet wave-wave interactions occur in the simulations. Triad interactions, diffraction, and wave setup also were not activated in the model. We used the Janssen frictional dissipation option, which has a default friction coefficient of 0.067 m^2/s^3. No model calibration was performed in this study, although several numerical experiments were implemented to test various assumptions in the wave modeling (e.g., not to use winds).

5.3.1 Wind effects

The decision not to model the effect of winds on wave growth over the continental shelf in our Coos County study (Allan and others, 2012) was based on two observations:

1. To develop our combined wave time series described previously, we performed a "statistical" wave transformation between buoy 46002 and the buoys at the edge of the continental shelf and found that in general the wave heights during storm events decreased even with hundreds of kilometers of additional fetch. Without understanding the details of this phenomenon (e.g., white capping versus wind wave growth) and with no data for calibration we felt that attempting to model wind growth would add to the uncertainty of our input wave conditions.
2. We also have previous experience with SWAN wave modeling in the region (U.S. Pacific Northwest) in which sensitivity runs including wind were performed with only minor impact on results (Ruggiero and others, 2010a).

To test the validity of the assumptions made in our original Coos County study, several wave modeling experiments were performed in order to specifically examine the role of additional wind wave development over the shelf. The basic question that was addressed is: How much do wind fields result in wave growth between the location of the GROW stations that were purchased - an off-shelf location roughly equivalent to the offshore extent of the Tillamook (46089) buoy shown in **Figure 4-1** and the inner shelf. The latter was defined as the 100 m (300 ft) isobath. To address this question, hindcast waves were modeled for the months of January and February (i.e., peak of the winter season) and for two representative years (2006 and 2010). The wave modeling was accomplished by running a regional Eastern North Pacific (ENP) model and a 3 arc-min grid for the Oregon coast, with the outer boundary coinciding with the Tillamook buoy station (**Figure 5-14**). The model runs were forced by analyzed Global Forecast System winds with a temporal resolution of 6 hours and a spatial resolution of 1 arc-degree. A similar run was undertaken without winds over the same 3 arc-min grid, just propagating the boundary conditions. Hindcast wave data were obtained from selected points across the shelf at contour depths of 500, 400, 300, 200, and 100 m along a cross-shore transects from the offshore GROW station (A and B in **Figure 5-14**).

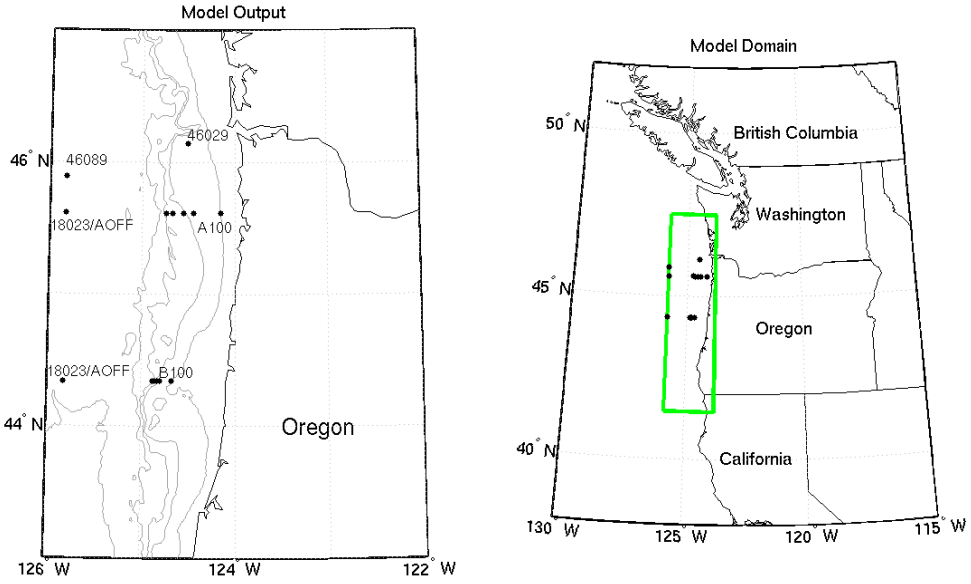

Figure 5-14. Left) Map showing the locations of the northern Oregon coast buoys, and transect lines (A and B), and Right) model domain.

Results from the model runs (with and without winds) are presented in **Figure 5-15** and **Figure 5-16**. Modeled and measured waves for two NDBC buoys (46089 and 46029) are included for comparative purposes (**Figure 5-17** and **Figure 5-18**). In general, our experiments indicated that although the addition of wind sometimes changed the timing of the large wave events, producing at times a relatively large % error for part of the "wave hydrograph," the peaks of the wave events showed very little difference between cases where wind was included or excluded (**Figure 5-15** and **Figure 5-16**). Furthermore, in the majority of cases, the differences in the derived wave heights between model runs including (excluding) wind (no wind) were on the whole minor. This finding was also observed in the derived peak wave periods, which appear to be virtually identical in all the plots. Of greater concern in these model tests, are the occasional large differences between the modeled runs (irrespective of whether wind/no wind is applied) and the actual measurements derived from NDBC wave buoys (**Figure 5-17** and **Figure 5-18**), as well as the GROW data derived for station 18023. These latter findings will be explored in more detail later in this section.

These experiments support our decision to not include wind growth in our model runs, and therefore quadruplet wave-wave interactions were also not incorporated in the simulations. Further, wave setup is not included in the simulations because we extract the transformed wave parameters at the 20-m depth contour and use the Stockdon and others (2006) empirical model to compute wave runup (which incorporates setup) along the coast.

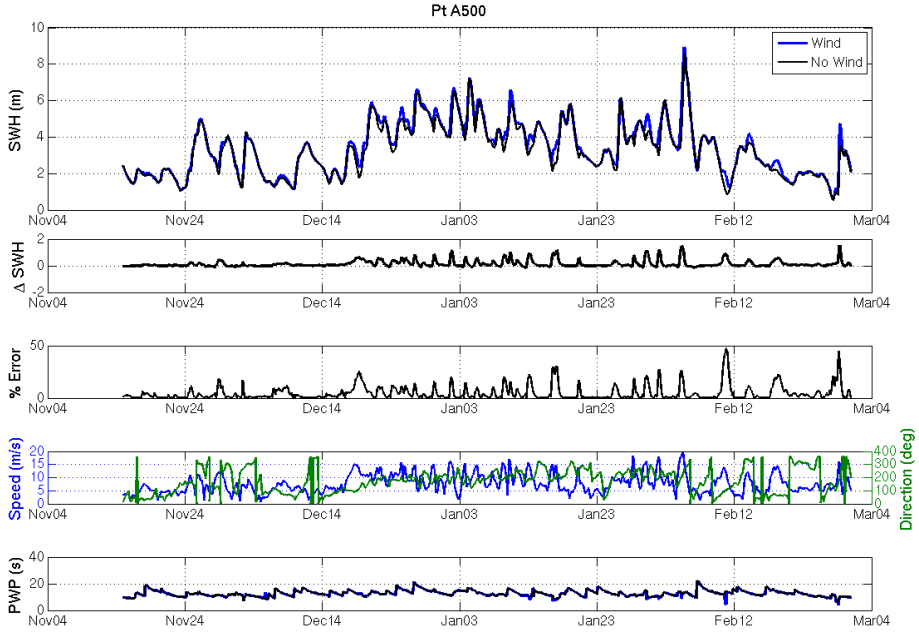

Figure 5-15. Model-model comparison at 500-m depth on transect A for the 2006 simulation.

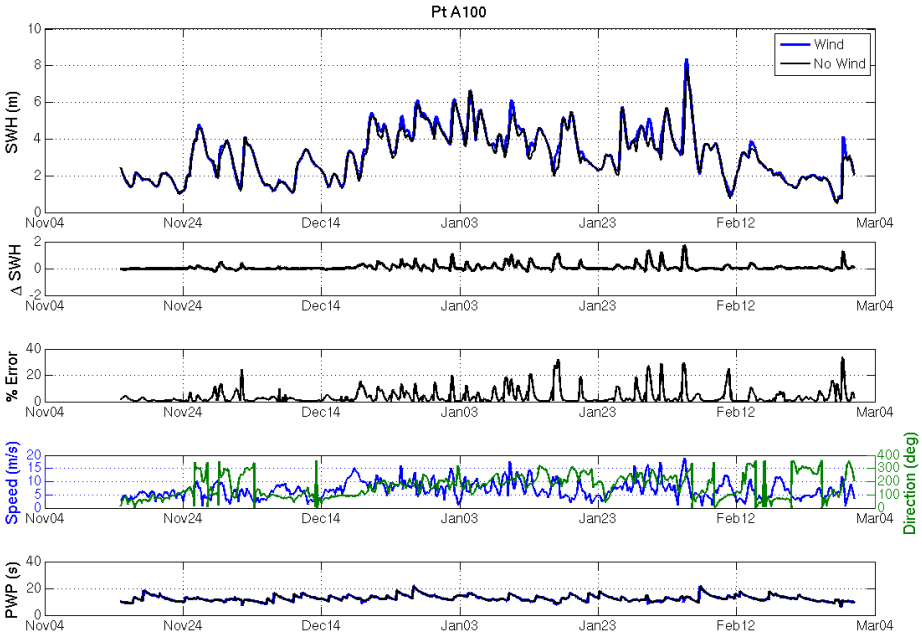

Figure 5-16. Model-model comparison at 100-m depth on transect A for the 2006 simulation.

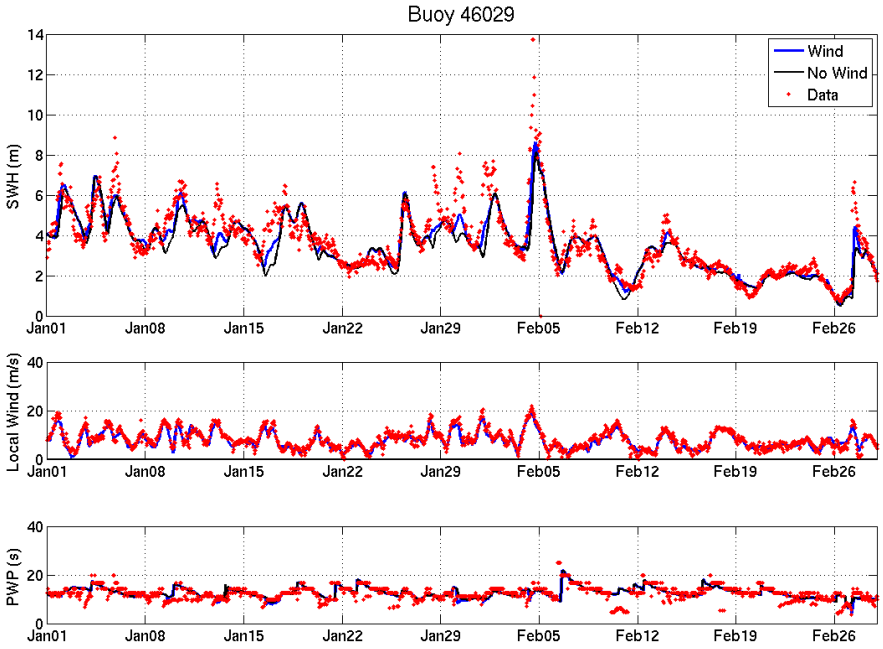

Figure 5-17. Model data comparison at NDBC buoy #46029 for the 2006 simulations.

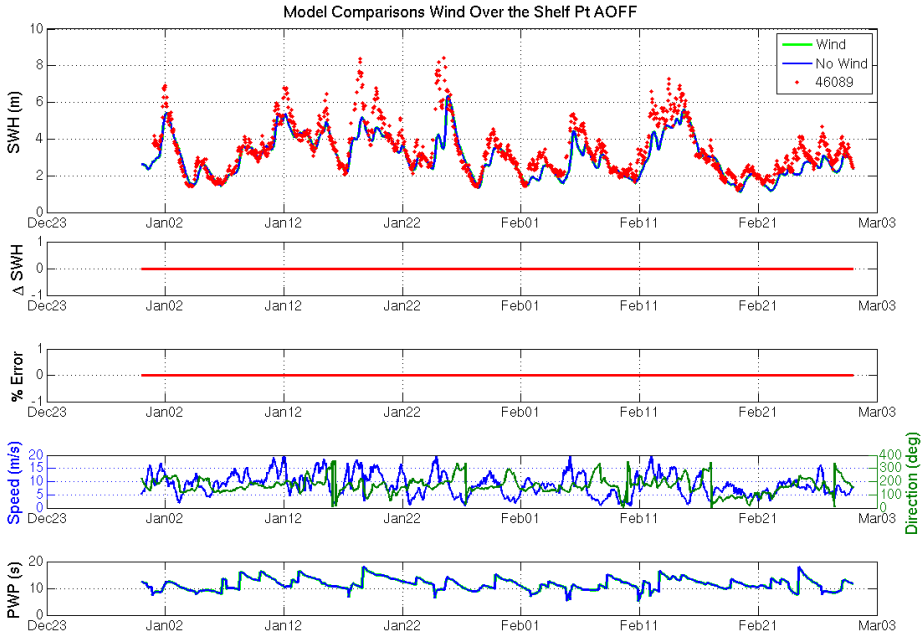

Figure 5-18. Model data comparison at Station Aoff (GROW station location) versus 46089 for the 2010 simulations.

5.3.2 Frictional and whitecapping dissipation of the wave energies

Additional testing was undertaken to explore the effect of not including friction and whitecapping. **Figure 5-19** and **Figure 5-20** provide two test-case conditions, associated with a significant wave height of 10 m and peak period of 20 s, with the waves approaching from a direction of 285 degrees (NW), while the second case is for a significant wave height of 14 m, peak period of 14 s, with the waves approaching from a direction of 270 degrees (W). **Figure 5-19** indicates that for this particular condition, the modeled results are relatively similar until immediately prior to wave breaking, where significant differences arise. However, as the significant wave height increases (**Figure 5-20**) the effect of excluding bottom friction and whitecapping becomes considerably larger. The exclusion of these processes results in an overestimation of wave heights prior to breaking. Therefore, we have chosen to include frictional dissipation and dissipation due to whitecapping in our modeling.

5.3.3 Look up table development

Having demonstrated that winds have little impact in terms of additional wave development across the continental shelf of Oregon, our next goal was to develop an efficient methodology that could be used to minimize the total number of SWAN runs needed to perform the actual wave modeling and transformations, while ensuring that we resolve the influence of varying parameters on the wave transformations. To do this we discretized the significant wave height (H_s), peak period (T_p), wave direction (D_p), and water level (WL) time series.

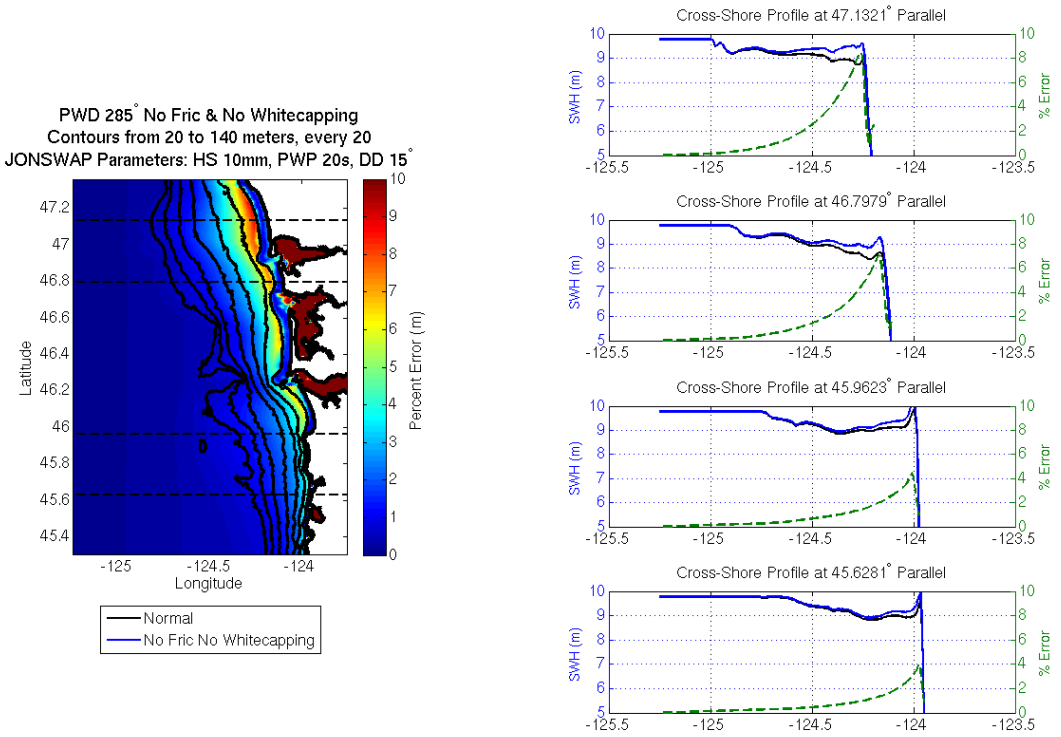

Figure 5-19. The impact of ignoring bottom frictional dissipation and dissipation due to whitecapping for a 10-m significant wave height with a peak period of 20 s approaching from a direction of 285 degrees.

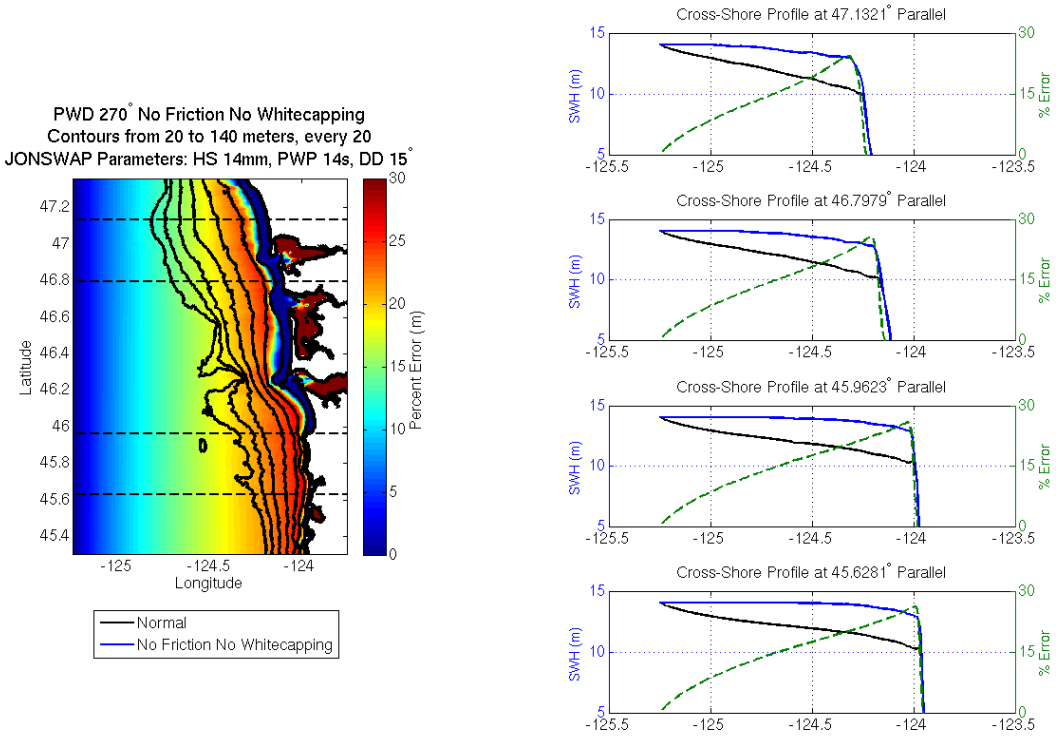

Figure 5-20. The impact of ignoring bottom frictional dissipation and dissipation due to whitecapping for a 14-m significant wave height with a peak period of 14 s approaching from a direction of 270 degrees.

For the direction bins (D_p), the bin widths were made approximately proportional to the probability distribution function of the GROW time series (and the synthesized wave climate time series). In application of this approach in our Clatsop County study, 10 directional bins were created that have approximately an equal probability of occurrence (**Figure 5-21**). As defined, the bin edges are: *Dp* = [170, 225, 240, 251, 260, 268, 277, 288, 304, 331, 370] and were subsequently refined in SWAN to *Dp* = [170, 225, 240, 250, 260, 270, 280, 290, 305, 330, 370], resulting in 11 direction cases for our SWAN runs. At the bin edges, linear interpolation is used to derive the wave parameters. From initial sensitivity runs undertaken as part of our Clatsop County study, we have determined that these bin widths are more than adequate. **Figure 5-22** shows the result of interpolating over a 20-degree bin spacing.

For the purposes of the Lincoln County work, we further refined our original approach to include an additional three directional bins. This was accomplished by refining the spread of the bins to better reflect the observed conditions offshore Lincoln County. The final bin edges are defined as: D_p = [175, 205, 225, 240, 250, 260, 270, 280, 290, 300, 315, 335, 365].

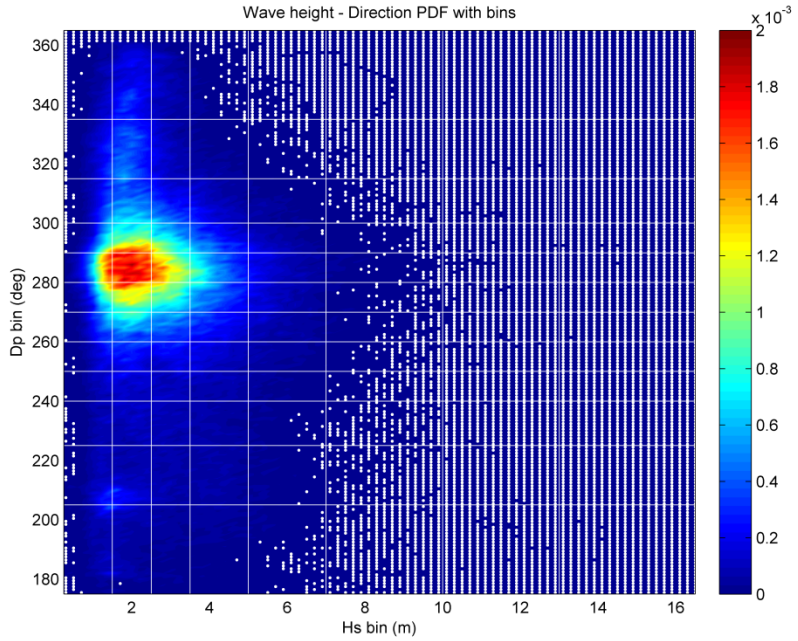

Figure 5-21. Joint probability of wave height and dominant direction derived from the GROW time series. Overlaid in white are the wave height and direction bins for use in the wave modeling on the Lincoln coast.

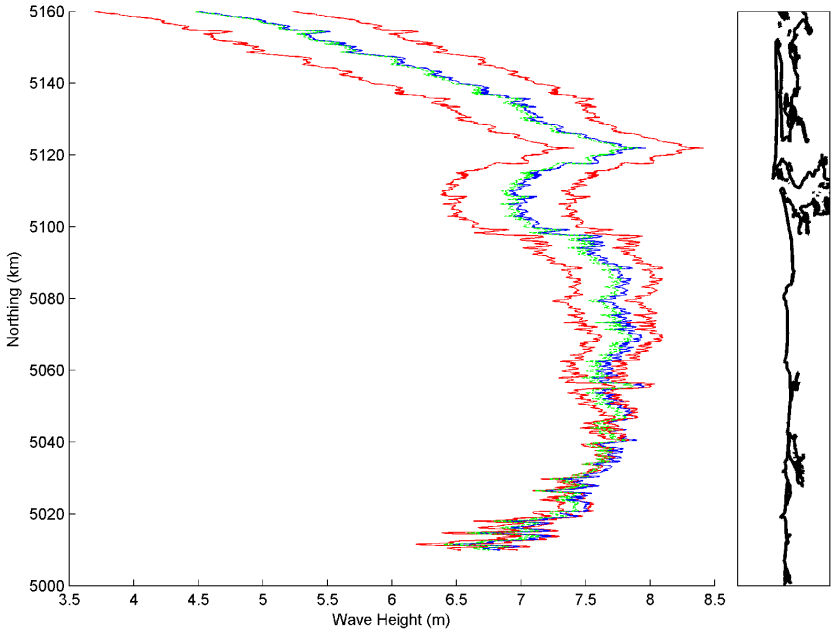

Figure 5-22. SWAN wave modeling and calculated alongshore wave variability using the look-up table approach. The left red line represents the alongshore variable wave height at the 20-m depth contour for an incident angle of 240 degrees (H_s = 10, T_p = 15 s) and the right red line is for an angle of 260 degrees. The blue line is the wave height for an angle of 250 degrees as modeled in SWAN while the green line is the linearly interpolated wave heights using the look-up table. Note that this is a preliminary SWAN model run, meant for testing the interpolation scheme, and the lateral boundary conditions are not dealt with in the same manner as in our production SWAN runs.

For the significant wave heights bins, we identified the following deepwater significant wave heights for inclusion in SWAN: H_s = [0.25; 1.5;2.5; 3.5; 5;7; 10;13; 16.5], which gives us 9 cases. Based on our sensitivity tests, we found that a bin width of 3 m for large waves is sufficient for resolving the linearly interpolated wave conditions (**Figure 5-23**). In the case of the deepwater peak periods, our analyses identified the following period bins for inclusion in SWAN: T_p = [2;4; 6;9; 11; 13; 15; 17; 20; 23; 26], which provides a total of 11 additional cases. Based on our sensitivity tests, we found that the linear interpolation approach for wave period is not quite as good as for direction and wave height. Because wave period affects breaking, shoaling, and whitecapping, there is significant variability in the wave transformations as a function of wave period. For our sensitivity run of H_s=10m, and D_p = 260 degrees, **Figure 5-24** illustrates the impact of linear interpolation. However, for the most part in our parameter space we will have interpolation errors only around 10%. In this particular example the maximum error is only approximately 4 %.

Figure 5-25 presents the joint probability of wave height and peak period from the GROW time series. The white dots represent bin centers, from a much smaller mesh, in which this combination of H_s and T_p does not exist in the GROW time series. The red line represents the theoretical wave steepness limit below which waves are non-physical. We can use this information to reduce the overall matrix of model runs.

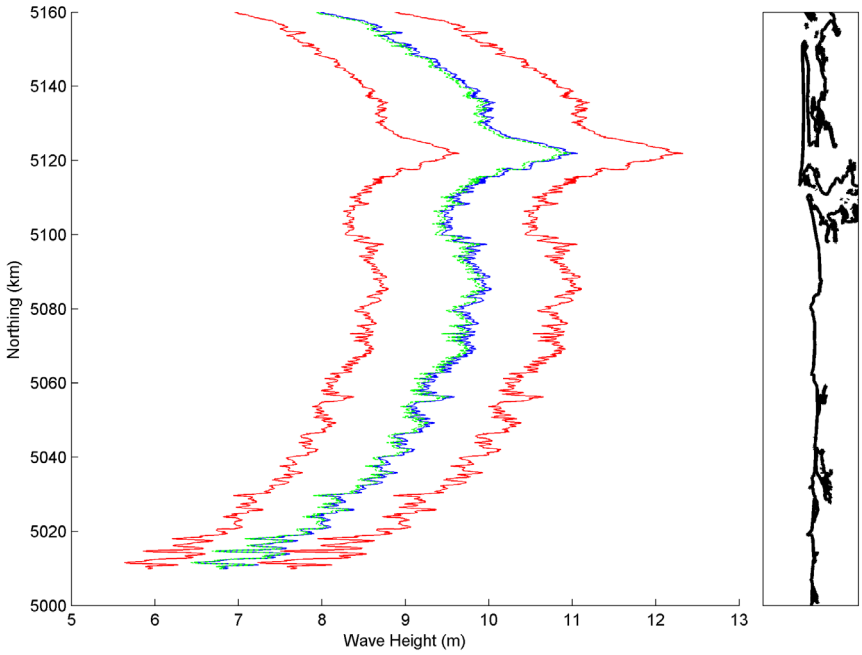

Figure 5-23. SWAN wave modeling and calculated alongshore wave variability using the look-up table approach for an 11-m and 15-m wave. In this example the red lines are the alongshore varying wave height for an 11-m and 15-m incident wave height in 20 m. The blue line is the modeled transformed 13 m wave height while the green represents a linear interpolation between the 11- and 15-m results.

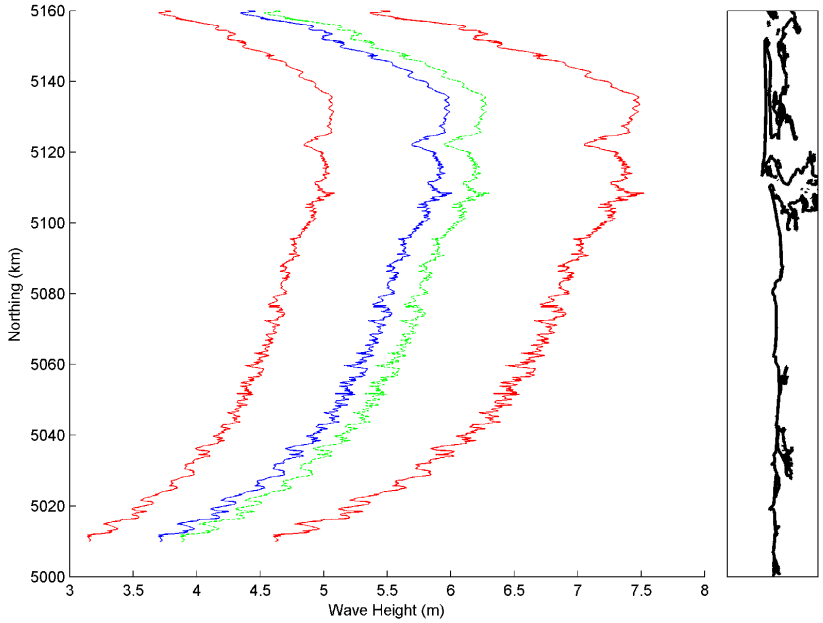

Figure 5-24. SWAN wave modeling and calculated alongshore wave variability using the look-up table approach for a 10-m wave. In this example the red lines are the alongshore varying wave height for a 10-m wave arriving from 260 degrees for 20 s and 24 s. The blue line is the modeled wave height for 22 s and the green line represents a linear interpolation.

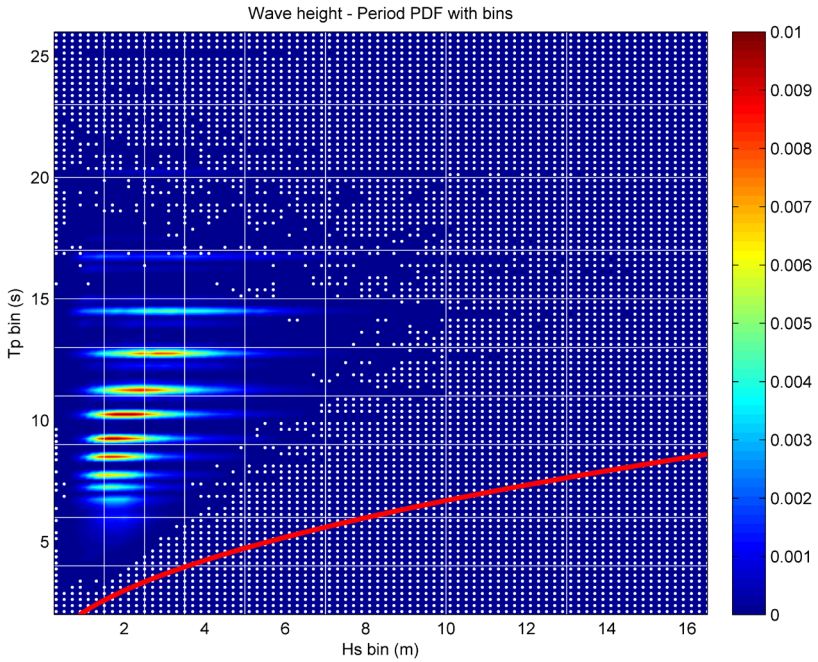

Figure 5-25. Joint probability of wave height and peak period from the GROW time series. The white dots represent bin centers, from a much smaller mesh, in which this combination of H_s and T_p does not exist in the GROW time series. The red line represents the theoretical wave steepness limit below which waves are non-physical.

Figure 5-26 is the joint probability of peak period and dominant wave height shown here for completeness. Finally, we illustrate our bin choice on the individual parameter PDFs in **Figure 5-27** (buoy data).

In summary, the lookup tables were generated using all wave parameter cases and two contrasting water levels. Our sensitivity tests indicated that varying water levels have a negligible impact on the model and linearly transformed waves. The following matrix of SWAN runs is considered for lookup table development for transforming waves offshore from Lincoln County:

D_p = [175, 205, 225, 240, 250, 260, 270, 280, 290, 300, 315, 335, 365] — 11 cases
H_s = [0.25, 1.5, 2.5, 3.5, 5, 7, 10, 13, 16.5] — 9 cases
T_p = [2, 4, 6, 9, 11, 13, 15, 17, 20, 23, 26] — 11 cases
WL = [-1.5, 4.5] — 2 cases

In total, this equates to 2,574 model cases that can be used for linearly interpolating the waves from a time series of data. However, **Figure 5-25** indicates that several H_s–T_p combinations are physically not realistic. Multiplying these bins by the D_p and WL bins means that we can eliminate 390 bins for a new total of only 2,184 model runs.

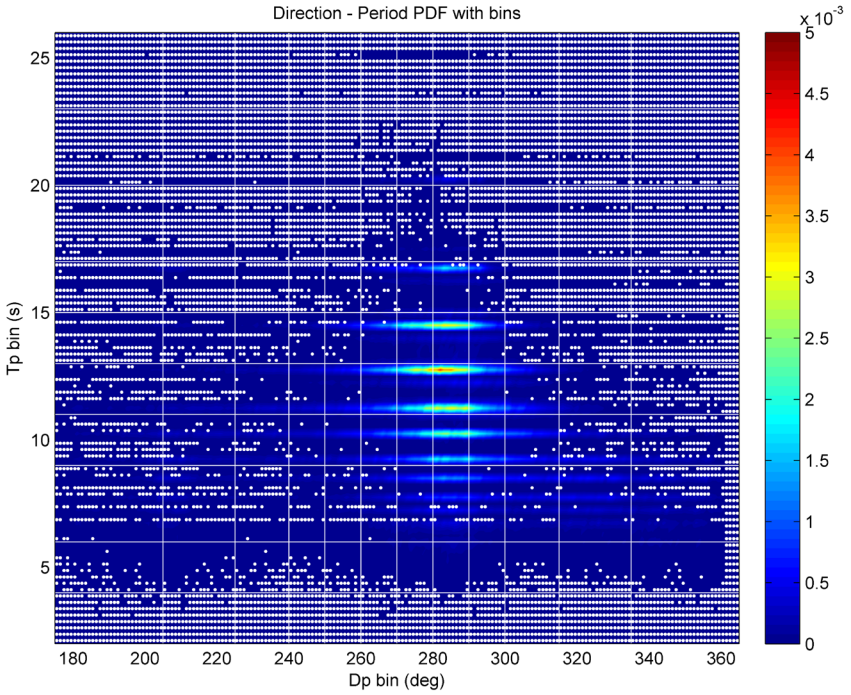

Figure 5-26. Joint probability of dominant direction and peak period from the GROW time series. The white dots represent bin centers, from a much smaller mesh, in which this combination of D_p and T_p does not exist in the GROW time series. The white lines depict the boundaries of the bin edges.

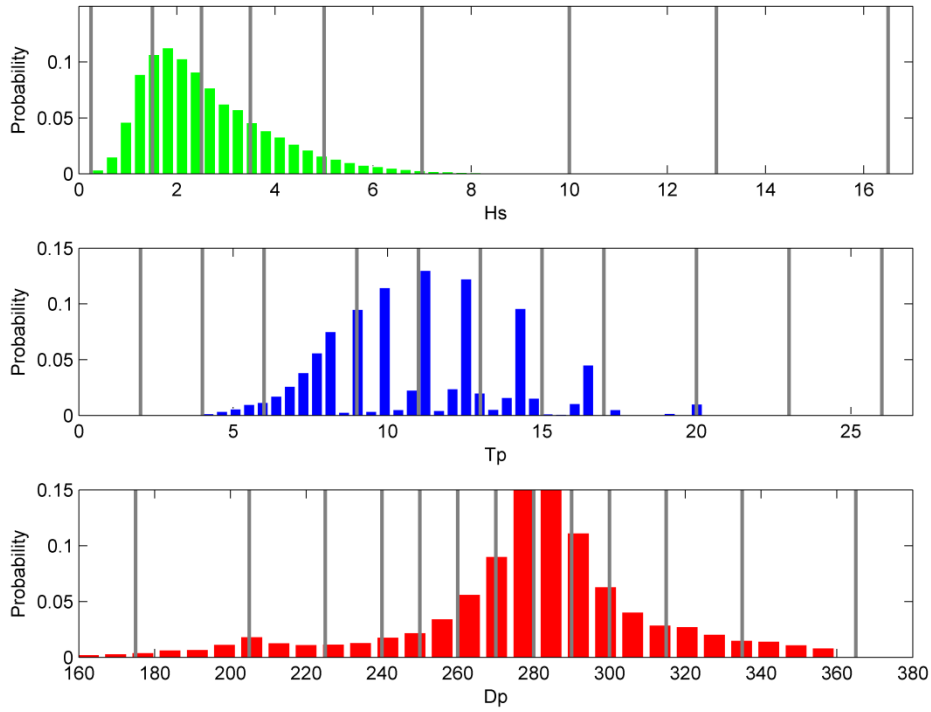

Figure 5-27. Individual parameter PDFs and bin edges using the combined buoy wave time series.

5.4 Summary of SWAN results

Significant alongshore variability is apparent in many of the conditions examined with SWAN (**Figure 5-28**). Differences on the order of 3 m in significant wave height along the 20-m isobaths are not uncommon in Lincoln County. To calculate the wave runup along the County's shoreline we subsequently extracted the wave characteristics along the 20-m contour, or the seaward most location where the wave breaking parameter equaled 0.4, throughout the model domain (right panel **Figure 5-28**). Because all of the parametric runup models used in this study rely on information on the deep-water equivalent wave height and peak periods as inputs, we then computed the linear wave theory shoaling coefficient and back shoaled our transformed waves to deep-water. These transformed deep-water equivalent waves were then used to calculate the wave runup and generate the TWL conditions used in the subsequent extreme value analysis.

To confirm that our approach of interpolating wave transformations using lookup tables yields acceptable results, we ran several additional SWAN runs that were not part of our original matrix. These additional runs extended across a range of conditions, including extreme events capable of forcing high water levels at the coast. We then compare the results from using the lookup tables to these additional direct SWAN computations at the 20 m contour location. **Figure 5-29** to **Figure 5-31** show a sample of these results for wave heights, peak periods, and directions respectively, for a SWAN run driven with an offshore boundary condition of H_s = 11.5, T_p = 18.5, D_p = 320, and a water level of 4.5-m NAVD88. In all cases, the percentage error between the lookup table and direct computation is low, averaging well less than 5%. In only a few locations, near model boundaries or inlets, are the errors significant. None of the transects analyzed in detail for extreme flooding later in this report are near those problem locations.

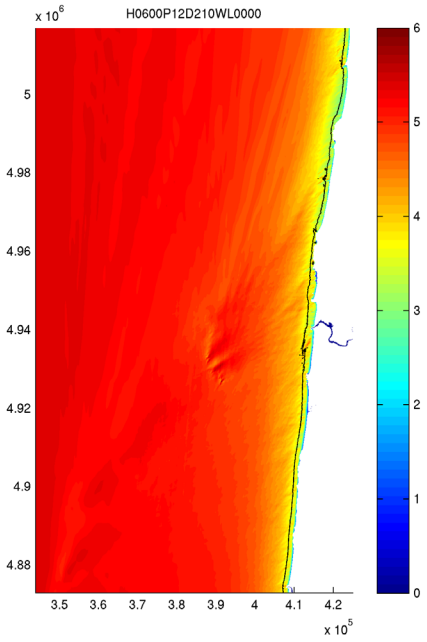

Figure 5-28. Example SWAN simulation offshore from Lincoln County (offshore significant wave height 6 m, peak wave period 12 s, and peak wave direction of 210 degrees). Significant wave height in the modeling domain is shown in colors. Dissipation processes generate differences in the inner shelf wave height.

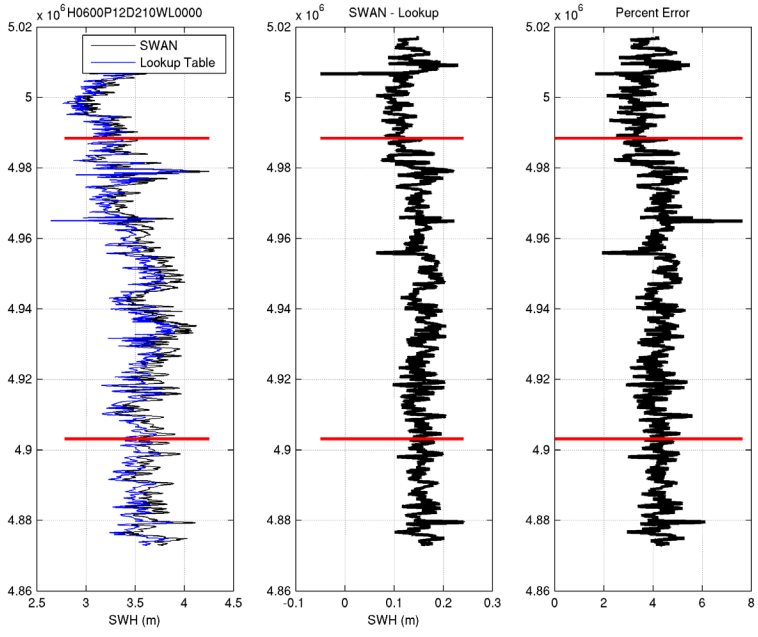

Figure 5-29. Comparison of alongshore varying wave height at the 20-m contour extracted from the lookup tables (blue line) and from a direct SWAN computation (black line) with an offshore boundary condition characterized as H_s = 6 m, T_p = 12, D_p = 210, and a water level of 0-m NAVD88. Solid red line denotes Lincoln County boundary.

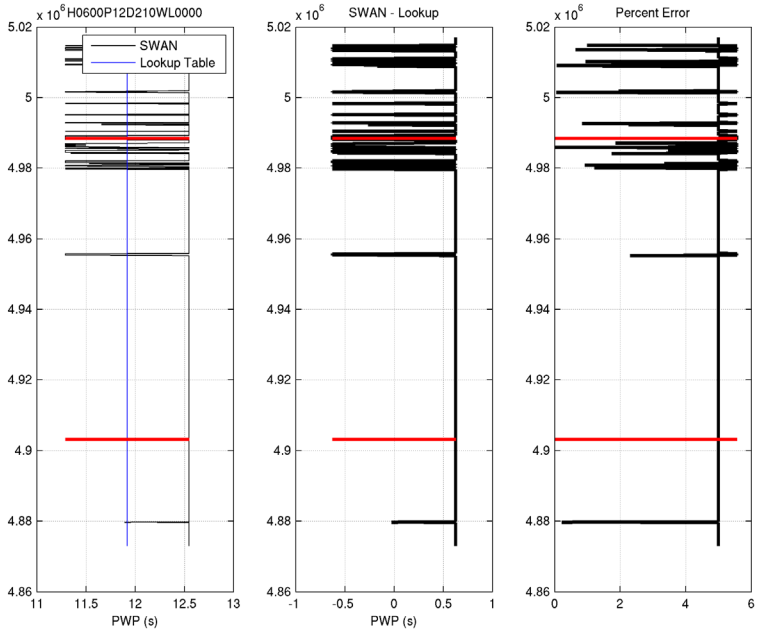

Figure 5-30. Comparison of alongshore varying wave period at the 20-m contour extracted from the lookup tables (blue line) and from a direct SWAN computation (black line) with an offshore boundary condition characterized as H_s = 6 m, T_p = 12 s, D_p = 320, and a water level of 0m NAVD88. Solid red line denotes Lincoln County boundary.

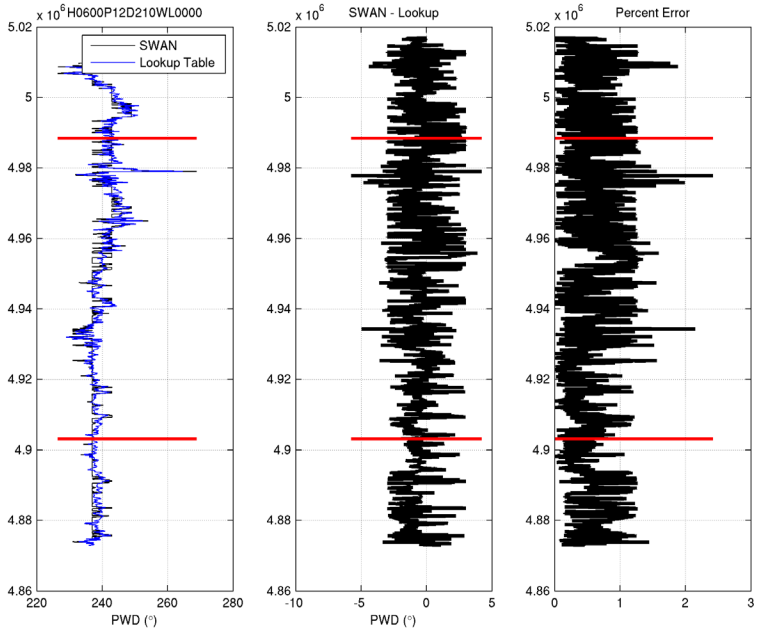

Figure 5-31. Comparison of alongshore varying wave direction at the 20-m contour extracted from the lookup tables (blue line) and from a direct SWAN computation (black line) with an offshore boundary condition characterized as H_s = 6 m, T_p = 12 s, D_p = 320, and a water level of 0m NAVD88. Solid red line denotes Lincoln County boundary.

6.0 WAVE RUNUP AND OVERTOPPING

Wave runup is the culmination of the wave breaking process whereby the swash of the wave above the still water level is able to run up the beach face, where it may encounter a dune, structure or bluff, potentially resulting in the erosion, or overtopping and flooding of adjacent land (**Figure 6-1**). Runup, *R*, or wave setup plus swash, is generally defined as the time-varying location of the intersection between the ocean and the beach, and as summarized is a function of several key parameters. These include the deepwater wave height (H_o or H_s), peak spectral wave period (T_p) and the wave length (L_o) (specifically the wave steepness, H_o/L_o), and through a surf similarity parameter called the Iribarren number,

$$\xi_o = \frac{\beta}{\sqrt{H_o/L_o}},$$

which accounts for the slope (β) of a beach or an engineering structure, as well as the steepness of the wave.

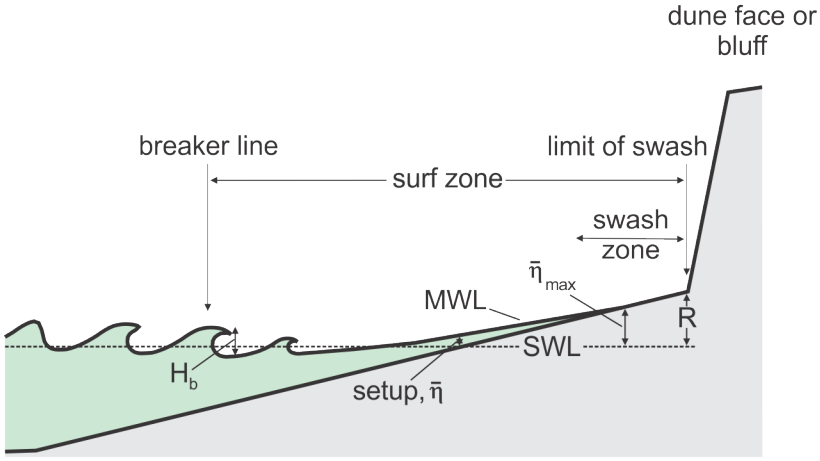

Figure 6-1. Conceptual model showing the components of wave runup associated with incident waves (modified from Hedges and Mase, 2004).

The total runup, *R*, produced by waves includes three main components:

- wave setup, $\bar{\eta}$;
- a dynamic component to the still water level, $\hat{\eta}$; and
- incident wave swash, S_{inc}.

$$R = \bar{\eta} + \hat{\eta} + S_{inc} \qquad (6.1)$$

Along the Pacific Northwest Coast of Oregon and Washington, the dynamic component of still water level, $\hat{\eta}$, has been demonstrated to be a major component of the total wave runup due to relatively high contributions from infragravity energy (Ruggiero and others, 2004). This process occurs due to a transfer of energy from the incident wind-generated waves to the longer-period infragravity wave energy, the division being placed at ~20-s periods. On the dissipative beaches of the Oregon coast, it is the infragravity energy that increases swash runup levels during major storms that is ultimately responsible for erosion and overwash events. The combination of these processes produces "sneaker waves," yielding the most extreme swash runup levels.

A variety of models have been proposed for calculating wave runup on beaches (Ruggiero and others, 2001; Hedges and Mase, 2004; Northwest Hydraulic

Consultants, 2005; Stockdon and others, 2006). Here we explore two approaches available for runup calculations along Lincoln County, Oregon. These included the runup model developed by Stockdon and others (2006) and the direct integration method (DIM) described in NHC (2005).

6.1 Runup Models for Beaches

6.1.1 Stockdon runup model

For sandy beaches, Stockdon and others (2006) developed an empirical model based on analyses of 10 experimental runup data sets obtained from a wide variety of beach and wave conditions, including data from Oregon (Ruggiero and others, 2004), and by separately parameterizing the individual runup processes: setup and swash. Stockdon and others (2006) proposed the following general relationship for the elevation of the 2% exceedance elevation of swash maxima, R_2, for any data run:

$$R_2 = 1.1[\overline{\eta} + \frac{S}{2}] \quad (6.2)$$

where:

$$S = \sqrt{(S_{inc})^2 + (\widehat{\eta})^2} \quad (6.3)$$

and:

$$\overline{\eta}, S_{inc}, \widehat{\eta} = f(H_o, T_o, \beta)$$

where β is the slope of the beach face, and S reflects both the dynamic, $\widehat{\eta}$, and incident swash, S_{inc}, components. The 1.1 coefficient value was determined because the swash level assumes a slightly non-Gaussian distribution. The final parameterized runup equation is:

$$R_{2\%} = 1.1\left(0.35\tan\beta\,(H_oL_o)^{\frac{1}{2}} + \frac{[H_oL_o(0.563\tan\beta^2 + 0.004)]^{\frac{1}{2}}}{2}\right) \quad (6.4)$$

which may be applied to natural sandy beaches over a wide range of morphodynamic conditions. In developing equation 6.4, Stockdon and others (2006) defined the slope of the beach as the average slope over a region ±2σ around the wave setup, $\overline{\eta}$, where σ is the standard deviation of the continuous water level record, η(t). Simply put, the setup reflects the height of the mean-water level (MWL) excursion above the SWL, such that the slope is determined to span the region around this MWL. For Lincoln County, the slope of the beach was determined by fitting a linear regression through those data points spanning the region located between 2 to 4 m.

Combining equation 6.4 with the measured water level at tide gauges produces the total water level, TWL at the shore, important for determining the erosion or flood risk potential. Given that equation 6.4 has been derived from quantitative runup measurements spanning a range of beach slopes (beach slopes ranged from 0.01 to 0.11 and Iribarren numbers [**ξ**], ranged from 0.1 [fully dissipative conditions] to ~2.2 [reflective conditions], Table 1 of Stockdon and others [2006]), the model is valid for the range of slopes and conditions observed along the Lincoln County coastline and elsewhere on the Oregon coast.

6.1.2 Direct Integration method—beaches

The FEMA coastal flood mapping guidelines (NHC, 2005) for the U.S West Coast presents an alternative method for calculating runup. According to NHC (2005), the direct integration method (DIM) approach allows for the wave and bathymetric characteristics to be taken into consideration, specifically the spectral shape of the waves and the actual bathymetry can be represented. Here we review the parameterized set of

runup equations that may be used to calculate runup on beaches. The equations are based on a parameterized JONSWAP spectra and uniform beach slopes.

Similar to equation 6.1, the runup of waves using DIM can be defined according to its three components that include the wave setup, $\overline{\eta}$, a dynamic nent, $\widehat{\eta}$, and the incident band swash, S_{inc}. Wave setup can be calculated using:

$$\overline{\eta} = 4.0\, F_H F_T F_{Gamma} F_{slope} \tag{6.5}$$

while the root mean square (rms) of the dynamic component, $\widehat{\eta}_{rms}$, may be estimated using:

$$\widehat{\eta}_{rms} = 2.7\, G_H G_T G_{Gamma} G_{slope} \tag{6.6}$$

where the units of $\overline{\eta}$ and $\widehat{\eta}_{rms}$ are in *feet* and the factors (F) are for the wave height (F_H and G_H), wave period (F_T and G_T), JONSWAP spectrum narrowness (F_{Gamma} and G_{Gamma}), and the nearshore slope (F_{slope} and G_{slope}). These factors are summarized as a series of simple equations in Table D.4.5-1 (NHC, 2005). For the purposes of defining an average slope, NHC recommended that the nearshore slope be based on the region between the runup limit and twice the wave breaking depth, h_b, where:

$$h_b = H_b / k \tag{6.7}$$

and

$$H_b = 0.39 g^{0.2} \left(T_p H_o^2\right)^{0.4} \tag{6.8}$$

where H_b is the breaker height calculated using equation 6.8 (Komar, 1998), g is acceleration due to gravity (9.81 m/s), and for the purposes here k (breaker depth index) can be taken to be 0.78. Thus, one important distinction between the DIM and Stockdon methods for calculating runup, is the method used to define the beach slope; the former accounts for a larger portion of the nearshore slope, while the latter is based on the slope calculated around the mid beach-face.

To derive the statistics of the oscillating wave setup and the incident swash components, the recommended approach is to base the calculations on the standard deviations (σ) of each component. The standard deviation of the incident wave oscillation (σ_2) on natural beaches may be calculated from:

$$\sigma_2 = 0.3 \xi_o H_o \tag{6.9}$$

Because the standard deviation of the wave setup fluctuations (σ_1) is proportional to equation 6.6, the total oscillating component of the dynamic portion of the wave runup can be derived from:

$$\widehat{\eta_T} = 2.0 \sqrt{\sigma_1^2 + \sigma_2^2} \tag{6.10}$$

Combining the results of equations 6.10 and 6.5 yields the 2% wave runup, and when combined with the tidal component results in the total water level, TWL.

6.1.3 Comparison between the Stockdon and DIM runup calculations

Fundamentally, the wave runup model proposed by Stockdon and others (2006) and the DIM method described in NHC (2005) are similar, because both models account for the three components of runup described in equation 6.1. Here we examine the runup results derived from both models based on a range of conditions characteristic of the Clatsop County shoreline (**Figure 6-2** and **Figure 6-3**). We focus on our Clatsop results, because this is where we first tested both approaches, before settling on one approach for calculating all subsequent runup for the Oregon coast.

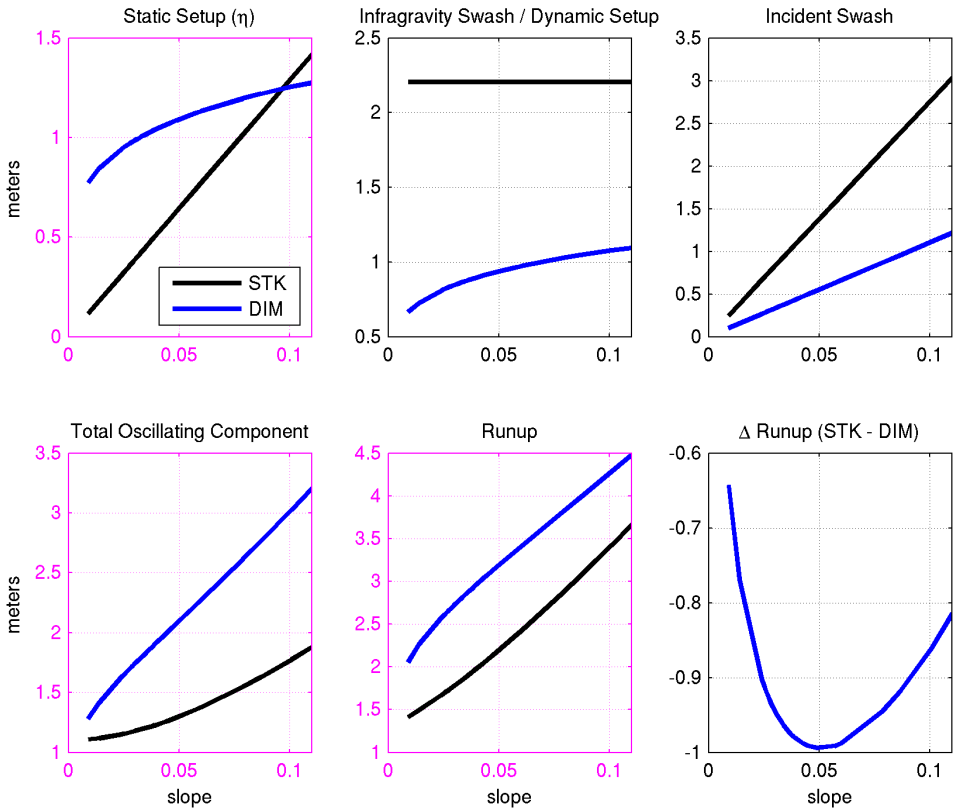

Figure 6-2. Calculated setup, swash and runup using the Stockdon and DIM runup equations. In this example, slope values are defined similarly for both methods, at a mid-beach elevation range of 2-4 m (6.6–13 ft). A 6 m (19.7 ft) significant wave height, 12-s peak wave period, and 270-degree wave direction were used to drive the models. Due to the semi-empirical nature of the equations, only the magnitudes of the subplots outlined in magenta are directly comparable (the two panels showing swash results are not directly comparable). The total oscillating component compares the results from equation 6.3 (S/2) with equation 6.10.

Figure 6-2 provides a comparison of the various calculated parameters (setup, infragravity swash, incident swash, total oscillating component, and runup) determined using the Stockdon and DIM approaches. In this example, we use the same slope defined for the mid-beach region in order to provide a direct comparison between DIM and Stockdon. Upper estimates have been truncated to tan β = 0.11, which reflects the slope limit on which Stockdon has been tested. In contrast, it is unclear the range of slope conditions on which DIM may be applied as there is no quantitative field testing of this particular formulation. As can be seen in **Figure 6-2**, although there are notable differences in the various parameterizations, the derived runup (bottom, middle plot) is similar. Nevertheless, as can be seen from the ΔR plot (bottom right), the DIM approach tends to estimate a slightly higher runup when compared to Stockdon, which in this example reaches a maximum of ~1 m (3.3 ft) for a beach slope of 0.04 to 0.05. Thus, overall, we can conclude that the two approaches are performing in a similar fashion when tested using the same slope.

Figure 6-3 presents a similar suite of comparisons under the same hydrodynamic conditions. Therefore the Stockdon and others (2006) results are identical to **Figure 6-2** in all panels. However, in this example we now account for the appropriate nearshore slope in the DIM runup calculations as defined above in

Section 6.1.2. This was originally done by computing the DIM runup components for this hydrodynamic condition using the full nearshore slope at 85 transects spread along the Clatsop County coastline (Allan and others, 2014). The DIM values are, however, plotted against the foreshore beach slopes defined for all 85 transects in order to make the comparisons with Stockdon meaningful. As can be seen in **Figure 6-3**, application of the nearshore slope significantly changes the magnitudes of all the runup components, and in particular reduces the calculated runup when compared to Stockdon for most foreshore slopes. In general, at lower slopes ($\tan\beta < 0.05$) runup calculated by DIM is slightly higher than Stockdon, which reverses at steeper slopes ($\tan\beta > 0.05$). This pattern is consistent with analyses performed by Allan and others (2012) in Coos County.

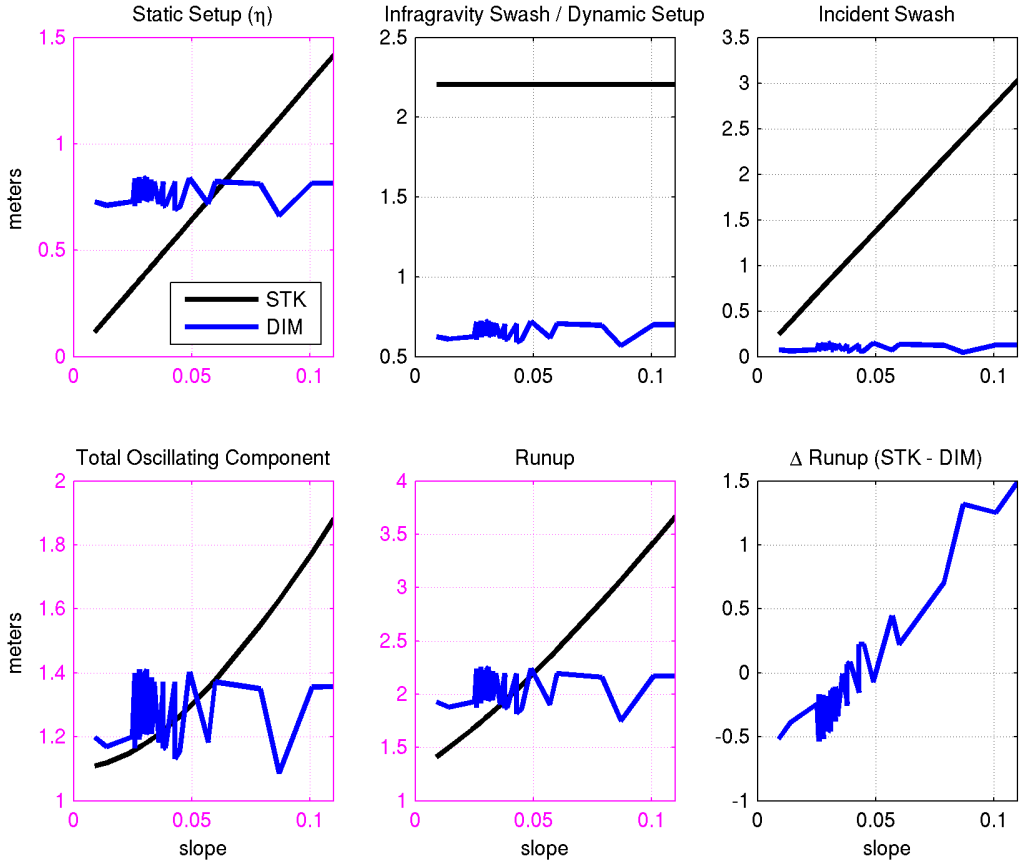

Figure 6-3. Total water level calculations using the Stockdon (foreshore slope) and DIM runup equations (nearshore slope). A 6 m (19.7 ft) significant wave height, 12-s peak wave period, and 270-degree wave direction was used to drive the models. Due to the semi-empirical nature of these equations only the magnitudes of the subplots outlined in magenta are directly comparable. The results for DIM are sorted in ascending order as a function of foreshore beach slope.

Most interesting in the comparisons shown in **Figure 6-3**, is that the DIM runup components actually do not vary as a function of the foreshore slope. The total runup (**Figure 6-3**, bottom-center) produced by DIM is relatively constant, oscillating between 1.7 and 2.3 m (5.6 and 7.5 ft). The oscillations are due primarily to the variability in the nearshore slopes, which are a function of wave height (equations 6.7-6.8). Because waves in the PNW are relatively large and upper shoreface slopes relatively shallow, the DIM runup

values are controlled by the nearshore slope with little influence from the upper beach. This lack of dependence on the foreshore is in contrast to field measurements made in Oregon (Ruggiero and others, 2004) in which runup is clearly a function of the foreshore slope. Because the Stockdon model has been extensively validated against measured runup data, including measurements on the Oregon coast (e.g., Ruggiero and others, 2001; Ruggiero and others, 2004) together with qualitative observations of runup during storms by DOGAMI staff at multiple sites along the coast, 1% extreme values of TWLs calculated for sandy beaches along the Lincoln County coast will be based primarily on the Stockdon and others (2006) model.

6.2 "Barrier" Runup Calculations

6.2.1 Introduction

According to NHC (2005), an alternate approach is recommended for use in calculating runup on steep barriers. By definition, *barriers include "steep dune features and coastal armoring structures such as revetments"* (NHC, 2005, p. D.45-10), although little guidance is offered in terms of the range of slopes to which this alternate approach would apply. Throughout this document we use the generic term *barrier* to define the range of morphological and engineering conditions where barrier runup calculations may apply. In general, runup on barriers depends not only on the height and steepness of the incident waves defined through the Iribarren number or breaker parameter ($\xi_{m-1,0}$), but also on the geometry (e.g., the slope of the barrier and/or if a berm is present), design characteristics of the structure and its permeability.

The recommended approach for calculating runup on barriers is to use the TAW (Technical Advisory Committee for Water Retaining Structures) method, which provides a mechanism for calculating the runup, adjusted for various reduction factors that include the surface roughness, the influence of a berm (if present), and effects associated with the angle of wave approach (van der Meer, 2002; Northwest Hydraulic Consultants, 2005; Pullen and others, 2007). According to NHC (2005) the TAW method is useful as it includes a wide range of conditions for calculating the wave runup (e.g., both smooth and rough slopes), and because it agrees well with both small- and large-scale experiments.

Figure 6-4 is a conceptual model of the various components required to determine the extent of runup on barriers. Of importance is first determining the 2% dynamic water level ($DWL_{2\%}$) at the barrier, which includes the combined effects of the measured still water level (SWL), the wave setup ($\overline{\eta}$) and the dynamic portion ($\hat{\eta}$) of the runup (**Figure 6-4**), which is then used to establish the spectral significant wave height (H_{mo}) at the toe of the "barrier" (NHC, 2005).

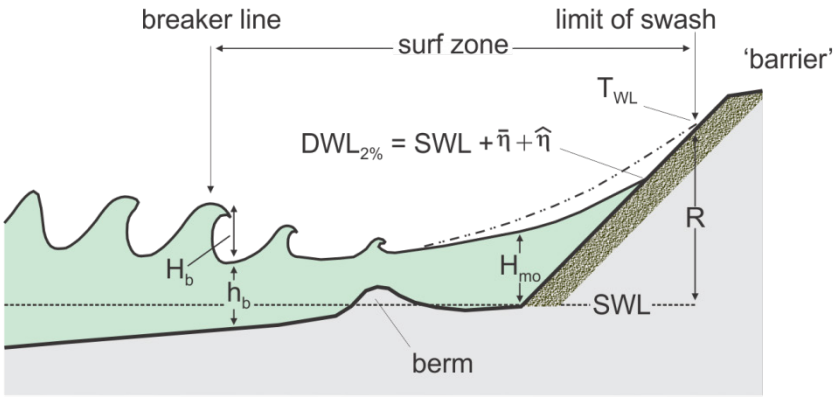

Figure 6-4. Wave runup on a beach backed by a structure or bluff (modified from NHC, 2005).

The general formula for calculating the 2% wave runup height on barriers is given in a non-dimensional form by equation 6.11:

$$\frac{R_{2\%}}{H_{mo}} = c_1 . \gamma_b . \gamma_f . \gamma_\beta . \xi_{m-1,0} \qquad (6.11)$$

with a maximum of:

$$\frac{R_{2\%}}{H_{mo}} = \gamma_f . \gamma_\beta \left(c_2 - \frac{c_3}{\sqrt{\xi_{m-1,0}}} \right)$$

where:
$R_{2\%}$ = wave runup height exceeded by 2% of the incoming waves
H_{mo} = spectral significant wave height at the structure toe
c_1, c_2, and c_3 = empirical coefficients with:
γ_b = influence factor for a berm (if present)
γ_f = influence factor for roughness element of slope
γ_β = influence factor for oblique wave attack
$\xi_{m-1,0}$ = breaker parameter

$$\left(tan\beta / \left(H_{mo} / L_{m-1,0} \right)^{0.5} \right)$$

tan β = slope of the "barrier,"
$L_{m-1,0}$ = the deepwater wave length $\left(g T_{m-1,0}^2 / 2\pi \right)$,
$T_{m-1,0}$ can be calculated from $T_p/1.1$, where T_p is the peak spectral wave period.

Substituting the empirical coefficients derived from wave tank experiments and incorporating a 5% upper exceedance limit into the general equations of 6.11 (van der Meer, 2002; Pullen and others, 2007), runup on barriers may be calculating using:

$$R_{2\%} = H_{mo} \left(1.75 . \gamma_b . \gamma_f . \gamma_\beta . \xi_{m-1,0} \right), \qquad (6.12)$$

$$where\ 0 < \gamma_b . \xi_{m-1,0} < 1.8$$

with a maximum of:

$$R_{2\%} = H_{mo} \left(1.0 . \gamma_f . \gamma_\beta \left(4.3 - \frac{1.6}{\sqrt{\xi_{m-1,0}}} \right) \right), where\ \gamma_b . \xi_{m-1,0} \geq 1.8$$

There are, however, notable differences between equation 6.12 originally described by van der Meer (2002) and Pullen and others (2007) from that presented in equation D.4.5-19 in the FEMA West Coast methodology (NHC, 2005). For example, equation D.4.5-19 in the NHC report contains a slightly higher coefficient value (1.77), along with one additional reduction factor (porosity) for calculating runup when the breaker parameter is less than 1.8. Similarly, for conditions where the breaker parameter exceeds 1.8 and the maximum runup equation is used, equation D.4.5-19 in the NHC report contains two extra reduction factors (berm and porosity reduction factors) that are not included in the original solution, which potentially could have a very significant effect on the calculated runup. On the basis of these differences, we have used the original solution presented as equation 6.12 by van der Meer (2002) and Pullen and others (2007).

6.2.2 Specific procedure for calculation "barrier" runup

For those cases where the TAW method is used for determining runup on barriers (i.e., beaches backed by structures, cobble berms, and/or bluffs), we have followed the general approach laid out in section D.4.5.1.5.2 in NHC (2005), with the exception that we use Stockdon to define the $DWL_{2\%}$ (instead of DIM) at the structure toe, and TAW to calculate the incident swash on the barrier (i.e., equation 6-12). Because waves are depth limited at the barrier toe, H_{mo} may be estimated from $DWL_{2\%}$ using a breaker index of 0.78 (i.e., $H_{mo} = DWL_{2\%} * 0.78$). In performing these various derivations, $DWL_{2\%}$ was first determined using equation 6.13:

$$DWL_{2\%} = SWL + 1.1 * \left(\overline{\eta} + \frac{\widehat{\eta}}{2}\right) - D_{low} \qquad (6.13)$$

where:
SWL = measured tide

$\overline{\eta} = 0.35 * \tan\beta\sqrt{H_s * L}$ *Eqn. 10 of Stockdon and others (2006)*

$\widehat{\eta} = 0.06 * \sqrt{H_s * L}$ *Eqn. 12 of Stockdon and others (2006)*

D_{low} = the toe of the structure or bluff
$\tan\beta$ = the beach slope defined for the region between 2 and 4 m.

Having calculated $DWL_{2\%}$ and H_{mo}, the TAW runup calculation can be implemented. equation 6.12 requires information on the slope of the barrier, used in the breaker parameter ($\xi_{m\text{-}1,0}$) calculation, which can be somewhat challenging to define. This is especially the case if the morphology of the barrier exhibits a composite morphology characterized by different slopes, such that errors in estimating the slope will translate to either significant underestimation or overestimation of the runup. According to van der Meer (2002) and Pullen and others (2007), because the runup process is influenced by the change in slope from the breaking point to the maximum wave runup, the characteristic slope should be specified for this same region. On the Oregon coast, the most common composite slope example is the case where a broad, dissipative sand beach fronts a structure or bluff that is perched relatively high on the back of the beach (structure toe > ~4-5 m). In this example, the wave runup is first influenced by the sandy beach slope and finally by the slope of the structure itself. To address this type of situation, we define a "local barrier slope," as the portion of the barrier that ranges from the calculated storm TWL (calculated initially using equation 6.4) down to a lower limit defined by the wave setup plus the SWL (i.e., $(1.1 * \overline{\eta}) + SWL$). In a few cases, the TWL was found to exceed the barrier crest in which case we used the structure crest as the upper limit for defining the local slope. This process is repeated for every storm condition. Having determined the barrier slope, the TAW runup is calculated using equation 6.12 and reduced based on the appropriate site specific reduction factors.

Of the 313 primary transects established along the length of Lincoln County, 47 were characterized with having a prominent rock (shore) platform located within the intertidal zone and seaward of the bluff (**Figure 6-5**). For these sites, we calculated the wave induced setup at the seaward toe of the platform by solving for the propagation of a wave over the transect, using the wave breaking models proposed by Alsina and Baldock (2007) and Janssen and Battjes (2007). The calculated wave-induced setup was then integrated into equation 6.13, replacing the wave setup ($\overline{\eta}$) component calculated using Stockdon.

Under certain conditions, we identified events that generated extreme runup that made little physical sense. For these (rare) cases, we calculated the TAW runup using an iterative approach based on procedures outlined in the Eurotop (2007) manual. Because the maximum wave runup is the desired outcome and is unknown when initially defining the slope, the process is iterative requiring two steps. First, the breaking limit is defined as $1.5H_{mo}$ *below* the SWL, while $1.5H_{mo}$ *above* the SWL defines the upper limit of the first slope estimate (**Figure 6-6**). Having determined the first slope estimate, the TAW runup is

calculated using equation 6.12 and reduced based on the appropriate reduction factors. A second slope estimate is then performed based on the initial runup calculation, while a third iteration is not necessary based on our tests because this method converges quickly. The breaking limit is again defined as $1.5H_{mo}$ *below* the SWL, while $R_{2\%}$ *above* the SWL defines the upper limit, and the final barrier runup estimate is again calculated using equation 6.12 and reduced based on the appropriate reduction factors.

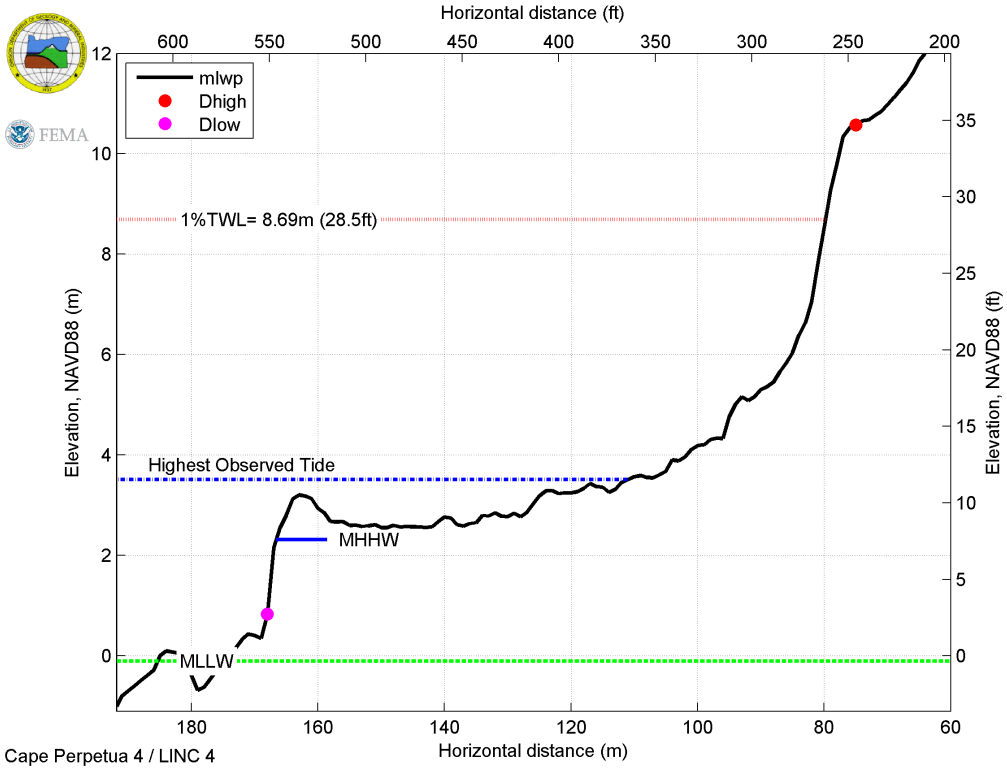

Figure 6-5. Example profile (Linc 4) where a broad rock platform fronts a bluff.

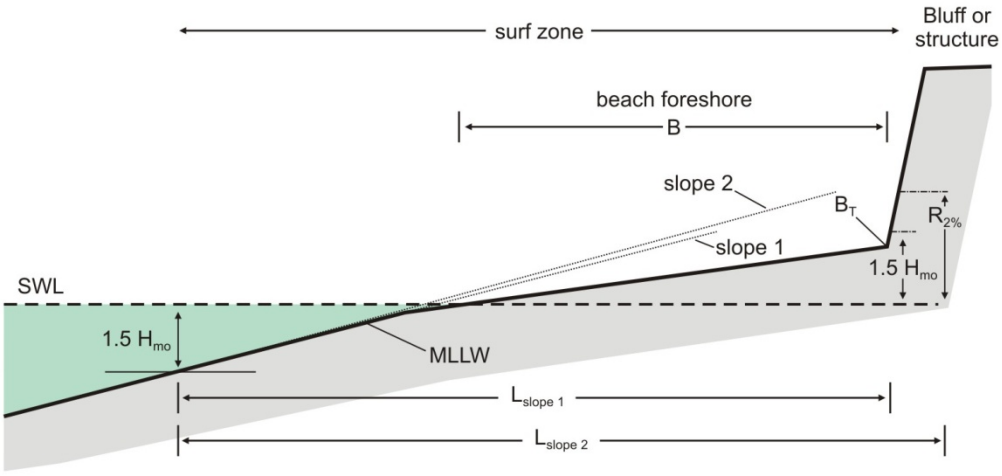

Figure 6-6. Determination of an average slope based on an iterative approach. The first estimate is initially based on 1.5H_{mo} ± SWL, while the second estimate is based on 1.5H_{mo} below the SWL and the calculated $R_{2\%}$ above the SWL that is based on the first slope estimate.

Finally, it is important to note that the runup estimates based on the "barrier" runup calculations is sensitive to the slope. Similar to our study in Coos, Clatsop, and Tillamook Counties, we identified several sites (primarily beaches backed by bluffs) along the Lincoln coast where the final TWLs calculated using TAW was unreasonably low. These few cases are entirely due to there being a very wide dissipative surf zone at these transect locations that results in very low slopes being defined. For these sites where the calculated TWLs seemed unreasonably low (relative to the morphology of the beach and observations of storm wave runup along this shore and elsewhere), we have defaulted to the TWLs calculated using the Stockdon and others model.

6.2.3 "Barrier" runup reduction factors

Table 6-1 below presents information pertaining to the suite of parameters used to define wave runup (R) and ultimately the 1% TWLs along the Lincoln County coast. In the case of bluff roughness along the Lincoln shore, we used a value of 0.6 for those situations where a bluff face was highly vegetated. These bluffs are typically located at or near their stable angle of repose and are covered with Salal plants (*Gaultheria shallon*), forming a deep, nearly impenetrable thicket. The decision to use 0.6 was based on discussions with Dr. WG McDougal (Coastal Engineer, OSU and Technical Coordinator of the North Pacific FEMA West Coast Guidelines, pers. comm., April 2010). Because much of the Lincoln County shoreline is characterized by beaches backed by near-vertical to vertical bluffs, we used a reduction factor of 0.95 because these sites were akin to a seawall situation. For those beaches backed by a significant riprap structure, we used a reduction factor of 0.55. In other cases, this was increased to 0.6 to 0.8, depending on whether the beach was backed by gravels/cobbles, a vegetated bluff face, or poor quality riprap. Wave direction (γ_β) reduction factors were determined based on the shoreline orientation at every transect site and the actual wave directions measured during each storm condition. The reduction factor was calculated using equation D.4.5-22 (NHC, 2005, p. D.4.5-13). Finally, of the 313 primary transects established along the Lincoln County coast, 47 of these are characterized with having a broad rock (basalt) platform within the intertidal zone that is akin to a protective berm. For these sites, we calculated a berm reduction factor using equation D.4.5-21 (NHC, 2005, p. D.4.5-13).

Table 6-1. Parameters used to define runup (*R*) and total water levels (TWLs) on beaches backed by dunes, structures, and bluffs.

Reach	Transect	D_{HIGH} (m)	D_{LOW} (m)	Beach Slope (tan β)	Wave Dir. (γ_β)	Rough -ness (γ_r)	Approach	Description
Cape Perpetua	LINC1	18.025	1.217	0.066	270.6	0.95	1	narrow rock platform backed by high cliffs
	LINC2	30.946	3.107	0.018	270.3	0.95	1	sand beach backed by high cliffs
	LINC3	39.090	1.902	0.021	271.8	0.95	1	broad rock platform backed by high cliffs
	LINC4	10.580	0.836	0.036	280.4	0.95	1	broad rock platform backed by high cliffs
Yachats	LINC5	12.193	2.735	0.035	282.4	0.95	1	rock platform backed by moderately high bluff
	LINC6	9.761	0.360	0.081	282.0	0.95	1	rock platform backed by moderately low bluff
	LINC7	8.538	-0.574	0.057	286.9	0.95	1	rock platform backed by moderately low bluff
	LINC8	**8.660**	**-0.821**	**0.031**	**295.7**	**0.95**	**2**	**sand beach fronts rock platform and backshore**
	LINC9	**9.057**	**4.019**	**0.006**	**270.4**	**0.95**	**1**	**sandy beach backed by bluff**
	LINC10	**12.935**	**5.284**	**0.046**	**270.1**	**0.95**	**1**	**rock platform and sandy beach backed by bluff**
	LINC11	13.090	5.605	0.110	274.5	0.55	1	sand beach backed by riprap
	LINC12	8.697	2.916	0.018	278.3	0.95	1	narrow rock platform backed by low bluff
	LINC13	8.012	3.761	0.038	282.8	0.95	1	broad rock platform backed by low bluff
	LINC14	8.944	4.202	0.023	284.7	0.95	1	sand beach fronts rock platform backed by low bluff
Waldport	LINC15	11.154	2.339	0.035	281.7	0.90	1	sand beach fronts rock platform backed by low bluff
	LINC16	**9.271**	**4.411**	**0.035**	**282.6**	**0.95**	**1**	**sand beach fronts low vertical bluff**
	LINC17	7.115	2.673	0.023	282.6	0.55	1	sand beach fronts riprap structure
	LINC18	**6.575**	**4.450**	**0.020**	**282.5**	**0.95**	**1**	**sand beach fronts low vertical bluff**
	LINC19	7.084	3.275	0.024	282.3	0.70	1	sand beach fronts riprap structure
	LINC20	6.414	3.539	0.026	282.5	0.90	1	sand beach fronts low vertical bluff
	LINC21	**6.485**	**3.797**	**0.024**	**279.9**	**0.90**	**1**	**sand beach fronts low vertical bluff**
	LINC22	**6.243**	**3.750**	**0.026**	**280.0**	**0.95**	**1**	**sand beach fronts low vertical bluff**
	LINC23	6.844	4.406	0.025	279.8	0.95	1	sand beach fronts low vertical bluff
	LINC24	6.347	3.458	0.031	279.7	0.90	1	sand beach fronts low vertical bluff
	LINC25	6.488	4.003	0.019	276.9	0.90	1	sand beach fronts riprap structure
	LINC26	**8.247**	**5.181**	**0.028**	**276.8**	**0.95**	**1**	**sand beach fronts low vertical bluff**
	LINC27	**7.369**	**5.345**	**0.033**	**279.9**	**0.95**	**1**	**sand beach fronts low vertical bluff**
	LINC28	**6.870**	**5.409**	**0.034**	**281.7**	**0.95**	**1**	**sand beach fronts low vertical bluff**
	LINC29	**6.481**	**5.146**	**0.038**	**279.5**	**0.95**	**1**	**sand beach fronts low vertical bluff**
	LINC30	**7.542**	**3.905**	**0.037**	**279.4**	**0.90**	**1**	**sand beach fronts low vertical bluff**
	LINC31	6.742	4.116	0.041	279.3	0.90	1	sand beach fronts low vertical bluff
	LINC32	**9.283**	**3.288**	**0.032**	**279.4**	**0.90**	**1**	**sand beach fronts low vertical bluff**
	LINC33	**7.880**	**4.211**	**0.035**	**288.5**	**0.90**	**1**	**sand beach fronts low vertical bluff**
	LINC34	**6.987**	**4.117**	**0.037**	**277.9**	**0.90**	**1**	**sand beach fronts low vertical bluff**
	LINC35	6.581	4.164	0.028	278.0	0.70	1	sand beach fronts riprap structure
	LINC36	**7.938**	**4.172**	**0.037**	**274.6**	**0.90**	**1**	**sand beach fronts low vertical bluff**
	LINC37	7.807	3.938	0.042	274.6	0.55	1	sand beach fronts riprap structure
	LINC38	9.099	3.606	0.042	277.6	0.55	1	sand beach fronts riprap structure
	LINC39	**8.511**	**4.777**	**0.041**	**279.1**	**0.95**	**1**	**sand beach fronts moderately low bluff**
	LINC40	**8.408**	**4.185**	**0.034**	**279.0**	**0.90**	**1**	**sand beach fronts moderately low bluff**
	LINC41	11.324	3.246	0.029	279.2	0.70	1	sand beach fronts riprap structure
	LINC42	10.700	4.363	0.034	279.9	0.70	1	sand beach fronts riprap structure
	LINC43	**10.635**	**4.878**	**0.034**	**280.0**	**0.95**	**1**	**sand beach fronts moderately high**

Reach	Transect	D_{HIGH} (m)	D_{LOW} (m)	Beach Slope (tan β)	Wave Dir. (γ_β)	Rough -ness (γ_r)	Approach	Description
								vertical bluff
	LINC44	11.648	4.390	0.034	282.2	0.70	1	sand beach fronts riprap structure
	LINC45	6.933	4.142	0.035	282.3	0.80	1	sand beach fronts riprap structure
	LINC46	8.937	5.919	0.042	280.5	1.00	3	dune-backed beach
	LINC47	6.181	5.441	0.031	279.9	1.00	3	dune-backed beach
	LINC48	8.599	5.958	0.047	295.1	1.00	3	dune-backed beach
	LINC49	**10.191**	**4.743**	**0.048**	**278.2**	**0.95**	**1**	**sand beach fronts moderately high vertical bluff**
	LINC50	7.258	6.361	0.050	278.4	1.00	3	dune-backed beach
	LINC51	8.129	4.496	0.045	278.3	0.80	1	sand beach fronts riprap structure
	LINC52	7.937	5.417	0.034	278.5	1.00	3	dune-backed beach
	LINC53	7.271	4.136	0.026	277.8	0.70	1	sand beach fronts riprap structure
	LINC54	9.015	5.728	0.042	276.9	1.00	3	dune-backed beach
	LINC55	**10.356**	**4.290**	**0.021**	**276.8**	**0.95**	**1**	**sand beach fronts moderately high vertical bluff**
	LINC56	9.322	4.620	0.036	276.7	1.00	3	dune-backed beach
	LINC57	6.811	3.678	0.016	275.6	0.70	1	sand beach fronts riprap structure
	LINC58	**7.091**	**4.326**	**0.023**	**271.8**	**0.95**	**1**	**sand beach fronts low vertical bluff**
	LINC59	7.480	4.272	0.034	277.1	0.70	1	sand beach fronts riprap structure
	LINC60	**8.898**	**4.906**	**0.036**	**279.4**	**0.60**	**1**	**sand beach fronts moderately high vertical bluff**
	LINC61	**10.859**	**6.219**	**0.053**	**283.1**	**0.95**	**3**	**sand dune fronts moderately high vertical bluff**
	LINC62	**12.513**	**5.358**	**0.048**	**281.0**	**0.95**	**3**	**sand dune fronts moderately high vertical bluff**
	LINC63	10.828	5.021	0.054	276.5	1.00	3	sand dune fronts moderately high vertical bluff
	LINC64	**13.583**	**5.199**	**0.025**	**276.1**	**0.95**	**1**	**sand beach fronts moderately high vertical bluff**
	LINC65	7.290	3.992	0.027	273.3	1.00	3	sand dune fronts moderately high vertical bluff
	LINC66	5.528	4.690	0.033	272.6	1.00	3	dune-backed beach
	LINC67	**11.260**	**5.405**	**0.030**	**303.2**	**0.95**	**1**	**sand beach fronts moderately high vertical bluff**
Alsea Spit	LINC68	11.754	5.501	0.057	239.6	1.00	3	dune-backed beach
	LINC69	17.199	6.833	0.098	270.1	1.00	3	dune-backed beach
	LINC70	12.411	4.253	0.037	272.0	1.00	3	dune-backed beach
	LINC71	14.596	4.038	0.050	273.2	1.00	3	dune-backed beach
	LINC72	7.173	5.397	0.050	274.3	1.00	3	dune-backed beach
	LINC73	11.202	4.940	0.035	276.7	1.00	3	dune-backed beach
	LINC74	8.746	8.015	0.069	277.7	1.00	3	dune-backed beach
	LINC75	7.264	5.675	0.040	276.8	1.00	3	dune-backed beach
	LINC76	5.936	4.498	0.032	276.9	0.95	1	sand beach fronts low vertical bluff
	LINC77	**10.139**	**4.995**	**0.029**	**275.2**	**0.95**	**1**	**sand beach fronts low vertical bluff**
	LINC78	**10.670**	**5.427**	**0.037**	**268.1**	**0.95**	**3**	**sand beach fronts low vertical bluff**
	LINC79	**12.084**	**5.488**	**0.035**	**270.3**	**0.95**	**3**	**sand dune fronts moderately high vertical bluff**
	LINC80	**15.499**	**5.539**	**0.038**	**272.2**	**0.95**	**3**	**sand dune fronts moderately high vertical bluff**
	LINC81	**11.427**	**5.430**	**0.035**	**272.6**	**0.95**	**3**	**sand dune fronts moderately high vertical bluff**
	LINC82	**16.323**	**5.360**	**0.029**	**266.4**	**0.95**	**1**	**sand beach fronts moderately high vertical bluff**
	LINC83	**16.819**	**4.606**	**0.023**	**271.3**	**0.95**	**1**	**sand beach fronts moderately high vertical bluff**

Reach	Transect	D_{HIGH} (m)	D_{LOW} (m)	Beach Slope (tan β)	Wave Dir. (γ_β)	Rough -ness (γ_r)	Approach	Description
	LINC84	**15.558**	**5.676**	**0.034**	**268.1**	**0.95**	**1**	**sand beach fronts moderately high vertical bluff**
	LINC85	**9.209**	**4.129**	**0.023**	**267.2**	**0.95**	**1**	**sand beach fronts moderately high vertical bluff**
	LINC86	8.697	6.101	0.038	252.1	1.00	3	dune-backed beach, backed further by bluffs
	LINC87	**12.566**	**4.395**	**0.033**	**268.2**	**0.95**	**1**	**sand beach fronts high vertical bluff**
	LINC88	**13.829**	**4.077**	**0.023**	**275.2**	**0.95**	**1**	**sand beach fronts high vertical bluff**
South Beach	**LINC89**	**21.717**	**4.764**	**0.032**	**279.8**	**0.95**	**1**	**sand beach fronts high vertical bluff**
	LINC90	**19.753**	**3.760**	**0.043**	**280.7**	**0.95**	**1**	**sand beach fronts high vertical bluff**
	LINC91	**21.883**	**4.663**	**0.045**	**282.6**	**0.95**	**1**	**sand beach fronts high vertical bluff**
	LINC92	**20.049**	**4.386**	**0.048**	**284.7**	**0.95**	**1**	**sand beach fronts high vertical bluff**
	LINC93	**11.324**	**4.036**	**0.035**	**285.6**	**0.95**	**1**	**sand beach fronts high vertical bluff**
	LINC94	**17.328**	**4.572**	**0.046**	**286.3**	**0.95**	**1**	**sand beach fronts high vertical bluff**
	LINC95	**23.471**	**5.384**	**0.058**	**286.2**	**0.95**	**1**	**sand beach fronts high vertical bluff**
	LINC96	**21.673**	**4.943**	**0.045**	**286.6**	**0.95**	**1**	**sand beach fronts high vertical bluff**
	LINC97	**14.112**	**6.249**	**0.092**	**286.2**	**0.95**	**1**	**sand beach fronts high vertical bluff**
	LINC98	**26.503**	**5.508**	**0.065**	**285.2**	**0.95**	**1**	**sand beach fronts high vertical bluff**
	LINC99	4.038	3.789	0.010	278.4	1.00	3	dune-backed beach
	LINC100	7.415	6.243	0.070	273.1	1.00	3	dune-backed beach
	LINC101	8.522	5.974	0.054	274.5	1.00	3	dune-backed beach
	LINC102	**9.045**	**4.878**	**0.049**	**275.4**	**0.95**	**1**	**sand beach fronts low vertical bluff**
	LINC103	14.179	3.348	0.039	277.7	0.55	1	sand beach fronts riprap structure
	LINC104	**13.334**	**4.655**	**0.041**	**278.3**	**0.95**	**1**	**sand beach fronts moderately high vertical bluff**
	LINC105	12.719	3.805	0.046	278.4	0.55	1	sand beach fronts riprap structure
	LINC106	**13.949**	**3.912**	**0.037**	**278.8**	**0.95**	**1**	**sand beach fronts moderately high vertical bluff**
	LINC107	**13.931**	**4.477**	**0.040**	**280.0**	**0.95**	**1**	**sand beach fronts moderately high vertical bluff**
	LINC108	6.915	6.915	0.053	279.3	1.00	3	sand beach backed by cobbles
	LINC109	**12.735**	**3.943**	**0.039**	**278.2**	**0.95**	**1**	**sand beach fronts high vertical bluff**
	LINC110	**16.781**	**3.881**	**0.038**	**274.2**	**0.95**	**1**	**sand beach fronts high vertical bluff**
	LINC111	**14.614**	**4.267**	**0.036**	**279.7**	**0.95**	**1**	**sand beach fronts high vertical bluff**
	LINC112	**23.387**	**3.480**	**0.039**	**280.3**	**0.95**	**1**	**sand beach fronts high vertical bluff**
	LINC113	**15.564**	**4.846**	**0.037**	**279.9**	**0.95**	**1**	**sand beach fronts high vertical bluff**
	LINC114	**7.175**	**6.571**	**0.051**	**278.7**	**1.00**	**3**	**dune-backed beach**
	LINC115	**8.087**	**4.814**	**0.046**	**278.1**	**0.95**	**1**	**sand beach fronts high vertical bluff**
	LINC116	18.160	4.228	0.046	276.7	0.70	1	sand beach fronts riprap structure
	LINC117	**18.878**	**4.050**	**0.041**	**271.8**	**0.95**	**1**	**sand beach fronts high vertical bluff**
	LINC118	**7.696**	**4.679**	**0.042**	**273.6**	**0.95**	**1**	**sand beach fronts low vertical bluff**
	LINC119	**22.033**	**4.185**	**0.033**	**276.2**	**0.95**	**1**	**sand beach fronts high vertical bluff**
	LINC120	24.971	4.060	0.039	276.4	0.55	1	sand beach fronts riprap structure
	LINC121	**23.486**	**4.583**	**0.040**	**276.5**	**0.95**	**1**	**sand beach fronts high vertical bluff**
	LINC122	**25.845**	**4.857**	**0.036**	**276.6**	**0.95**	**1**	**sand beach fronts high vertical bluff**
	LINC123	**23.811**	**4.813**	**0.041**	**275.4**	**0.95**	**1**	**sand beach fronts high vertical bluff**
	LINC124	**11.830**	**4.445**	**0.031**	**270.2**	**0.95**	**1**	**sand beach fronts high vertical bluff**
	LINC125	**19.537**	**3.964**	**0.025**	**274.3**	**0.95**	**1**	**sand beach fronts high vertical bluff**
	LINC126	6.579	5.934	0.053	272.3	1.00	3	dune-backed beach
	LINC127	7.909	6.129	0.059	274.4	1.00	3	dune-backed beach
	LINC128	9.796	7.038	0.058	278.1	1.00	3	dune-backed beach
	LINC129	15.373	5.863	0.055	271.8	1.00	3	dune-backed beach
	LINC130	12.478	5.151	0.039	246.8	1.00	3	dune-backed beach

Reach	Transect	D_{HIGH} (m)	D_{LOW} (m)	Beach Slope (tan β)	Wave Dir. (γ_β)	Rough -ness (γ_r)	Approach	Description
Newport	LINC131	13.140	5.881	0.041	263.7	1.00	3	dune-backed beach
	LINC132	**10.388**	**4.379**	**0.035**	**275.8**	**0.95**	**1**	**sand beach fronts high vertical bluff**
	LINC133	**16.665**	**4.258**	**0.030**	**278.3**	**0.95**	**1**	**sand beach fronts high vertical bluff**
	LINC134	**18.413**	**5.257**	**0.037**	**279.7**	**0.95**	**1**	**sand beach fronts high vertical bluff**
	LINC135	**18.755**	**3.455**	**0.028**	**281.0**	**0.95**	**1**	**sand beach fronts high vertical bluff**
	LINC136	**6.669**	**3.303**	**0.012**	**278.4**	**0.95**	**1**	**sand beach fronts seawall**
	LINC137	**23.345**	**5.020**	**0.035**	**277.1**	**0.95**	**1**	**sand beach fronts high vertical bluff**
	LINC138	**12.967**	**5.597**	**0.040**	**278.2**	**0.95**	**3**	**sand dune fronts high bluff**
	LINC139	**15.506**	**4.190**	**0.031**	**277.4**	**0.95**	**3**	**sand dune fronts high bluff**
	LINC140	**18.965**	**4.738**	**0.038**	**276.7**	**0.95**	**1**	**sand beach fronts high vertical bluff**
	LINC141	**24.141**	**5.329**	**0.023**	**276.9**	**0.95**	**3**	**sand dune fronts high bluff**
	LINC142	**8.015**	**4.395**	**0.021**	**267.2**	**0.95**	**3**	**dune-backed beach, backed further by bluffs**
	LINC143	**18.671**	**4.548**	**0.027**	**263.8**	**0.95**	**3**	**dune-backed beach, backed further by bluffs**
	LINC144	7.781	3.596	0.028	260.8	1.00	3	dune-backed beach, backed further by bluffs
	LINC145	6.064	3.189	0.027	257.3	1.00	3	sand dune fronts high bluff
	LINC146	**21.800**	**3.604**	**0.021**	**256.5**	**0.95**	**3**	**sand dune fronts high bluff**
	LINC147	**24.604**	**4.021**	**0.045**	**231.4**	**0.95**	**3**	**sand dune fronts high bluff**
Yaquina Head	**LINC148**	**21.012**	**5.592**	**0.085**	**259.6**	**0.95**	**1**	**narrow rock platform backed by high cliffs**
	LINC149	19.945	0.739	0.020	268.4	0.95	1	narrow rock platform backed by high cliffs
Beverly Beach	**LINC150**	**12.395**	**5.351**	**0.044**	**301.1**	**0.95**	**1**	**sand beach and platform fronts high vertical bluff**
	LINC151	**12.037**	**4.125**	**0.027**	**293.8**	**0.95**	**1**	**sand beach and platform fronts high vertical bluff**
	LINC152	**16.648**	**4.071**	**0.037**	**283.2**	**0.95**	**1**	**sand beach fronts moderately high vertical bluff**
	LINC153	**8.459**	**4.074**	**0.040**	**283.7**	**0.70**	**1**	**sand beach fronts moderately high vertical bluff**
	LINC154	7.662	3.824	0.037	284.0	0.70	1	sand beach backed by cobble berm/riprap
	LINC155	**22.818**	**4.776**	**0.053**	**283.5**	**0.95**	**1**	**sand beach fronts high vertical bluff**
	LINC156	**36.791**	**4.980**	**0.042**	**284.1**	**0.95**	**1**	**sand beach fronts high vertical bluff**
	LINC157	**14.831**	**3.994**	**0.035**	**285.2**	**0.95**	**1**	**sand beach fronts high vertical bluff**
	LINC158	**15.853**	**5.141**	**0.061**	**272.6**	**0.95**	**1**	**sand beach fronts high vertical bluff**
	LINC159	**13.518**	**5.000**	**0.053**	**282.1**	**0.95**	**1**	**sand beach fronts high vertical bluff**
	LINC160	14.915	3.525	0.043	282.8	0.70	1	sand beach fronts riprap structure
	LINC161	8.559	5.320	0.088	279.8	0.70	1	sand beach backed by cobble berm
	LINC162	**18.977**	**5.346**	**0.047**	**280.9**	**0.95**	**1**	**sand beach fronts high vertical bluff**
	LINC163	**23.622**	**5.016**	**0.062**	**278.2**	**0.95**	**1**	**sand beach fronts high vertical bluff**
	LINC164	**12.086**	**4.816**	**0.051**	**275.3**	**0.95**	**1**	**sand beach fronts high vertical bluff**
	LINC165	**22.688**	**5.331**	**0.047**	**274.2**	**0.95**	**1**	**sand beach fronts high vertical bluff**
	LINC166	**21.825**	**4.401**	**0.036**	**274.8**	**0.95**	**1**	**sand beach fronts high vertical bluff**
	LINC167	**17.714**	**4.820**	**0.041**	**274.5**	**0.95**	**1**	**sand beach fronts high vertical bluff**
	LINC168	**15.690**	**5.194**	**0.043**	**275.6**	**0.95**	**1**	**sand beach fronts high vertical bluff**
	LINC169	**18.825**	**4.807**	**0.039**	**267.0**	**0.95**	**1**	**sand beach fronts high vertical bluff**
	LINC170	**33.129**	**4.713**	**0.046**	**239.4**	**0.95**	**1**	**sand beach fronts high vertical bluff**
	LINC171	**28.516**	**4.251**	**0.041**	**232.1**	**0.95**	**1**	**sand beach fronts high vertical bluff**

Reach	Transect	D_{HIGH} (m)	D_{LOW} (m)	Beach Slope (tan β)	Wave Dir. (γ_β)	Rough-ness (γ_r)	Approach	Description
Otter Rock	LINC172	21.009	4.444	0.051	267.6	0.95	1	rock platform and sandy beach backed by bluff
	LINC173	25.393	3.221	0.027	268.7	0.95	1	rock platform backed by bluff
	LINC174	23.010	3.156	0.008	270.6	0.95	1	rock platform backed by bluff
	LINC175	23.244	2.644	0.015	269.5	0.95	1	rock platform backed by bluff
	LINC176	24.099	2.344	0.015	268.5	0.95	1	rock platform backed by bluff
Cape	LINC177	116.753	1.237	0.036	264.4	0.95	1	narrow rock platform backed by high cliffs
Foulweather	**LINC178**	**103.606**	**3.516**	**0.047**	**261.2**	**0.95**	**1**	**narrow rock platform backed by high cliffs**
Miroco	LINC179	19.740	1.743	0.065	269.9	0.95	1	basalt ramp with low tide cliff
	LINC180	21.948	0.397	0.110	274.9	0.95	1	basalt ramp with low tide cliff
	LINC181	16.989	1.637	0.121	276.0	0.95	1	basalt ramp with low tide cliff
Rocky Creek	LINC182	14.183	1.467	0.043	275.6	0.95	1	basalt ramp with low tide cliff
	LINC183	14.596	2.088	0.076	277.3	0.95	1	basalt ramp with low tide cliff
Whale Cove	LINC184	15.310	1.302	0.040	267.3	0.95	1	basalt ramp with low tide cliff
	LINC185	13.989	0.314	0.011	271.3	0.95	1	basalt ramp with low tide cliff
	LINC186	16.676	2.155	0.080	277.7	0.95	1	basalt ramp with low tide cliff
	LINC187	14.648	1.253	0.022	290.2	0.95	1	basalt ramp with low tide cliff
	LINC188	10.068	1.250	0.023	296.0	0.95	1	basalt ramp with low tide cliff
	LINC189	12.439	0.868	0.038	293.7	0.95	1	basalt ramp with low tide cliff
Depoe Bay	LINC190	31.062	1.745	0.028	277.2	0.95	1	narrow rock platform backed by basalt ramp
	LINC191	26.414	1.966	0.069	275.5	0.95	1	narrow rock platform backed by basalt cliff
	LINC192	17.251	1.018	0.020	271.5	0.95	1	moderately wide rock platform backed by basalt cliff
	LINC193	15.543	1.512	0.027	269.0	0.95	1	moderately wide rock platform backed by basalt cliff
	LINC194	14.360	1.173	0.056	269.4	0.95	1	basalt cliff
	LINC195	15.519	1.013	0.021	270.1	0.95	1	basalt cliff
	LINC196	14.959	2.163	0.043	269.9	0.95	1	moderately wide rock platform backed by basalt cliff
	LINC197	14.091	3.035	0.088	270.2	0.95	1	narrow rock platform backed by basalt cliff
	LINC198	15.074	0.249	0.055	270.6	0.95	1	moderately wide rock platform backed by basalt cliff
	LINC199	13.910	1.321	0.110	274.9	0.95	1	basalt cliff
	LINC200	18.001	0.092	0.110	276.3	0.95	1	basalt cliff
	LINC201	**21.750**	**5.697**	**0.060**	**284.5**	**0.95**	**1**	**moderately wide rock platform backed by basalt cliff**
	LINC202	19.540	2.624	0.060	284.9	0.95	1	moderately wide rock platform backed by basalt cliff

Reach	Transect	D_{HIGH} (m)	D_{LOW} (m)	Beach Slope (tan β)	Wave Dir. (γ_β)	Rough -ness (γ_r)	Approach	Description
Fogarty Creek	**LINC203**	**16.484**	**3.988**	**0.031**	**301.8**	**0.95**	**1**	**bluff fronted by sand and gravel beach and shore platform**
	LINC204	5.960	4.247	0.025	288.0	0.55	1	riprap fronted by sand and gravel beach and shore platform
	LINC205	17.253	3.999	0.106	286.9	0.95	1	bluff fronted by sand and gravel beach and shore platform
	LINC206	20.951	2.861	0.072	271.7	0.55	1	riprap fronted by sand and gravel beach and shore platform
	LINC207	**13.485**	**3.282**	**0.025**	**286.2**	**0.95**	**1**	**bluff fronted by sand and gravel beach and shore platform**
	LINC208	**18.792**	**3.215**	**0.022**	**288.0**	**0.95**	**1**	**bluff fronted by sand and gravel beach and shore platform**
	LINC209	**20.005**	**4.334**	**0.051**	**313.2**	**0.95**	**1**	**bluff fronted by sand and gravel beach and shore platform**
	LINC210	**18.034**	**3.436**	**0.040**	**292.0**	**0.95**	**1**	**bluff fronted by sand and gravel beach and shore platform**
Gleneden Beach / Siletz Spit	LINC211	15.137	3.330	0.071	291.7	0.55	1	mixed sand and gravel beach fronts riprap structure
	LINC212	10.448	4.393	0.081	292.0	0.55	1	mixed sand and gravel beach fronts riprap structure
	LINC213	10.398	4.798	0.054	292.0	0.95	1	mixed sand and gravel beach fronts bluff
	LINC214	9.392	5.565	0.080	290.8	0.70	1	mixed sand and gravel beach fronts riprap structure
	LINC215	9.145	5.009	0.075	289.4	0.70	1	mixed sand and gravel beach fronts riprap structure
	LINC216	13.620	5.545	0.110	288.2	0.55	1	mixed sand and gravel beach fronts riprap structure
	LINC217	**15.570**	**5.785**	**0.092**	**287.5**	**0.95**	**1**	**mixed sand and gravel beach fronts bluff**
	LINC218	14.340	4.998	0.108	285.2	0.55	1	mixed sand and gravel beach fronts riprap structure
	LINC219	13.497	4.328	0.089	285.3	0.55	1	mixed sand and gravel beach fronts riprap structure
	LINC220	21.776	4.896	0.110	285.1	0.55	1	mixed sand and gravel beach fronts riprap structure
	LINC221	8.111	6.149	0.064	285.7	0.55	3	mixed sand and gravel beach fronts dune
	LINC222	**15.448**	**5.300**	**0.073**	**285.2**	**0.95**	**1**	**mixed sand and gravel beach fronts bluff**
	LINC223	13.416	2.809	0.059	284.3	0.55	1	mixed sand and gravel beach fronts riprap structure
	LINC224	**15.850**	**5.409**	**0.052**	**285.2**	**0.95**	**1**	**mixed sand and gravel beach fronts bluff**
	LINC225	15.390	5.384	0.079	285.0	0.55	1	mixed sand and gravel beach fronts riprap structure
	LINC226	**13.513**	**5.449**	**0.054**	**284.5**	**0.95**	**1**	**mixed sand and gravel beach fronts bluff**
	LINC227	**13.125**	**4.887**	**0.043**	**282.6**	**0.95**	**1**	**mixed sand and gravel beach fronts seawall**
	LINC228	**24.807**	**5.201**	**0.066**	**283.7**	**0.95**	**1**	**mixed sand and gravel beach fronts bluff**
	LINC229	40.682	6.543	0.083	283.7	0.55	3	mixed sand and gravel beach fronts riprap structure
	LINC230	15.605	7.001	0.077	284.1	1.00	3	dune-backed beach overlying riprap structure

Reach	Transect	D_{HIGH} (m)	D_{LOW} (m)	Beach Slope (tan β)	Wave Dir. (γ_β)	Rough -ness (γ_r)	Approach	Description
	LINC231	9.419	7.592	0.079	284.6	1.00	3	dune-backed beach overlying riprap structure
	LINC232	15.636	7.219	0.079	283.8	1.00	3	dune-backed beach overlying riprap structure
	LINC233	8.342	5.217	0.075	283.3	1.00	3	dune-backed beach overlying riprap structure
	LINC234	10.097	8.183	0.094	283.3	1.00	3	dune-backed beach overlying riprap structure
	LINC235	9.877	7.347	0.085	283.8	1.00	3	dune-backed beach overlying riprap structure
	LINC236	8.964	6.356	0.078	283.8	1.00	3	dune-backed beach overlying riprap structure
	LINC237	10.662	6.537	0.085	282.9	1.00	3	dune-backed beach overlying riprap structure
	LINC238	9.091	9.091	0.109	281.9	1.00	3	dune-backed beach overlying riprap structure
	LINC239	9.962	7.637	0.095	281.2	1.00	3	dune-backed beach overlying riprap structure
	LINC240	8.306	8.017	0.065	281.4	1.00	3	dune-backed beach overlying riprap structure
	LINC241	9.086	6.925	0.065	281.6	1.00	3	dune-backed beach overlying riprap structure
	LINC242	9.039	7.673	0.075	281.2	1.00	3	dune-backed beach overlying riprap structure
	LINC243	8.765	8.765	0.105	281.8	1.00	3	dune-backed beach
	LINC244	6.000	6.000	0.066	279.5	1.00	3	dune-backed beach
Lincoln City	LINC245	6.231	4.263	0.038	277.8	1.00	3	sand beach fronts high bluffs
	LINC246	6.254	6.254	0.067	278.6	1.00	3	sand beach fronts high bluffs
	LINC247	24.270	7.000	0.076	275.4	1.00	3	sand beach fronts high bluffs
	LINC248	**7.621**	**5.472**	**0.067**	**276.0**	**0.95**	**1**	**sand beach fronts seawall**
	LINC249	**27.100**	**5.166**	**0.042**	**288.5**	**0.95**	**1**	**sand beach fronts high bluffs**
	LINC250	10.979	5.279	0.067	277.1	0.70	1	sand beach fronts riprap
	LINC251	**7.300**	**4.153**	**0.032**	**277.4**	**0.95**	**1**	**sand beach fronts seawall**
	LINC252	**7.415**	**5.758**	**0.081**	**276.9**	**0.95**	**1**	**sand beach fronts seawall**
	LINC253	**32.943**	**6.413**	**0.070**	**272.9**	**0.95**	**3**	**sand beach fronts high bluffs**
	LINC254	**34.319**	**5.667**	**0.062**	**272.9**	**0.95**	**1**	**sand beach fronts high bluffs**
	LINC255	**7.410**	**4.866**	**0.048**	**291.4**	**0.95**	**1**	**sand beach fronts seawall and high bluffs**
	LINC256	**12.766**	**4.785**	**0.046**	**274.5**	**0.95**	**1**	**sand beach fronts seawall and high bluffs**
	LINC257	**37.604**	**6.525**	**0.068**	**274.7**	**0.95**	**3**	**sand beach fronts high bluffs**
	LINC258	**38.806**	**4.899**	**0.053**	**280.5**	**0.95**	**1**	**sand beach fronts high bluffs**
	LINC259	**7.575**	**4.883**	**0.078**	**282.6**	**0.95**	**1**	**sand beach fronts seawall**
	LINC260	**40.100**	**5.800**	**0.079**	**283.6**	**0.95**	**1**	**sand beach fronts moderately high bluffs**
	LINC261	**24.403**	**6.770**	**0.065**	**284.5**	**0.95**	**1**	**sand beach fronts moderately high bluffs**
	LINC262	18.974	4.487	0.072	289.1	0.70	1	sand beach fronts riprap
	LINC263	**7.835**	**5.492**	**0.081**	**283.7**	**0.95**	**1**	**sand beach fronts seawall**
	LINC264	9.440	4.957	0.078	282.8	0.70	1	sand beach fronts riprap
	LINC265	**6.798**	**4.406**	**0.036**	**287.8**	**0.95**	**1**	**sand beach fronts seawall**
	LINC266	6.700	3.383	0.026	283.6	0.70	1	sand beach fronts riprap
	LINC267	7.069	4.537	0.039	281.4	1.00	3	sand beach fronts riprap
	LINC268	**7.897**	**4.423**	**0.037**	**282.8**	**0.95**	**1**	**sand beach fronts seawall**
	LINC269	10.260	6.259	0.070	282.4	1.00	3	dune-backed beach

Reach	Transect	D_{HIGH} (m)	D_{LOW} (m)	Beach Slope (tan β)	Wave Dir. (γ_β)	Rough -ness (γ_r)	Approach	Description
	LINC270	14.128	5.222	0.069	281.2	0.90	1	sand beach fronts riprap and bluffs
	LINC271	**18.857**	**5.554**	**0.060**	**281.0**	**0.95**	**1**	**sand beach fronts moderately high bluffs**
	LINC272	8.800	4.829	0.054	280.7	0.70	1	sand beach fronts riprap and bluffs
	LINC273	27.820	5.684	0.089	280.5	0.80	1	sand beach fronts riprap and bluffs
	LINC274	10.235	6.466	0.079	280.0	0.80	1	sand beach fronts riprap and bluffs
	LINC275	**13.002**	**6.350**	**0.084**	**279.6**	**0.80**	**1**	**sand beach fronts riprap and bluffs**
	LINC276	12.510	4.815	0.076	277.7	0.55	1	sand beach fronts riprap and bluffs
	LINC277	**19.421**	**5.586**	**0.072**	**280.0**	**0.95**	**1**	**sand beach fronts moderately high bluffs**
	LINC278	**7.419**	**4.556**	**0.054**	**285.7**	**0.95**	**1**	**sand beach fronts seawall**
	LINC279	9.806	4.226	0.039	274.2	0.70	1	sand beach fronts riprap and bluffs
	LINC280	**7.671**	**4.584**	**0.048**	**280.6**	**0.95**	**1**	**sand beach fronts seawall**
	LINC281	**8.843**	**5.283**	**0.048**	**274.7**	**0.95**	**1**	**sand beach fronts low bluff**
	LINC282	**10.062**	**5.779**	**0.041**	**280.0**	**0.95**	**1**	**sand beach fronts moderately high bluffs**
	LINC283	**9.471**	**5.500**	**0.051**	**281.4**	**0.90**	**1**	**sand beach fronts riprap/low seawall and bluffs**
	LINC284	**12.776**	**5.865**	**0.061**	**279.8**	**0.95**	**1**	**sand beach fronts moderately high bluffs**
	LINC285	**9.284**	**5.358**	**0.055**	**278.6**	**0.95**	**1**	**sand beach fronts seawall and bluffs**
	LINC286	9.531	5.057	0.054	280.7	0.70	1	sand beach fronts riprap and bluffs
	LINC287	11.137	4.982	0.050	281.5	0.70	1	sand beach fronts riprap and bluffs
	LINC288	**6.865**	**5.143**	**0.064**	**282.1**	**0.95**	**1**	**sand beach fronts moderately high bluffs**
	LINC289	**18.092**	**4.752**	**0.049**	**281.5**	**0.95**	**1**	**sand beach fronts moderately high bluffs**
	LINC290	**28.243**	**5.285**	**0.073**	**281.4**	**0.95**	**1**	**sand beach fronts moderately high bluffs**
	LINC291	10.575	4.853	0.058	281.1	0.80	1	sand beach fronts riprap and bluffs
	LINC292	13.387	5.078	0.091	279.2	0.55	1	sand beach fronts riprap and bluffs
	LINC293	**11.936**	**4.686**	**0.051**	**279.1**	**0.95**	**1**	**sand beach fronts low bluff**
	LINC294	8.286	5.341	0.047	283.1	1.00	3	sand beach fronts dune and low bluff
	LINC295	**9.221**	**5.021**	**0.044**	**277.0**	**0.95**	**1**	**sand beach fronts low bluff**
	LINC296	8.311	4.358	0.047	273.9	0.55	1	sand beach fronts riprap and bluffs
	LINC297	13.363	4.891	0.055	272.3	0.90	1	sand beach fronts collapsed riprap and bluff
	LINC298	11.517	4.279	0.056	271.7	0.55	1	sand beach fronts riprap and bluffs
	LINC299	**10.933**	**4.898**	**0.043**	**270.7**	**0.95**	**1**	**sand beach fronts seawall and bluffs**
	LINC300	**11.270**	**5.022**	**0.054**	**271.4**	**0.95**	**1**	**sand beach fronts seawall and bluffs**
	LINC301	11.929	4.800	0.052	270.0	0.55	1	sand beach fronts riprap and bluffs
	LINC302	**20.930**	**5.449**	**0.076**	**268.5**	**0.95**	**1**	**sand beach fronts high bluffs**
Salmon River	LINC303	47.701	3.136	0.070	276.9	0.95	1	dune-backed beach backed by bluff
	LINC304	26.308	5.173	0.102	279.0	0.95	3	dune-backed beach backed by bluff
	LINC305	57.755	3.220	0.017	279.5	0.95	1	inter-tidal rocky area backed by bluffs
	LINC306	**32.488**	**5.553**	**0.070**	**279.3**	**0.95**	**1**	**dune-backed beach backed by bluff**
	LINC307	**23.641**	**4.128**	**0.038**	**276.0**	**0.95**	**1**	**dune-backed beach backed by bluff**
	LINC308	6.251	5.058	0.066	272.2	1.00	3	dune-backed beach
Cascade Head	LINC309	48.172	1.609	0.027	268.8	0.95	1	plunging cliff
	LINC310	43.560	1.207	0.028	274.1	0.95	1	plunging cliff
	LINC311	24.427	0.358	0.022	270.3	0.80	1	boulder beach backed by bluffs
	LINC312	93.240	2.125	0.026	271.8	0.95	1	plunging cliff
	LINC313	139.103	0.000	0.023	273.7	0.95	1	plunging cliff

Reach	Transect	D_{HIGH} (m)	D_{LOW} (m)	Beach Slope (tan β)	Wave Dir. (γ_β)	Rough-ness (γ_r)	Approach	Description
Supplemental Transects	LINC_9_290	5.986	3.518	0.025	270.4	0.55	1	sandy beach backed by bluff
	LINC_26_457	7.145	4.451	0.032	276.8	0.95	1	sand beach fronts low vertical bluff
	LINC_26_459	6.682	4.453	0.038	276.8	0.90	1	sand beach fronts low vertical bluff
	LINC_43_554	8.895	3.653	0.028	280.0	0.95	1	sand beach fronts moderately high vertical bluff
	LINC_44_573	8.826	3.259	0.043	282.2	0.70	1	sand beach fronts riprap structure
	LINC_44_575	8.786	4.080	0.039	282.2	0.70	1	sand beach fronts riprap structure
	LINC_99_1257	4.984	4.196	0.030	278.4	1.00	3	Ona Beach - dune-backed beach
	LINC_99_1274	4.300	3.583	0.028	278.4	1.00	3	Ona Beach - dune-backed beach
	LINC_106_1340	12.480	4.428	0.069	278.8	0.95	1	sand beach fronts moderately high vertical bluff
	LINC_106_1343	8.969	4.267	0.048	278.8	0.95	1	sand beach fronts moderately high vertical bluff
	LINC_106_1345	11.830	3.936	0.042	278.8	0.95	1	sand beach fronts moderately high vertical bluff
	LINC_109_1366	7.444	4.984	0.056	278.2	0.95	1	sand beach fronts high vertical bluff
	LINC_109_1367	8.862	4.690	0.053	278.2	0.95	1	sand beach fronts high vertical bluff
	LINC_121_1528	8.926	5.145	0.083	276.5	0.95	1	creek (South Beach)
	LINC_167_2257	4.221	4.221	0.050	274.5	1.00	3	Spencer Creek, Beverly Beach
	LINC_195_2790	13.245	2.217	0.063	270.1	0.95	1	plunging cliff, north of Depoe Bay
	LINC_204_2928	3.239	3.239	0.085	288.0	1.00	3	Fogarty Creek
	LINC_250_3385	7.779	5.140	0.085	277.1	0.70	1	sand beach fronts riprap

Notes:

D_{HIGH} denotes the crest of the dune, bluff, or structure; D_{LOW} denotes the toe of the dune (i.e., E_j), bluff, or structure;

Beach slope reflects the calculated slope spanning the region between 2- and 4-m elevation;

Wave direction denotes the shoreline orientation used to calculate the wave reduction (γ_β) factor used in TAW runup calculations;

Roughness (γ_r) defines the backshore roughness used in TAW runup calculations. Bold values indicate sites where the local slope goes to 1 due to the presence of a vertical bluff; and

Approach defines the final runup approach used to calculate the wave runup, where STK = Stockdon, Snsh/TAW = nearshore slope and TAW, and LocSlp/TAW = the local barrier slope and TAW.

6.3 Lincoln County Wave Runup and Total Water Level Calculations

The complete hourly combined time series is run through the lookup tables to derive alongshore varying transformed wave time series. Using the transformed wave conditions, and the measured alongshore varying beach and barrier slopes, initial TWL time series based on the Stockdon approach are developed at all transect locations. From these time series we identify the ~150 highest independent TWLs at each transect over the length of the record. Wave runup is then computed for each of these storm input conditions (about 5 events per year) at every profile site shown in **Figure 3-1** to **Figure 3-4** using a combination of the Stockdon and others (2006) runup equation for dune-backed beaches (equation 6.4) and TAW (equation 6-12) for wave runup on a barrier. The specific approaches used in our calculations are defined above in Table 6-1. For both models, the calculated runup is combined with the SWL (measured tides) to develop the TWL conditions used to generate the 10-, 50-, and 100-year return level event as well as the 500-year return event. The input wave conditions from the SWAN modeling used in the various calculations were determined for each transect location by extending the shore-perpendicular transects from the backshore to where they intersected the 20-m contour, or the seaward most location of H_{mo}/depth = 0.4, whichever was farther offshore (but almost always shallower than 30 m). This ensured that only minor dissipation due to wave breaking influenced the model results. These intersections are where wave statistics from the SWAN output were extracted.

Having calculated the storm-induced TWLs, we used the generalized extreme value (GEV) family of distributions (specifically the peak over threshold (POT) approach) to estimate the 100-year and 500-year total water levels for each of the beach profile sites. Specific information about the extreme value techniques used to estimate these TWLs is described in Section 4.6. **Figure 6-7** gives an example of the extreme value (GPD-Poisson) model for the LINC 6 profile site in which the 100-year event is calculated to be 9.8 m (32 ft) and the 500-year event is estimated to be 10.8 m (35.4 ft). The results for all of the profiles can be found in **Table 6-2**.

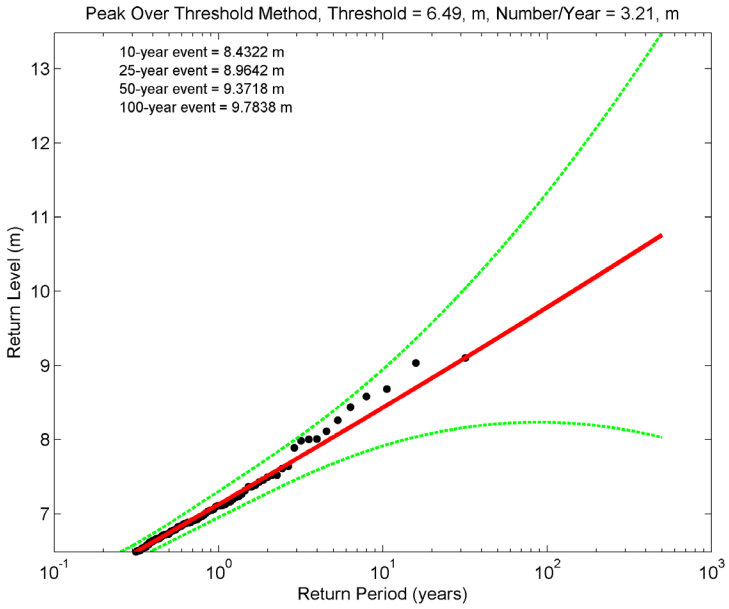

Figure 6-7. Example peak over threshold (POT) extreme value theory results for the Lincoln 6 transect site (with 95% confidence levels) located in the Waldport sub-littoral cell. Note that the y-axis vertical datum is relative to NAVD88.

Table 6-2. 100-year (1%) and 500-year (0.2%) total water levels calculated for the Lincoln County transect sites.

Reach	Transect	D_{HIGH} (m)	D_{LOW} (m)	100-Year (m)	500-Year (m)	Description
Cape Perpetua	LINC1	18.025	1.217	9.27	10.61	narrow rock platform backed by high cliffs
	LINC2	30.946	3.107	11.14	13.05	sand beach backed by high cliffs
	LINC3	39.090	1.902	9.20	9.22	broad rock platform backed by high cliffs
	LINC4	10.580	0.836	8.69	10.36	broad rock platform backed by high cliffs
Yachats	LINC5	12.193	2.735	8.51	8.53	broad rock platform backed by moderately high bluff
	LINC6	9.761	0.360	9.78	10.76	broad rock platform backed by moderately low bluff
	LINC7	8.538	-0.574	8.23	8.88	broad rock platform backed by moderately low bluff
	LINC8	8.660	-0.821	7.25	7.75	sand beach fronts broad rock platform and backshore
	LINC9	9.057	4.019	8.06	8.61	sandy beach backed by bluff
	LINC10	12.935	5.284	10.66	15.07	rock platform and sandy beach backed by bluff
	LINC11	13.090	5.605	12.30	13.41	sand beach backed by riprap
	LINC12	8.697	2.916	10.42	12.44	narrow rock platform backed by low bluff
	LINC13	8.012	3.761	10.61	15.55	broad rock platform backed by low bluff
	LINC14	8.944	4.202	8.78	9.48	sand beach fronts broad rock platform backed by low bluff
Waldport	LINC15	11.154	2.339	9.30	9.54	sand beach fronts broad rock platform backed by low bluff
	LINC16	9.271	4.411	10.79	12.48	sand beach fronts low vertical bluff
	LINC17	7.115	2.673	9.02	9.32	sand beach fronts riprap structure
	LINC18	6.575	4.450	9.32	12.13	sand beach fronts low vertical bluff
	LINC19	7.084	3.275	9.25	9.55	sand beach fronts riprap structure
	LINC20	6.414	3.539	10.29	10.83	sand beach fronts low vertical bluff
	LINC21	6.485	3.797	10.17	10.73	sand beach fronts low vertical bluff
	LINC22	6.243	3.750	11.39	12.16	sand beach fronts low vertical bluff
	LINC23	6.844	4.406	8.22	10.31	sand beach fronts low vertical bluff
	LINC24	6.347	3.458	11.70	12.75	sand beach fronts low vertical bluff
	LINC25	6.488	4.003	8.56	8.97	sand beach fronts riprap structure
	LINC26	8.247	5.181	8.04	9.84	sand beach fronts low vertical bluff
	LINC27	7.369	5.345	7.68	8.80	sand beach fronts low vertical bluff
	LINC28	6.870	5.409	7.17	7.66	sand beach fronts low vertical bluff
	LINC29	6.481	5.146	8.21	9.34	sand beach fronts low vertical bluff
	LINC30	7.542	3.905	12.50	14.63	sand beach fronts low vertical bluff
	LINC31	6.742	4.116	10.65	11.50	sand beach fronts low vertical bluff
	LINC32	9.283	3.288	13.45	15.25	sand beach fronts low vertical bluff
	LINC33	7.880	4.211	11.58	13.79	sand beach fronts low vertical bluff
	LINC34	6.987	4.117	10.97	11.85	sand beach fronts low vertical bluff
	LINC35	6.581	4.164	8.54	11.20	sand beach fronts riprap structure
	LINC36	7.938	4.172	10.92	11.97	sand beach fronts low vertical bluff
	LINC37	7.807	3.938	9.58	10.94	sand beach fronts riprap structure
	LINC38	9.099	3.606	10.01	11.25	sand beach fronts riprap structure
	LINC39	8.511	4.777	10.02	10.64	sand beach fronts moderately low bluff
	LINC40	8.408	4.185	11.11	12.55	sand beach fronts moderately low bluff
	LINC41	11.324	3.246	11.11	12.32	sand beach fronts riprap structure
	LINC42	10.700	4.363	10.64	15.76	sand beach fronts riprap structure
	LINC43	10.635	4.878	9.96	13.20	sand beach fronts moderately high vertical bluff
	LINC44	11.648	4.390	9.09	11.28	sand beach fronts riprap structure
	LINC45	6.933	4.142	10.47	11.99	sand beach fronts riprap structure
	LINC46	8.937	5.919	7.67	8.39	dune-backed beach
	LINC47	6.181	5.441	7.07	7.67	dune-backed beach

Reach	Transect	D_{HIGH} (m)	D_{LOW} (m)	100-Year (m)	500-Year (m)	Description
	LINC48	8.599	5.958	7.67	8.25	dune-backed beach
	LINC49	10.191	4.743	10.90	11.82	sand beach fronts moderately high vertical bluff
	LINC50	7.258	6.361	7.96	8.60	dune-backed beach
	LINC51	8.129	4.496	10.29	11.25	sand beach fronts riprap structure
	LINC52	7.937	5.417	7.25	7.86	dune-backed beach
	LINC53	7.271	4.136	8.39	10.62	sand beach fronts riprap structure
	LINC54	9.015	5.728	7.75	8.56	dune-backed beach
	LINC55	10.356	4.290	9.37	10.17	sand beach fronts moderately high vertical bluff
	LINC56	9.322	4.620	7.63	8.72	dune-backed beach
	LINC57	6.811	3.678	8.92	12.45	sand beach fronts riprap structure
	LINC58	7.091	4.326	9.34	10.00	sand beach fronts low vertical bluff
	LINC59	7.480	4.272	8.94	11.19	sand beach fronts riprap structure
	LINC60	8.898	4.906	7.43	8.09	sand beach fronts moderately high vertical bluff
	LINC61	10.859	6.219	7.94	8.64	sand dune fronts moderately high vertical bluff
	LINC62	12.513	5.358	7.58	8.20	sand dune fronts moderately high vertical bluff
	LINC63	10.828	5.021	8.25	9.21	sand dune fronts moderately high vertical bluff
	LINC64	13.583	5.199	6.94	7.79	sand beach fronts moderately high vertical bluff
	LINC65	7.290	3.992	6.94	7.64	sand dune fronts moderately high vertical bluff
	LINC66	5.528	4.690	7.07	7.64	dune-backed beach
	LINC67	11.260	5.405	7.60	8.94	sand beach fronts moderately high vertical bluff
Alsea Spit	LINC68	11.754	5.501	8.31	9.02	dune-backed beach
	LINC69	17.199	6.833	10.92	12.05	dune-backed beach
	LINC70	12.411	4.253	7.51	8.40	dune-backed beach
	LINC71	14.596	4.038	7.84	8.46	dune-backed beach
	LINC72	7.173	5.397	7.78	8.30	dune-backed beach
	LINC73	11.202	4.940	7.24	7.93	dune-backed beach
	LINC74	8.746	8.015	9.17	10.22	dune-backed beach
	LINC75	7.264	5.675	7.73	8.70	dune-backed beach
	LINC76	5.936	4.498	9.22	11.23	sand beach fronts low vertical bluff
	LINC77	10.139	4.995	8.92	12.12	sand beach fronts low vertical bluff
	LINC78	10.670	5.427	7.48	8.32	sand beach fronts low vertical bluff
	LINC79	12.084	5.488	7.23	7.85	sand dune fronts moderately high vertical bluff
	LINC80	15.499	5.539	7.30	7.95	sand dune fronts moderately high vertical bluff
	LINC81	11.427	5.430	7.05	7.58	sand dune fronts moderately high vertical bluff
	LINC82	16.323	5.360	7.01	7.69	sand beach fronts moderately high vertical bluff
	LINC83	16.819	4.606	10.05	14.70	sand beach fronts moderately high vertical bluff
	LINC84	15.558	5.676	7.16	7.67	sand beach fronts moderately high vertical bluff
	LINC85	9.209	4.129	10.60	12.58	sand beach fronts moderately high vertical bluff
	LINC86	8.697	6.101	7.39	7.99	dune-backed beach, backed further by bluffs
	LINC87	12.566	4.395	11.05	13.06	sand beach fronts high vertical bluff
	LINC88	13.829	4.077	10.99	13.06	sand beach fronts high vertical bluff
South Beach	LINC89	21.717	4.764	8.82	10.64	sand beach fronts high vertical bluff
	LINC90	19.753	3.760	13.44	15.02	sand beach fronts high vertical bluff
	LINC91	21.883	4.663	11.73	14.26	sand beach fronts high vertical bluff
	LINC92	20.049	4.386	13.32	16.00	sand beach fronts high vertical bluff
	LINC93	11.324	4.036	12.85	15.47	sand beach fronts high vertical bluff
	LINC94	17.328	4.572	11.33	12.62	sand beach fronts high vertical bluff
	LINC95	23.471	5.384	11.06	14.81	sand beach fronts high vertical bluff
	LINC96	21.673	4.943	10.51	12.49	sand beach fronts high vertical bluff
	LINC97	14.112	6.249	13.23	18.78	sand beach fronts high vertical bluff
	LINC98	26.503	5.508	10.75	13.15	sand beach fronts high vertical bluff
	LINC99	4.038	3.789	6.02	6.39	dune-backed beach
	LINC100	7.415	6.243	9.13	10.16	dune-backed beach
	LINC101	8.522	5.974	8.03	8.66	dune-backed beach
	LINC102	9.045	4.878	10.31	10.96	sand beach fronts low vertical bluff
	LINC103	14.179	3.348	10.15	11.44	sand beach fronts riprap structure

Reach	Transect	D_{HIGH} (m)	D_{LOW} (m)	100-Year (m)	500-Year (m)	Description
	LINC104	13.334	4.655	11.12	12.76	sand beach fronts moderately high vertical bluff
	LINC105	12.719	3.805	9.72	10.77	sand beach fronts riprap structure
	LINC106	13.949	3.912	12.80	14.59	sand beach fronts moderately high vertical bluff
	LINC107	13.931	4.477	11.06	12.45	sand beach fronts moderately high vertical bluff
	LINC108	6.915	6.915	7.94	8.56	sand beach backed by cobbles
	LINC109	12.735	3.943	11.81	12.71	sand beach fronts high vertical bluff
	LINC110	16.781	3.881	12.68	14.53	sand beach fronts high vertical bluff
	LINC111	14.614	4.267	11.84	14.10	sand beach fronts high vertical bluff
	LINC112	23.387	3.480	13.77	15.21	sand beach fronts high vertical bluff
	LINC113	15.564	4.846	10.75	14.86	sand beach fronts high vertical bluff
	LINC114	7.175	6.571	7.74	8.17	dune-backed beach
	LINC115	8.087	4.814	10.87	11.97	sand beach fronts high vertical bluff
	LINC116	18.160	4.228	12.86	17.56	sand beach fronts riprap structure
	LINC117	18.878	4.050	12.88	14.78	sand beach fronts high vertical bluff
	LINC118	7.696	4.679	10.79	12.15	sand beach fronts low vertical bluff
	LINC119	22.033	4.185	11.65	13.56	sand beach fronts high vertical bluff
	LINC120	24.971	4.060	11.50	17.32	sand beach fronts riprap structure
	LINC121	23.486	4.583	11.84	14.11	sand beach fronts high vertical bluff
	LINC122	25.845	4.857	9.71	12.32	sand beach fronts high vertical bluff
	LINC123	23.811	4.813	9.24	9.44	sand beach fronts high vertical bluff
	LINC124	11.830	4.445	11.74	14.66	sand beach fronts high vertical bluff
	LINC125	19.537	3.964	10.96	12.24	sand beach fronts high vertical bluff
	LINC126	6.579	5.934	8.45	9.56	dune-backed beach
	LINC127	7.909	6.129	9.30	11.16	dune-backed beach
	LINC128	9.796	7.038	8.75	10.05	dune-backed beach
	LINC129	15.373	5.863	9.34	11.56	dune-backed beach
	LINC130	12.478	5.151	7.70	8.72	dune-backed beach
Newport	LINC131	13.140	5.881	7.56	8.42	dune-backed beach
	LINC132	10.388	4.379	10.64	11.56	sand beach fronts high vertical bluff
	LINC133	16.665	4.258	11.34	13.60	sand beach fronts high vertical bluff
	LINC134	18.413	5.257	8.37	10.26	sand beach fronts high vertical bluff
	LINC135	18.755	3.455	11.92	12.17	sand beach fronts high vertical bluff
	LINC136	6.669	3.303	11.33	12.48	sand beach fronts seawall
	LINC137	23.345	5.020	9.33	11.65	sand beach fronts high vertical bluff
	LINC138	12.967	5.597	7.54	8.30	sand dune fronts high bluff
	LINC139	15.506	4.190	6.83	7.26	sand dune fronts high bluff
	LINC140	18.965	4.738	9.91	10.28	sand beach fronts high vertical bluff
	LINC141	24.141	5.329	6.76	7.43	sand dune fronts high bluff
	LINC142	8.015	4.395	6.73	7.41	dune-backed beach, backed further by bluffs
	LINC143	18.671	4.548	6.97	7.69	dune-backed beach, backed further by bluffs
	LINC144	7.781	3.596	6.97	7.68	dune-backed beach, backed further by bluffs
	LINC145	6.064	3.189	7.11	7.98	sand dune fronts high bluff
	LINC146	21.800	3.604	6.78	7.57	sand dune fronts high bluff
	LINC147	24.604	4.021	7.59	8.15	sand dune fronts high bluff
Yaquina	LINC148	21.012	5.592	11.63	12.11	narrow rock platform backed by high cliffs
Head	LINC149	19.945	0.739	16.54	16.89	narrow rock platform backed by high cliffs
Beverly	LINC150	12.395	5.351	9.06	11.29	sand beach and platform fronts high vertical bluff
Beach	LINC151	12.037	4.125	10.46	11.73	sand beach and platform fronts high vertical bluff
	LINC152	16.648	4.071	11.84	13.07	sand beach fronts moderately high vertical bluff
	LINC153	8.459	4.074	9.68	10.50	sand beach fronts moderately high vertical bluff
	LINC154	7.662	3.824	9.34	9.75	sand beach backed by cobble berm/riprap
	LINC155	22.818	4.776	11.97	13.40	sand beach fronts high vertical bluff
	LINC156	36.791	4.980	9.72	11.34	sand beach fronts high vertical bluff
	LINC157	14.831	3.994	13.60	16.81	sand beach fronts high vertical bluff
	LINC158	15.853	5.141	12.15	13.58	sand beach fronts high vertical bluff
	LINC159	13.518	5.000	11.10	11.83	sand beach fronts high vertical bluff

Reach	Transect	D_{HIGH} (m)	D_{LOW} (m)	100-Year (m)	500-Year (m)	Description
	LINC160	14.915	3.525	11.48	12.66	sand beach fronts riprap structure
	LINC161	8.559	5.320	10.08	11.74	sand beach backed by cobble berm
	LINC162	18.977	5.346	10.56	14.96	sand beach fronts high vertical bluff
	LINC163	23.622	5.016	13.98	17.09	sand beach fronts high vertical bluff
	LINC164	12.086	4.816	13.24	16.07	sand beach fronts high vertical bluff
	LINC165	22.688	5.331	10.25	14.81	sand beach fronts high vertical bluff
	LINC166	21.825	4.401	12.86	15.83	sand beach fronts high vertical bluff
	LINC167	17.714	4.820	11.04	14.93	sand beach fronts high vertical bluff
	LINC168	15.690	5.194	9.31	12.30	sand beach fronts high vertical bluff
	LINC169	18.825	4.807	9.33	9.78	sand beach fronts high vertical bluff
	LINC170	33.129	4.713	10.45	11.74	sand beach fronts high vertical bluff
	LINC171	28.516	4.251	11.35	13.32	sand beach fronts high vertical bluff
Otter Rock	LINC172	21.009	4.444	11.15	15.16	rock platform and sandy beach backed by bluff
	LINC173	25.393	3.221	10.14	10.68	rock platform backed by bluff
	LINC174	23.010	3.156	14.69	15.94	rock platform backed by bluff
	LINC175	23.244	2.644	15.14	16.32	rock platform backed by bluff
	LINC176	24.099	2.344	15.79	18.91	rock platform backed by bluff
Cape Foulweather	LINC177	116.753	1.237	14.99	15.37	narrow rock platform backed by high cliffs
	LINC178	103.606	3.516	14.60	16.58	narrow rock platform backed by high cliffs
Miroco	LINC179	19.740	1.743	13.90	14.59	basalt ramp with low tide cliff
	LINC180	21.948	0.397	12.19	12.44	basalt ramp with low tide cliff
	LINC181	16.989	1.637	13.07	13.35	basalt ramp with low tide cliff
Rocky Creek	LINC182	14.183	1.467	13.28	13.86	basalt ramp with low tide cliff
	LINC183	14.596	2.088	11.75	12.22	basalt ramp with low tide cliff
Whale Cove	LINC184	15.310	1.302	14.44	15.12	basalt ramp with low tide cliff
	LINC185	13.989	0.314	16.92	17.75	basalt ramp with low tide cliff
	LINC186	16.676	2.155	11.63	11.91	basalt ramp with low tide cliff
	LINC187	14.648	1.253	13.77	14.33	basalt ramp with low tide cliff
	LINC188	10.068	1.250	14.36	15.07	basalt ramp with low tide cliff
	LINC189	12.439	0.868	14.21	14.82	basalt ramp with low tide cliff
Depoe Bay	LINC190	31.062	1.745	12.19	12.60	narrow rock platform backed by basalt ramp
	LINC191	26.414	1.966	10.31	12.46	narrow rock platform backed by basalt cliff
	LINC192	17.251	1.018	9.90	10.99	moderately wide rock platform backed by basalt cliff
	LINC193	15.543	1.512	12.88	13.18	moderately wide rock platform backed by basalt cliff
	LINC194	14.360	1.173	14.59	15.06	basalt cliff
	LINC195	15.519	1.013	14.74	15.59	basalt cliff
	LINC196	14.959	2.163	15.30	19.11	moderately wide rock platform backed by basalt cliff
	LINC197	14.091	3.035	11.94	13.17	narrow rock platform backed by basalt cliff
	LINC198	15.074	0.249	11.76	12.58	moderately wide rock platform backed by basalt cliff
	LINC199	13.910	1.321	13.81	13.88	basalt cliff
	LINC200	18.001	0.092	14.82	15.23	basalt cliff
	LINC201	21.750	5.697	10.12	12.89	moderately wide rock platform backed by basalt cliff
	LINC202	19.540	2.624	14.16	15.53	moderately wide rock platform backed by basalt cliff
Fogarty Creek	LINC203	16.484	3.988	9.93	10.65	bluff fronted by sand and gravel beach andshore platform
	LINC204	5.960	4.247	6.84	7.60	riprap fronted by sand and gravel beach andshore platform
	LINC205	17.253	3.999	10.61	11.39	bluff fronted by sand and gravel beach andshore platform

Reach	Transect	D_{HIGH} (m)	D_{LOW} (m)	100-Year (m)	500-Year (m)	Description
	LINC206	20.951	2.861	12.98	14.42	riprap fronted by sand and gravel beach andshore platform
	LINC207	13.485	3.282	12.06	12.67	bluff fronted by sand and gravel beach andshore platform
	LINC208	18.792	3.215	11.82	12.58	bluff fronted by sand and gravel beach andshore platform
	LINC209	20.005	4.334	12.75	14.79	bluff fronted by sand and gravel beach andshore platform
	LINC210	18.034	3.436	13.70	14.99	bluff fronted by sand and gravel beach andshore platform
Siletz Spit	LINC211	15.137	3.330	12.55	14.05	mixed sand and gravel beach fronts riprap structure
	LINC212	10.448	4.393	12.68	15.47	mixed sand and gravel beach fronts riprap structure
	LINC213	10.398	4.798	11.44	13.04	mixed sand and gravel beach fronts bluff
	LINC214	9.392	5.565	10.56	12.93	mixed sand and gravel beach fronts riprap structure
	LINC215	9.145	5.009	11.68	13.05	mixed sand and gravel beach fronts riprap structure
	LINC216	13.620	5.545	11.52	13.31	mixed sand and gravel beach fronts riprap structure
	LINC217	15.570	5.785	13.83	16.04	mixed sand and gravel beach fronts bluff
	LINC218	14.340	4.998	12.86	14.65	mixed sand and gravel beach fronts riprap structure
	LINC219	13.497	4.328	11.77	12.95	mixed sand and gravel beach fronts riprap structure
	LINC220	21.776	4.896	12.68	13.94	mixed sand and gravel beach fronts riprap structure
	LINC221	8.111	6.149	8.80	9.98	mixed sand and gravel beach fronts dune
	LINC222	15.448	5.300	12.41	14.32	mixed sand and gravel beach fronts bluff
	LINC223	13.416	2.809	12.08	13.12	mixed sand and gravel beach fronts riprap structure
	LINC224	15.850	5.409	10.26	14.13	mixed sand and gravel beach fronts bluff
	LINC225	15.390	5.384	8.93	9.69	mixed sand and gravel beach fronts riprap structure
	LINC226	13.513	5.449	11.01	15.46	mixed sand and gravel beach fronts bluff
	LINC227	13.125	4.887	10.28	11.14	mixed sand and gravel beach fronts seawall
	LINC228	24.807	5.201	14.20	17.75	mixed sand and gravel beach fronts bluff
	LINC229	40.682	6.543	9.46	10.28	mixed sand and gravel beach fronts riprap structure
	LINC230	15.605	7.001	9.04	9.76	dune-backed beach overlying riprap structure
	LINC231	9.419	7.592	10.10	11.81	dune-backed beach overlying riprap structure
	LINC232	15.636	7.219	9.02	9.71	dune-backed beach overlying riprap structure
	LINC233	8.342	5.217	8.96	9.80	dune-backed beach overlying riprap structure
	LINC234	10.097	8.183	10.60	12.04	dune-backed beach overlying riprap structure
	LINC235	9.877	7.347	9.26	9.83	dune-backed beach overlying riprap structure
	LINC236	8.964	6.356	9.12	9.91	dune-backed beach overlying riprap structure
	LINC237	10.662	6.537	10.14	11.47	dune-backed beach overlying riprap structure
	LINC238	9.091	9.091	11.43	12.54	dune-backed beach overlying riprap structure
	LINC239	9.962	7.637	10.84	12.29	dune-backed beach overlying riprap structure
	LINC240	8.306	8.017	9.01	10.34	dune-backed beach overlying riprap structure
	LINC241	9.086	6.925	9.18	10.72	dune-backed beach overlying riprap structure
	LINC242	9.039	7.673	10.04	11.92	dune-backed beach overlying riprap structure
	LINC243	8.765	8.765	11.26	12.78	dune-backed beach
	LINC244	6.000	6.000	9.22	10.57	dune-backed beach

Reach	Transect	D_{HIGH} (m)	D_{LOW} (m)	100-Year (m)	500-Year (m)	Description
Lincoln City	LINC245	6.231	4.263	7.27	8.00	sand beach fronts high bluffs
	LINC246	6.254	6.254	8.87	9.88	sand beach fronts high bluffs
	LINC247	24.270	7.000	8.82	9.49	sand beach fronts high bluffs
	LINC248	7.621	5.472	10.95	13.63	sand beach fronts seawall
	LINC249	27.100	5.166	9.58	13.17	sand beach fronts high bluffs
	LINC250	10.979	5.279	9.28	10.93	sand beach fronts riprap
	LINC251	7.300	4.153	11.95	14.27	sand beach fronts seawall
	LINC252	7.415	5.758	11.58	13.81	sand beach fronts seawall
	LINC253	32.943	6.413	8.51	9.01	sand beach fronts high bluffs
	LINC254	34.319	5.667	9.42	11.41	sand beach fronts high bluffs
	LINC255	7.410	4.866	9.83	10.35	sand beach fronts seawall and high bluffs
	LINC256	12.766	4.785	10.63	11.43	sand beach fronts seawall and high bluffs
	LINC257	37.604	6.525	8.86	9.69	sand beach fronts high bluffs
	LINC258	38.806	4.899	10.58	11.20	sand beach fronts high bluffs
	LINC259	7.575	4.883	13.74	15.15	sand beach fronts seawall
	LINC260	40.100	5.800	10.56	12.35	sand beach fronts moderately high bluffs
	LINC261	24.403	6.770	8.65	9.66	sand beach fronts moderately high bluffs
	LINC262	18.974	4.487	11.23	12.32	sand beach fronts riprap
	LINC263	7.835	5.492	11.43	12.05	sand beach fronts seawall
	LINC264	9.440	4.957	10.40	11.15	sand beach fronts riprap
	LINC265	6.798	4.406	9.99	10.91	sand beach fronts seawall
	LINC266	6.700	3.383	9.37	9.99	sand beach fronts riprap
	LINC267	7.069	4.537	7.34	8.12	sand beach fronts riprap
	LINC268	7.897	4.423	10.24	11.30	sand beach fronts seawall
	LINC269	10.260	6.259	8.75	9.58	dune-backed beach
	LINC270	14.128	5.222	11.31	13.11	sand beach fronts riprap and bluffs
	LINC271	18.857	5.554	11.80	17.20	sand beach fronts moderately high bluffs
	LINC272	8.800	4.829	8.94	9.12	sand beach fronts riprap and bluffs
	LINC273	27.820	5.684	11.70	14.14	sand beach fronts riprap and bluffs
	LINC274	10.235	6.466	9.37	10.16	sand beach fronts riprap and bluffs
	LINC275	13.002	6.350	9.80	10.70	sand beach fronts riprap and bluffs
	LINC276	12.510	4.815	10.83	12.78	sand beach fronts riprap and bluffs
	LINC277	19.421	5.586	11.57	14.42	sand beach fronts moderately high bluffs
	LINC278	7.419	4.556	12.95	15.10	sand beach fronts seawall
	LINC279	9.806	4.226	9.81	11.32	sand beach fronts riprap and bluffs
	LINC280	7.671	4.584	12.52	15.21	sand beach fronts seawall
	LINC281	8.843	5.283	9.11	11.06	sand beach fronts low bluff
	LINC282	10.062	5.779	7.14	7.57	sand beach fronts moderately high bluffs
	LINC283	9.471	5.500	8.28	9.44	sand beach fronts riprap/low seawall and bluffs
	LINC284	12.776	5.865	8.15	8.78	sand beach fronts moderately high bluffs
	LINC285	9.284	5.358	9.38	11.79	sand beach fronts seawall and bluffs
	LINC286	9.531	5.057	7.62	8.12	sand beach fronts riprap and bluffs
	LINC287	11.137	4.982	8.19	9.29	sand beach fronts riprap and bluffs
	LINC288	6.865	5.143	12.01	13.19	sand beach fronts moderately high bluffs
	LINC289	18.092	4.752	10.87	11.91	sand beach fronts moderately high bluffs
	LINC290	28.243	5.285	12.36	13.34	sand beach fronts moderately high bluffs
	LINC291	10.575	4.853	10.61	11.53	sand beach fronts riprap and bluffs
	LINC292	13.387	5.078	11.92	13.47	sand beach fronts riprap and bluffs
	LINC293	11.936	4.686	12.02	13.50	sand beach fronts low bluff
	LINC294	8.286	5.341	7.65	8.19	sand beach fronts dune and low bluff
	LINC295	9.221	5.021	10.86	14.65	sand beach fronts low bluff
	LINC296	8.311	4.358	8.51	9.39	sand beach fronts riprap and bluffs
	LINC297	13.363	4.891	10.52	11.16	sand beach fronts collapsed riprap and bluff
	LINC298	11.517	4.279	9.35	9.92	sand beach fronts riprap and bluffs
	LINC299	10.933	4.898	9.97	10.55	sand beach fronts seawall and bluffs
	LINC300	11.270	5.022	11.45	12.43	sand beach fronts seawall and bluffs

Reach	Transect	D_{HIGH} (m)	D_{LOW} (m)	100-Year (m)	500-Year (m)	Description
	LINC301	11.929	4.800	9.16	11.16	sand beach fronts riprap and bluffs
	LINC302	20.930	5.449	12.80	14.03	sand beach fronts high bluffs
Salmon River	LINC303	47.701	3.136	8.19	8.66	dune-backed beach backed by bluff
	LINC304	26.308	5.173	10.51	11.42	dune-backed beach backed by bluff
	LINC305	57.755	3.220	10.20	11.06	inter-tidal rocky area backed by bluffs
	LINC306	32.488	5.553	10.89	13.22	dune-backed beach backed by bluff
	LINC307	23.641	4.128	12.25	13.86	dune-backed beach backed by bluff
	LINC308	6.251	5.058	9.29	10.62	dune-backed beach
Cascade Head	LINC309	48.172	1.609	14.13	14.28	plunging cliff
	LINC310	43.560	1.207	13.83	14.01	plunging cliff
	LINC311	24.427	0.358	12.91	13.46	boulder beach backed by bluffs
	LINC312	93.240	2.125	12.40	12.68	plunging cliff
	LINC313	139.103	0.000	17.29	17.49	plunging cliff
Supplemental Transects	LINC_9_294	5.986	3.518	7.90	9.05	sandy beach backed by bluff
	LINC_26_457	7.145	4.451	9.94	11.89	sand beach fronts low vertical bluff
	LINC_26_459	6.682	4.453	10.42	11.80	sand beach fronts low vertical bluff
	LINC_43_554	8.895	3.653	11.44	12.24	sand beach fronts moderately high vertical bluff
	LINC_44_573	8.826	3.259	11.03	12.85	sand beach fronts riprap structure
	LINC_44_575	8.786	4.080	9.86	10.56	sand beach fronts riprap structure
	LINC_99_1257	4.984	4.196	6.54	7.06	Ona Beach - dune-backed beach
	LINC_99_1274	4.300	3.583	6.46	6.84	Ona Beach - dune-backed beach
	LINC_106_1340	12.480	4.428	13.34	14.17	sand beach fronts moderately high vertical bluff
	LINC_106_1343	8.969	4.267	11.63	13.72	sand beach fronts moderately high vertical bluff
	LINC_106_1345	11.830	3.936	11.70	12.91	sand beach fronts moderately high vertical bluff
	LINC_109_1366	7.444	4.984	10.44	15.52	sand beach fronts high vertical bluff
	LINC_109_1367	8.862	4.690	10.85	13.29	sand beach fronts high vertical bluff
	LINC_121_1528	8.926	5.145	13.22	15.10	creek (South Beach)
	LINC_167_2257	4.221	4.221	7.60	8.42	Spencer Creek, Beverly Beach
	LINC_195_2790	13.245	2.217	12.63	13.56	plunging cliff, north of Depoe Bay
	LINC_204_2928	3.239	3.239	9.07	9.80	Fogarty Creek
	LINC_250_3385	7.779	5.140	10.92	13.45	sand beach fronts riprap

Notes:

100-year and 500-year total water level (TWL) values relative to NAVD88 vertical datum.

D_{HIGH} is the crest of the dune, bluff, or barrier determined for the eroded profile. *Red text denotes that the crest is overtopped.*

6.4 Overtopping Calculations

Overtopping of natural features such as foredunes, spits and coastal engineering structures and barriers occurs when the wave runup superimposed on the tide exceeds the crest of the foredune or structure (**Figure 6-8**). Hazards associated with wave overtopping can be linked to a number of simple direct flow parameters including (Pullen and others, 2007):

- mean overtopping discharge, q;
- overtopping velocities over the crest and farther landward, V;
- landward extent of green water and splash overtopping $y_{G,\ outer}$; and
- overtopping flow depth, h at a distance y landward of the foredune crest or "barrier."

NHC (2005) notes that there are three physical types of wave overtopping:

1. *Green water or bore overtopping* occurs when waves break onto or over the foredune or barrier and the overtopping volume is relatively continuous;
2. *Splash overtopping* occurs when the waves break seaward of the foredune or barrier, or where the foredune or barrier is high relative to the wave height and overtopping consists of a stream of droplets. Splash overtopping can be a function of its momentum due to the runup swashing up the barrier and/or may be enhanced due to onshore direct winds; and
3. *Spray overtopping* is generated by the effects of wind blowing droplets and spray that are derived from the wave crests.

Mapping these respective flood inundation zones requires an estimate of the velocity, V, the overtopping discharge, q, of the water that is carried over the crest, the inland extent of green water and splash overtopping, and the envelope of the water surface that is defined by the water depth, h, landward of the barrier crest. According to NHC (2005) these hazard zones are ultimately defined based on the following two derivations:

- Base Flood Elevations (BFEs) are determined based on the water surface envelope landward of the barrier crest; and
- Hazard zones are determined based on the landward extent of green water and splash overtopping, and on the depth and flow velocity in any sheet flow areas beyond that, defined as $hV^2 = 5.7\ m^3/s^2$ *or* $200\ ft^3/s^2$.

A distinction can be made between whether green water (or bore) or splash overtopping predominates at a particular location that is dependent on the ratio of the calculated wave runup height relative to the barrier crest elevation, R/Z_c. When $1 < R/Z_c < 2$, splash overtopping dominates and for $R/Z_c > 2$, bore propagation occurs. In both cases, R and Z_c are relative to the 2% dynamic water level ($DWL_{2\%}$) at the barrier (Figure D.4.5-12 in NHC [2005, p. D.4.5-22]).

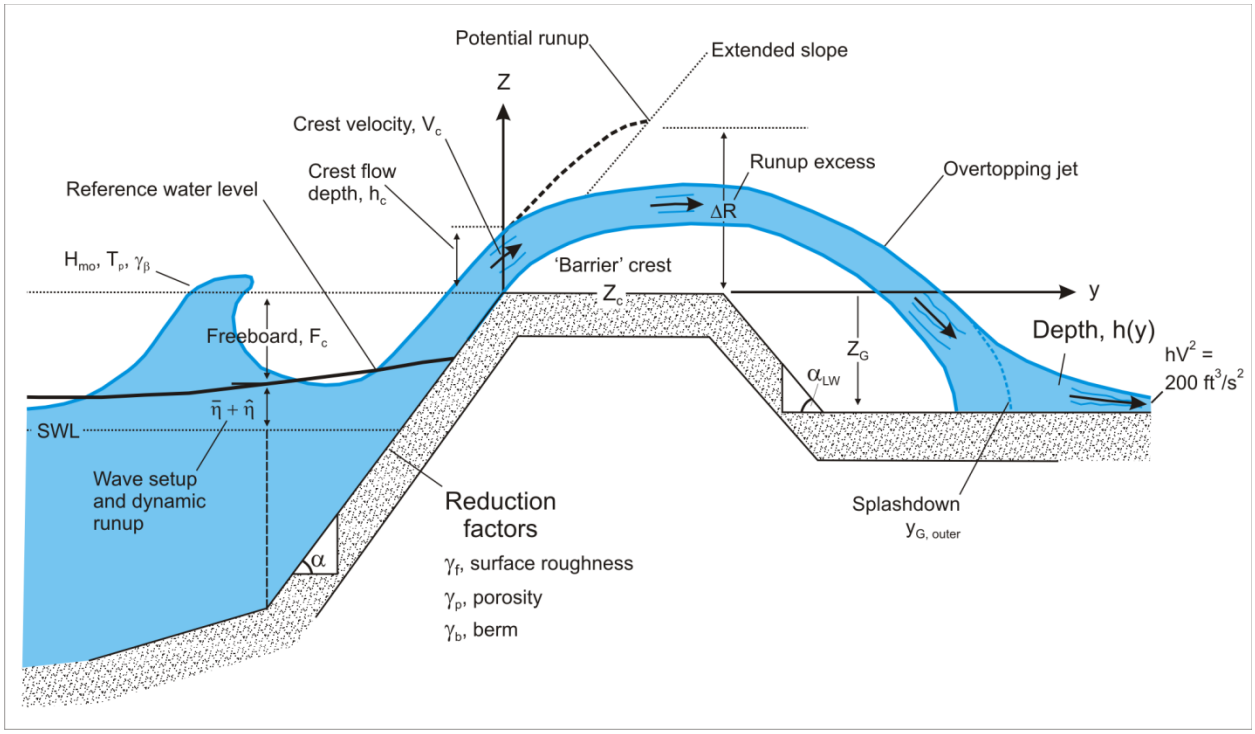

Figure 6-8. Nomenclature of overtopping parameters available for mapping base flood elevations (BFEs) and flood hazard zones (after NHC, 2005).

6.4.1 Mean overtopping rate at the "barrier" crest

Wave overtopping of dunes and barrier is a function of both hydraulic and barrier structure parameters whereby:

$$q = f(H_{mo}, T_p, \beta, F_c, DWL_{2\%}, geometry) \qquad (6.14)$$

where q is the overtopping discharge (expressed as cubic meters per second per meter, $m^3/s/m$ [$ft^3/s/ft$]), H_{mo} is the significant wave height at the toe of the structure, T_p is the peak period, β is the angle of wave attack, F_c is the freeboard, and $DWL_{2\%}$ is 2% dynamic water level at the toe of the structure (**Figure 6-8**).

Prior to calculating the mean overtopping rate at the barrier crest it is necessary to first distinguish between four contrasting types of wave breaking situations that may impact a particular barrier or dune overtopping situation. There four conditions include *non-breaking* or *breaking* on a normally sloped barrier (where 0.067 < tan α <0.67), and *reflecting* or *impacting* on steeply sloping or vertical barriers (where tan $\alpha \geq 0.67$). Of these, the breaking wave situation is the dominant condition in Lincoln County, where the waves have already broken across the surf zone and are reforming as bores prior to swashing up the beach face or barrier.

For beaches and normally sloping barriers (where 0.067 < tan α < 0.67), a distinction can be made between situations where waves break directly on the barrier versus those conditions where the waves have not yet broken. These conditions can be determined using the surf similarity parameter (Iribarren number) defined here in terms of the beach or structure slope (tan α), and the wave steepness ($S_{op} = H_{mo}/L_o$):

$$\xi_{op} = \frac{tan\alpha}{\sqrt{\frac{H_{mo}}{L_o}}} = \frac{tan\alpha}{\sqrt{S_{op}}} \qquad (6.15)$$

Breaking on normally sloping surfaces generally occurs where the surf similarity number, $\xi_{op} \leq 1.8$, while non-breaking conditions occur when $\xi_{op} > 1.8$. As noted above, for the Lincoln County coastline the identified Iribarren numbers almost always fell below

the 1.8 criteria indicating that the incident waves are always broken prior to reaching the beach or the barrier face.

At the beach or barrier crest, the relative freeboard (F_c/H_{mo}), **Figure 6-8**, is a particularly important parameter because changing these two parameters controls the volume of water that flows over the barrier crest. For example, increasing the wave height or period increases the overtopping discharge, as does reducing the beach or barrier crest height or raising the water level.

A variety of prediction methods are available for calculating the overtopping discharge and are almost entirely based on laboratory experiments based on a range of structure slopes (slopes between 1:1 and 1:8, with occasional tests at slopes around 1:15 or lower). Factors that will serve to reduce the potential overtopping discharge include the barrier *surface roughness* (γ_f), the presence of a *berm* (γ_b), *wave approach directions* (γ_β), and the *porosity* of the barrier (γ_p) (**Figure 6-8**). In terms of porosity, increasing this variable effectively reduces the wave runup and overtopping discharge because more of the water is able to be taken up by the voids between the clasts and particles. As noted by NHC (2005), the effect of the *porosity* factor makes it convenient to distinguish between impermeable and permeable structures. Methods for determining the various reduction factors are described in Table D.4.5-3 in NHC (2005, p. D.4.5-13), with one difference whereby the approach recommended for determining the wave approach (γ_β) reduction factor for wave overtopping calculations is based on the following equation:

$$\gamma_\beta = \begin{Bmatrix} 1 - 0.0033|\beta|, (0 \le |\beta| \le 80°) \\ 1 - 0.0033|80|, (|\beta| \ge 80°) \end{Bmatrix} \quad (6.16)$$

Table D.4.5-3 in NHC (2005, p. D.4.5-13) identifies four general categories of overtopping applications: overtopping on a normally sloping barrier (e.g., riprap structure), steep sloping or vertical barrier (e.g., seawall or bluff where some waves broken); steep sloping or vertical barrier (all waves broken), and shallow foreshore slopes subject to large Iribarren numbers.

For a normally sloping barrier, where 0.05 < tan α < 0.67 and the Iribarren number (ξ_{op}) ≤ 1.8 (breaking wave condition), the following formulation can be used to determine the mean overtopping discharge (both dimensional [q] and non-dimensional [Q] forms) at the barrier crest:

$$q = Q\sqrt{\frac{gH_{mo}\tan\alpha}{S_{op}}} \text{ where:} \quad (6.17)$$

$$Q = 0.06e^{-4.7F'}, \text{ and}$$

$$F' = \frac{F_c}{H_{mo}}\frac{\sqrt{S_{op}}}{\tan\alpha}\frac{1}{\gamma_f\gamma_b\gamma_\beta\gamma_p}$$

For non-breaking conditions (Iribarren number (ξ_{op}) > 1.8):

$$q = Q\sqrt{gH_{mo}^3} \text{ where:} \quad (6.18)$$

$$Q = 0.2e^{-2.3F'}, \text{ and}$$

$$F' = \frac{F_c}{H_{mo}}\frac{1}{\gamma_f\gamma_\beta}$$

For steep sloping or vertical barrier, where tan α > 0.67 and $h_* \ge 0.3$ (reflecting condition, where

$$h_* = \frac{h}{H_{mo}}\left(\frac{2\pi h}{gT_m^2}\right)$$

and h is the water depth at the structure toe), the following formulation can be used:

$$q = Q\sqrt{gH_{mo}^3} \text{ where:} \quad (6.19)$$

$$Q = 0.05e^{-2.78F_c/H_{mo}}$$

For impacting conditions (h_* < 0.3):

$$q = Q\sqrt{gh^3}\,h_*^2 \text{ where:} \quad (6.20)$$

$$Q = 1.37 * 10^{-4}(F')^{-3.24}, \text{ and}$$

$$F' = \frac{F_c}{H_{mo}}\,h_*$$

For steep sloping or vertical barrier (all waves are broken) where the structure toe < $DWL_{2\%}$ water level and where $(F_c/H_{mo})*h_* \leq 0.03$:

$$q = Q\sqrt{gh^3}\,h_*^2 \text{ where:} \quad (6.21)$$

$$Q = 0.27 * 10^{-4} e^{-3.24\,(F_c/H_{mo})h_*}$$

For steep sloping or vertical barrier (all waves are broken) where the structure toe > $DWL_{2\%}$ water level:

$$q = Q\sqrt{gh^3}\,h_*^2 \text{ where:} \quad (6.22)$$

$$Q = 0.06e^{-4.7\,F_c S_{op}^{-0.17}}$$

We have implemented two additional overtopping calculations following discussions with Dr. W.G. McDougal, which may be applied to beaches subject to gently sloping ($\tan\beta < 0.4$), dissipative foreshores:

$$q = Q\sqrt{gh^3}h_*^2 \text{ where:} \quad (6.23)$$

$$Q = 0.21\sqrt{gH_{mo}^3}e^{-F'} \text{ and}$$

$$F' = \frac{F_c}{\gamma_f \gamma_\beta H_{mo}(0.33 + 0.022\xi_{op})}$$

and cases where there is negative freeboard. The latter occurs when the dynamic water level ($DWL_{2\%}$) is higher than the barrier crest, which produces a negative freeboard (i.e., $-F_c$). In this situation we apply the well-known weir type formula to define the volume of water that is overflowing the crest (Eurotop, 2007). The formulation used is:

$$q = Q_s + q_w \text{ where:} \quad (6.24)$$

$$Q_s = 0.4583(-F_C)\sqrt{-F_C g} \text{ and}$$

$$Q_w = 0.21\sqrt{gH_{mo}^3} \text{ and}$$

$$q_w = Q_w\sqrt{gh^3}h_*^2$$

6.4.2 Overtopping limits and flood hazard zones landward of the "barrier" crest

Estimates of the landward limit of the splashdown distance associated with wave overtopping and the landward limit of the hazard zone require several calculation steps. These include:

1. The following three initial parameters are first calculated:
   a. excess potential runup: $\Delta R = R - Z_c$;
   b. crest flow rate, $V_c \cos\alpha$ (where $V_c = 1.1\sqrt{g\Delta R}$ for cases where splash overtopping, and $V_c = 1.8\sqrt{g\Delta R}$ for bore overtopping); and
   c. initial flow depth, h_c (where $h_c = 0.38\Delta R$).
2. The associated onshore wind component, *Wy* is determined from available wind data. For the purposes of this study, we used *Wy = 19.6 m/s (64.3 ft/s)*, which was determined from an analysis of winds (mean from a select number of storms) measured at the Cape Arago C-MAN station operated by the NDBC. In the absence of wind data, NHC (2005) recommends a wind speed of 13.4 m/s (44 ft/s).
3. The enhanced onshore water velocity component $(V_c \cos\alpha)'$ is then calculated using equation 6.25:

$$\text{For vertical bluffs and seawalls;} \quad (6.25)$$
$$(V_c \cos\alpha)' = 0.3 * W_y$$

$$\text{All other cases: } (V_c \cos\alpha)' = V_c \cos\alpha + 0.3(W_y - V_c \cos\alpha)$$

4. The effective angle, α_{eff}, is calculated from:

$$\tan\alpha_{eff} = \frac{V_c sin\alpha}{(V_c cos\alpha)'}.$$

5. Having determined the above parameters, the outer limit of the splash region, $y_{G\ outer}$ is calculated using equation 6.26. Here we have used an algorithm developed by Dr. Bill McDougal (Coastal Engineer, OSU and Technical Coordinator of the North Pacific FEMA West Coast Guidelines) of the form:

$$y_{G\ outer} = \frac{(V_c \cos\alpha)'}{g} * V_c \sin\alpha - mBackshore * (V_c \cos\alpha)' * \left(1 + \sqrt{1 - \frac{2g * bBackshore}{(V_c \sin\alpha - mBackshore * (V_c \cos\alpha)'^2)}}\right) \quad (6.26)$$

and

$$Z_G = bBackshore + (mBackshore * y_{G\ outer}) \quad (6.27)$$

where *bBackshore* is the intercept for the backshore slope adjacent to the barrier crest and *mBackshore* is the slope of the backshore. equation 6.26 is ultimately based on Figure D.4.5-15 *in* NHC (2005, p. D.4.5-30).

6. The total energy, E, of the splashdown is calculated from $E = \Delta R - Z_G$.
7. Finally, the initial splashdown velocity, V_o (where $V_o = 1.1\sqrt{gE}$), and depth, h_o (where $h_o = 0.19E$) are calculated. In the case of green water or bore overtopping, the splashdown velocity, V_o, can be calculated from $V_o = 1.1\sqrt{g\Delta R}$, while the flow depth is determined as $h_o = 0.38E$.

Having determined the initial splashdown velocity, V_o, and flow depth, h_o, the landward extent of the overland flow is calculated using an approach modified from that originally proposed by Cox and Machemehl (1986). The version presented in NHC (2005) effectively calculates the flow depth, h, with distance, y, from the barrier crest, such that the flow depth decays asymptotically as y-distance increases away from the barrier crest, eventually approaching zero. The NHC (2005) equation is shown as equation 6.28:

$$h(y) = \left[\sqrt{h_o} - \frac{5(y - y_o)}{A\sqrt{gT^2}}\right]^2 \quad (6.28)$$

where h_o is determined from step 7 above and for an initial approximation the non-dimensional A parameter may be taken as unity. For sloping backshores, the A parameter in equation 6.28 can be modified such that $A_m = A(1 - 2 * \tan\alpha_{LW})$, and the value in parentheses is limited to the range 0.5 to 2. According to NHC (2005) if the maximum distance of splash or bore propagation calculated using equation 6.28 does not appear reasonable or match field observations, the A parameter can be adjusted in order to increase or decrease the landward wave propagation distance. In addition, for green water or bore propagation the A parameter value is taken, initially, to be 1.8.

For the purposes of this study we have adopted a modified version of equation 6.28 developed by Dr. W.G. McDougal of the form:

$$h(y) = \left[h_o^{1/2} - \frac{y - y_o}{2\alpha(\alpha + 1)^{\frac{3}{2}}(1 - 2m)\, g^{0.5}T}\right]^2 \quad (6.29)$$

where m is the slope of the backshore and α is a constant that can be varied in order to increase or decrease the landward wave propagation distance.

Finally, the landward limit of the hazard zone defined as $hV^2 = 5.7\ m^3/s^2$ *(or 200* ft^3/s^2*)* is determined, whereby h is the water depth given by the modified Cox and Machemehl (1986) method (equation 6.29) and $V = V_o$ calculated from step 7 above.

6.4.3 Initial testing of the landward limit of wave overtopping

Our initial computations of the landward extent of wave overtopping using the steps outlined above yielded narrow hazard zones for our original coastal FIRM study in Coos County. In order to calibrate equation 6.29, we performed wave overtopping calculations and inundation for a site on the northern Oregon coast, where there are field observations of wave overtopping. The site is Cape Lookout State Park located on the northern Oregon coast in Lincoln County (Allan and others, 2006; Allan and Komar, 2002a; Komar and others, 2003). The southern portion of Cape Lookout State Park is characterized by a wide, gently sloping, dissipative sand beach backed by a moderately steep gravel berm and, ultimately, by a low foredune that has undergone significant erosion since the early 1980s (Komar and others, 2000).

On March 2-3, 1999, the crest of the cobble berm/dune at Cape Lookout State Park was overtopped during a major storm; the significant wave heights reached 14.1 m (46.3 ft), while the peak periods were 14.3 seconds measured by a deepwater NDBC wave buoy (Allan and Komar, 2002b). Wave overtopping of the dune and flooding extended ~70 m (230 ft) into the park (Dr. P. Komar, Emeritus Professor, College of Oceanic and Atmospheric Sciences, pers. comm., 2010), evidence for which included photos and field evidence including pockmarks at the base of the tree trunks located in the park. These pock-marks were caused by cobbles having been carried into the park from the beach by the overtopping waves, where they eventually slammed into the base of the trees as ballistics. Because the average beach slopes at Cape Lookout State park are analogous to those observed elsewhere along the Lincoln County coastline and because large wave events associated with extratropical storms affect significant stretches (100s to 1,000 kilometers) of the coast at any single point in time, we believe these data provide a reasonable means in which to investigate a range of alpha (α) values that may be used to determine the landward extent of wave inundation in the park.

Using beach morphology data (slope [tan β] = 0.089, barrier crest = 5.5 m [18 ft]) from Cape Lookout State Park and deepwater wave statistics from a nearby NDBC wave buoy (#46050), we experimented with a range of alpha values (**Figure 6-9**) in order to replicate the landward extent of the inundation. As can be seen in **Figure 6-8**, in order to emulate the landward extent of flooding observed at Cape Lookout our analyses yielded an alpha of 0.58. Using α = 0.58, we in turn calculated the extent of the hazard zone where $h(y)$ = 200 ft^3/s^2, which was found to be ~34 m from the crest of the cobble berm/dune, consistent with damage to facilities in the park.

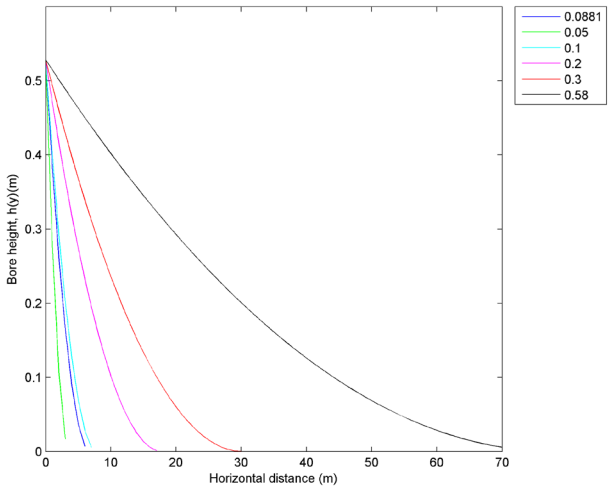

Figure 6-9. Calculations of bore height decay from wave overtopping at Cape Lookout State Park at the peak of the 2-3 March 1999 storm based on a range of alpha (α) values.

6.4.4 Wave overtopping and hazard zone limits calculated for Lincoln County

Table 6-3 presents the results of the calculated splashdown distances ($y_{G\ outer}$) and the landward extent of the flow (hV^2) where the flows approach 5.7 m^3/s^2 (or 200 ft^3/s^2). **Table 6-3** includes a more conservative splashdown distance, based on an enhanced wind velocity of 19.6 m/s (64.3 ft/s); this contrasts with the default wind speed of 13.4 m/s (44 ft/s) suggested by NHC (2005). This enhanced wind velocity was determined from an analysis of wind speeds measured by the Cape Arago C-MAN station (http://www.ndbc.noaa.gov/station_page.php?station=CARO3) located adjacent to the mouth of Coos Bay (Allan and others 2012b). Essentially, Allan and others examined the wind speeds identified at Cape Arago for a range of storm events and identified a wide range of values, with a maximum mean wind speed of 19.6 m/s (64.3 ft/s). Because the measured wind speeds reflect a 2-minute average such that higher wind speeds have been measured throughout the entire record (e.g., the maximum 2-minute average wind speed is 29.3 m/s (96 ft/s), while the maximum 5-s wind gust reached 38.1 m/s [125.0 ft/s]), we believe it is justified to use the more conservative enhanced wind velocity of 19.6 m/s (64.3 ft/s). Furthermore, comparisons by Allan and others (2012b) indicated that the relative difference between the value suggested by NHC (2005) and the enhanced wind used here differs by about 30%. As can be seen from the **Table 6-3**, the calculated splashdown distances ($y_{G\ outer}$) indicate splash distances that range from as little as 0.1 m (0.33 ft) to a maximum of 10.4 m (34 ft); the mean splash distance is 3.8 m (12.5 ft), while the standard deviation is 2.3 m (7.5 ft). Thus, adopting the reduced wind velocity would cause the zones to narrow by ~3.1 m for the highest splash distance; for the majority of cases (mean + 1σ) this would equate to a reduction of 1.8 m (6 ft). Overall, these differences are negligible given the tremendous uncertainties in calculating splash and overtopping (NHC, 2005).

Hazard zone calculations shown in **Table 6-3** indicate a similarly broad range of values that vary from negligible (i.e., effectively where the 1% TWL intersects with the backshore, plus the width of the splash zone where applicable) to as much as 164 m (538 ft) wide, with the widest zones having occurred where overtopping significantly exceeds the eroded beach crest elevations such as along the Yachats to Waldport shoreline. Unlike the Tillamook County coastline, there is very little field-based information of past storm wave overtopping events to corroborate the magnitude of the results identified in **Table 6-3**. The depth of flooding at each mapped overtopping zone is indicated in **Table 6-4**.

Table 6-3. Splashdown and hazard zone limits calculated for Lincoln County detailed coastal sites. Values reported in the table reflect the maximum values derived from all the storm runup and overtopping calculations. Note: Dist_3, Dist_2 and Dist_1 reflect the landward extent at which the calculated bore height decreases from 0.9 m (3 ft), to 0.6 m (2 ft) and, finally, 0.3 m (1 ft). In all cases, the hazard zones are ultimately defined relative to the location of the dune/structure crest.

Profiles	Transect	Splashdown $y_{G\ outer}$ (m)	Bore Ht (m)	Dist_3 (≥0.91 m)	Dist_2 (>0.61 <0.91 m)	Dist_1 (≤0.31 m)	$hV^2 > 5.7\ m^3/s^2$ (m)
Yachats	LINC12	0.73	0.31			0.89	2.51
	LINC13	0.70	0.13				
Waldport	LINC16	4.71	0.43			16.52	31.33
	LINC17	5.30	0.46			14.51	26.89
	LINC18	5.30	0.59			25.46	44.39
	LINC19	3.34	0.41			10.78	20.67
	LINC20	3.46	0.73		3.28	13.17	21.84
	LINC21	4.74	0.59			37.13	64.67
	LINC22	6.02	0.88		24.02	59.26	94.79
	LINC23	4.14	0.44			20.57	38.59
	LINC24	5.46	1.06	10.59	35.64	68.29	105.39
	LINC25	3.02	0.44			14.90	28.14
	LINC27	3.81	0.28				
	LINC28	0.71	0.04				
	LINC29	4.19	0.37			9.91	20.04
	LINC30	7.17	1.07	11.46	37.73	71.97	110.97
	LINC31	4.46	0.79		18.84	58.85	96.15
	LINC32	5.53	0.73		11.64	48.47	80.53
	LINC33	5.45	0.68		4.54	29.07	49.05
	LINC34	5.82	0.76		11.65	41.64	68.62
	LINC35	2.90	0.38			7.44	14.81
	LINC36	4.93	0.55			33.66	59.58
	LINC37	3.38	0.34			5.94	12.73
	LINC38	4.92	0.35			6.46	13.63
	LINC39	5.03	0.48			17.79	32.62
	LINC40	4.41	0.47			24.41	45.14
	LINC45	2.83	0.58			38.16	66.68
	LINC47	0.87	0.18				
	LINC49	1.37	0.09				
	LINC50	0.70	0.13				
	LINC51	4.38	0.42			11.71	22.29
	LINC53	0.38	0.20				
	LINC57	6.12	0.41			11.56	22.21
	LINC58	3.74	0.36			6.24	12.76
	LINC59	2.74	0.27				
	LINC66	0.45	0.29				
Alsea	LINC76	6.56	0.89		18.52	44.59	71.13
	LINC85	2.69	0.21				
South Beach	LINC93	4.65	0.42			17.14	32.78
	LINC99	1.48	0.40			9.76	19.03
	LINC100	3.88	0.46			20.77	38.50
	LINC102	3.74	0.28				
	LINC108	2.37	0.26				
	LINC114	0.29	0.10				
	LINC115	5.73	0.66		2.35	19.90	33.79
	LINC118	4.78	0.53			20.09	35.92
	LINC126	3.25	0.44			17.77	33.45
	LINC127	1.48	0.27				

Profiles	Transect	Splashdown $y_{G\ outer}$ (m)	Bore Ht (m)	Dist_3 (≥0.91 m)	Dist_2 (>0.61 <0.91 m)	Dist_1 (≤0.31 m)	$hV^2 > 5.7\ m^3/s^2$ (m)
Newport	LINC132	0.44	0.02				
	LINC136	7.10	1.04	7.69	22.68		****
Beverly Beach	LINC153	3.30	0.24				
	LINC154	0.71	0.30			0.00	0.67
	LINC161	4.54	0.41			8.72	16.87
Whale Cove	LINC185	4.17	0.43			6.69	12.71
Fogarty Creek	LINC204	2.09	0.16				
Gleneden Beach/Siletz Spit	LINC214	1.26	0.20				
	LINC215	5.84	0.59			33.72	58.75
	LINC221	1.07	0.14				
	LINC231	0.13	0.12				
	LINC234	0.82	0.09				
	LINC236	0.86	0.04				
	LINC238	2.77	0.48			14.97	27.39
	LINC239	0.14	0.16				
	LINC240	2.12	0.19				
	LINC241	1.05	0.04				
	LINC242	1.23	0.19				
	LINC243	3.58	0.55			23.14	40.93
	LINC244	5.36	0.81		12.55	36.42	59.15
Lincoln City	LINC248	5.33	0.63		2.07	33.63	57.60
	LINC251	6.50	0.92	0.29	24.17	55.29	87.66
	LINC252	4.81	0.63		1.51	23.22	39.75
	LINC259	6.98	1.12	2.96	8.15	14.91	22.81
	LINC263	5.50	0.67		4.89	32.83	55.46
	LINC264	1.96	0.17				
	LINC265	4.97	0.57			25.61	44.97
	LINC266	3.76	0.47			17.50	32.22
	LINC267	0.09	0.05				
	LINC268	4.49	0.45			14.70	27.47
	LINC278	6.72	1.01	6.57	30.69	62.13	96.79
	LINC280	6.17	0.87		16.73	41.47	66.38
	LINC281	0.97	0.04				
	LINC295	3.25	0.27				
	LINC300	1.43	0.04				
	LINC308	1.41	0.57			20.66	36.24
Supplemental Transects	LINC_9_294	7.24	0.68		6.01	37.95	64.01
	LINC_26_457	4.21	0.45			32.03	59.80
	LINC_26_459	5.35	0.72		9.15	39.32	65.43
	LINC_43_554	4.45	0.46			16.53	30.78
	LINC_44_573	3.78	0.43			13.86	26.25
	LINC_44_575	6.91	0.54			22.31	39.75
	LINC_99_1257	1.59	0.32			1.55	3.87
	LINC_99_1274	0.23	0.41			10.74	20.70
	LINC_106_1343	5.99	0.70		5.412	28.70	48.16
	LINC_109_1366	4.682	0.51			13.452	24.226
	LINC_109_1367	5.660	0.61		0.070	10.431	17.996
	LINC_121_1528	7.109	1.01	3.2099	15.343	31.1538	48.564
	LINC_167_2257	0.589	0.64		2.399	33.7496	57.7204
	LINC_204_2928	3.447	2.16	93.52	125.506	167.191	214.993
	LINC_250_3385	8.233	0.78		13.058	42.724	70.022

NOTES: **** The maximum inundation was mapped to a TWL contour of 8.56 m. This was derived using multiple steps in order to account for a parking lot with various walls and step elevation gains.

Table 6-4. Depth of flooding at the overtopping zones landward of the structure crest.

Profiles	Transect	Dist_3 (≥0.91 m)	Dist_2 (>0.61 <0.91 m)	Dist_1 (≤0.31 m)	hV^2 > 5.7m3/s2 (m)	Comments
Yachats	LINC12			0.31	0.31	narrow D1 added to splashdown; HV2 too narrow to map
Waldport	LINC16			0.31	0.31	
	LINC17			0.31	0.31	
	LINC18			0.31	0.31	HV2 zone cut short by topo barrier
	LINC19			0.31	0.31	
	LINC20		0.61	0.31	0.31	narrow D2 added to D1
	LINC21		0.61	0.31	0.31	narrow D2 added to D1; HV2 cut short by topo barrier
	LINC22	0.91	0.61	0.31	0.31	narrow D3 added to D2
	LINC23			0.31	0.31	
	LINC24	0.91	0.61	0.31	0.31	narrow D3 added to D2
	LINC25			0.31	0.31	
	LINC29			0.31	0.31	narrow D1 added to HV2
	LINC30	0.91	0.61	0.31	0.31	narrow D3 added to D2
	LINC31		0.61	0.31	0.31	
	LINC32		0.61	0.31	0.31	
	LINC33		0.61	0.31	0.31	narrow D2 added to D1
	LINC34		0.61	0.31	0.31	narrow D2 added to D1
	LINC35			0.31	0.31	narrow D1 added to HV2
	LINC36			0.31	0.31	
	LINC37			0.31	0.31	narrow D1 added to HV2
	LINC38			0.31	0.31	narrow D1 added to HV2
	LINC39			0.31	0.31	
	LINC40			0.31	0.31	
	LINC45			0.31	0.31	HV2 zone cut short by topo barrier
	LINC51			0.31	0.31	narrow D1 added to HV2
	LINC57			0.31	0.31	
	LINC58			0.31	0.31	narrow D1 added to HV2
Alsea	LINC76		0.61	0.31	0.31	D2, D1, and HV2 cut short by topo barrier
South Beach	LINC93			0.31	0.31	
	LINC99			0.31	0.31	this transect is not shown on the FIRM
	LINC100			0.31	0.31	narrow D1 added to HV2
	LINC115		0.61	0.31	0.31	narrow D2 added to D1; D1 and HV2 cut short by topo barrier
	LINC118			0.31	0.31	
	LINC126			0.31	0.31	
Newport	LINC136		0.61	0.31	0.31	narrow D2 added to D1; HV2 cut short by topo barrier
Beverly Beach	LINC154				0.31	narrow HV2 added to splashdown
	LINC161			0.31	0.31	narrow D1 added to HV2
Whale Cove	LINC185			0.31	0.31	narrow D1 added to HV2
Gleneden Beach/Siletz	LINC215			0.31	0.31	D1 and HV2 cut short by topo barrier
Lincoln City	LINC248		0.61	0.31	0.31	narrow D2 added to splashdown; D1 and HV2 cut short by topo barrier
	LINC251	0.91	0.61	0.31	0.31	narrow D3 added to D2; HV2 cut short by topo barrier
	LINC252		0.61	0.31	0.31	narrow D2 added to D1; D2, D1, and HV2 cut short by topo barrier

Profiles	Transect	Dist_3 (≥0.91 m)	Dist_2 (>0.61 <0.91 m)	Dist_1 (≤0.31 m)	hV^2 > 5.7m3/s2 (m)	Comments
	LINC259	0.91	0.61	0.31	0.31	D3, D2, D1, and HV2 cut short by topo barrier; narrow D3, D2, and D1 added to HV2
	LINC263		0.61	0.31	0.31	narrow D2 added to D1
	LINC265			0.31	0.31	
	LINC266			0.31	0.31	
	LINC268			0.31	0.31	
	LINC278	0.91	0.61	0.31	0.31	D3, D2, D1 and HV2 cut short by topo barrier
	LINC280		0.61	0.31	0.31	D2, D1 and HV2 cut short by topo barrier
Supplemental Transects	LINC_9_294		0.61	0.31	0.31	narrow D2 added to D1; HV2 cut short by topo barrier
	LINC_26_459	0.91	0.61	0.31	0.31	narrow D3 added to D2; HV2 cut short by topo barrier
	LINC_43_554			0.31	0.31	
	LINC_44_573			0.31	0.31	
	LINC_44_575			0.31	0.31	
	LINC_99_1257			0.31	0.31	D1and HV2 too narrow to map
	LINC_99_1274			0.31	0.31	narrow D1 added to HV2
	LINC_106_1343		0.61	0.31	0.31	narrow D2 added to D1; HV2 cut short by topo barrier
	LINC_109_1366			0.31	0.31	D1 and HV2 cut short by topo barrier
	LINC_109_1367		0.61	0.31	0.31	narrow D2 added to D1; D1 and HV2 cut short by topo barrier
	LINC_121_1528	0.91	0.61	0.31	0.31	narrow D3 added to D2; D1 and HV2 cut short by topo barrier
	LINC_167_2257		0.61	0.31	0.31	narrow D2 and HV2 added to D1
	LINC_204_2928	0.91	0.61	0.31	0.31	narrow D2 and HV2 added to D1
	LINC_250_3385		0.61	0.31	0.31	D1 and HV2 cut short by topo barrier

7.0 COASTAL EROSION CAUSED BY INDIVIDUAL STORMS

In order to estimate beach (or bluff) erosion and the resulting profile changes that occur during a particular storm, it is important to first establish the initial profile conditions that existed prior to that storm. As outlined in Section 3.2, this initial profile morphology is represented by the most likely winter profile (MLWP), which forms the basis for determining profile changes that could eventuate as a result of a particularly severe storm(s). Having established the MLWP for a site, the profile is then modified according to the amount of erosion estimated to occur during a specified storm as a result of the increased water levels (tide + surge + ENSO) as well as from wave processes, specifically the wave runup. This section explores two approaches described in the revised FEMA guidelines, which may be used to establish the eroded profiles along the Lincoln County coastline. The second half of the section describes the specific approach adopted for Lincoln County and the results from our erosion analyses.

7.1 Models of Foredune Erosion

7.1.1 The Komar and others (1999) model

The erosion potential of sandy beaches and foredunes along the Pacific Northwest coast of Oregon and Washington is a function of the total water level produced by the combined effect of the wave runup plus the tidal elevation (E_T), exceeding some critical elevation of the fronting beach, typically the elevation of the beach-dune junction (E_J). This basic concept is depicted conceptually in **Figure 7-1A** based on the model developed by Ruggiero and others (1996), and in the case of the erosion of a foredune backing the beach the application of a geometric model (**Figure 7-1B**) formulated by Komar and others (1999). Clearly, the more extreme the total water level elevation, the greater the resulting erosion that occurs along both dunes and bluffs.

As can be seen from **Figure 7-1B**, estimating the maximum potential dune erosion (DE_{MAX}) is dependent on first determining the total water level elevation, TWL, diagrammed in **Figure 7-1A** which includes the combined effects of extreme high tides plus storm surge plus wave runup, relative to the elevation of the beach-dune junction (E_J). Therefore, when the TWL > E_J the foredune retreats landward by some distance, until a new beach-dune junction is established, whose elevation approximately equals the extreme water level. Because beaches along the high-energy Oregon coast are typically wide and have a nearly uniform slope (tan β), the model assumes that this slope is maintained, and the dunes are eroded landward until the dune face reaches point B in **Figure 7-1B**. As a result, the model is geometric in that it assumes an upward and landward shift of a triangle, one side of which corresponds to the elevated water levels, and then the upward and landward translation of that triangle and beach profile to account for the total possible retreat of the dune (Komar and others, 1999). An additional feature of the geometric model is its ability to accommodate further lowering of the beach face due to the presence of a rip current, which has been shown to be important to occurrences on the Oregon coast of localized "hot spot" erosion and property impacts (Komar, 1997). This feature of the model is represented by the beach-level change ΔBL shown in **Figure 7-1B**, which causes the dune to retreat some additional distance landward until it reaches point C. As can be seen from **Figure 7-1B**, the distance from point A to point C depicts the total retreat, DE_{MAX}, expected during a particularly severe storm event (or series of storms) that includes the localized effect enhancement by a rip current. Critical then in applying the model to evaluate the susceptibility of coastal properties to erosion, is an evaluation of the occurrence of extreme tides (E_T), the runup of waves, and the joint probabilities of these processes along the coast (Ruggiero and others, 2001), this having been the focus of Section 6 described previously.

The geometric model gives the maximum potential equilibrium cross-shore change in the shoreline position landward of the MLWP resulting from a storm. However, in reality it is unlikely that this extreme degree of response is ever fully realized,

because of the assumptions that had been made in deriving the geometric model with the intent of evaluating the maximum potential dune erosion. As noted by Komar and others (1999), in the first instance the geometric model projects a mean linear beach slope. As a result, if the beach is more concave, it is probable that the amount of erosion would be less, though not by much. Perhaps of greater significance is that the geometric model assumes an instantaneous erosional response, with the dunes retreating landward as a result of direct wave attack. However, the reality of coastal change is that it is far more complex, there in fact being a lag in the erosional response behind the forcing processes. As noted by Komar and others (1999), the extreme high runup elevations typically occur for only a relatively short period of time (e.g., the period of time in which the high wave runup elevations coincide with high tides). Because the elevation of the tide varies with time (e.g., hourly), the amount of erosion can be expected to be much less when the water levels are lower. Thus, it is probable that several storms during a winter may be required to fully realize the degree of erosion estimated by the geometric model; this did, for example, occur during the winter of 1998-99, with the last in the series of 5 storms having been the most extreme and erosive (Allan and Komar, 2002). In addition, as beaches erode, the sediment is removed offshore (or farther along the shore) into the surf zone where it accumulates in near shore sand bars. This process helps to mitigate the incoming wave energy by causing the waves to break farther offshore, dissipating some of the wave energy, and forming the wide surf zones that are characteristic of the Oregon coast. In turn, this process helps to reduce the rate of beach erosion that occurs. In summary, the actual amount of beach erosion and dune recession is dependent on many factors, the most important of which include the incident wave conditions, the TWL, and the duration of the storm event(s).

Figure 7-1. (A) The foredune erosion model. (B) The geometric model used to assess the maximum potential beach erosion in response to an extreme storm (Komar and others, 1999).

7.1.2 The Kriebel and Dean (1993) model

Kriebel and Dean (1993), hereafter known as K&D, developed a dune erosion model that is broadly similar to the Komar and others (1999) geometric model. At its core is the assumption that the beach is in statistical equilibrium with respect to the prevailing wave climate and mean water levels (Bruun, 1962). As water levels increase, the beach profile is shifted upward by an amount equal to the change in water level (S) and landward by an amount R_∞ until the volume of sand eroded from the subaerial beach matches the volume deposited offshore in deeper water (**Figure 7-2**); *note that DE_{MAX} and R_∞ are essentially synonymous with each other*. One important feature in the K&D model relative to Bruun (1962) is that it relies on the equilibrium beach profile theory proposed by Dean (1977) to account for the erosion following an increase in the water level. The Dean model is a simplified equilibrium form for open-coast beach profiles expressed as a power-law curve of the form:

$$h = Ay^{2/3} \text{ or equivalently as } x = \left(\frac{h}{A}\right)^{3/2} \qquad (7.1)$$

where h is the water depth at a distance x offshore from the still-water level and A is a parameter that governs the overall steepness (and slope) of the profile and is a function of the beach grain size. Thus, incorporating the assumed components of Bruun (1962) and Dean (1977), the maximum erosion potential, R_∞, was determined by K&D to be a function of the increase in mean water level (S) caused by a storm, the breaking wave water depth (h_b), surf zone width (W_b), berm or dune height (B or D), and the slope (β_f) of the upper foreshore beach face. The breaking wave depth (h_b) may be calculated from the wave breaker height (equation 6.8) multiplied by 0.78 (the breaker index).

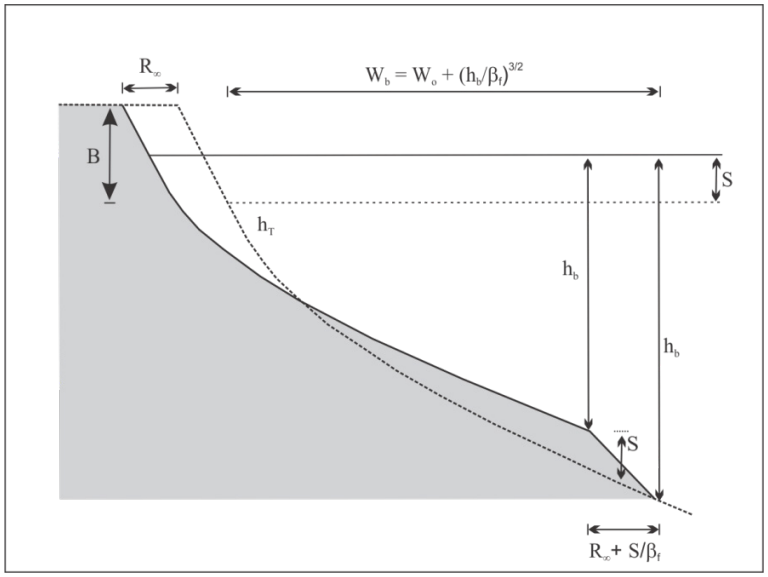

Figure 7-2. Maximum potential erosion (R_∞) due to a change in water levels (after Kriebel and Dean, 1993).

As a result of the above concepts, K&D developed two approaches for determining the maximum erosion potential. These include:

- A beach backed by a low sand berm

$$R_\infty = \frac{S\left(W_b - h_b/\beta_f\right)}{B + h_b - S/2} \qquad (7.2)$$

- A beach backed by high sand dune

$$R_\infty = \frac{S\left(W_b - h_b/\beta_f\right)}{D + h_b - S/2} \qquad (7.3)$$

Like the Komar and others (1999) model, the Kriebel and Dean (1993) dune erosion model estimates the *maximum potential erosion* (DE_{MAX}) associated with a major storm, and assume that a particular storm will last sufficiently long enough to fully erode the dune. In reality, DE_{MAX} is almost never fully realized because storms rarely last long enough to fully erode the dune to the extent of the model predictions. Because the duration of a storm is a major factor controlling beach and dune erosion, K&D developed an approach to account for the duration effects of storms with respect to the response time scale required to fully erode a beach profile. The time scale for the erosion of a dune to the extent R given by equation (7.2) can be estimated using equation 7.4:

$$T_S = C_1 \frac{H_b^{3/2}}{g^{1/2} A^3} \left(1 + \frac{h_b}{B} + \frac{\beta_f W_b}{h_b}\right)^{-1} \qquad (7.4)$$

where T_S is the time scale of response, C_1 is an empirical constant (320), H_b is the breaker height, h_b is the breaker depth, g is acceleration due to gravity, B is the berm elevation, β_f is the slope of the foreshore, W_b is the surf zone width and A is the beach profile parameter that defines an equilibrium profile. Using equation 7.4 yields typical response times for complete profile erosion that are on the order of 10 to 100 hours (NHC, 2005). In general, as the surf zone width increases due to larger wave heights, smaller grain-sizes or gentler slopes, the response time increases. In addition, the response time will also increase as the height of the berm increases.

The beach profile response is determined by a convolution integral. According to NHC (2005), the time dependency of the storm hydrograph may be approximated by:

$$f(t) = sin^2\left(\pi \frac{t}{T_D}\right) \; for \; 0 < t < T_D \qquad (7.5)$$

where t is time from the start of the storm and T_D is the storm duration. The convolution integral is:

$$DE(t) = \frac{DE_{MAX}}{T_S} \int_0^t f(\tau) e^{-(t-\tau)/T_S} \, d\tau \qquad (7.6)$$

which integrates to:

$$\frac{DE(t)}{DE_{MAX}} = 0.5 \left\{ 1 - \frac{\beta^2}{1+\beta^2} \exp\left(-\frac{t}{T_S}\right) - \frac{1}{1+\beta^2} \left[\cos\left(\frac{2\pi t}{T_D}\right) + \beta \sin\left(\frac{2\pi t}{T_D}\right) \right] \right\} \qquad (7.7)$$

where $\beta = 2\pi T_S / T_D$ and DE_{MAX} is the maximum potential recession that would occur if the storm duration was infinite. Thus, if the storm duration, T_D, is long relative to the time scale of profile response, T_S, then a significant portion of the estimated erosion determined by the K&D or geometric model will occur. As the ratio of these two values decreases, the amount of erosion will also decrease. The time required for maximum beach and dune recession is determined by setting the derivative of equation 7.7 to zero and solving for time. This yields:

$$exp\left(-\frac{t_m}{T_D}\right) = cos\left(\frac{2\pi t_m}{T_S}\right) - \frac{T_D}{2\pi T_S} sin\left(\frac{2\pi t_m}{T_S}\right) \qquad (7.8)$$

in which t_m is the time that the maximum erosion occurs with respect to the beginning of the storm. Unfortunately, this equation can only be solved by approximation or numerically. Thus the maximum recession associated with a duration limited storm can be calculated by:

$$\alpha = \frac{DE_m}{DE_{MAX}} = 0.5 \left[1 - cos\left(2\pi \frac{t_m}{T_D}\right)\right] \qquad (7.9)$$

where α is the duration reduction factor and DE_m is the maximum recession that occurs for a given storm duration that occurs at time t_m. As a result, the duration limited recession is:

$$DE_m = \alpha DE_{MAX} \qquad (7.10)$$

7.2 Erosion Modeling on Lincoln County beaches

In order to determine the duration reduction factor, α, the duration of each storm event has to be first identified. The approach used here involved an analysis of the number of hours a specific total water level (TWL) event was found to exceed a particular beach profile's beach-dune junction elevation, applying the Ruggiero and others (2001) analysis approach. **Figure 7-3** is an example of the approach we used, which is based on a script developed in MATLAB. In essence, the blue line is the TWL time series for a particular profile ±3 days from the event. The script moves backwards and forwards in time from the identified event until the TWL falls below the critical threshold shown as the black line in **Figure 7-3**, which reflects the beach-dune junction elevation. The duration of the storm was then determined as the period where the TWL exceeds the threshold and includes the shoulders of the event (i.e., when the TWL first falls below the critical threshold). This process was undertaken for every storm and for each of the profile sites. One limitation of this approach that was encountered is that it is possible for the duration to be underestimated if the TWL dips below the threshold for an hour or more and then rises again above the threshold, as seen in the example in **Figure 7-3**.

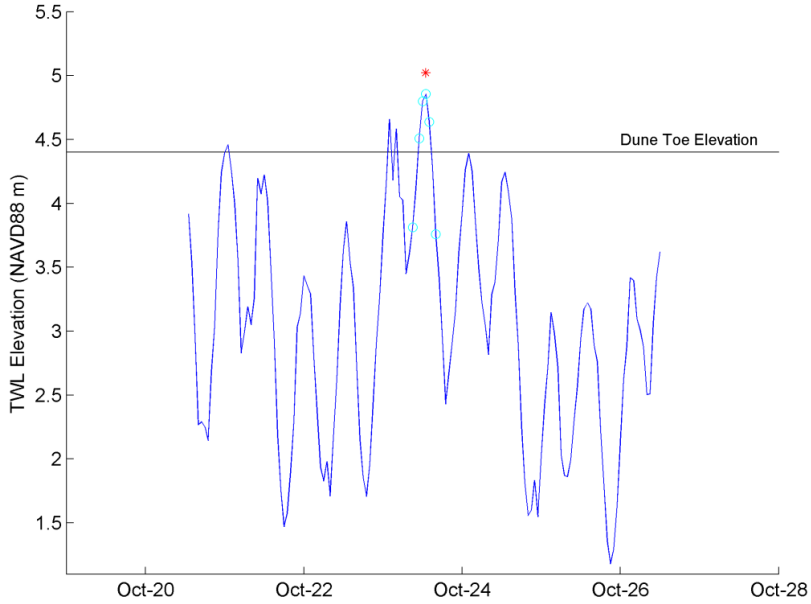

Figure 7-3. Example plot of the approach used to define storm duration along the Coos County shoreline. Note: The red asterisk denotes the location of the storm peak. The blue circles denote the hours when the event exceeded the critical beach-dune junction toe elevation (including the shoulders) that are used to define the "duration" of the event.

As described previously, the breaker height, H_b, was calculated using equation 6.8 and the breaker depth, h_b, was claculated using a breaker index of 0.78. The berm elevation was established at 3 m (typical for PNW beaches), while the surf zone width, W_b, was determined for each breaker depth value by interpolating along a profile line of interest (**Figure 7-4**). Although we have grain size information available that could have been used to define the A-parameter for Lincoln County, the approach we took was to iteritively determine an equilibrium A value based on the actual beach profile data. Here we used

the profile data seaward to the 8 m (26.3 ft) water depth; a range of A values were fit to the data until a value was found that best matched the profile morphology. This approach was adopted for all the profile sites. **Figure 7-5** presents the alongshore varying dune erosion parameters (beach slope, A, surfzone width and breaker depth) calculated for each transect site and averaged over every storm. These data are also summarized in **Table 7-1**.

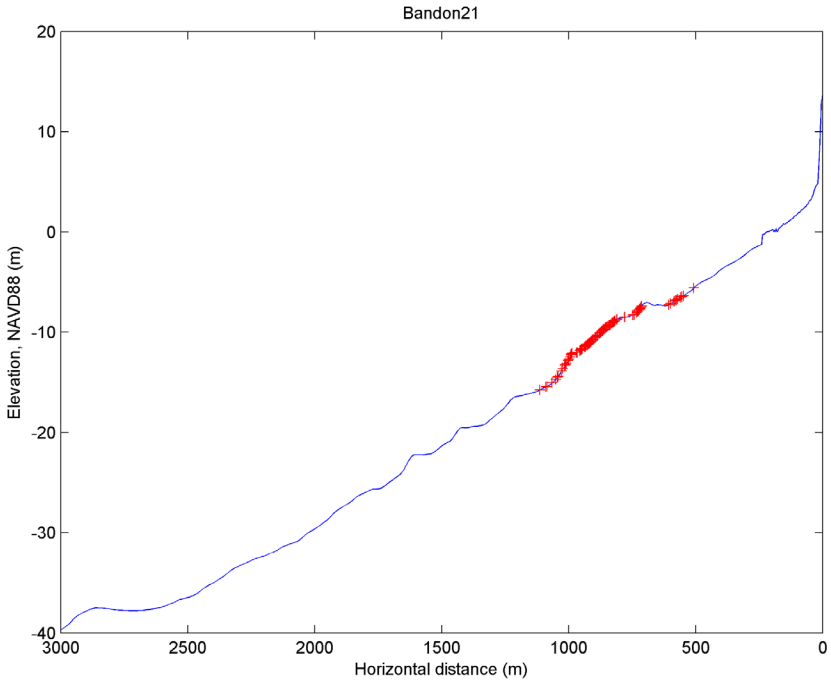

Figure 7-4. Example transect from Coos County showing the locations of h_b (red crosses), used to define the cross-shore width (W_b) of the surf zone.

Figure 7-6 presents the alongshore varying time scale for the erosion of a dune (T_S), storm duration (T_D), and duration reduction factor (α) values determined for those transect sites characterized as "dune-backed" in Lincoln County. In all cases, we used the surf zone width, breaking depth, and water levels determined at the respective transect site (along with information pertaining to the site's beach/dune morphology) to calculate T_S, and T_D for each storm, while the final parameter, Tm, was solved numerically using equation 7.8 in order to define the duration reduction factor (α). These data have subsequently been averaged for each of the transect locations and are ultimately included in **Table 7-1** and presented in **Figure 7-5** and **Figure 7-6**.

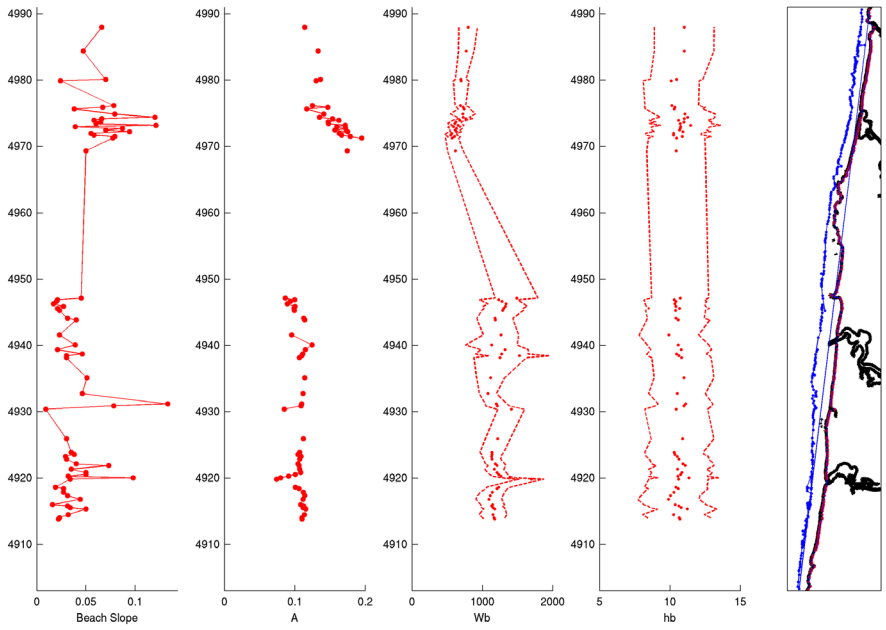

Figure 7-5. Plot showing the dune erosion parameters (tan β, A, W_b, and h_b) used to calculate the profile responses (T_S), storm durations (T_D), alpha, and the storm-induced dune erosion. For W_b and h_b we show the mean value and ±1 standard deviation computed using all of the storms.

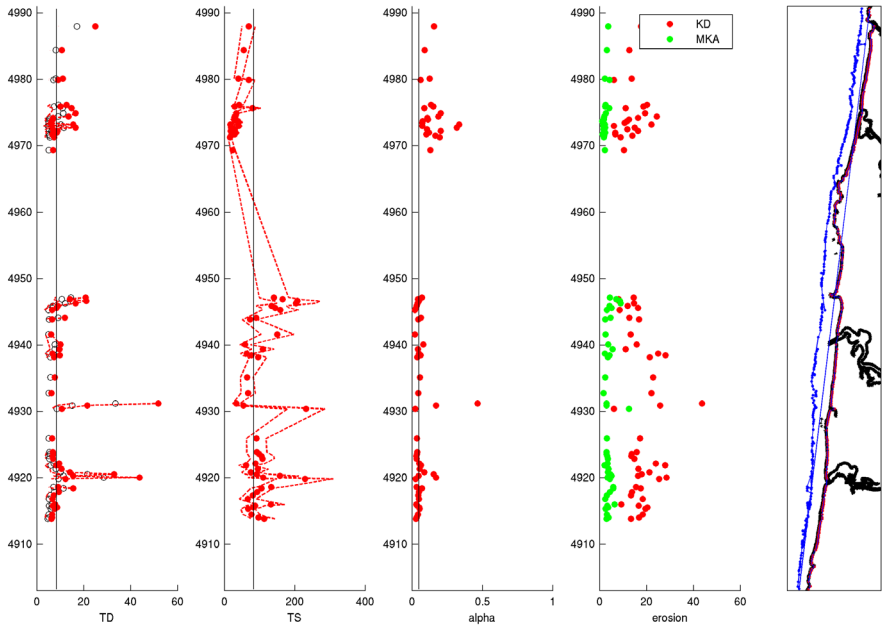

Figure 7-6. Plot showing the storm duration hours (T_D), the calculated time scale of profile response hours (T_S), alpha, and the storm induced K&D and geometric model erosion adjusted using equation 7.10 for the dune-backed profiles along the Lincoln County shore.

Having defined the duration reduction factor (α) for each transect location, the storm-induced erosion was calculated using equation 7.10. As can be seen in **Table 7-1**, calculations of the maximum potential dune erosion (DE_{MAX}) using the Komar and others (1999) geometric model yielded results that are considerably smaller than those derived using the Kriebel and Dean (1993) approach. These differences are largely due to the effect of the surfzone width parameter and the low nearshore slopes used in the K&D calculations. Our initial calculations of storm-induced erosion based on the K&D approach indicated several sites with anomalously large estimates of dune erosion (>20 m [65.6 ft]), when compared with actual field observations observed by DOGAMI staff over the past two decades. In contrast, storm-induced erosion estimates based on the duration-reduced maximum potential dune erosion (DE_{MAX}) calculated using the geometric model produced very negligible erosion responses that made little physical sense. As a result, our final calculation of the storm-induced erosion (DE_m) is based on the K&D approach. To reduce the large erosion responses observed at several of the transect sites, we ultimately defined an alongshore averaged duration reduction factor (α) of 0.048 (**Table 7-1**), which was used to calculate the storm-induced erosion (DE_m) at each of the dune-backed transect sites present along Lincoln County. As can be seen from **Table 7-1**, this resulted in erosion responses that range from a minimum of 6.1 m (20 ft) to as much as 28.6 m (94 ft), while the mean storm-induced erosion response is calculated to be 15.9 m (52.2 ft). These results are entirely consistent with actual field observations derived from both GPS beach surveys and from previous analyses of topographic change data measured using lidar (Allan and Harris, 2012; Allan and Stimely, 2013).

Table 7-1. Calculated storm-induced erosion parameters for dune-backed beaches in Lincoln County. Note: MKA denotes the geometric model and K&D is the Kriebel and Dean model.

Profiles	LINC	A	W_B	T_D	T_S	α	MKA (DE_{MAX})	MKA (DE_m)	K&D (DE_{MAX})	K&D (DE_m)
Waldport	46	0.110	1174.213	6.254	112.595	0.027	61.585	2.952	279.615	13.402
	47	0.110	1162.531	6.524	96.762	0.033	78.303	3.753	349.842	16.768
	48	0.113	1151.659	6.461	76.779	0.040	64.001	3.067	383.149	18.364
	50	0.115	1172.353	7.628	66.855	0.054	52.312	2.507	407.751	19.543
	52	0.112	1148.904	8.631	81.813	0.050	76.500	3.667	425.161	20.378
	54	0.113	1132.761	6.758	86.926	0.038	66.782	3.201	347.994	16.679
	56	0.108	1146.402	7.810	132.124	0.029	131.282	6.292	193.313	9.265
	61	0.111	1092.746	6.658	66.280	0.048	49.876	2.391	381.781	18.298
	62	0.114	1112.522	7.230	80.716	0.043	65.429	3.136	277.459	13.298
	63	0.112	1140.974	9.418	92.712	0.049	91.317	4.377	288.851	13.844
	65	0.106	1205.937	15.531	105.369	0.069	121.451	5.821	364.578	17.474
	66	0.101	1229.905	9.084	132.926	0.033	121.443	5.821	324.604	15.558
Alsea Spit	68	0.074	1696.319	12.263	229.230	0.026	91.699	4.395	528.502	25.331
	69	0.080	1390.111	43.755	109.951	0.169	70.146	3.362	595.797	28.556
	70	0.091	1264.845	15.522	157.713	0.047	107.020	5.129	339.884	16.290
	71	0.101	1231.422	32.861	92.148	0.154	95.353	4.570	375.547	18.000
	72	0.108	1206.390	14.139	74.447	0.087	73.870	3.541	441.213	21.147
	73	0.107	1170.509	10.479	94.886	0.053	80.195	3.844	343.478	16.463
	74	0.106	1206.966	8.180	61.005	0.063	41.826	2.005	582.597	27.923
	75	0.105	1181.921	9.453	88.157	0.051	69.915	3.351	499.454	23.938
	78	0.107	1137.010	6.907	107.993	0.031	71.811	3.442	309.379	14.828
	79	0.109	1132.195	6.600	105.013	0.031	68.353	3.276	281.803	13.507
	80	0.105	1136.127	7.045	98.514	0.035	59.973	2.874	283.994	13.612
	81	0.107	1135.176	6.841	92.138	0.036	61.521	2.949	330.456	15.838
	86	0.112	1218.870	6.498	90.533	0.035	64.222	3.078	359.735	17.242
South Beach	99	0.085	1409.922	10.603	232.321	0.022	261.729	12.544	126.961	6.085
	100	0.109	1214.019	21.515	53.491	0.171	61.845	2.964	537.126	25.744
	101	0.110	1197.355	51.744	33.806	0.466	60.561	2.903	911.994	23.500
	108	0.112	1078.607	6.165	67.452	0.044	34.452	1.651	460.730	22.082
	114	0.114	1117.255	7.606	63.952	0.056	49.584	2.377	475.530	22.792
	126	0.107	1251.976	7.355	95.595	0.037	72.306	3.466	444.775	21.318
	127	0.110	1523.896	9.722	76.886	0.060	89.350	4.282	586.903	28.130
	128	0.111	1275.834	6.597	63.171	0.050	46.068	2.208	520.884	24.965
	129	0.115	1319.143	9.592	108.763	0.042	113.604	5.445	230.262	11.036
	130	0.125	1129.031	10.142	58.796	0.080	74.935	3.592	330.725	15.851
Newport	131	0.096	1264.451	6.021	150.393	0.020	52.382	2.511	275.353	13.197
	138	0.114	1185.666	6.504	72.649	0.043	49.510	2.373	350.891	16.818
	139	0.113	1178.765	11.990	89.730	0.063	96.440	4.622	262.746	12.593
	141	0.100	1288.890	6.528	158.593	0.020	64.801	3.106	177.486	8.507
	142	0.099	1301.964	8.325	144.551	0.028	106.181	5.089	341.868	16.385
	143	0.100	1324.013	8.872	133.415	0.032	87.870	4.212	249.824	11.974
	144	0.089	1336.901	16.507	203.245	0.039	186.588	8.943	305.525	14.644
	145	0.094	1277.656	21.084	207.235	0.049	181.042	8.677	170.899	8.191
	146	0.100	1231.155	14.081	165.305	0.041	146.796	7.036	168.727	8.087
	147	0.087	1486.445	20.735	140.543	0.069	90.192	4.323	303.821	14.562

Profiles	LINC	A	W_B	T_D	T_S	α	MKA (DE_{MAX})	MKA (DE_m)	K&D (DE_{MAX})	K&D (DE_m)
Siletz Spit	221	0.175	615.471	6.943	23.739	0.129	45.249	2.169	214.905	10.300
	230	0.195	570.125	7.343	15.406	0.197	37.919	1.817	186.694	8.948
	231	0.179	600.450	7.235	18.800	0.165	39.314	1.884	291.213	13.958
	232	0.167	547.828	6.475	29.452	0.100	25.021	1.199	138.708	6.648
	233	0.163	564.506	8.493	31.656	0.120	47.987	2.300	138.689	6.647
	234	0.175	628.619	8.762	17.585	0.205	37.946	1.819	341.996	16.392
	235	0.157	610.918	6.804	29.110	0.106	33.142	1.588	244.653	11.726
	236	0.172	629.220	16.520	18.864	0.319	50.345	2.413	311.879	14.948
	237	0.160	590.239	6.333	40.710	0.073	30.402	1.457	127.279	6.100
	238	0.172	655.309	15.560	16.703	0.333	46.096	2.209	461.574	22.123
	239	0.148	605.055	6.138	38.991	0.073	29.450	1.411	222.579	10.668
	240	0.147	622.777	6.209	38.421	0.075	21.124	1.012	242.899	11.642
	241	0.163	680.882	6.788	26.935	0.113	37.963	1.820	260.681	12.494
	242	0.154	766.033	6.946	29.043	0.108	36.094	1.730	341.341	16.360
	243	0.135	728.523	13.486	30.327	0.186	40.161	1.925	508.467	24.370
	244	0.141	723.353	16.513	33.544	0.203	55.093	2.641	402.971	19.314
Lincoln City	245	0.117	741.913	14.840	79.676	0.086	85.407	4.093	232.415	11.139
	246	0.147	724.434	10.004	28.641	0.151	49.800	2.387	389.588	18.673
	247	0.125	687.105	12.629	41.744	0.133	51.313	2.459	421.884	20.220
	267	0.130	698.340	9.037	69.223	0.062	88.467	4.240	127.960	6.133
	269	0.137	693.065	11.044	39.383	0.125	46.583	2.233	283.250	13.576
	294	0.133	771.132	10.642	54.779	0.089	63.828	3.059	263.473	12.628
Salmon River	308	0.114	798.418	24.872	69.194	0.155	76.351	3.659	368.048	17.640
Summary		**0.121**	**1038.609**	**11.468**	**83.462**	**0.048**	**72.610**	**3.480**	**339.002**	**15.951**

Note:

A is the beach profile parameter that defines an equilibrium profile; W_b is the surf zone width; T_D is the storm duration; T_S is the time scale of response; α is the duration reduction factor.

Figure 7-7 and **Figure 7-8** provide two examples where the most eroded winter profile is eroded to reflect the storm-induced erosion values identified in **Table 7-1**. The first example is the LINC 70 profile site (located near the south end of Alsea Spit) where the beach is backed by a prominent foredune. In this example, the calculated duration reduced recession is ~16.3 m (53.5 ft). The location of the beach-dune junction is depicted in **Figure 7-7** by the magenta dot, while the most eroded winter profile is shown as the solid black line. Because the underlying principle of the K&D and geometric models is for the slope to remain constant, the dune is eroded landward by shifting the location of the beach-dune junction landward by 16.9 m (55 ft) and upward to its new location where it forms an erosion scarp (**Figure 7-7**). Due to the high dune crest, overtopping does not occur at this location.

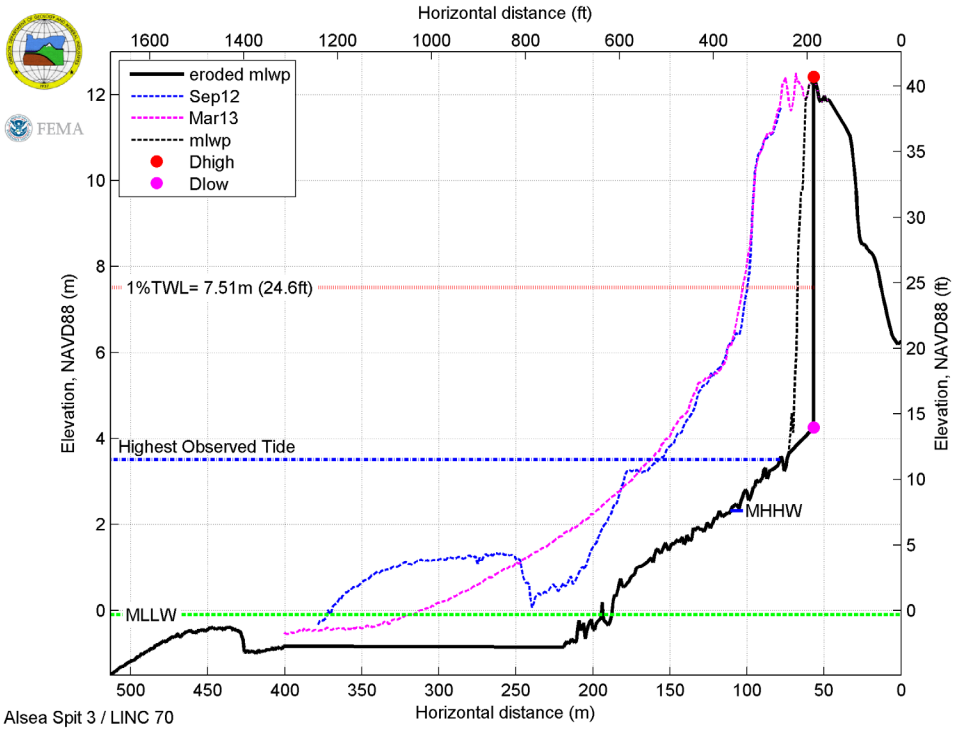

Figure 7-7. Application of the duration reduced erosion estimate to the most likely winter profile at LINC 70, near the south end of Alsea Spit.

Figure 7-8 provides an example where dune breaching and overtopping occurs in response to the calculated 1% TWL for the LINC 238 profile site. The calculated dune erosion for LINC 238 is ~22.1 m (72.5 ft). The original location of the beach-dune junction is located at an elevation of ~6.75 m (22 ft), **Figure 7-8**, and is shifted upward and landward to its new location depicted by the magenta dot; the most eroded winter profile is shown as the solid black line. As noted by NHC (2005), when dunes are subject to major overtopping events, breaching of the dune typically results in significant lowering of the dune morphology and the development of an overwash fan on the lee side of the dune. Because the present methodologies are unable to account for such responses, NHC recommends that the dune profile is adjusted by extending the most likely winter profile slope to the backside of the dune. This type of adjustment is demonstrated in **Figure 7-8**, where the entire foredune is assumed to be eroded and removed as a result of a major storm.

Unfortunately, there are no measured examples of the type of response depicted in **Figure 7-8** for the Lincoln County area against which to make comparisons. However, monitoring of beaches by DOGAMI on the Oregon coast provides some suggestion that this approach is probably reasonable. **Figure 7-9** is an example of beach profile changes measured along a barrier beach adjacent to Garrison Lake, Port Orford, located to the south of Bandon. In this example, the barrier beach, which has a crest elevation of 8-9 m NAVD88 (26–29 ft), is known to have been overtopped during several major storms in February/March 1999 (**Figure 7-10**) (Allan and others, 2003). Analyses of the mean shoreline position at this site indicate that changes in the morphology of the beach is controlled primarily by the occurrence of these major storms as well as by El Niño climate events that result in hotspot erosion. Examination of the beach profile changes along the Garrison Lake shore indicate that during major events characterized by overtopping, the crest of the barrier beach is lowered, with some of the eroded sand having been carried landward where they form washover fans, while the bulk is removed seaward to form sand bars. Ultimately, though, any dune located at the back of the profile is removed entirely, as the barrier rolls landward, consistent with the response depicted in **Figure 7-7**.

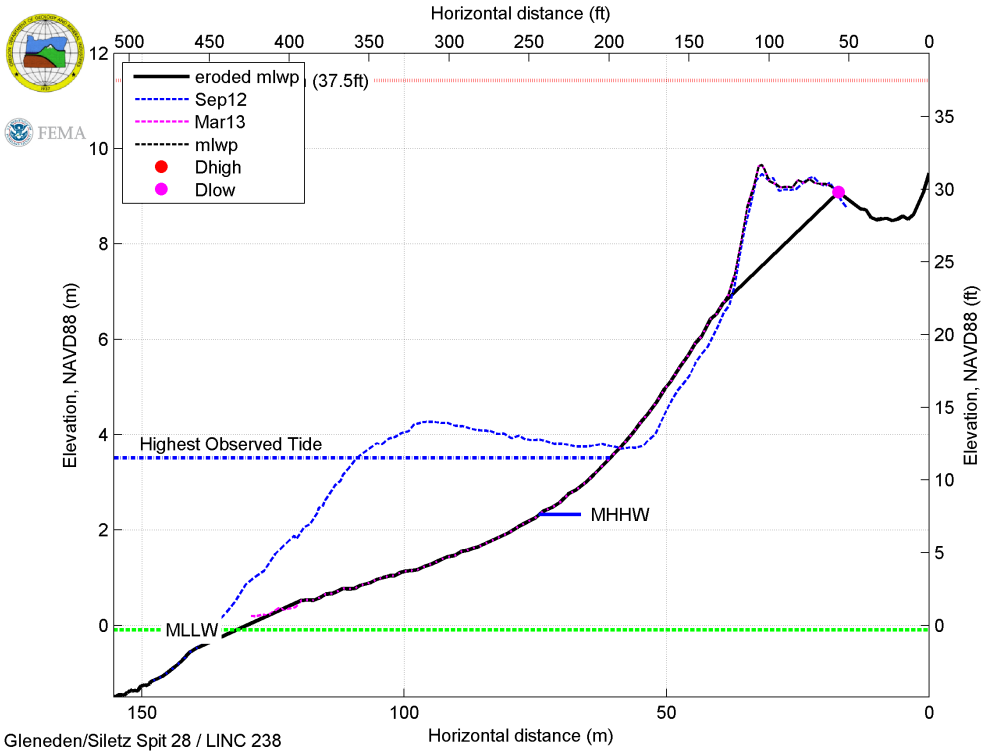

Figure 7-8. Application of the duration reduced erosion estimate to the most likely winter profile at LINC 238 where overtopping and breaching occurs.

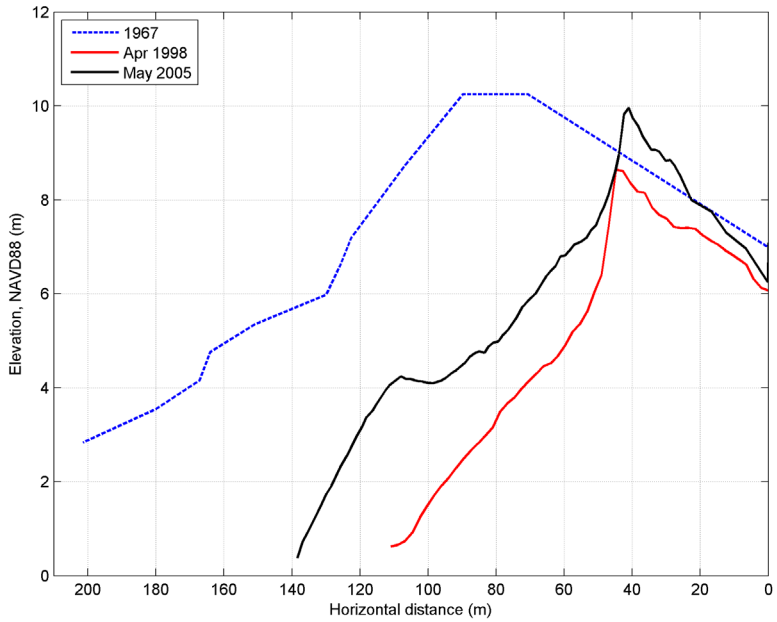

Figure 7-9. Example profile where a barrier beach is overtopped and eroded. This example is based on measured beach profile changes at Garrison Lake, Port Orford, on the southern Oregon coast. The 1967 morphology was derived from Oregon Department of Transportation surveys of the beach on September 25, 1967, used to define the Oregon statutory vegetation line.

.

Figure 7-10. Overtopping of the barrier beach adjacent to Garrison Lake during a major storm on February 16, 1999 (photo courtesy of a resident at Port Orford).

8.0 FLOOD MAPPING

8.1 Detailed Coastal Zone VE Flood Zone Mapping

Detailed mapping of the 1% chance flood event within selected areas of Lincoln County was performed using two contrasting approaches, controlled ultimately by the geomorphology of the beach and backshore. In all cases, we followed the methods described in section D.4.9 in the final draft guidelines of the Coastal Flood Hazard Analysis and Mapping for the Pacific Coast of the United States (NHC, 2005). Due to the complexities of each mapping approach for the 0.1% chance flood event, it was not possible to map reasonably the 0.2% chance event. The reasons for this are described in more detail in the following sections.

8.1.1 Bluff-backed beaches

For bluff-backed beaches the total water level (TWL) values calculated in Section 6.3 were extended into the bluff. The first step involved identifying specific contours of interest, which were extracted from the 1-meter resolution bare earth lidar grid DEM (surveyed in 2009). For the bluff-backed beaches the landward extent of the coastal Zone VE is defined by the contour representing the total water level (TWL) elevation calculated for each of the represented detailed surveyed transects (e.g., **Figure 8-1** and **Table 6-2**). FEMA Operating Guidance 9-13 (2013) dictates that areas near the landward extent of Zone VE, where the difference between the total water level (TWL) and ground elevation are less than 3 feet, be designated as Zone AE. However, due to the steepness of the shore-line along bluff-backed beaches such areas are too thin in Lincoln County to be visible at the prescribed map scale, and therefore Zone AE was not designated in these environments.

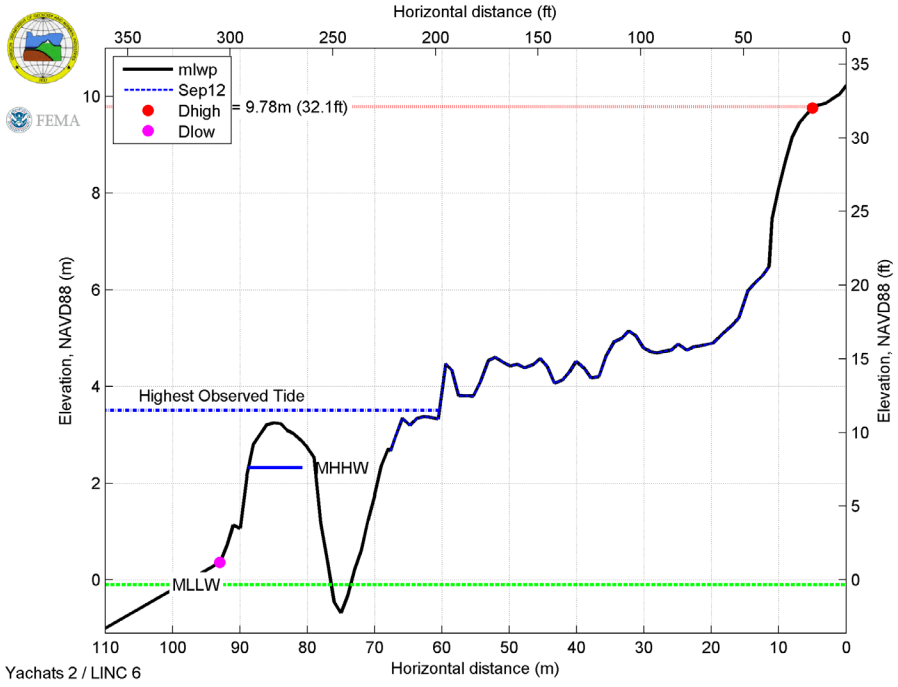

Figure 8-1. Example of a bluff-backed beach (LINC 6) where the calculated total water level and defined velocity (VE) zone extend into the bluff.

To define the velocity zones between transects, we used professional judgment to establish appropriate zone breaks between the various transects. For example, along-shore geomorphic barriers were identified within which the transect total water level (TWL) value is valid (**Figure 8-2**). Slope and hillshade derivatives of the lidar DEM, as well as 1-m orthophotos (acquired in 2009), provided the base reference. An effort was made to orient zone breaks perpendicular to the beach at the location of the geomorphic barrier. The seaward extent for the majority of Zone VE were inherited from the preliminary DFIRM (2011). In some cases adopting the effective extent produced inconsistent zone widths (too thin) and the boundaries were subsequently extended seaward.

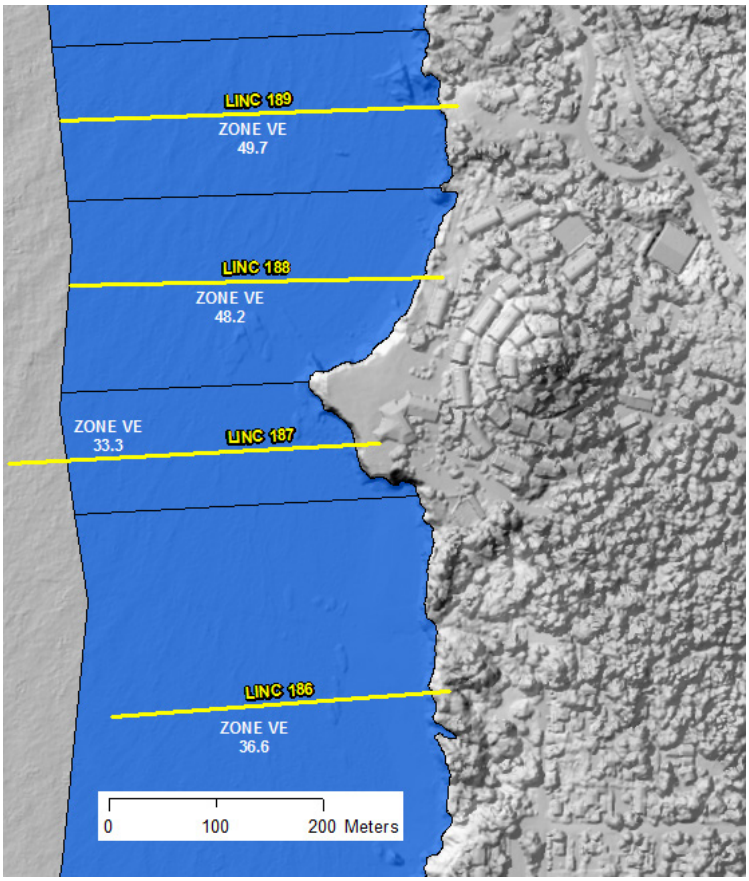

Figure 8-2. Example of alongshore zone breaks and their relationship to geomorphic barriers and surveyed transects. Surveyed transects are symbolized as yellow lines; zone breaks are solid black lines.

8.1.2 Dune-backed beaches

For dune-backed beaches, the VE flood zone was determined according to one or more criteria specified in the NHC (2005) guidelines. These include:

1. The ***wave runup zone***, which occurs where the total water level (TWL) exceeds the (eroded) ground profile by ≥ 0.91 m (3 ft);
2. The ***wave overtopping splash zone*** is the area landward of the dune/bluff/structure crest where splashover occurs. The landward limit of the splash zone is only mapped in cases where the wave runup exceeds the crest elevation by ≥ 0.91 m (3 ft);
3. The ***high-velocity flow zone*** occurs landward of the overtopping splash zone, where the product of flow times the flow velocity squared (hV^2) is ≥ 5.7 m^3/s^2 (or 200 ft^3/s^2);
4. The ***breaking wave height zone*** occurs where wave heights ≥ 0.91 m (3 ft) could occur and is mapped when the wave crest profile is 0.64 m (2.1 ft) or more above the static water elevation; and
5. The ***primary frontal dune (PFD) zone*** as defined in Part 44 of the U.S. Code of Federal Regulations, Section 59.1; FEMA Coastal Hazard Bulletin, No. 15.

Table 6-3 lists the overtopping calculations for those transects where overtopping occurs, including the calculated splashdown distances ($Y_{G\ outer}$), bore height associated with wave overtopping (h_o) and the landward extent of the high-velocity flow (hV^2) where the flows approach 5.7 m^3/s^2 (or 200 ft^3/s^2). As noted above, hV^2 reflects the farthest point landward of the dune/bluff/structure crest that experiences coastal flooding due to overtopping and is ultimately controlled by the extent of the landward flow where it approaches 5.7 m^3/s^2 (or 200 ft^3/s^2); values greater than 5.7 m^3/s^2 (or 200 ft^3/s^2) are located within the high-velocity flow (VE) zone, while lower values are located within the passive overland flooding (AE) zone. "Dist_3" (where the bore height is ≥ 3 ft) identifies the landward extent of flood zones where the bore height (h_o) was determined to be ≥ 0.91 m and were ultimately rounded up to the nearest whole foot (i.e., having an elevation of 0.91 m (3 ft) above the land surface). "Dist_2" (where the bore height is >2 <3 ft) identifies the landward extent of flood zones where the bore height (h_o) was determined to be between 0.61 and 0.91 m (2 and 3 ft high) and were ultimately rounded up to the nearest whole foot (i.e., having an elevation of 0.91 m (3 ft) above the land surface). "Dist_1" marks the seaward extent of flood zones where the bore height falls below 0.3 m (1 ft (i.e., having an elevation of 0.3 m [1 ft]) above the land surface (all values less than 0.3 m (1 ft) were rounded up to the nearest whole foot). Areas where flood zones exhibited bore height elevations of 0.61 m (2 ft) above the land surface were inferred as existing in the area between the two previously described regions (i.e., between "Distance from 'x' Where Bore >2 <3 ft" and "Distance from 'x' Where Bore <1").

Similar to the bluff-backed beaches, professional judgment was once again used to establish appropriate zone breaks between the detailed transects. This was achieved through a combination of having detailed topographic information of the backshore and from knowledge of the local geomorphology. Some interpretation was required to produce flood zones appropriate for the printed map scale. Elevations were identified from the 1-m resolution bare-earth lidar DEM to aid in establishing zone breaks due to changes in flood depth landward of the dune crest (**Figure 8-3**). Slope and hillshade derivatives of the lidar DEM, as well as 1-m orthophotos, provided base reference.

In overtopping splash transect situations, the flood zone was determined by adding the splashdown distances ($Y_{G\,outer}$) to the D_{HIGH} distance. For the majority of overtopping splash situations on the Lincoln coast, the splash distance are very short and not distinguishable at a mapping scale. Therefore, it was added to the VE zone extent (**Figure 8-4**).

For flood zones seaward of the dune crest, the calculated TWL values were used. As with the bluff-backed beaches, along-shore geomorphic barriers were identified within which the transect TWL value is valid. In all cases, an effort was made to orient zone breaks perpendicular to the beach at the location of the geomorphic barrier. The seaward extent of the flood zones were inherited from the preliminary DFIRM (2011).

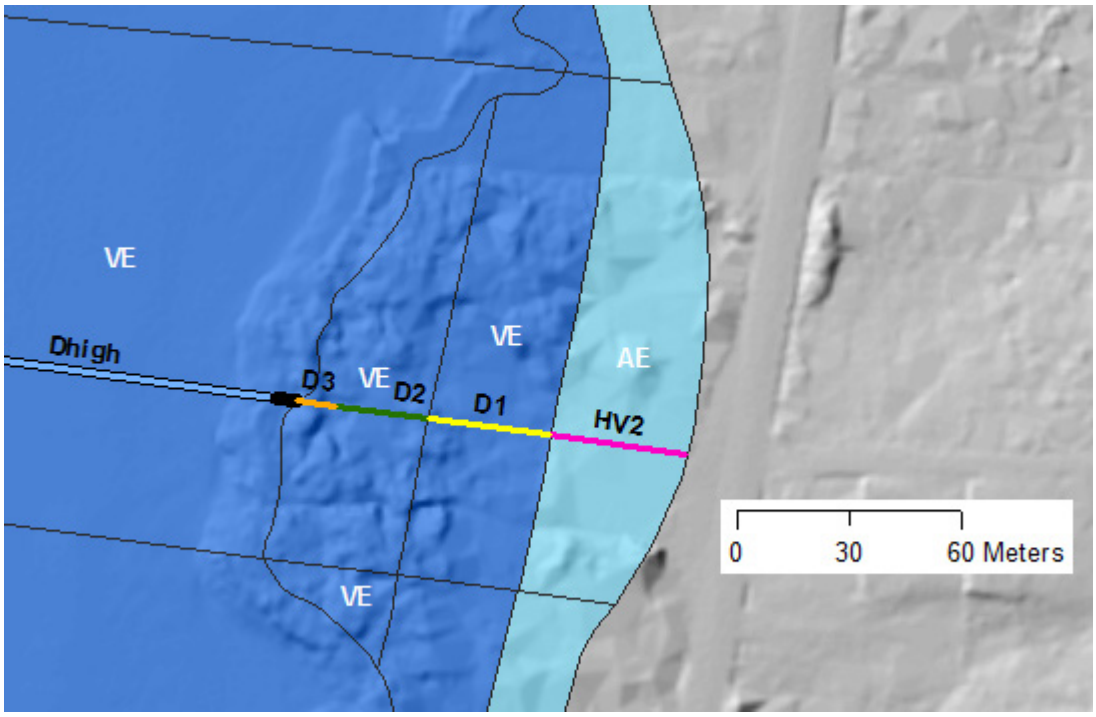

Figure 8-3. Overtopping along the LINC 24 transect (near Yachats), where D_{HIGH} is the area seaward of D_{HIGH} distance, Splash is the splashdown distance, D3 is depth > 3 ft, D2 is depth > 2 < 3 ft, D1 is depth ≤ 0.31 m, HV^2 is flow < 5.7 m^3/s^2 (or 200 ft^3/s^2). Zone breaks are solid black lines. Dark blue flood zones are VE zones; light blue are AE zones.

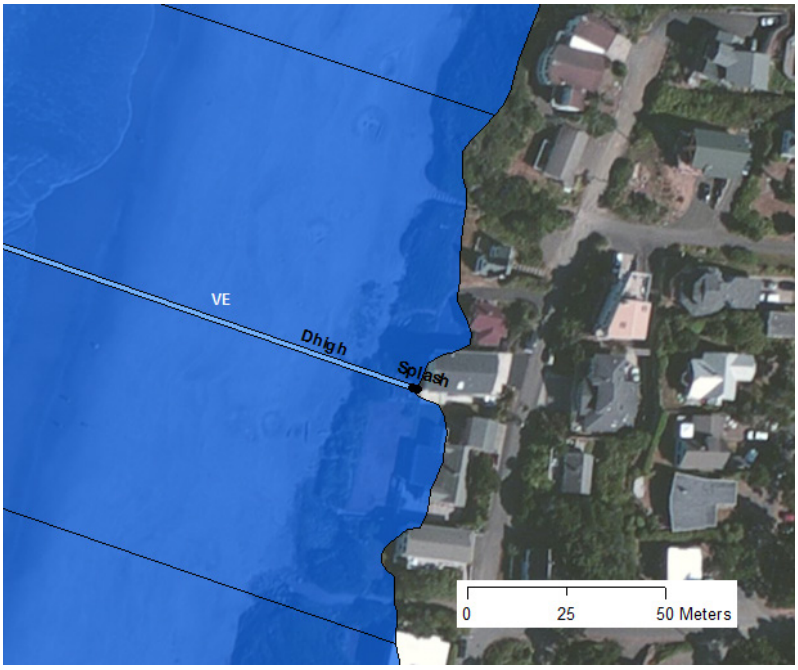

Figure 8-4. LINC 214 transect at Lincoln Beach with overtopping Splash zone. The short splash zone distance (black) was added to the extent of Zone VE.

The PFD is defined as "a continuous or nearly continuous mound or ridge of sand with relatively steep seaward and landward slopes immediately landward and adjacent to the beach and subject to erosion and overtopping from high tides and waves during major coastal storms. The landward limit of the primary frontal dune, also known as the toe or heel of the dune, occurs at a point where there is a distinct change from a relatively steep slope to a relatively mild slope. The primary frontal dune toe represents the landward extension of the Zone VE coastal high hazard velocity zone" (Part 44 of the U.S. Code of Federal Regulations, Section 59.1, as modified in FEMA Coastal Hazard Bulletin, No. 15, https://www.¬floodmaps.fema.gov/listserv/ch_jul02.shtml).

The approach developed by DOGAMI to define the morphology of the beach and dune system, including the location of the PFD follows procedures developed in our Coos Bay study (Allan and others 2012) and was based on detailed analyses of light detection and ranging (lidar) data measured by the USGS/NASA/NOAA in 1997, 1998, and 2002 and by DOGAMI in 2009. However, because the lidar data flown by the USGS/NASA/NOAA are of relatively poor resolution (~1 point/m^2) and reflect a single return (i.e., include vegetation where present), while the lidar data flown by DOGAMI have a higher resolution (8 points/m^2) and are characterized by multiple returns, enabling the development of a bare-earth DEM, determination of the PFD was based entirely on analysis of the 2009 lidar data.

Lidar data flown in 1997, 1998, and 2002 were downloaded from NOAA's Coastal Service Center, (http://www.csc.noaa.gov/digitalcoast/data/coastallidar/index.html), and gridded in ArcGIS using a triangulated irregular network (TIN) algorithm (Allan and Harris, 2012). Transects spaced 25 m apart were cast for the full length of the county coastline using the Digital Shoreline Analysis System (DSAS) developed by the USGS (Thieler and others, 2009); this process yielded 4,034 individual transects throughout Lincoln County. For each transect, xyz values for the 1997, 1998, 2002, and 2009 lidar data were extracted at 1-m intervals along each transect line and saved as a text file using a customized ArcGIS script.

Processing of the lidar data was undertaken in MATLAB using a beach profile analysis script developed by DOGAMI. This script requires the user to interactively define various morphological features including the dune/bluff/structure crest/top, bluff/structure slope, landward edge of the PFD(s), beach-dune juncture elevations for various years, and the slopes of the beach foreshore (Allan and Harris, 2012). Because the bulk of the Lincoln County coastline is backed by coastal bluffs, our analyses of the locations of the PFD focused only on those transects that were classified as being dune-backed. **Figure 8-5** provides an example from Lincoln #1609 located near the south end of Netarts Spit. In this example, the dune crest in 2009 is presently located at 10.59 m (34.7 ft); prior to 2009, the dune crest was as high as 11.7 m (38.4 ft). As can be seen from the figure, the seaward face of the dune has prograded seaward by ~13 m (43 ft) between 1997 and 2009; shoreline change (erosion/accretion) was determined based on the change in position of the 6 m (19.7 ft) contour elevation, which is an excellent proxy for determining the effects of storm erosion (Allan and others, 2003). **Figure 3-19** depict changes in the position of the 5 m (16 ft) contour along the length of the Lincoln County shoreline. As can be seen from the figures, erosion is generally most significant in those areas that are backed by sand dunes (e.g., Siletz Spit, **Figure 3-19**). In contrast, accretion dominates much of the Alsea Spit and along approximately 2.2 km (1.2 mi) of shoreline immediately south of Yaquina Bay (**Figure 3-19**).

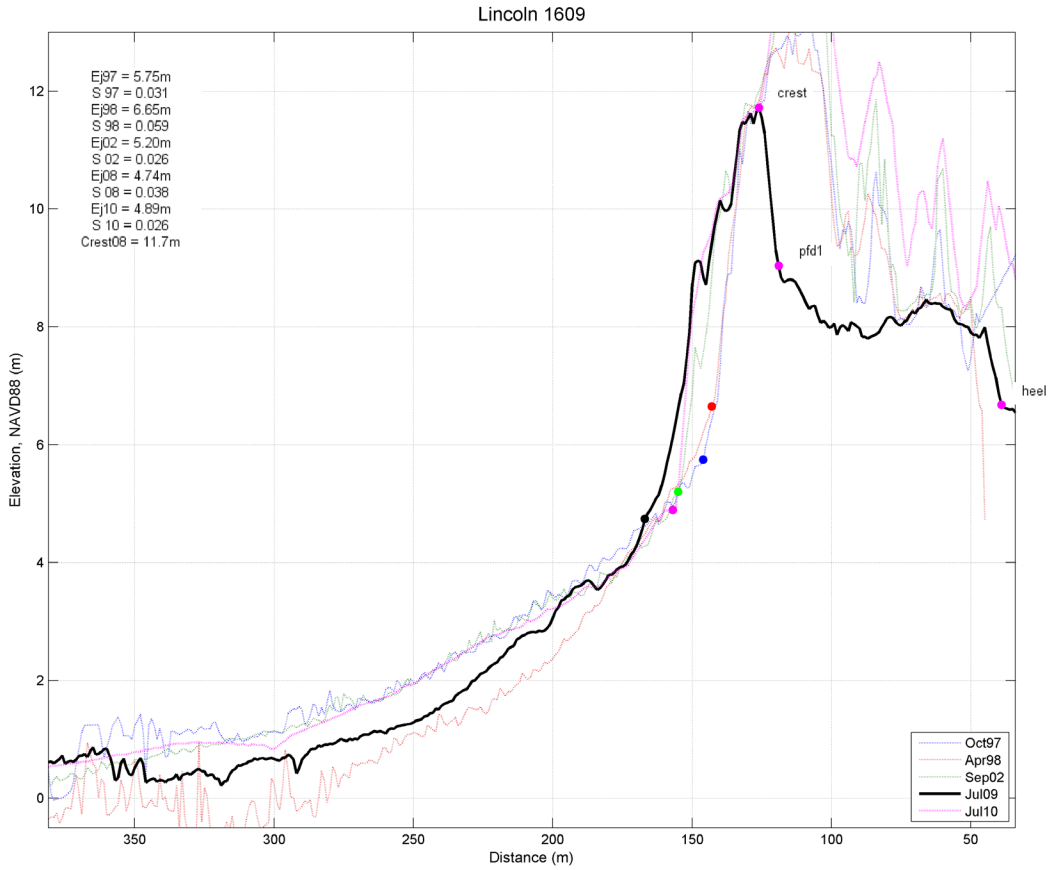

Figure 8-5. Example beach profile (#1609) located near Yaquina Bay State Park, south of the entrance to Yaquina Bay, and derived from 1997, 1998, 2002, and 2009 lidar data (Allan and Harris, 2012).

Having interpolated the lidar transect data in order to define the various morphological parameters, the actual locations of the PFDs were subsequently plotted in ArcGIS and overlaid on both current and historical aerial photos of the county, and shaded relief derived from the 2009 lidar. In many cases, multiple PFD locations were defined along a single transect. In a number of locations the PFD was found to be located either farther landward or seaward relative to adjacent PFD locations. This response is entirely a function of the degree to which the morphology of foredunes vary along a coast, and further the ambiguity of defining the PFD as defined above in the FEMA definition. Our observations of the PFD approach highlighted a number of uncertainties, including:

1. There were numerous examples of smaller dune features that have begun to develop in front of a main dune (or are the product of erosion of the dune), but have not yet attained dimensions and volumes where they would be considered an established dune or may continue to erode and could disappear entirely. However, the PFD approach does not adequately account for such features. In this example, the smaller dunes are almost certainly subject to erosion and periodic over-topping, and have morphologies that resemble the FEMA PFD definition. However, because they are subject to short-term erosion responses they are more ephemeral in nature and thus it is debatable whether they should be defined as

PFDs. Furthermore, over the life of a typical map (~10 years) these dunes could be eroded and removed entirely leaving a "gap" between the original polygon boundary and the eroding dune. For example, from repeated observations of beach profile transects on the northern Oregon coast, single storm events have been documented to remove as much as 9–25 m (30–82 ft) of the dune (Allan and Hart, 2007, 2008);

2. The PFD does not adequately account for a large established foredune, where the dune may have attained heights of 10–15 m (33–49 ft), with cross-shore dimensions on the order of 100–200 m (328–656 ft) wide due to prolonged aggradation and progradation of the beach. In this example, although there may be a clear landward heel located well inland away from the beach (e.g., profile #840 in **Figure 8-6**, which was derived from our Clatsop County study), the PFD is clearly not subject to "frequent" wave over-topping due to its height and erosion (because of its large volume of sand). Defining the PFD at the location of the heel is consistent within the definition provided by FEMA, but would almost certainly generate a very conservative V-zone.

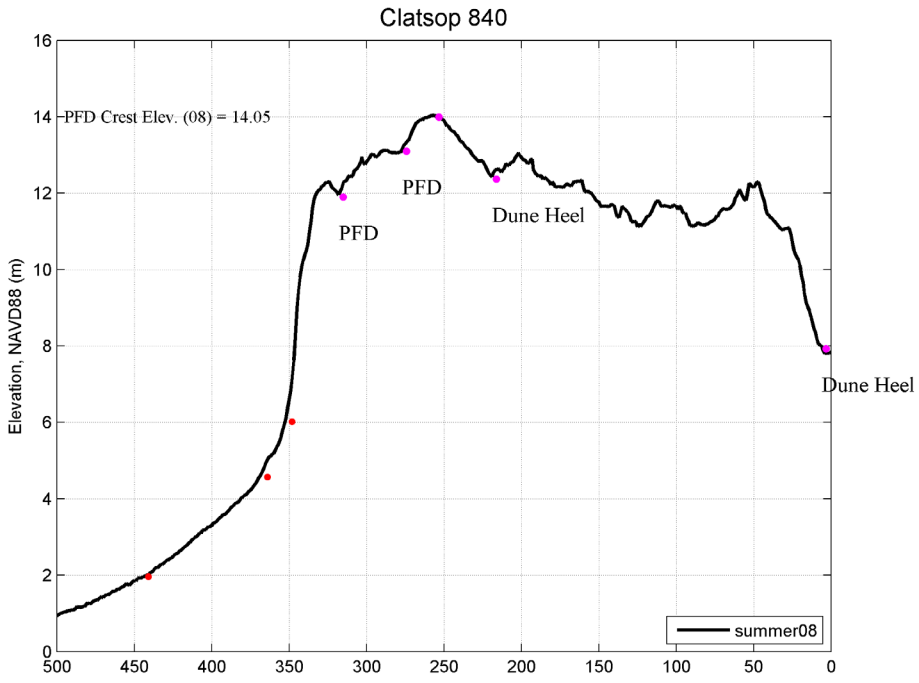

Figure 8-6. Example profile from the Clatsop Plains where considerable aggradation and progradation of the dune has occurred. In this example, the PFD could conceivably be drawn at a variety of locations and meet the FEMA definition.

3. Although numerous transects exhibited clear examples of single PFD locations, many others were characterized by more than one PFD. Profile #1929 (**Figure 8-7**) taken from our Tillamook County study is an example where multiple potential PFDs could be defined.

To account for these variations and uncertainties, the PFD shown on the profile plots (e.g., **Figure 8-5** to **Figure 8-7**) were re-examined and adjustments were made where necessary in order to define a single PFD line. For example, in a few locations along the Clatsop Plains, the PFD extent for a particular transect was physically moved so that it was more in keeping with the adjacent PFD locations to its immediate north and south. As can be seen in **Figure 8-8**, the final PFD designation was invariably some distance inland, often representing the clearest signal determined from all available data and adhering best to the FEMA definition.

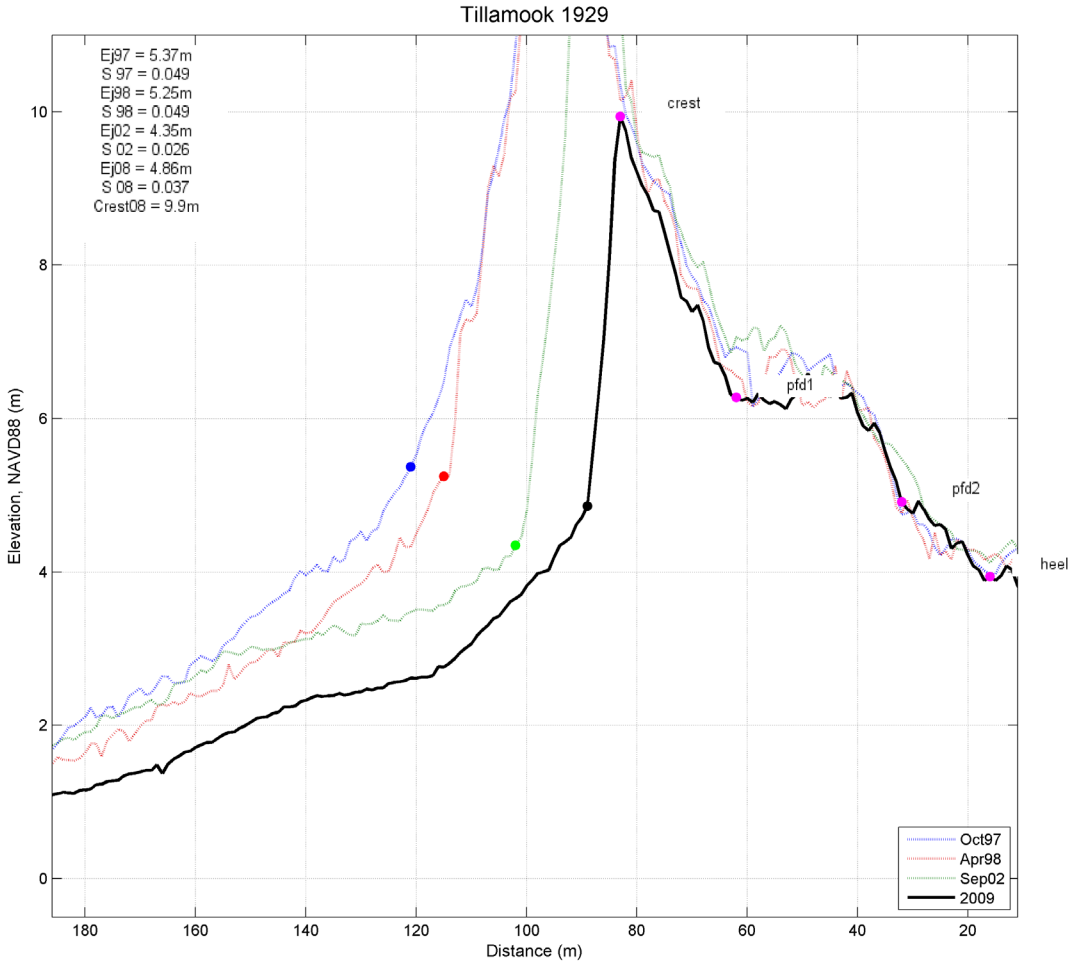

Figure 8-7. Example profile (#1929) from Netarts Spit showing the presence of at least two PFD locations.

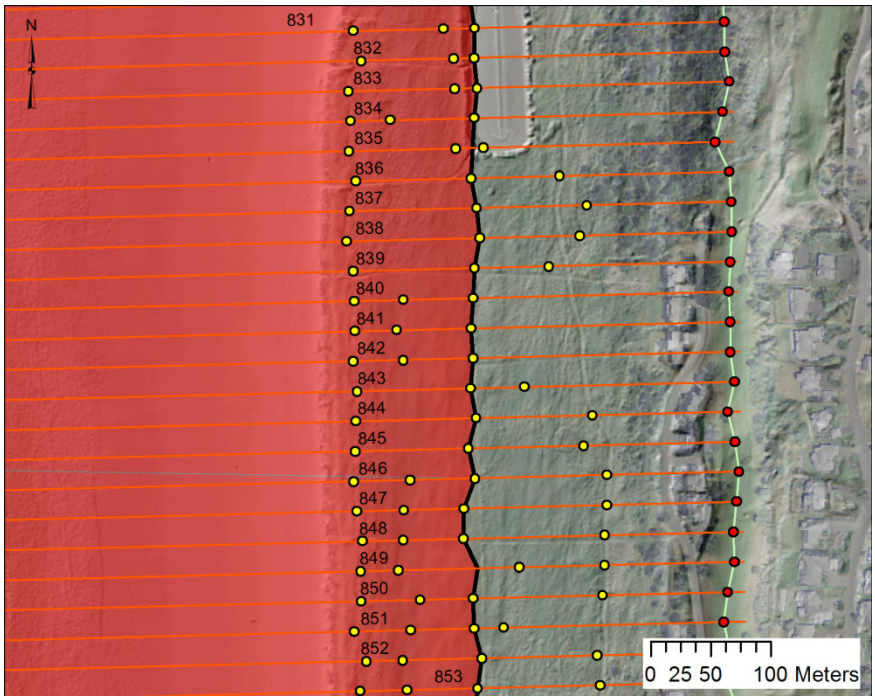

Figure 8-8. Plot showing identified PFD locations (yellow dots) along each transect, landward most dune heel (red dots), and derived PFD line (black line). Red zone depicts the VE zone having accounted for all possible criteria. Red lines depict the locations of the lidar transects, which were spaced 25 m (82 ft) apart.

The PFD was defined at a number of locations where significant human modification has occurred on the dune. In these areas, the natural dune system has been severely impacted and the PFD line does not represent a natural dune system. **Table 8-1** lists the transect locations where this situation occurs and also provides the VE zone extent used in place of the PFD.

Table 8-1. Transect locations where the PFD was not used for mapping due to significant human modification of the dune.

Transect	VE Zone Extent
LINC 52	runup
LINC 54	runup
LINC 127	wave overtopping splash zone
LINC 231	runup
LINC 234	runup

8.1.3 Mapping of estuarine flooding

Lincoln County includes three large estuarine features. Due to their complexity, Alsea Bay and Siletz Bay were redelineated using previously effective BFEs. Yaquina Bay, which was mapped in the previously effective FIRM using still water levels (SWL), was remapped using a different SWL determined in this new study.

Alsea Bay was completely redelineated (**Figure 8-9**). However, the northern end of Siletz Bay was incorporated as-is from the effective DFRIM due to the difficulty involved in redelineation (**Figure 8-10**); the remainder of the bay was redelineated. No new studies were performed at these locations, and the adjacent open coast detailed coastal analysis could not reasonably be used for mapping these estuaries.

As part of this new study, Yaquina Bay is mapped based on the new detailed coastal analyses of the open coast SWL, which results in coastal backwater flooding (**Figure 8-11**). Due to the lack of wave energy the SWL was used to map the coastal backwater effect of the 1% and 0.2% flood events into Yaquina Bay. Procedures for developing the SWL are described in Section 4.6. The 1% SWL value for the Lincoln County coast is 3.5 m (11.5 ft, NAVD88) and 0.2% SWL is estimated to be 3.6 m (11.8 ft, NAVD88).

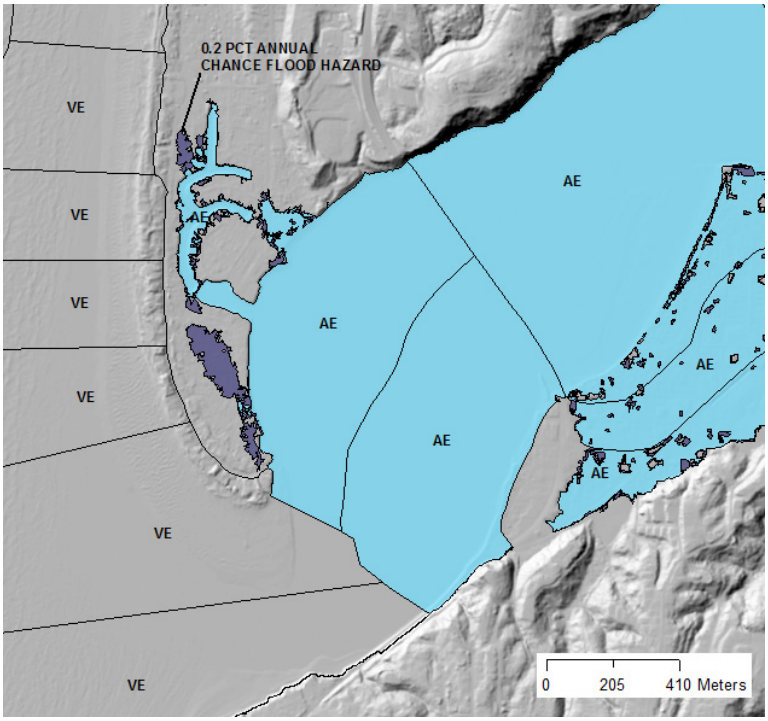

Figure 8-9. Redelineation at the mouth of Alsea Bay (Zone AE and 0.2 Percent Annual Chance Flood Hazard).

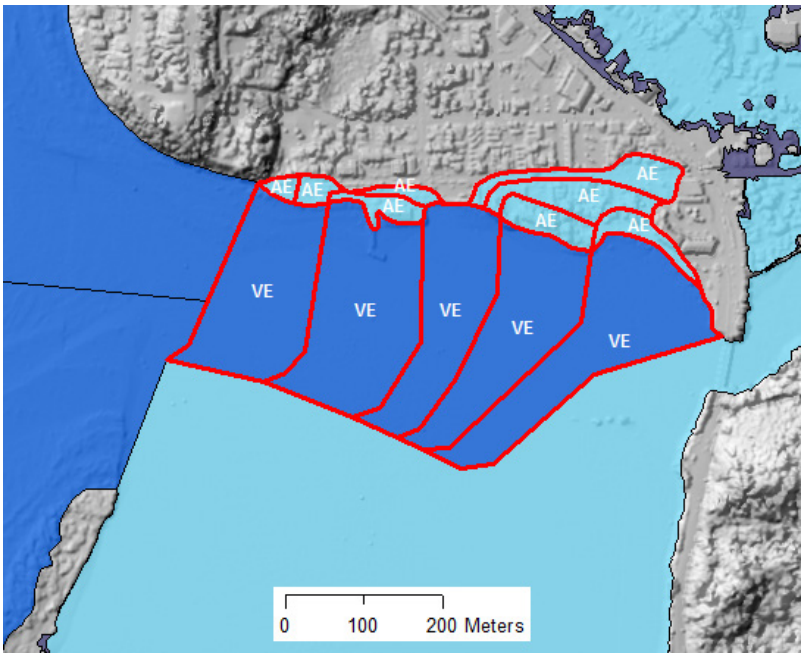

Figure 8-10. Siletz Bay, showing the effective flood zones incorporated "as is" (outlined in red).

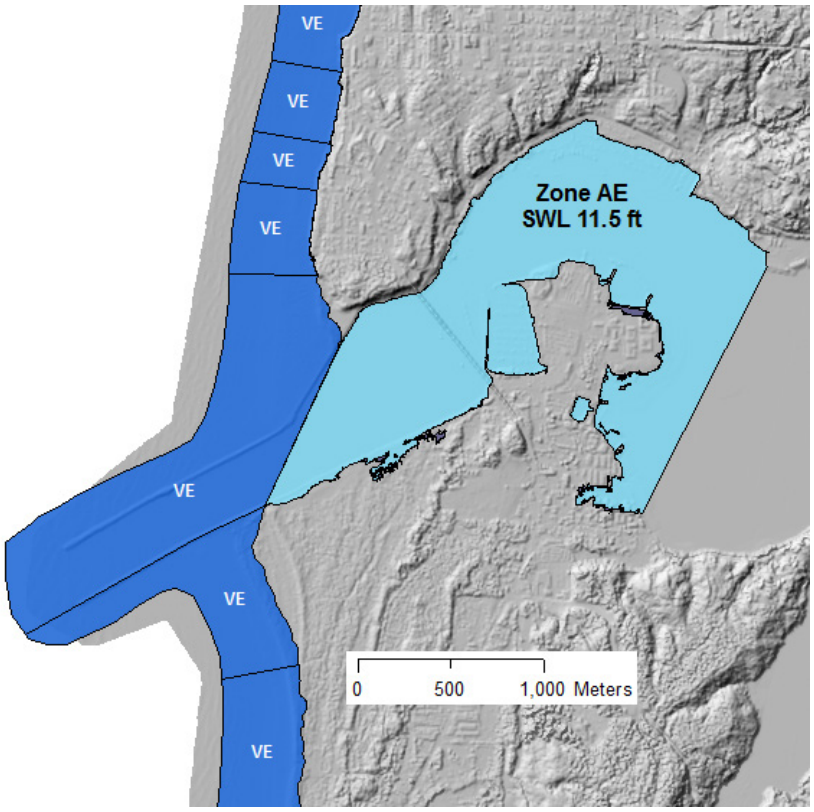

Figure 8-11. Coastal backwater flooding mapped from SWLs for Yaquina Bay. The 0.2% chance flooding (purple) is difficult to distinguish at this scale.

9.0 ACKNOWLEDGMENTS

Funding for this study was provided by the Federal Emergency Management Agency as part of the Flood Map Modernization program under Cooperating Technical Partner award EMS-2010-GR-0014. We are grateful to Dr. Bill McDougal for his technical advice throughout this project. We would especially like to acknowledge Joe Faries from Stantec and Dr. Paul Komar for their insightful review of the report.

10.0 REFERENCES

Aguilar-Tunon, N.A., and Komar, P.D., 1978, The annual cycle of profile changes of two Oregon beaches: Ore Bin, v. 40, no. 2, p. 25-39.

Allan, J.C., and Komar, P.D., 2002, Extreme storms on the Pacific Northwest Coast during the 1997-98 El Niño and 1998-99 La Niña: Journal of Coastal Research, v. 18, no. 1, p. 175-193.

Allan, J.C., Komar, P.D., and Priest, G.R., 2003, Shoreline variability on the high-energy Oregon coast and its usefulness in erosion-hazard assessments, *in* Byrnes, M.R., Crowell, M., and Fowler, C., eds., Shoreline mapping and change analysis: Technical considerations and management implications: Journal of Coastal Research, Special Issue No. 38, p. 83-105.

Allan, J.C., and Komar, P.D., 2006, Climate controls on U.S. West Coast erosion processes: Journal of Coastal Research, v. 22, no. 3, p. 511-529.

Allan, J.C., and Hart, R., 2007, Assessing the temporal and spatial variability of coastal change in the Neskowin littoral cell: Developing a comprehensive monitoring program for Oregon beaches: Oregon Department of Geology and Mineral Industries Open-File Report O-07-01, 27 p.

Allan, J.C., and Hart, R., 2008, Oregon beach and shoreline mapping and analysis program: 2007-2008 beach monitoring report: Oregon Department of Geology and Mineral Industries Open-File Report O-08-15, 60 p.

Allan, J.C., Komar, P.D., and Ruggiero, P., 2011, Storm surge magnitudes and frequenciy on the central Oregon coast, *in* Solutions to Coastal Disasters 2011, Anchorage, Alaska, American Society of Civil Engineers, p. 53-64.

Allan, J.C., and Harris, E.L., 2012, An "expanded" geospatial database of beach and bluff morphology determined from LIDAR data collected on the northern Oregon coast; Tillamook to Clatsop County: Oregon Department of Geology and Mineral Industries Open-File Report O-12-08, 23 p.

Allan, J.C., Komar, P.D., Ruggiero, P., and Witter, R.C., 2012a, The March 2011 Tōhoku tsunami and its impacts along the U.S. West Coast: Journal of Coastal Research, v. 28, no. 5, p. 1142-1153.

Allan, J.C., Ruggiero, P., and Roberts, J.T., 2012b, Coastal flood insurance study, Coos County, Oregon: Oregon Department of Geology and Mineral Industries Special Paper 44, 132 p.

Allan, J.C., and Stimely, L., 2013, Oregon Beach Shoreline Mapping and Analysis Program: Quantifying short to long-term beach and shoreline changes in the Gold Beach, Nesika, and Netarts littoral cells: Oregon Department of Geology and Mineral Industries Open-File Report O-13-07, 46 p.

Alsina, J.M., and Baldock, T.E., 2007, Improved representation of breaking wave energy dissipation in parametric wave transformation models: Coastal Engineering, v. 54, no. 10, p. 765-769.

Atwater, B.F., Satoko, M.-R., Satake, K., Yoshinobu, T., Kazue, U., and Yamaguchi, D.K., 2005, The orphan tsunami of 1700—Japanese clues to a parent earthquake in North America: U.S. Geological Survey Professional Paper 1707, 144 p.

Baird & Associates, 2005, Pacific Ocean wave information study: Validation of wave model results against satellite altimeter data. Prepared

for U.S. Army Corp of Engineers, Engineering Research and Development Center, Vicksburg, Miss.: Madison, Wisconsin, 13 p.

Bernstein, D.J., Freeman, C., Forte, M.F., Park, J.-Y., Gayes, P.T., and Mitasova, H., 2003, Survey design analysis for three-dimensional mapping of beach and nearshore morphology, *in* Fifth International Symposium on Coastal Engineering and Science of Coastal Sediment Processes (Coastal Sediments '03), Clearwater Beach, Fla., American Society of Civil Engineers, p. 12.

Booij, N., Ris, R.C., and Holthuijsen, L.H., 1999, A third-generation wave model for coastal regions, Part I: Model description and validation: Journal of Geophysical Research, v. 104, no. C4, p. 7649-7666.

Boon, J.D., 2004, Secrets of the tide: Tide and tidal current analysis and predictions, storm surges and sea level trends: Cambridge, U.K., Woodhead Publishing, 224 p.

Bruun, P., 1962, Sea level rise as a cause of shore erosion: Journal of Waterways, Harbors Division, Amer. Soc. Civil Engrs., v. 88, p. 117-130.

Burgette, R.J., Weldon, R.E., III, and Schmidt, D.A., 2009, Interseismic uplift rates for western Oregon and along-strike variation in locking on the Cascadia subduction zone: Journal of Geophysical Research, v. 114, no. B01408, p. 24.

Carignan, K.S., Taylor, L.A., Eakins, B.W., Warnken, R.R., Lim, E., and Grothe, P.R., 2009, Digital elevation model of central Oregon coast: Procedures, data sources and analysis: National Geophysical Data Center, Marine Geology and Geophysics Division NOAA Technical Memorandum NESDIS NGDC-25, 38 p.

Clemens, K.E., and Komar, P.D., 1988, Oregon beach-sands compositions produced by the mixing of sediments under a transgressing sea: Journal of Sedimentary Petrology, v. 58, no. 3, p. 519-529.

Coles, S., 2001, An introduction to statistical modeling of extreme values: London, Springer-Verlag, 208 p.

Cooper, W.S., 1958, Coastal sand dunes of Oregon and Washington: Geological Society of America Memoir 72, 169 p.

Davis, R.E., and Dolan, R., 1993, Nor'easters: American Scientist, v. 81, p. 428-439.

Dean, R.G., 1977, Equilibrium beach profiles: U.S. Atlantic and Gulf Coasts; Ocean Engineering Technical Report No. 12: Newark, Del., University of Delaware, Department of Civil Engineering and College of Marine Studies, 45 p.

Goldfinger, C., Nelson, C.H., and Johnson, J.G., 2003, Holocene earthquake records from the Cascadia Subduction Zone and Northern San Andreas fault based on precise dating of offshore turbidites: Annual Review of Earth and Planetary Sciences, v. 31, p. 555-577.

Goldfinger, C., 2009, Paleoseismically derived probabilities for Cascadia great earthquakes [abs.]: Geological Society of America Abstracts with Programs, v. 41, no. 7, p. 520.

Goldfinger, C., and others, 2012, Turbidite event history—Methods and implications for Holocene paleoseismicity of the Cascadia subduction zone: U.S. Geological Survey Professional Paper 1661-F, 170 p.

Haxell, J.H., and Holman, R.A., 2004, The sediment response of a dissipative beach to variations in wave climate: Marine Geology, v. 206, no. 1-4, p. 73-99.

Hedges, T.S., and Mase, H., 2004, Modified Hunt's equation incorporating wave setup: Journal of Waterway, Port, Coastal, and Ocean Engineering, v. 130, no. 3, p. 109-113.

Janssen, T.T., and Battjes, J.A., 2007, A note on wave energy dissipation over steep beaches: Coastal Engineering, v. 54, no. 9, p. 711-716.

Kelsey, H.M., Nelson, A.R., Hemphill-Haley, E., and Witter, R.C., 2005, Tsunami history of an Oregon coastal lake reveals a 4600 yr record of great earthquakes on the Cascadia subduction zone: Geological Society of America Bulletin, v. 117, no. 7/8, p. 1009-1032.

Komar, P.D., 1986, The 1982-83 El Nino and erosion on the coast of Oregon: Shore and Beach, v. 54, no. 2, p. 3-12.

Komar, P.D., Torstenson, R.W., and Shih, S.-M., 1991, Bandon, Oregon: Coastal development and the

potential for extreme ocean hazards: Shore & Beach, v. 59, no. 4, p. 14-22.

Komar, P.D., 1997, The Pacific Northwest Coast: Living with the shores of Oregon and Washington: Durham and London, Duke University Press, 195 p.

Komar, P.D., 1998, Beach processes and sedimentation (2nd ed.): Englewood Cliffs, New Jersey, Prentice Hall, Inc., 544 p.

Komar, P.D., McDougal, W.G., Marra, J.J., and Ruggiero, P., 1999, The rational analysis of setback distances: Applications to the Oregon coast: Shore & Beach, v. 67, p. 41-49.

Komar, P.D., 2004, Oregon's coastal cliffs: Processes and erosion impacts: United States Government Professional Paper 1693, 123 p.

Komar, P.D., McManus, J., and Styllas, M., 2004, Sediment Accumulation in Tillamook Bay, Oregon: Natural Processes versus Human Impacts: Journal of Geology, v. 112, p. 455-469.

Komar, P.D., Allan, J.C., and Ruggiero, P., 2011, Sea level variations along the U.S. Pacific Northwest Coast: Tectonic and climate controls: Journal of Coastal Research, v. 27, no. 5, p. 808-823.

Legaard, K.R., and Thomas, A.C., 2006, Spatial patterns in seasonal and interannual variability of chlorophyll and sea surface temperature in the California Current: Journal of Geophysical Research, v. 111, no. C06032.

Mori, N., Takahashi, T., Yasuda, T., and Yanagisawa, H., 2011, Survey of 2011 Tohoku Earthquake Tsunami Inundation and Run-up: Geophysical Research Letters, v. 38, no. L00G14, p. 6.

Morton, R.A., Leach, M.P., Paine, J.G., and Cardoza, M.A., 1993, Monitoring beach changes using GPS surveying techniques: Journal of Coastal Research, v. 9, no. 3, p. 702-720.

Northwest Hydraulic Consultants, Inc. (NHC), 2005, Final draft guidelines for coastal flood hazard analysis and mapping for the Pacific Coast of the United States, report prepared for FEMA: West Sacramento, Calif., Northwest Hydraulic Consultants, Inc., 344 p.

Oceanweather Inc., 2010, Global Reanalysis of Ocean Waves Fine Northeast Pacific Hindcast (GROW-FINE NEPAC): Oceanweather Inc., 39 p.

Orr, E.L., Orr, W.N., and Baldwin, E.M., 1992, Geology of Oregon (4th ed.): Dubuque, Iowa., Kendall/Hunt

Ozkan-Haller, H.T., Allan, J.C., Barth, J.A., Haller, M.C., Holman, R.A., and Ruggiero, P., 2009, Baseline observations and modeling for the Reedsport wave energy site: Oregon State University and the Oregon Department of Geology and Mineral Industries on behalf of Oregon Wave Energy Trust, 35 p.

Peterson, C., Scheidegger, K., Komar, P.D., and Niem, W., 1984, Sediment composition and hydrography in six high-gradient estuaries of the northwestern United States: Journal of Sedimentary Petrology, v. 54, no. 1, p. 86-97.

Peterson, C.D., Jackson, P.L., O'Neil, D.J., Rosenfeld, C.L., and Kimerling, A.J., 1990, Littoral cell response to interannual climatic forcing 1983-1987 on the central Oregon coast, USA: Journal of Coastal Research, v. 6, no. 1, p. 87-110.

Peterson, C.D., Darienzo, M.E., Hamilton, D., Pettit, D.J., Yeager, R.K., Jackson, P.L., Rosenfeld, C.L., and Terich, T.A., 1994, Beach-shoreline database, Pacific Northwest Region, USA: Oregon Department of Geology and Mineral Industries Open-File Report O-94-2, 29 p.

Priest, G.R., Saul, I., and Diebenow, J., 1993, Pilot erosion rate data study of the central Oregon coast, Lincoln County: Final technical report to the Federal Emergency Management Agency: Oregon Department of Geology and Mineral Industries Open-File Report O-93-10, 228 p.

Priest, G.R., Goldfinger, C., Wang, K., Witter, R.C., Zhang, Y., and Baptista, A.M., 2010, Confidence levels for tsunami-inundation limits in northern Oregon inferred from a 10,000-year history of great earthquakes at the Cascadia subduction zone: Natural Hazards, v. 54, p. 27-73.

Pullen, T.A., Allsop, N.W.H., Bruce, T., Kortenhaus, A., Schuttrümpf, H., and van der Meer, J.W., 2007, EurOtop - wave overtopping of sea defences and related structures: Assessment manual, 193 p.

Ris, R.C., Booij, N., and Holthuijsen, L.H., 1999, A third-generation wave model for coastal regions, Part II: Verification: Journal of Geophysical Research, v. 104, no. C4, p. 7667-7681.

Ruggiero, P., Komar, P.D., McDougal, W.G., and Beach, R.A., 1996, Extreme water levels, wave runup and coastal erosion, *in* Proceedings of the 25th International Conference on Coastal Engineering, Sept. 2-6, 1996, Orlando, Fla., American Society of Civil Engineers, p. 2793-2805.

Ruggiero, P., and Voigt, B., 2000, Beach monitoring in the Columbia River littoral cell, 1997-2000: Coastal Monitoring & Analysis Program, Washington Department of Ecology Publication No. 00-06-026, 113 p.

Ruggiero, P., Komar, P.D., McDougal, W.G., Marra, J.J., and Beach, R.A., 2001, Wave runup, extreme water levels and the erosion of properties backing beaches: Journal of Coastal Research, v. 17, no. 2, p. 407-419.

Ruggiero, P., Holman, R.A., and Beach, R.A., 2004, Wave run-up on a high-energy dissipative beach: Journal of Geophysical Research, v. 109, p. C06025.

Ruggiero, P., Kaminsky, G.M., Gelfenbaum, G., and Voight, B., 2005, Seasonal to interannual morphodynamics along a high-energy dissipative littoral cell: Journal of Coastal Research, v. 21, no. 3, p. 553-578.

Ruggiero, P., Buijsman, M.C., Kaminsky, G.M., and Gelfenbaum, G., 2010a, Modeling the effects of wave climate and sediment supply variability on large-scale shoreline change: Marine Geology, v. 273, p. 127-140.

Ruggiero, P., Komar, P.D., and Allan, J.C., 2010b, Increasing wave heights and extreme value projections: The wave climate of the U.S. Pacific Northwest: Coastal Engineering, v. 57, no. 5, p. 539-552.

Ruggiero, P., Kratzmann, M.G., Himmelstoss, E.A., Reid, D., Allan, J., and Kaminsky, G., 2013, National Assessment of Shoreline Change: Historical Shoreline Change along the Pacific Northwest coast (Oregon and Washington): U.S. Geological Survey Open-File Report 2012-1007, 62 p.

Satake, K., Shemazaki, K., Yoshinobu, T., and Ueda, K., 1996, Time and size of a giant earthquake in Cascadia inferred from Japanese tsunami records of January 1700: Nature, v. 379, no. 6562, p. 246-249.

Schlicker, H.G., Deacon, R.J., Olcott, G.W., and Beaulieu, J.D., 1973, Environmental geology of Lincoln County, Oregon: Oregon Department of Geology and Mineral Industries Bulletin 81, 171 p, 176 maps p.

Smith, J.M., Sherlock, A.R., and Resio, D.T., 2001, STWAVE: Steady-state spectral wave model user's manual for STWAVE, Version 3.0: U.S. Army Engineer Research and Development Center, Coastal and Hydraulics Laboratory Technical Report ERDC/CHL SR-01-1, 81 p.

Soler, T., Weston, N.D., and Foote, R.H., 2011, The "Online Positioning User Service" suite (OPUS-S, OPUS-RS, OPUS-DB), *in* Soler, T., ed., CORS and OPUS for Engineers: Tools for Surveying and Mapping Applications Reston, Va., American Society of Civil Engineers, p. 17-26.

Stembridge, J.E., 1975, Recent shoreline changes of the Alsea sandspit, Lincoln County, Oregon: Ore Bin, v. 37, no. 5, p. 77-82.

Stockdon, H.F., Holman, R.A., Howd, P.A., and Sallenger, A.H., 2006, Empirical parameterization of setup, swash, and runup: Coastal Engineering, v. 53, no. 7, p. 573-588.

Storlazzi, C.D., and Griggs, G.B., 2000, Influence of El Niño-Southern Oscillation (ENSO) events on the evolution of central California's shoreline: Bulletin of the Geological Society of America, v. 112, no. 2, p. 236-249.

Thieler, E.R., Himmelstoss, E.A., Zichichi, J.L., and Ayhan, E., 2009, Digital Shoreline Analysis System (DSAS) version 4.0—An ArcGIS extension for calculating shoreline change: U.S. Geological Survey Open-File Report 2008-1278.

Tillotson, K., and Komar, P.D., 1997, The wave climate of the Pacific Northwest (Oregon and Washington): A comparison of data sources: Journal of Coastal Research, v. 13, no. 2, p. 440-452.

Trenberth, K.E., 1999, The extreme weather events of 1997 and 1998: Consequences, v. 5, no. 1, p. 3-15.

Trimble, 2005, Trimble 5700 GPS system datasheet: Dayton, Ohio, Trimble Navigation Limited, Engineering & Construction Group, p. 2.

van der Meer, J.W., 2002, Technical report wave run-up and wave overtopping at dikes: Deflt, Netherlands, Technical Advisory Committee on Flood Defence, Road and Hydraulic Engineering Institute, 50 p.

Witter, R.C., Kelsey, H.M., and Hemphill-Haley, E., 2003, Great Cascadia earthquakes and tsunamis of the past 6700 years, Coquille River estuary, southern coastal Oregon: Geological Society of America Bulletin, v. 115, p. 1289-1306.

Witter, R.C., 2008, Prehistoric Cascadia tsunami inundation and runup at Cannon Beach, Clatsop County, Oregon: Oregon Department of Geology and Mineral Industries Open-File Report O-08-12, 36 p.

Witter, R.C., Zhang, Y.J., Goldfinger, C., Priest, G.R., and Wang, K., 2010, Validating numerical tsunami simulations in southern Oregon using late Holocene records of great Cascadia earthquakes and tsunamis [abs.]: Seismological Research Letters, v. 81, no. 2, p. 290.

Yamamoto, M., 2011, Tōhoku Tsunami March 11, 2011 as of 30 March 2011: United Nations Educational, Scientific and Cultural Organization, Intergovernmental Oceanographic Comission IOC/UNESCO Bulletin No. 13.

Zhang, K., Douglas, B.C., and Leatherman, S., 2001, Beach erosion potential for severe nor'easters: Journal of Coastal Research, v. 17, no. 2, p. 309-321.

11.0 APPENDICES

Appendix A: Ground Survey Accuracy Assessment Protocols

Appendix B: Lincoln County Beach and Bluff Profiles

11.1 Appendix A: Ground Survey Accuracy Assessment Protocols

See report by Watershed Sciences, Inc., dated December 21, 2009.

11.2 Appendix B: Tillamook County Beach and Bluff Profiles

11.2.1 Cape Perpetua

LINC 1

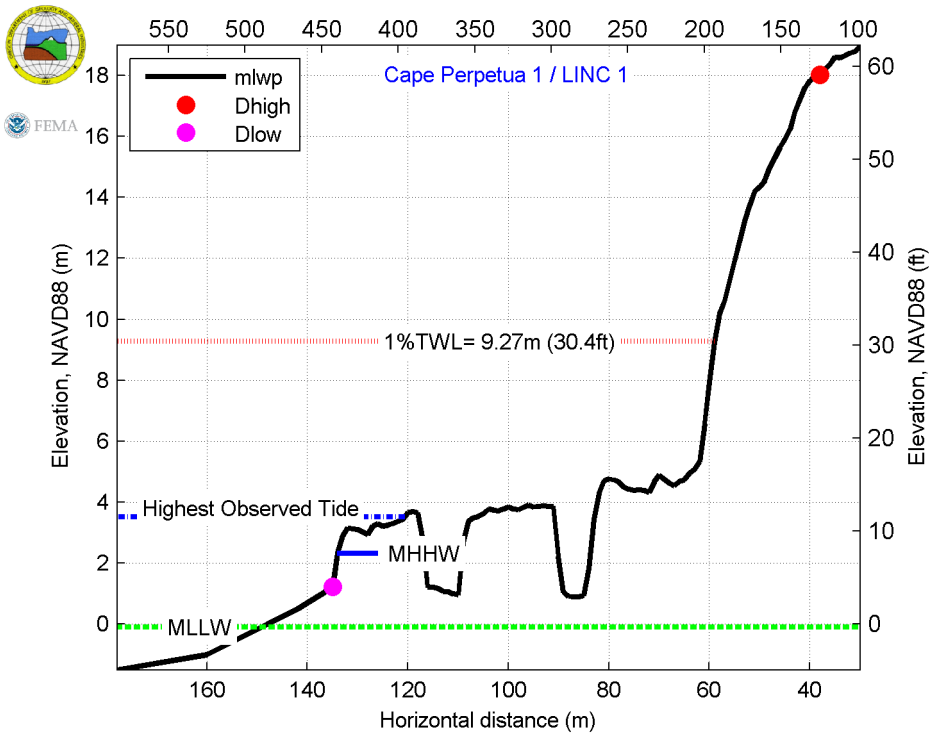

LINC 2

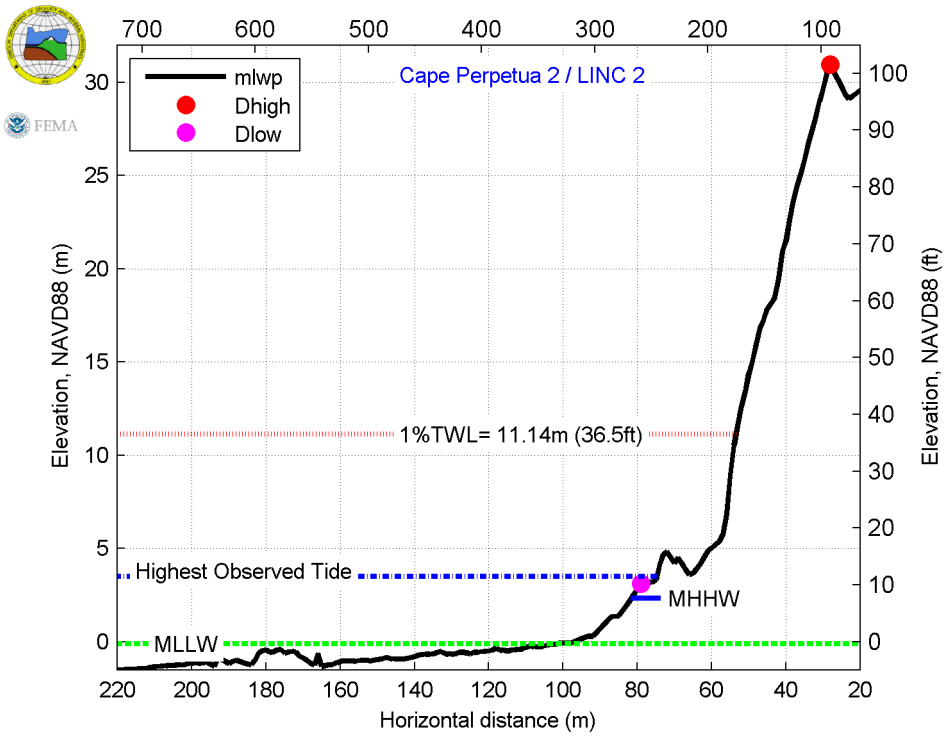
Cape Perpetua 2 / LINC 2
mlwp
Dhigh
Dlow
1%TWL= 11.14m (36.5ft)
Highest Observed Tide
MHHW
MLLW
Elevation, NAVD88 (m)
Elevation, NAVD88 (ft)
Horizontal distance (m)
700 600 500 400 300 200 100
220 200 180 160 140 120 100 80 60 40 20
30 25 20 15 10 5 0
100 90 80 70 60 50 40 30 20 10 0

LINC 3

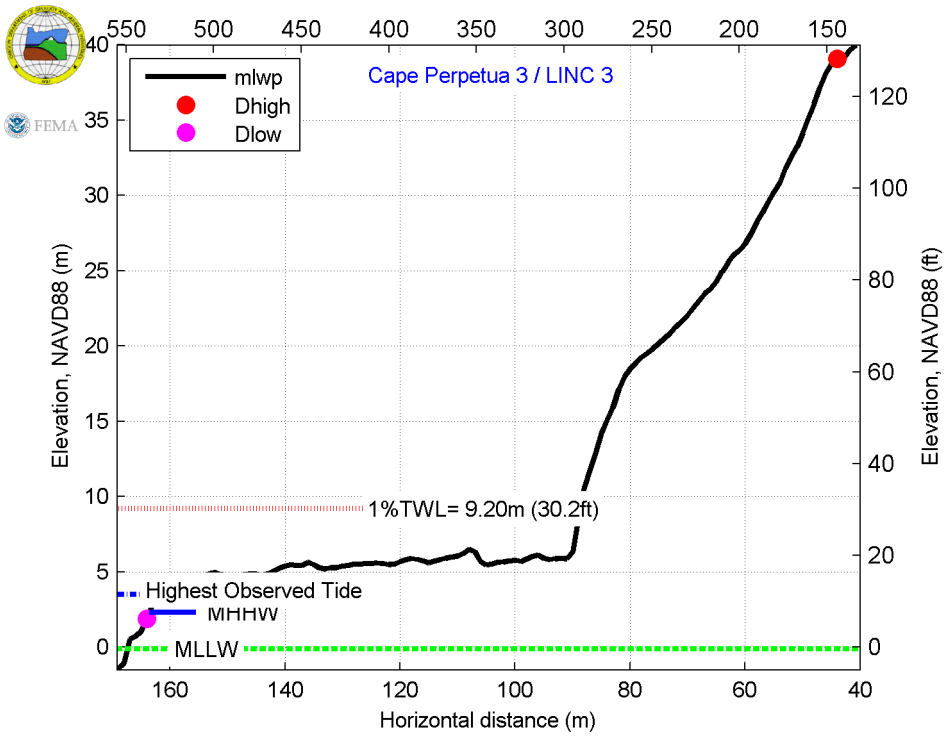
Cape Perpetua 3 / LINC 3
mlwp
Dhigh
Dlow
1%TWL= 9.20m (30.2ft)
Highest Observed Tide
MHHW
MLLW
Elevation, NAVD88 (m)
Elevation, NAVD88 (ft)
Horizontal distance (m)
550 500 450 400 350 300 250 200 150
160 140 120 100 80 60 40
40 35 30 25 20 15 10 5 0
120 100 80 60 40 20 0

LINC 4

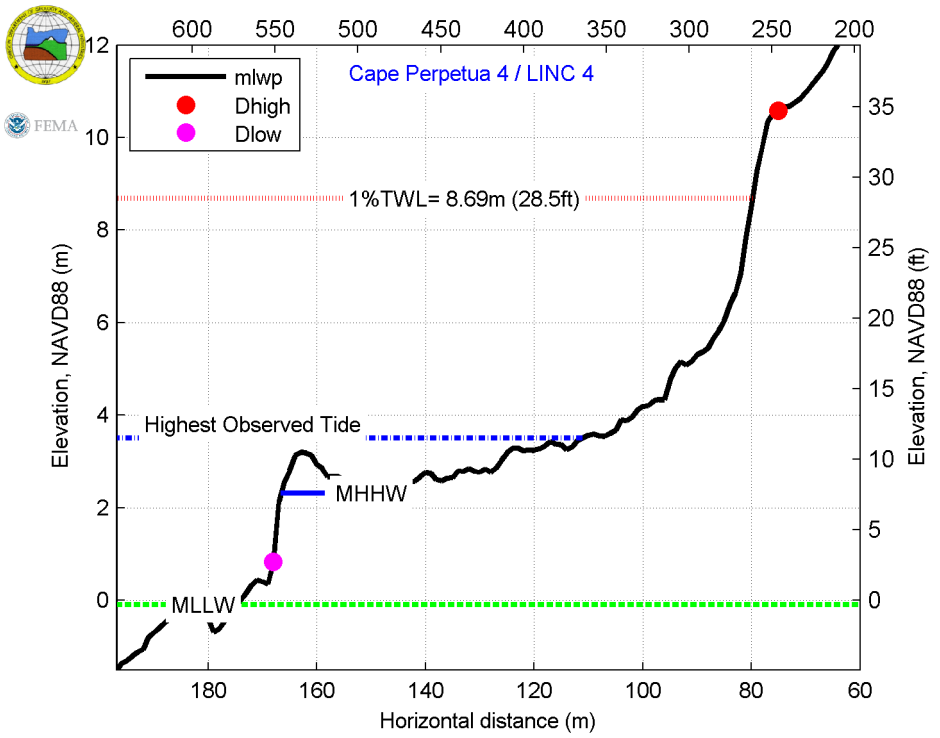
Cape Perpetua 4 / LINC 4
mlwp
Dhigh
Dlow
1%TWL= 8.69m (28.5ft)
Highest Observed Tide
MHHW
MLLW
Elevation, NAVD88 (m)
Elevation, NAVD88 (ft)
Horizontal distance (m)
600
550
500
450
400
350
300
250
200
180
160
140
120
100
80
60
0
2
4
6
8
10
12
0
5
10
15
20
25
30
35

11.2.2 Yachats

LINC 5

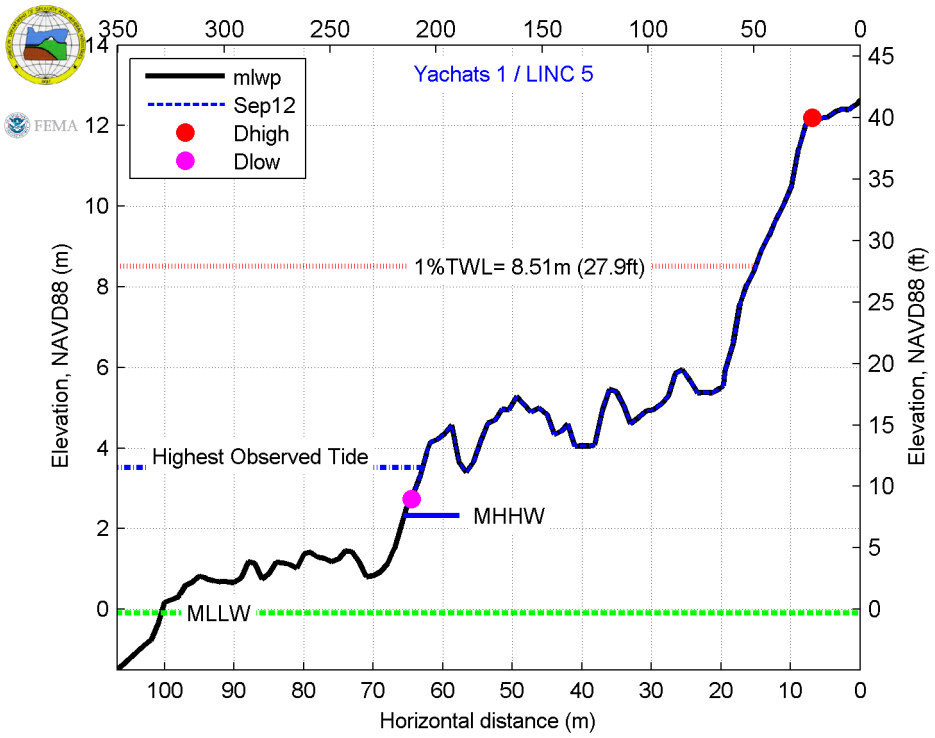

LINC 6

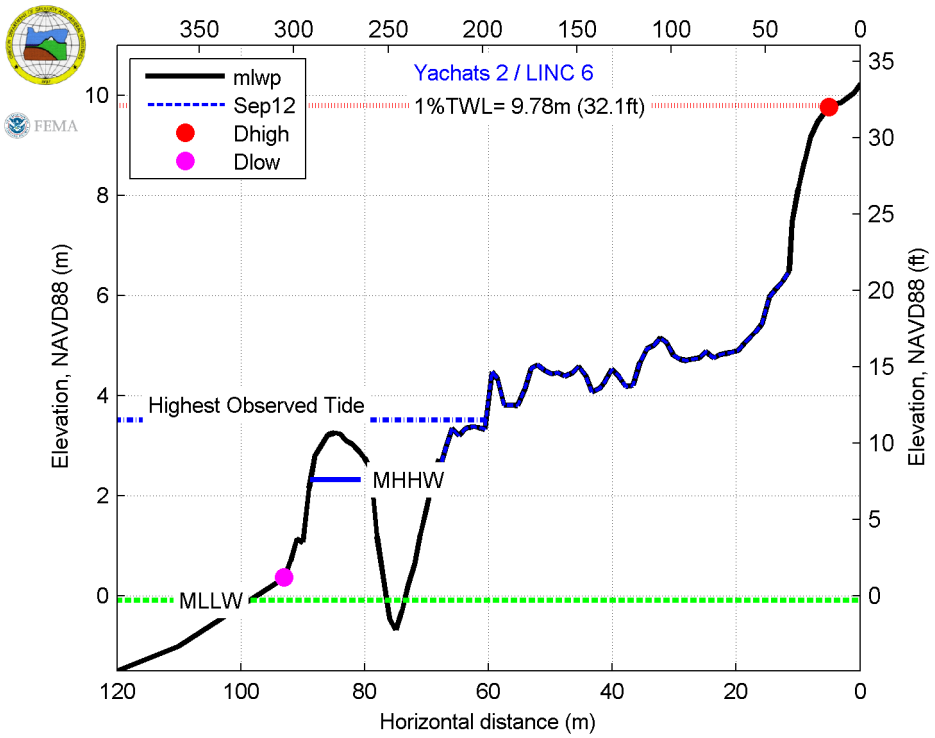

LINC 7

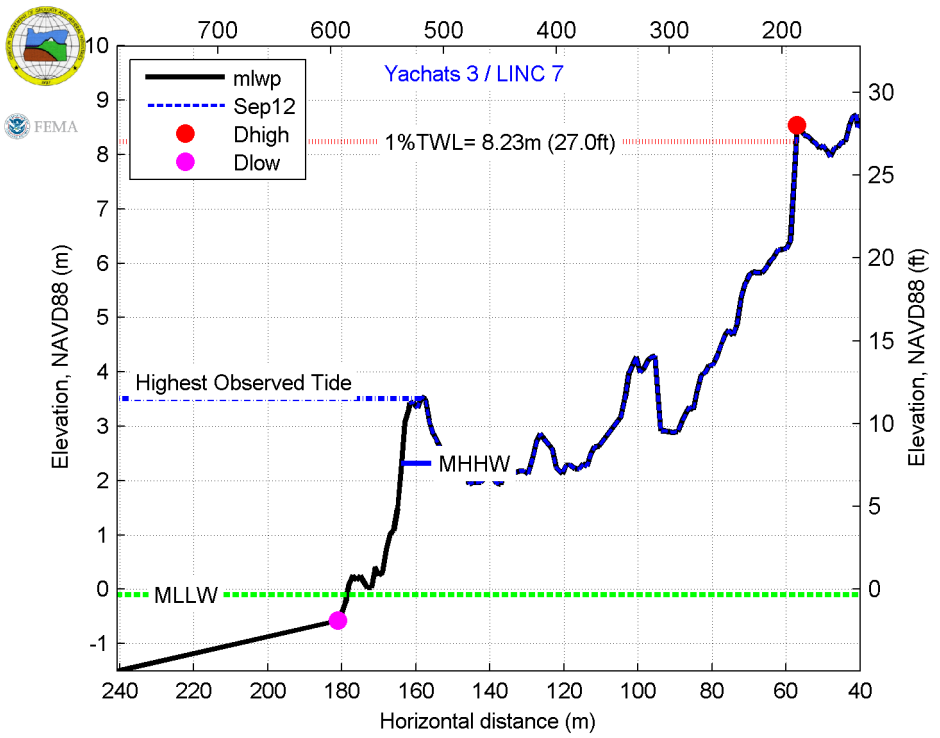
Yachats 3 / LINC 7
mlwp
Sep12
Dhigh
Dlow
1%TWL= 8.23m (27.0ft)
Highest Observed Tide
MHHW
MLLW
Elevation, NAVD88 (m)
Elevation, NAVD88 (ft)
Horizontal distance (m)
700 600 500 400 300 200
240 220 200 180 160 140 120 100 80 60 40
FEMA

LINC 8

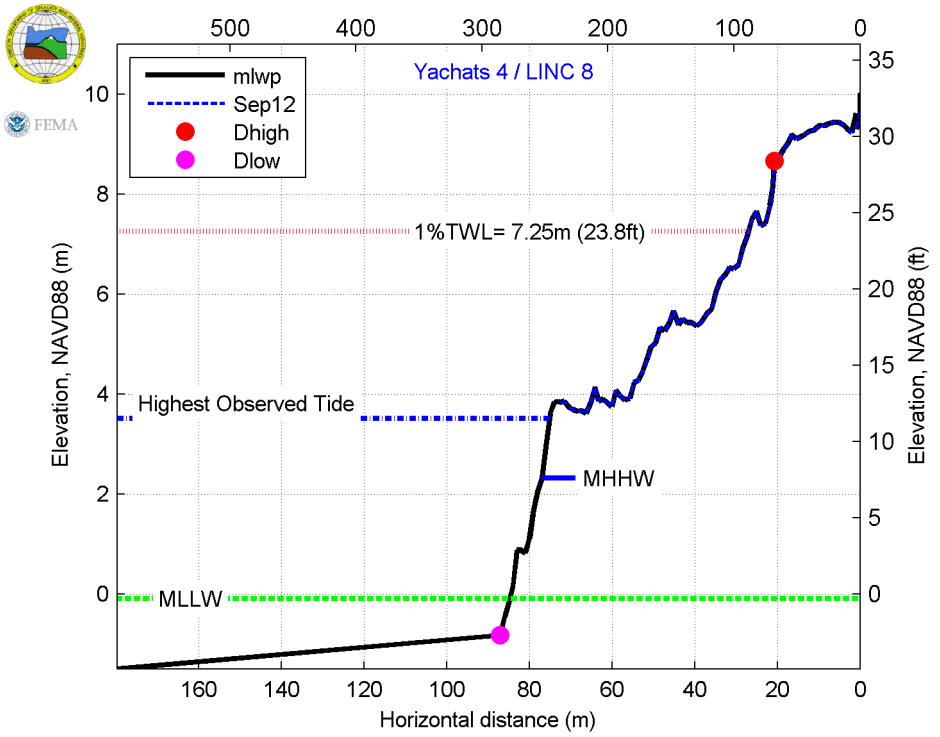
Yachats 4 / LINC 8
mlwp
Sep12
Dhigh
Dlow
1%TWL= 7.25m (23.8ft)
Highest Observed Tide
MHHW
MLLW
Elevation, NAVD88 (m)
Elevation, NAVD88 (ft)
Horizontal distance (m)
500 400 300 200 100 0
160 140 120 100 80 60 40 20 0
FEMA

LINC 9

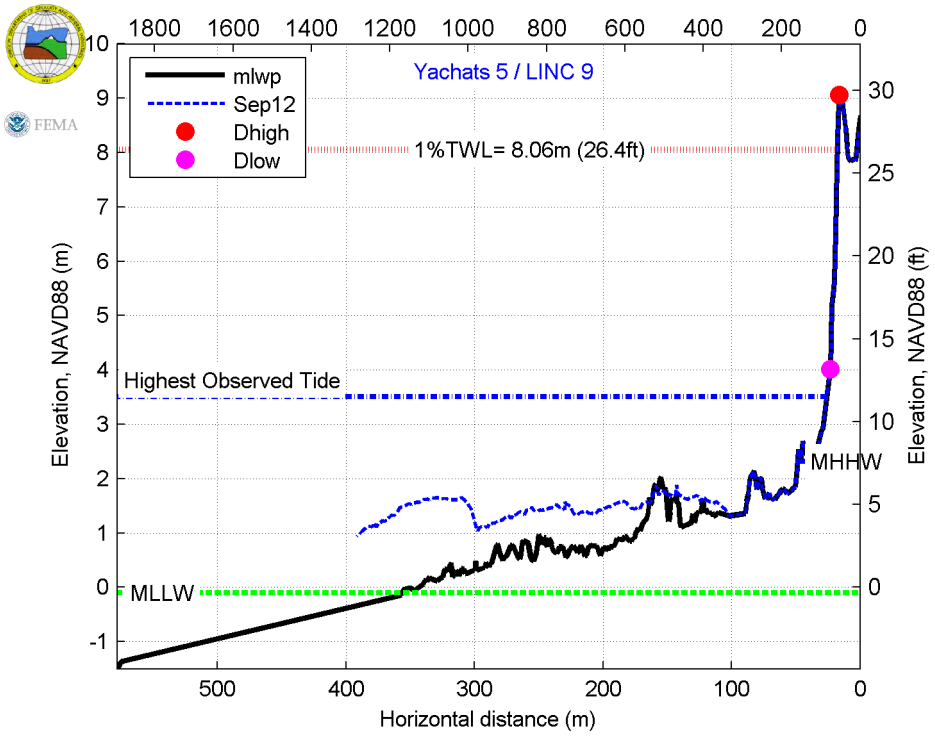

LINC 10

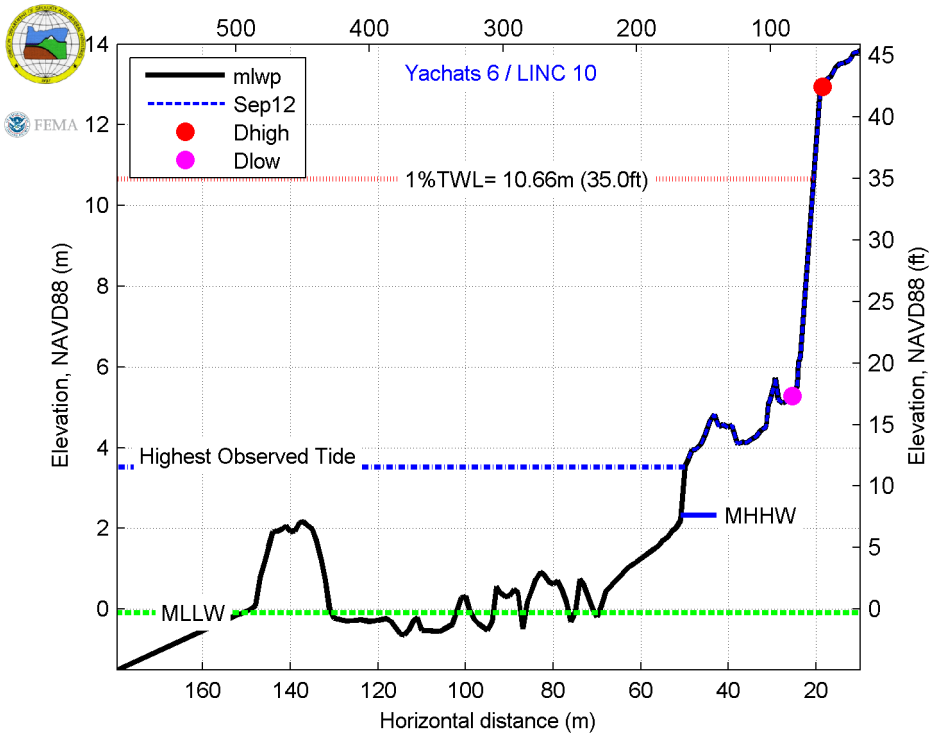

LINC 11

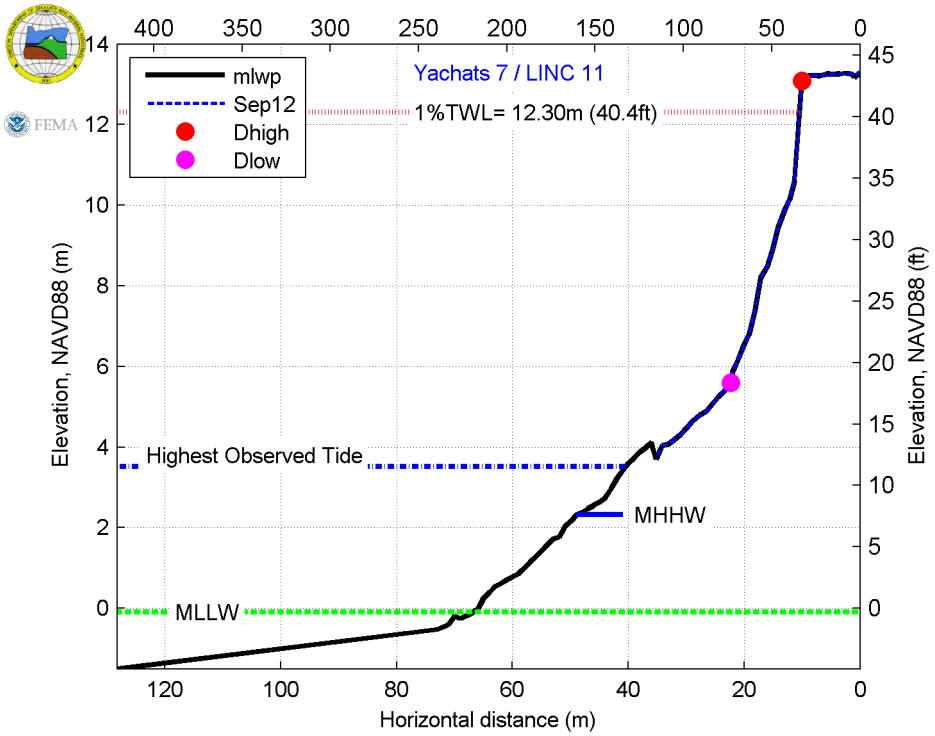

LINC 12

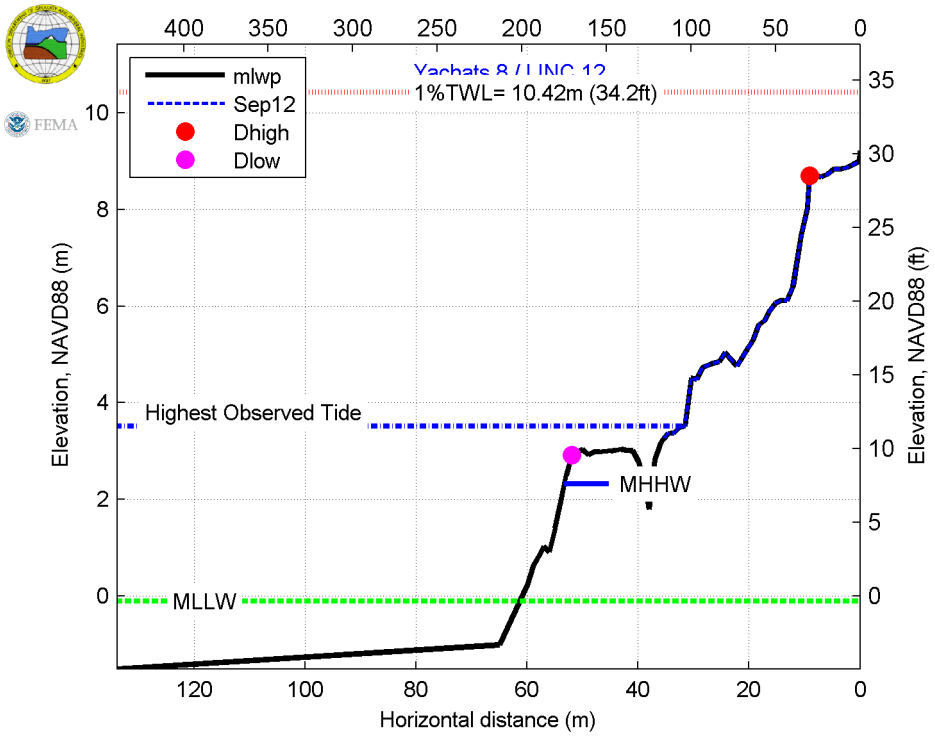

LINC 13

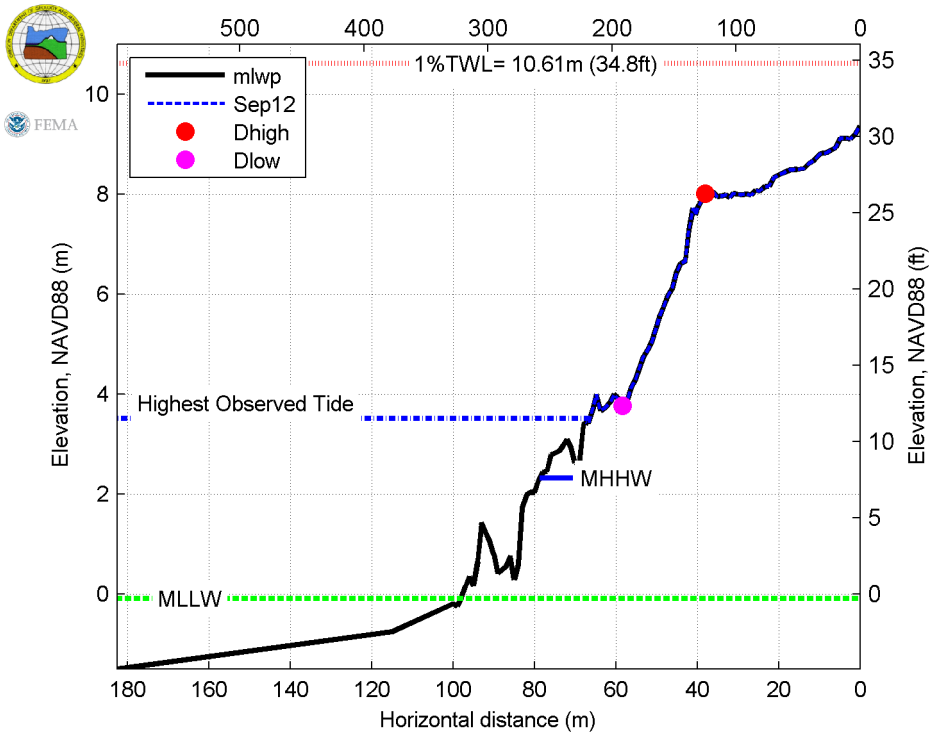

LINC 14

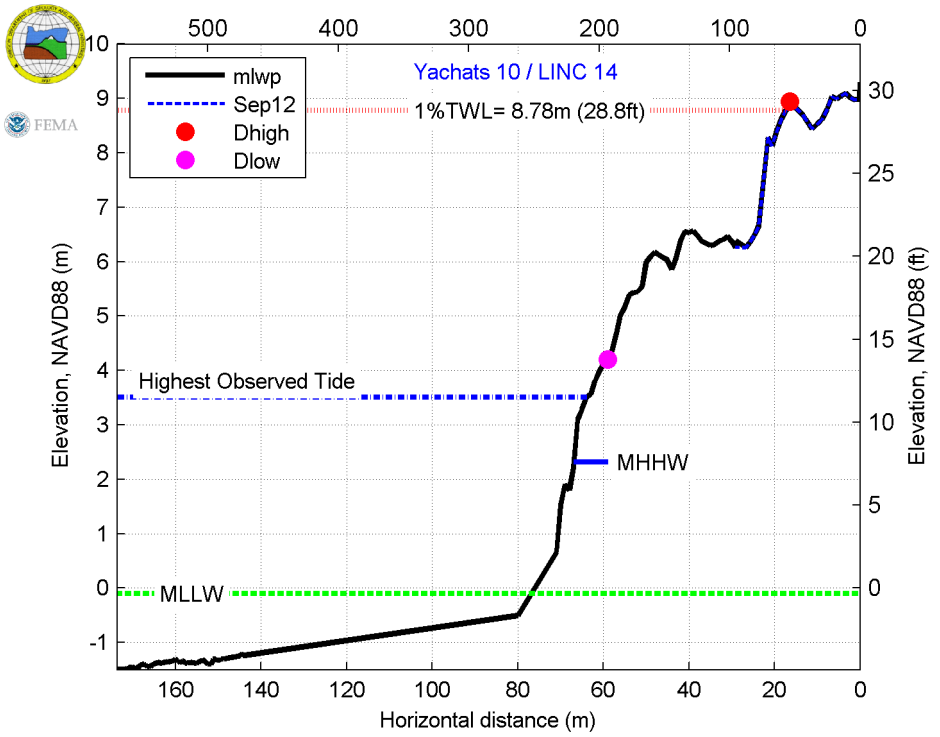

11.2.3 Waldport

LINC 15

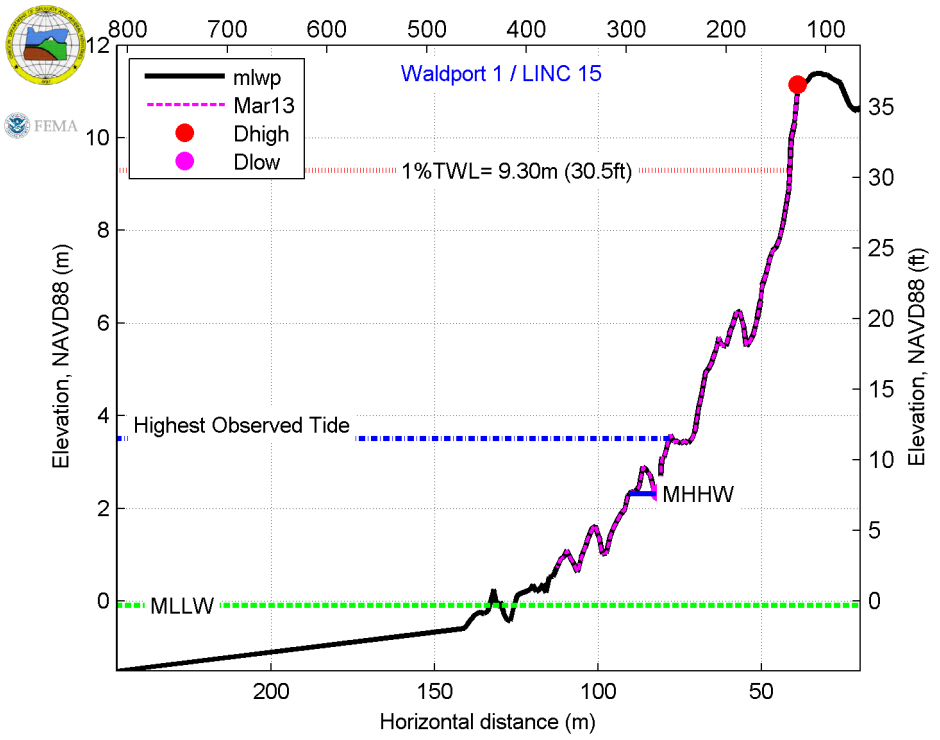

LINC 16

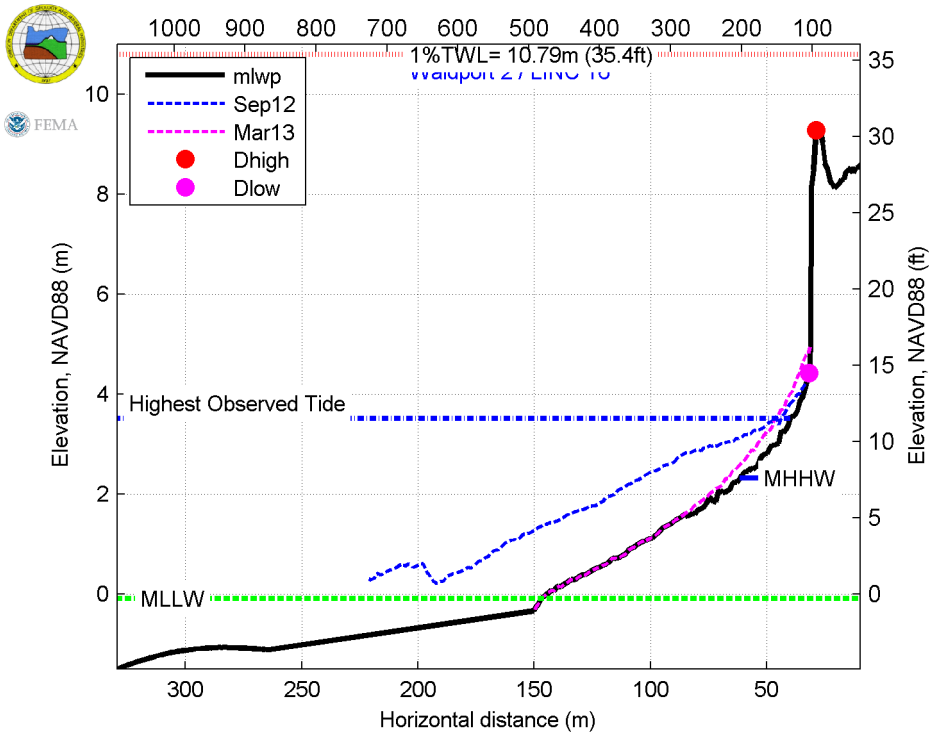

LINC 17

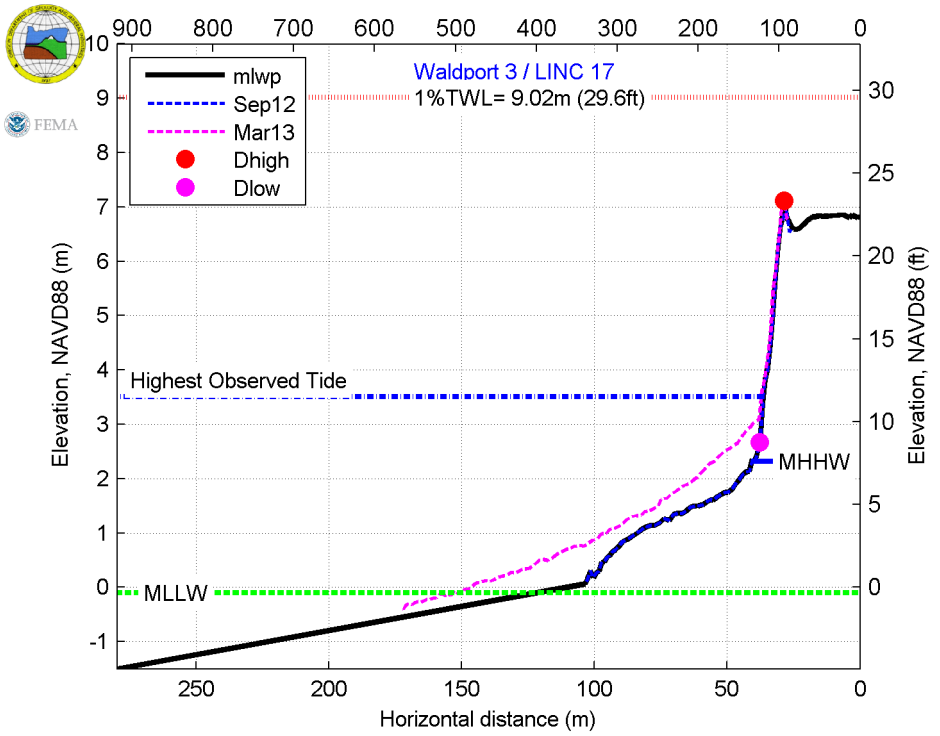

LINC 18

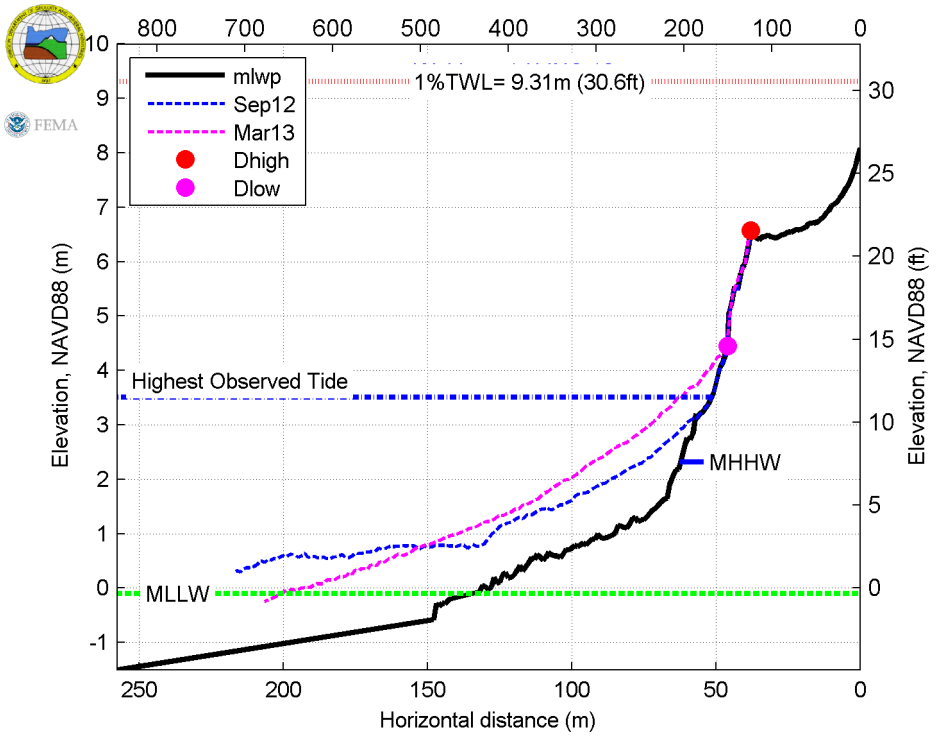

LINC 19

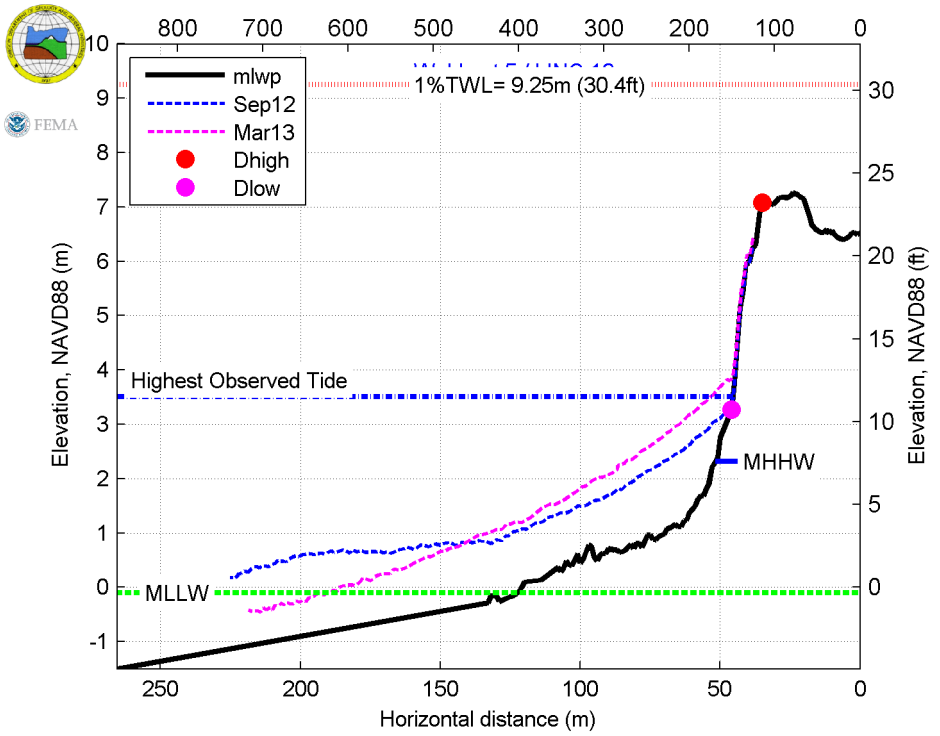

LINC 20

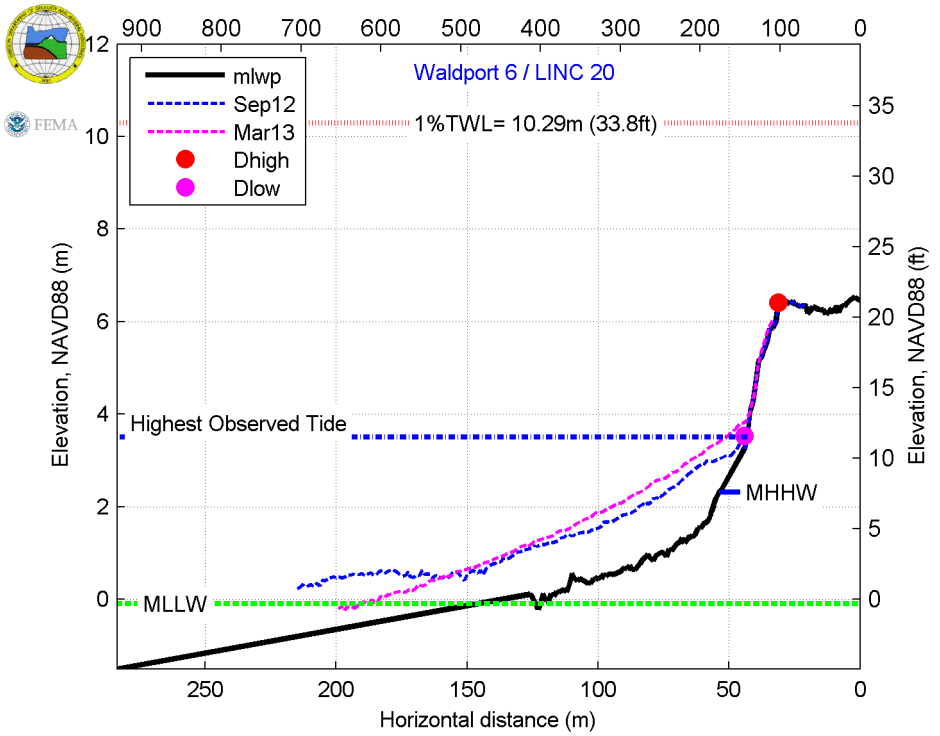

LINC 21

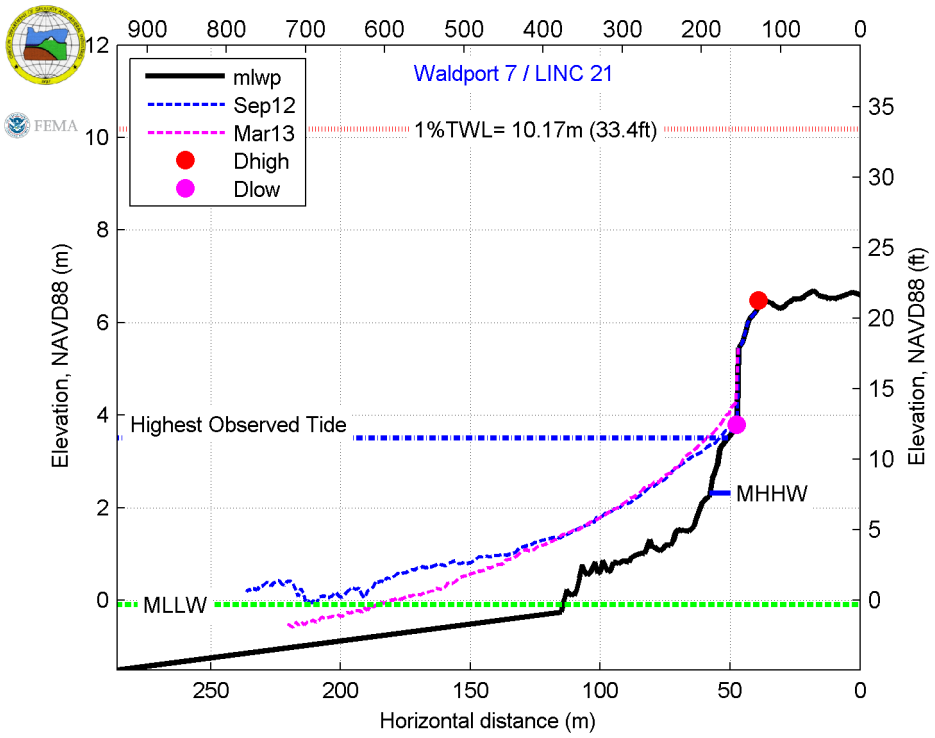

LINC 22

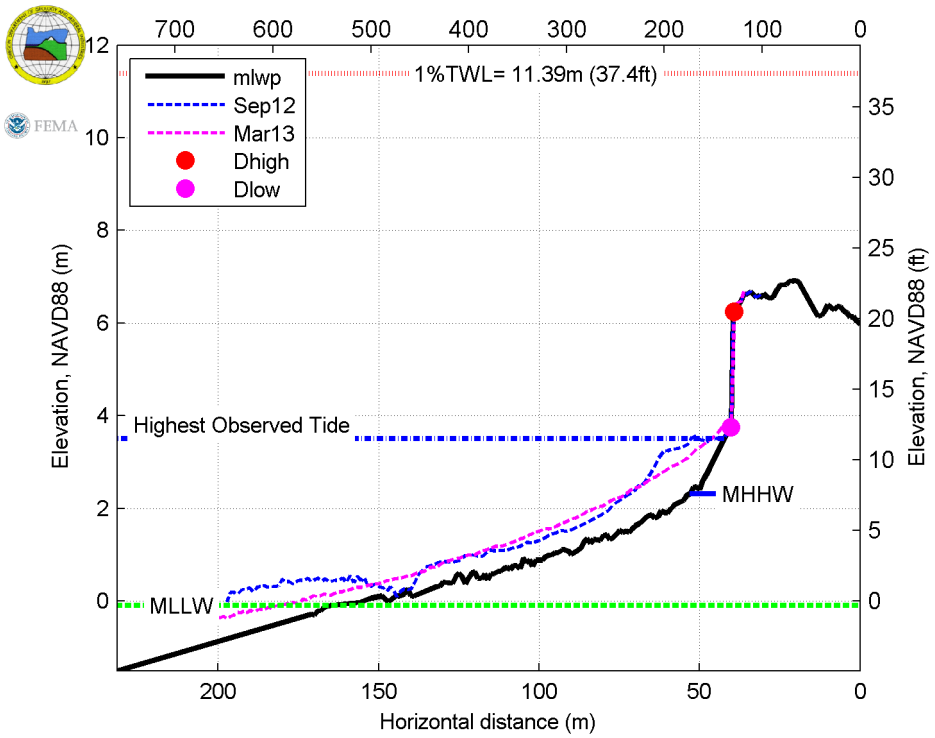

LINC 23

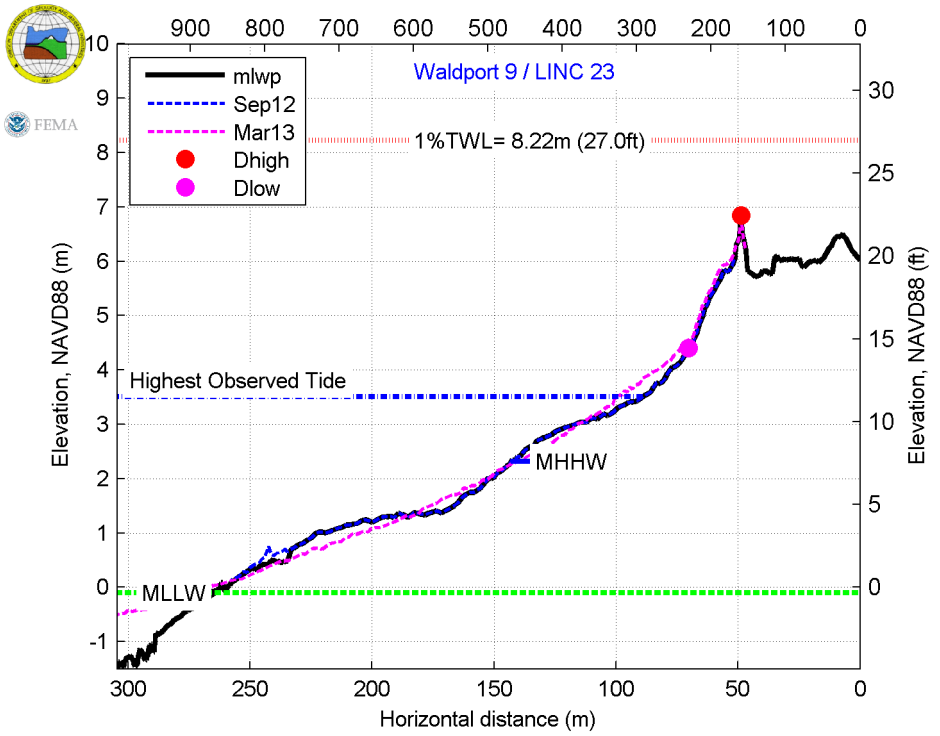

LINC 24

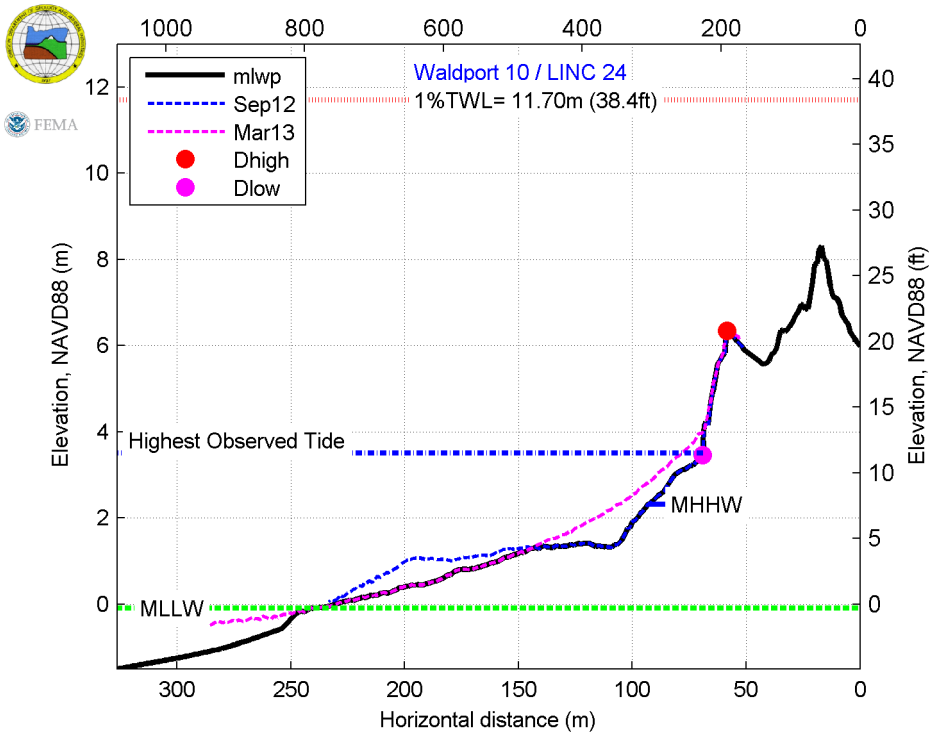

LINC 25

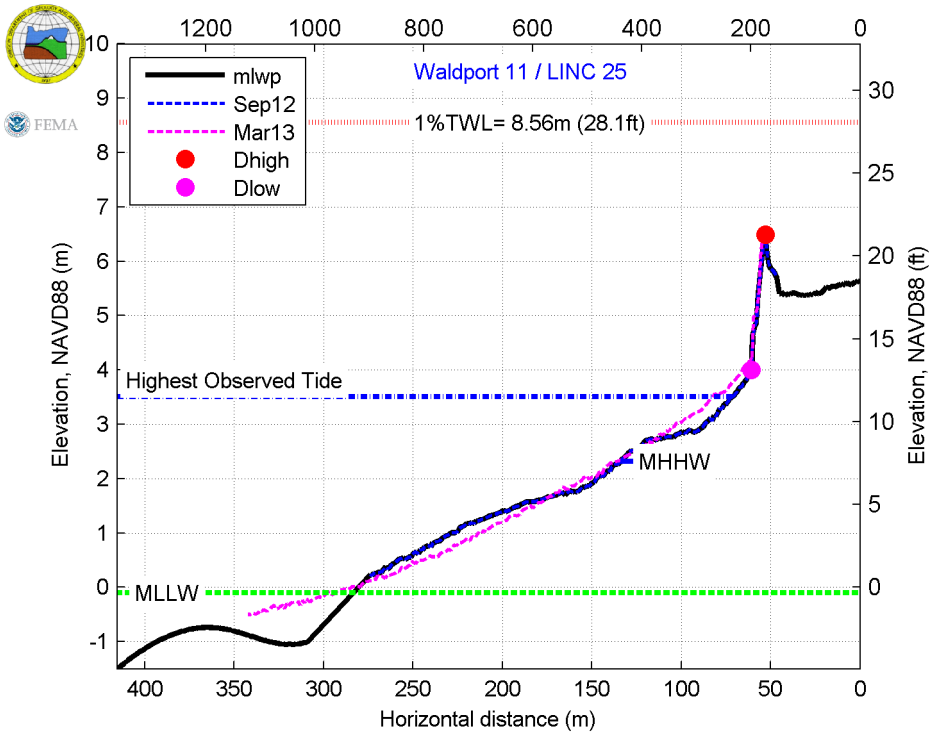

LINC 26

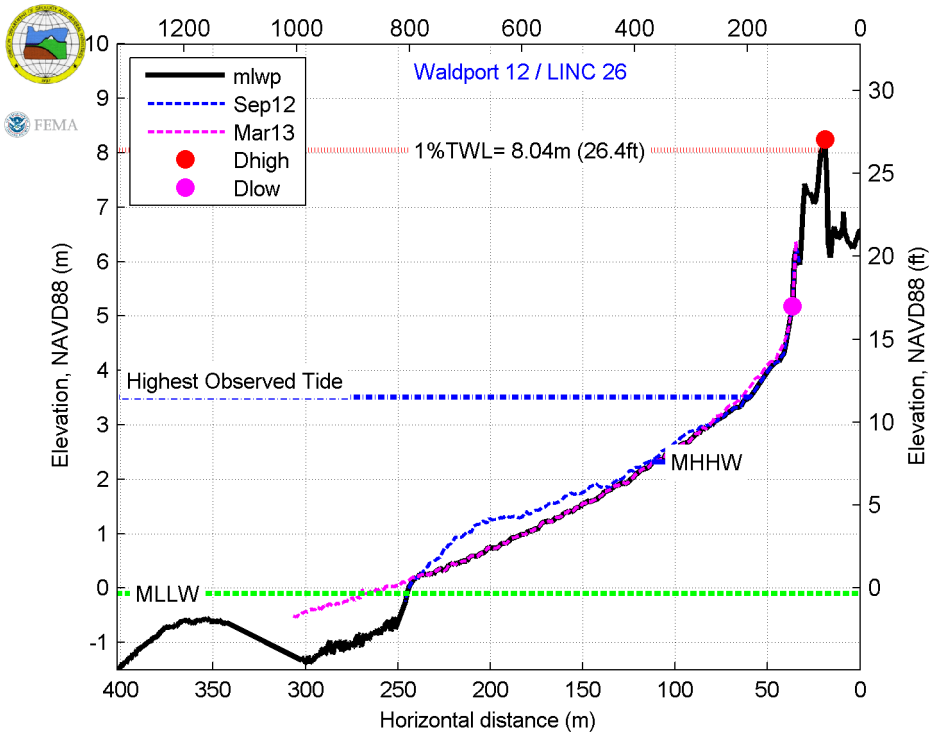

LINC 27

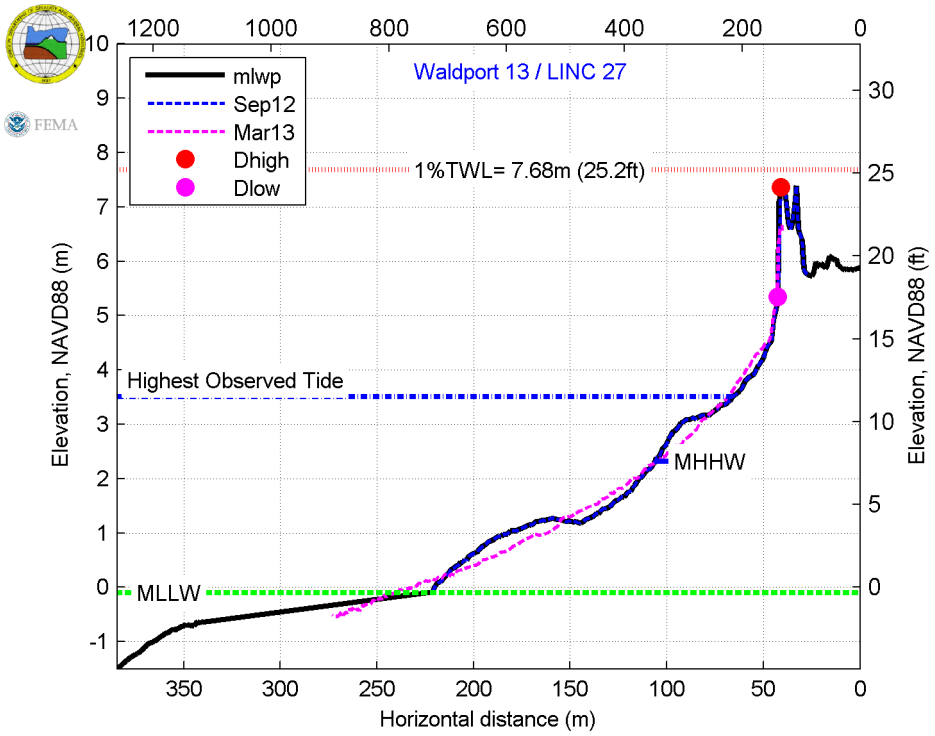

LINC 28

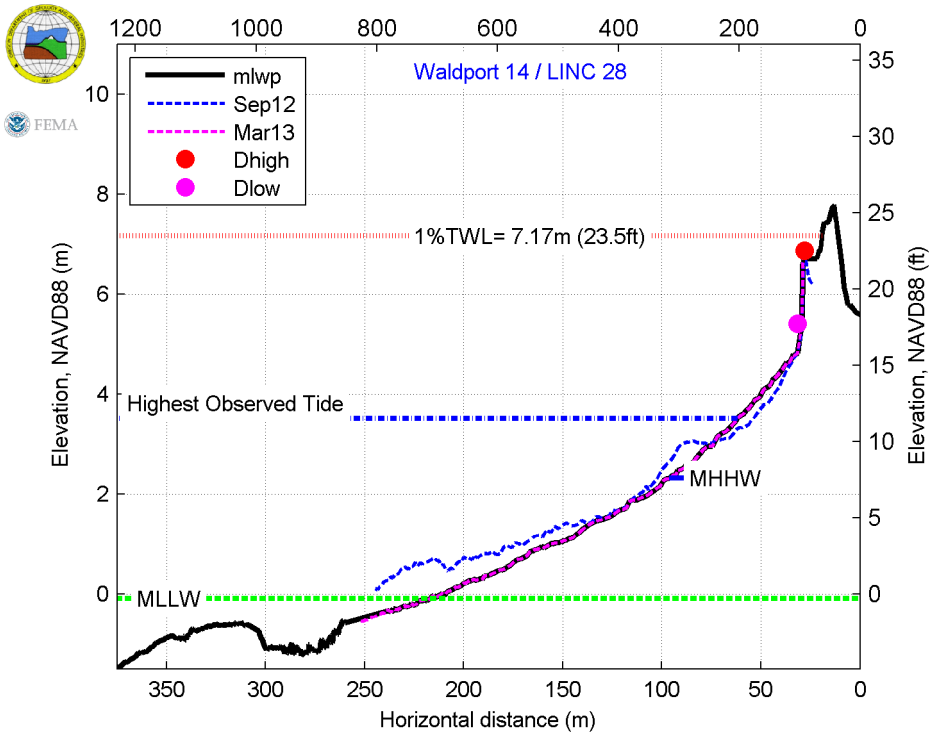

LINC 29

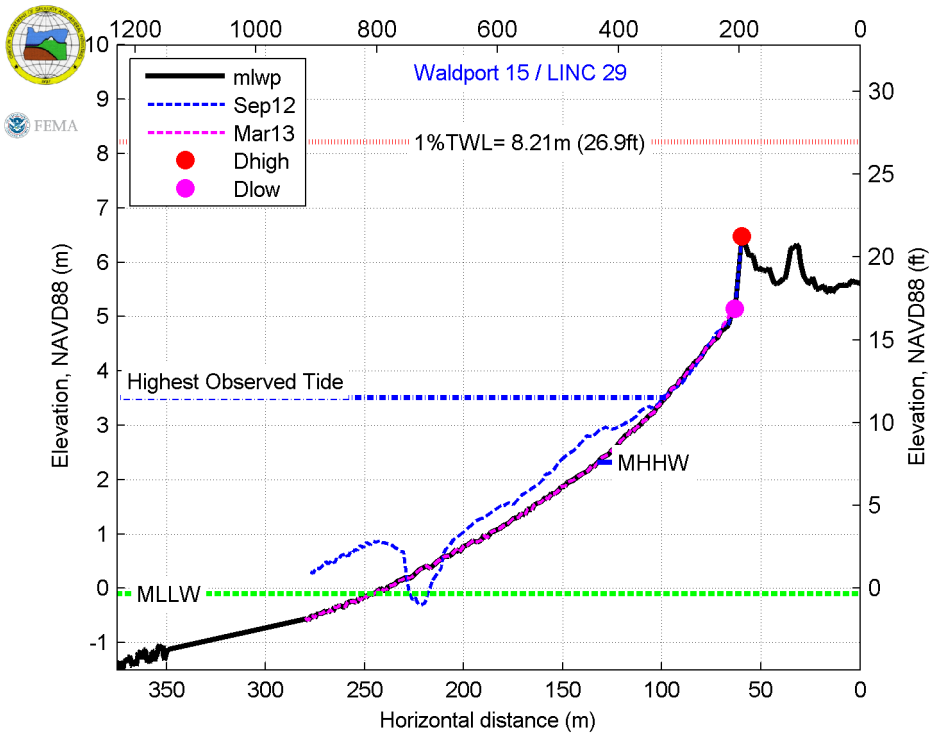

LINC 30

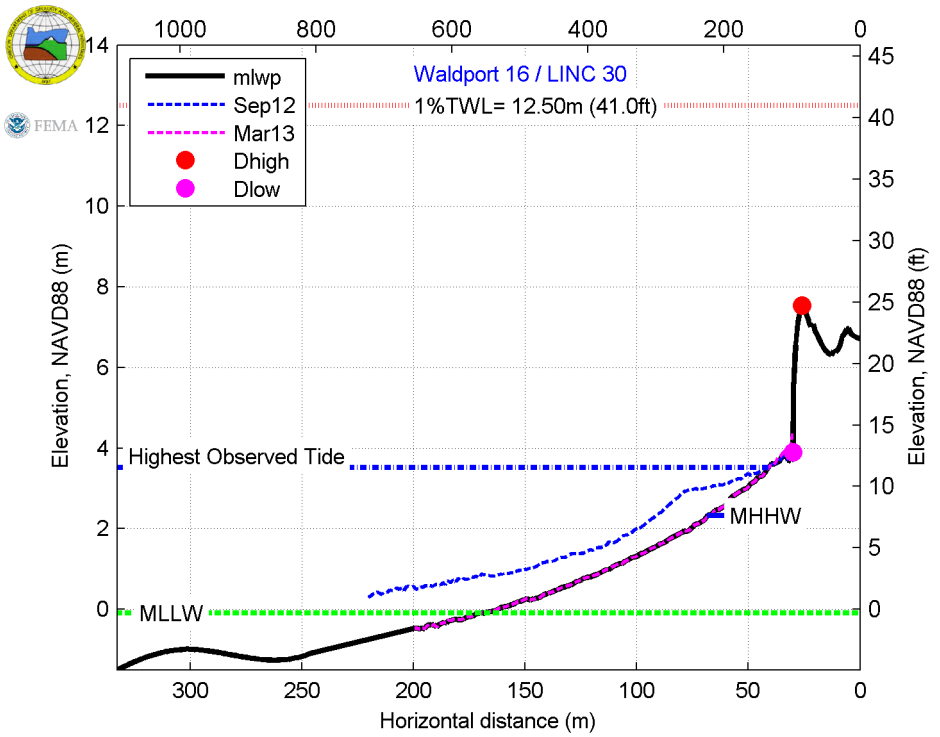

LINC 31

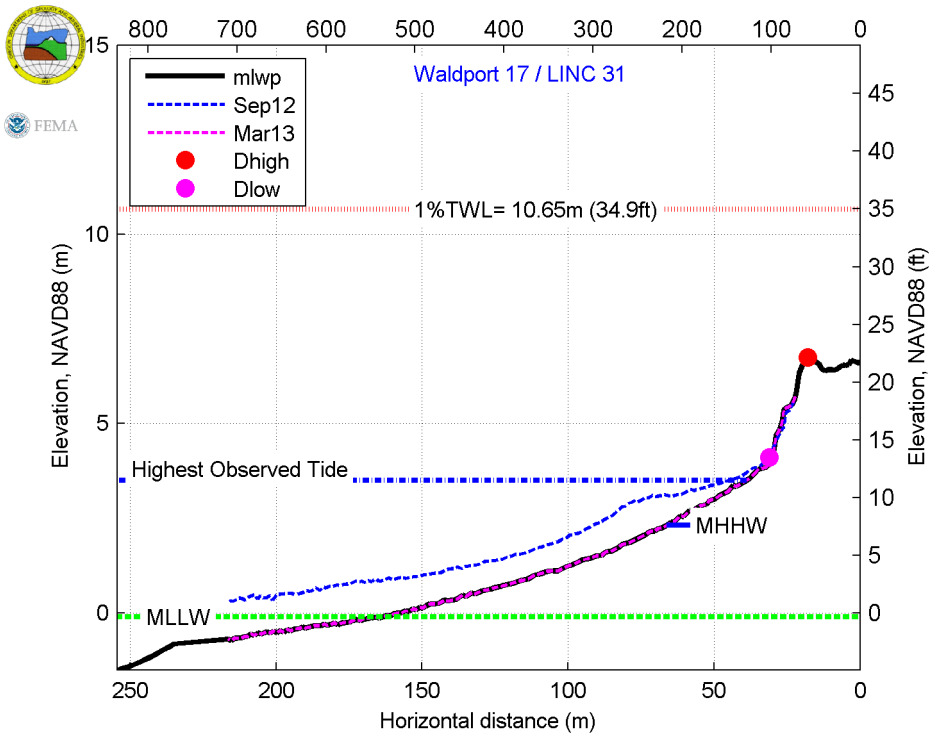

LINC 32

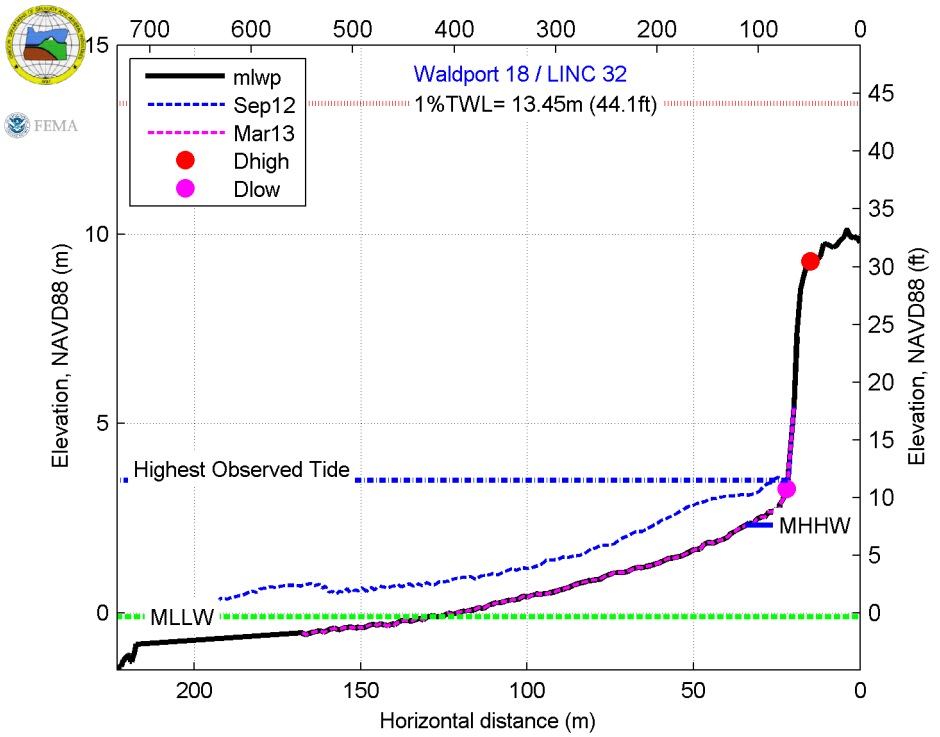

LINC 33

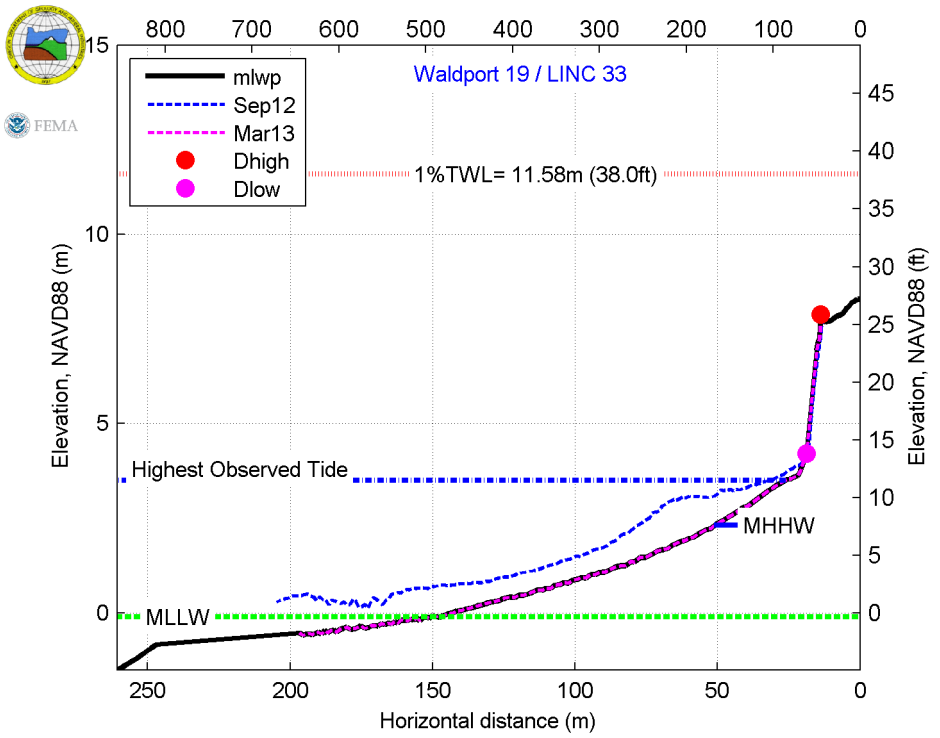

LINC 34

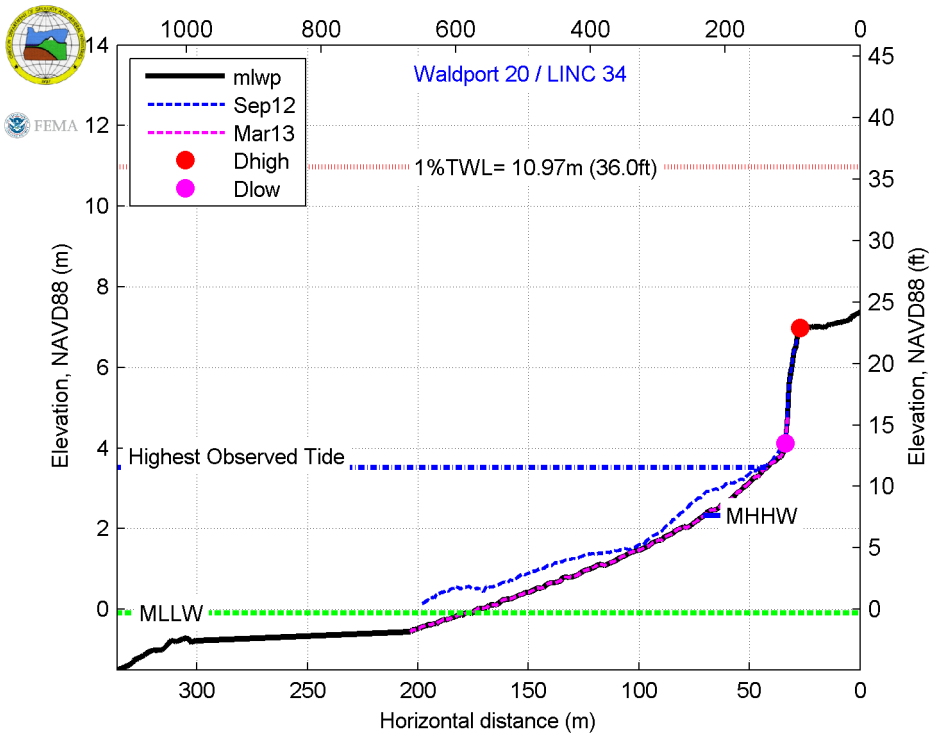

LINC 35

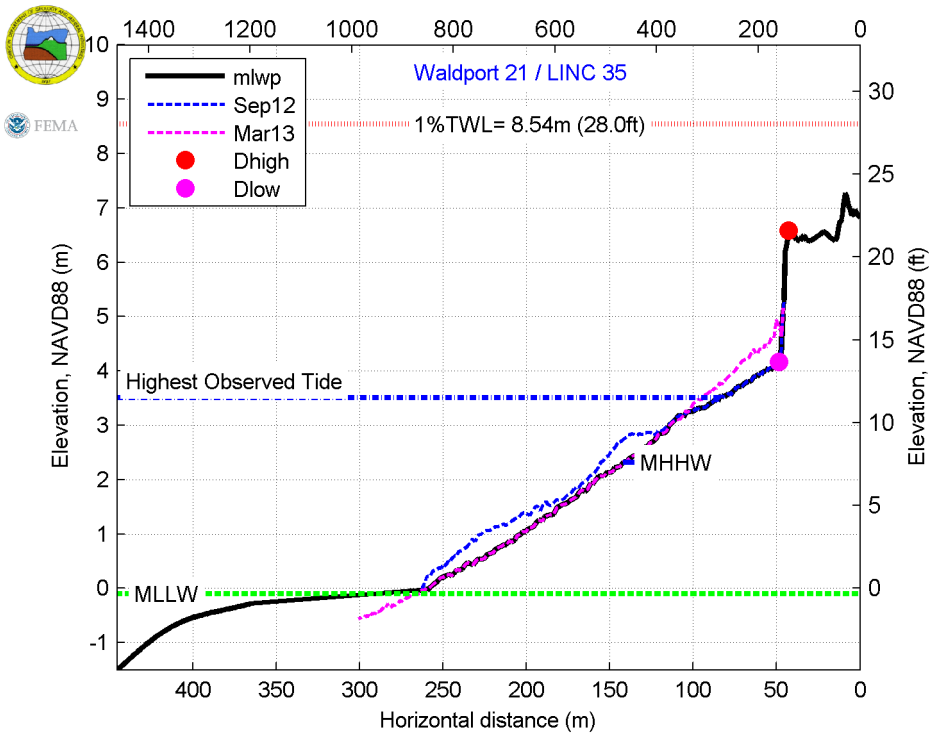

LINC 36

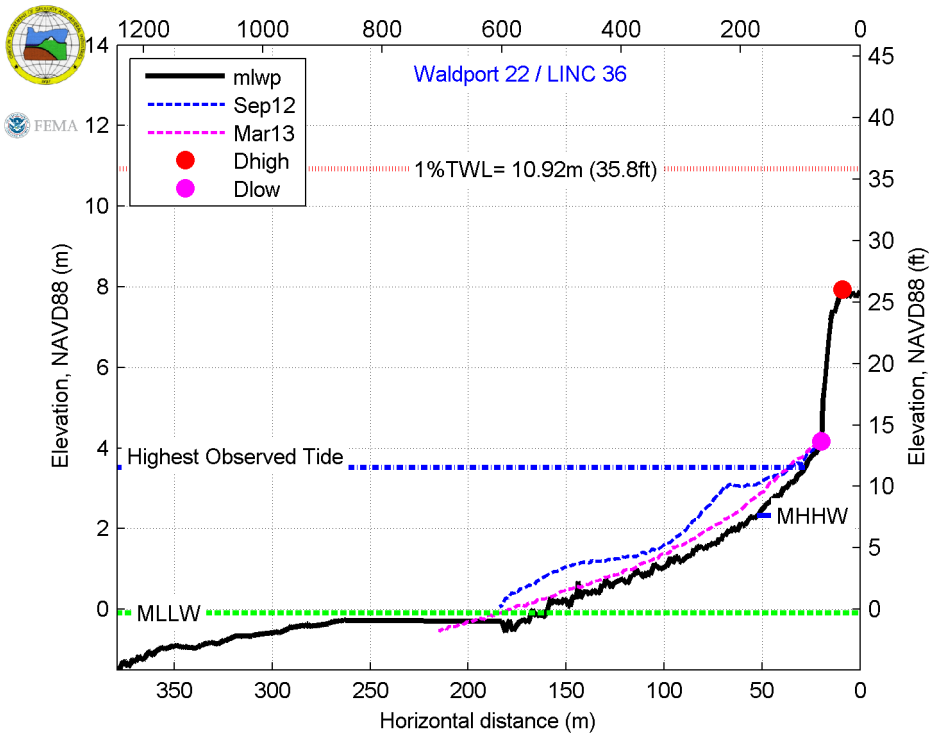

LINC 37

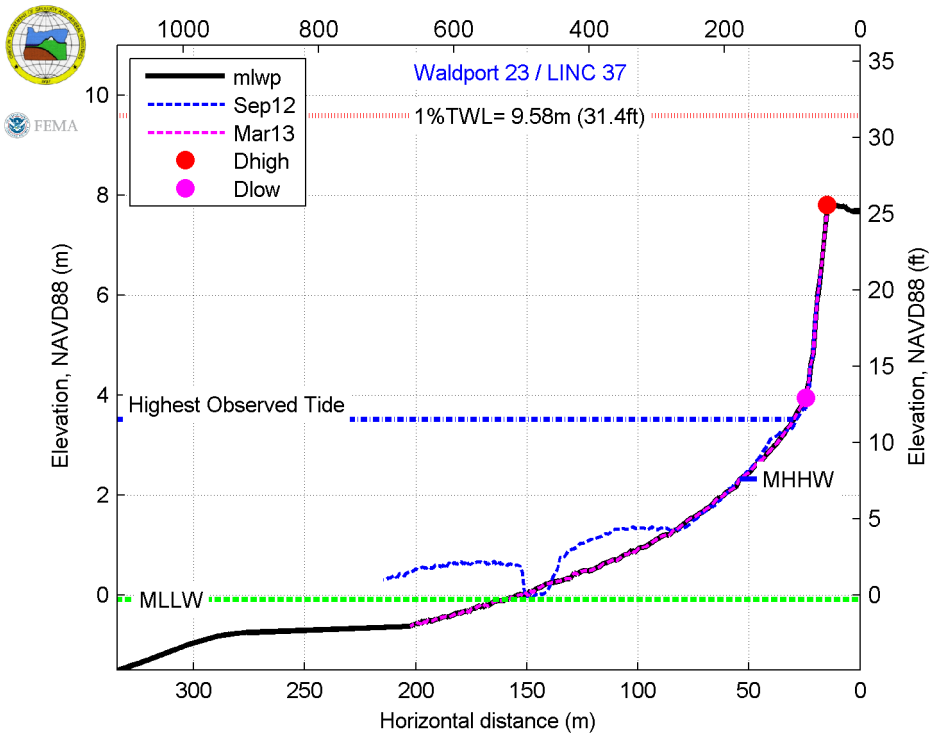

LINC 38

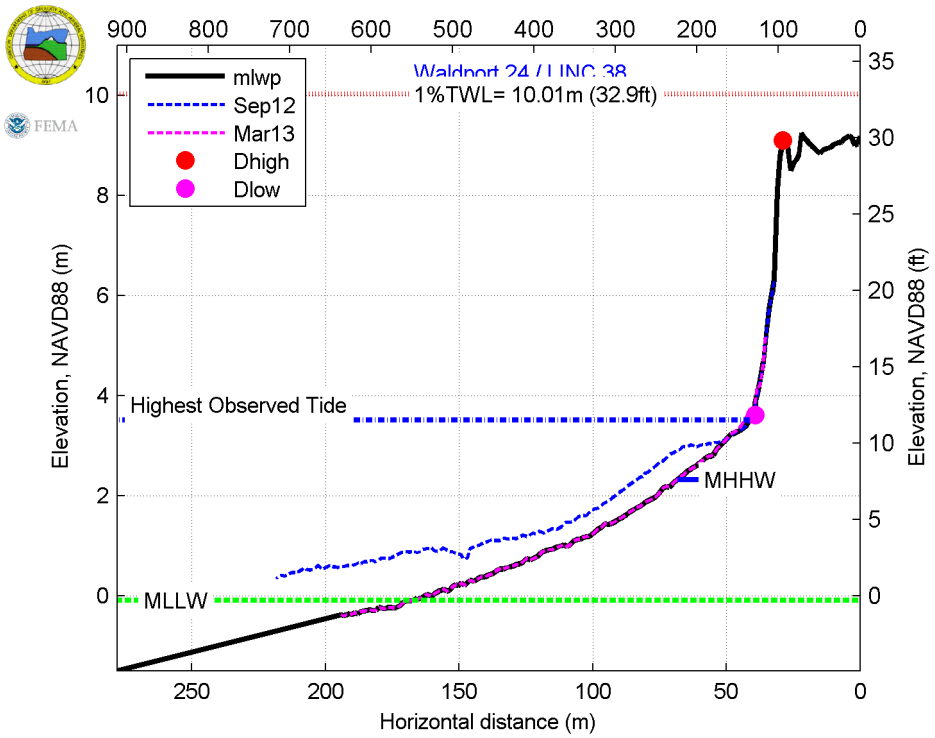

LINC 39

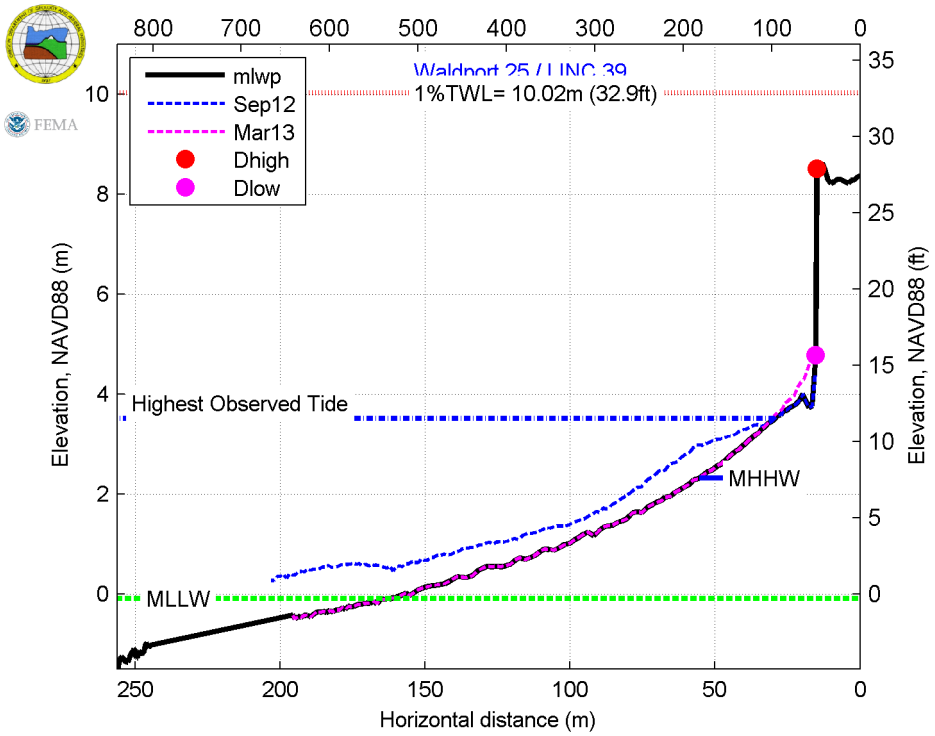

LINC 40

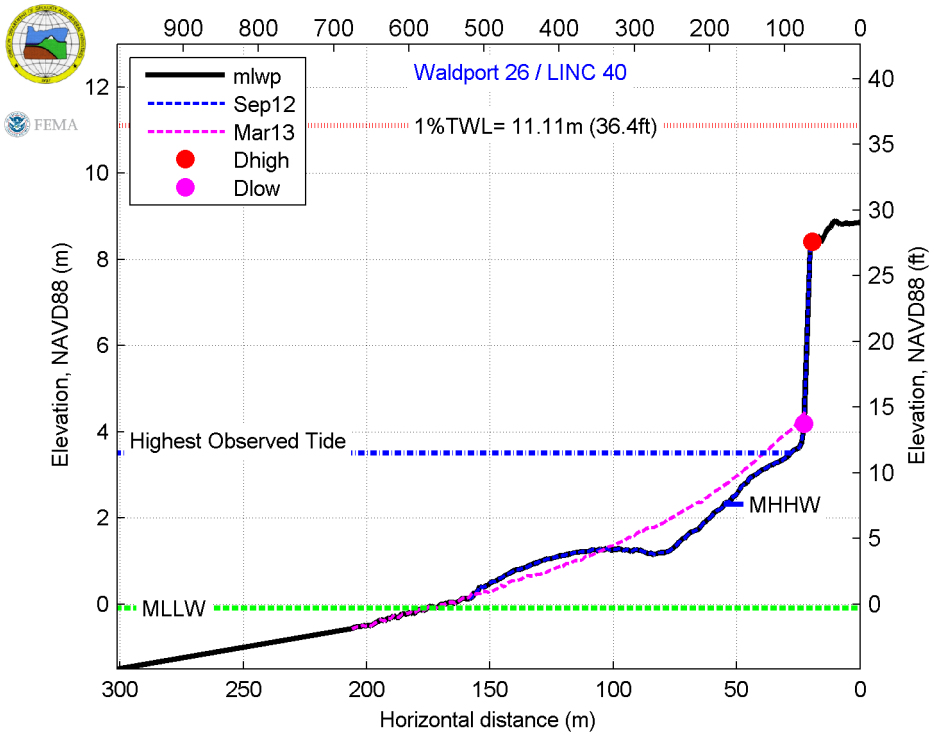

LINC 41

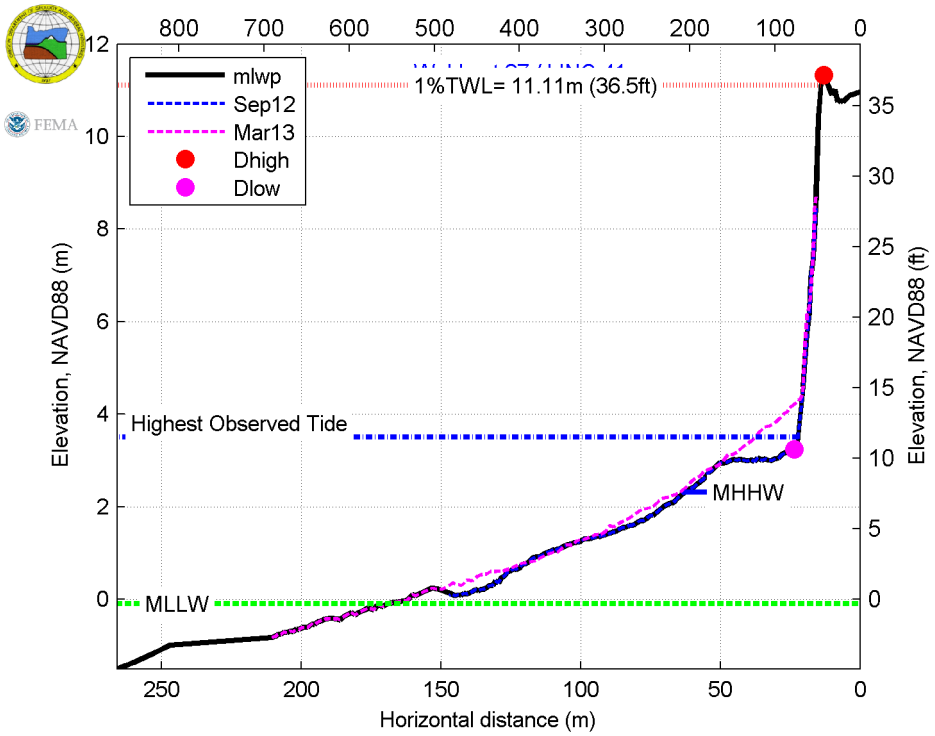

LINC 42

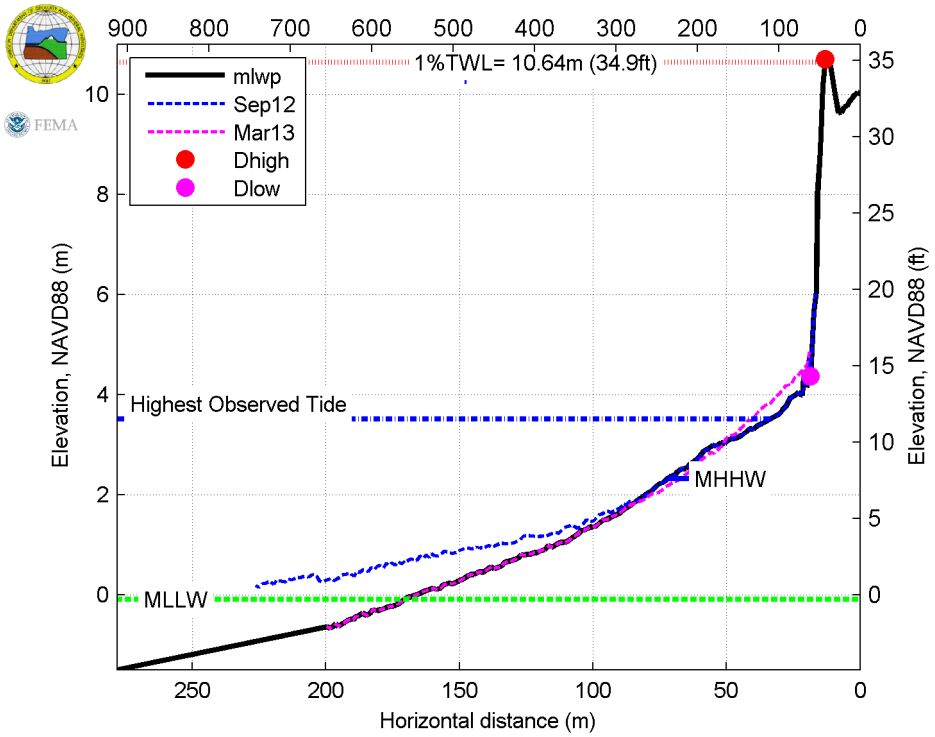

LINC 43

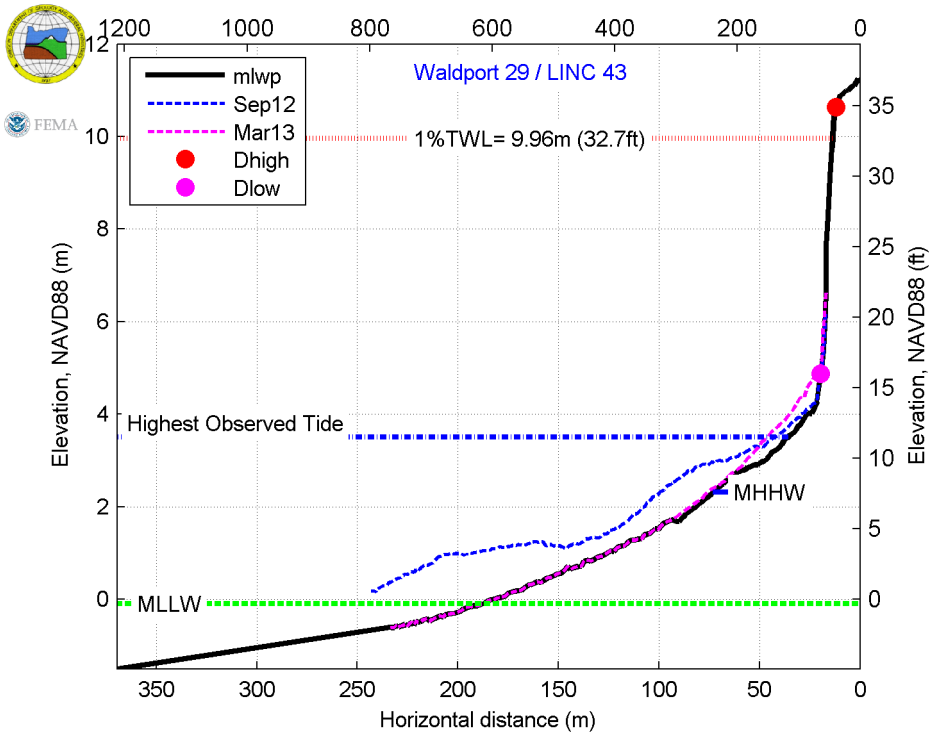

LINC 44

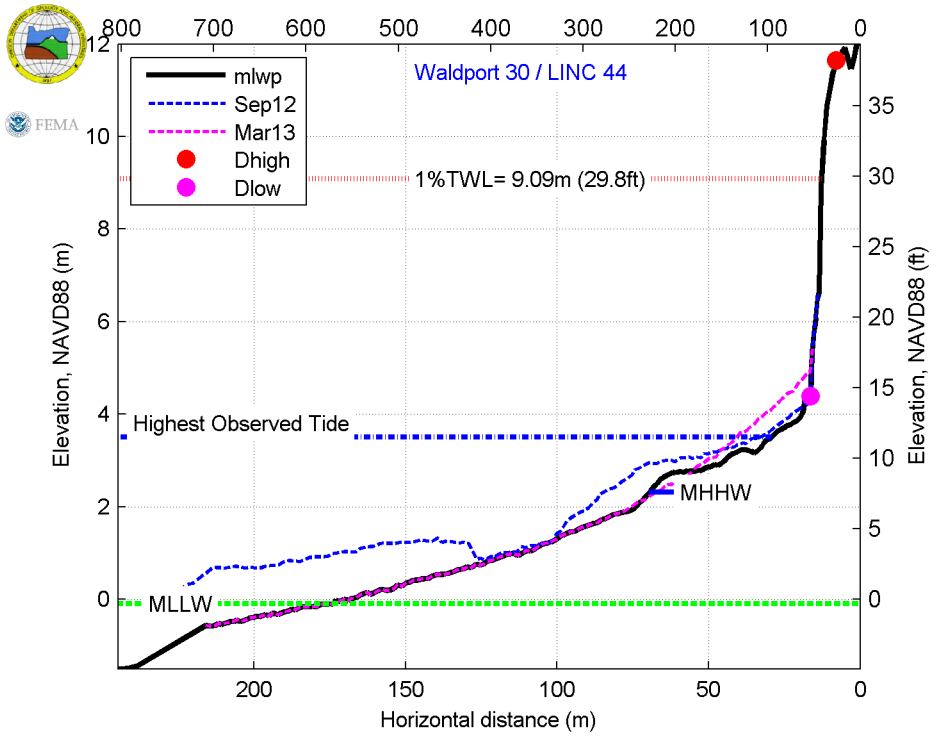

LINC 45

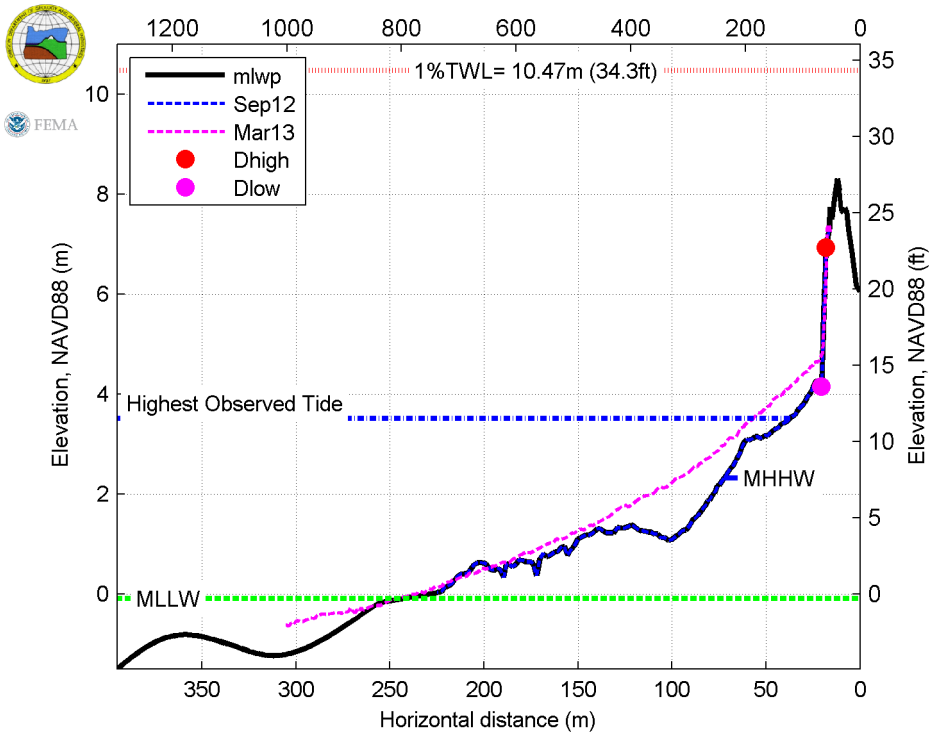

LINC 46

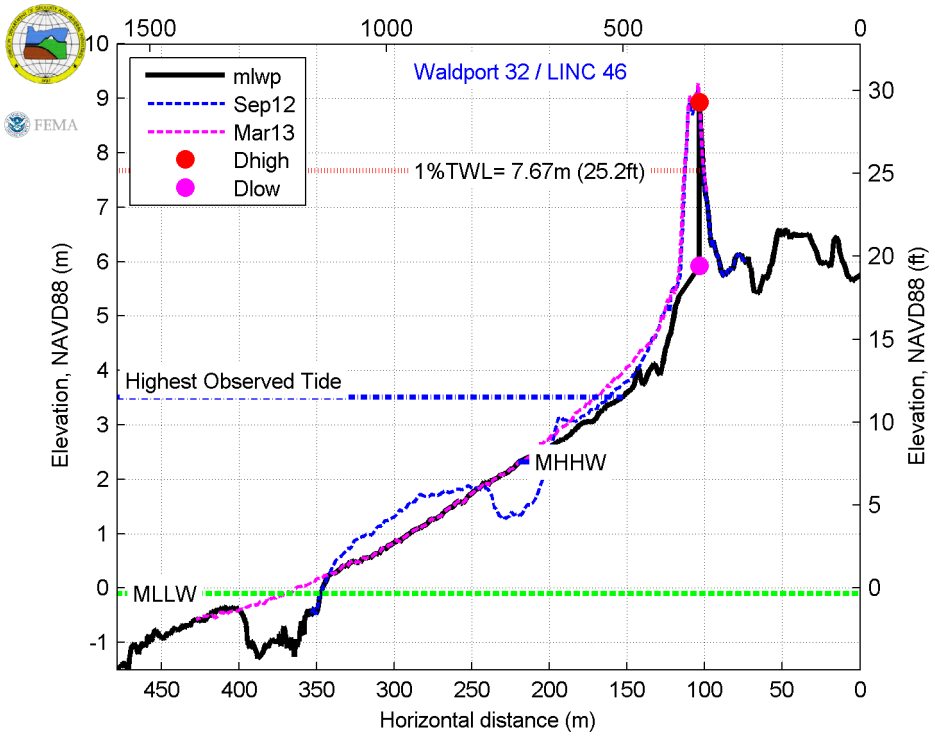

LINC 47

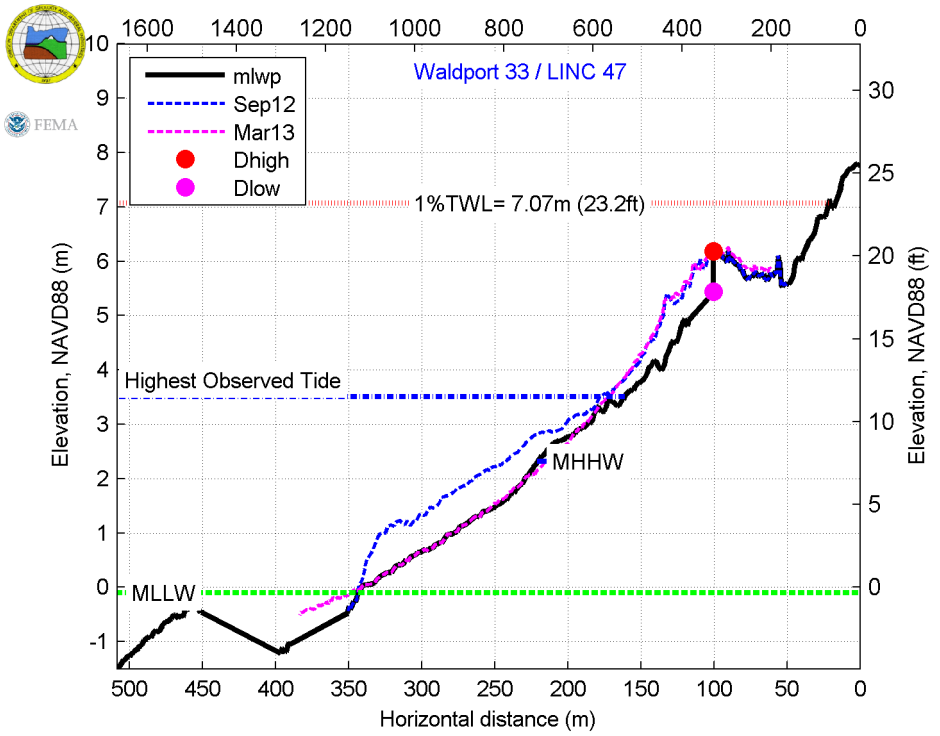

LINC 48

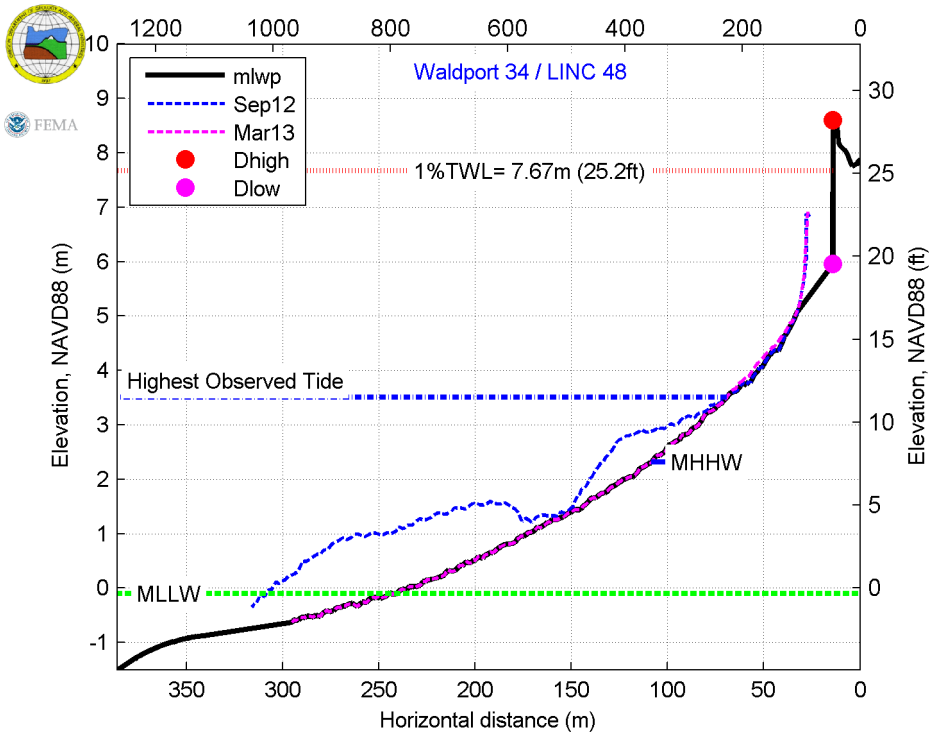

LINC 49

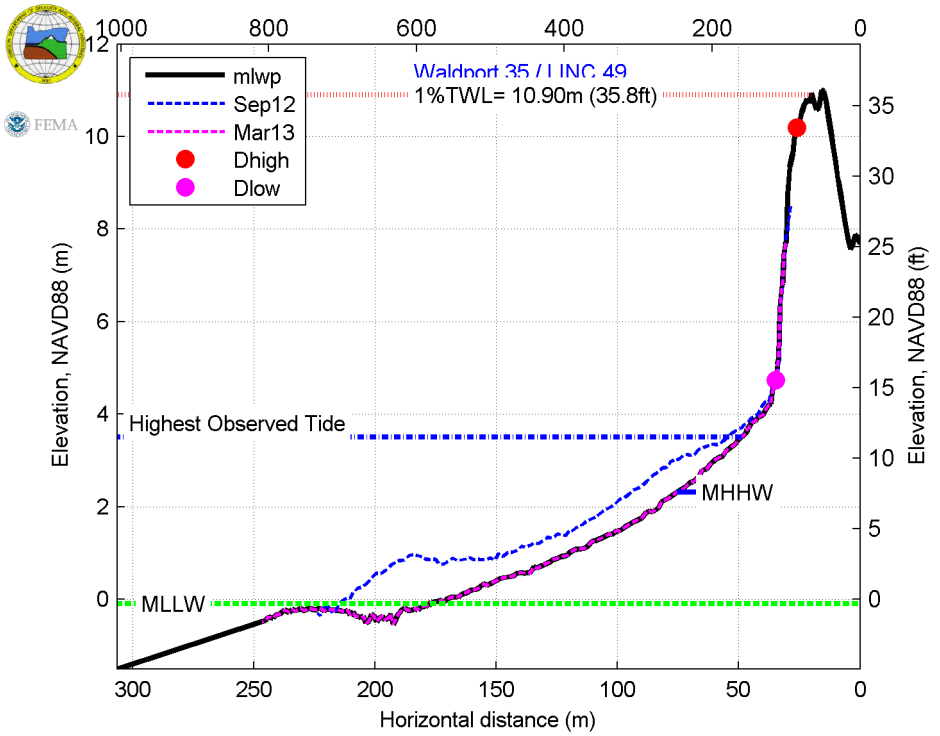

LINC 50

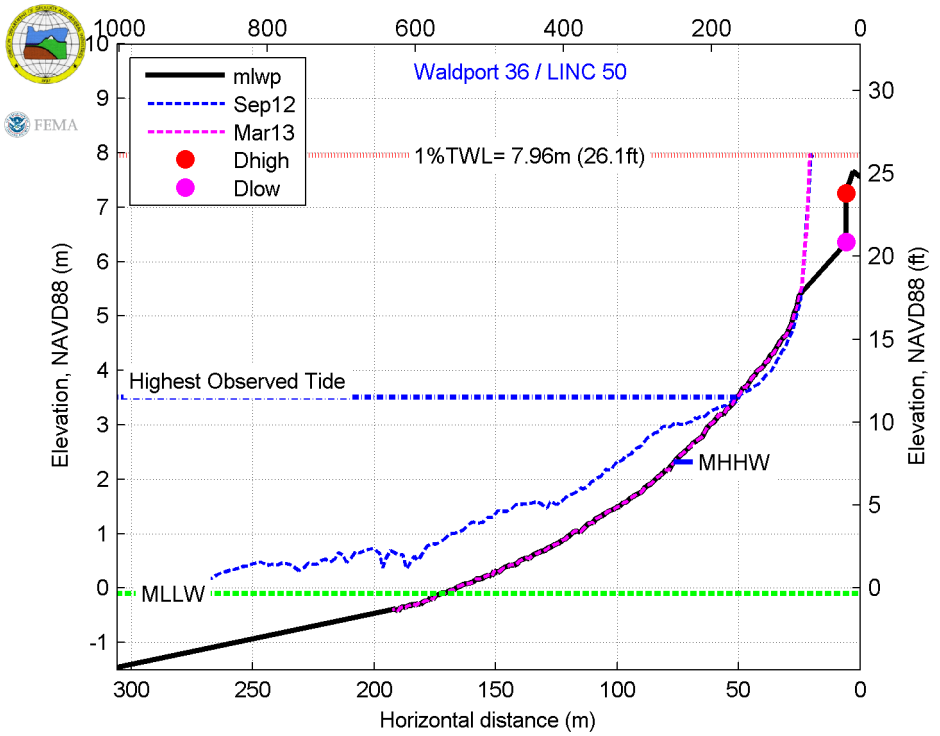

LINC 51

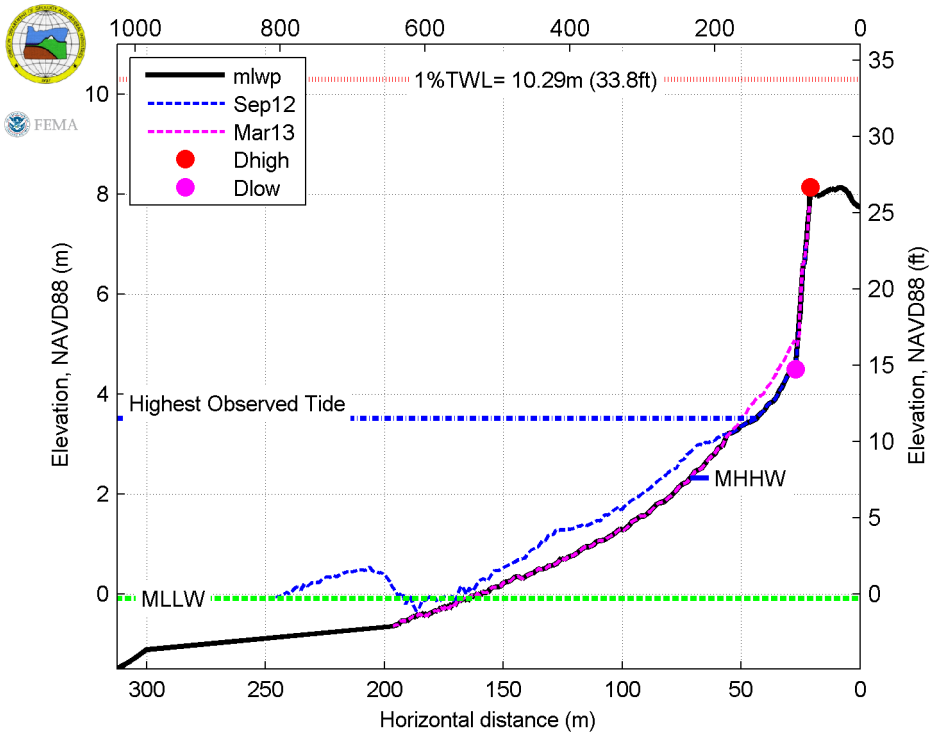

LINC 52

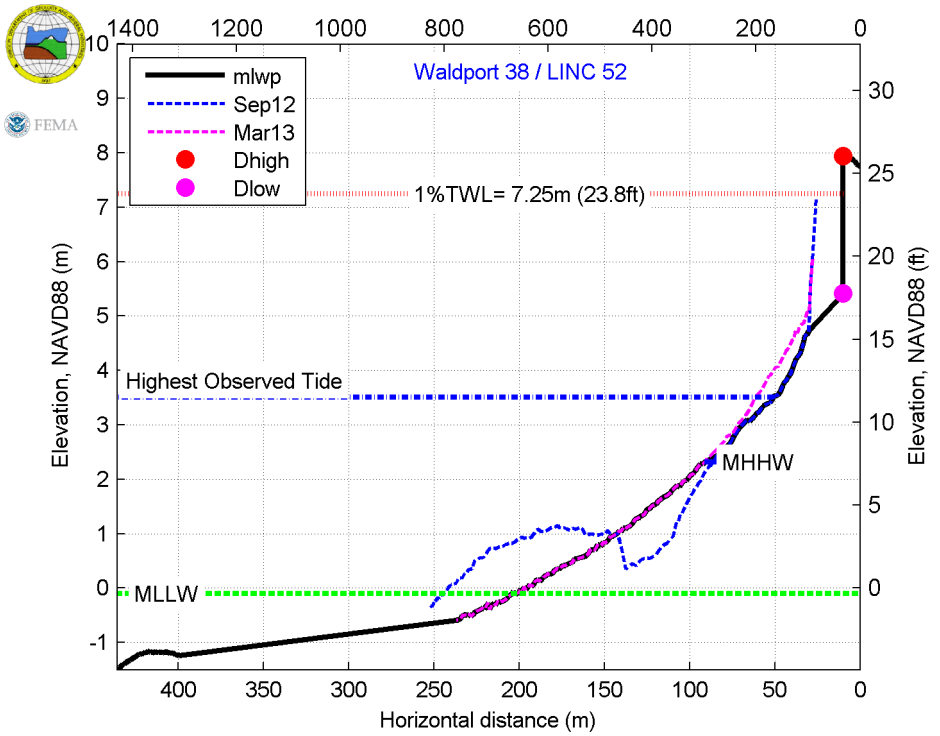

LINC 53

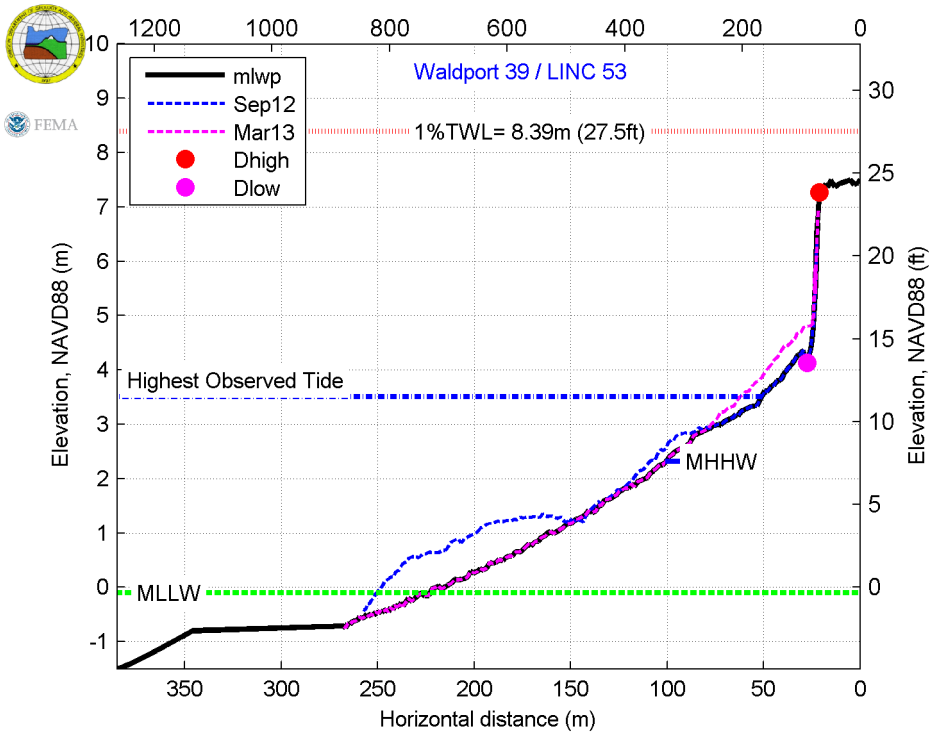

LINC 54

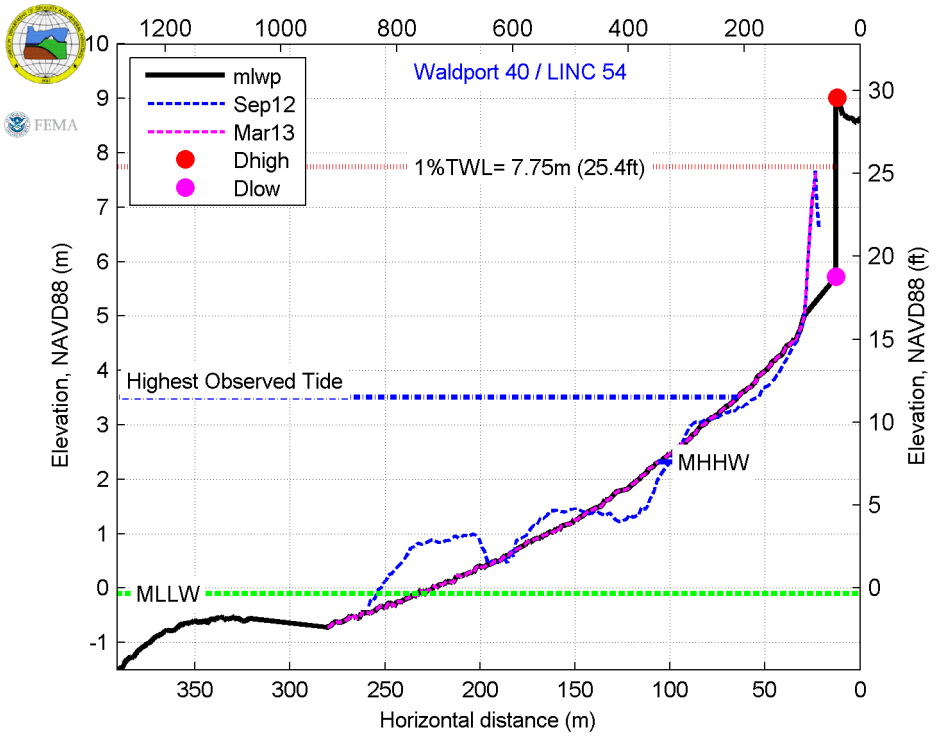

LINC 55

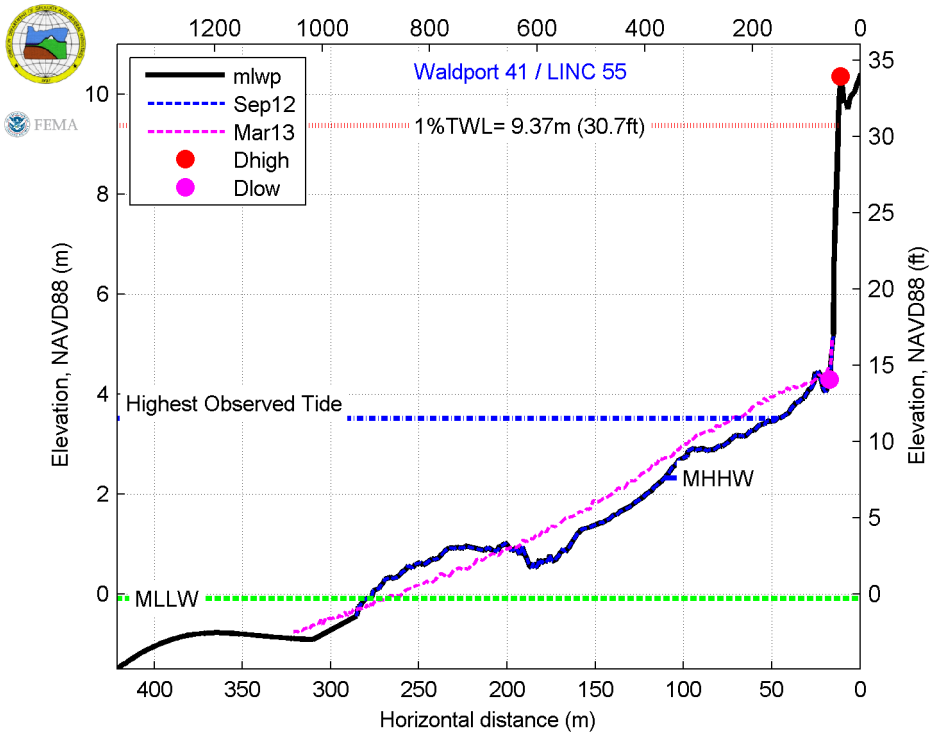

LINC 56

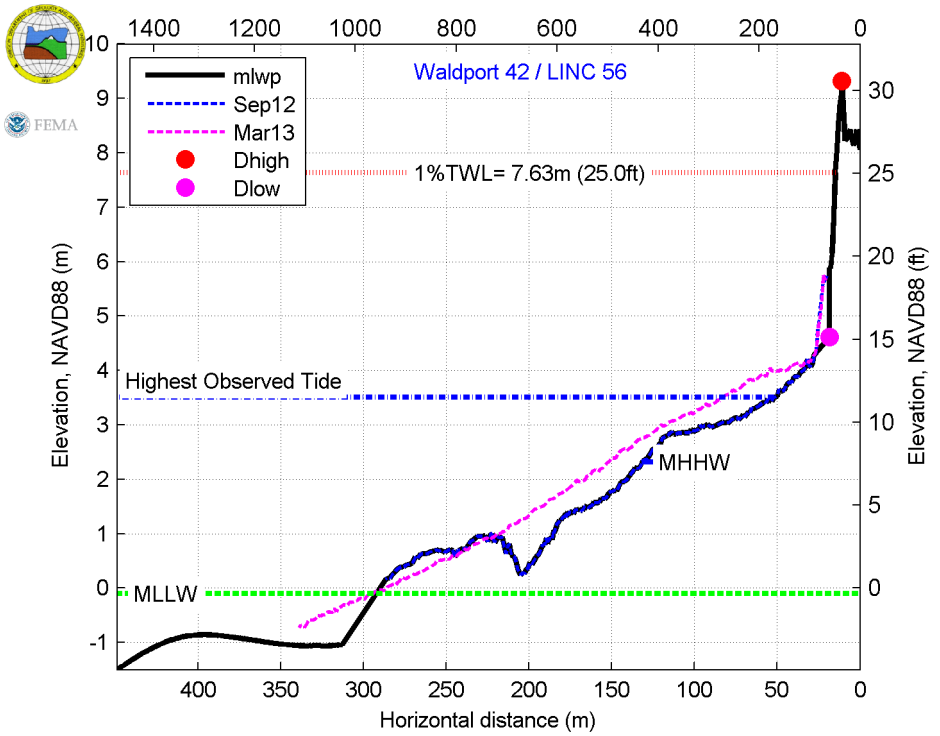

LINC 57

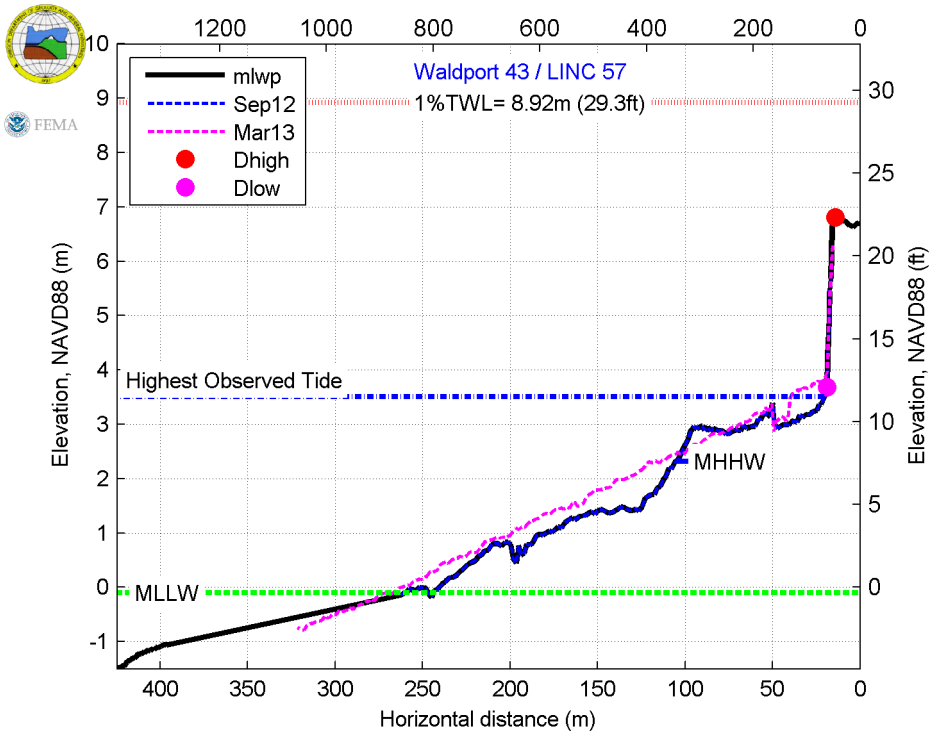

LINC 58

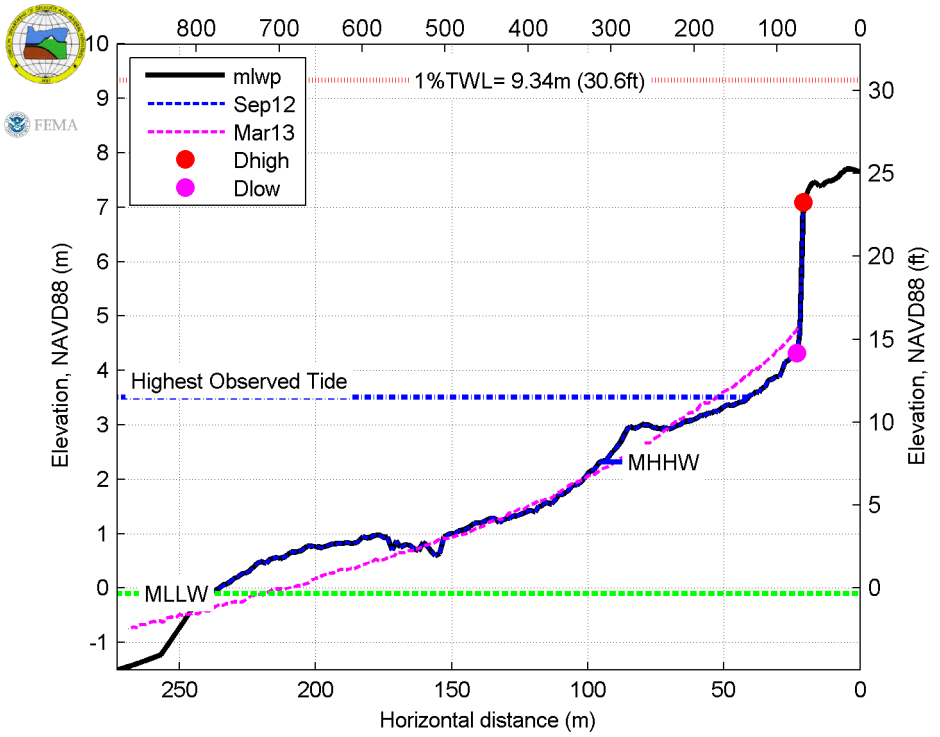

LINC 59

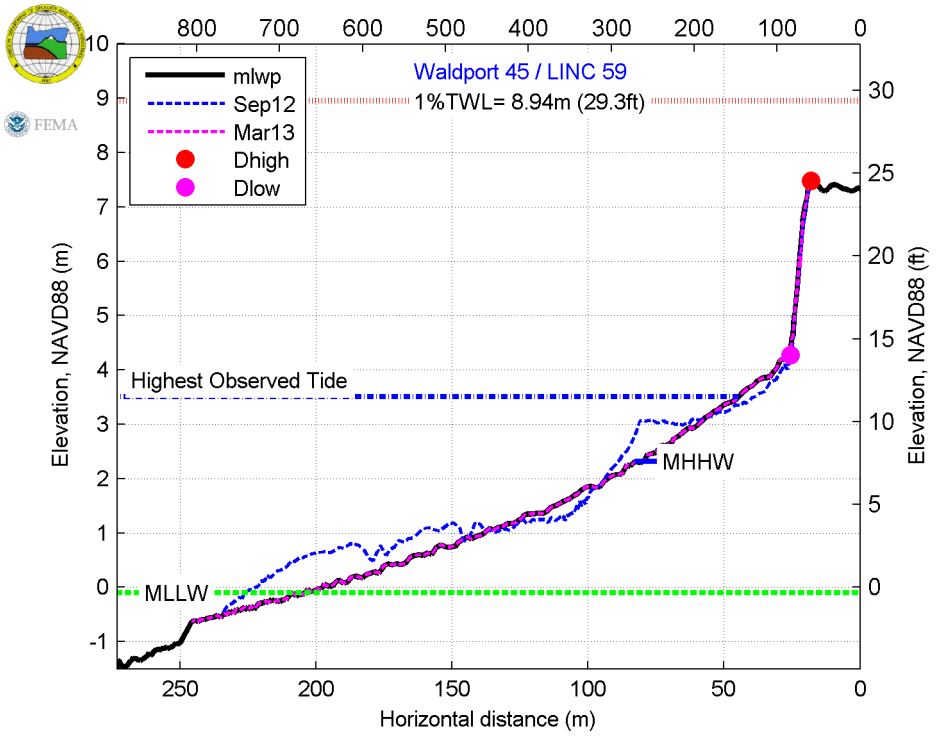

LINC 60

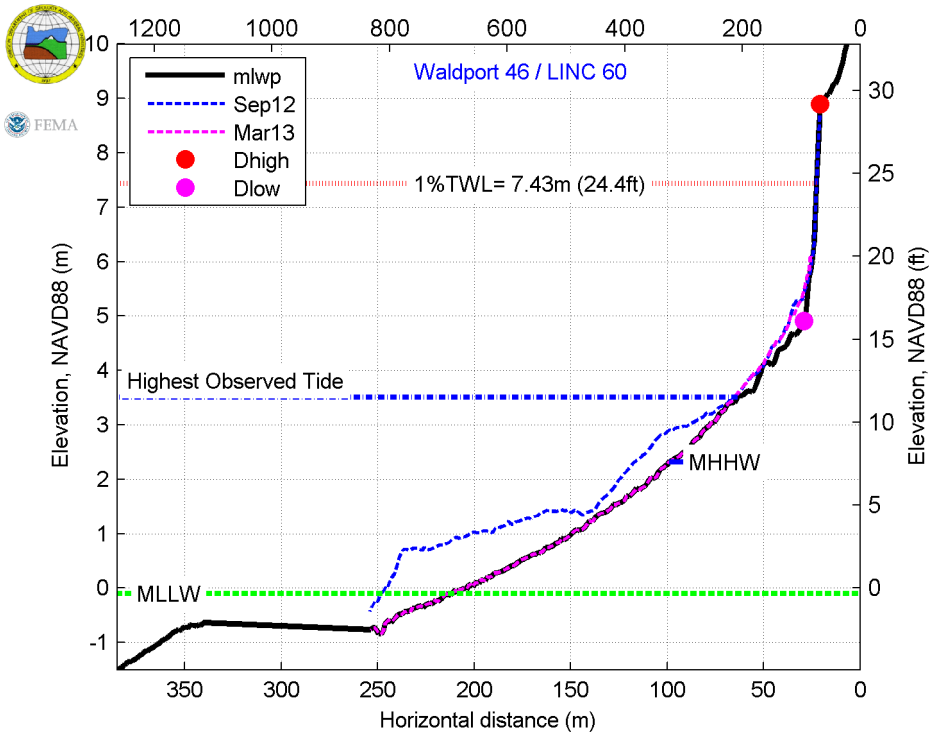

LINC 61

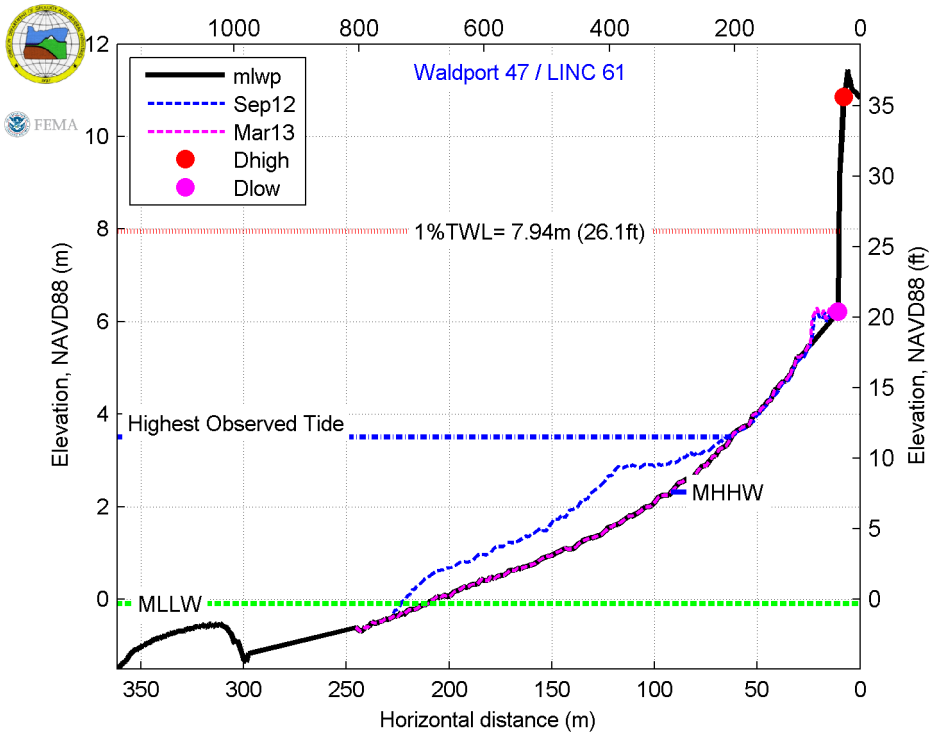

LINC 62

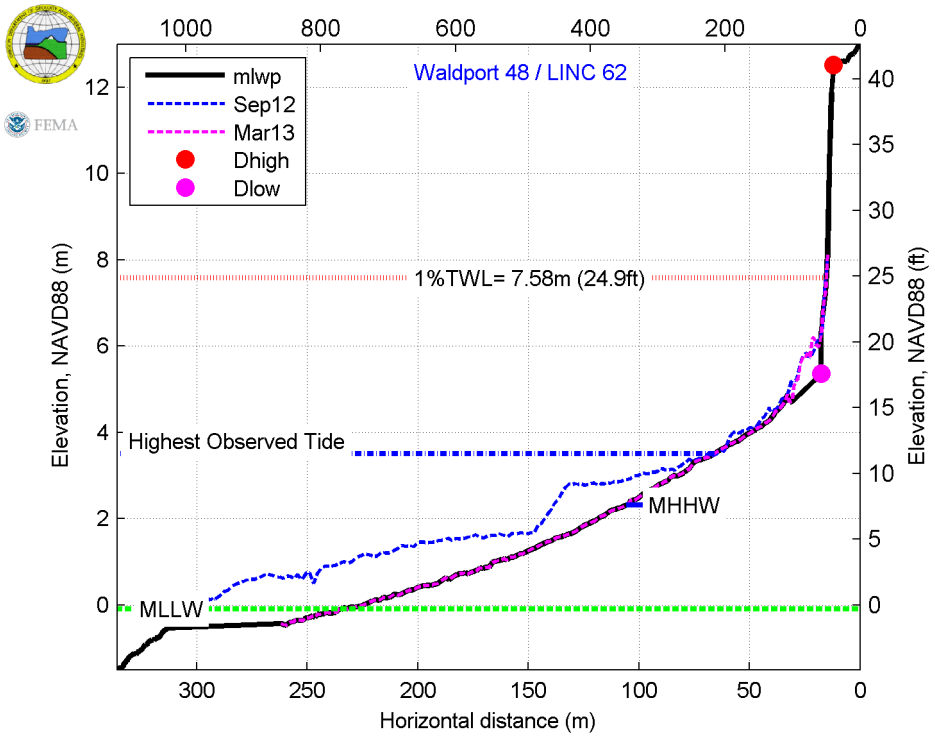

LINC 63

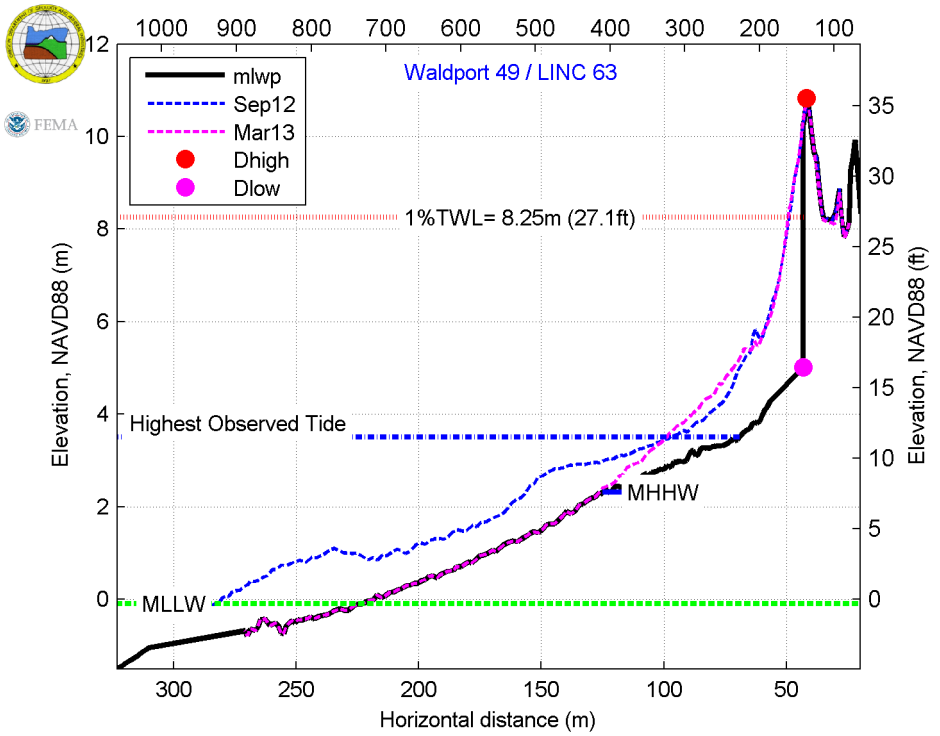

LINC 64

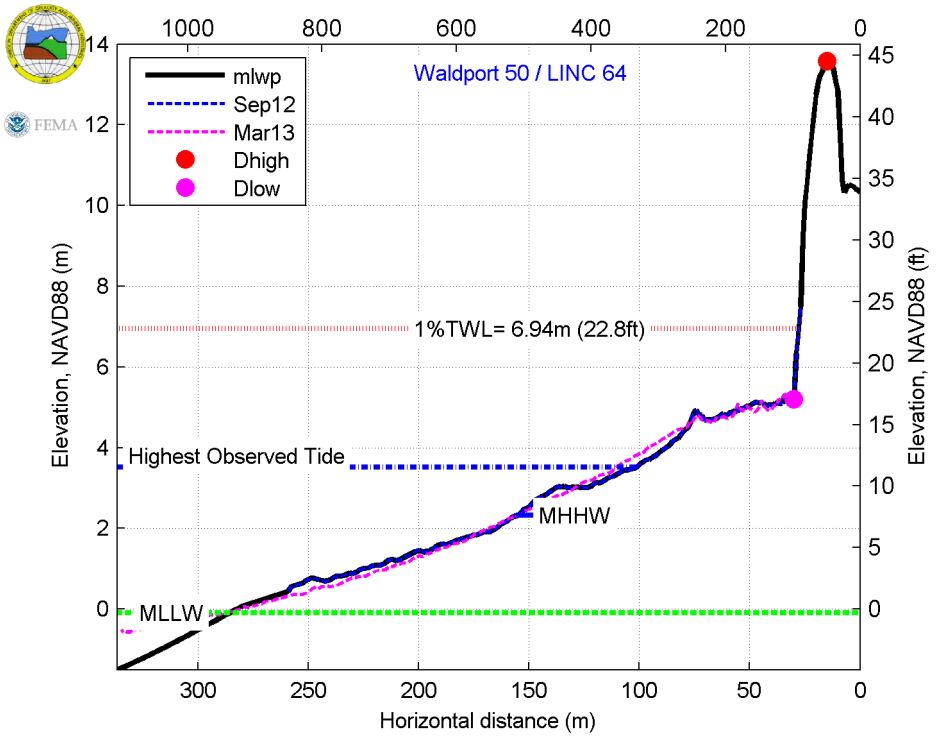

LINC 65

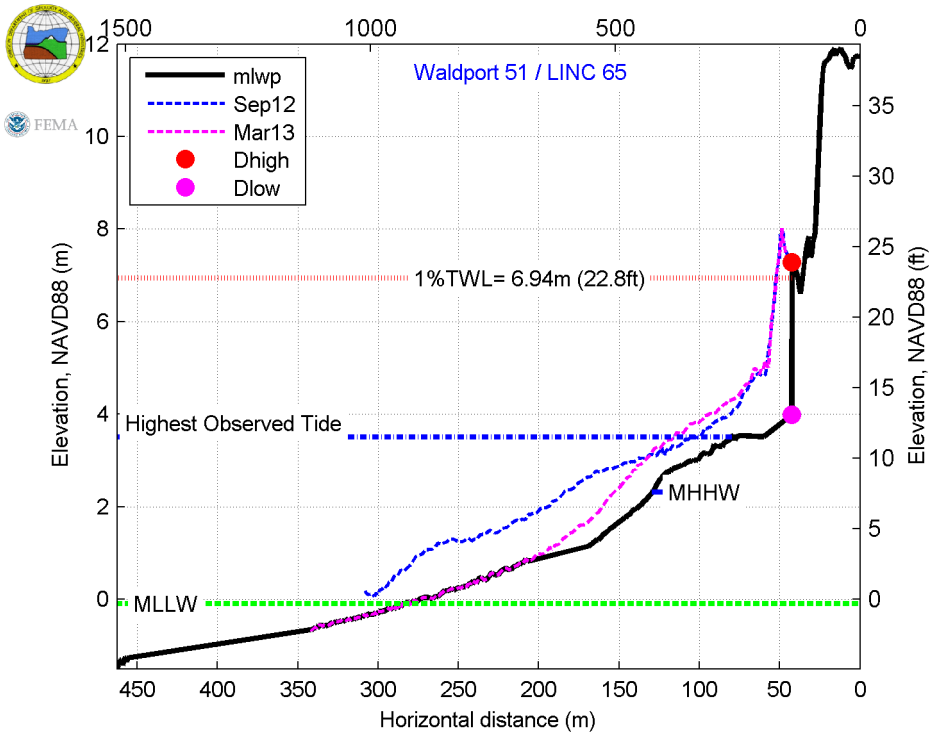

LINC 66

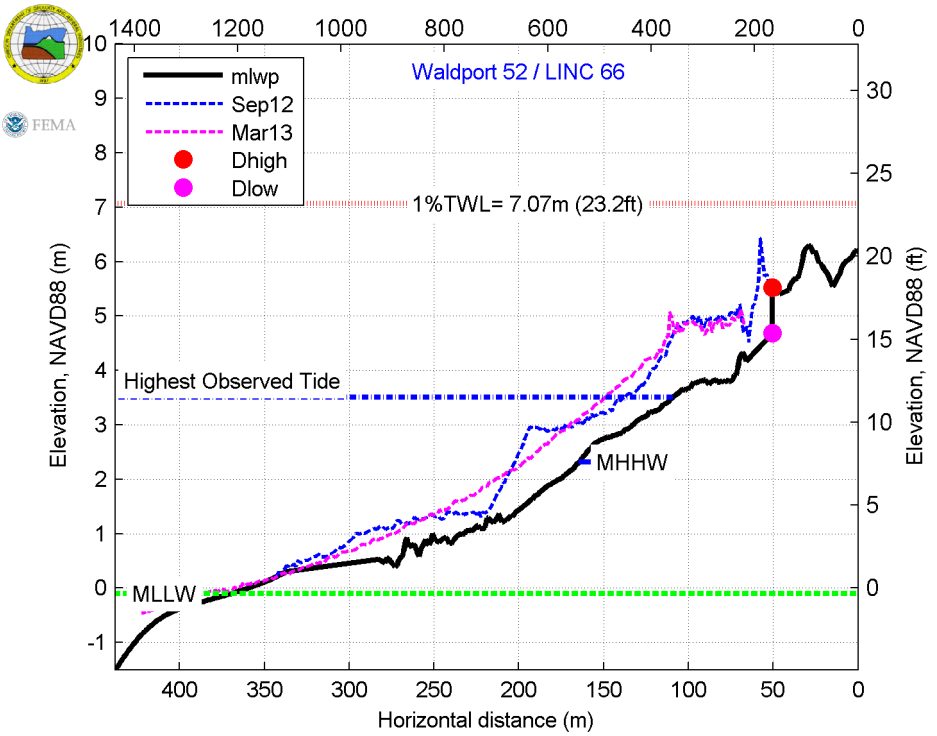

LINC 67

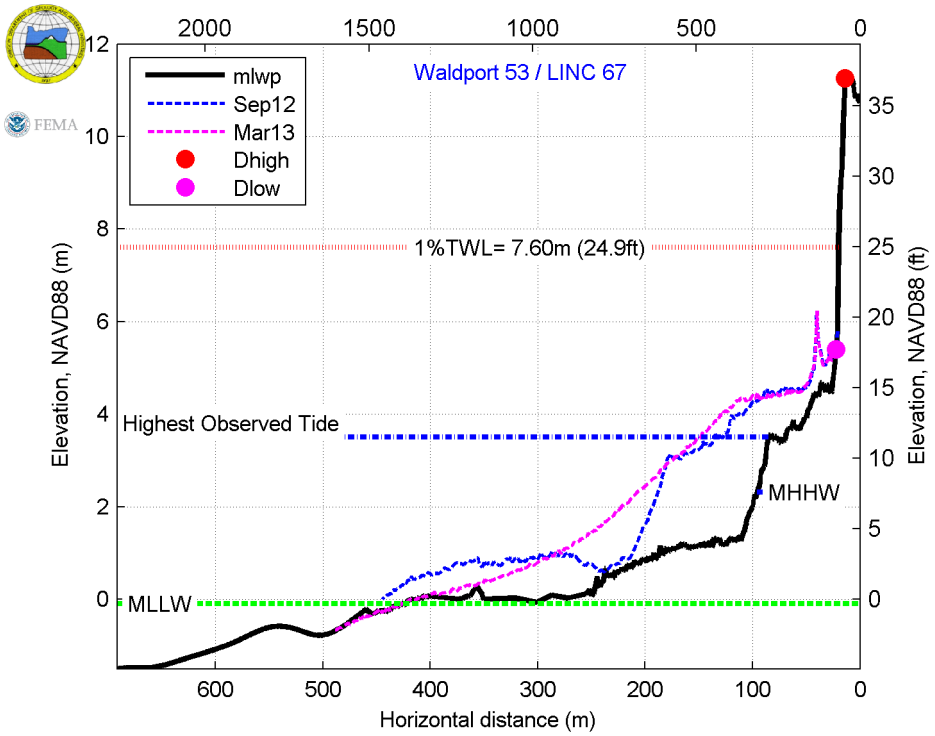
Waldport 53 / LINC 67
mlwp
Sep12
Mar13
Dhigh
Dlow
1%TWL= 7.60m (24.9ft)
Highest Observed Tide
MHHW
MLLW
Elevation, NAVD88 (m)
Elevation, NAVD88 (ft)
Horizontal distance (m)
2000
1500
1000
500
0
600
500
400
300
200
100
0
12
10
8
6
4
2
0
35
30
25
20
15
10
5
0

11.2.4 Alsea Spit

LINC 68

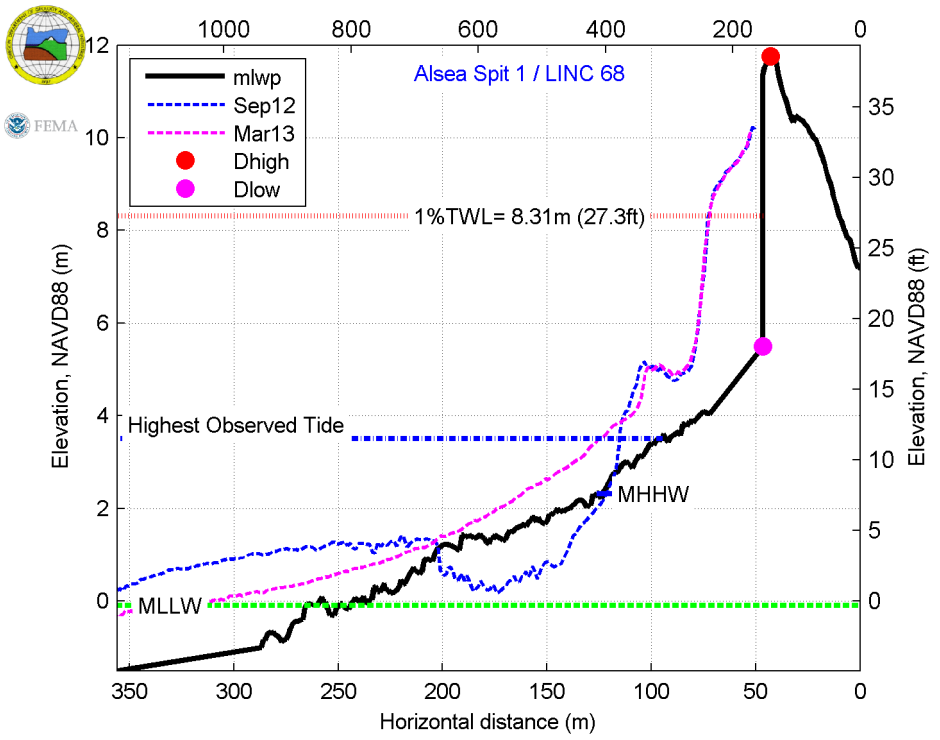

LINC 69

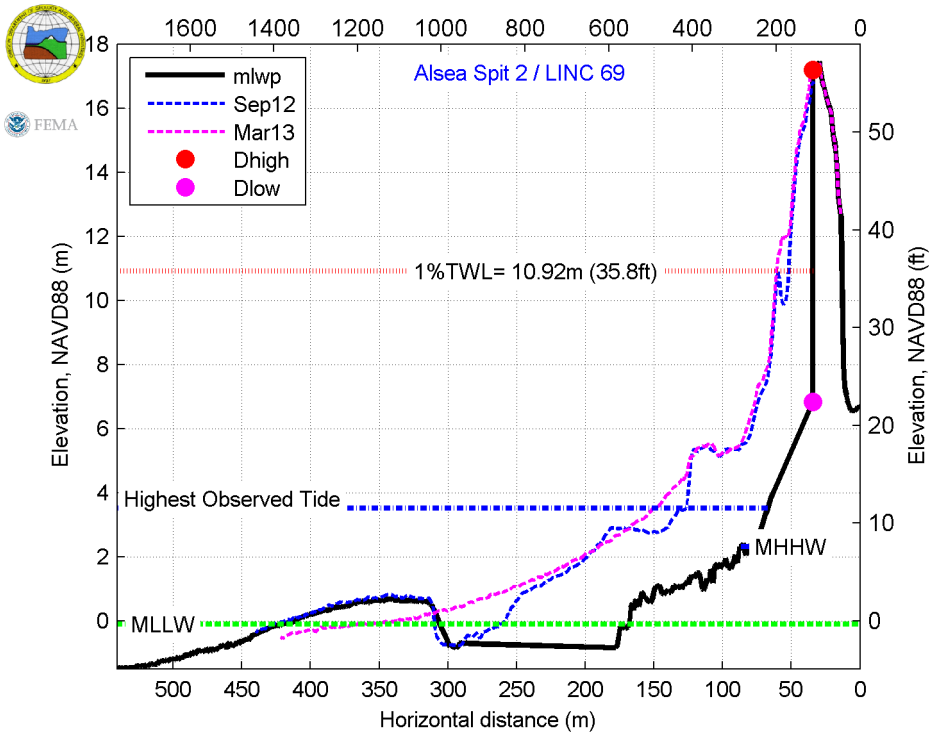

LINC 70

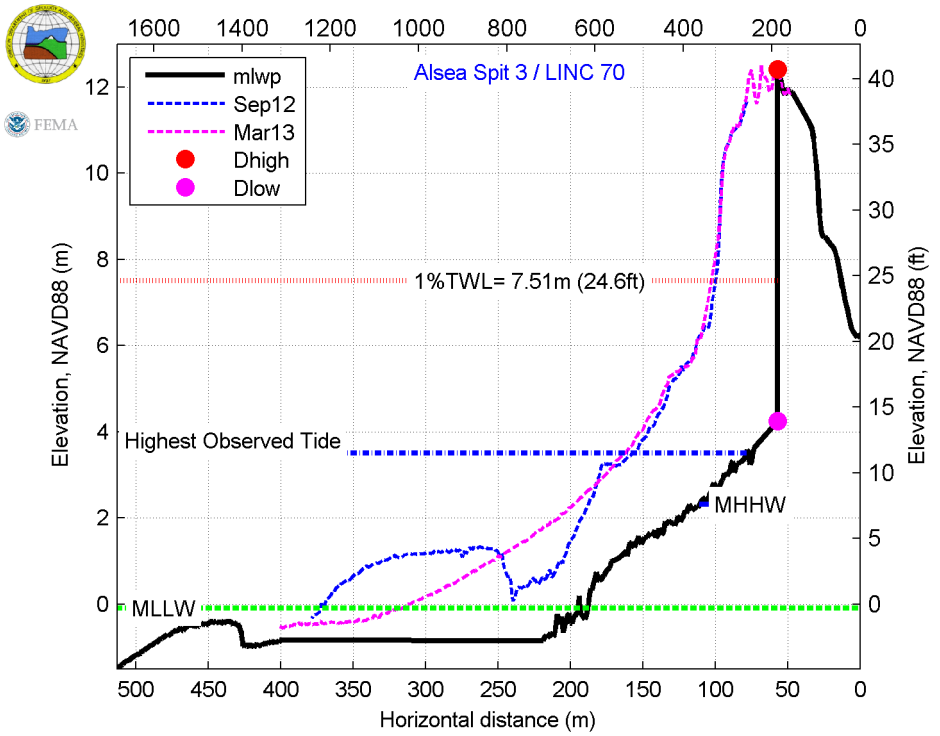

LINC 71

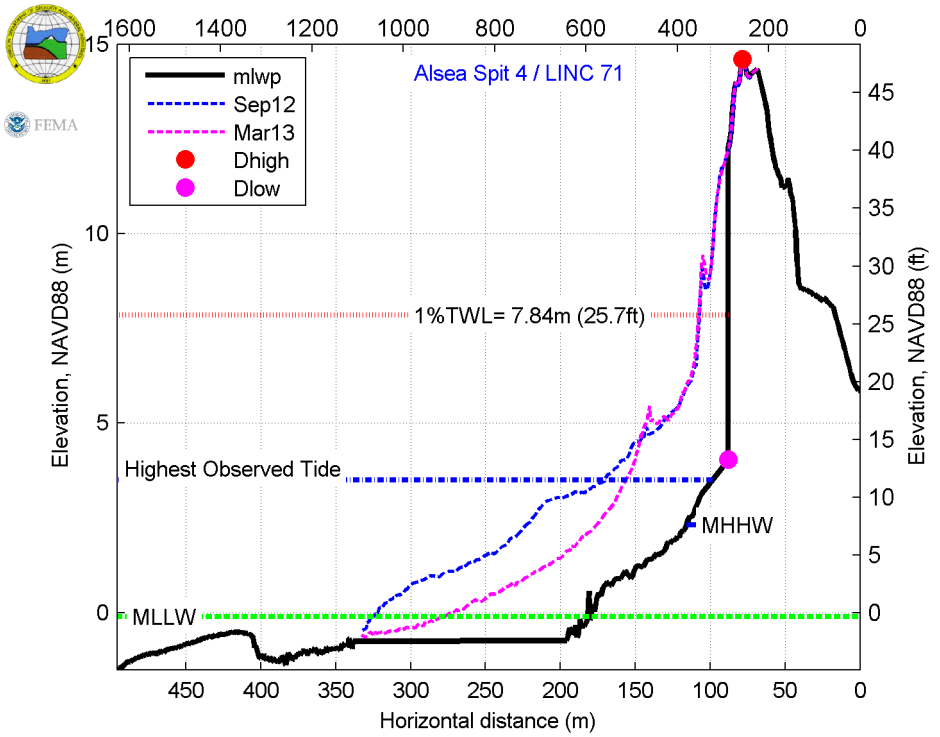

LINC 72

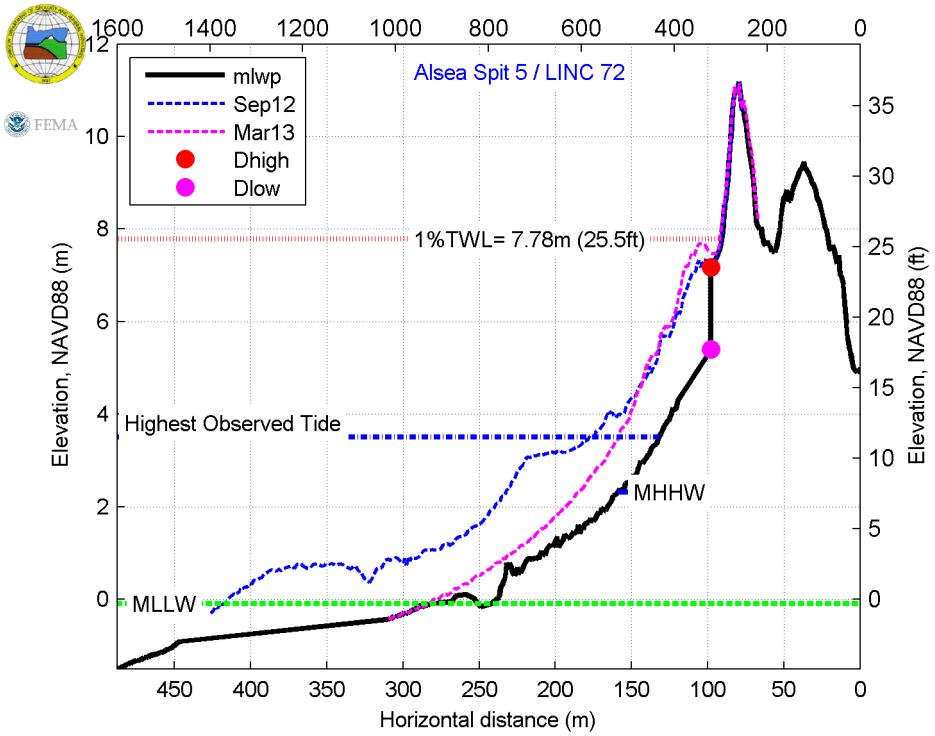

LINC 73

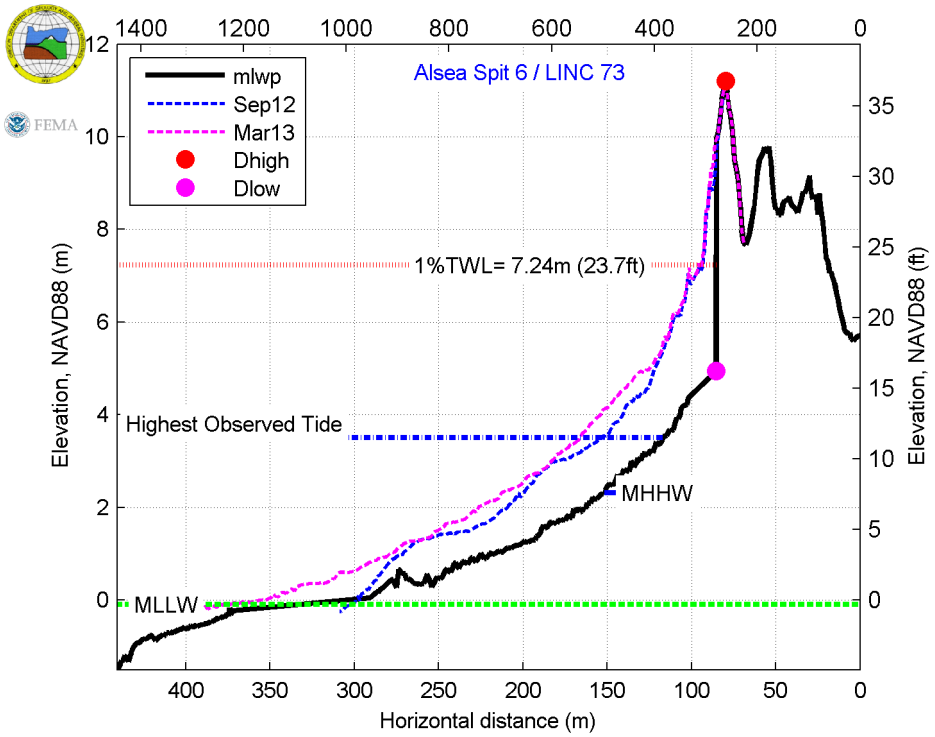

LINC 74

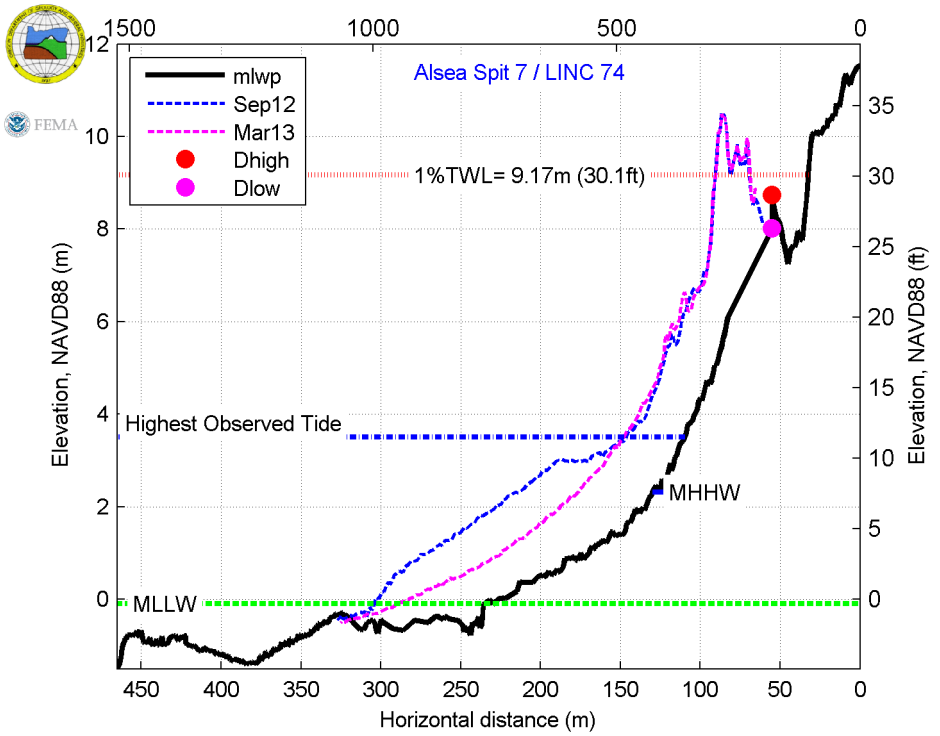

LINC 75

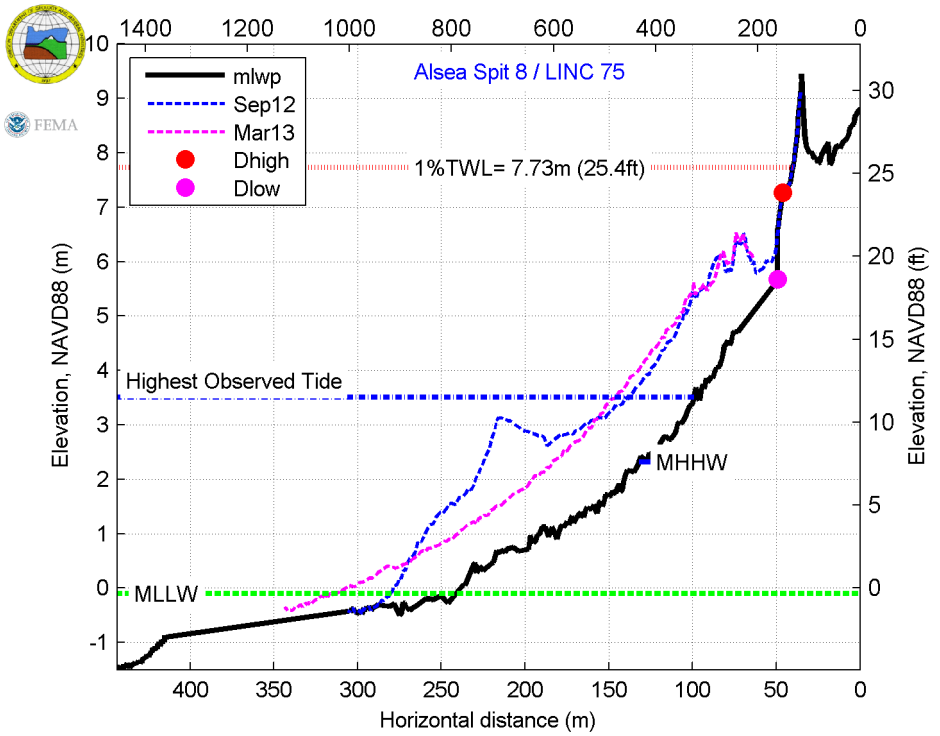

LINC 76

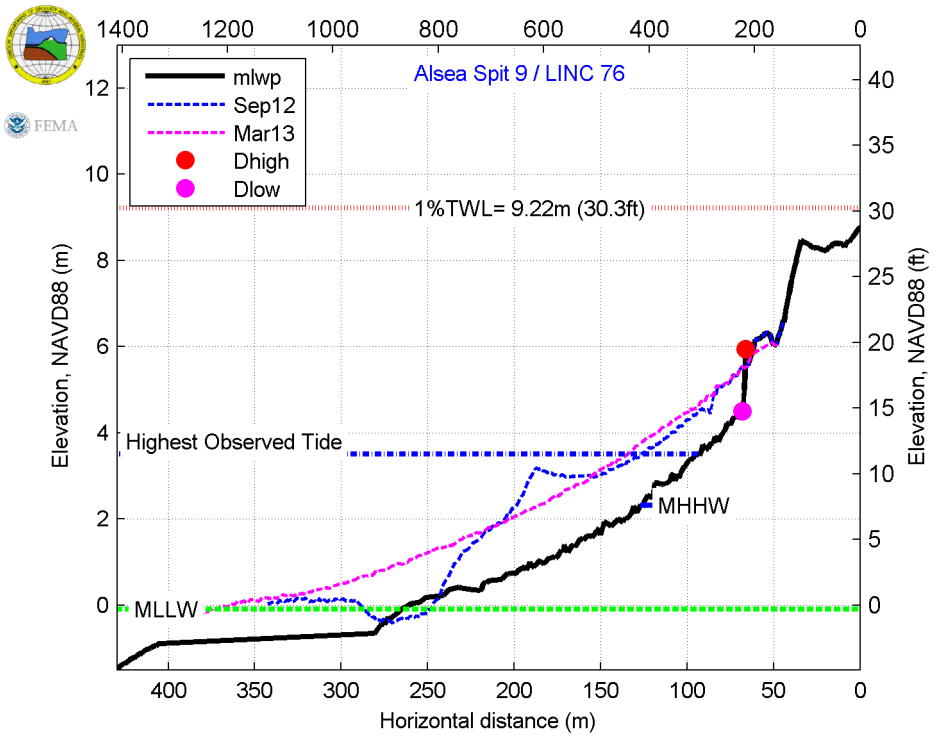

LINC 77

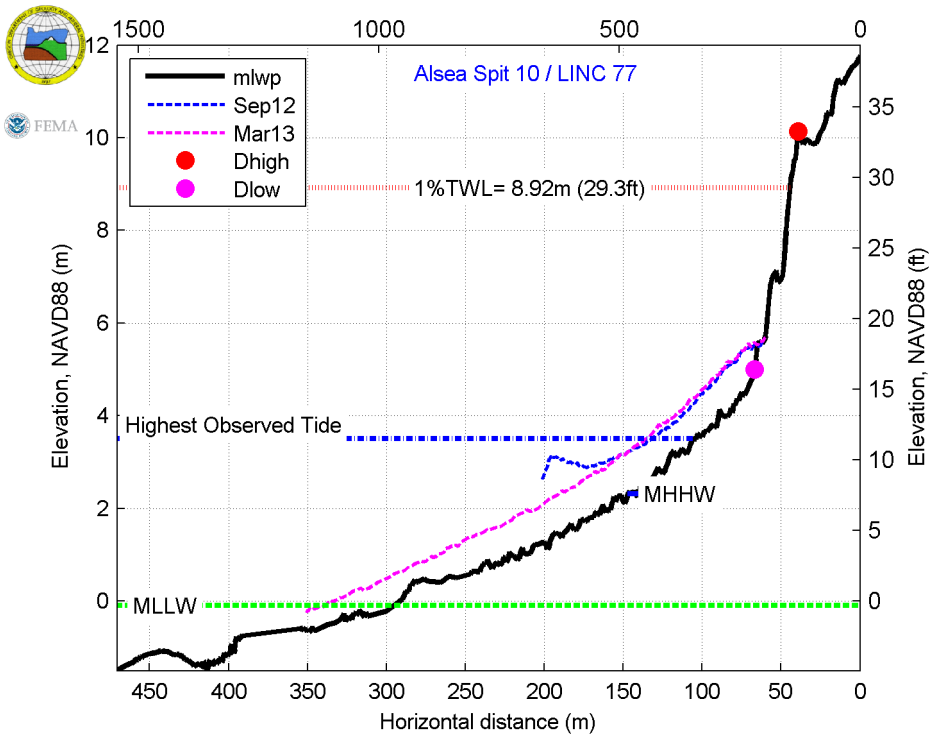

LINC 78

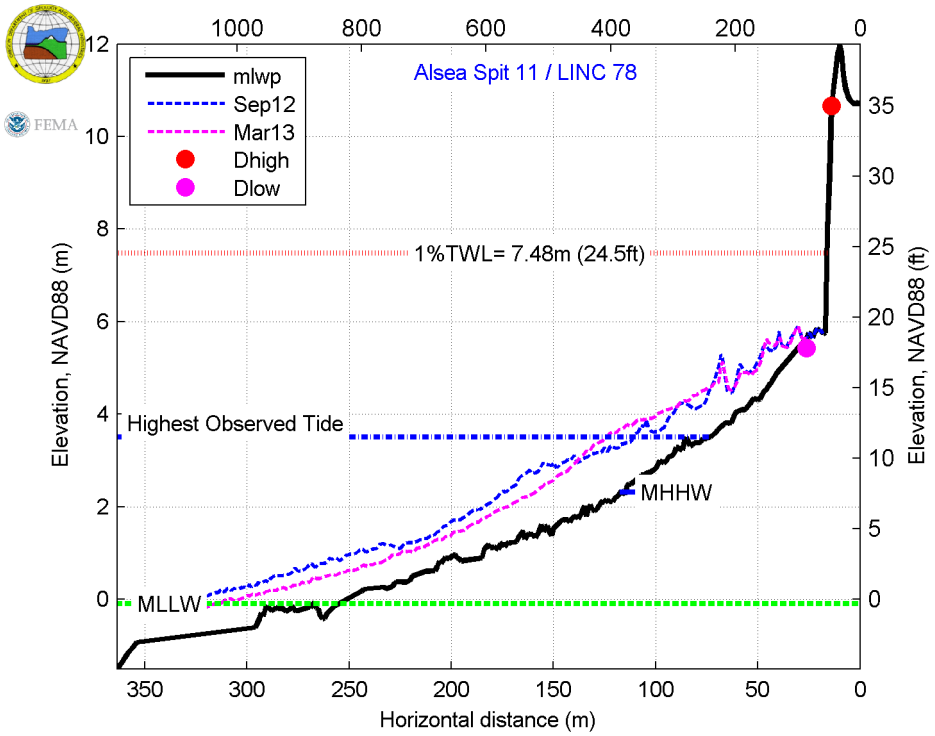

LINC 79

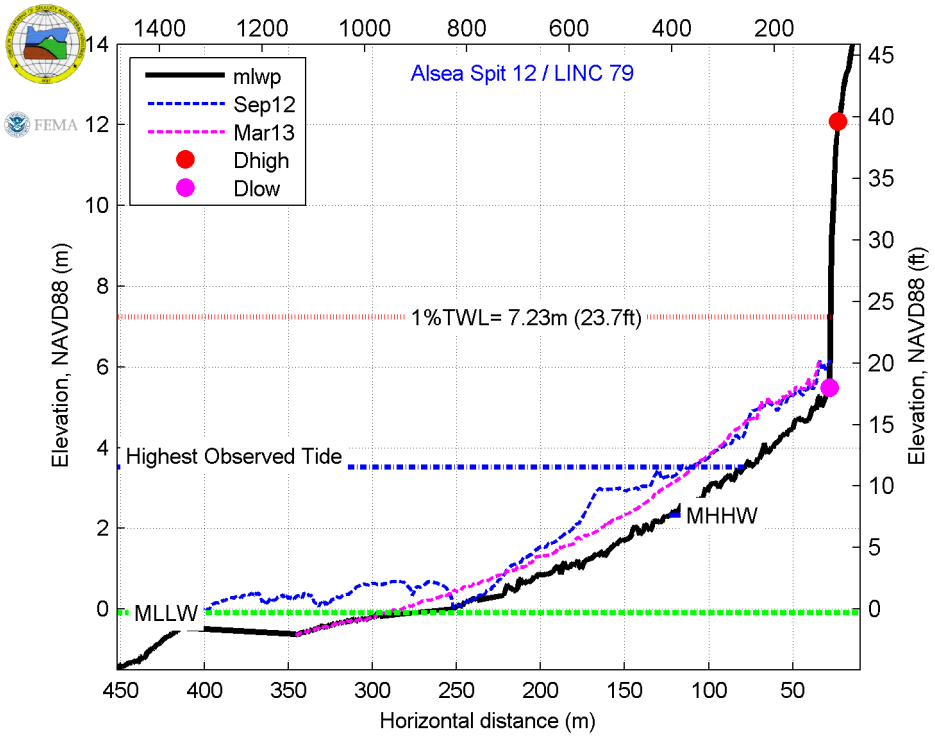

LINC 80

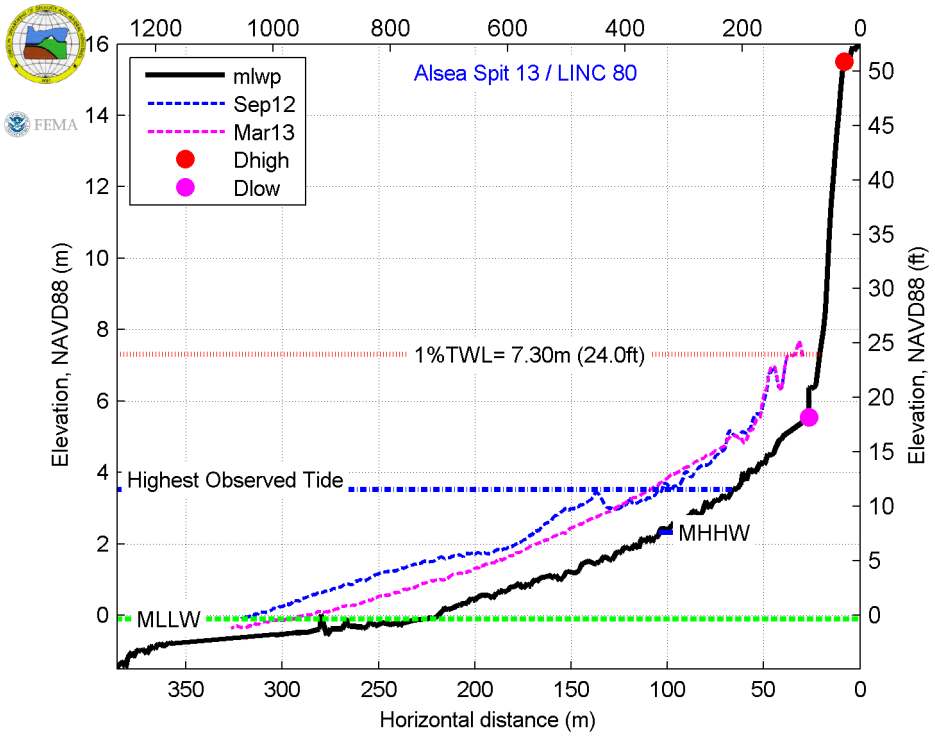

LINC 81

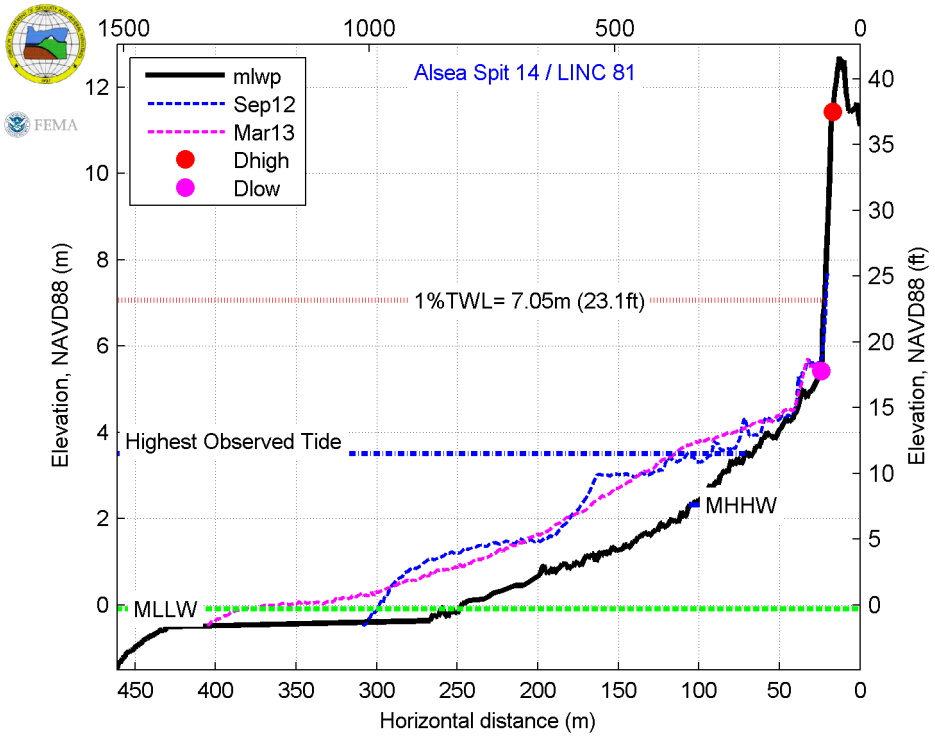

LINC 82

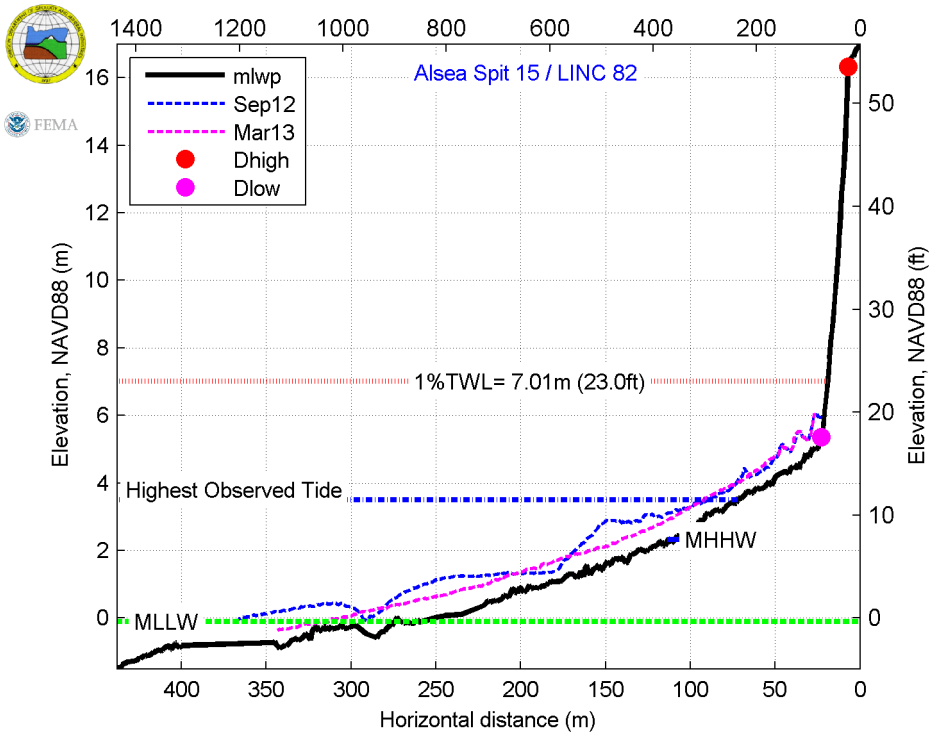

LINC 83

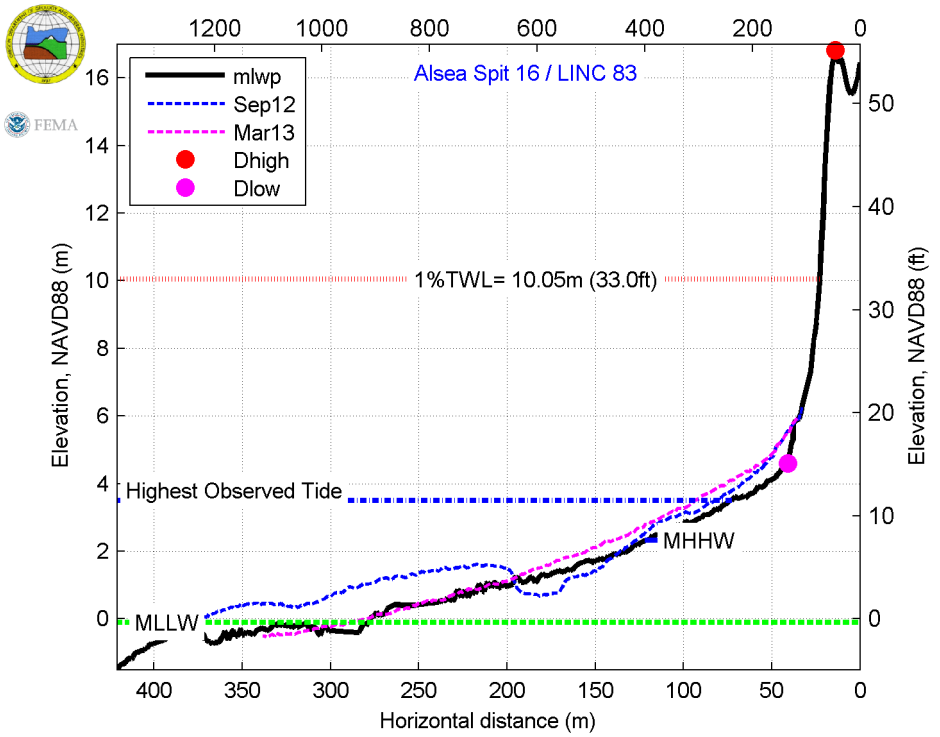

LINC 84

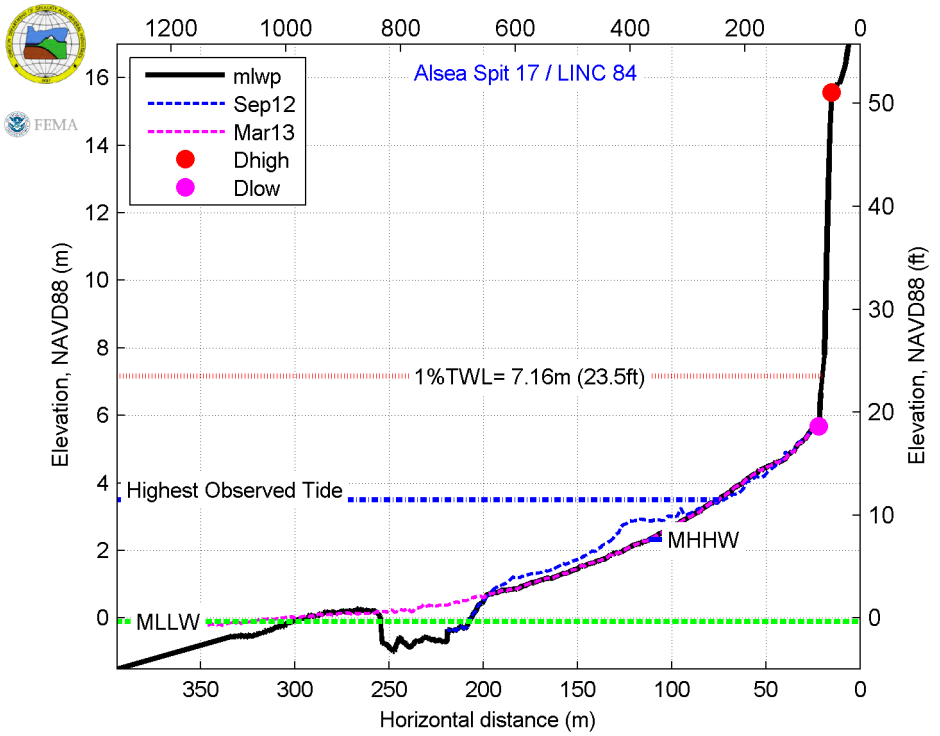

LINC 85

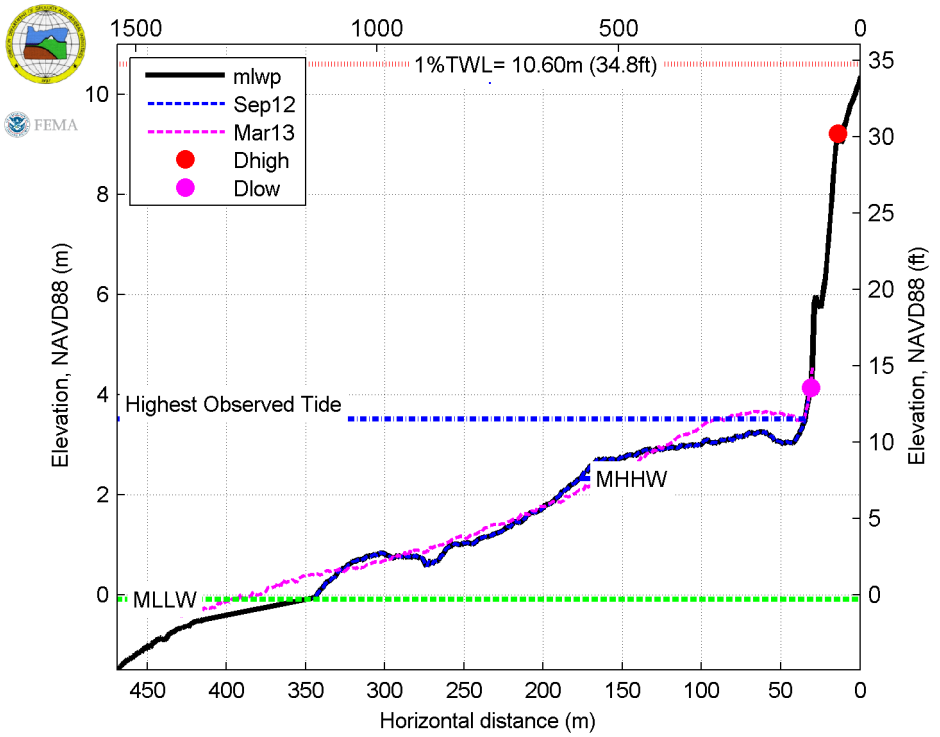

LINC 86

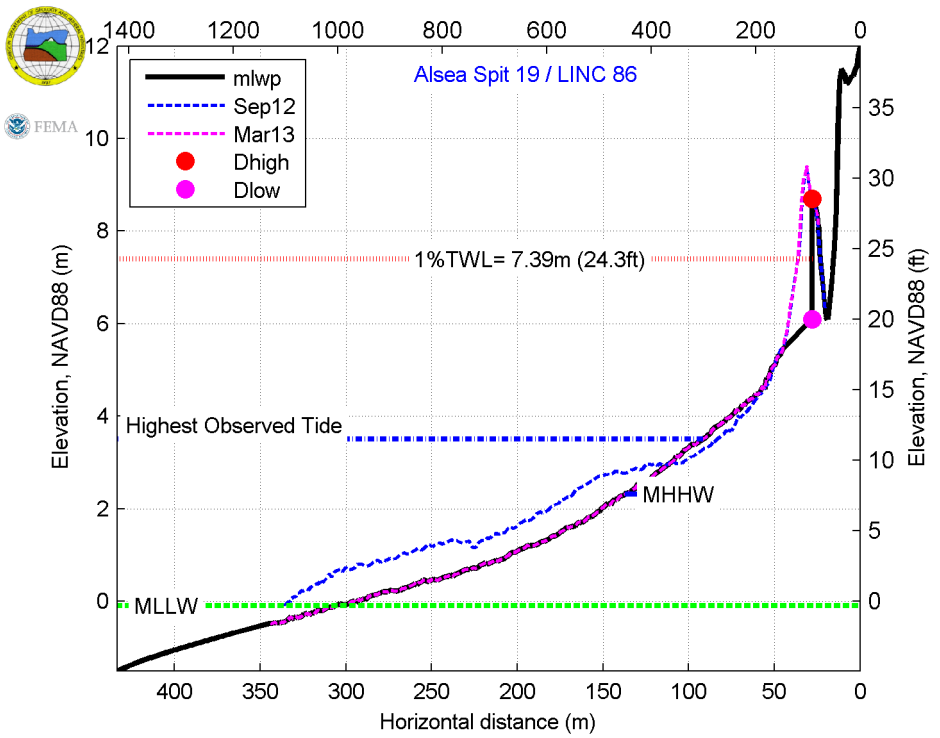

LINC 87

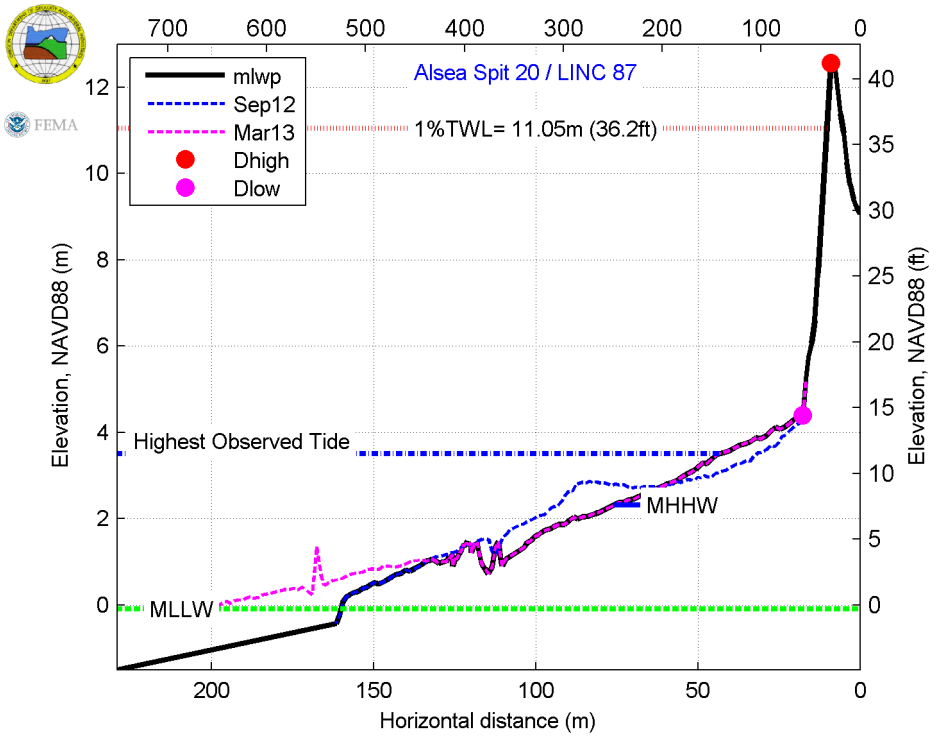

LINC 88

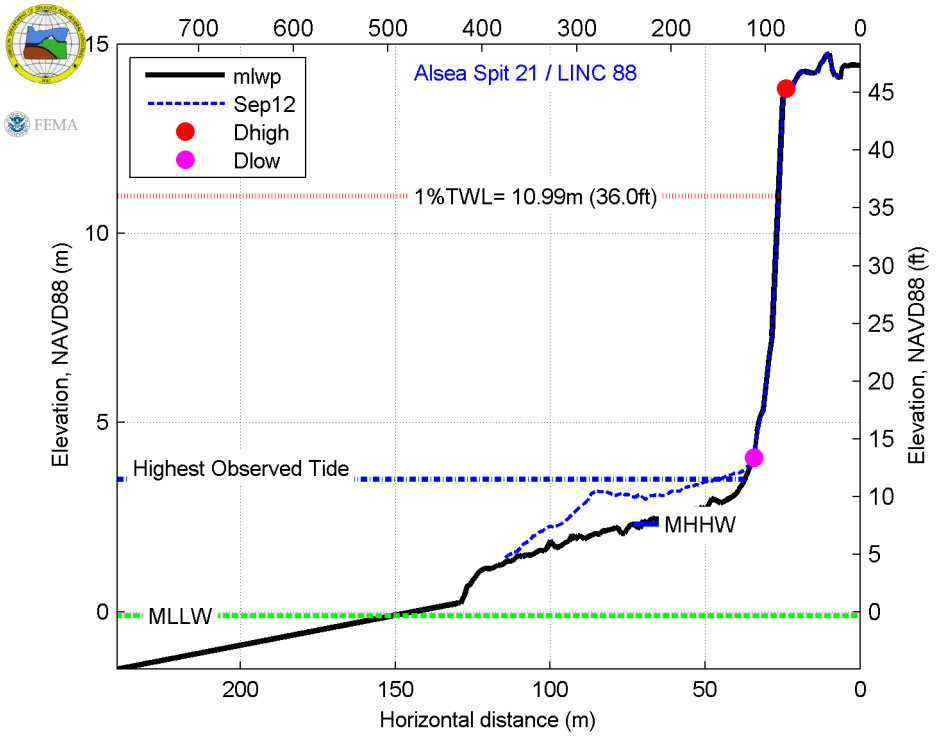
Alsea Spit 21 / LINC 88
mlwp
Sep12
Dhigh
Dlow
1%TWL= 10.99m (36.0ft)
Highest Observed Tide
MHHW
MLLW
Elevation, NAVD88 (m)
Elevation, NAVD88 (ft)
Horizontal distance (m)
700
600
500
400
300
200
100
0
200
150
100
50
0
15
10
5
0
45
40
35
30
25
20
15
10
5
0

11.2.5 South Beach

LINC 89

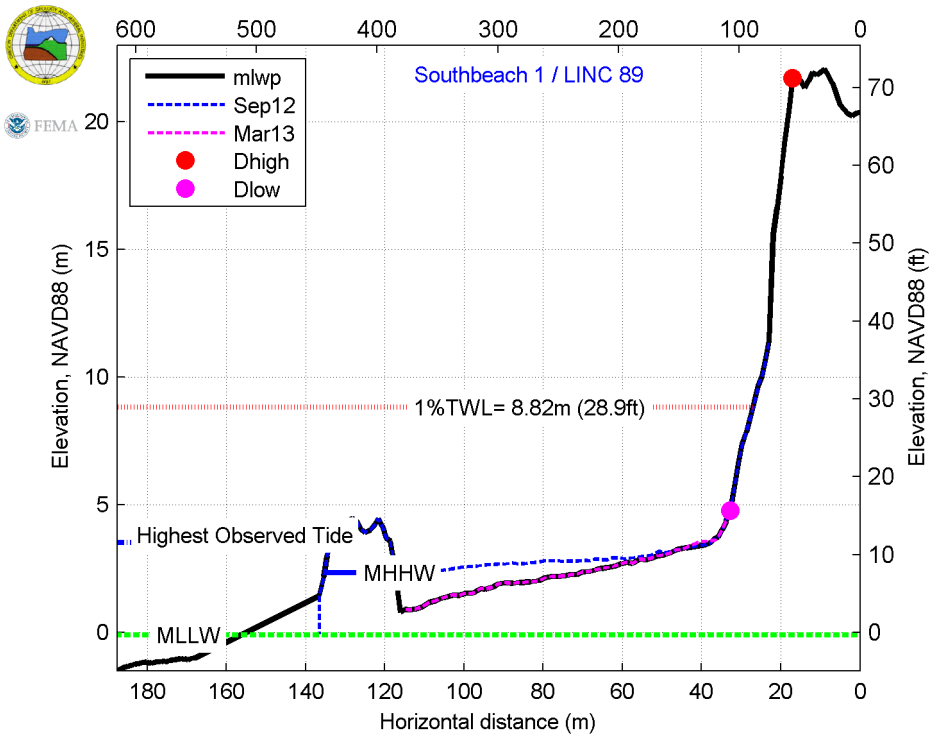

LINC 90

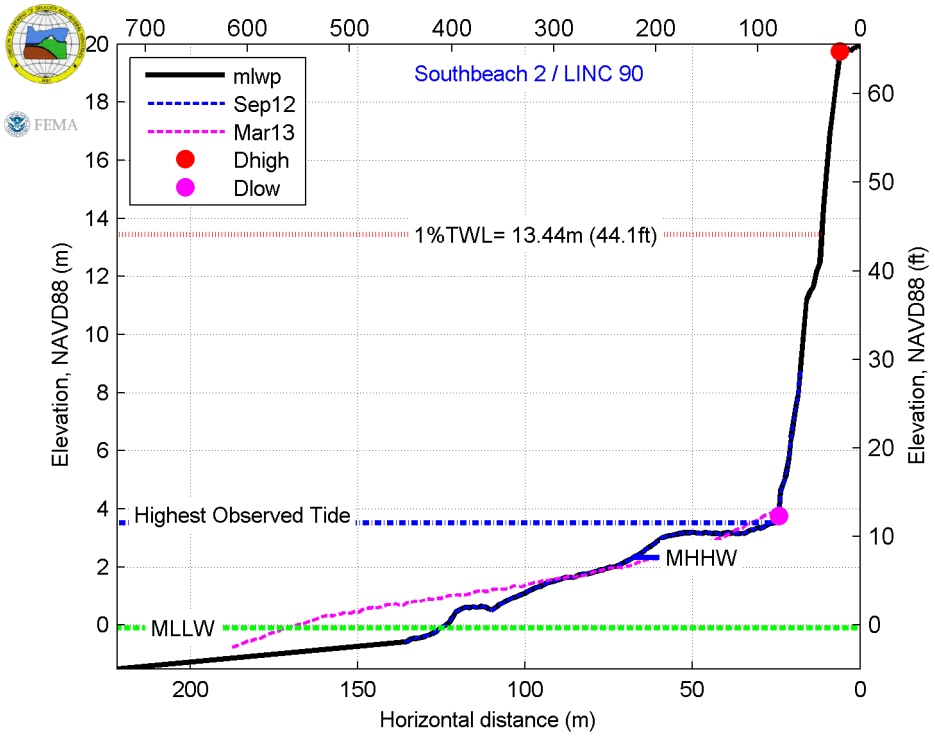

LINC 91

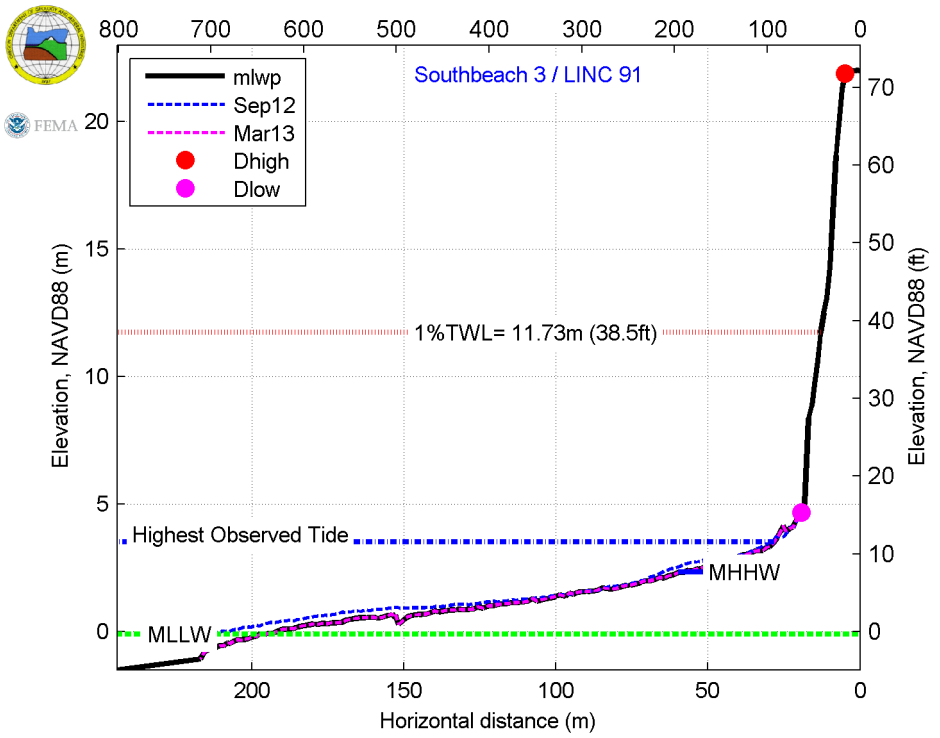

LINC 92

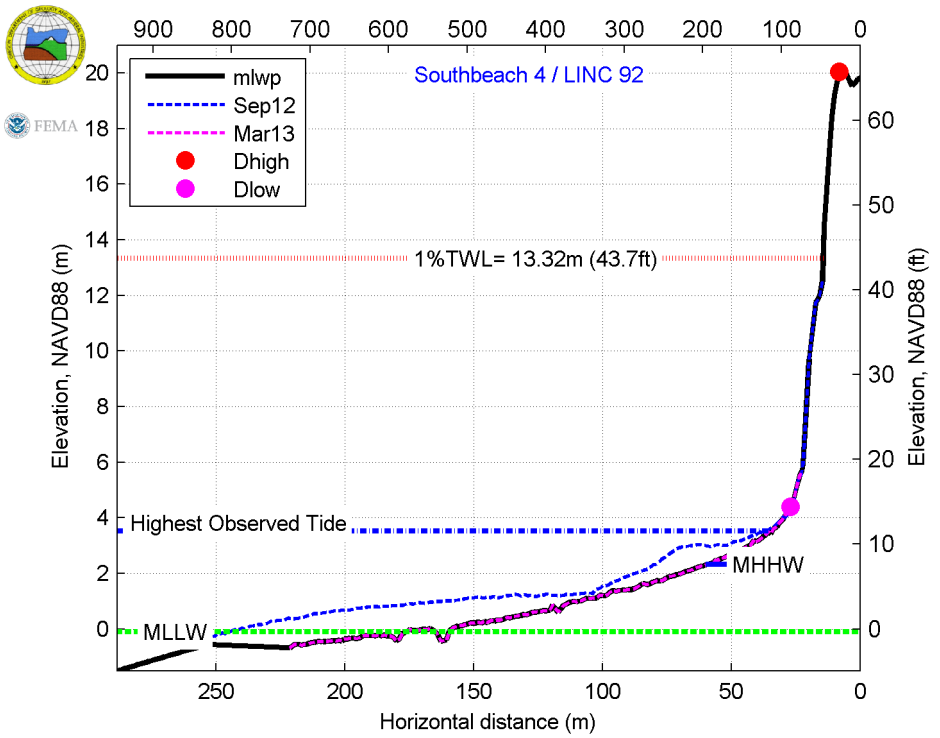

LINC 93

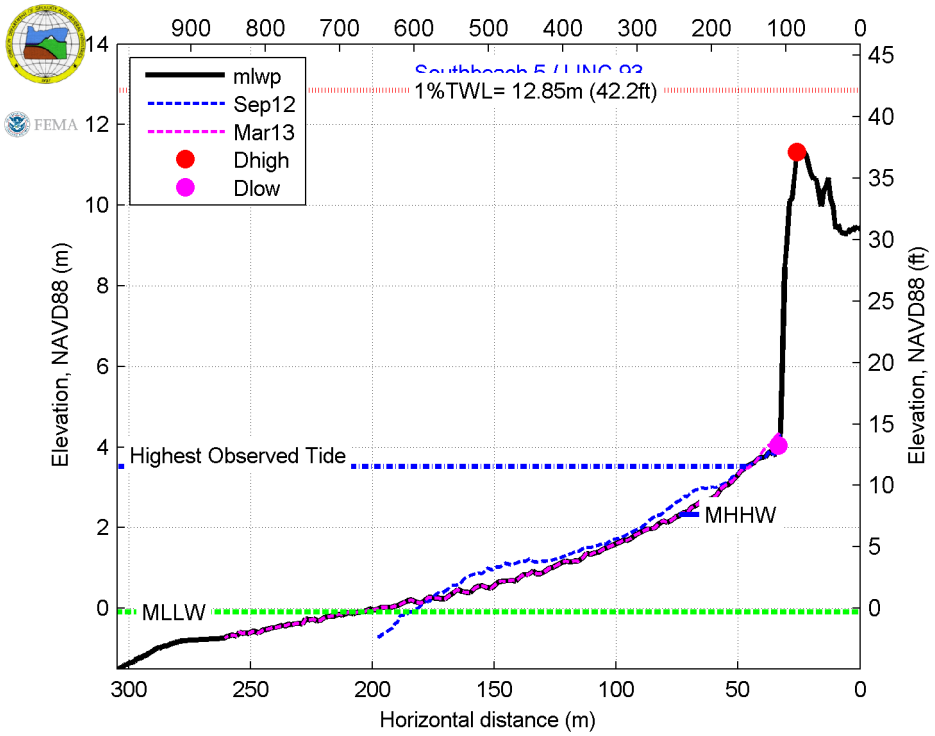

LINC 94

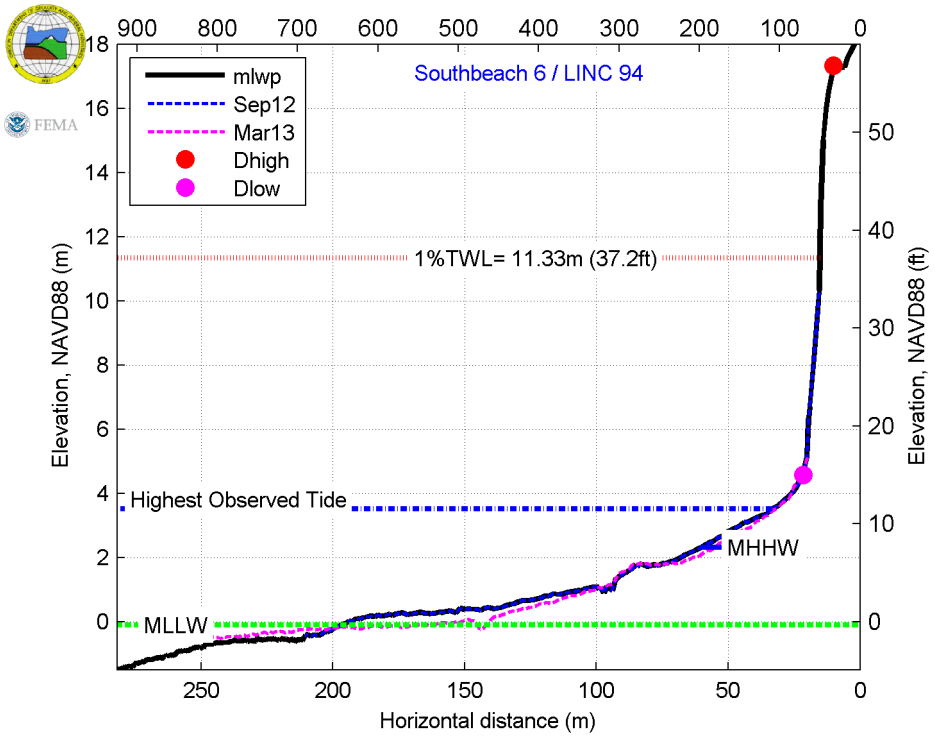

LINC 95

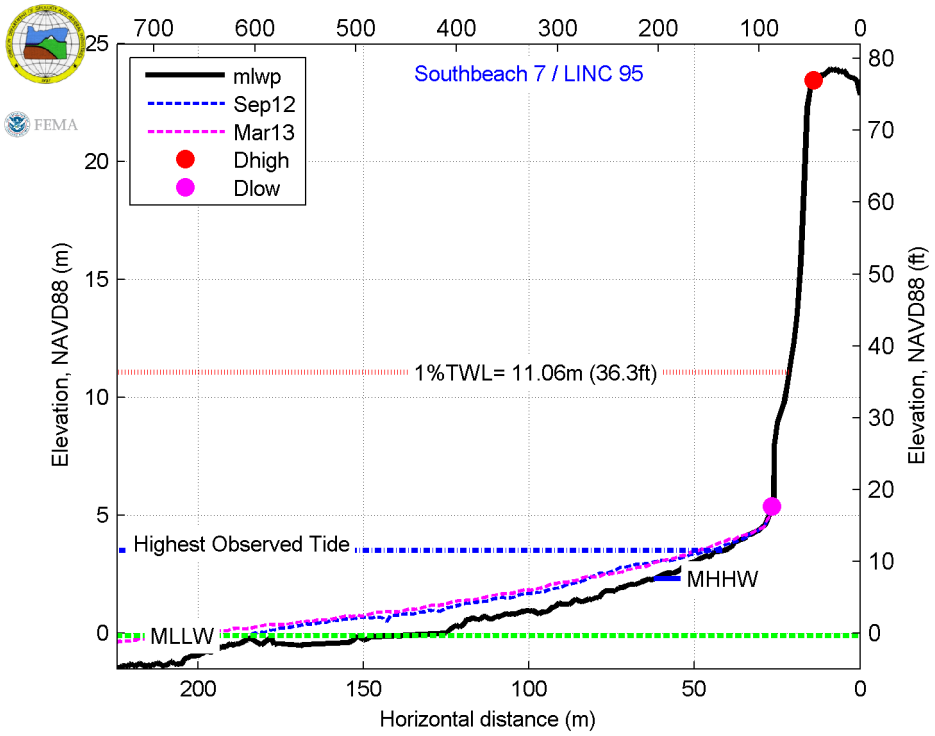

LINC 96

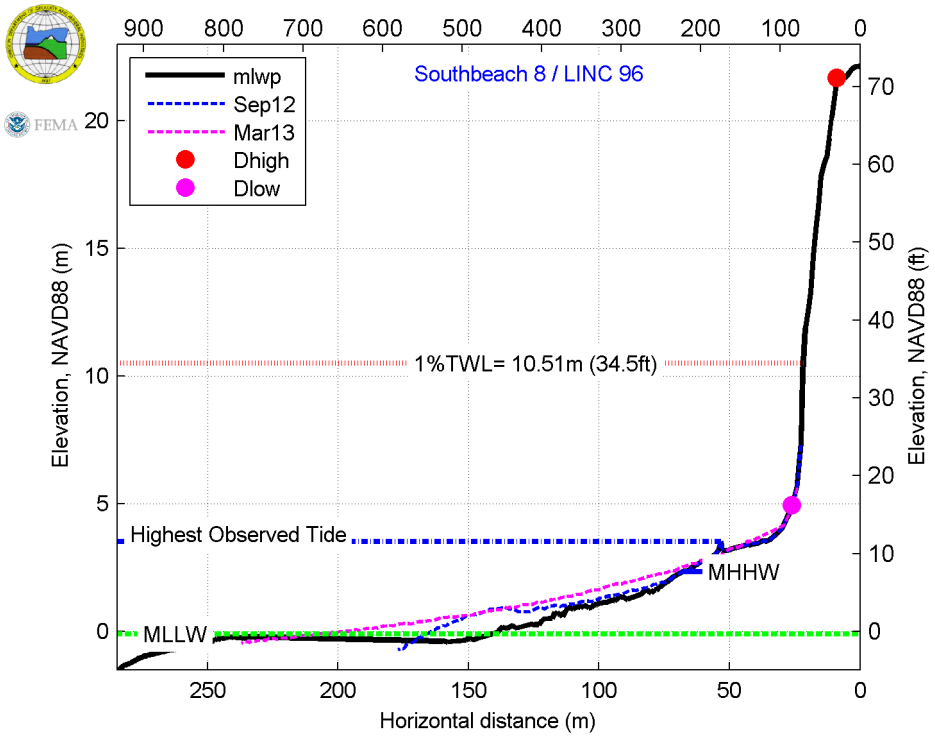

LINC 97

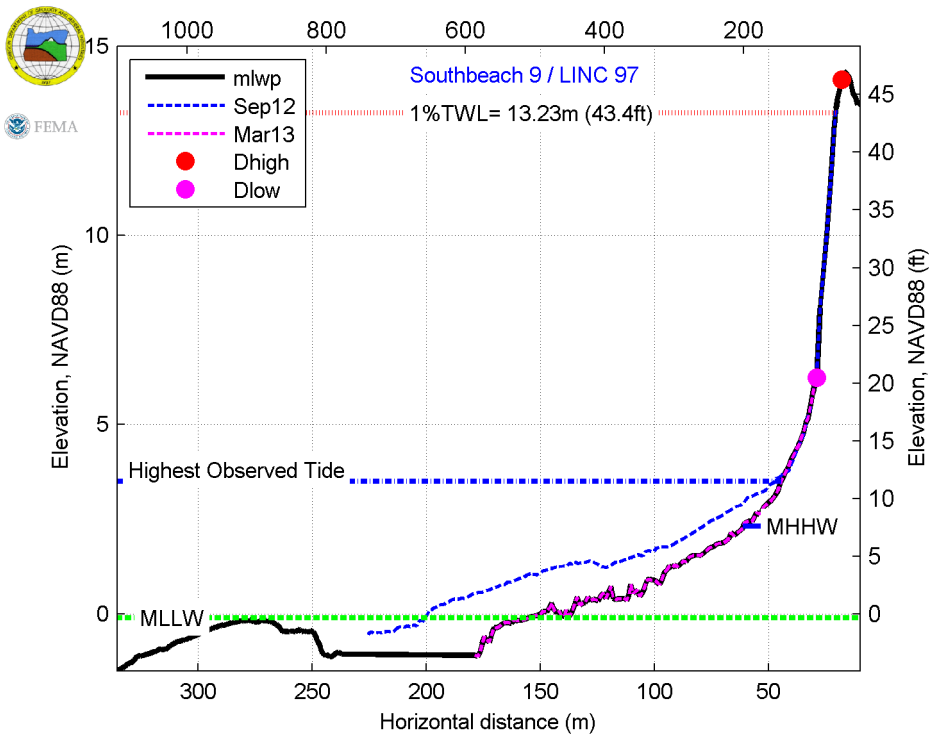

LINC 98

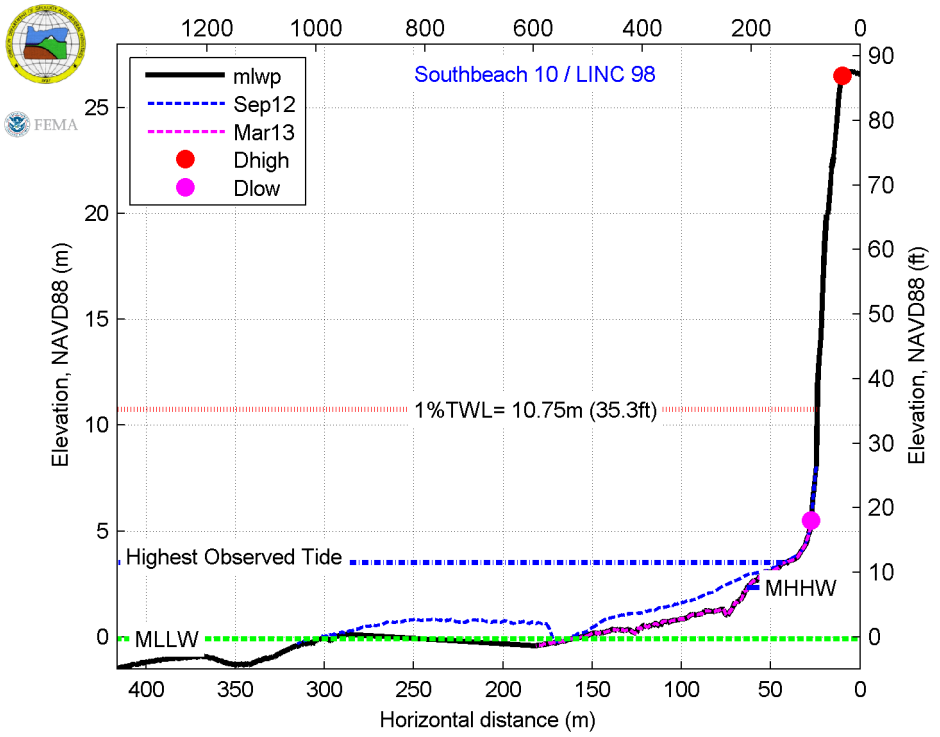

LINC 99

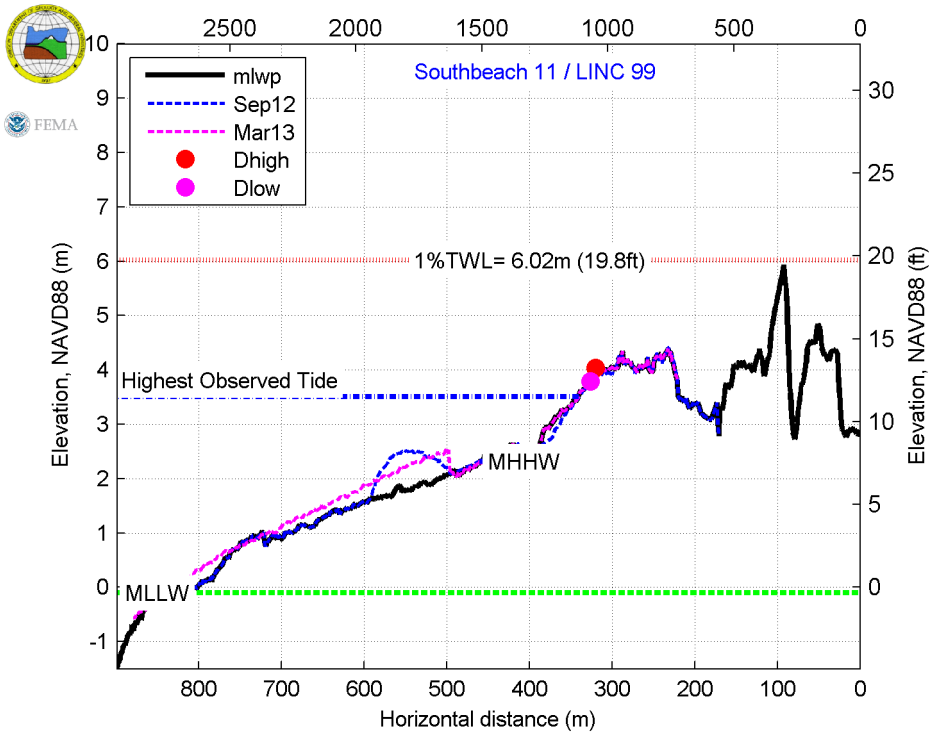

LINC 100

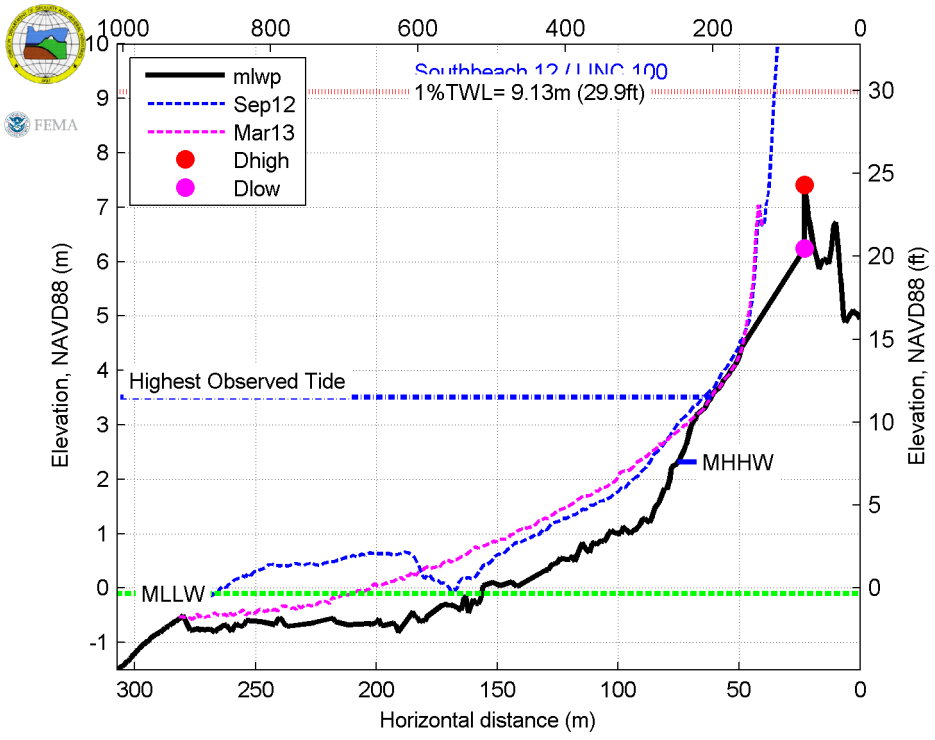

LINC 101

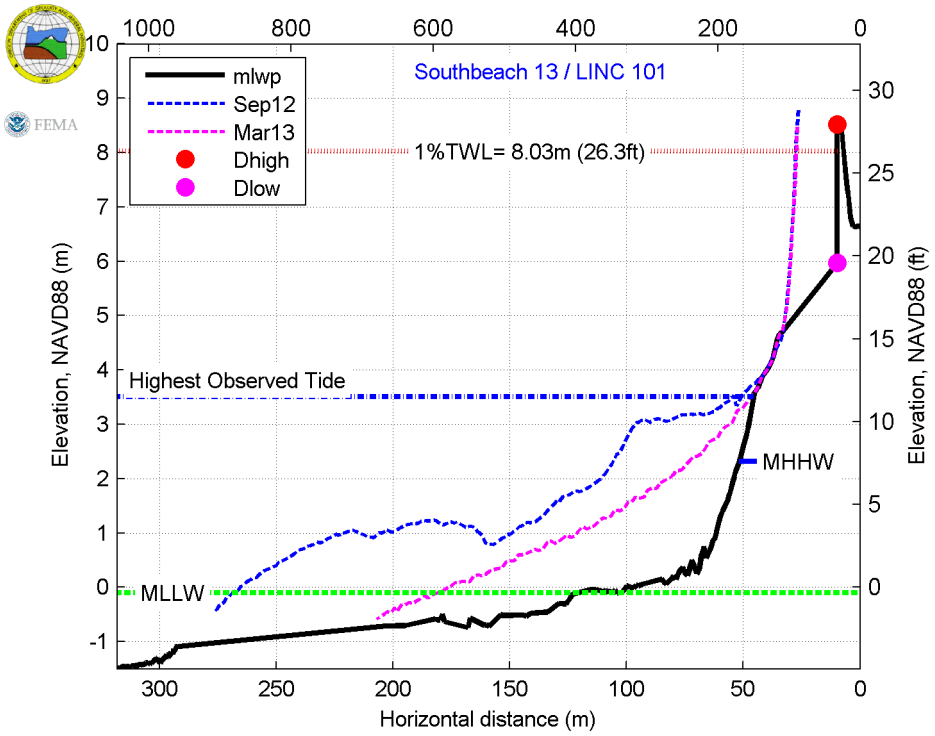

LINC 102

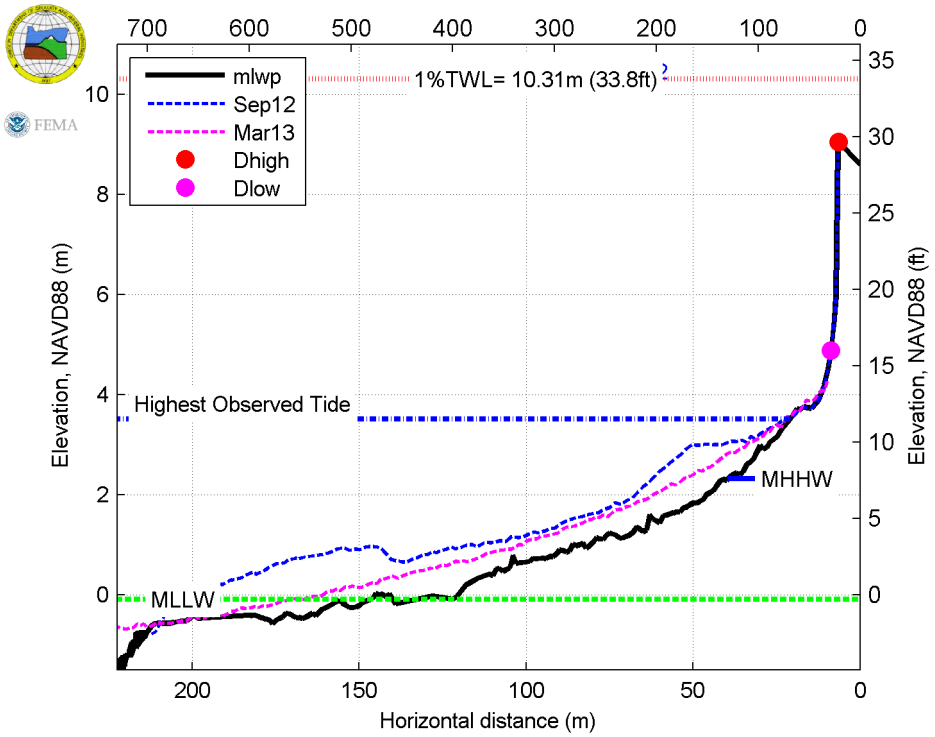

LINC 103

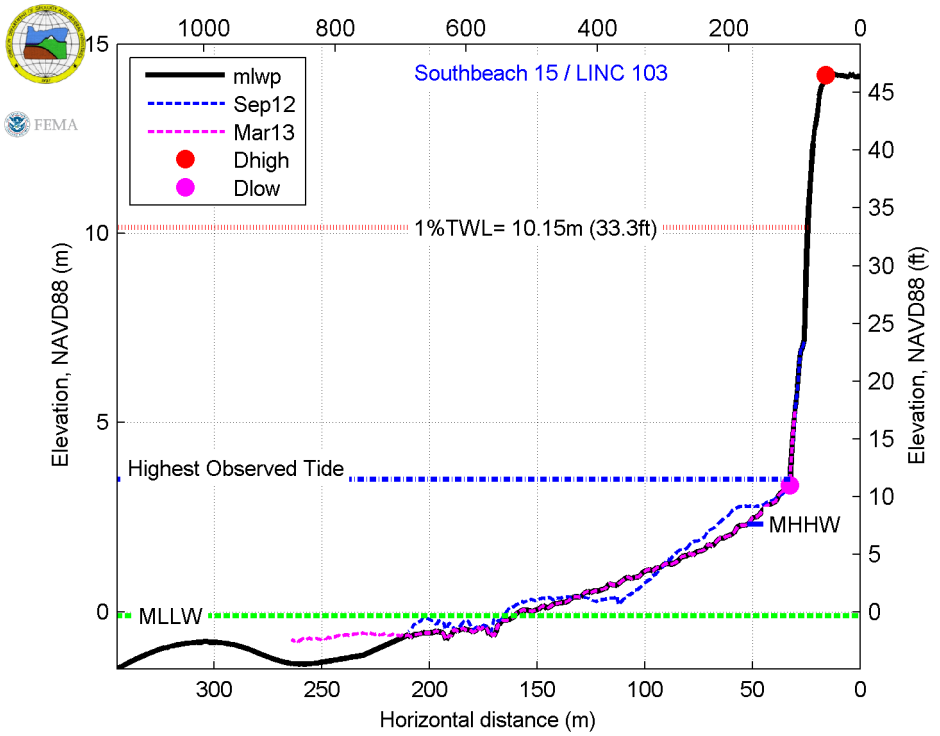

LINC 104

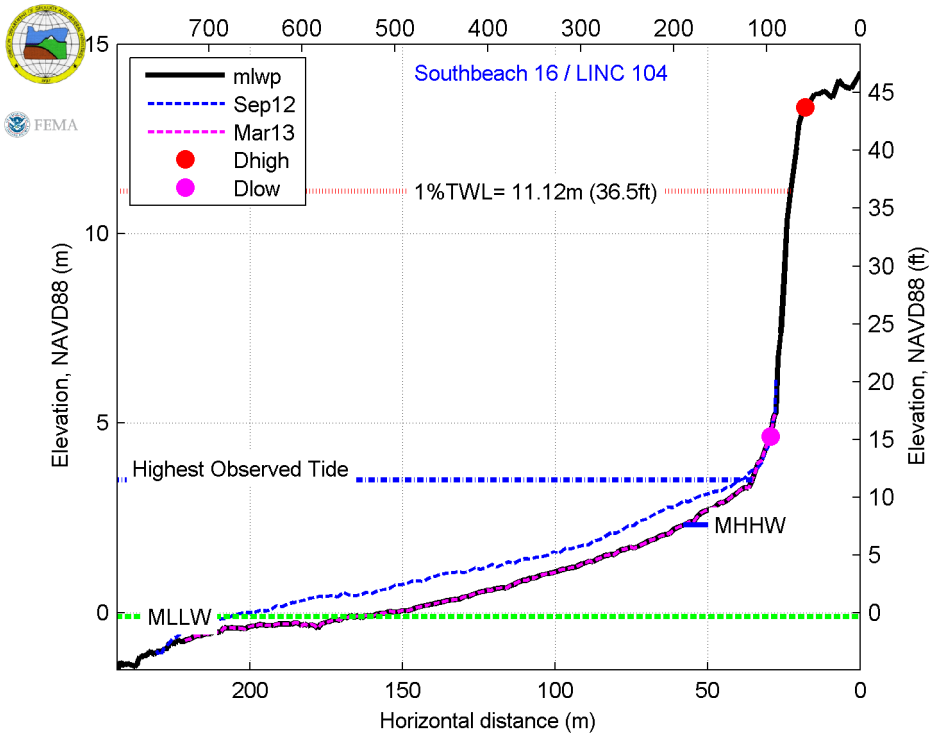

LINC 105

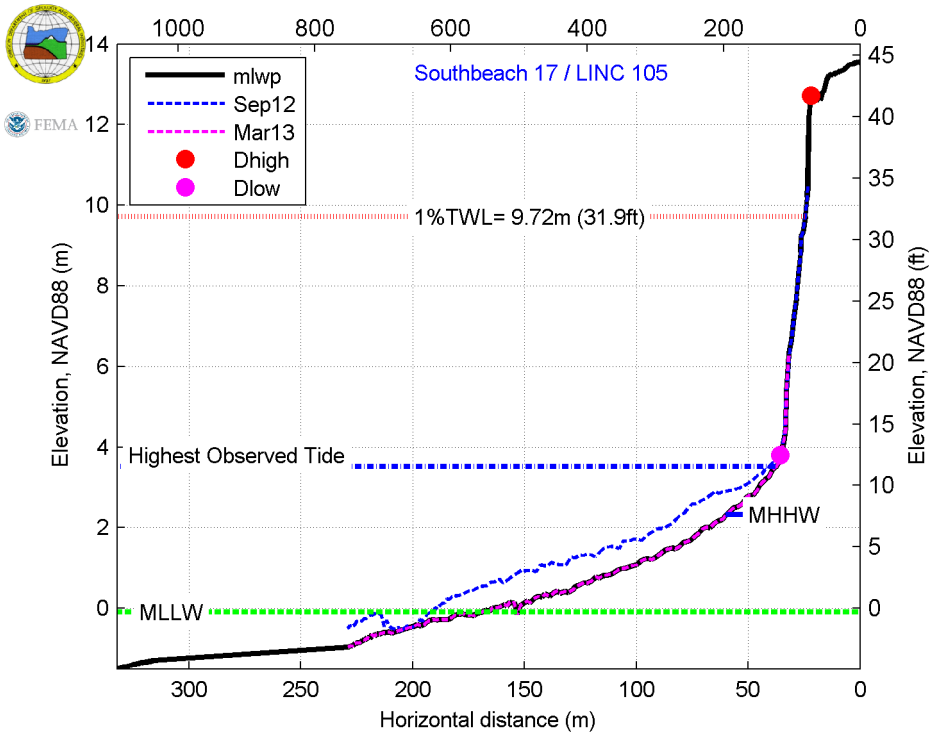

LINC 106

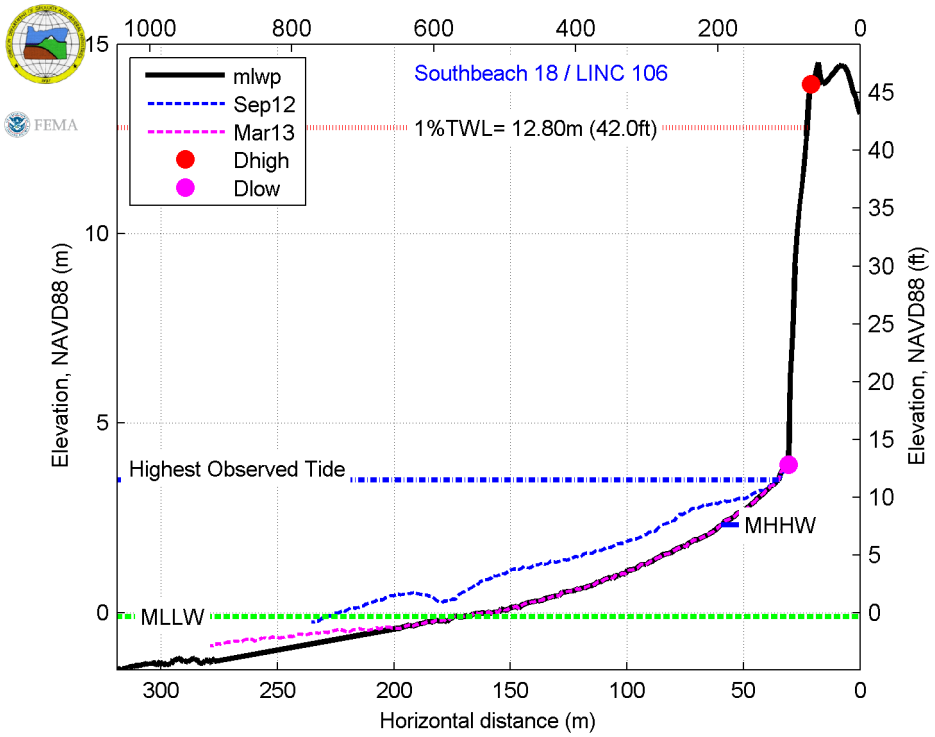

LINC 107

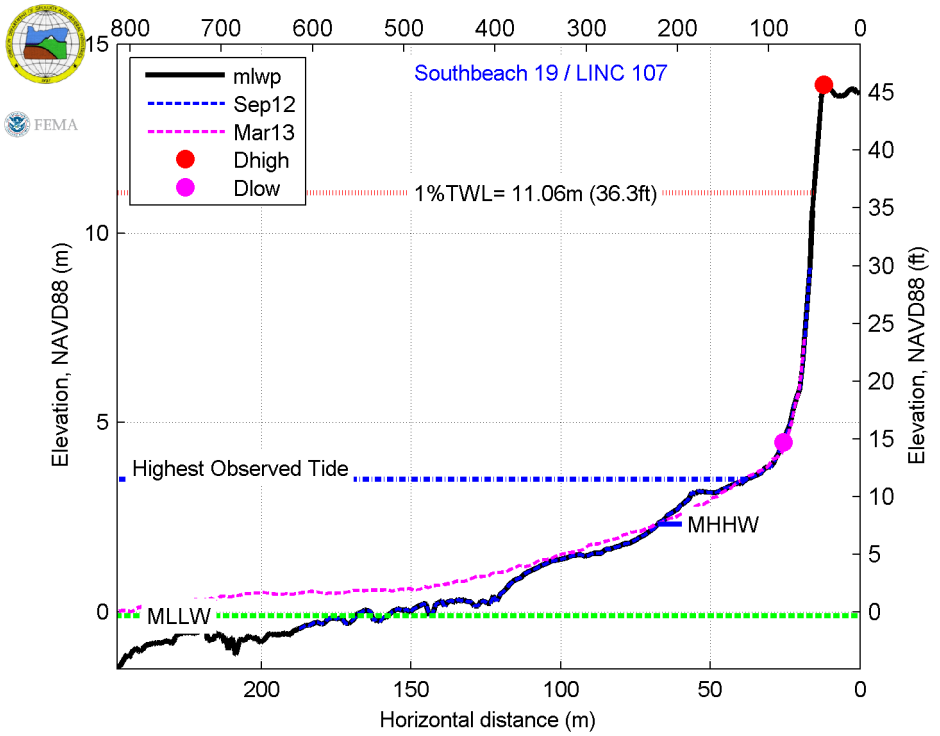

LINC 108

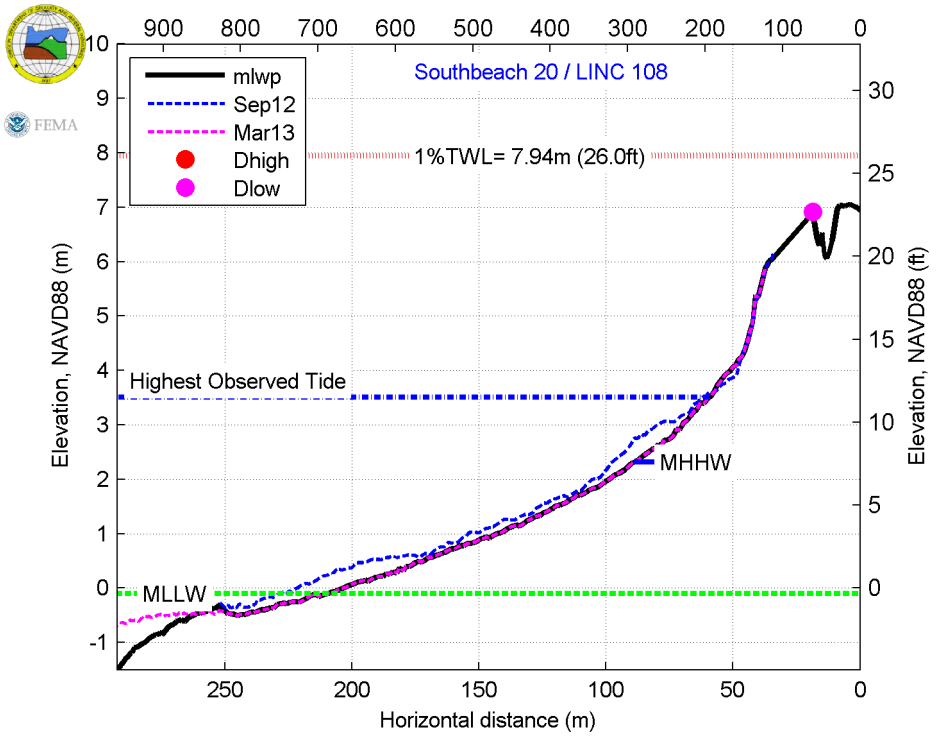

LINC 109

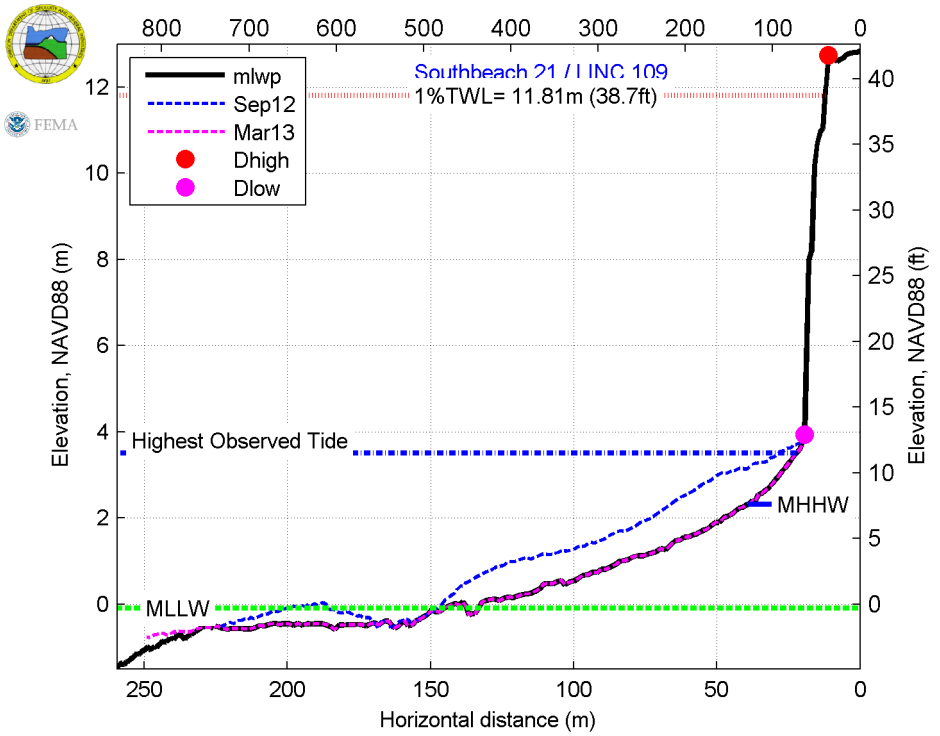

LINC 110

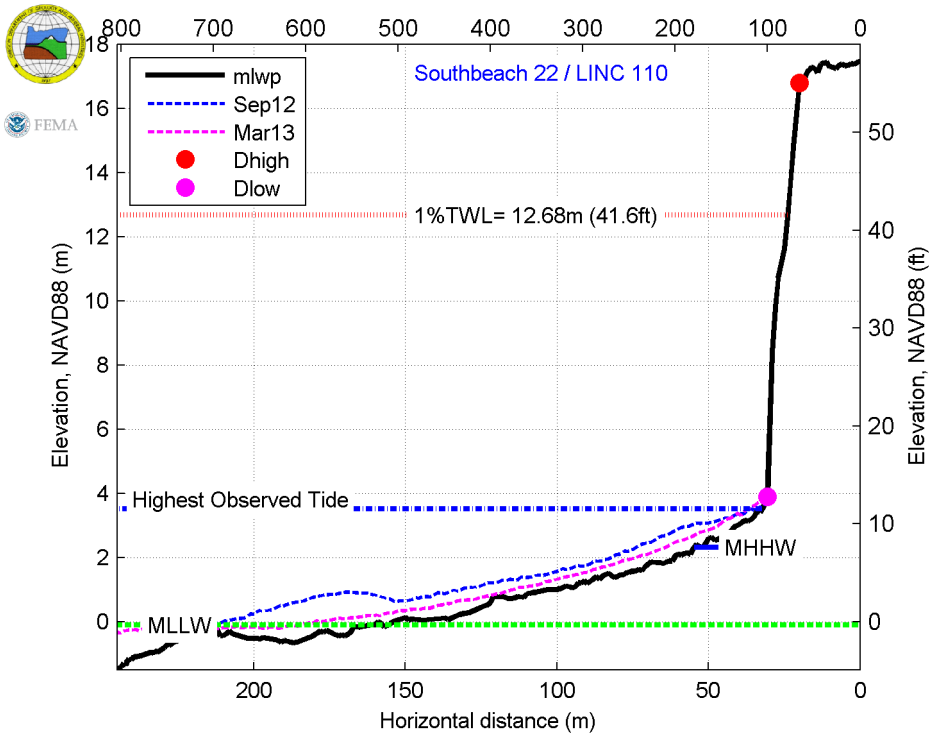

LINC 111

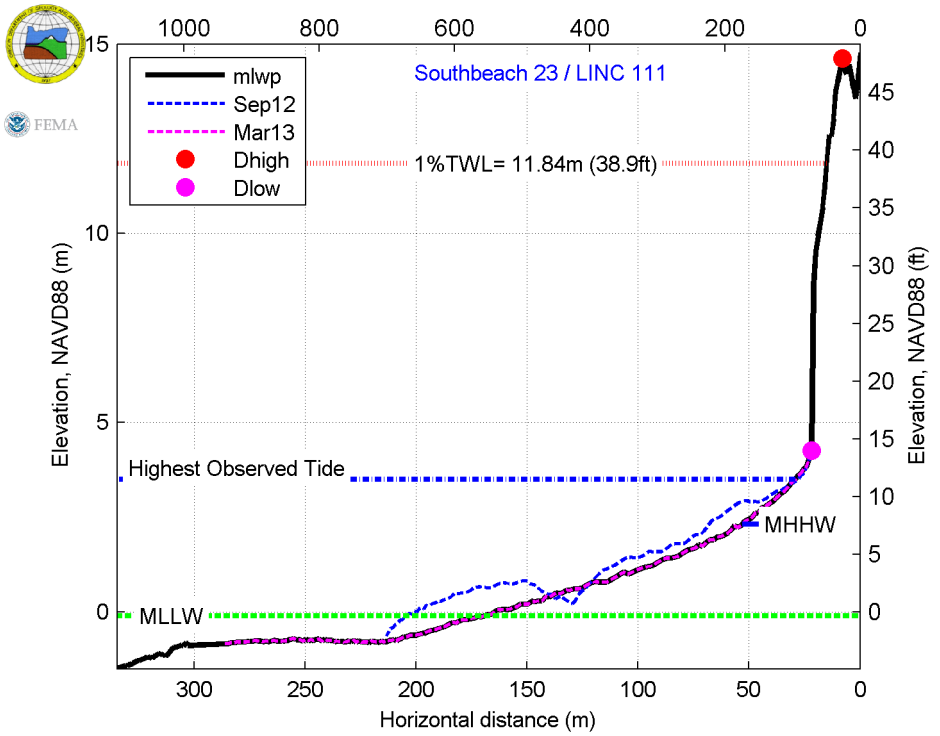

LINC 112

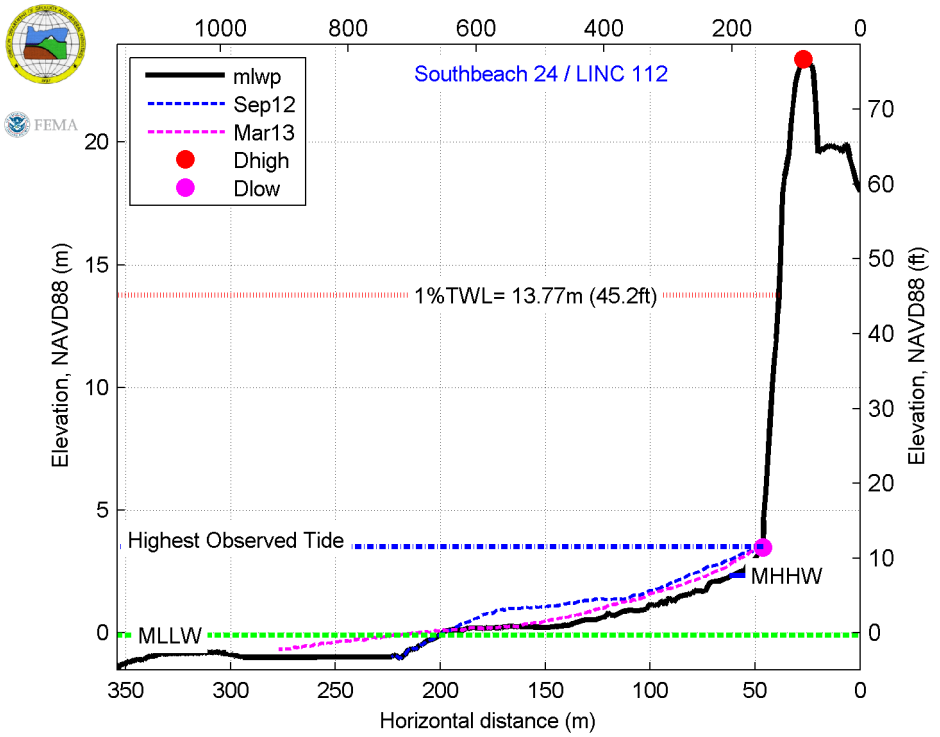

LINC 113

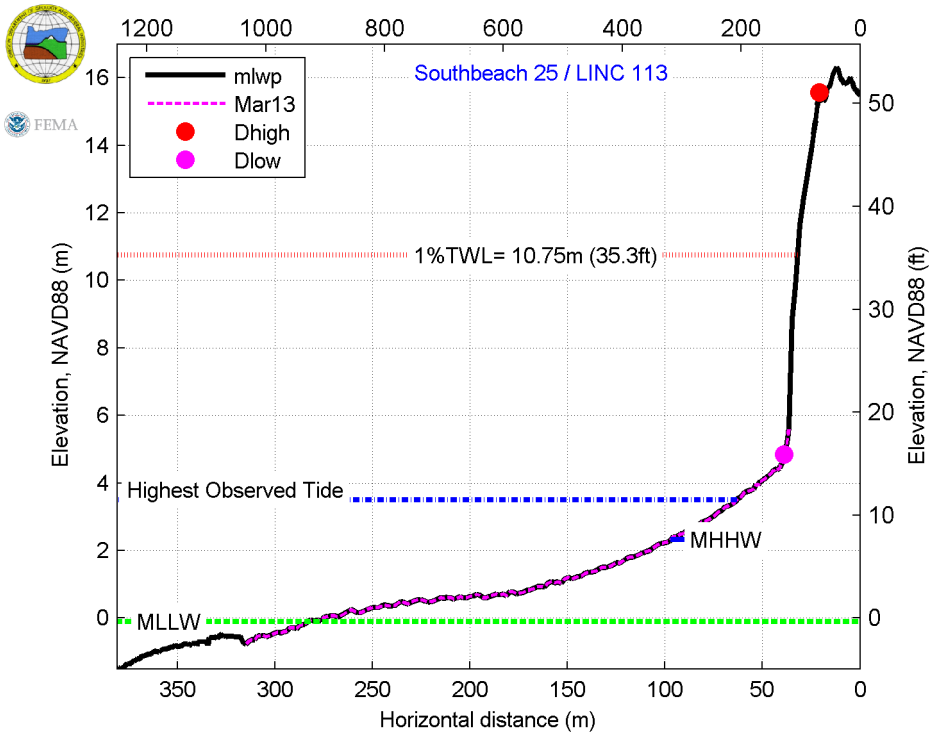

LINC 114

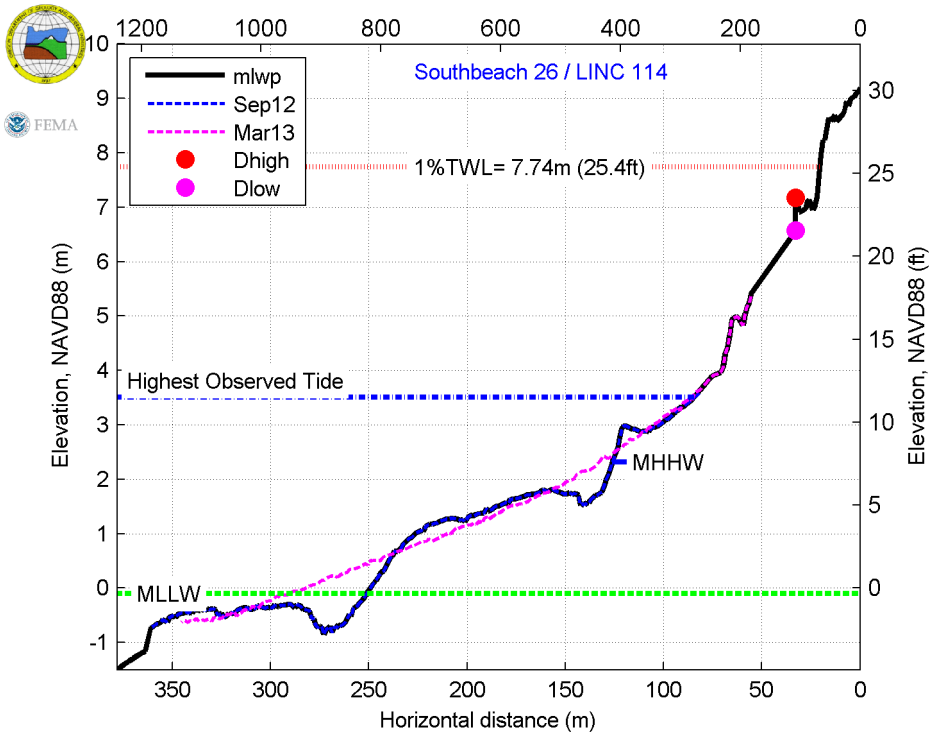

LINC 115

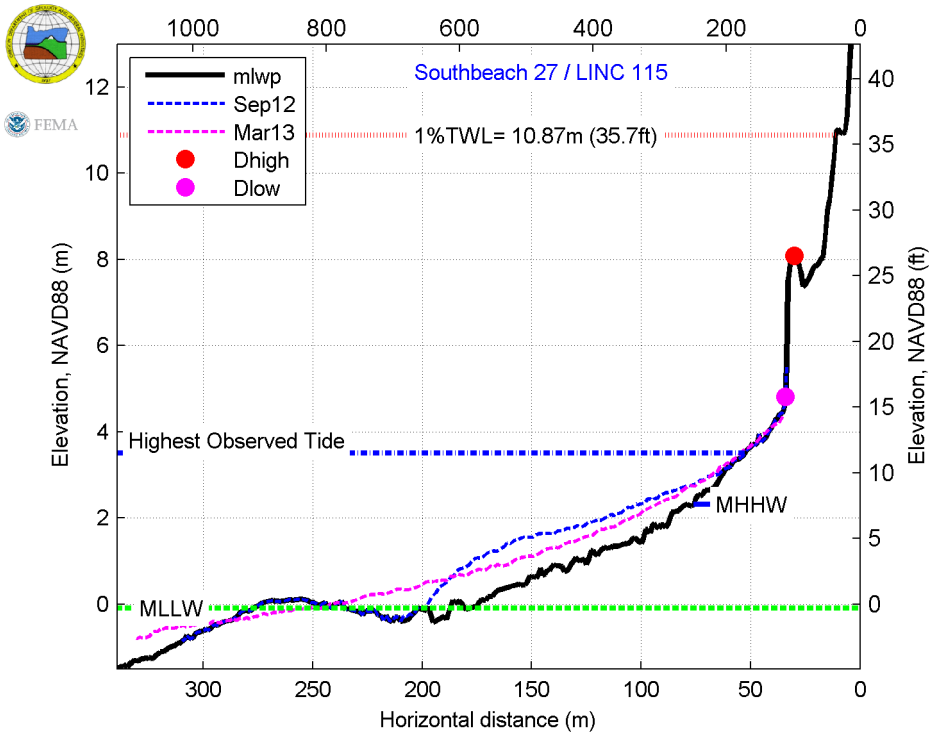

LINC 116

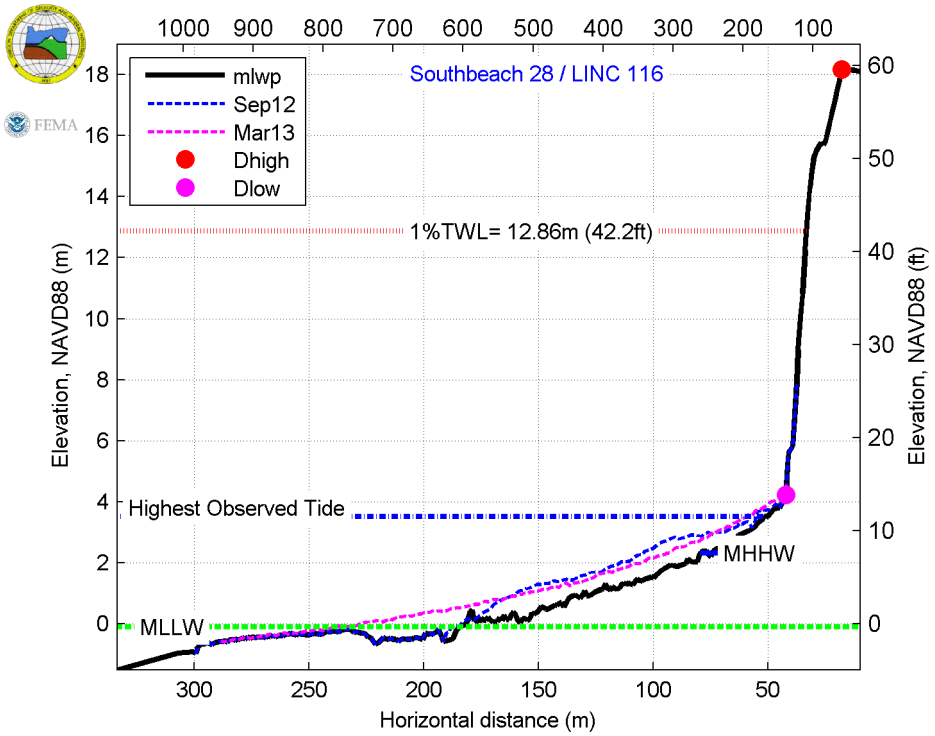

LINC 117

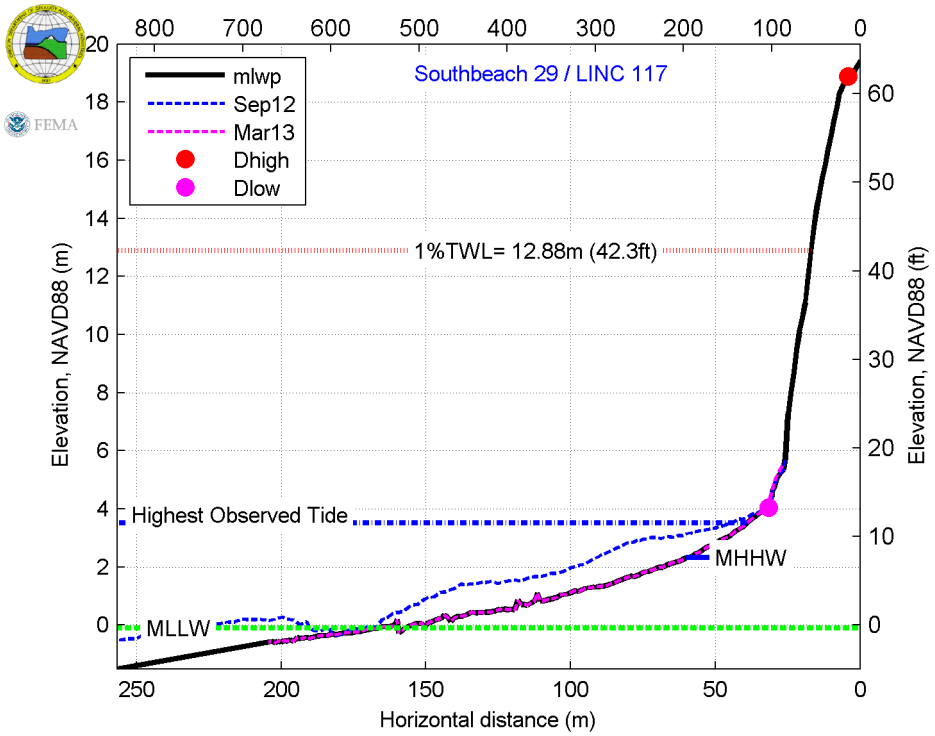

LINC 118

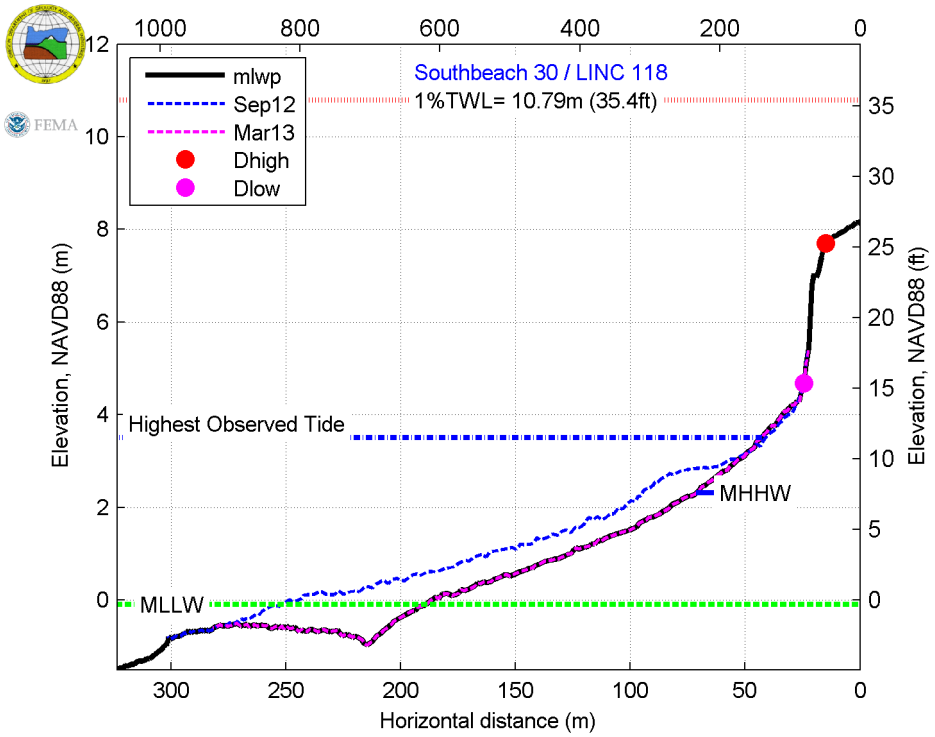

LINC 119

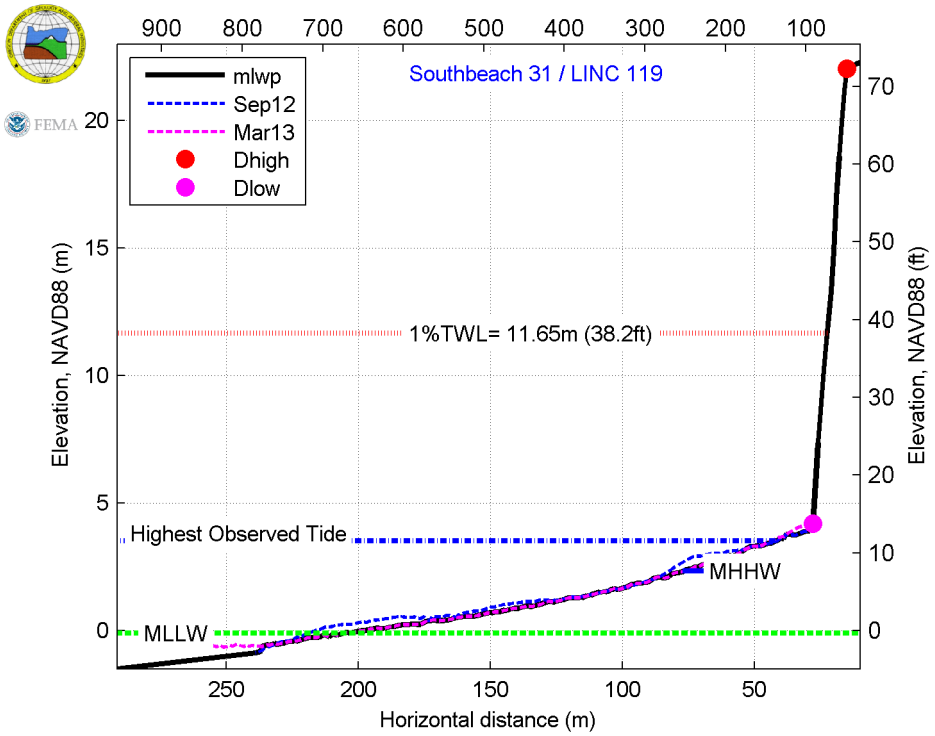

LINC 120

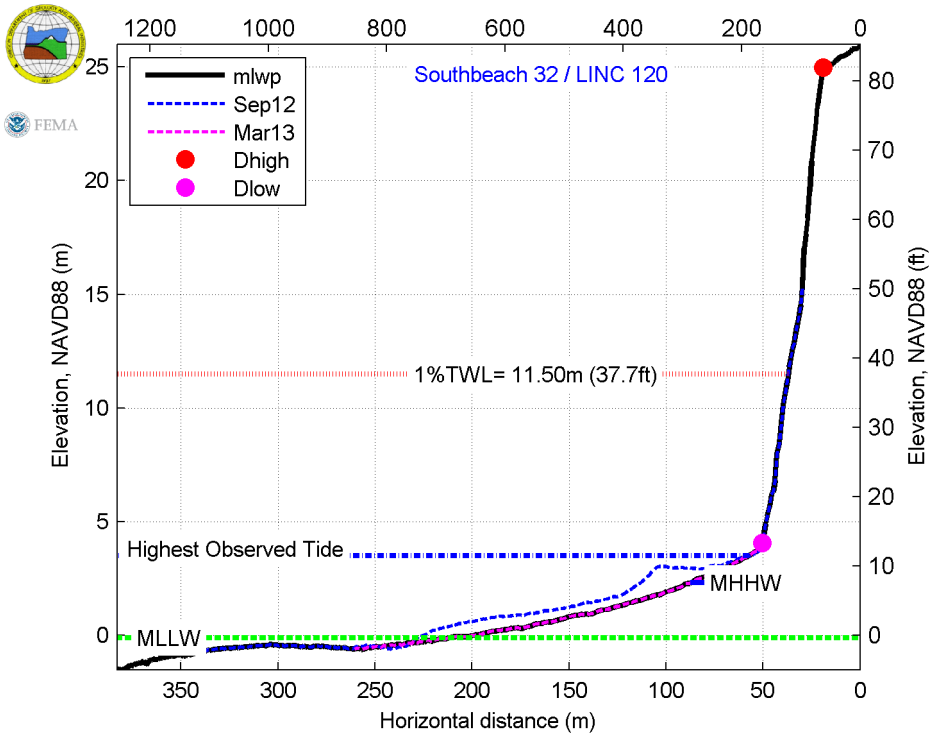

LINC 121

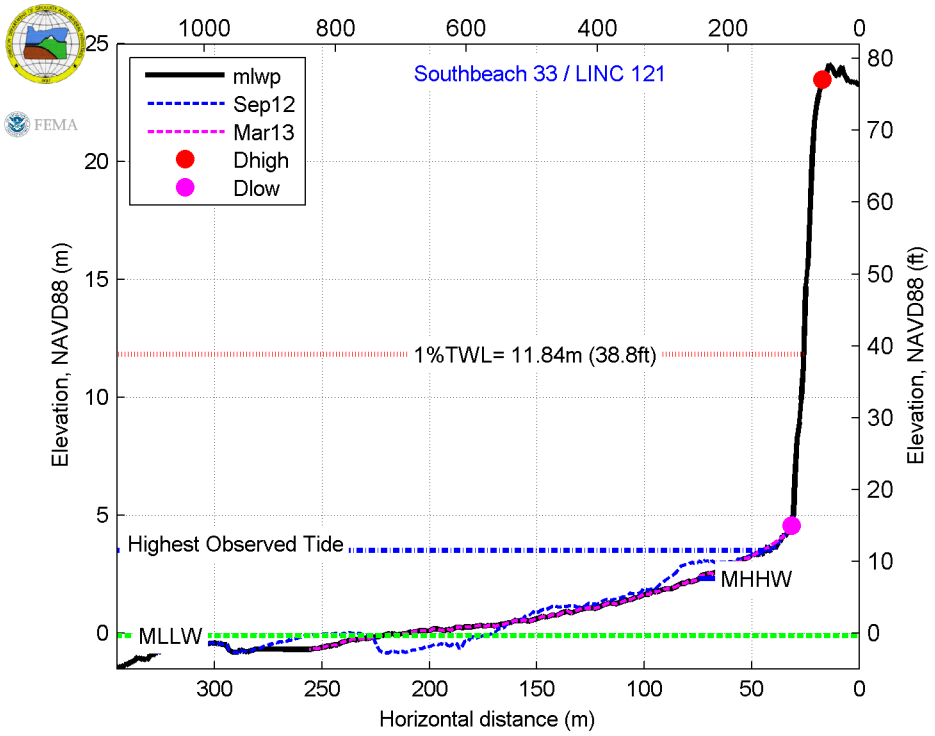

LINC 122

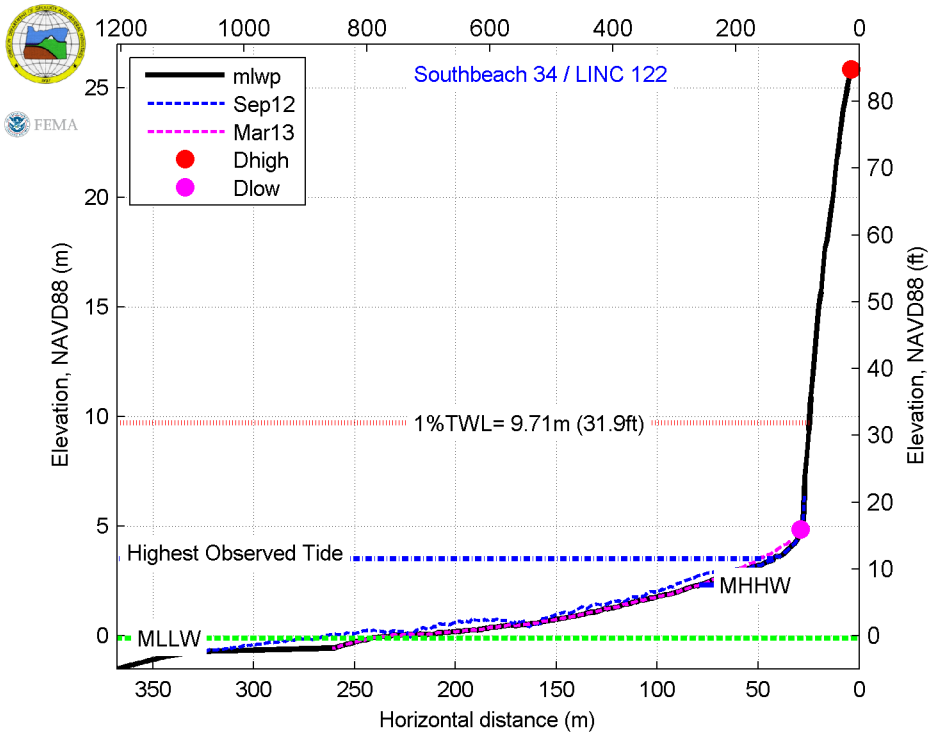

LINC 123

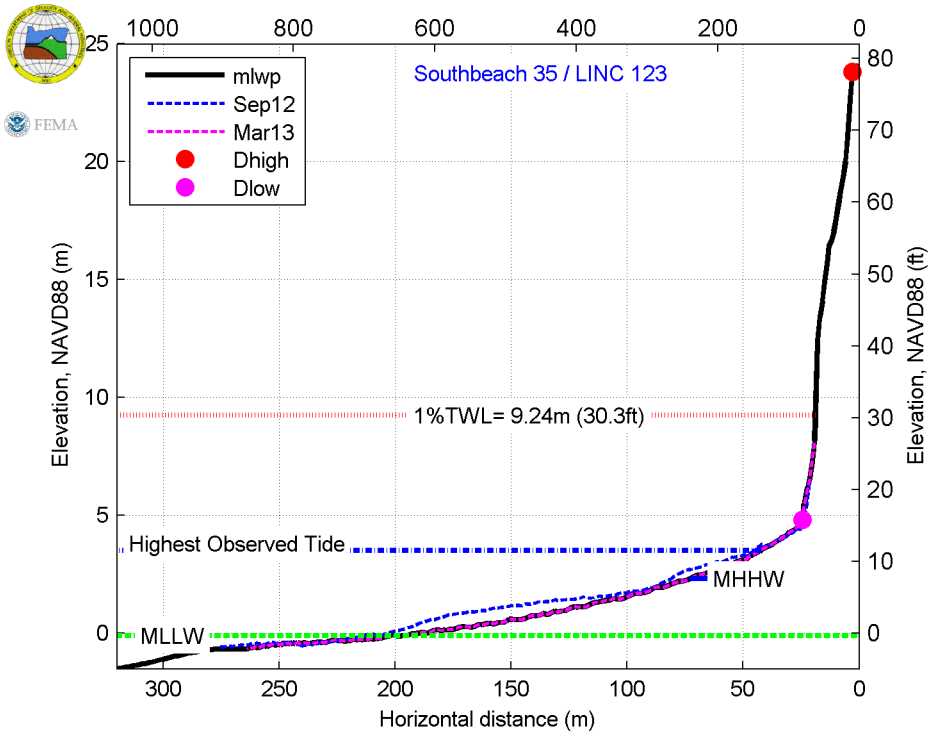

LINC 124

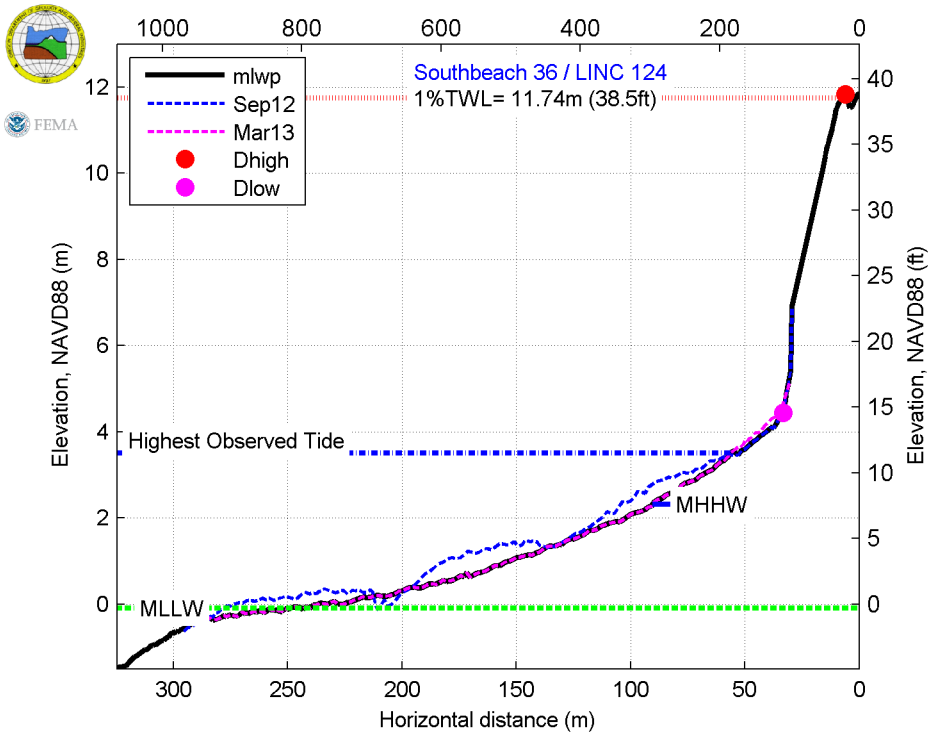

LINC 125

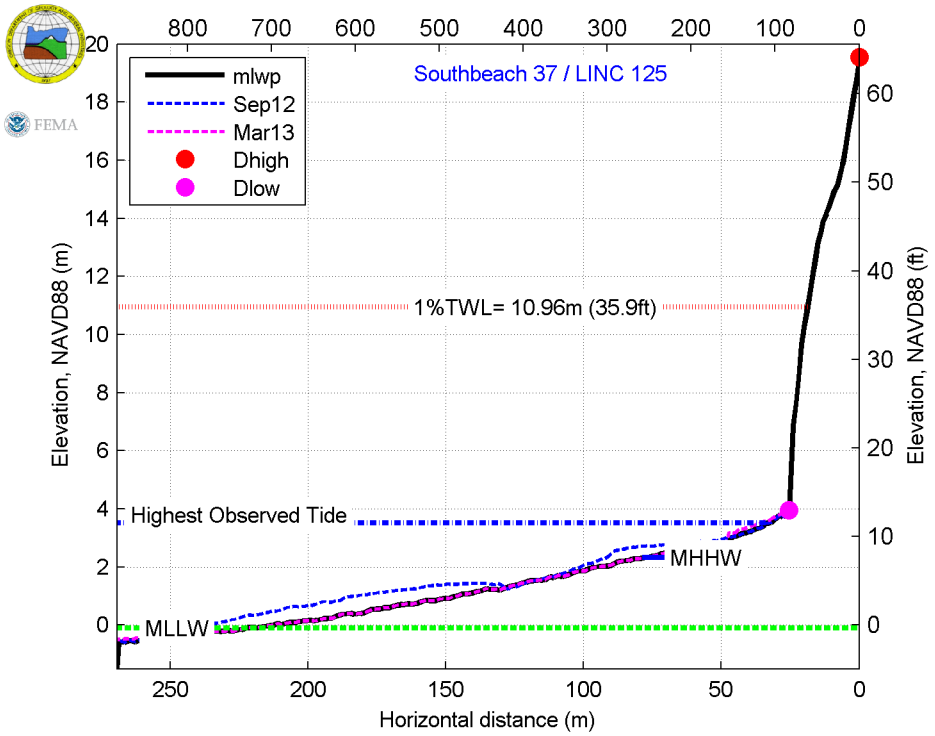

LINC 126

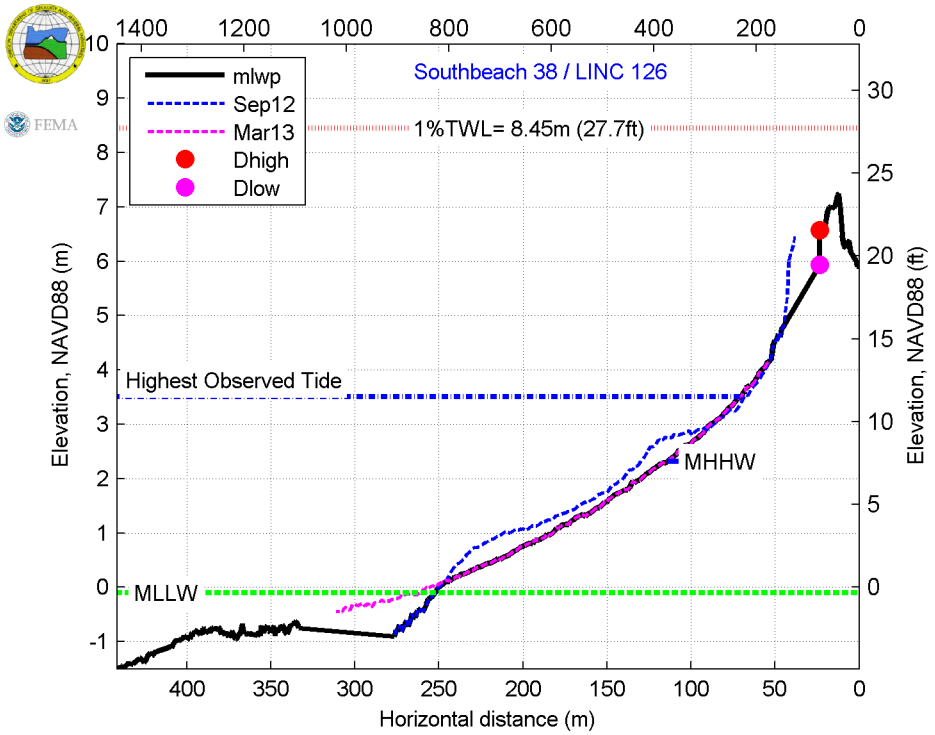

LINC 127

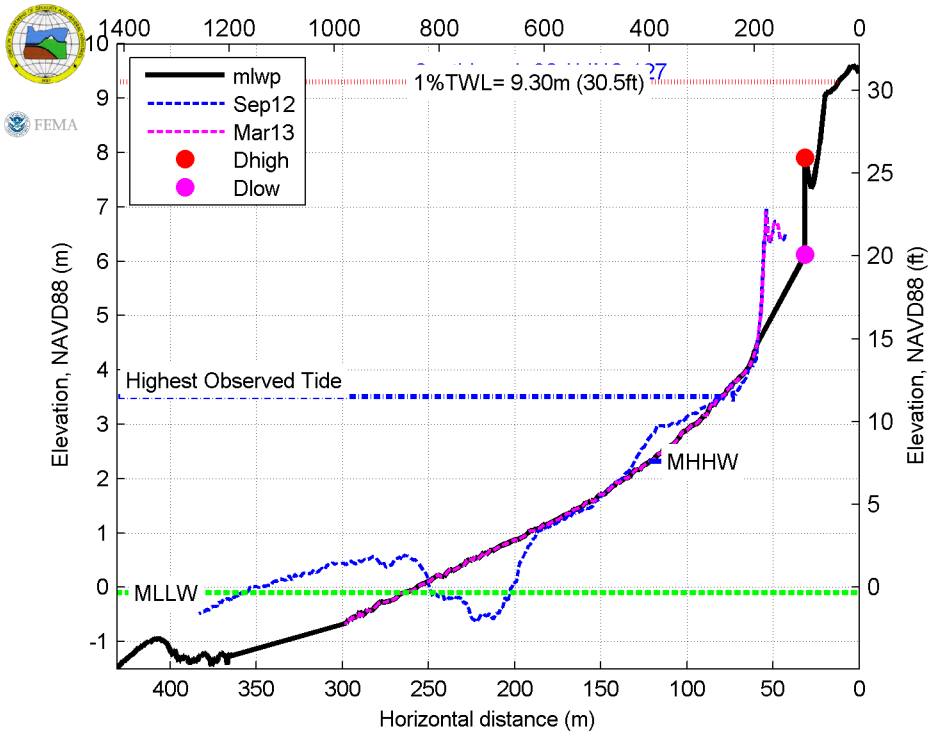

LINC 128

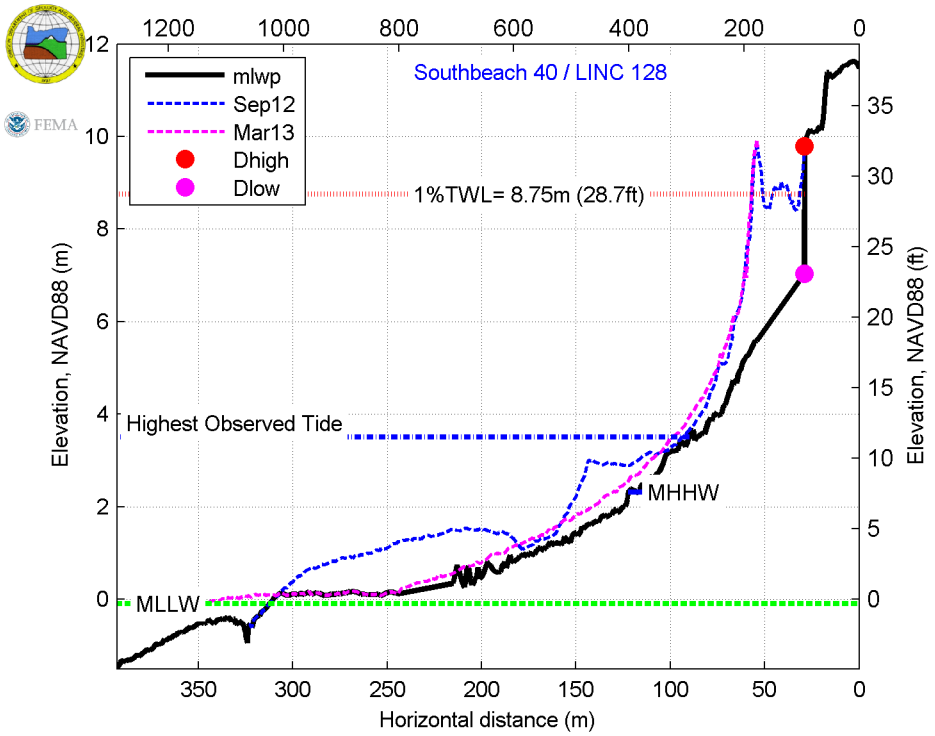

LINC 129

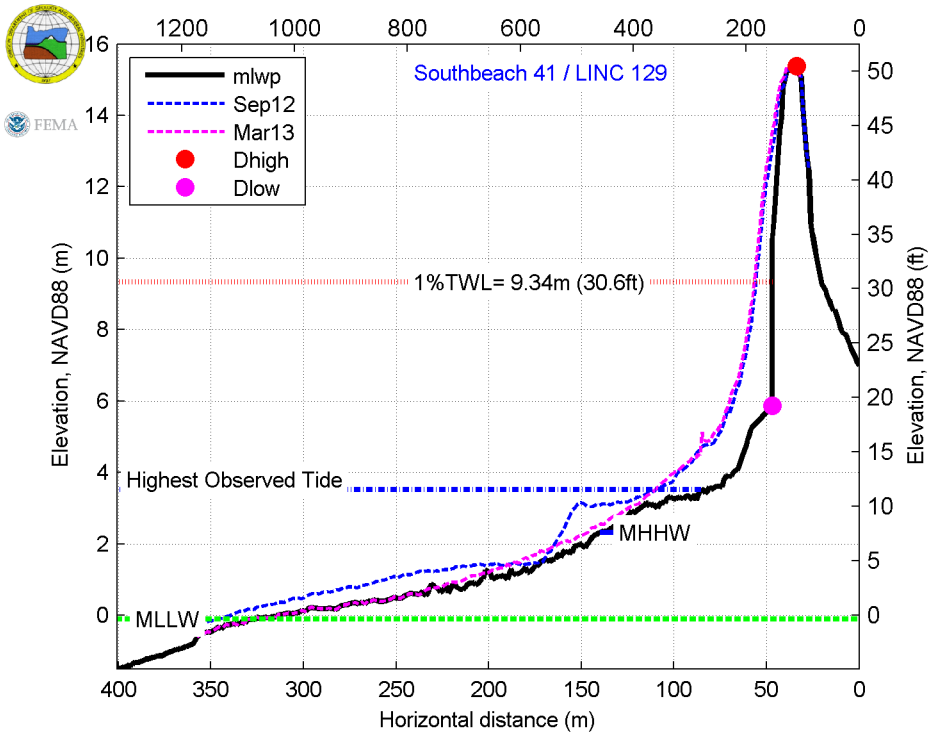

LINC 130

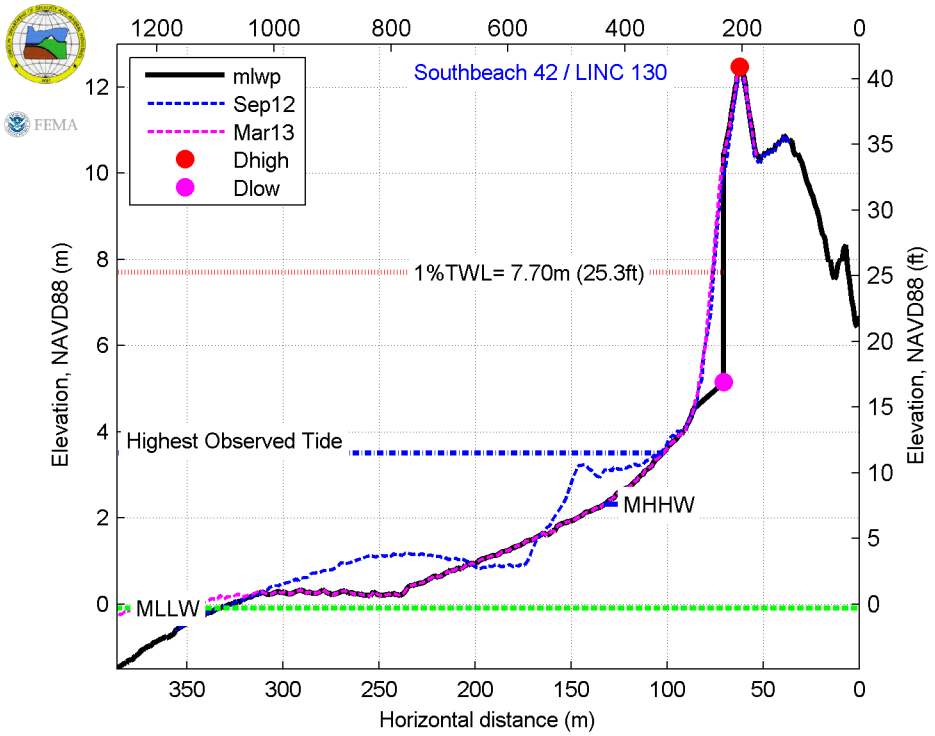

11.2.6 Newport

LINC 131

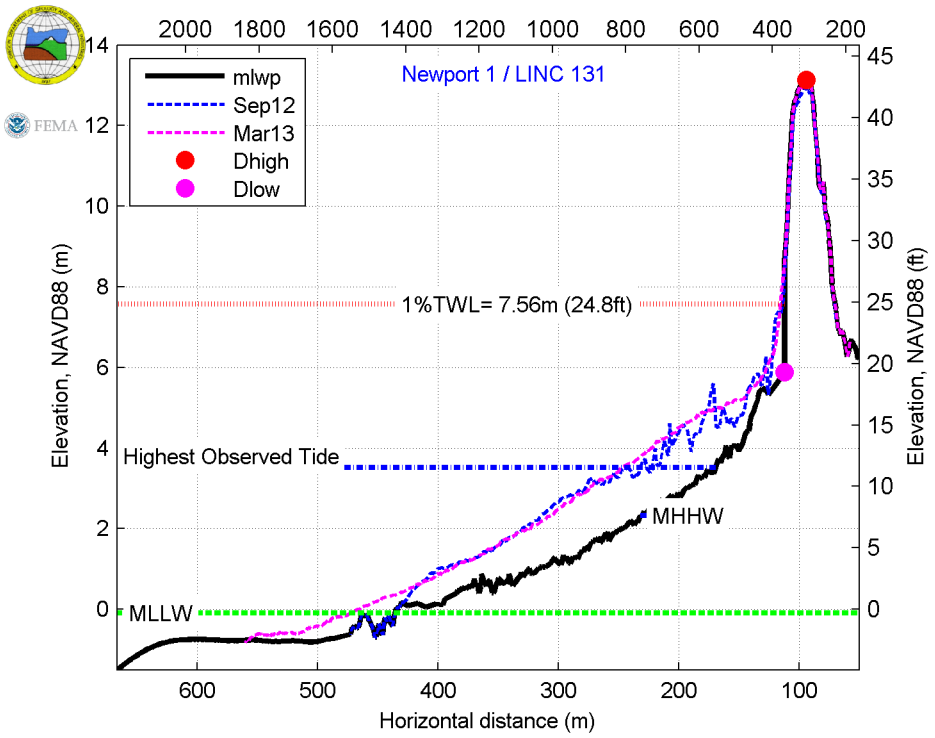

LINC 132

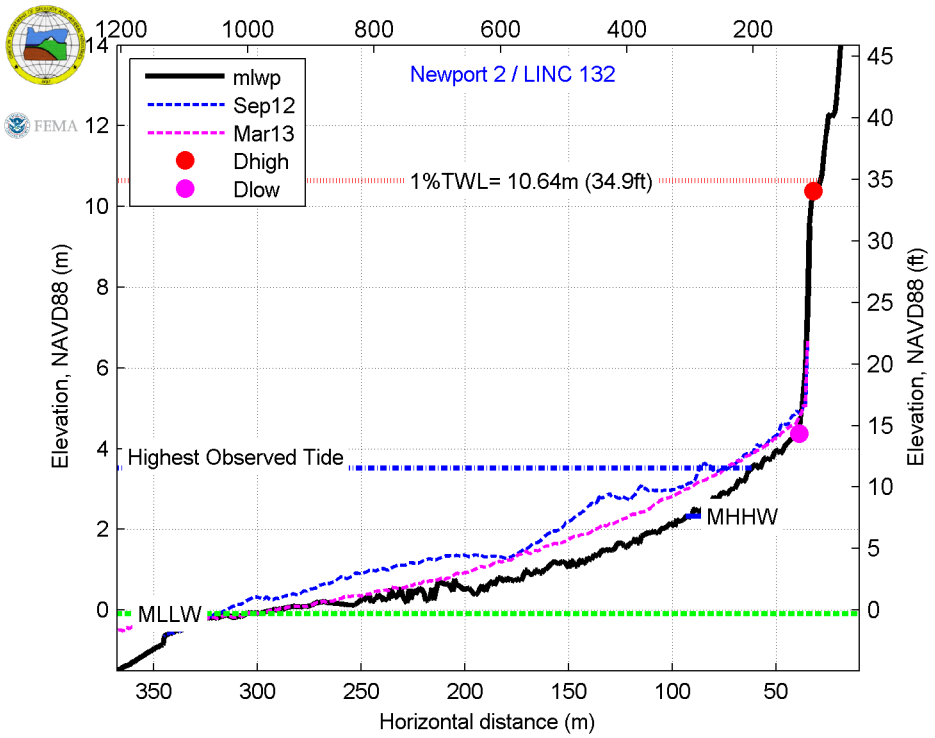

LINC 133

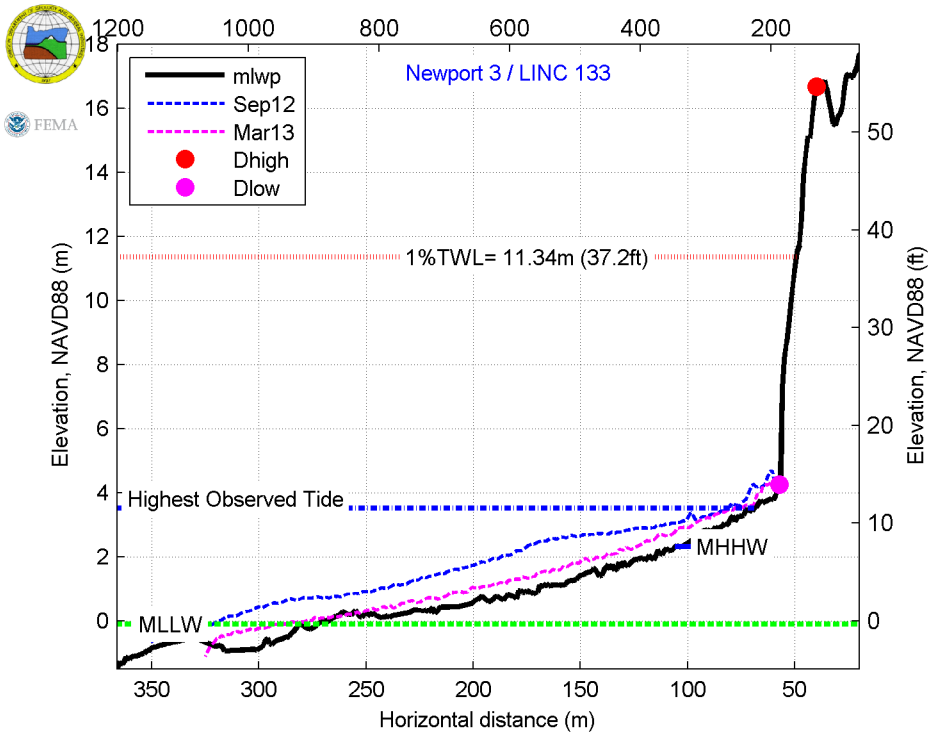

LINC 134

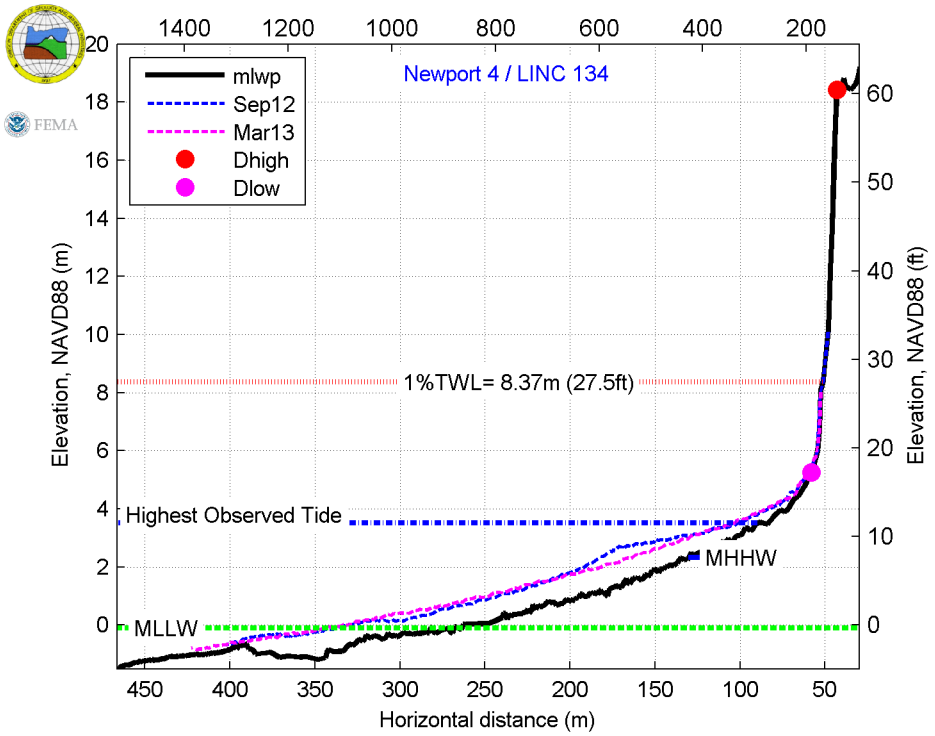

LINC 135

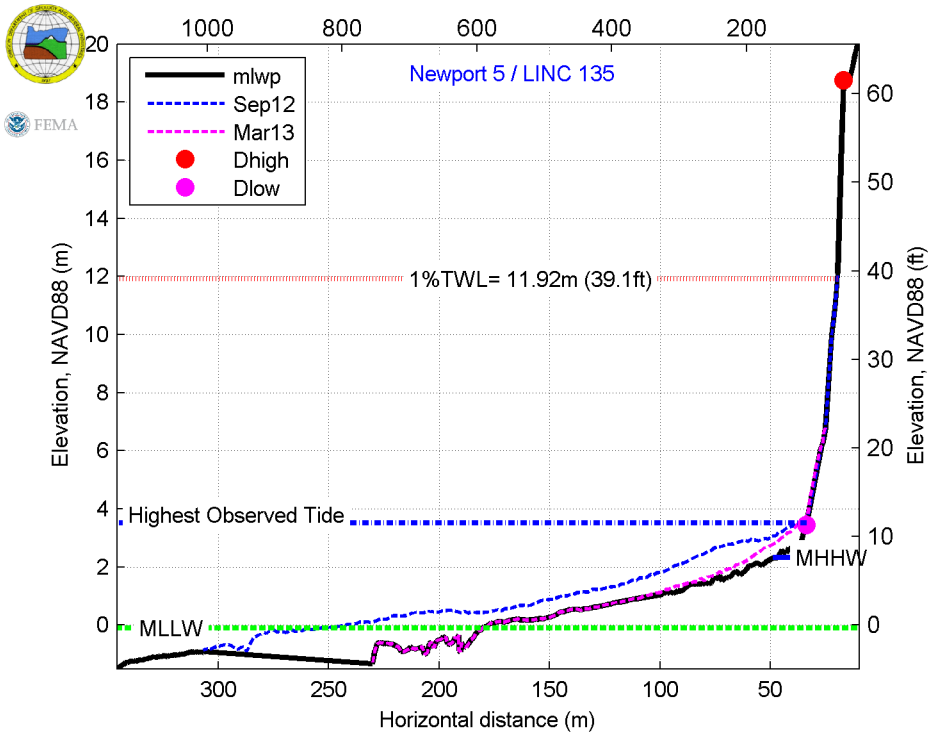

LINC 136

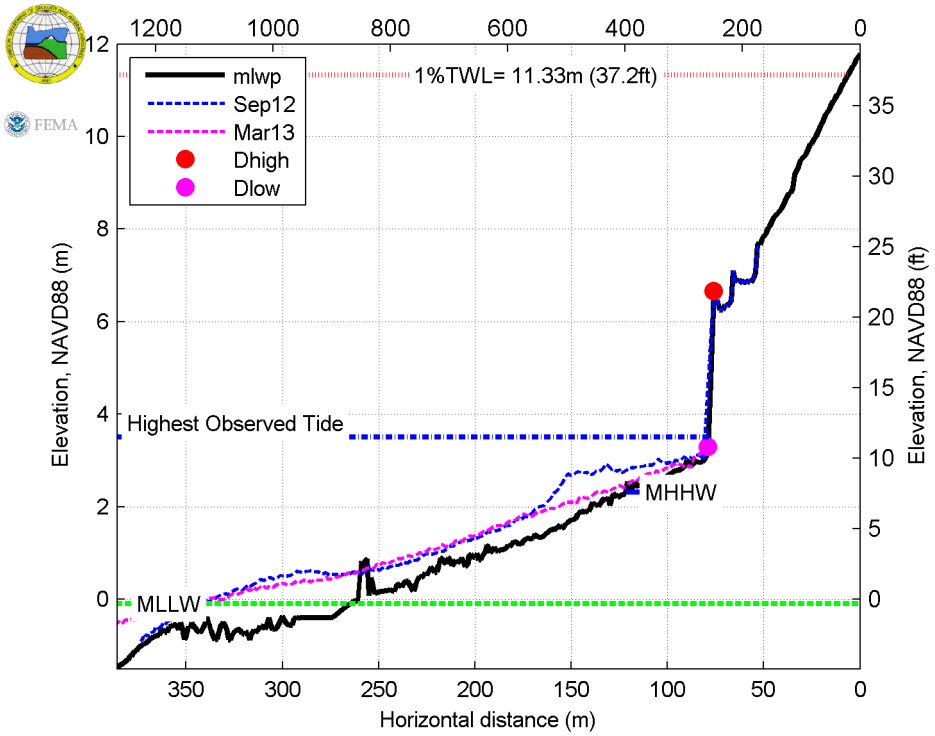

LINC 137

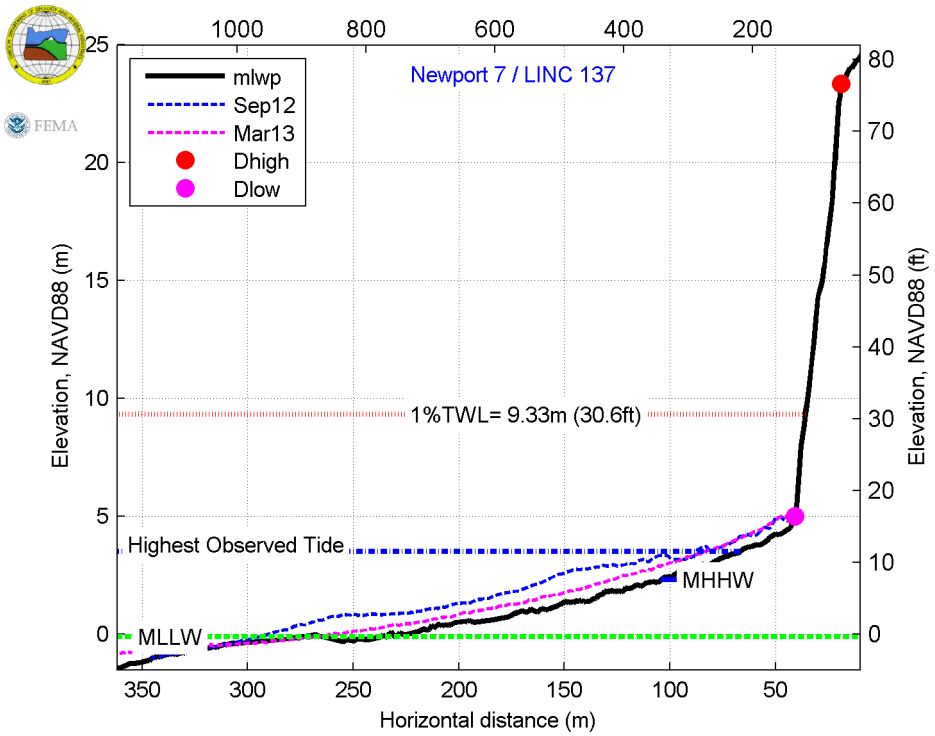

LINC 138

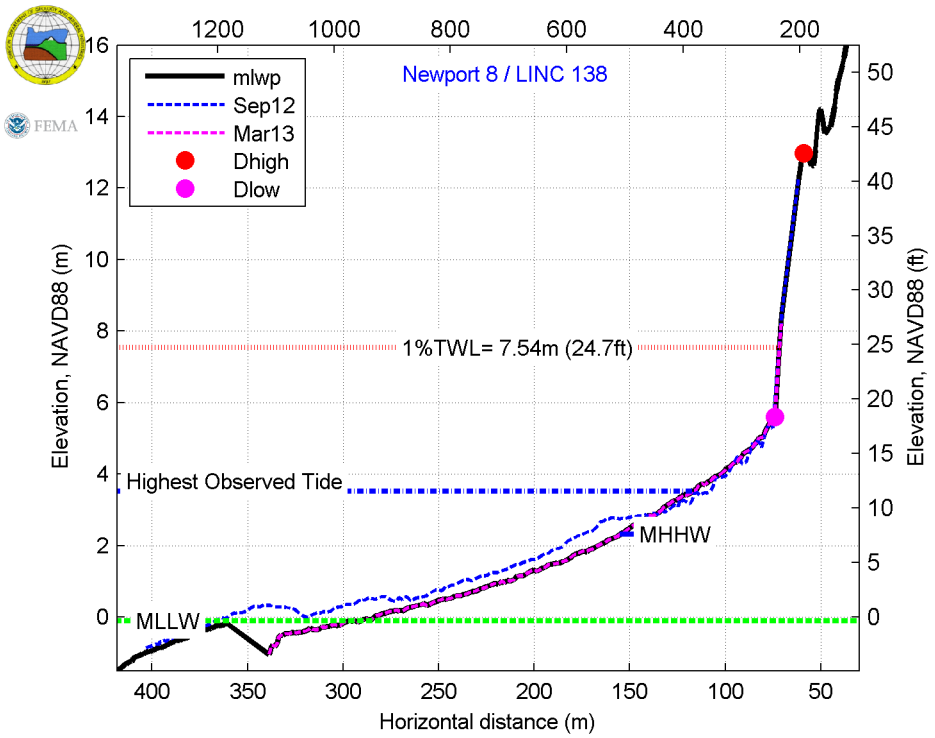

LINC 139

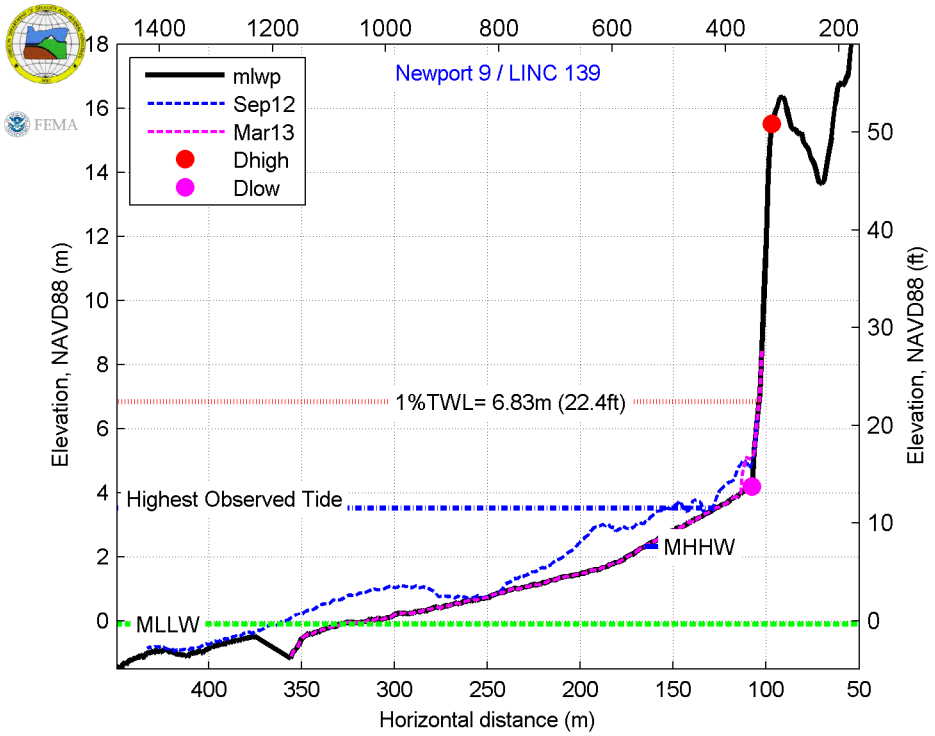

LINC 140

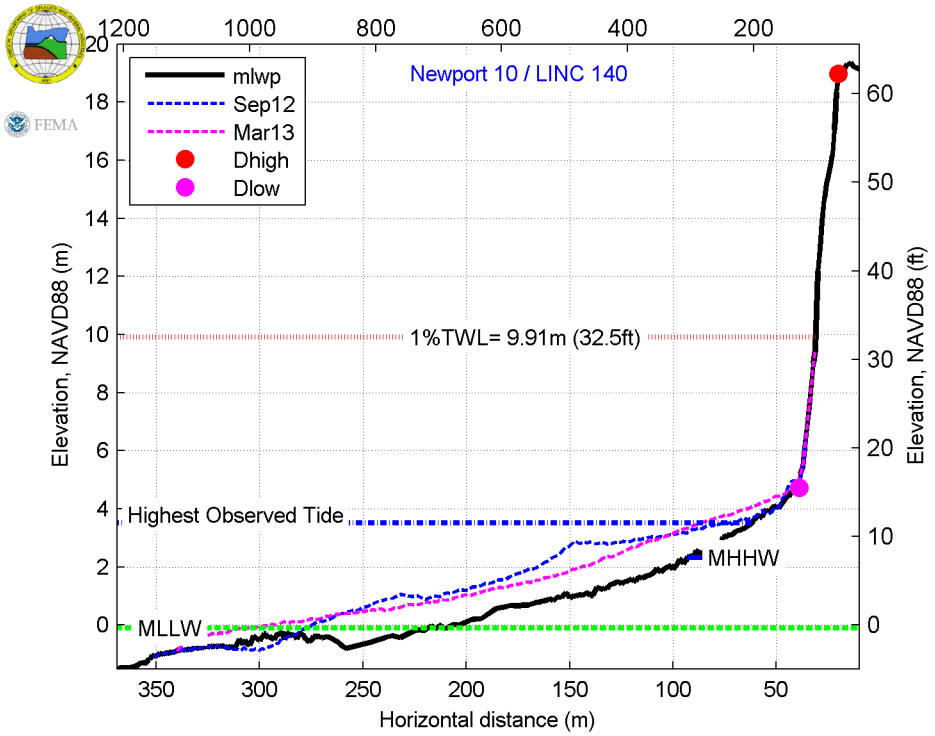

LINC 141

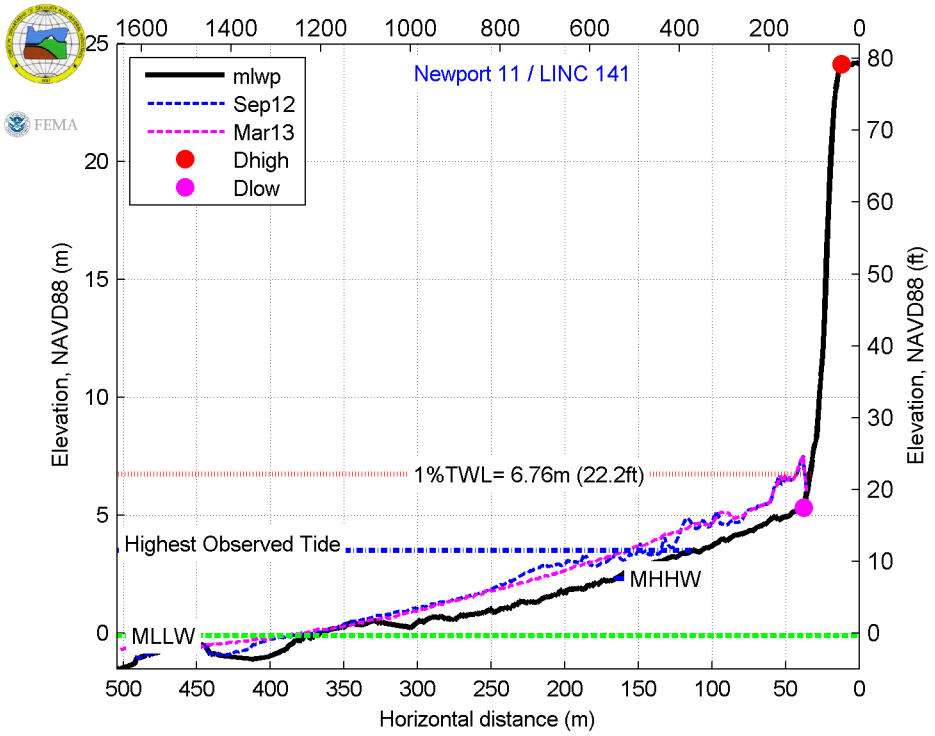

LINC 142

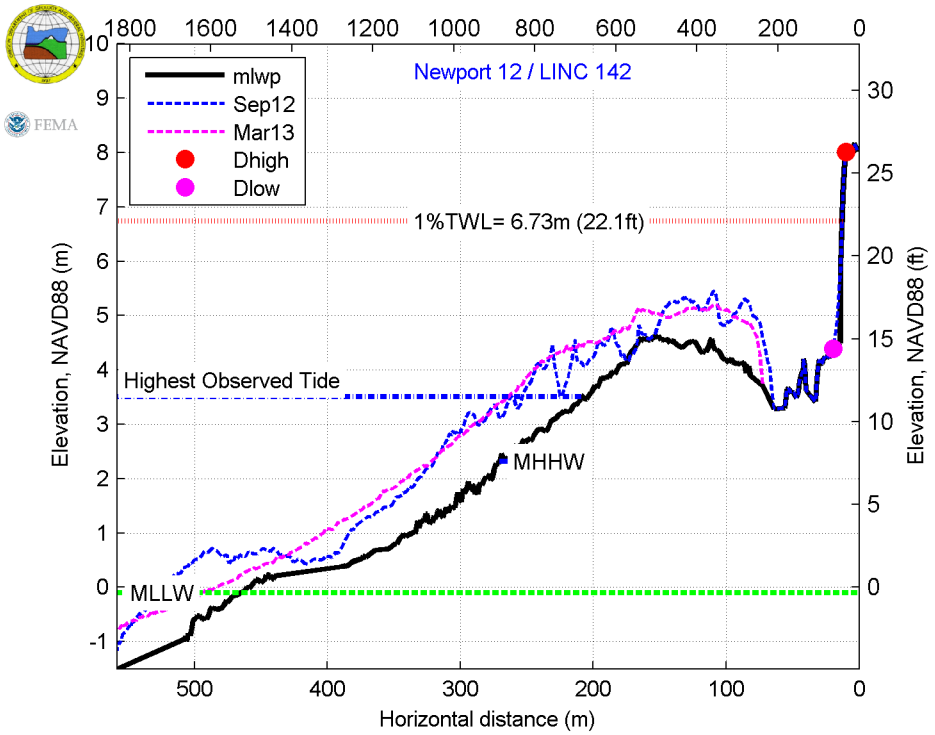

LINC 143

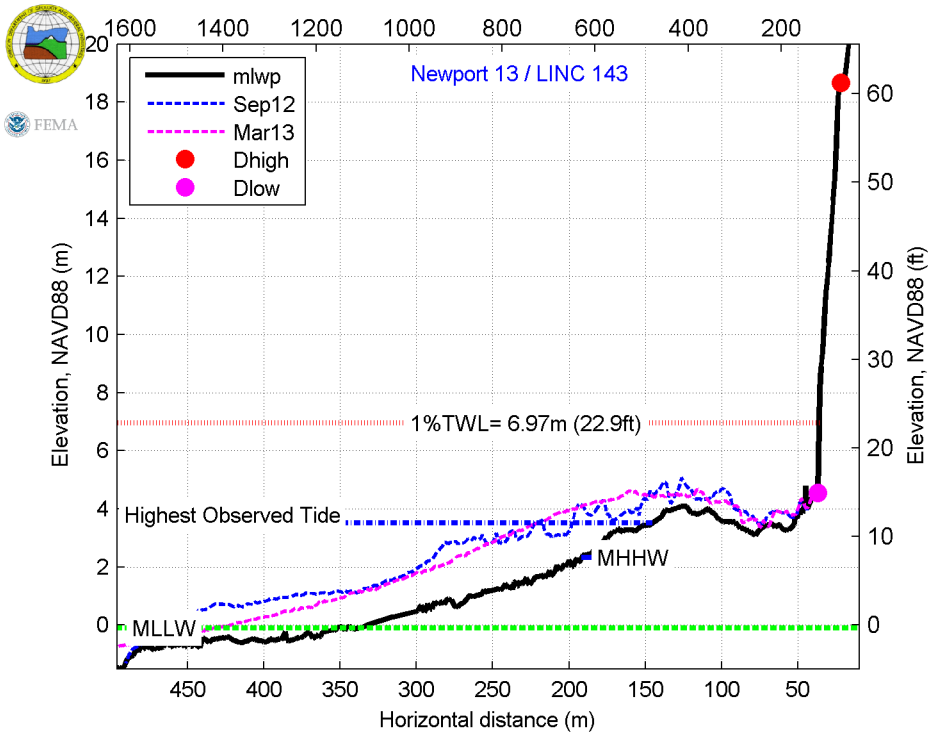

LINC 144

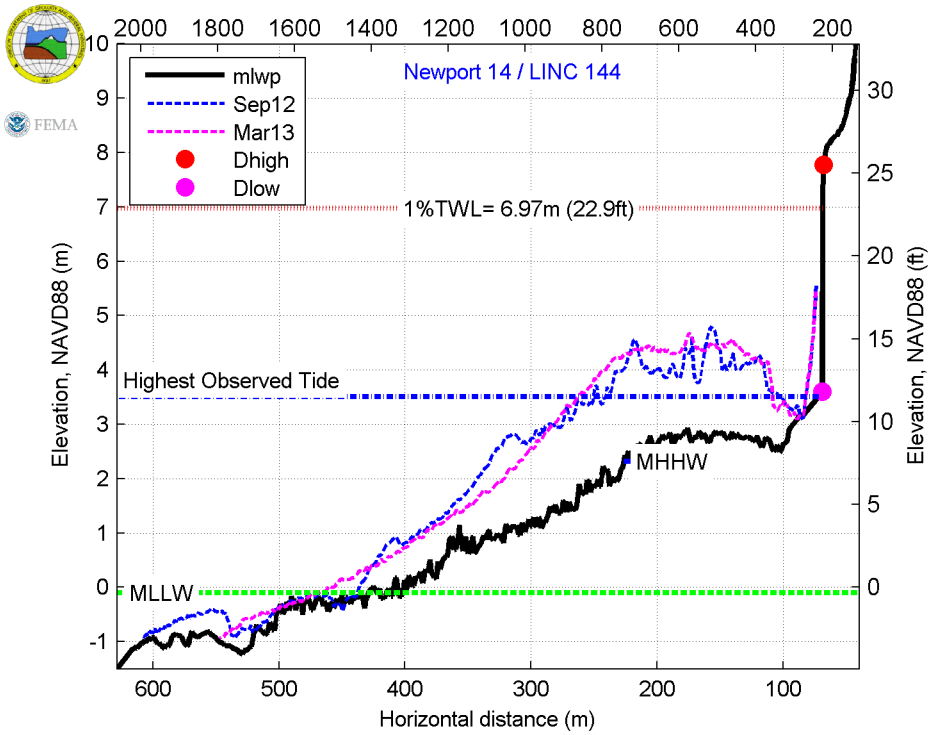

LINC 145

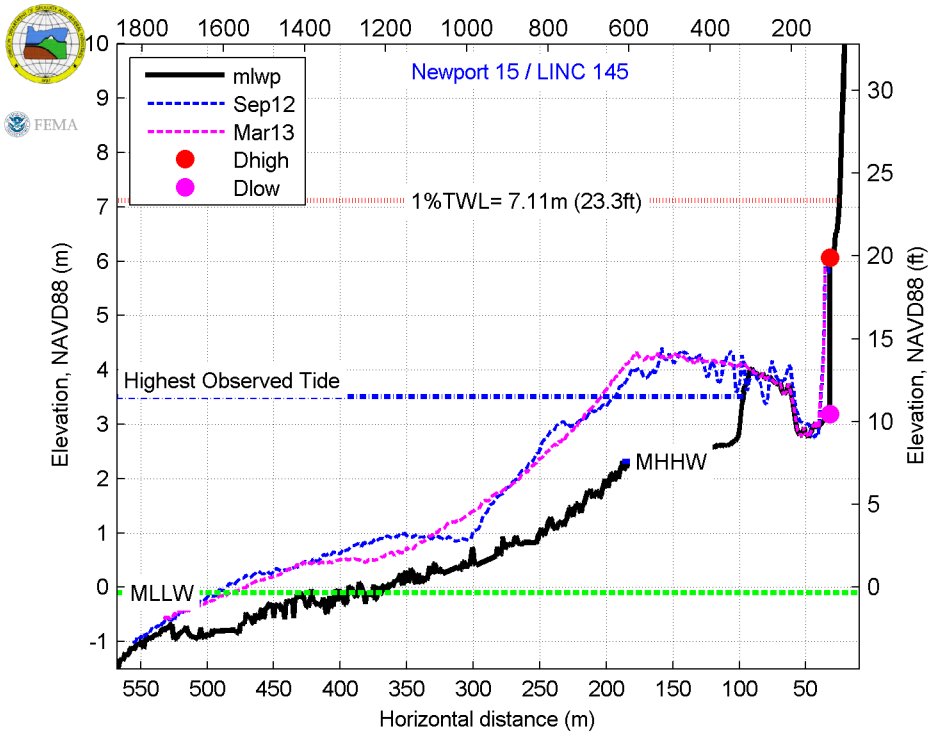

LINC 146

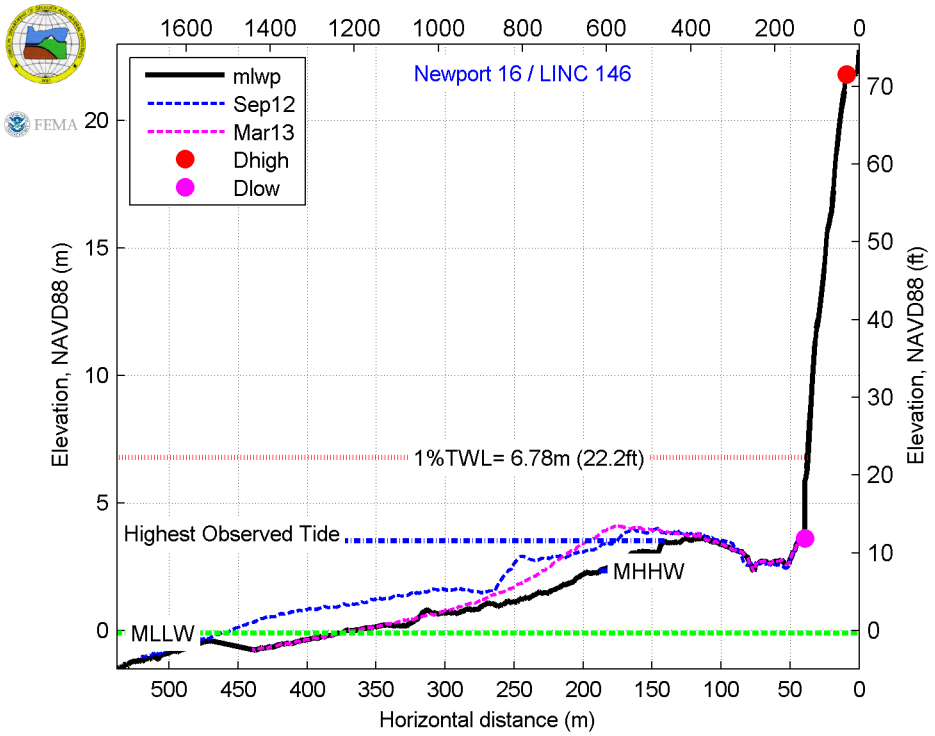

LINC 147

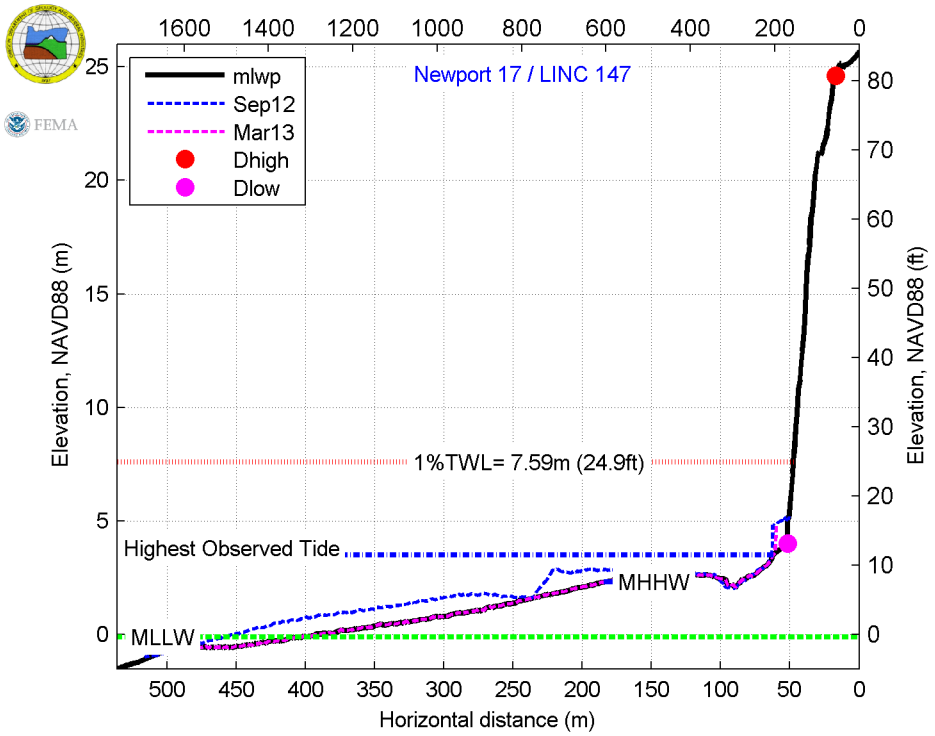
Newport 17 / LINC 147
mlwp
Sep12
Mar13
Dhigh
Dlow
1%TWL= 7.59m (24.9ft)
Highest Observed Tide
MHHW
MLLW
Elevation, NAVD88 (m)
Elevation, NAVD88 (ft)
Horizontal distance (m)
1600 1400 1200 1000 800 600 400 200 0
500 450 400 350 300 250 200 150 100 50 0
0 5 10 15 20 25
0 10 20 30 40 50 60 70 80

11.2.7 Yaquina Head

LINC 148

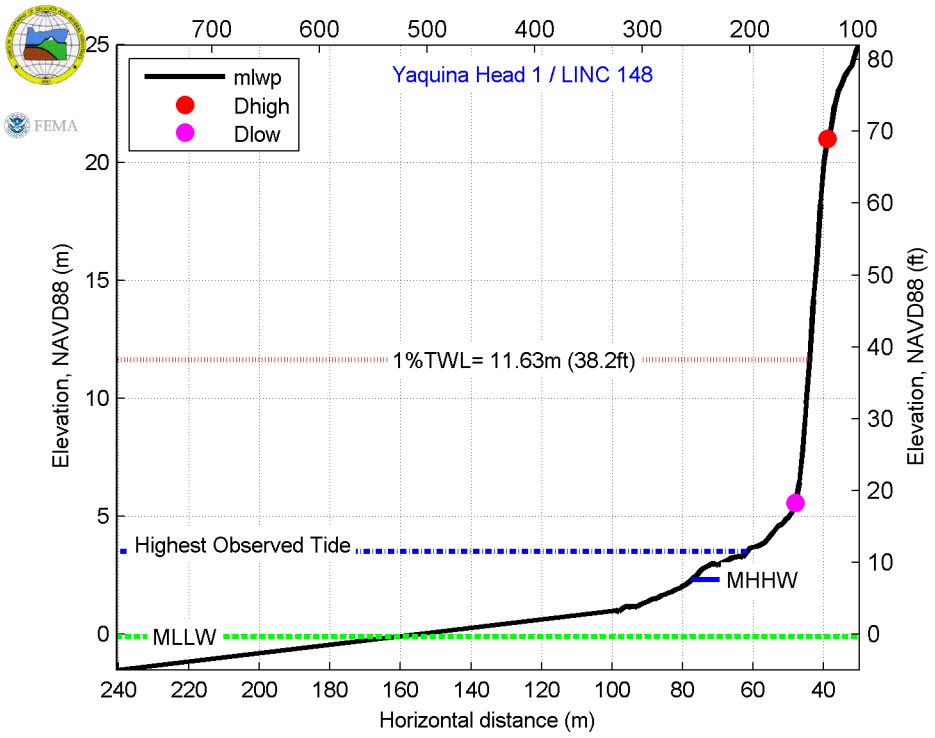

LINC 149

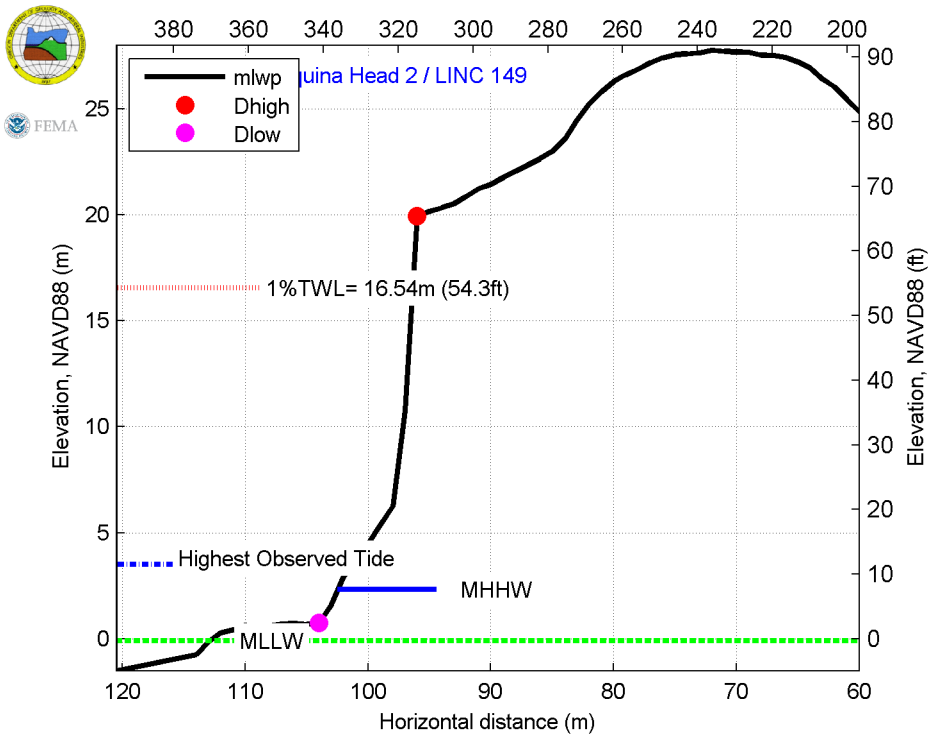

11.2.8 Beverly Beach

LINC 150

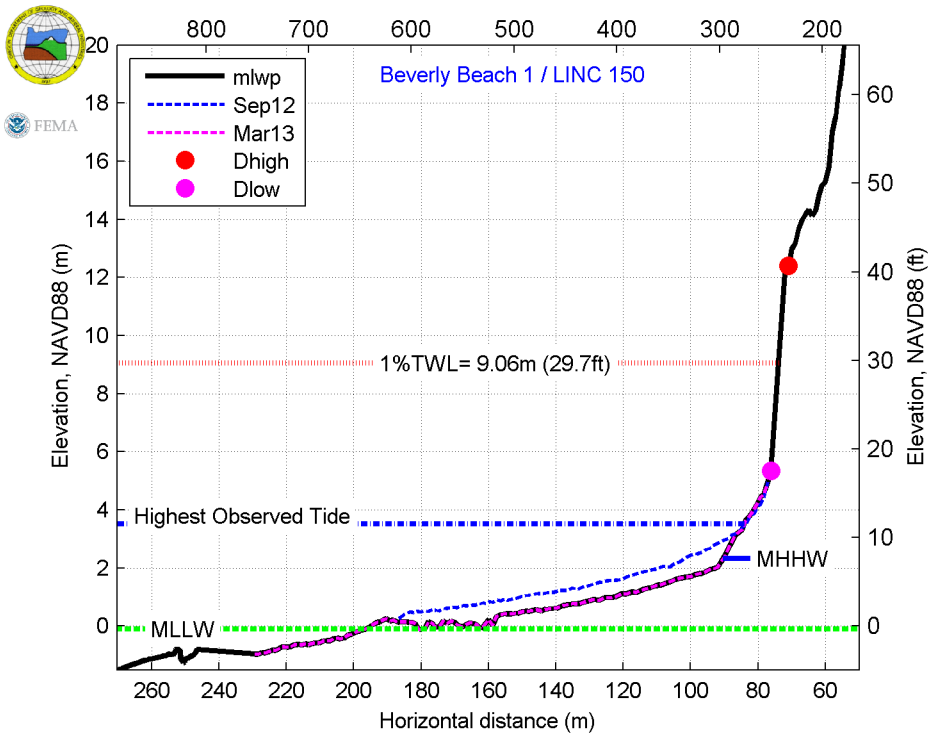

LINC 151

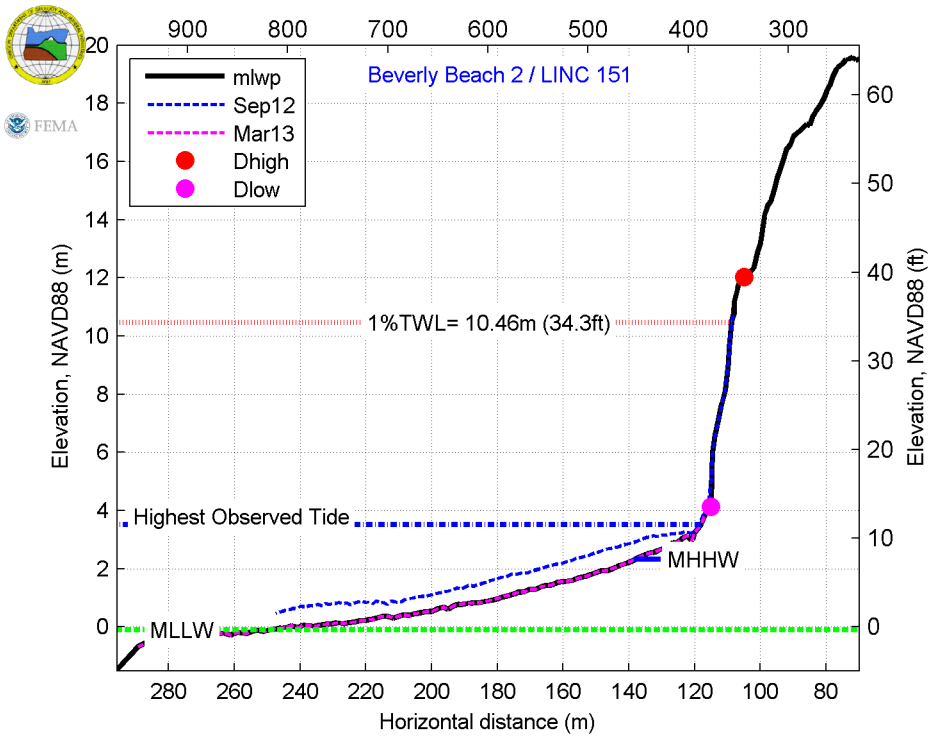

LINC 152

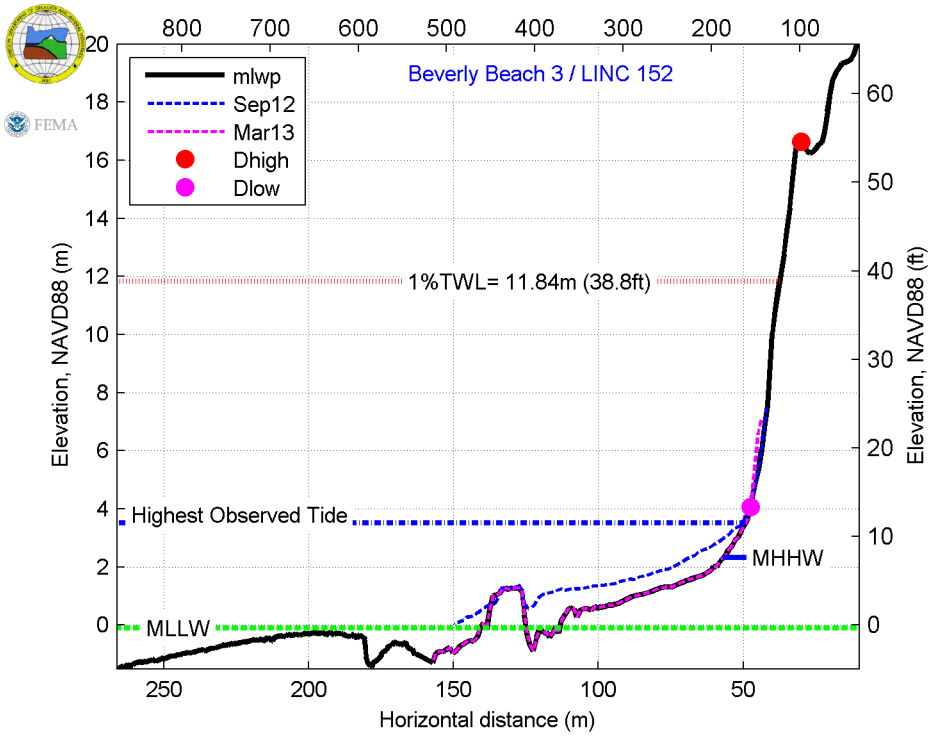

LINC 153

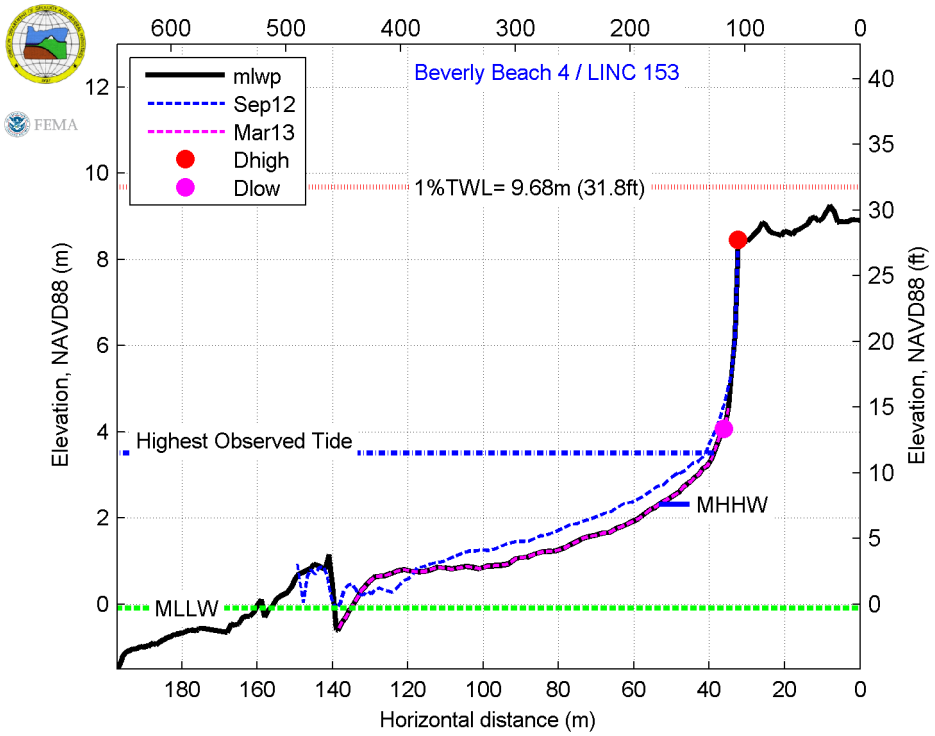

LINC 154

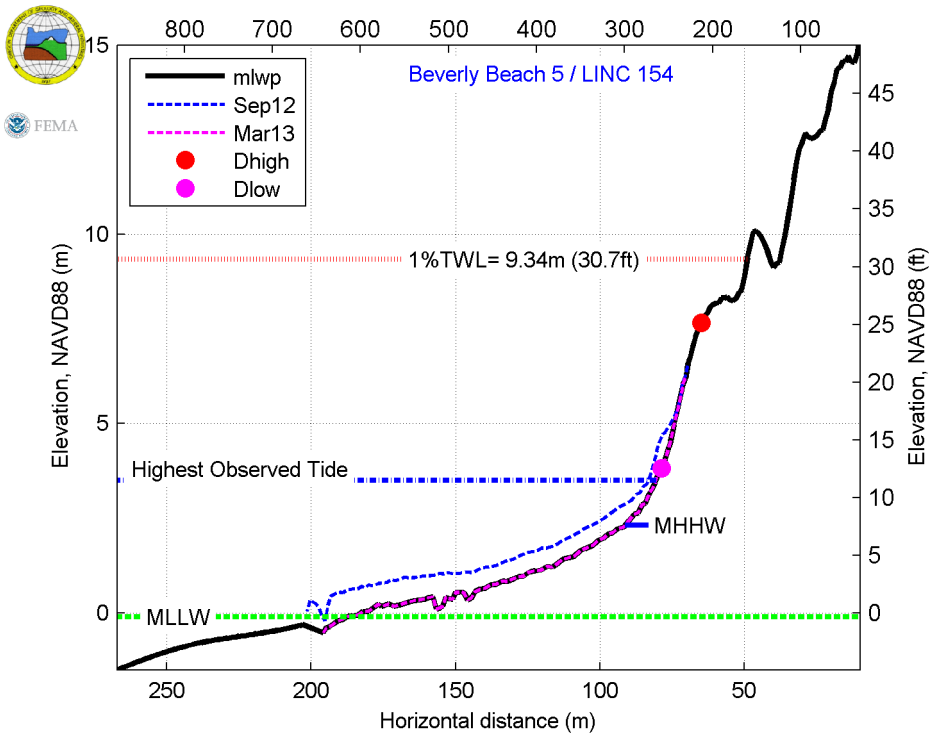

LINC 155

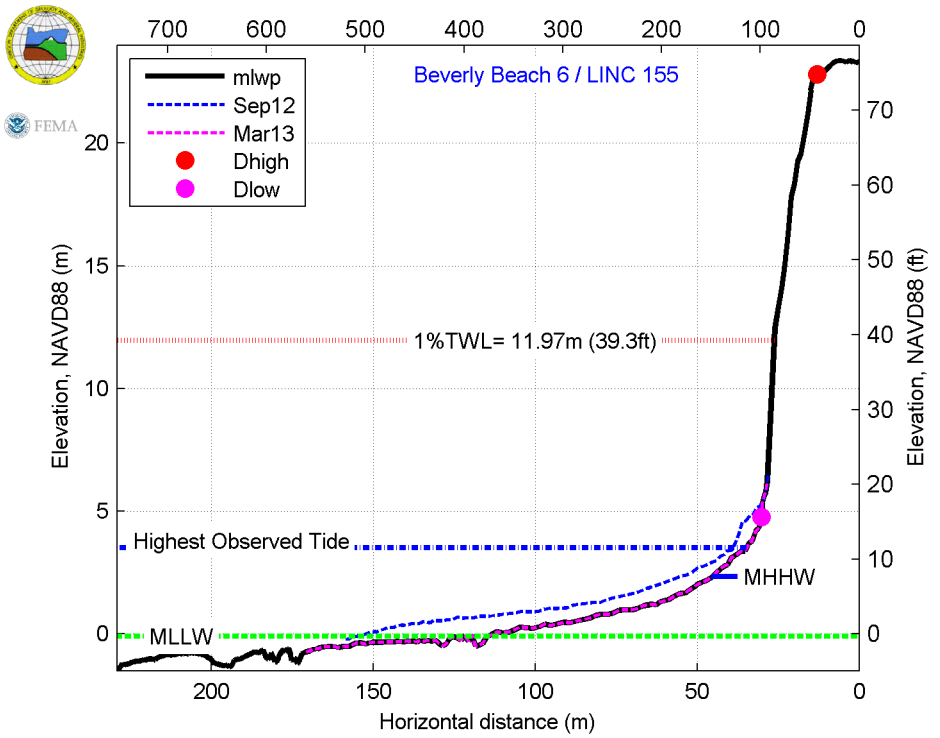

LINC 156

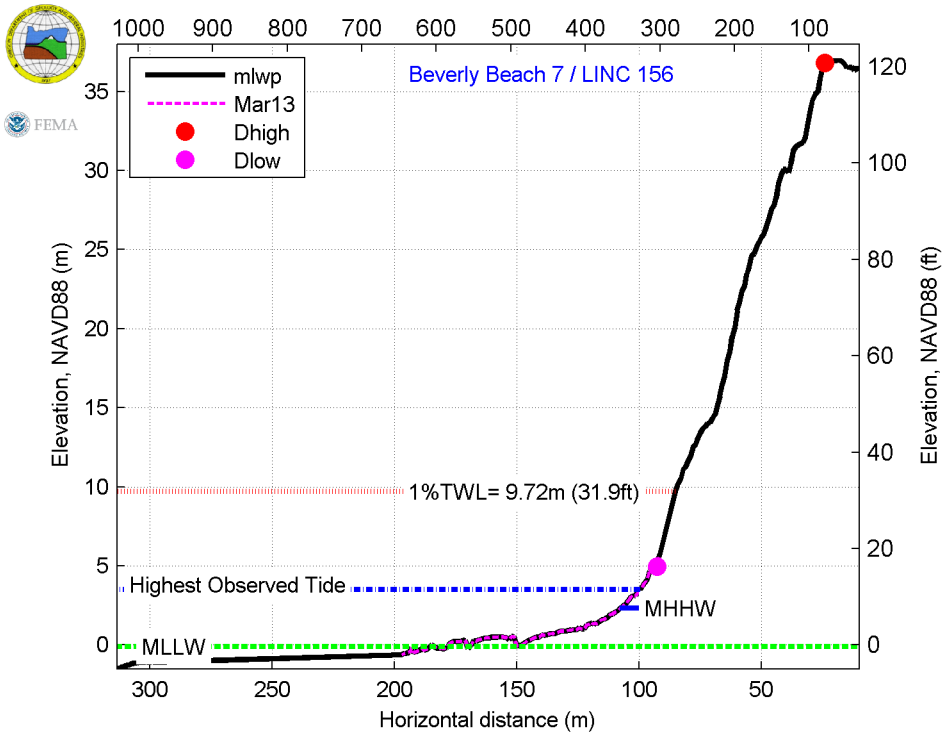

LINC 157

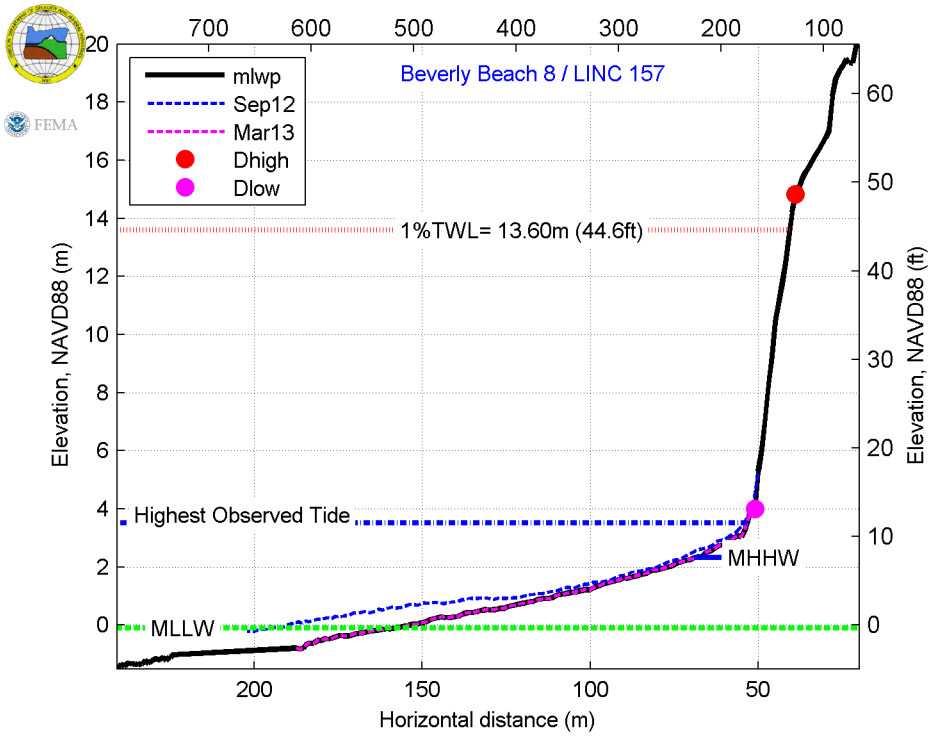

LINC 158

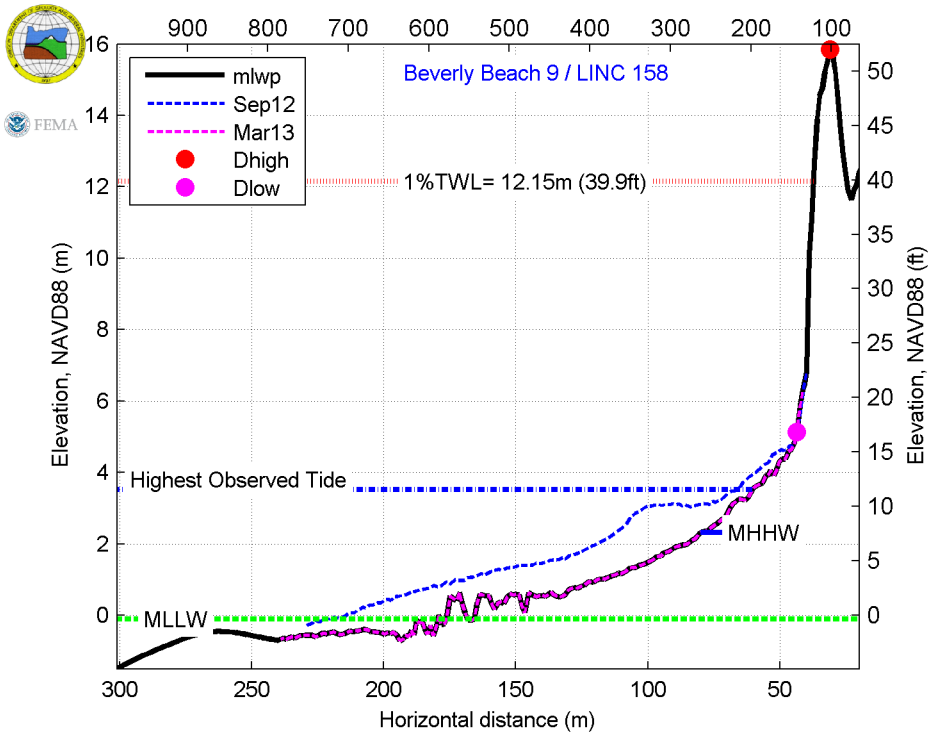

LINC 159

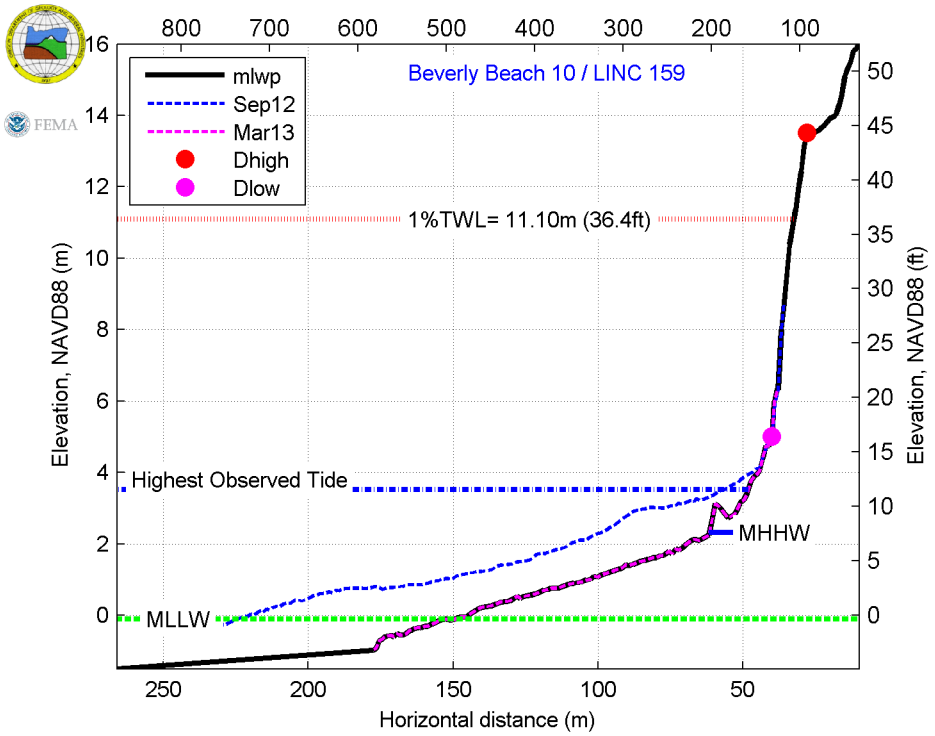

LINC 160

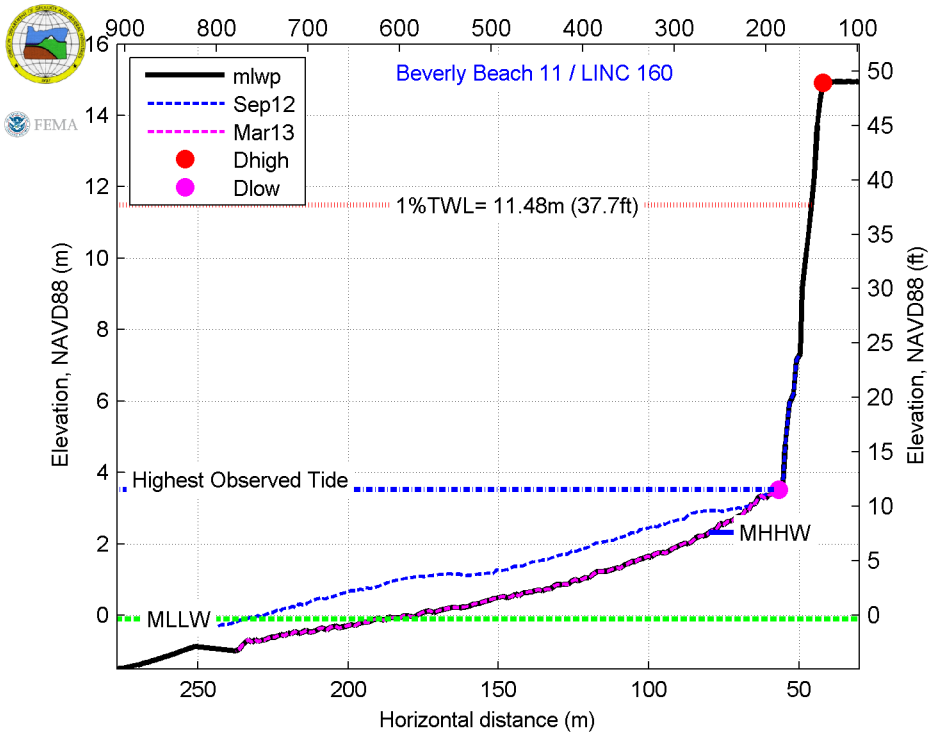

LINC 161

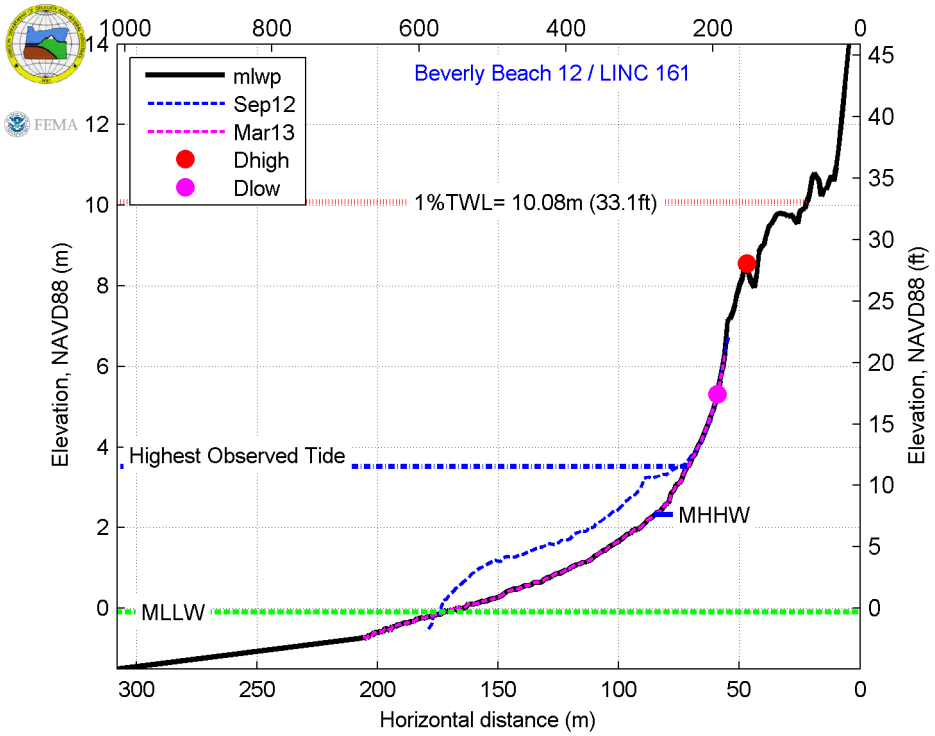

LINC 162

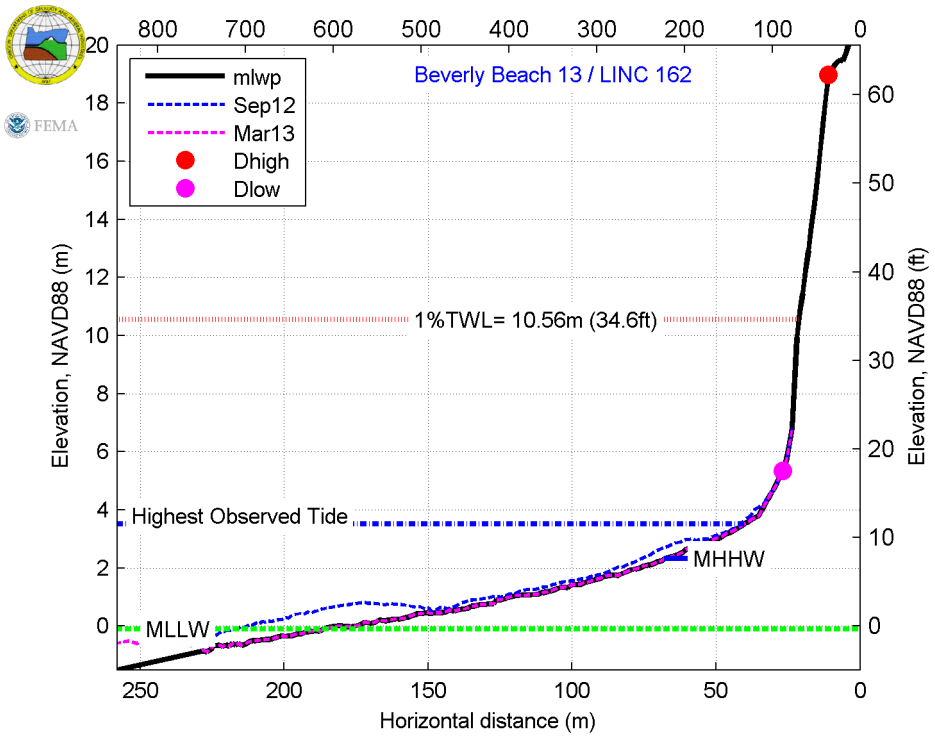

LINC 163

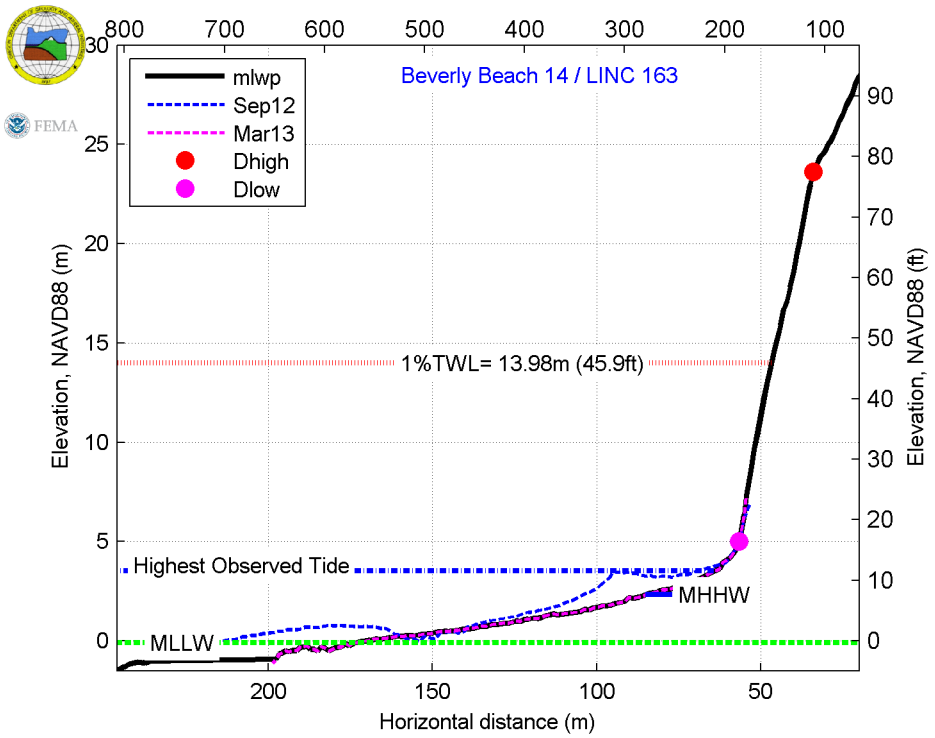

LINC 164

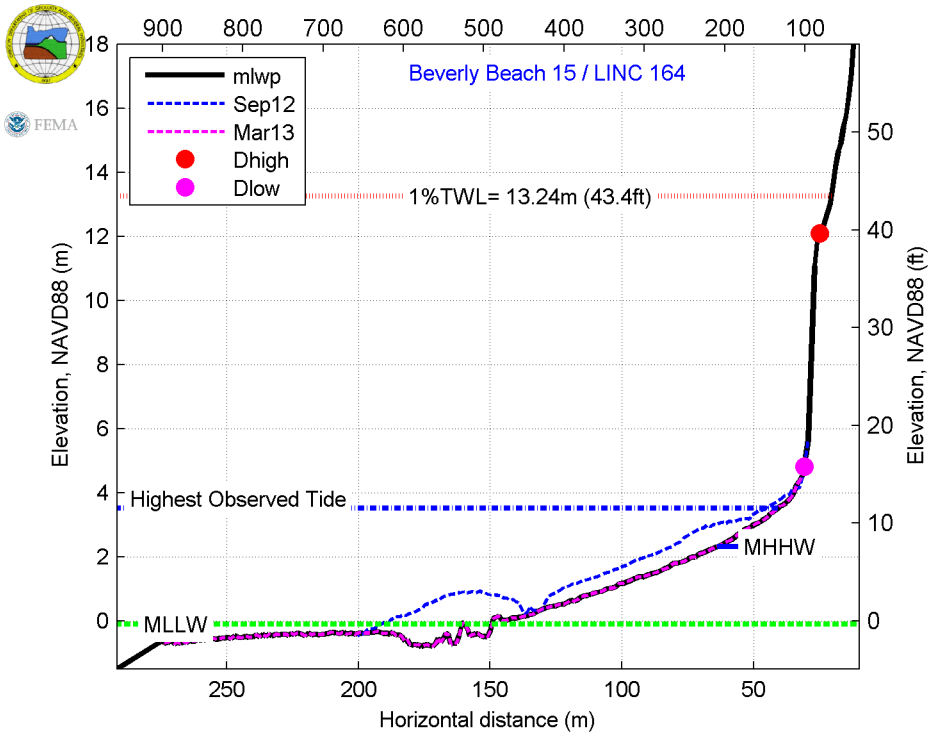

LINC 165

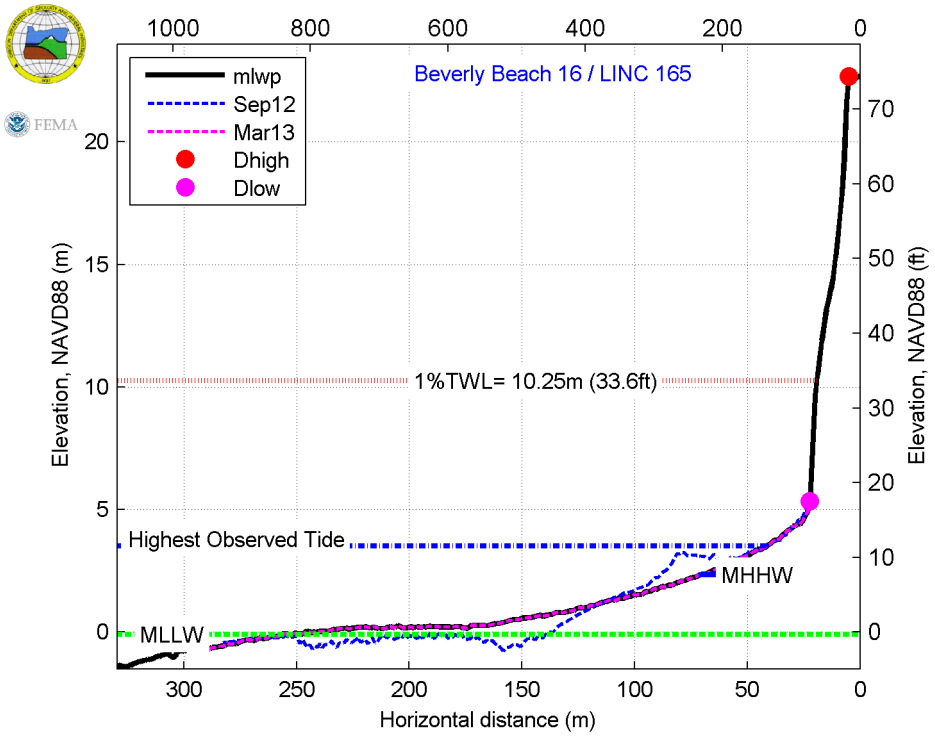

LINC 166

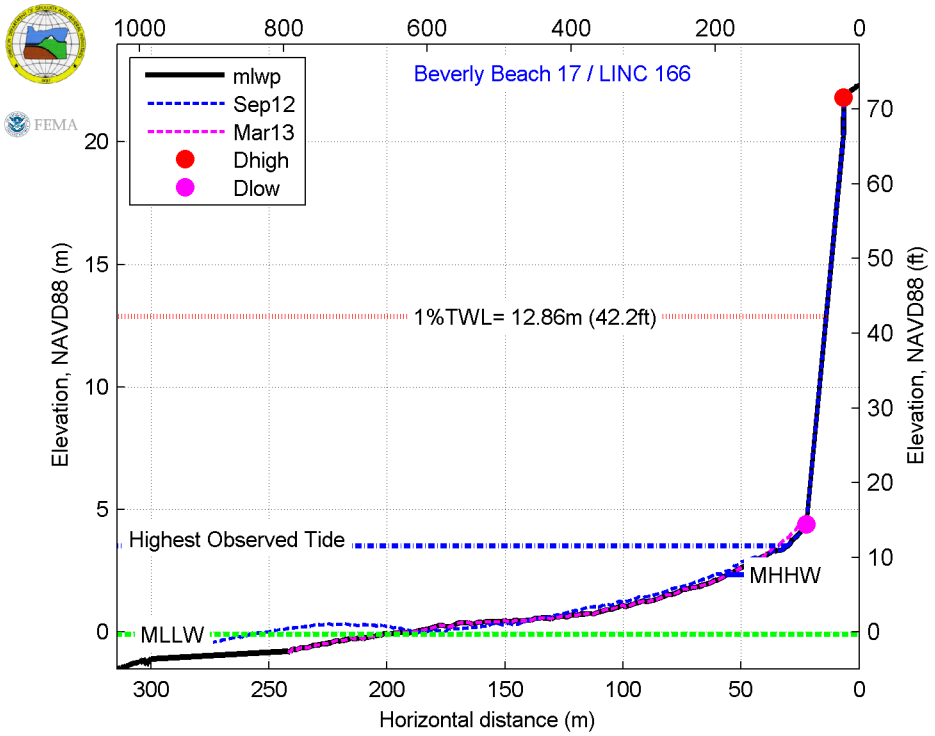

LINC 167

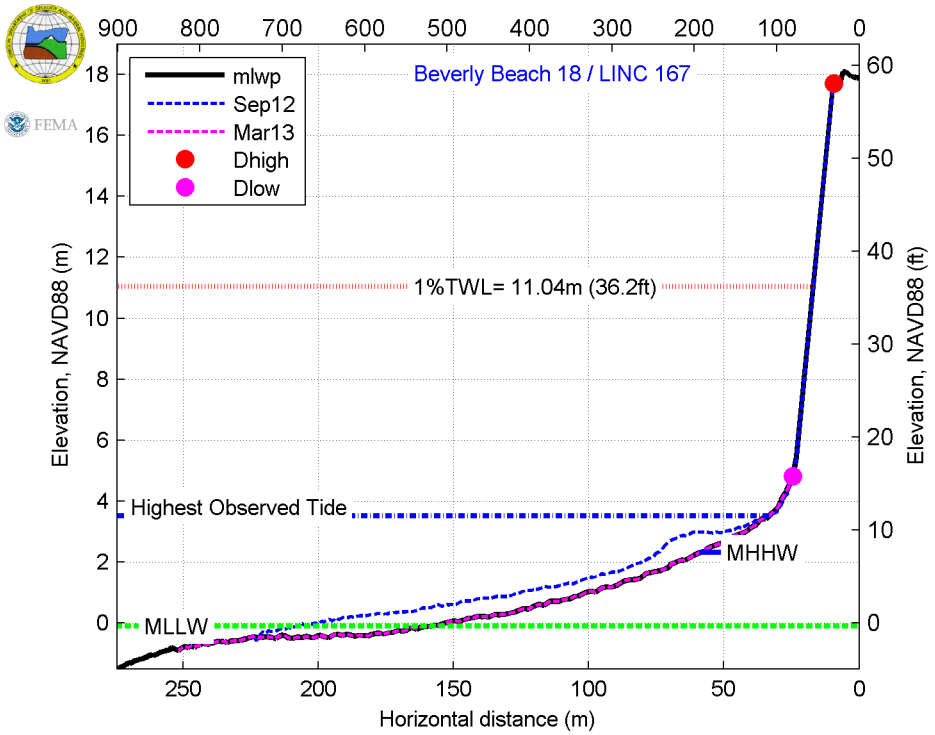

LINC 168

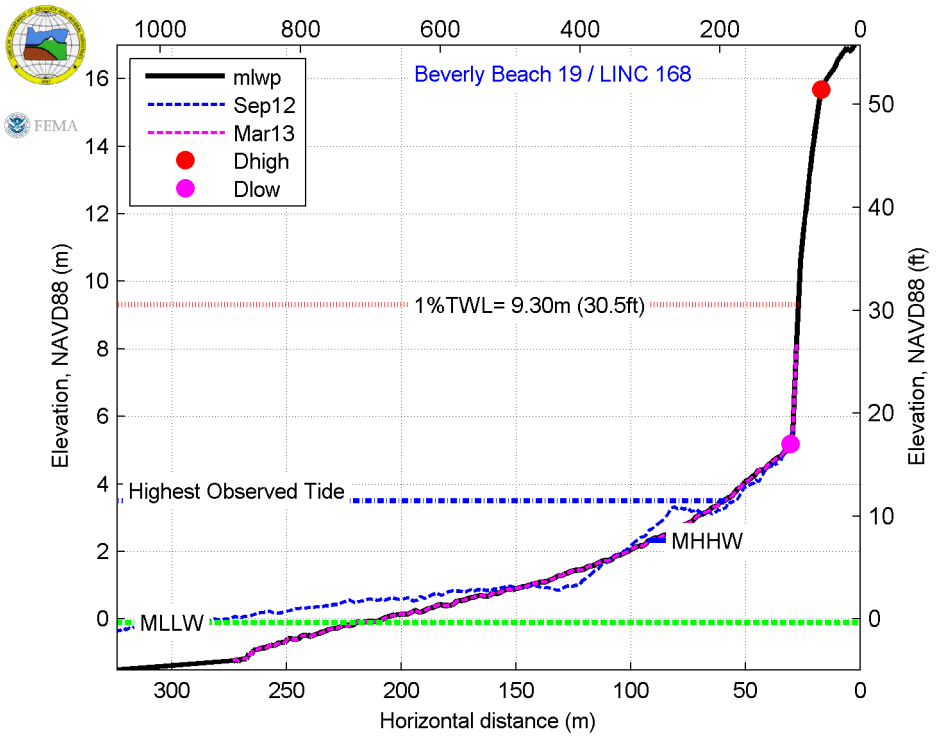

LINC 169

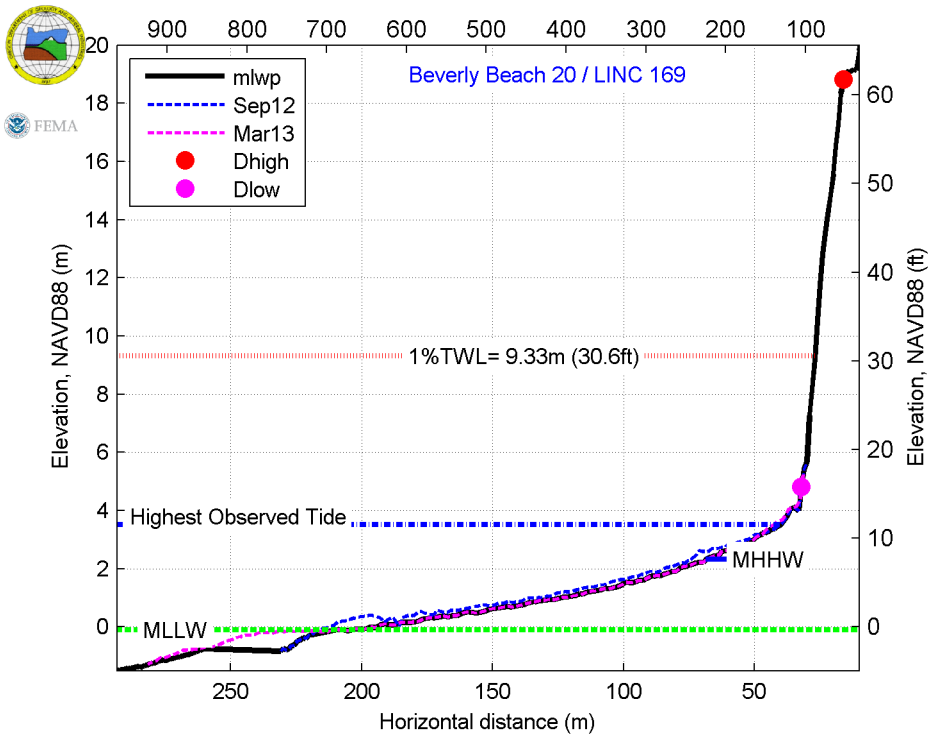

LINC 170

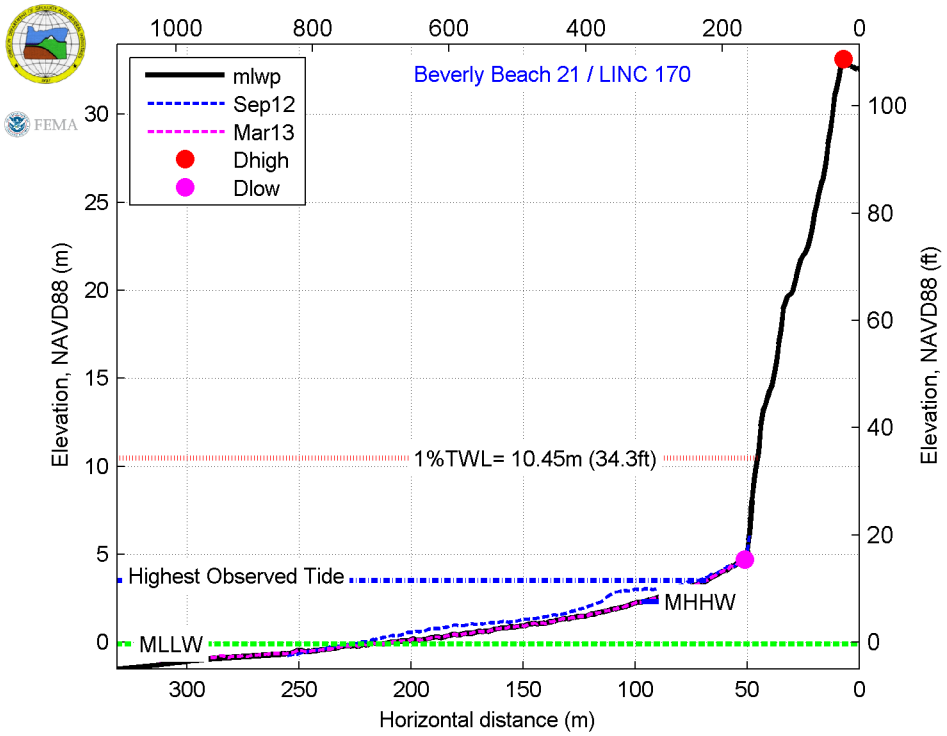

LINC 171

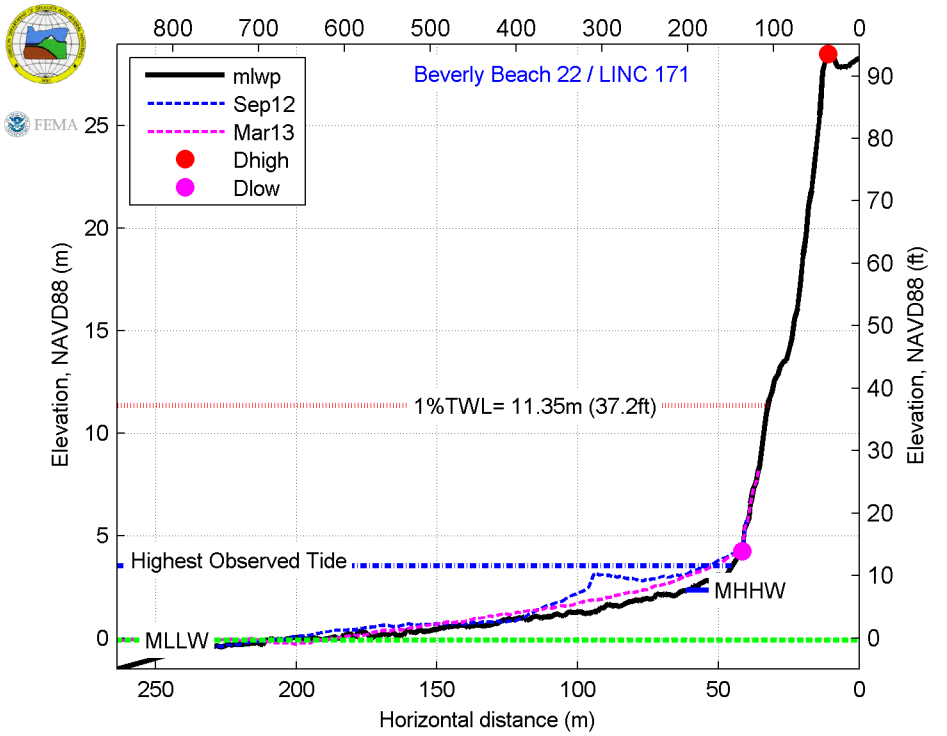

11.2.9 Otter Rock

LINC 172

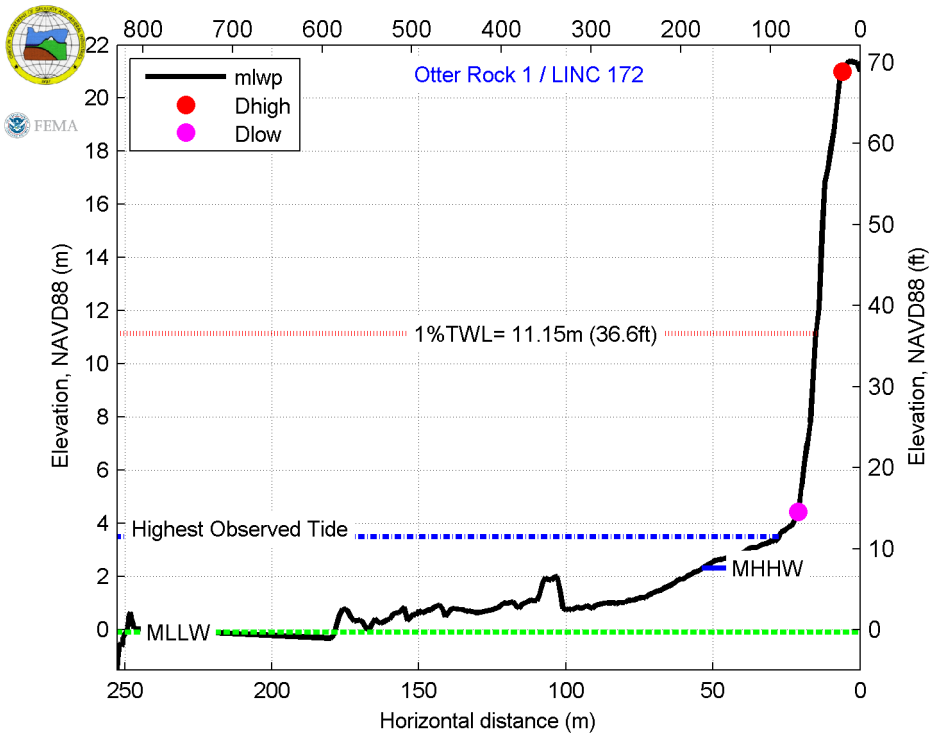

LINC 173

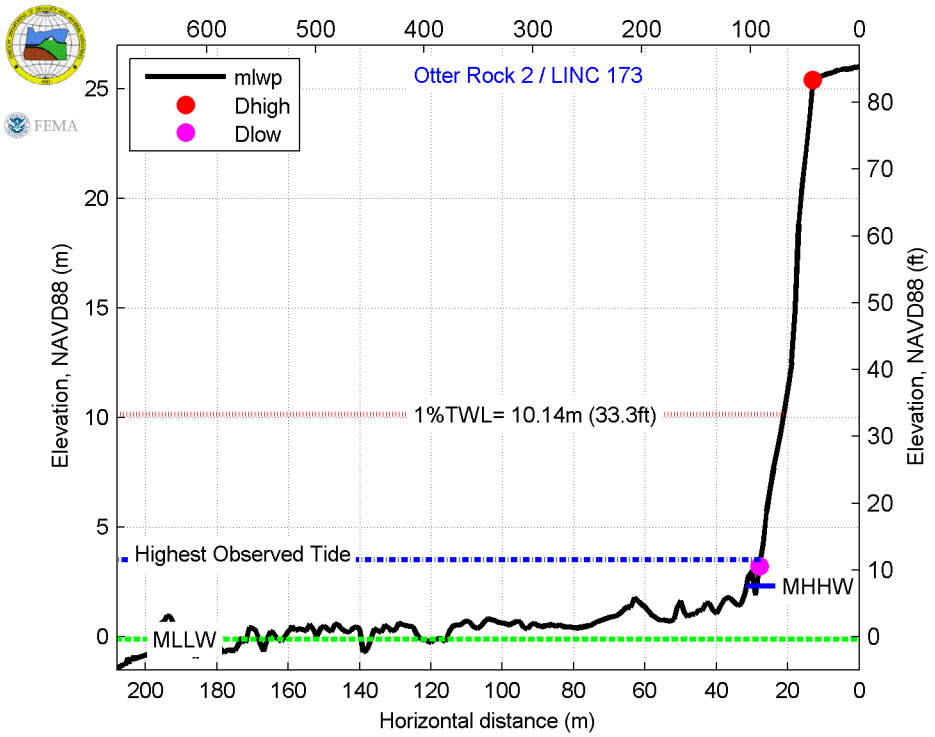

LINC 174

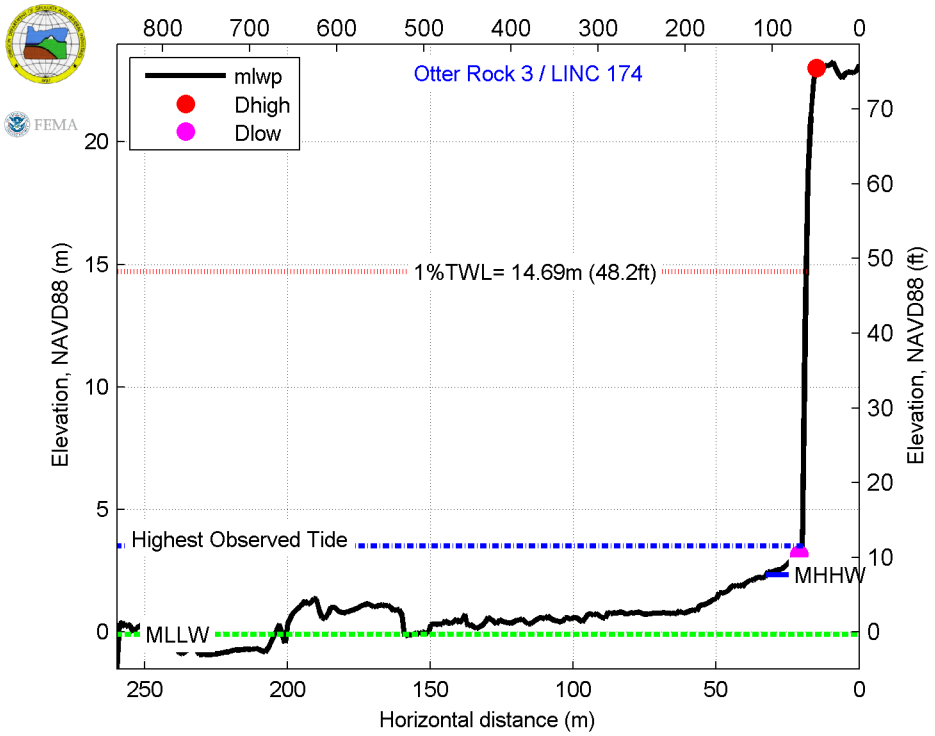

LINC 175

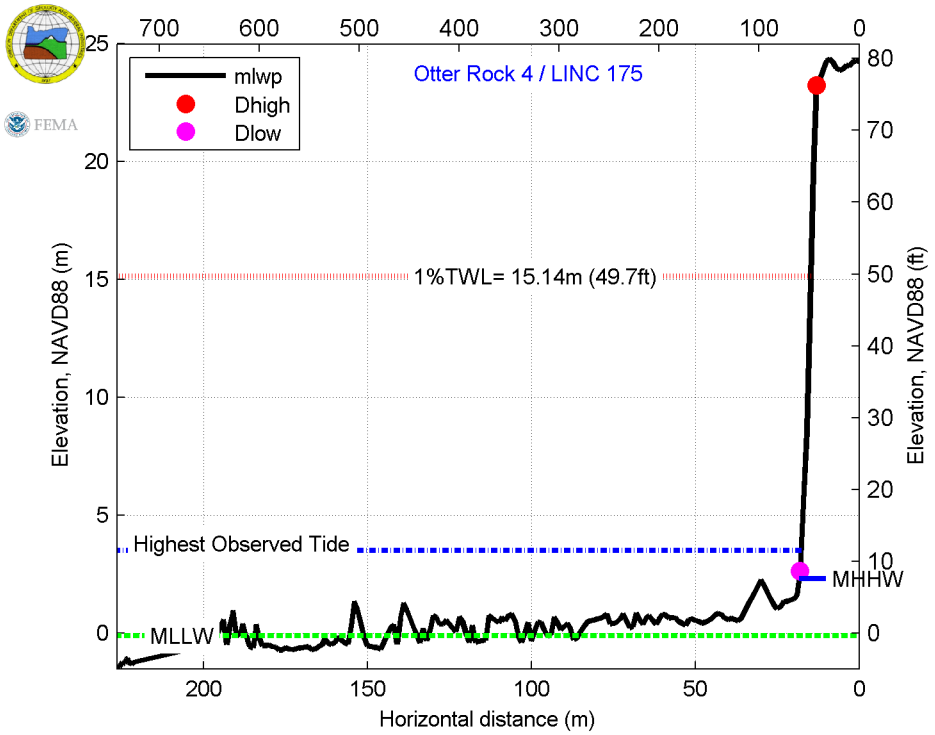

LINC 176

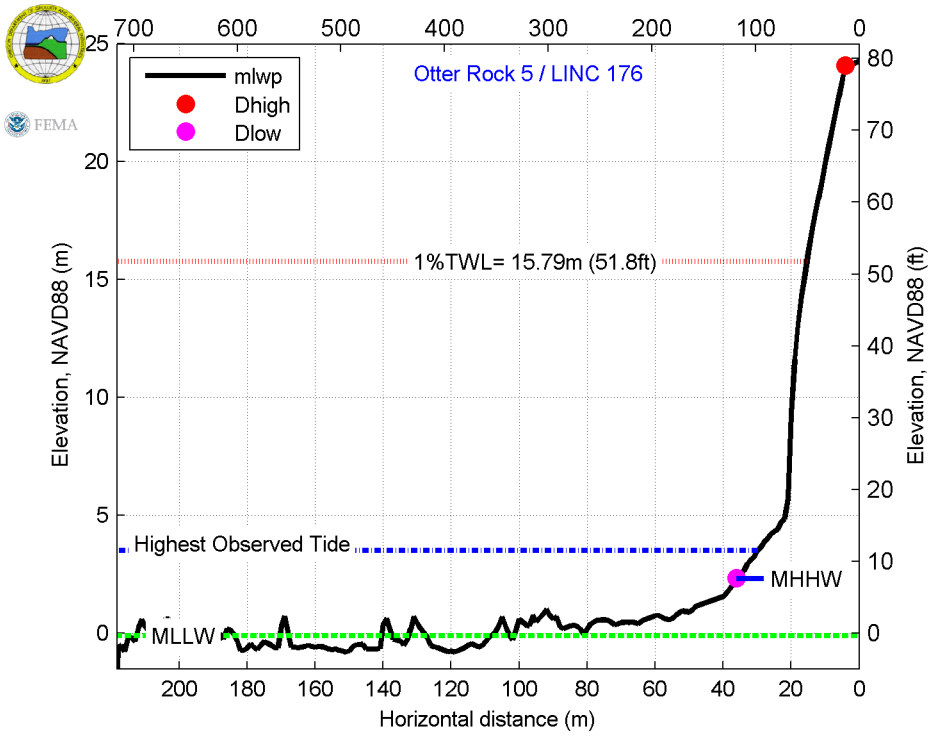
Otter Rock 5 / LINC 176
mlwp
Dhigh
Dlow
1%TWL= 15.79m (51.8ft)
Highest Observed Tide
MHHW
MLLW
Elevation, NAVD88 (m)
Elevation, NAVD88 (ft)
Horizontal distance (m)
700
600
500
400
300
200
100
0
25
20
15
10
5
0
80
70
60
50
40
30
20
10
0
200
180
160
140
120
100
80
60
40
20
0

11.2.10 Cape Foulweather

LINC 177

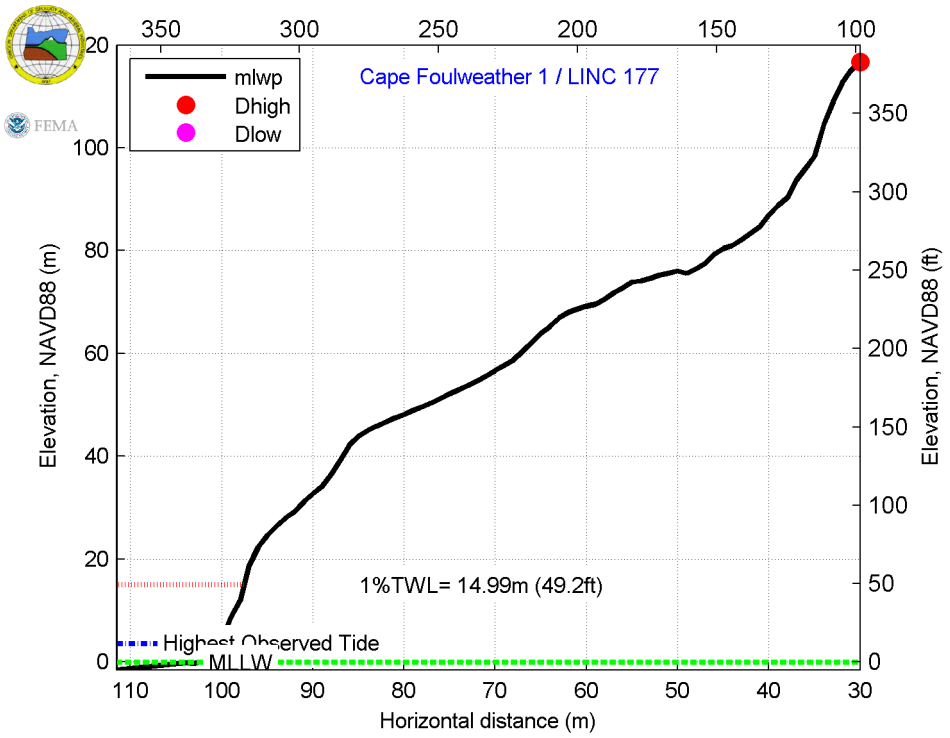

LINC 178

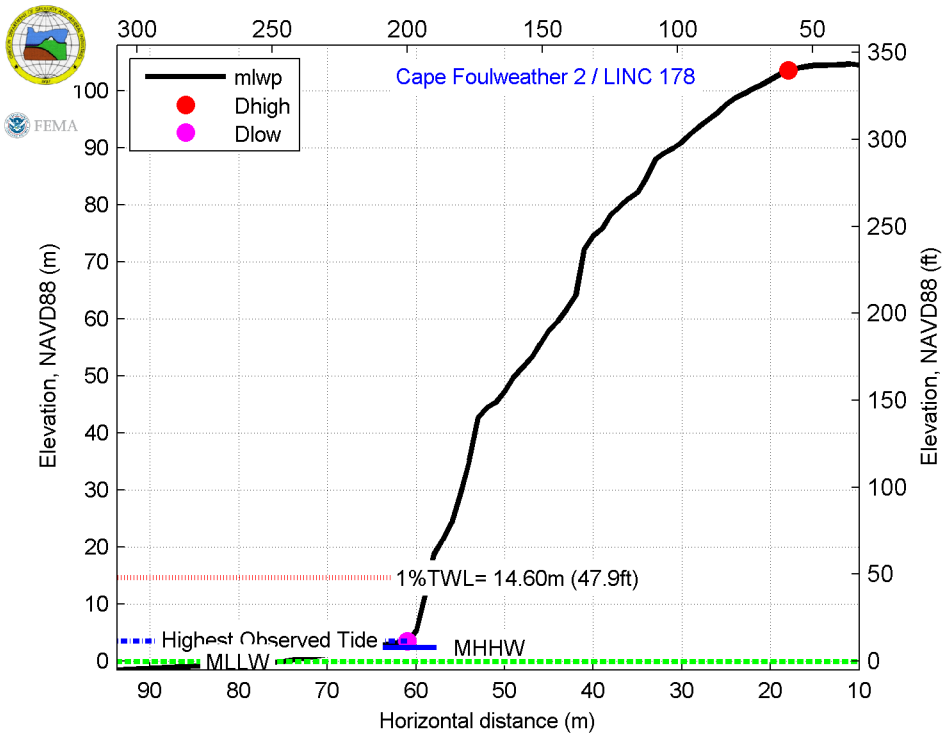

11.2.11 Miroco

LINC 179

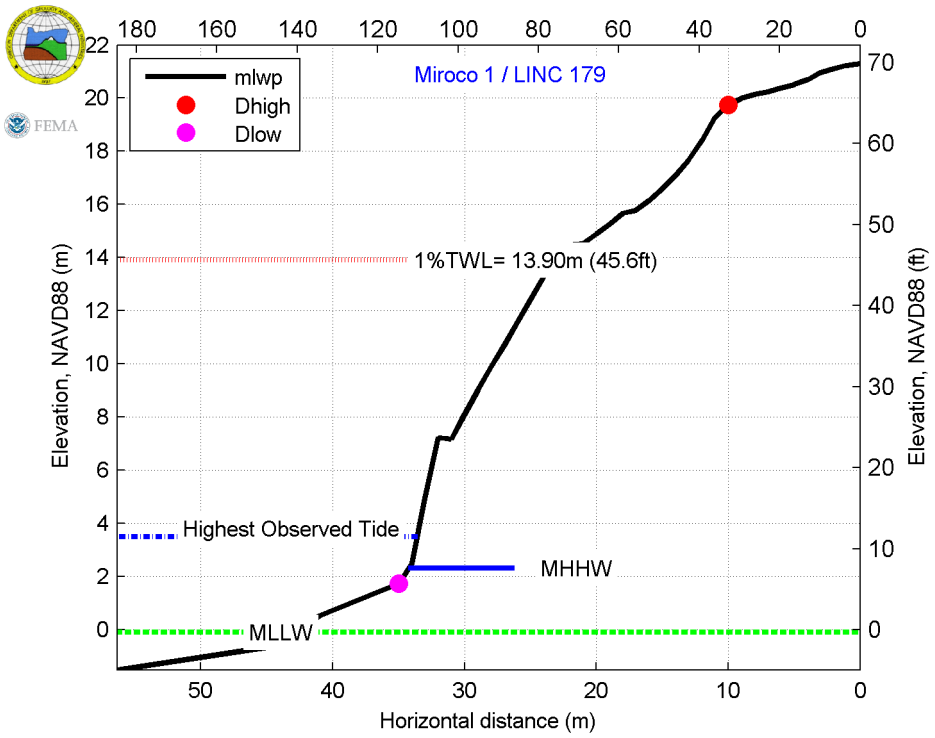

LINC 180

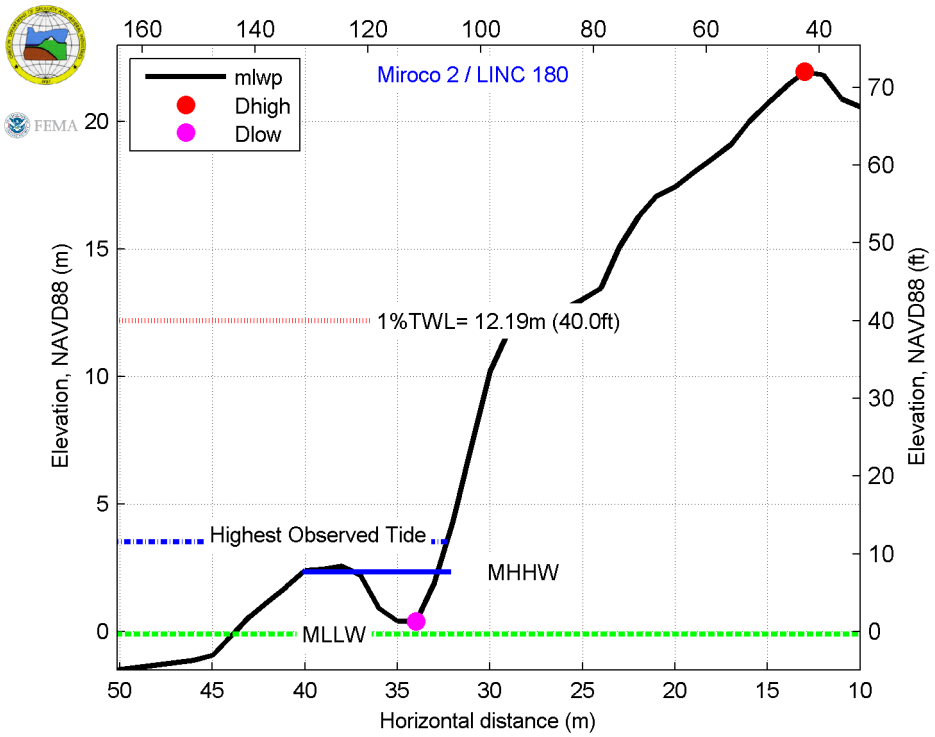

LINC 181

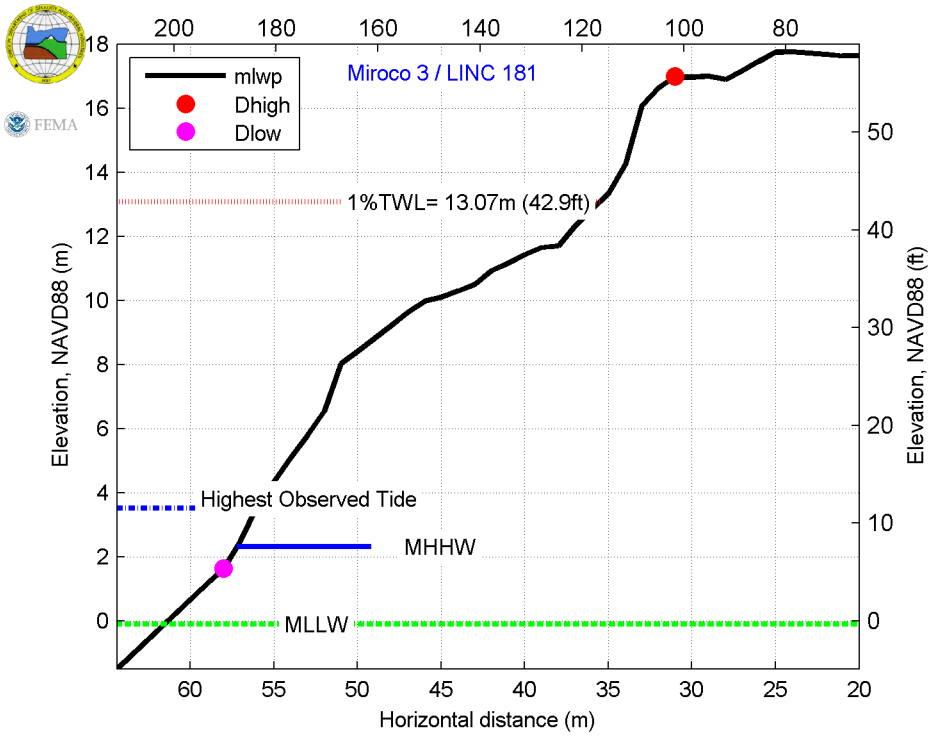
Miroco 3 / LINC 181
mlwp
Dhigh
Dlow
1%TWL= 13.07m (42.9ft)
Highest Observed Tide
MHHW
MLLW
Elevation, NAVD88 (m)
Elevation, NAVD88 (ft)
Horizontal distance (m)
200
180
160
140
120
100
80
60
55
50
45
40
35
30
25
20
18
16
14
12
10
8
6
4
2
0
50
40
30
20
10
0

11.2.12 Rocky Creek

LINC 182

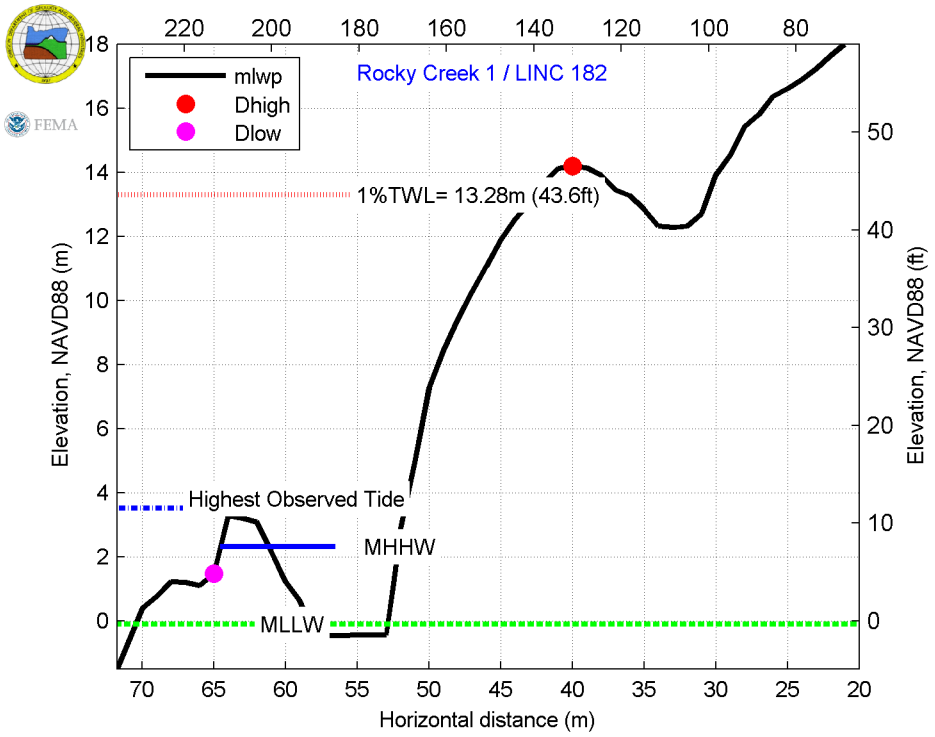

LINC 183

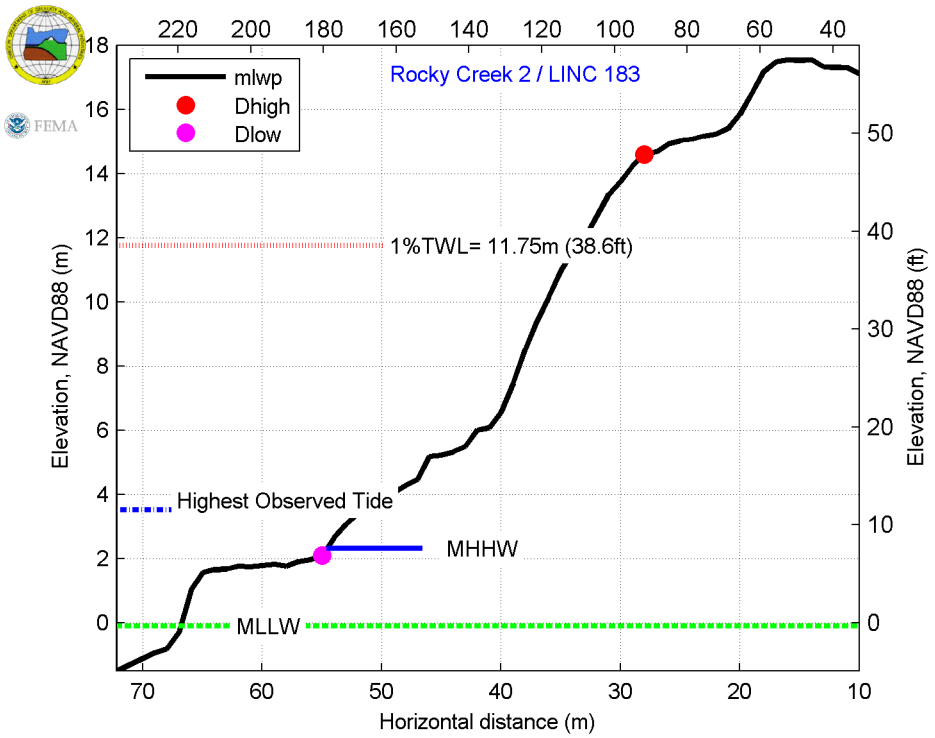

11.2.13 Whale Cove

LINC 184

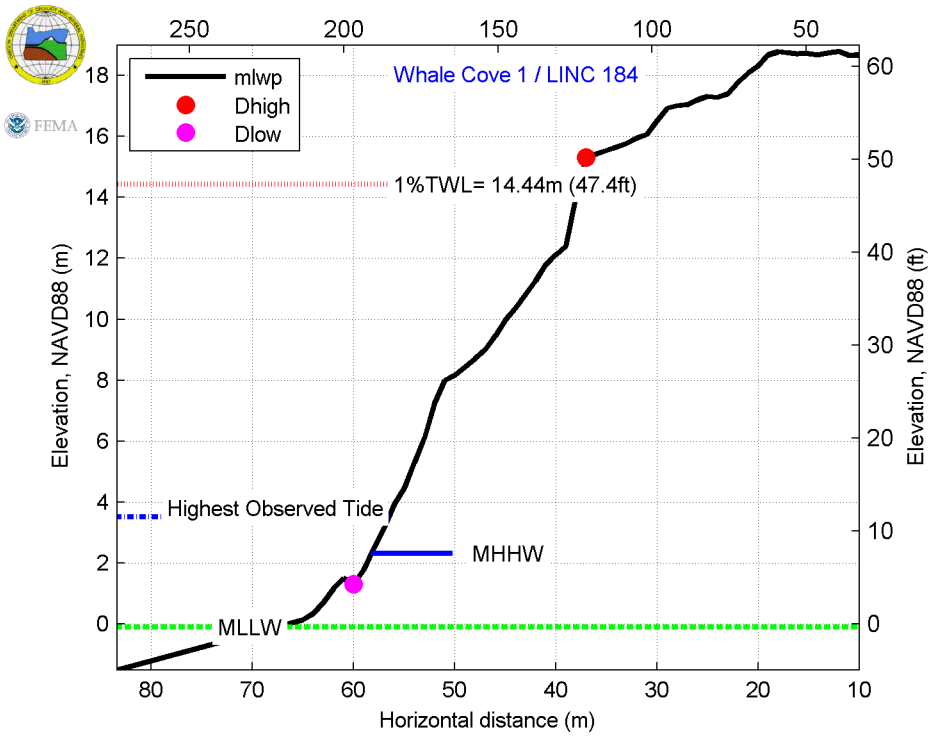

LINC 185

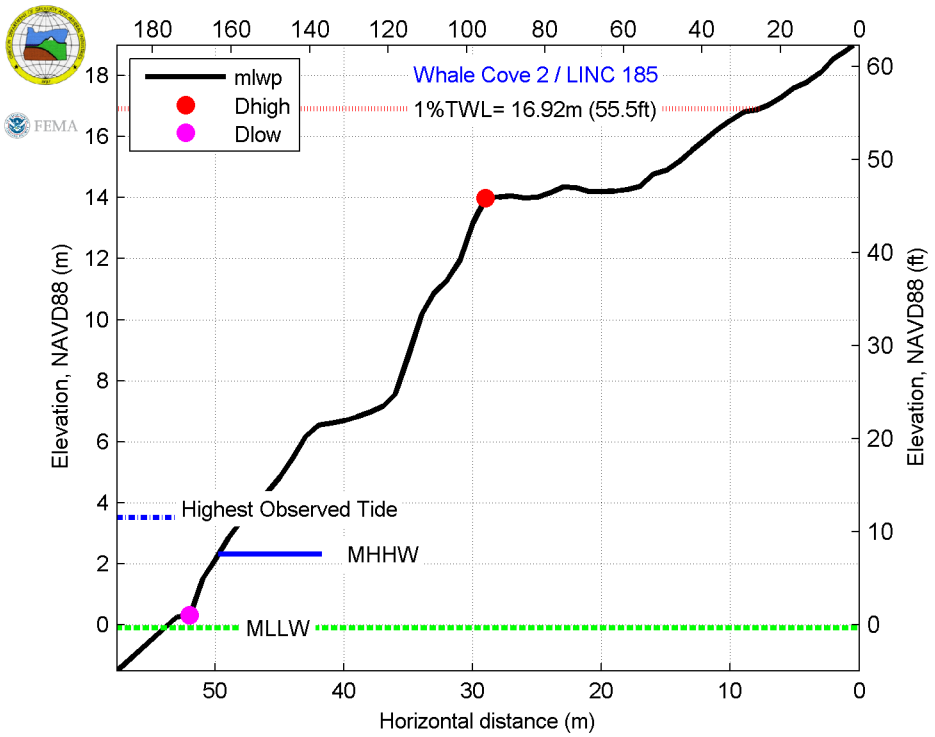

LINC 186

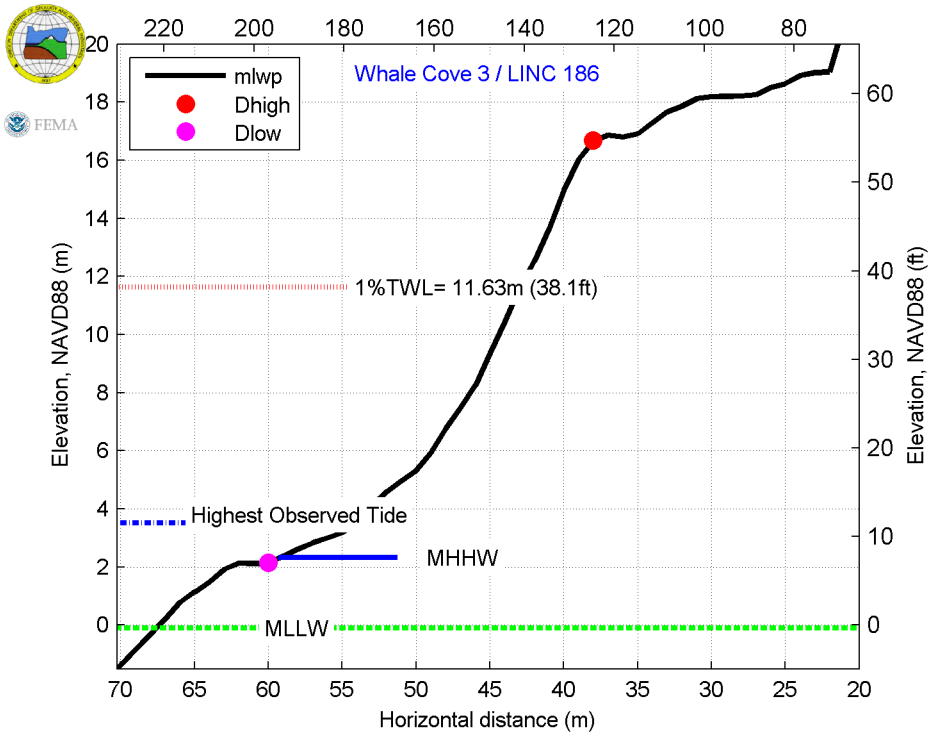

LINC 187

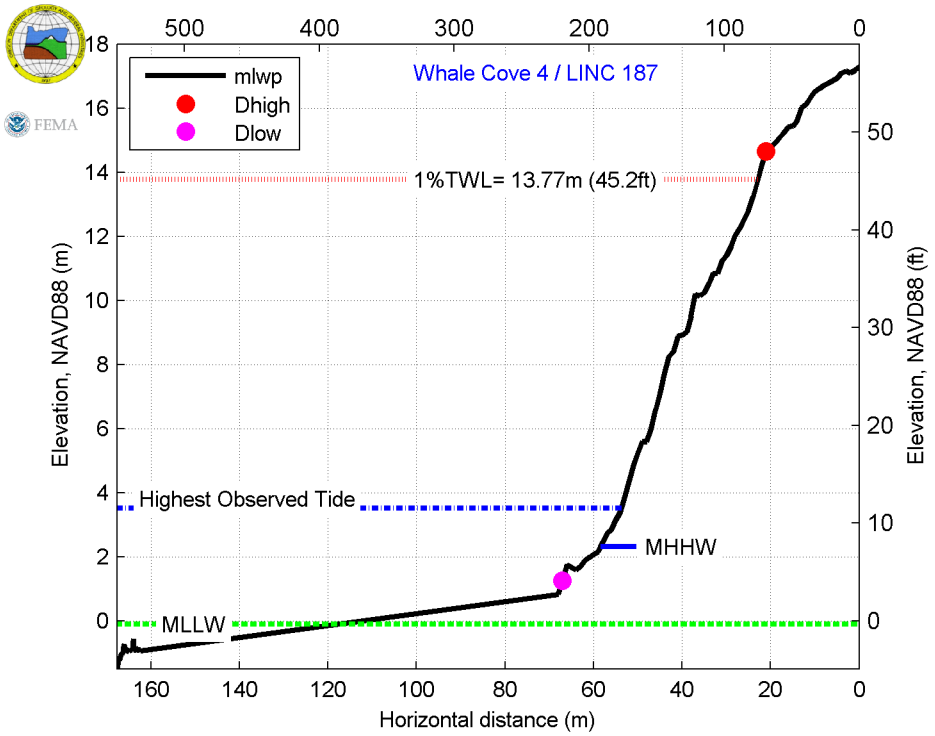

LINC 188

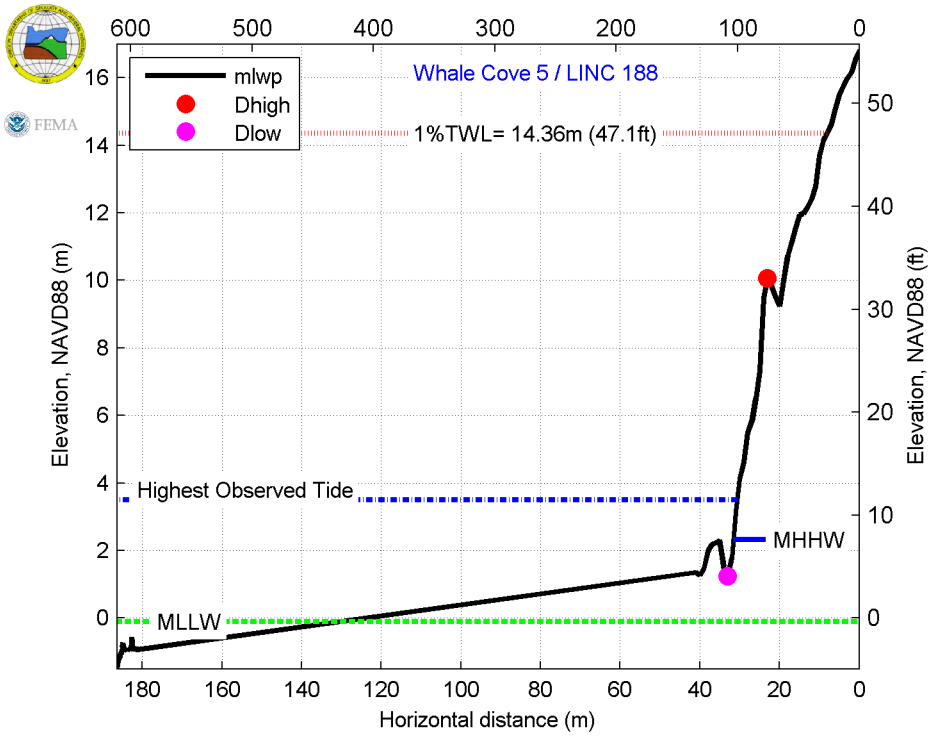

LINC 189

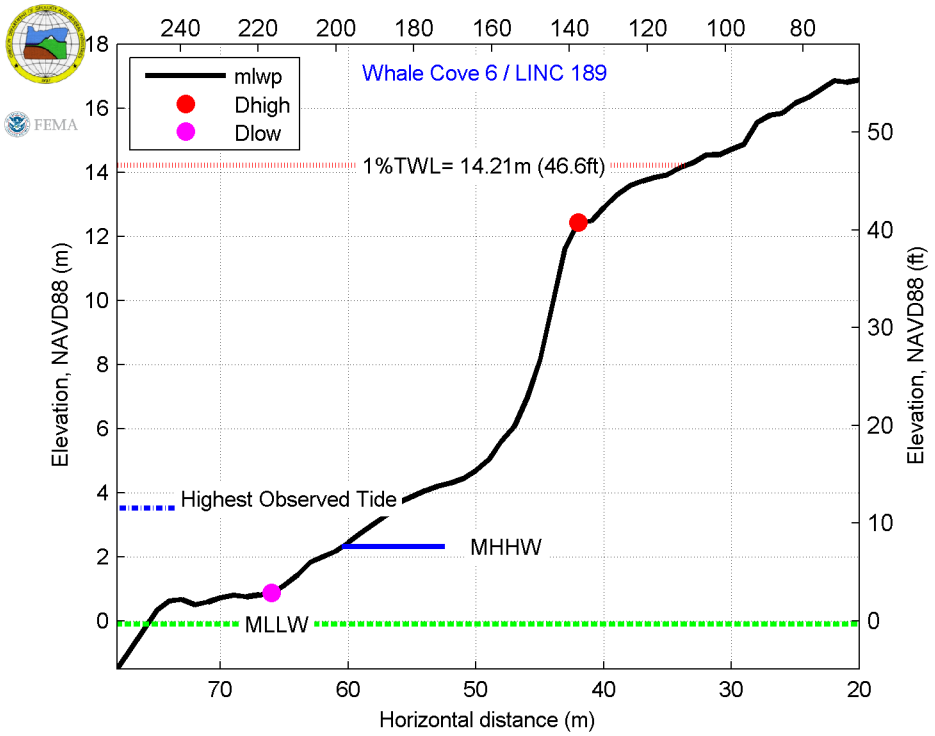

11.2.14 Depoe Bay

LINC 190

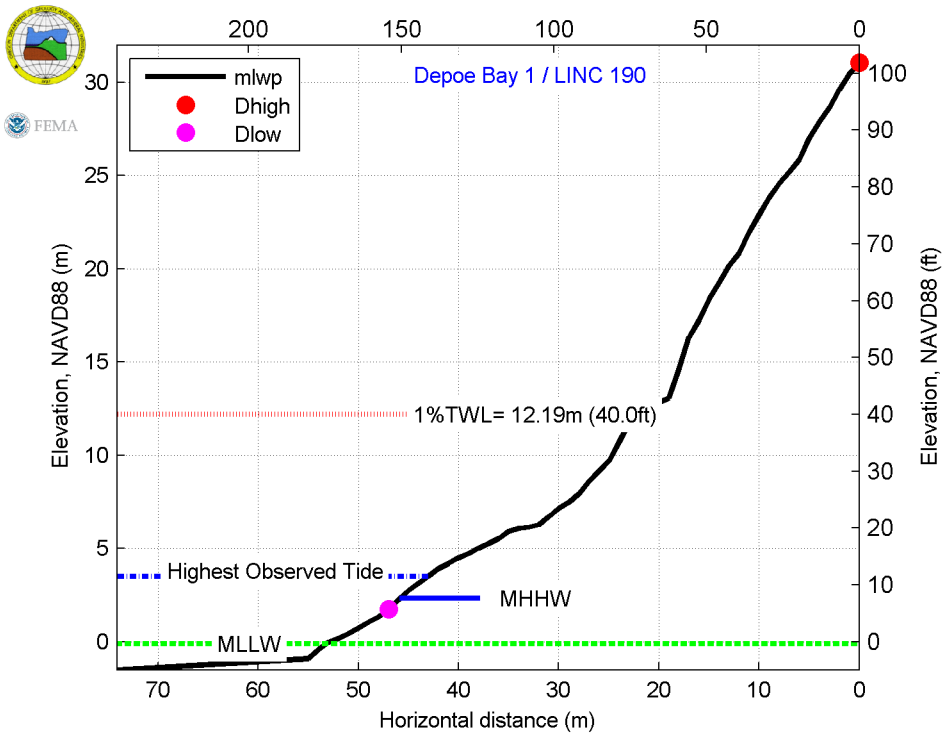

LINC 191

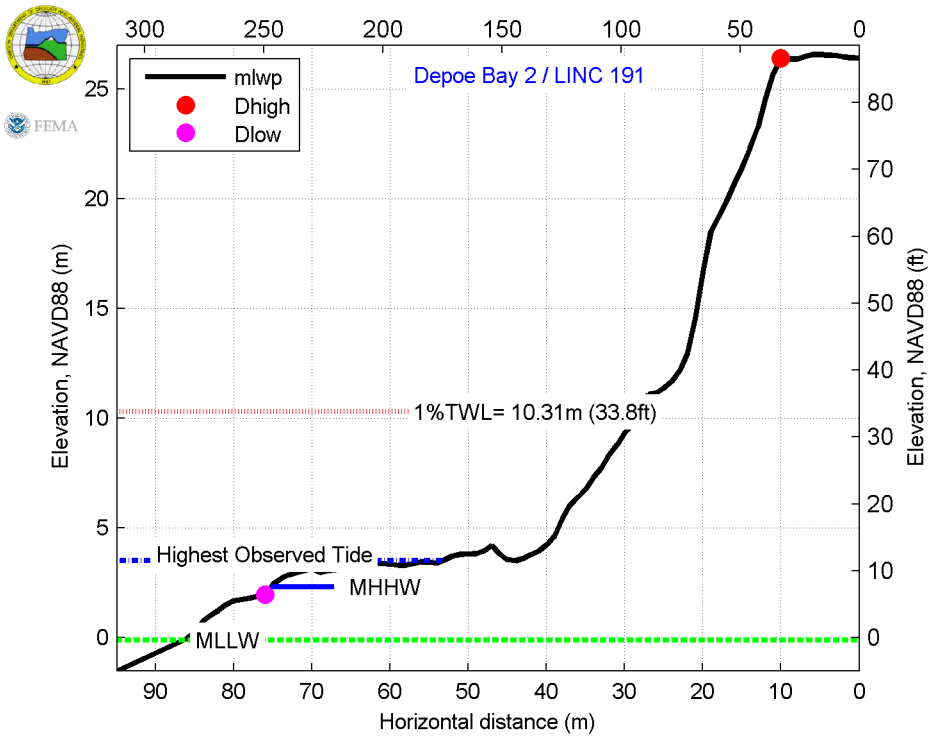

LINC 192

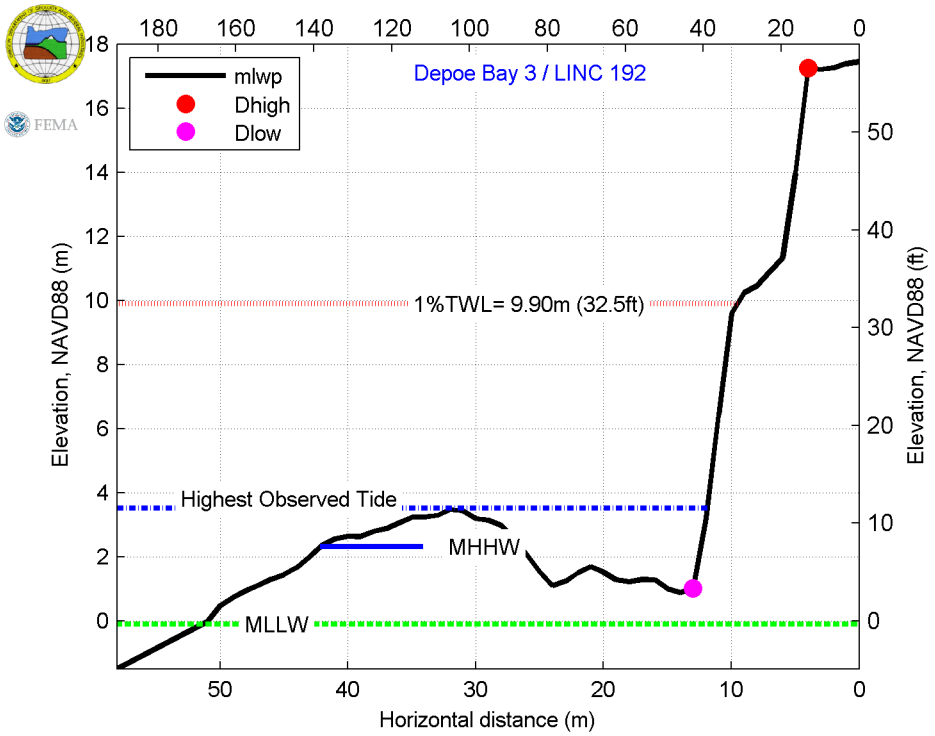

LINC 193

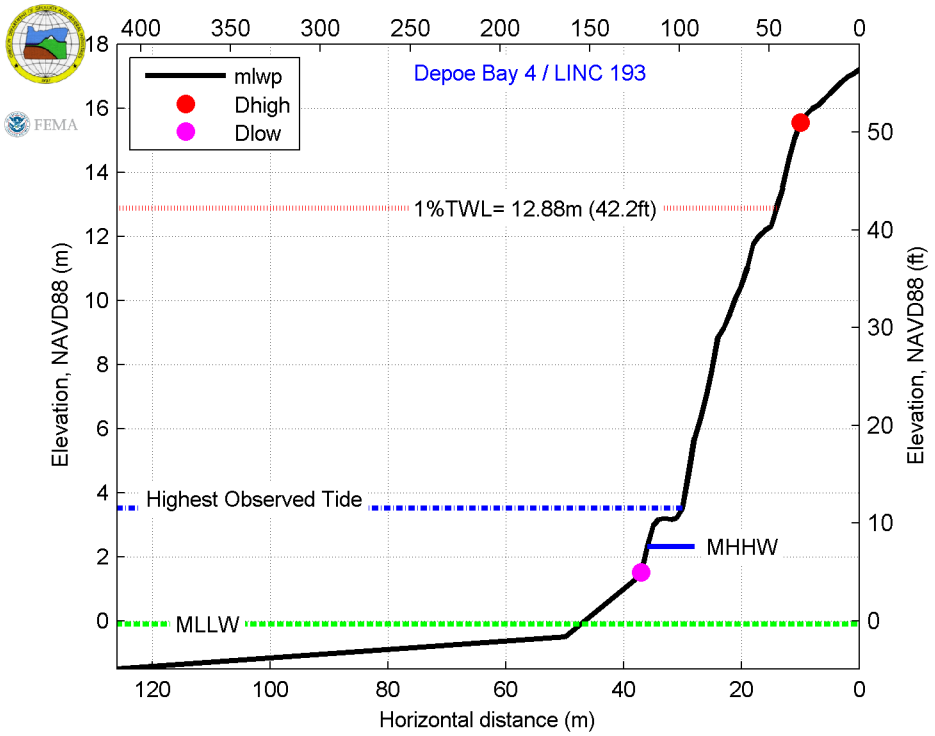

LINC 194

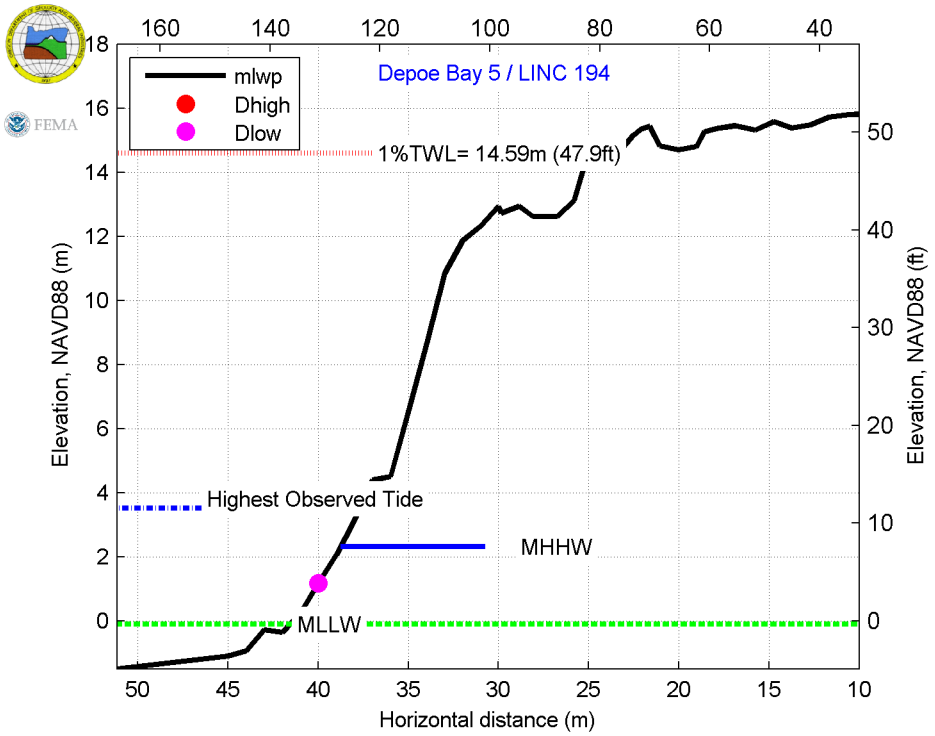

LINC 195

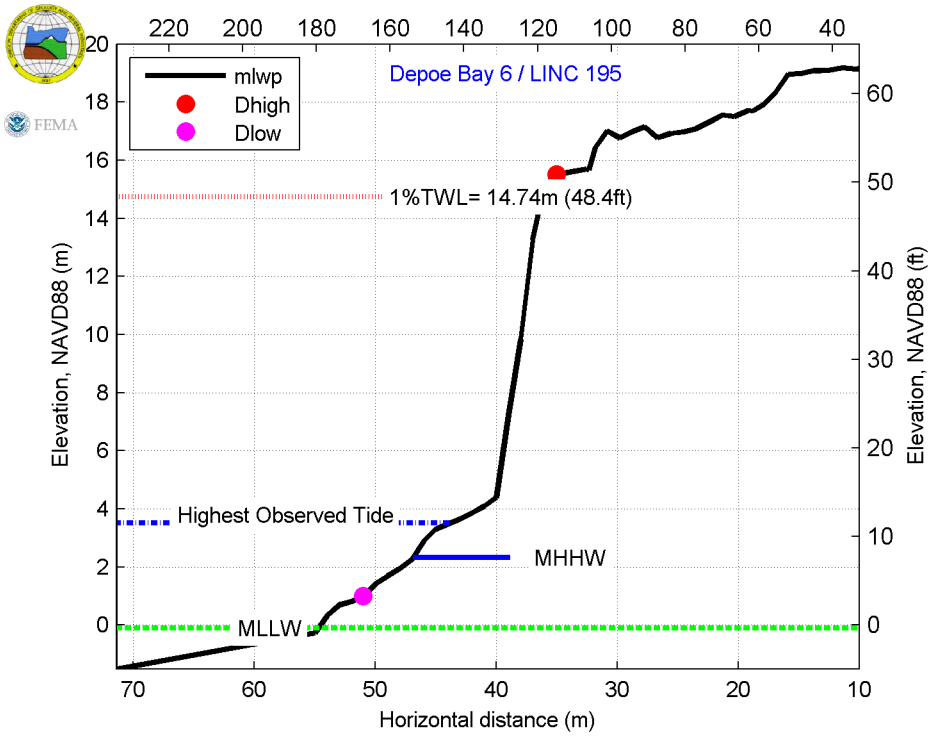

LINC 196

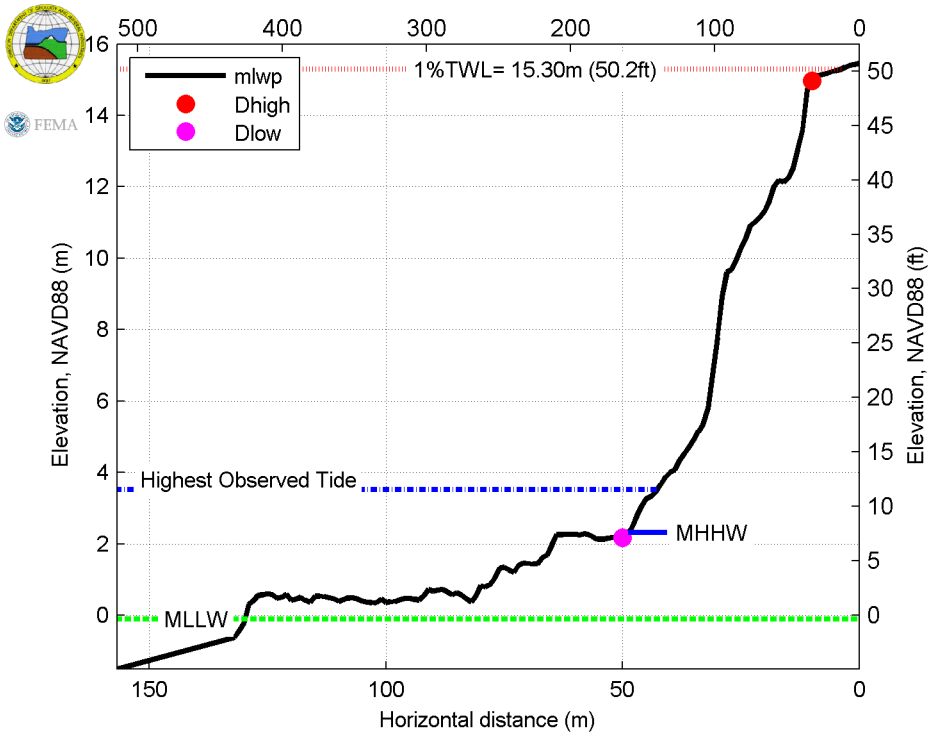

LINC 197

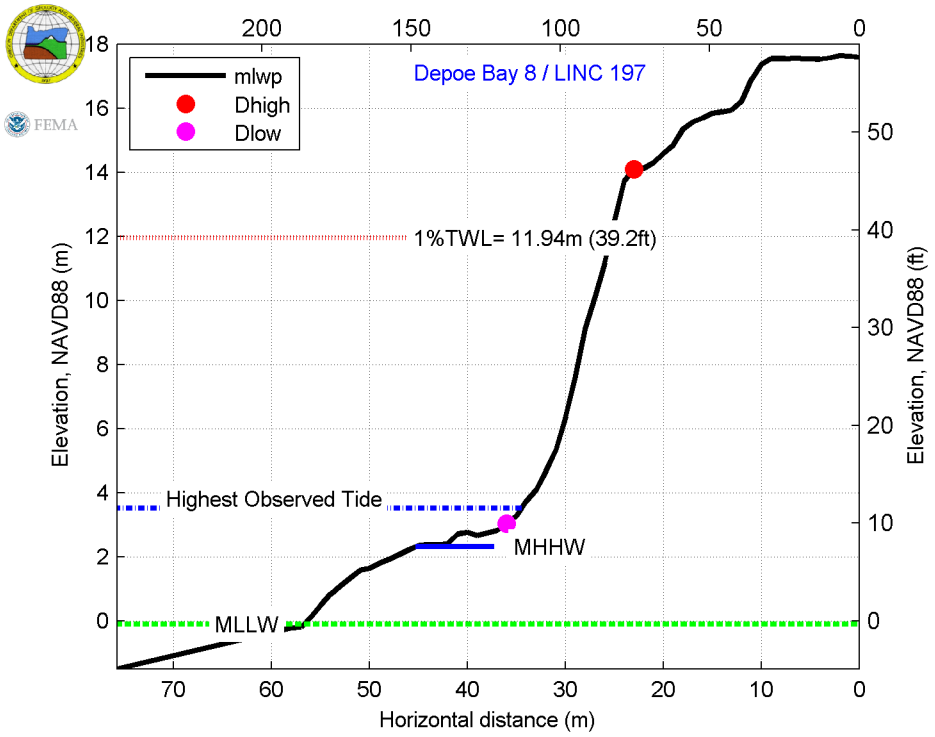

LINC 198

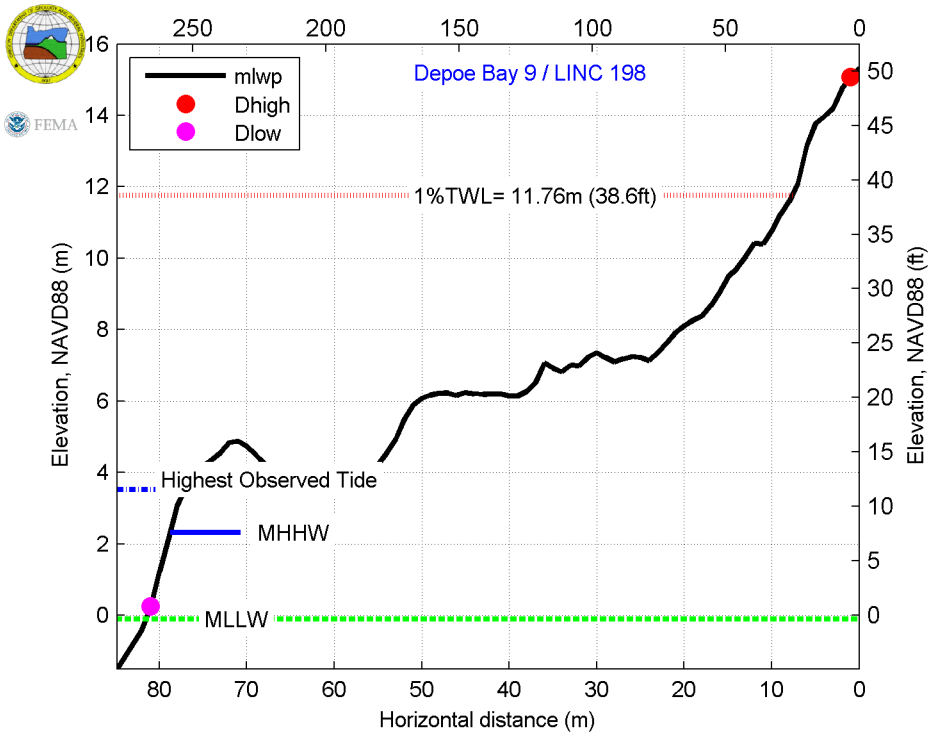

LINC 199

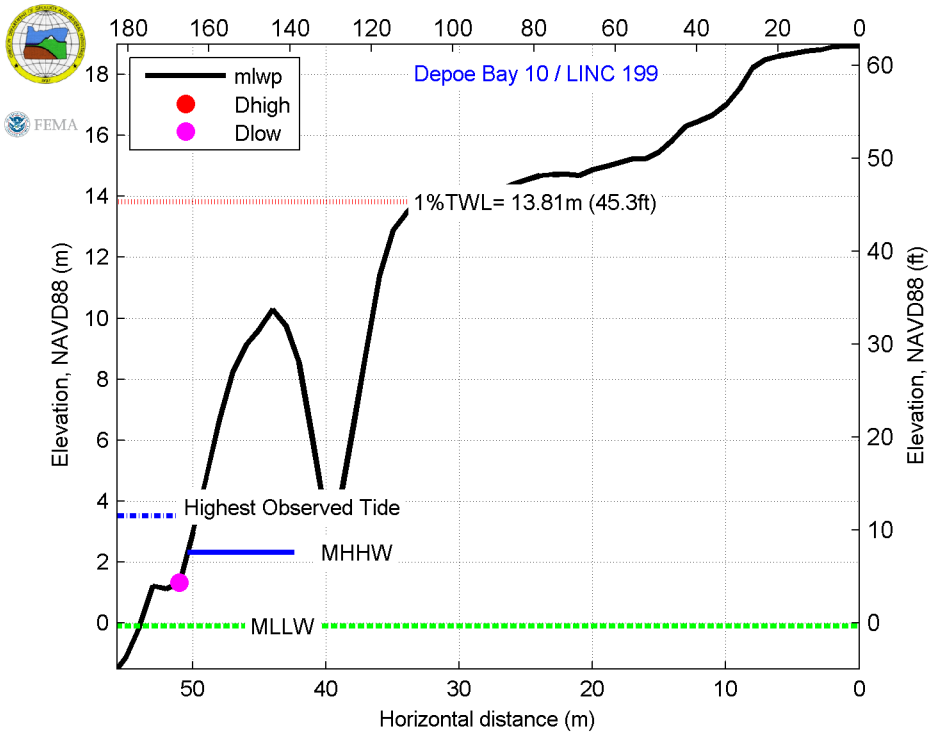

LINC 200

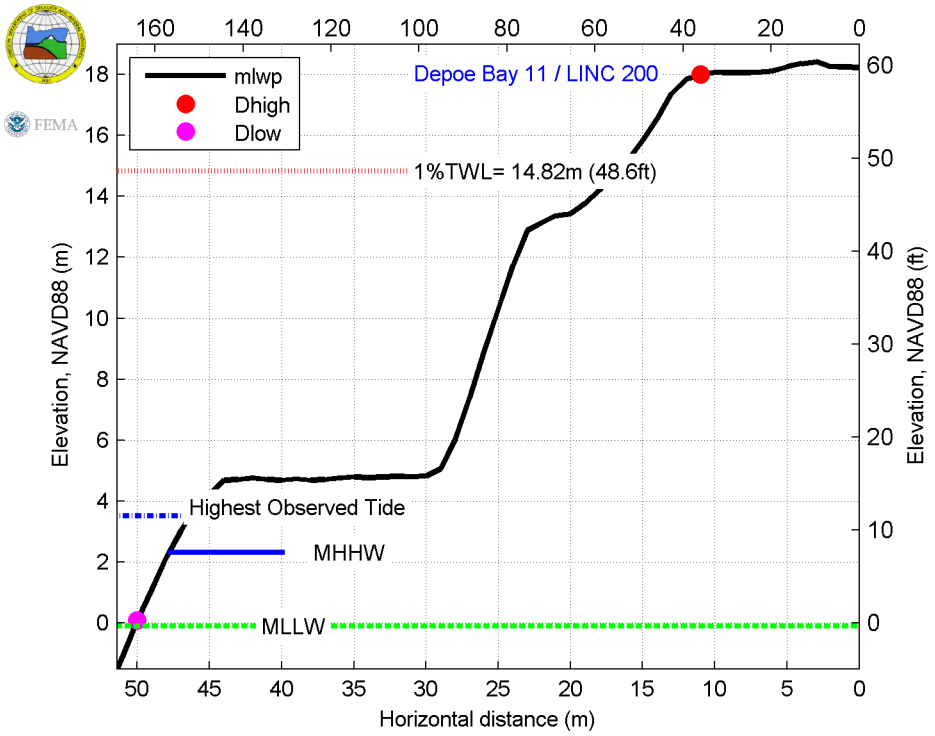

LINC 201

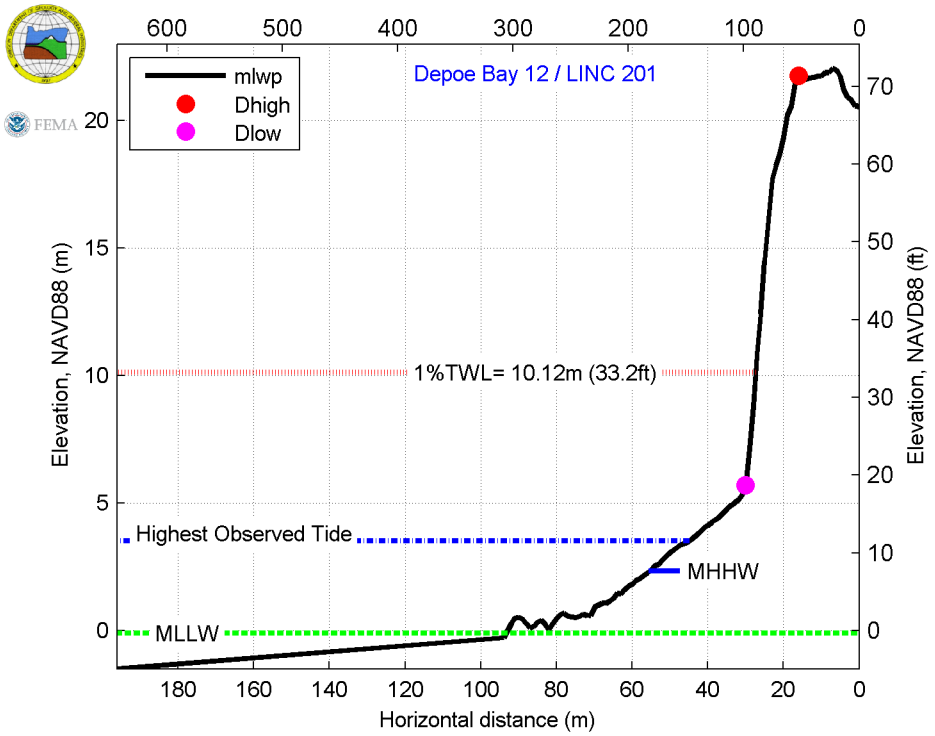

LINC 202

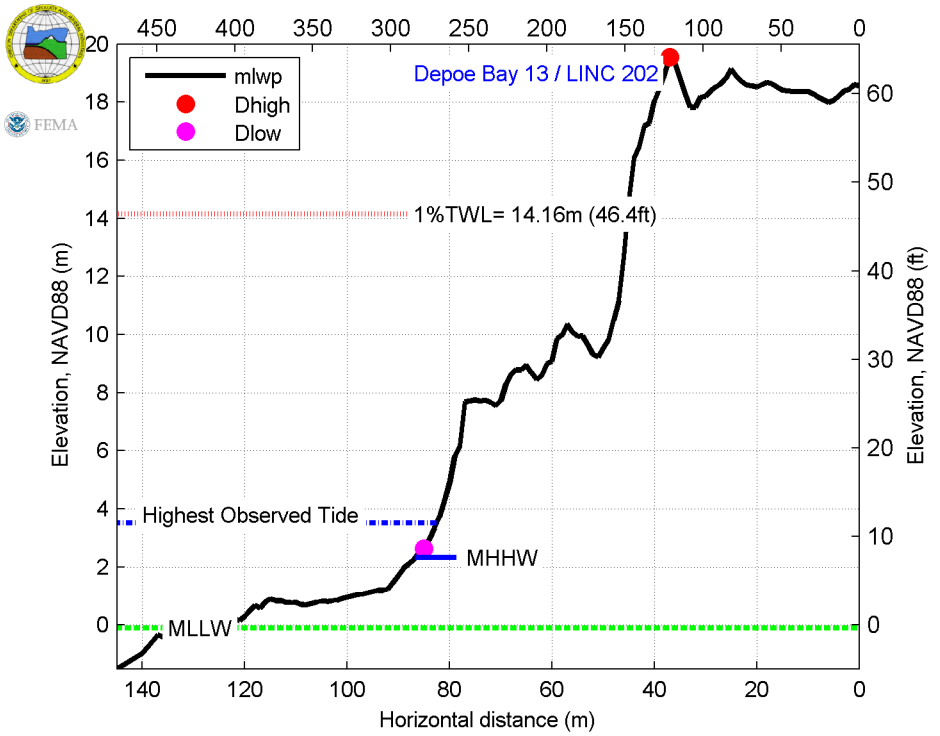
mlwp
Dhigh
Dlow
Depoe Bay 13 / LINC 202
1%TWL= 14.16m (46.4ft)
Highest Observed Tide
MHHW
MLLW
Elevation, NAVD88 (m)
Elevation, NAVD88 (ft)
Horizontal distance (m)
FEMA

11.2.15 Fogarty Creek

LINC 203

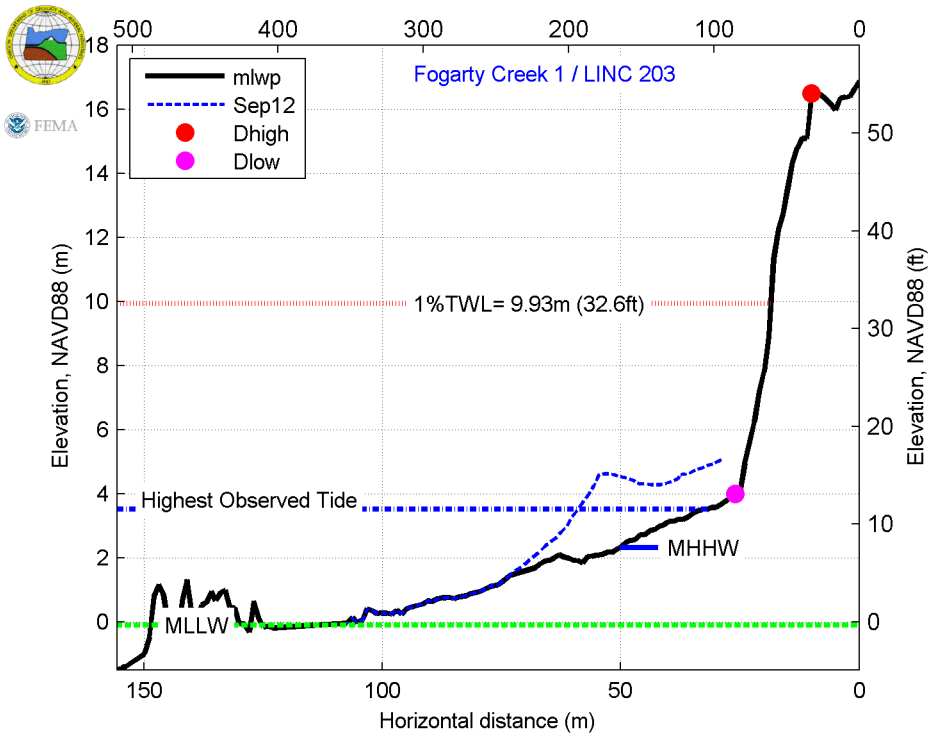

LINC 204

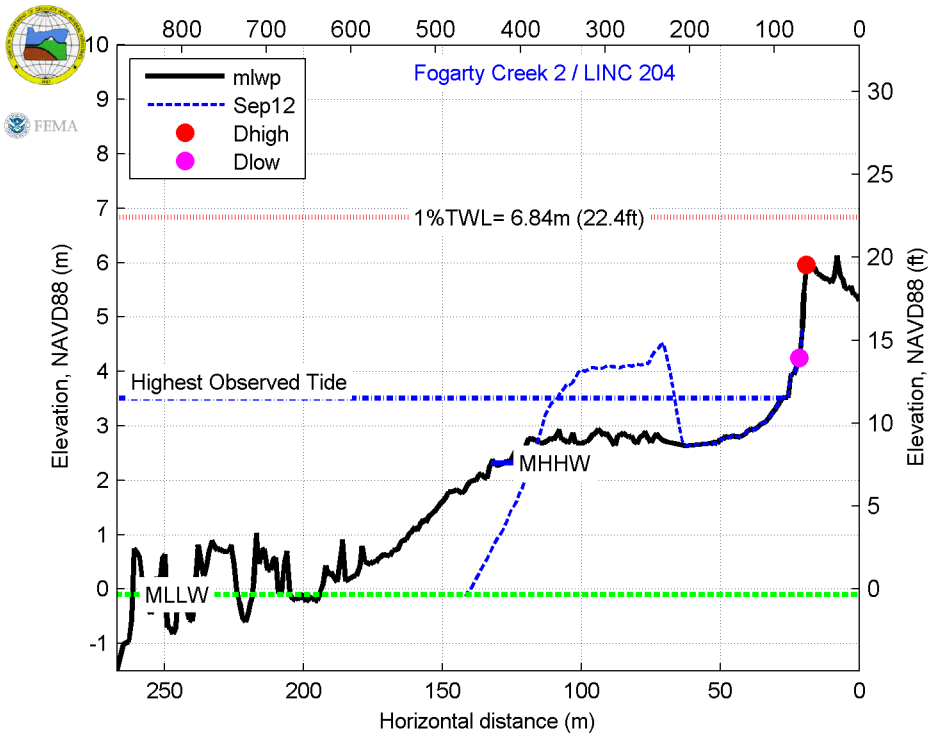

LINC 205

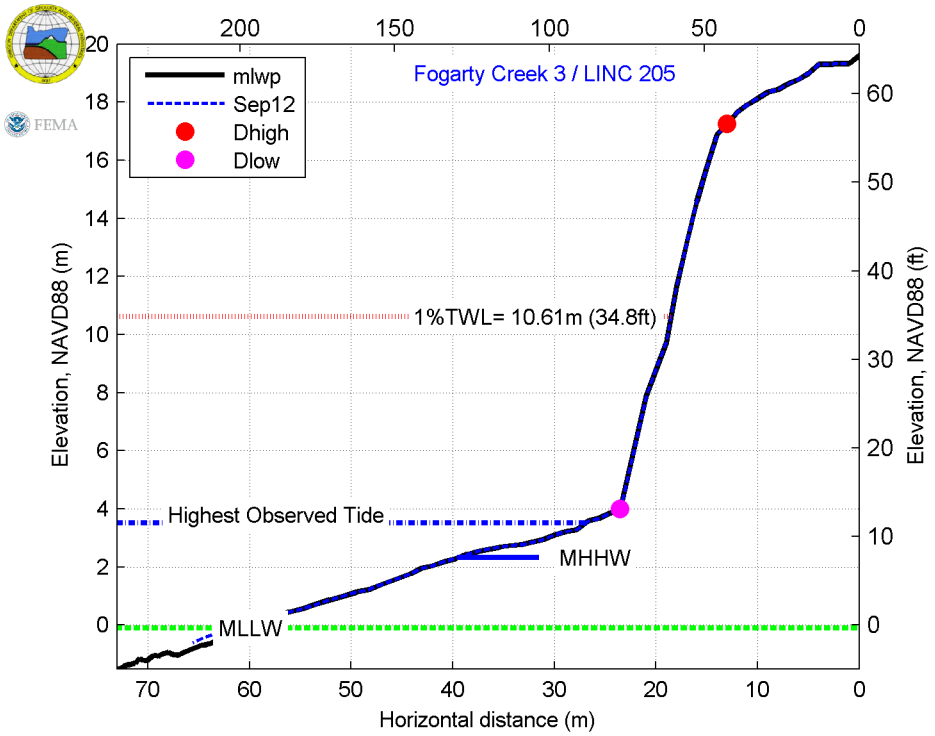

LINC 206

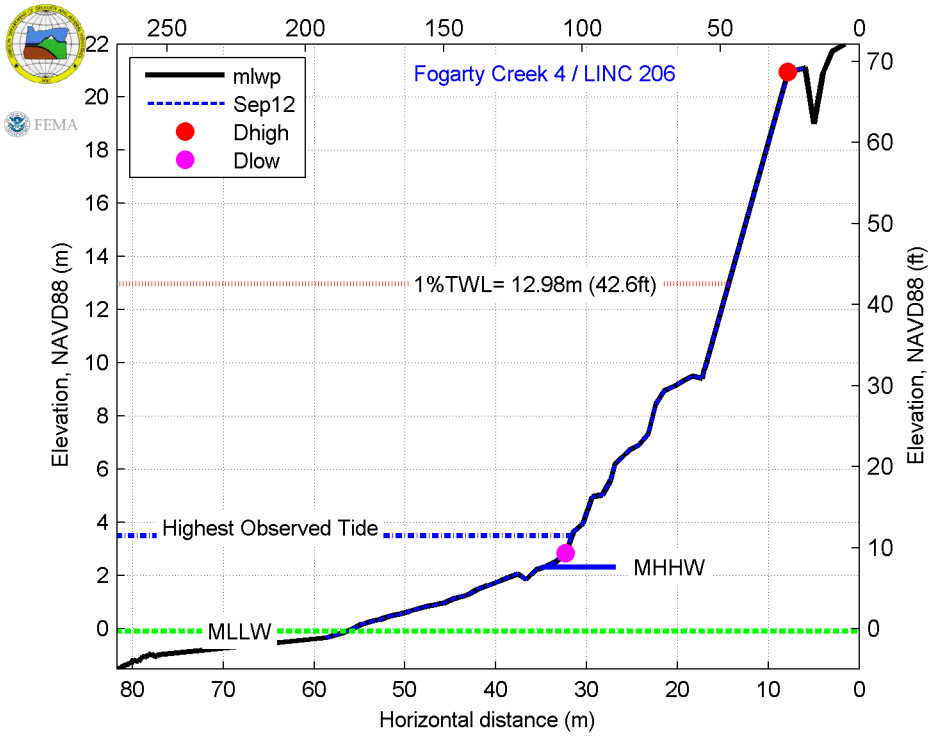

LINC 207

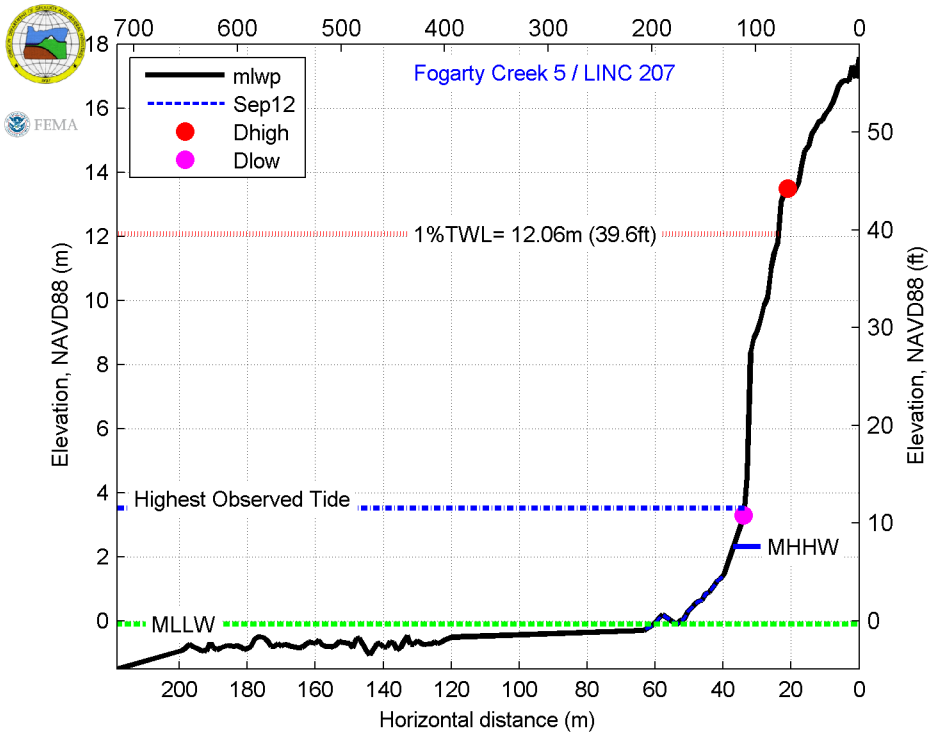

LINC 208

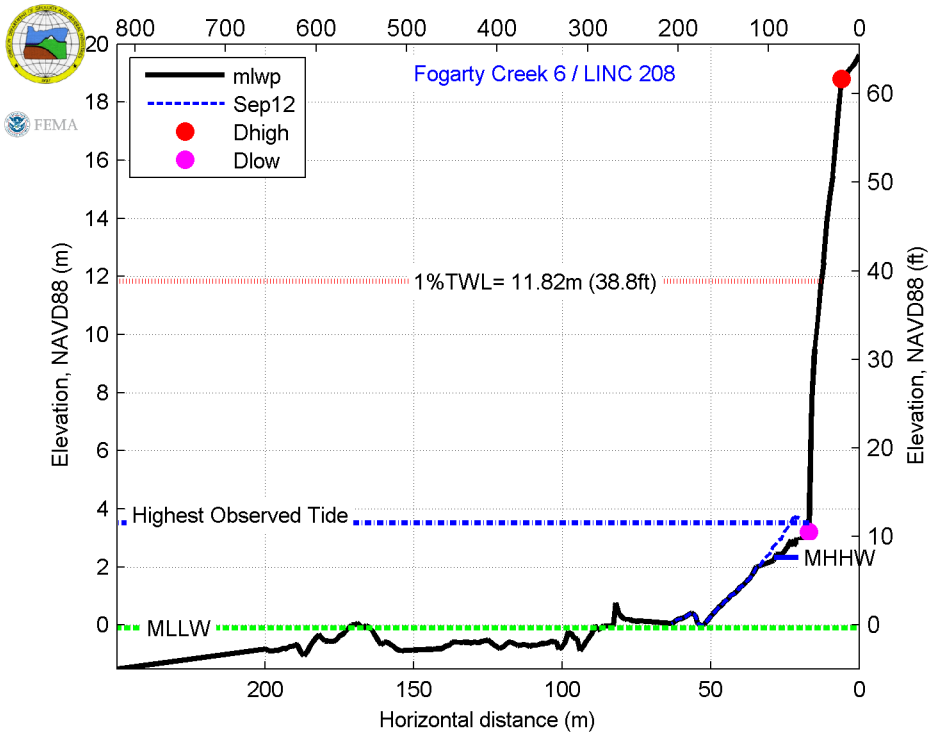

LINC 209

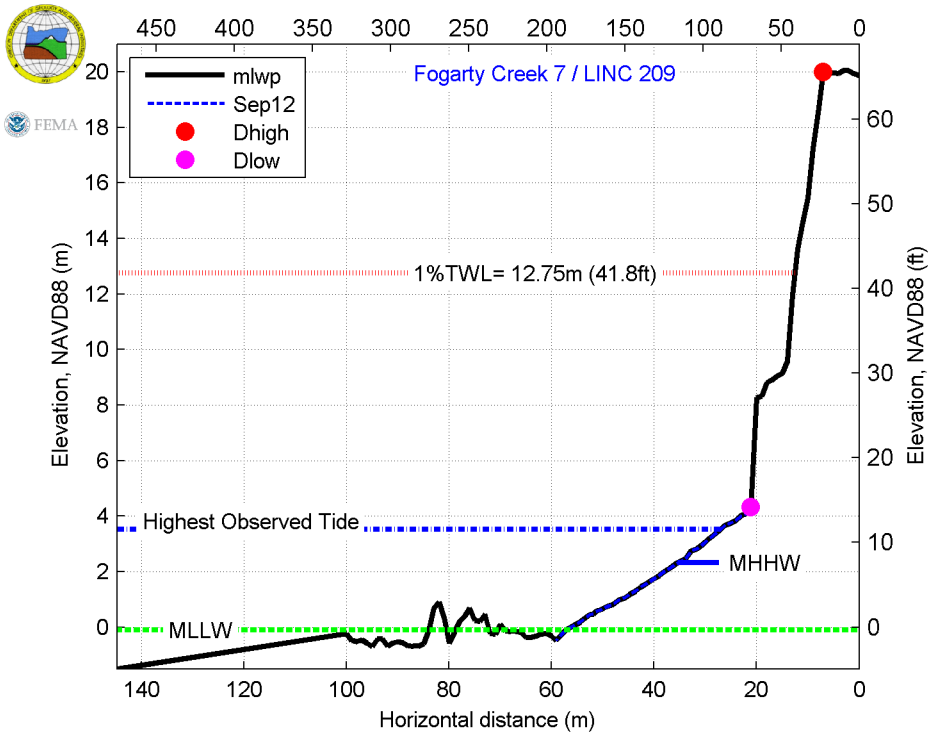

LINC 210

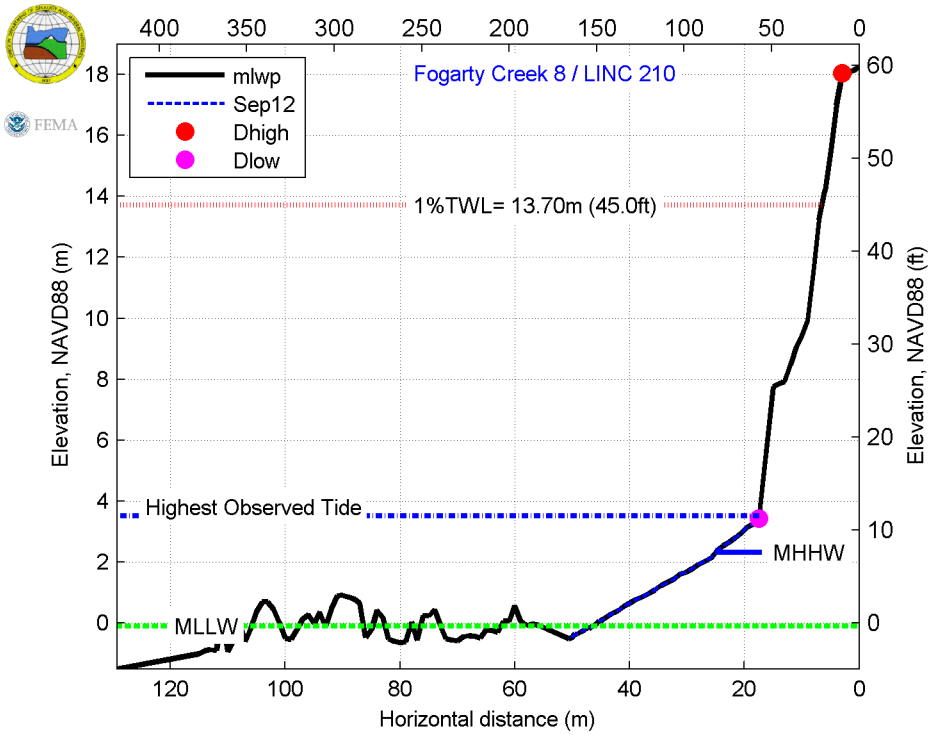

11.2.16 Siletz Spit

LINC 211

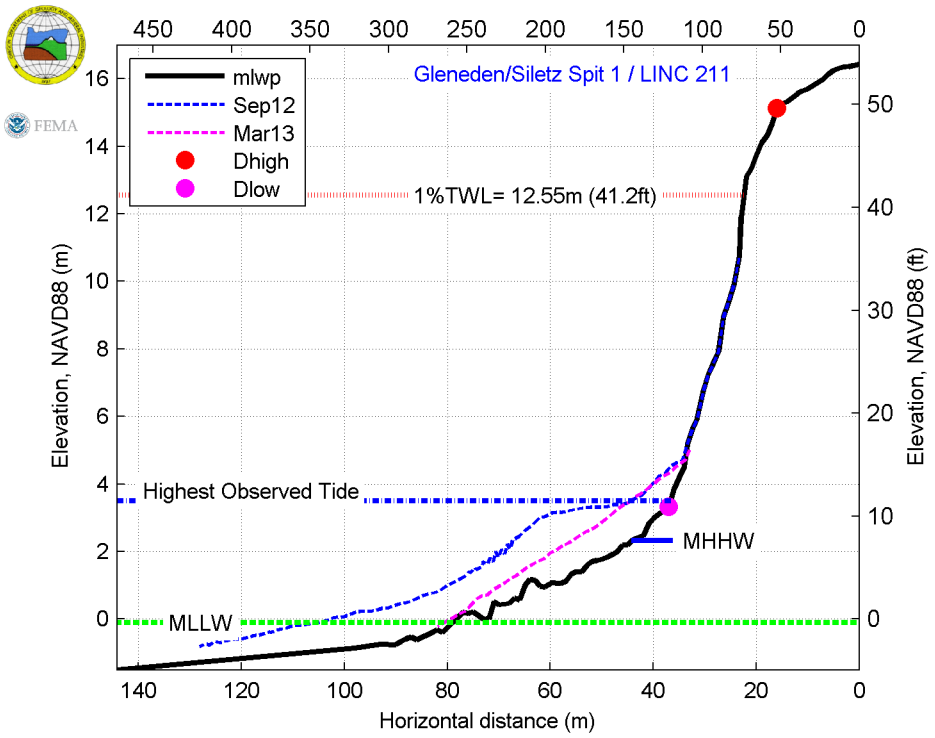

LINC 212

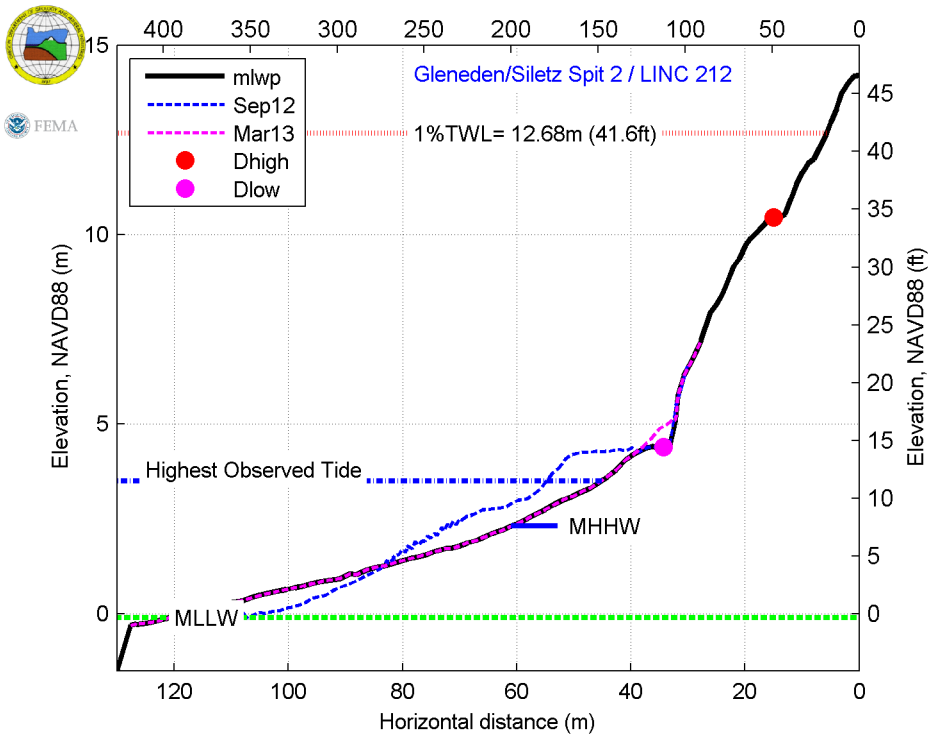

LINC 213

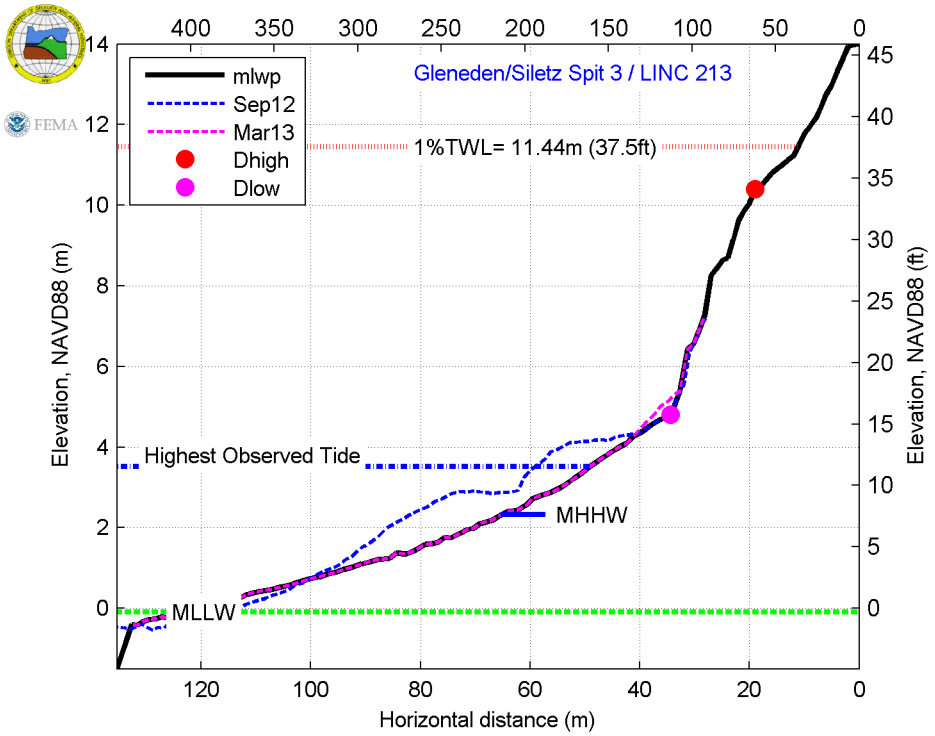

LINC 214

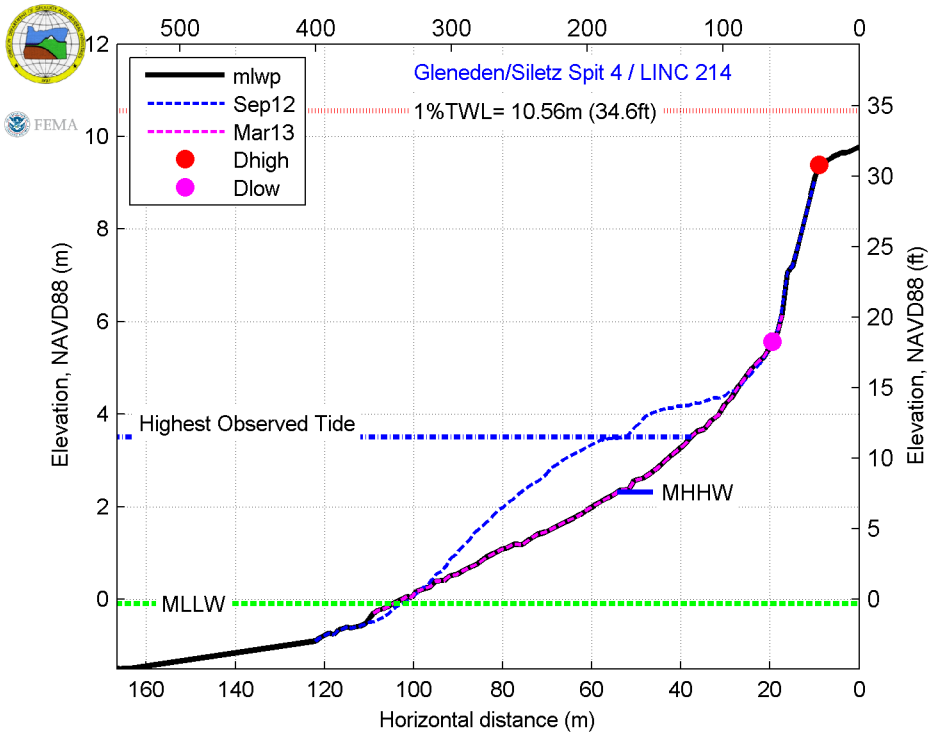

LINC 215

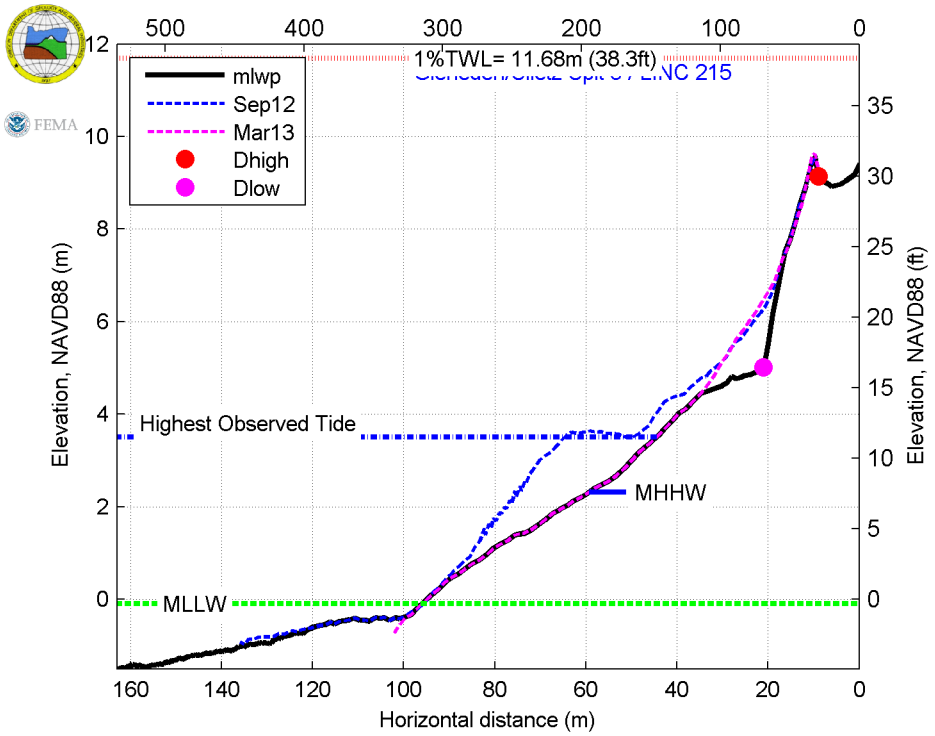

LINC 216

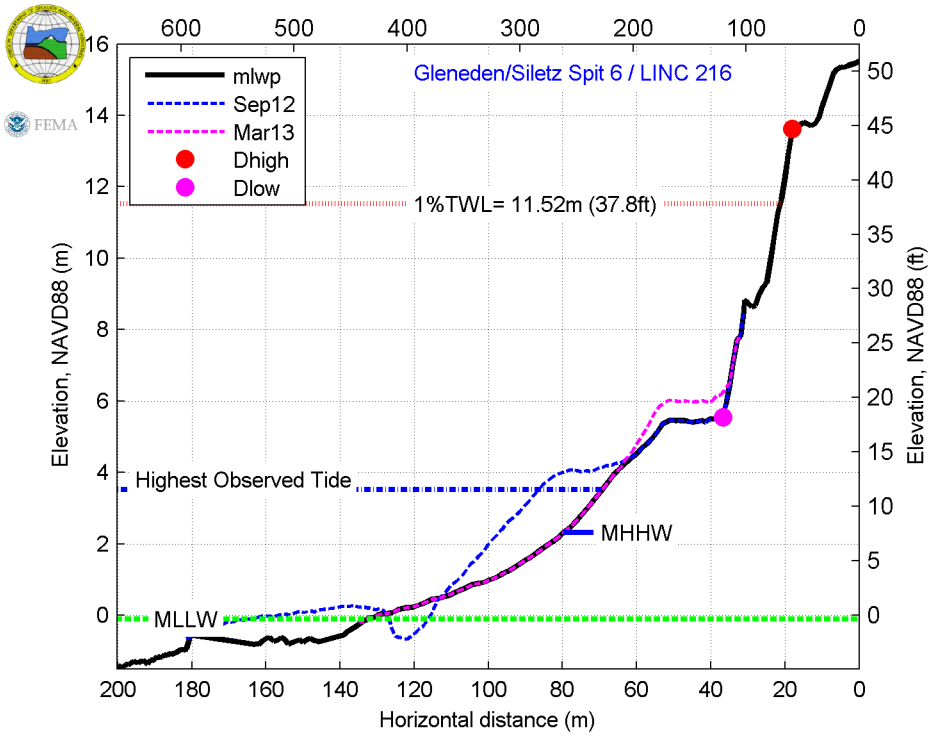

LINC 217

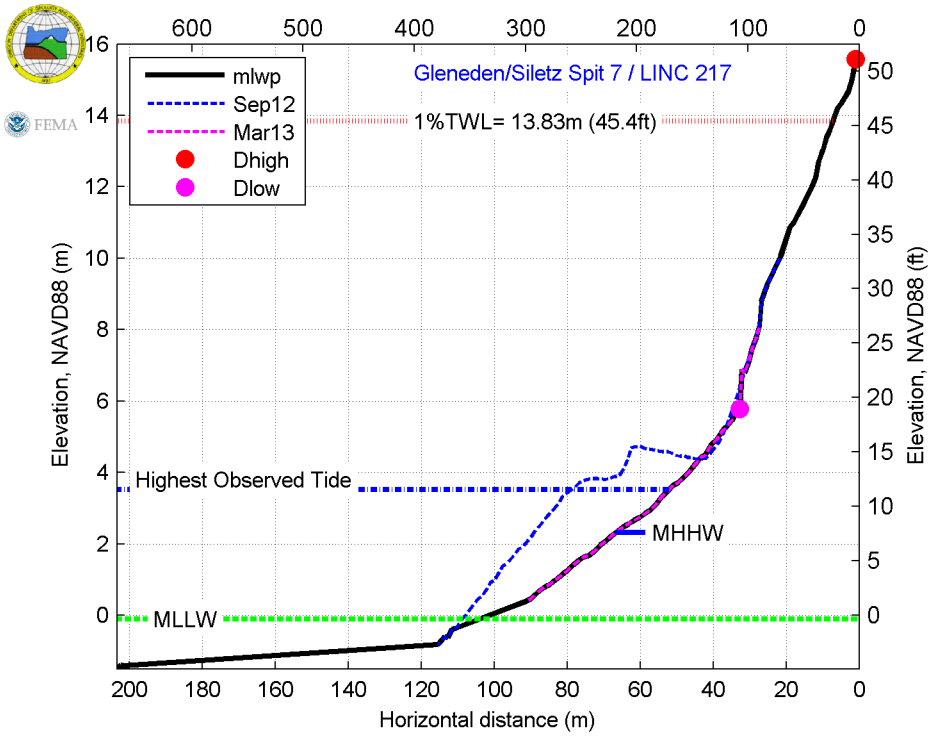

LINC 218

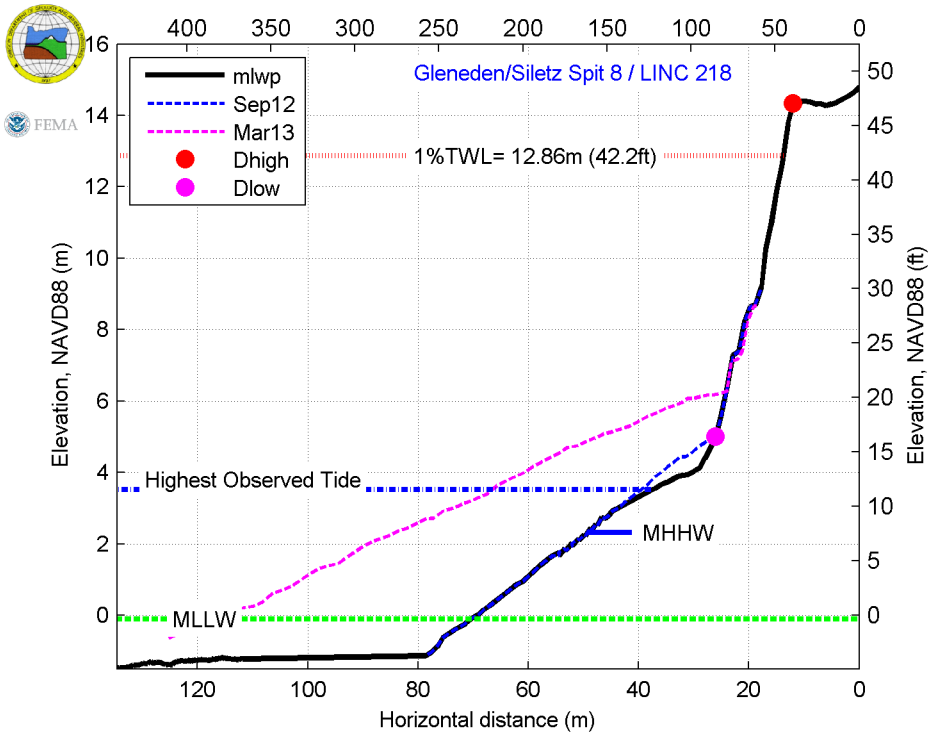

LINC 219

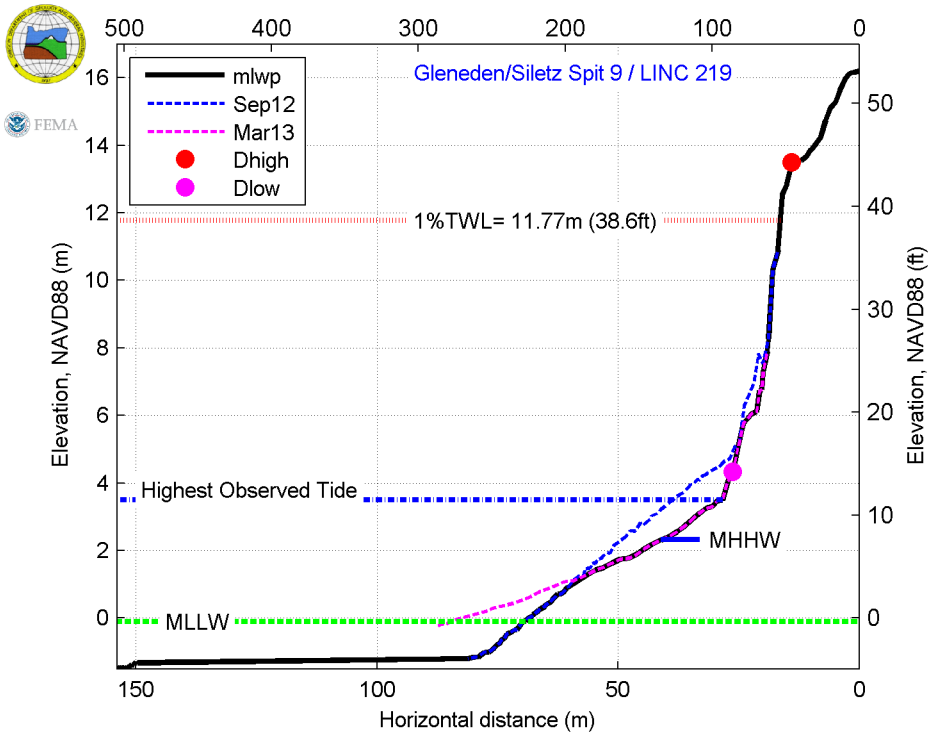

LINC 220

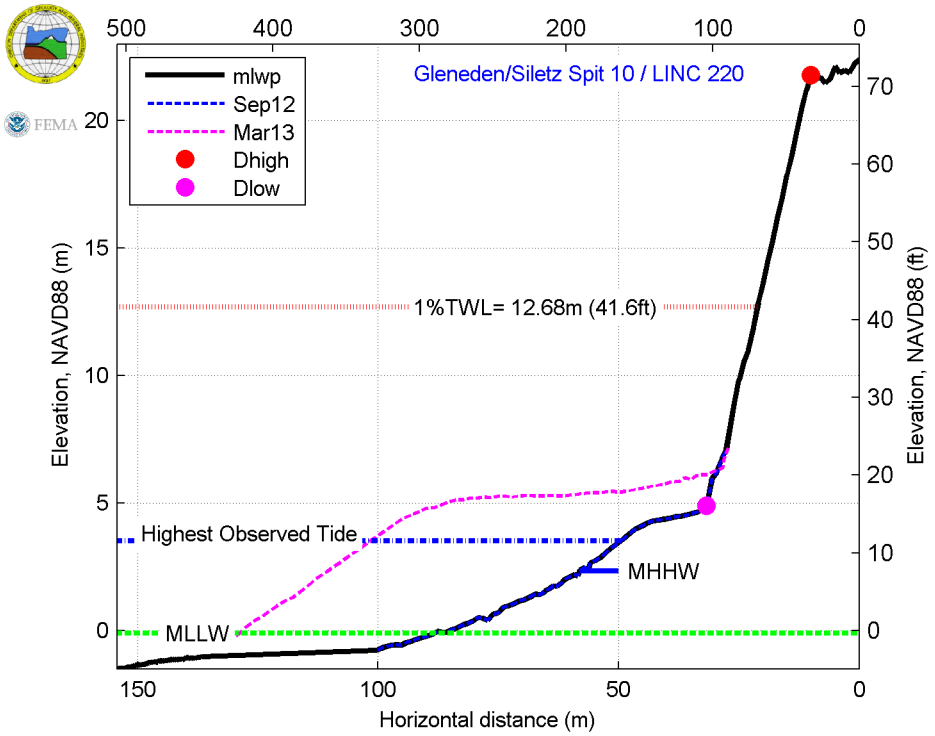

LINC 221

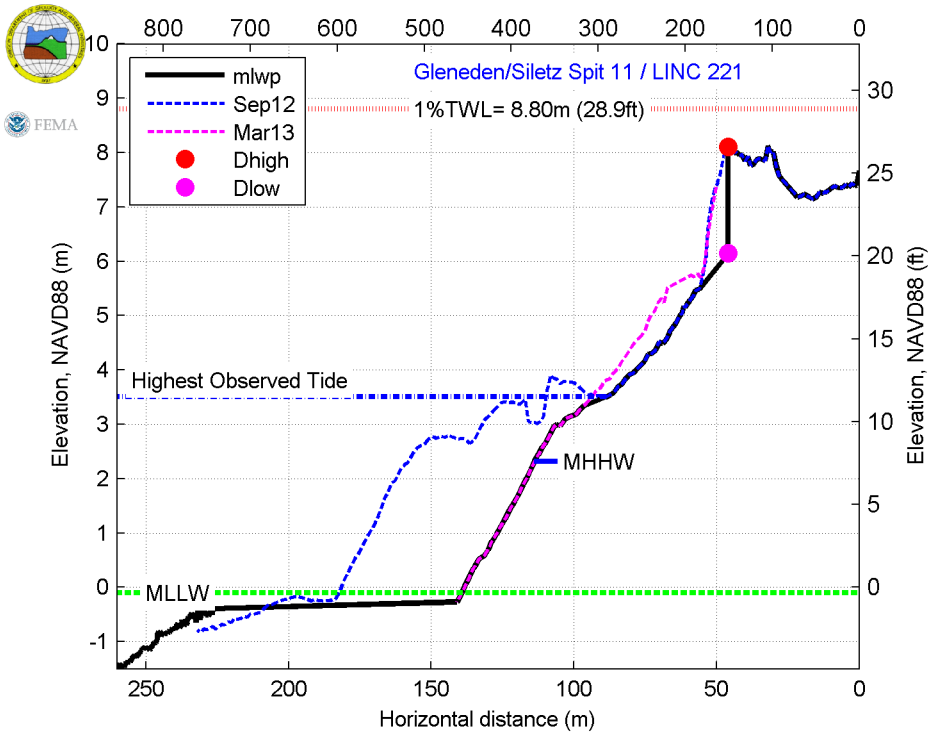

LINC 222

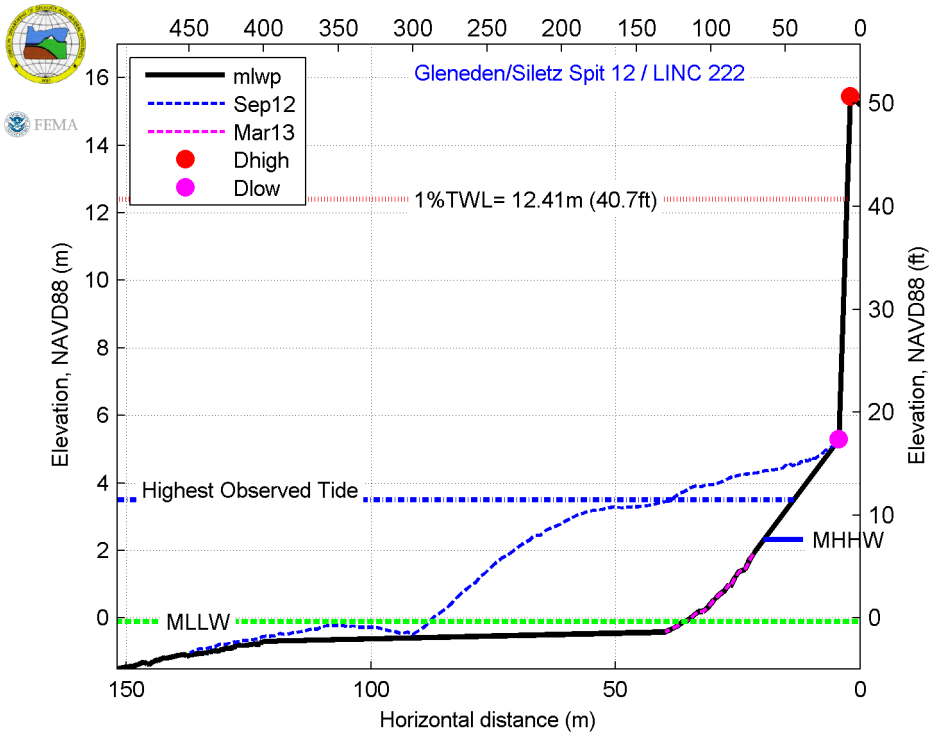

LINC 223

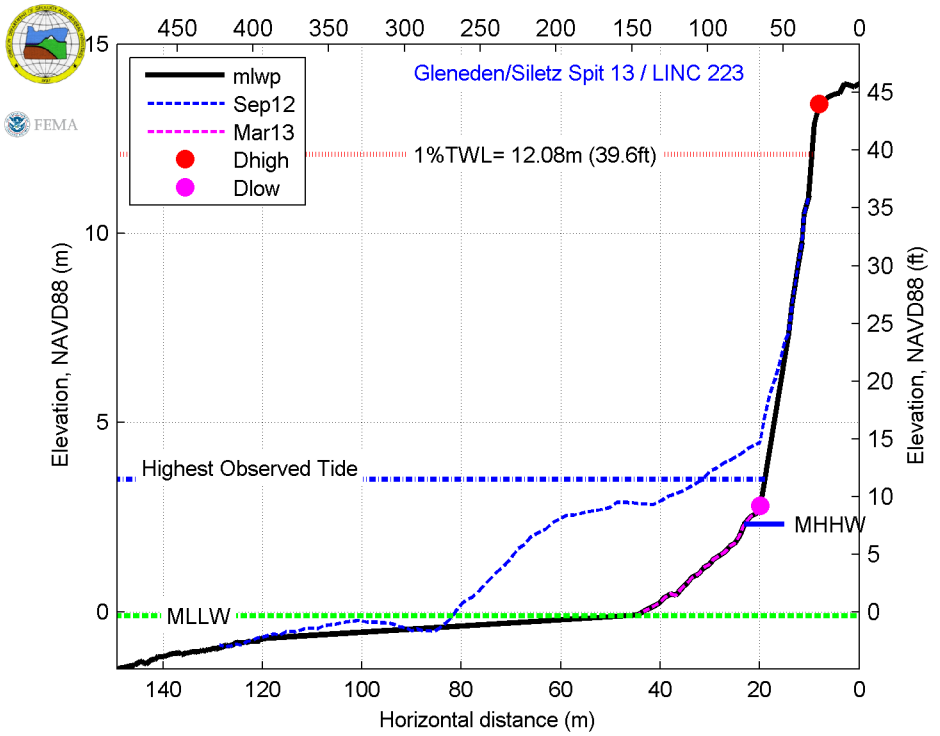

LINC 224

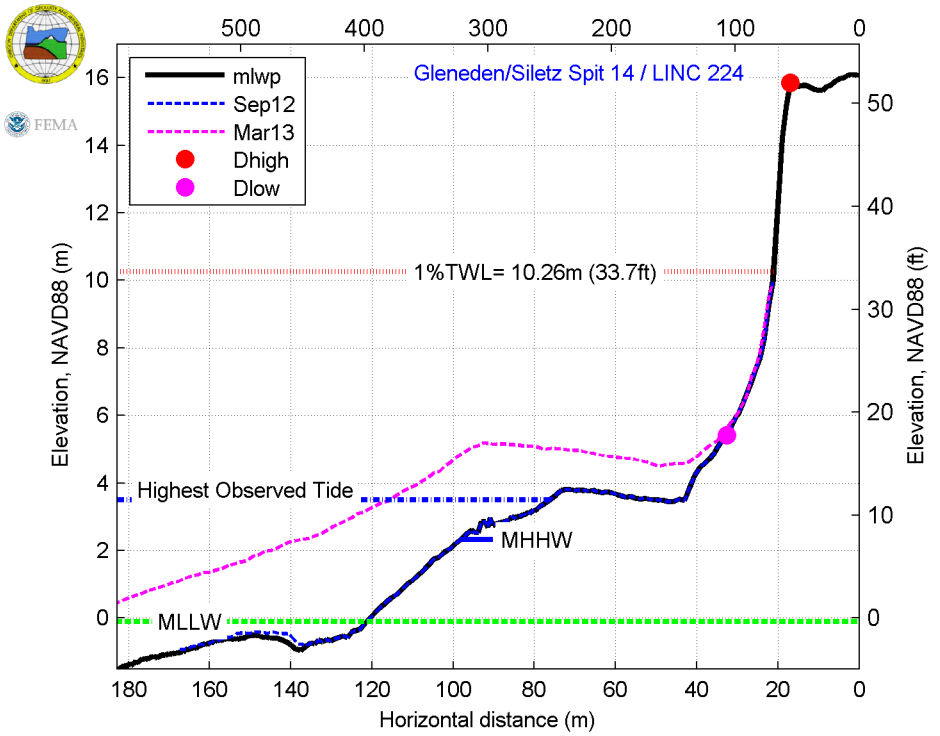

LINC 225

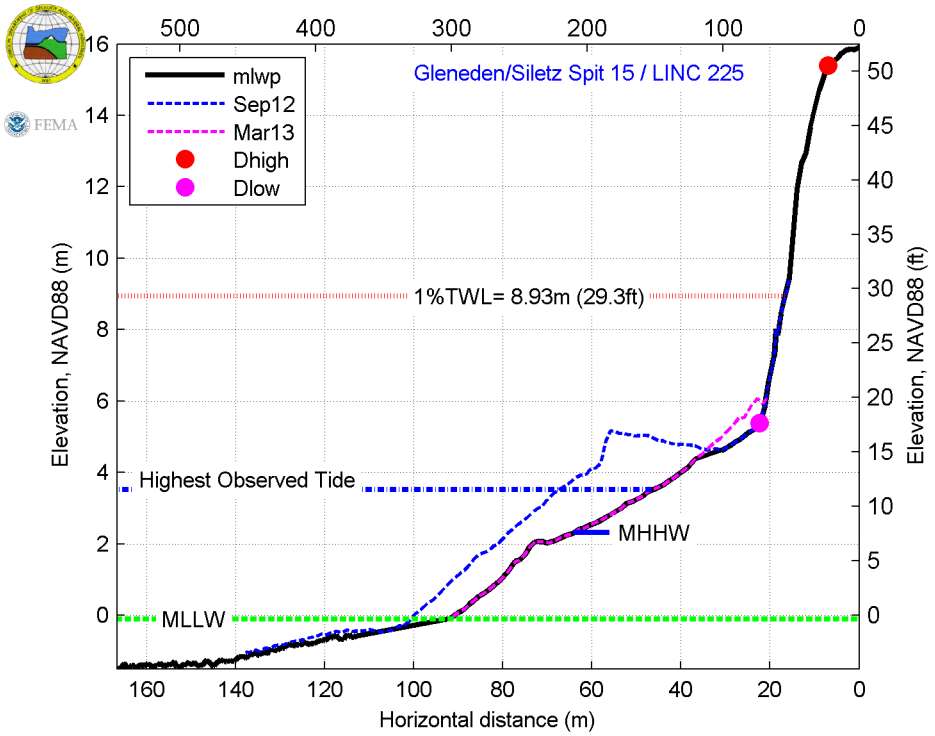

LINC 226

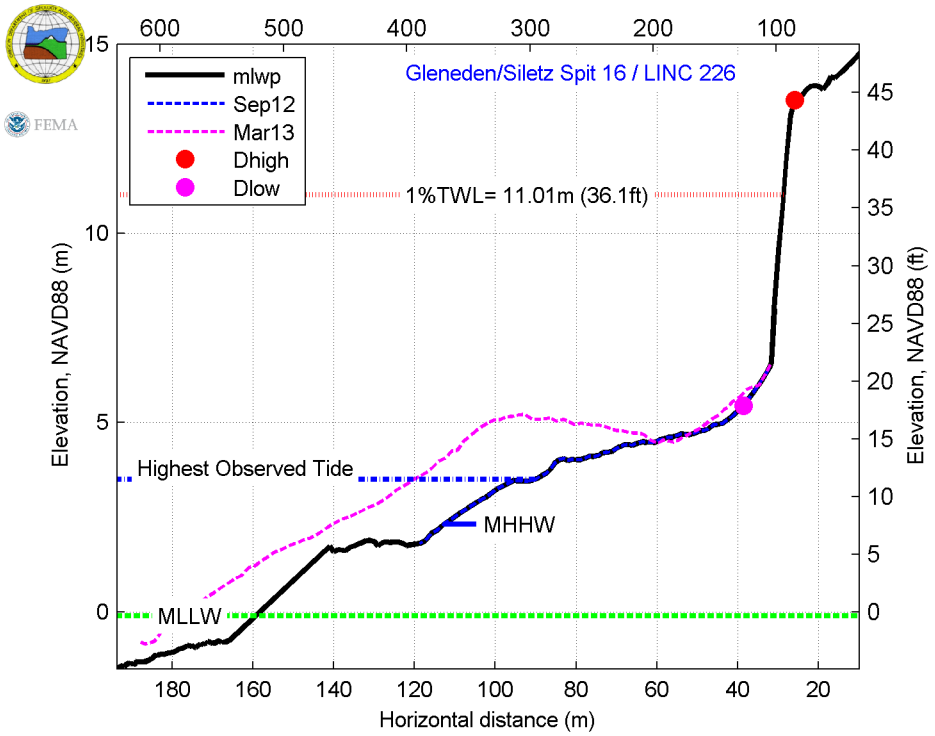

LINC 227

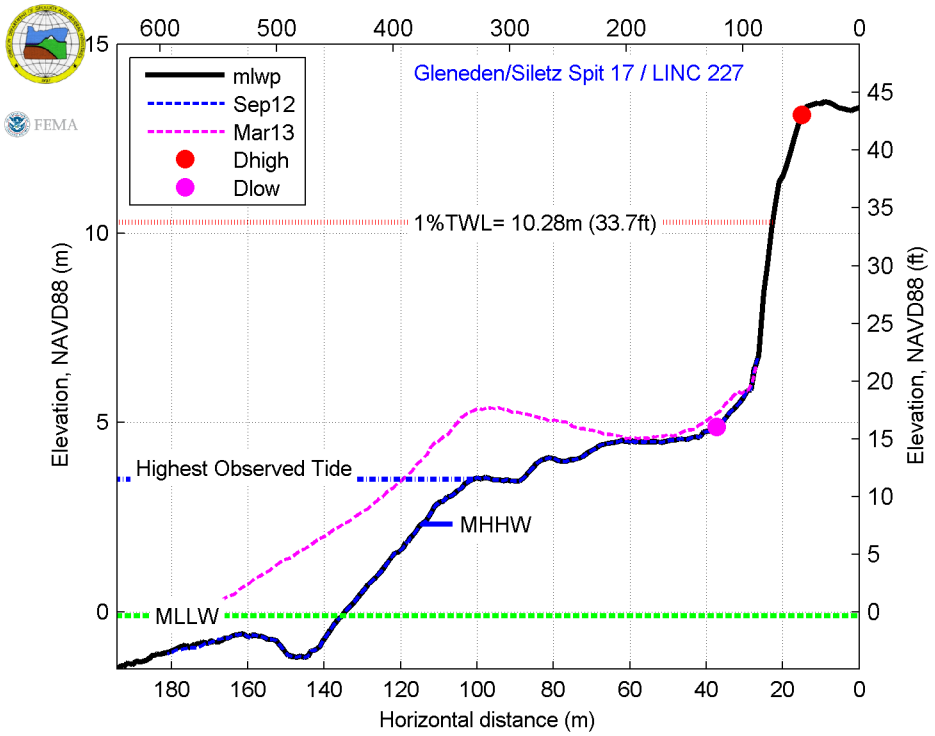

LINC 228

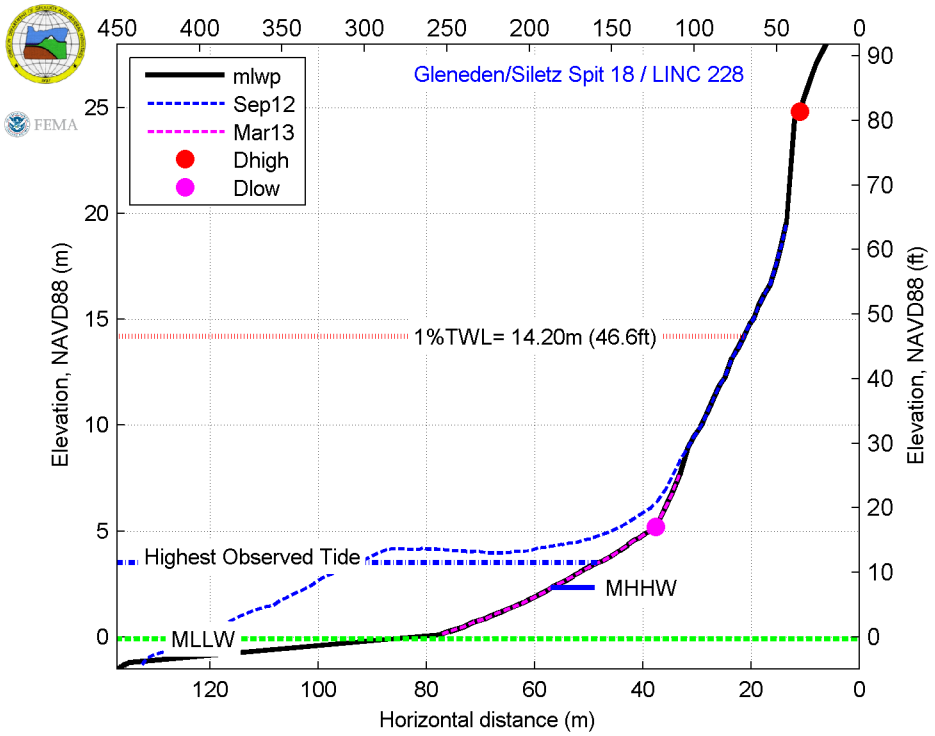

LINC 229

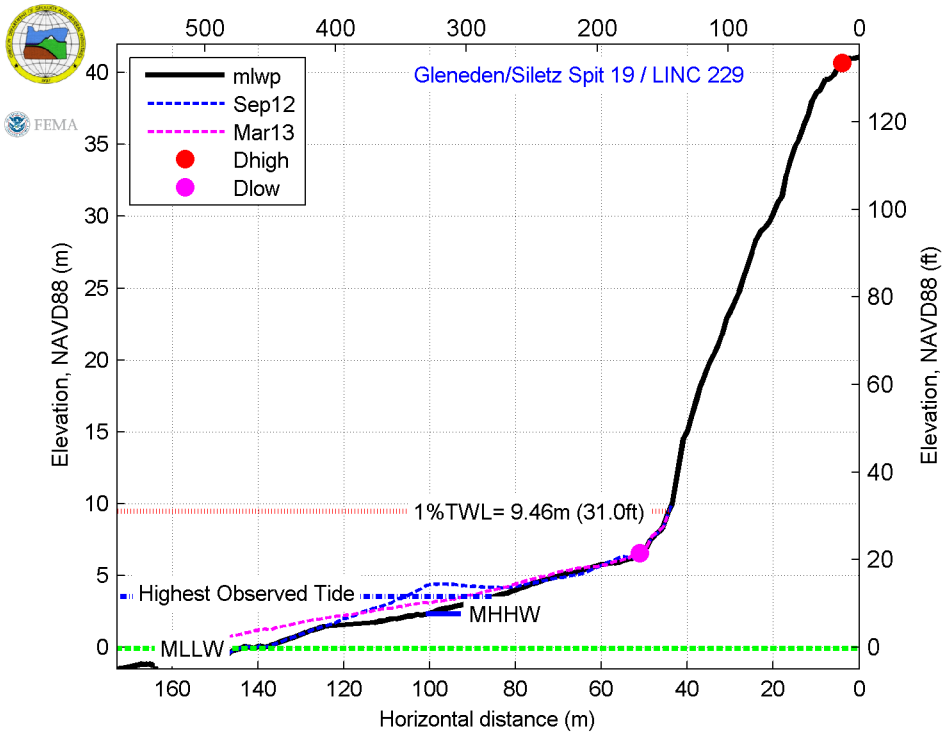

LINC 230

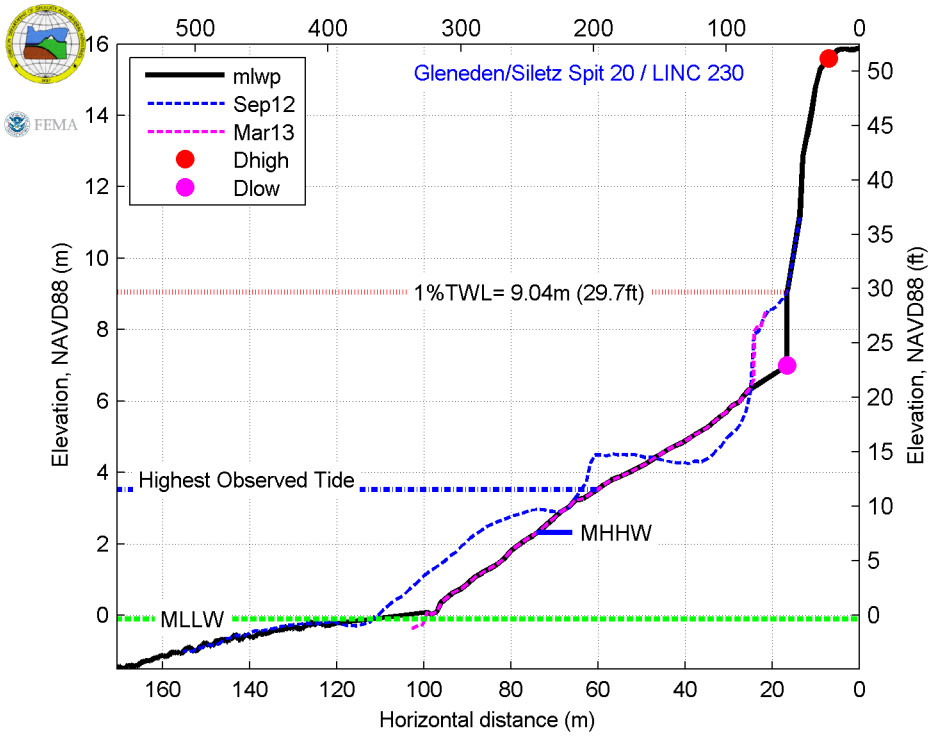

LINC 231

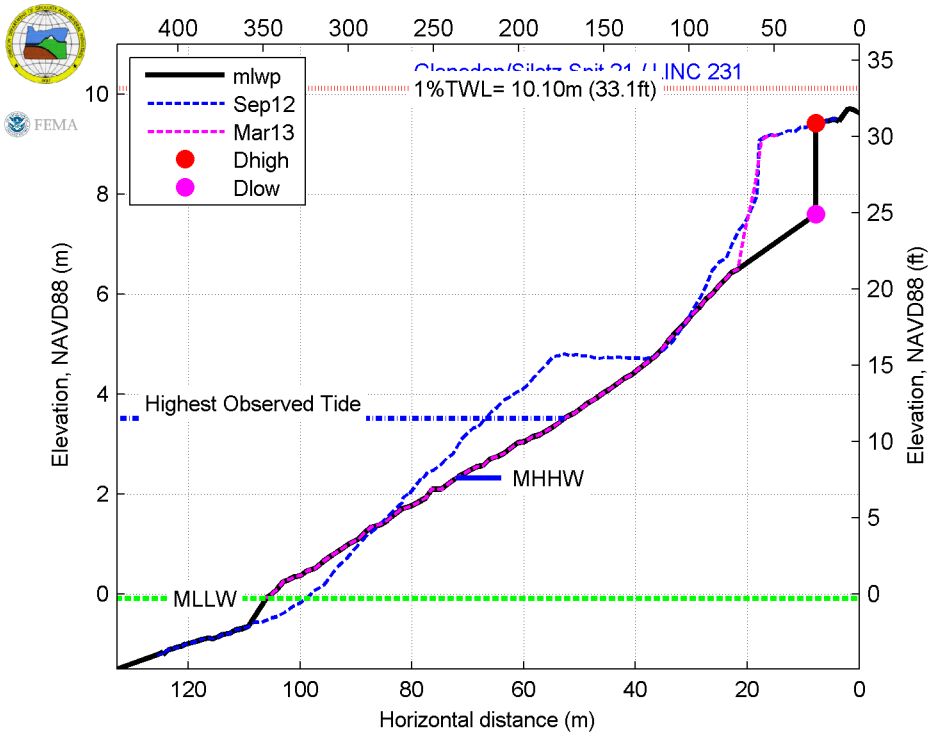

LINC 232

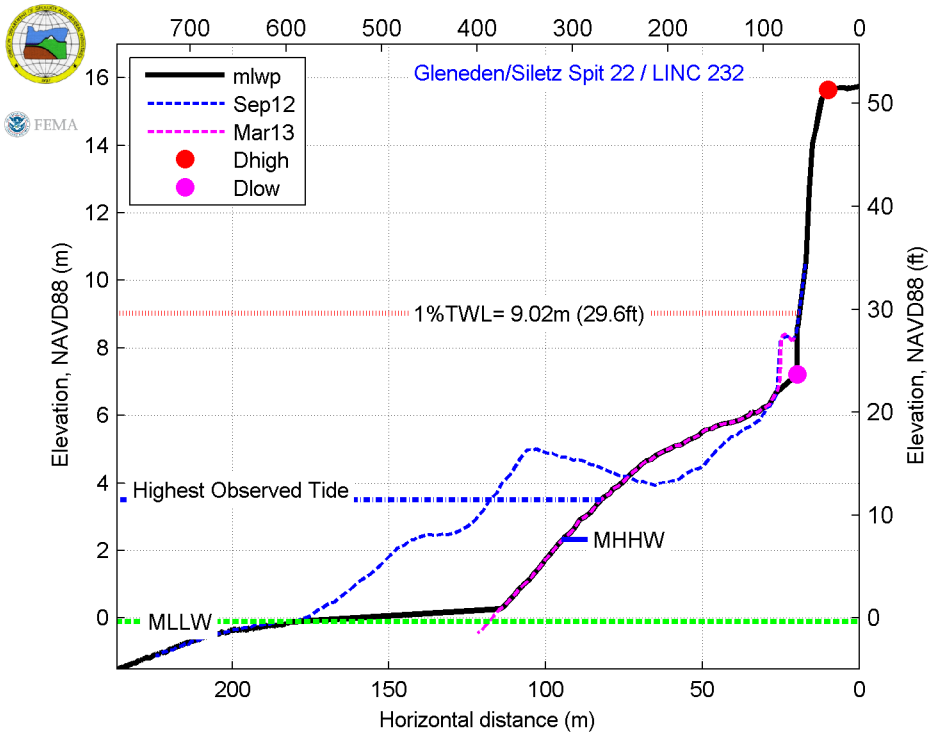

LINC 233

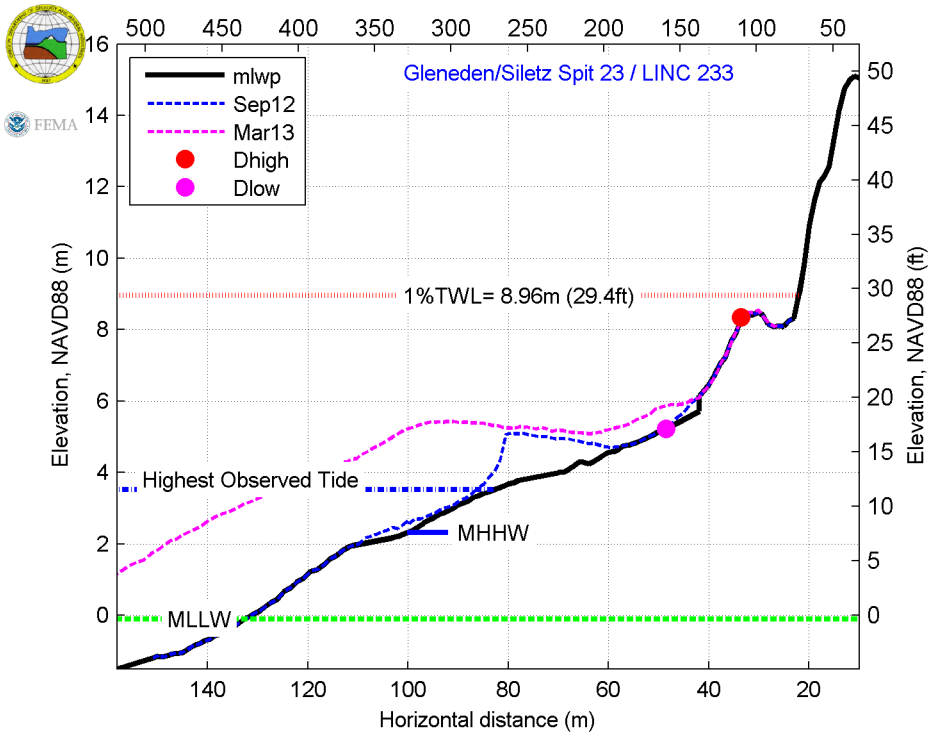

LINC 234

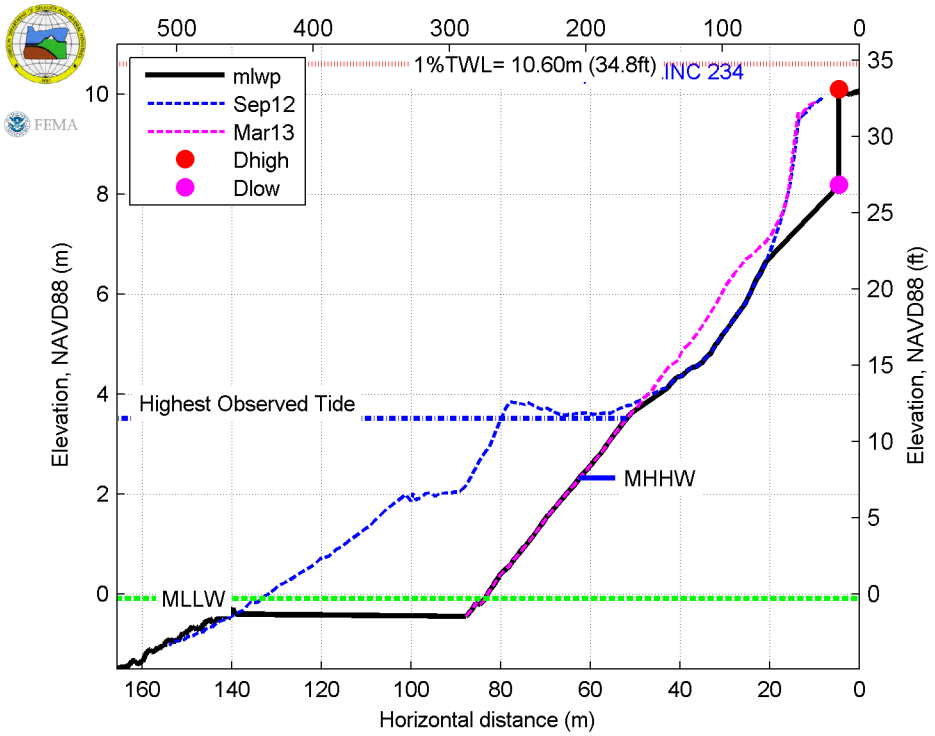

LINC 235

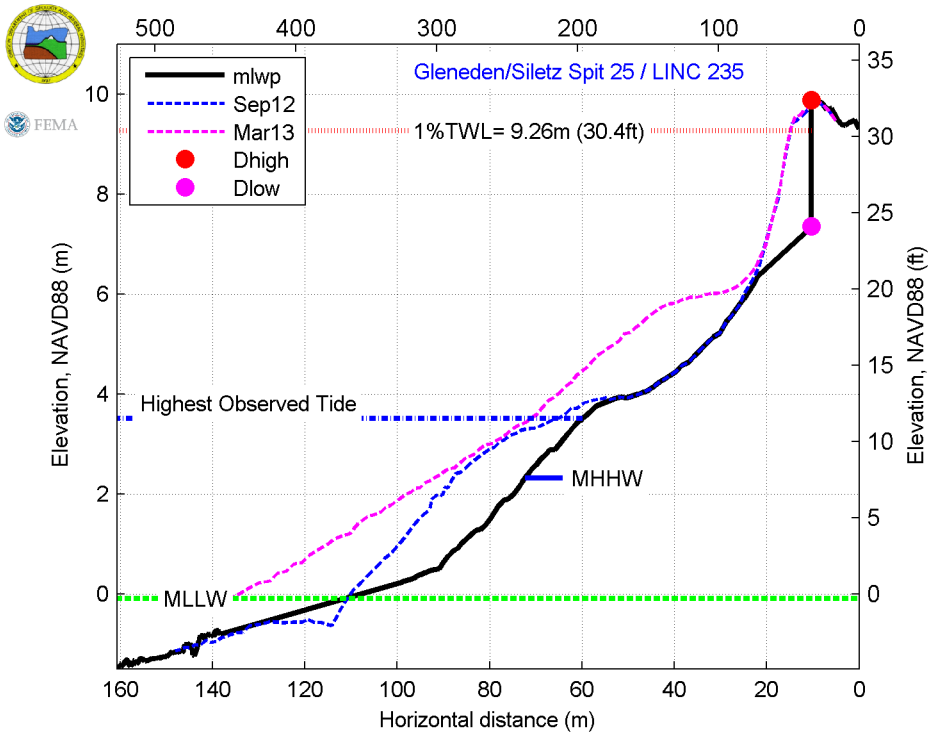

LINC 236

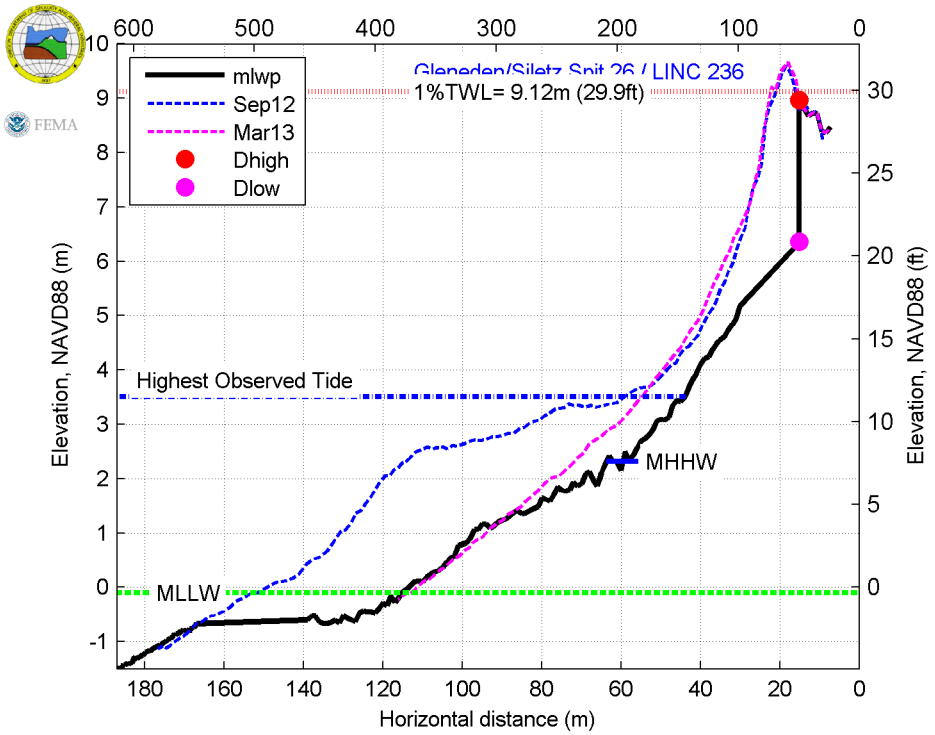

LINC 237

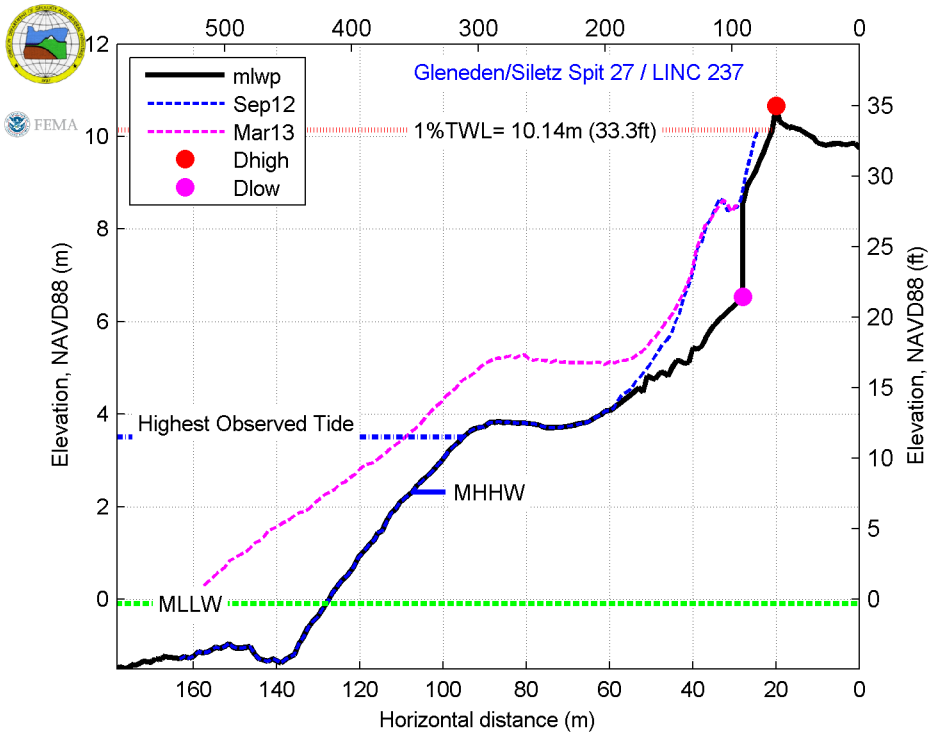

LINC 238

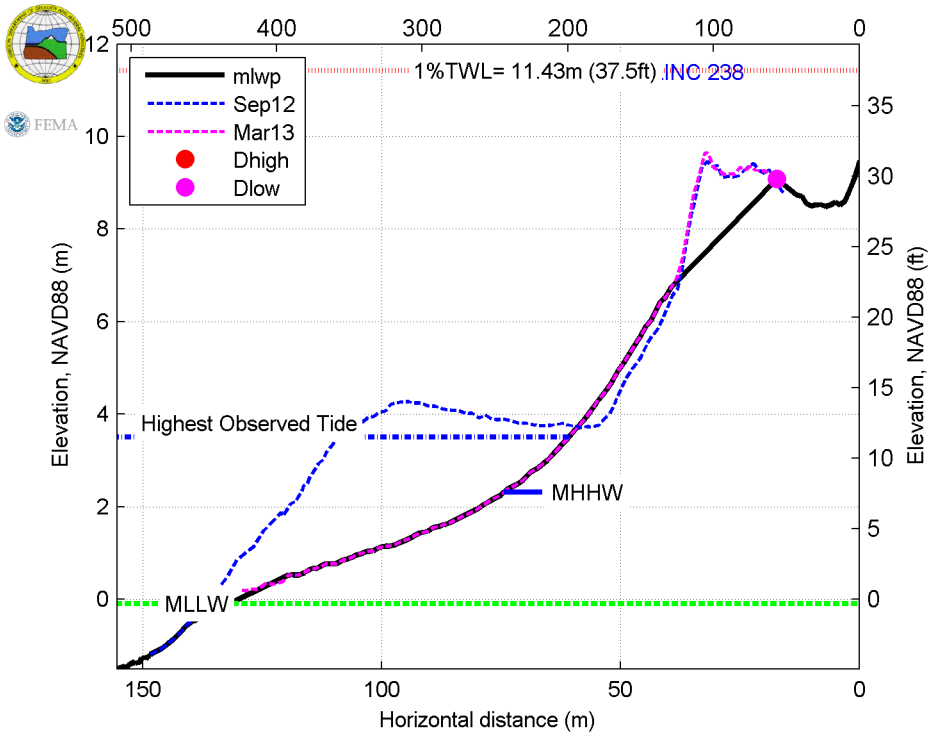

LINC 239

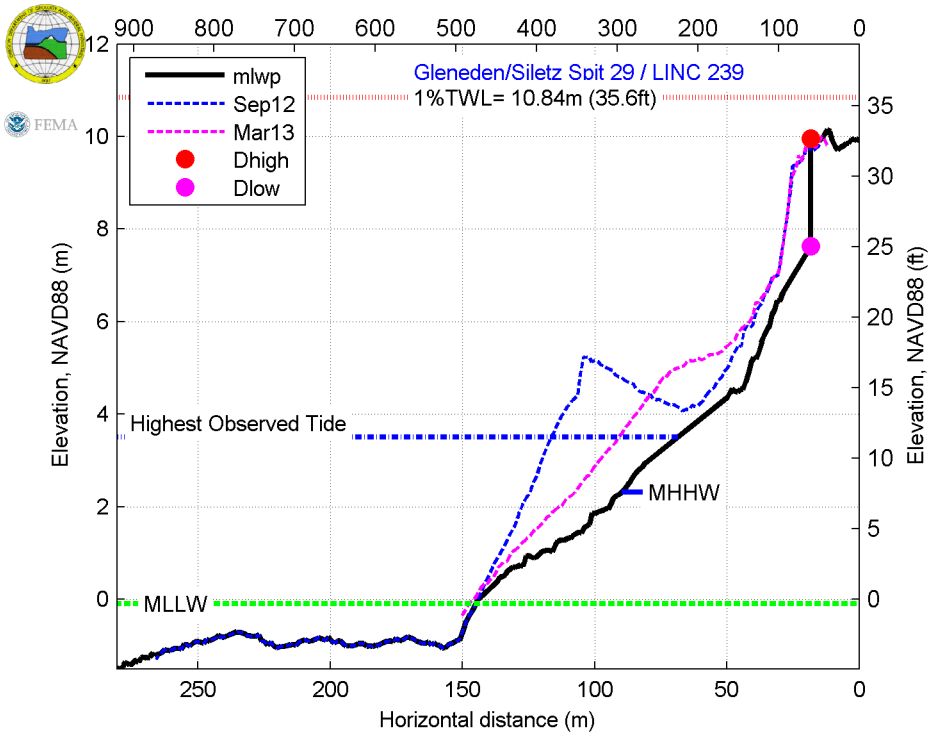

LINC 240

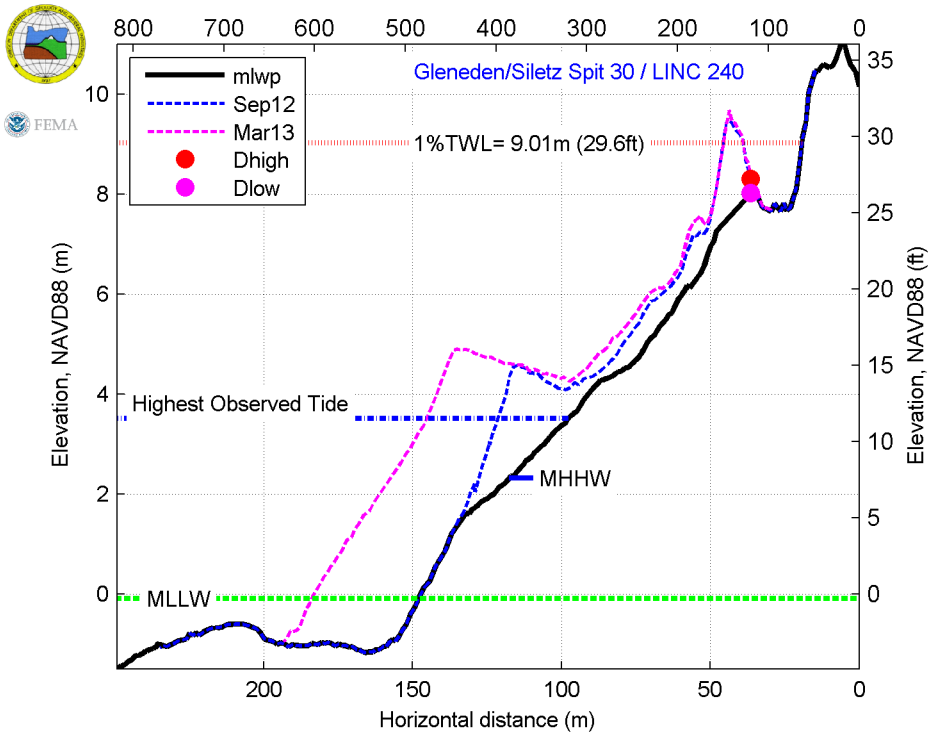

LINC 241

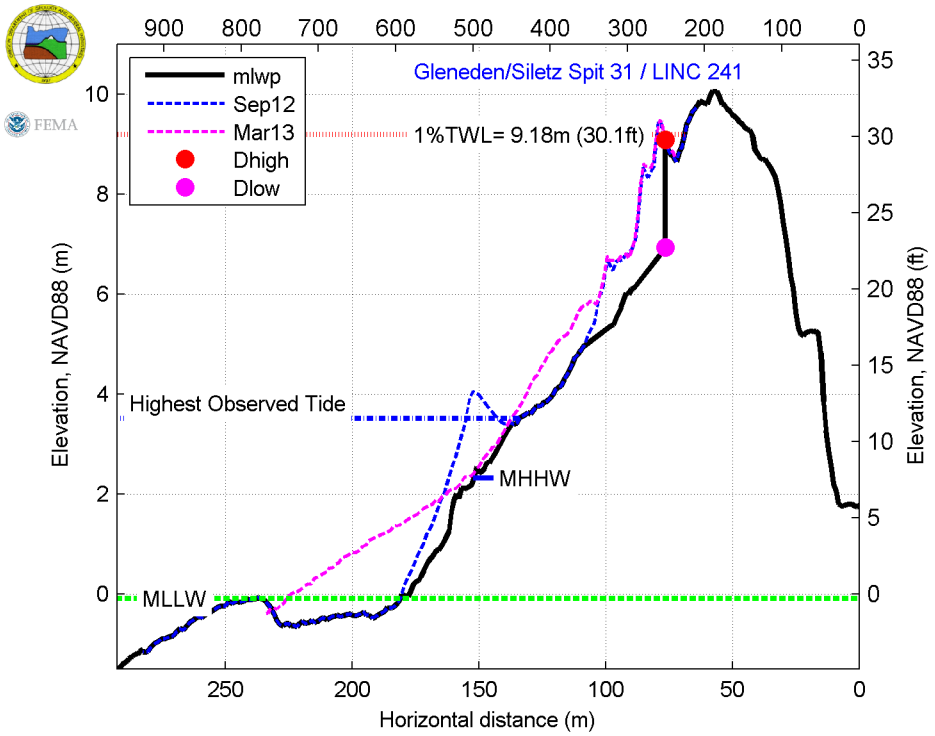

LINC 242

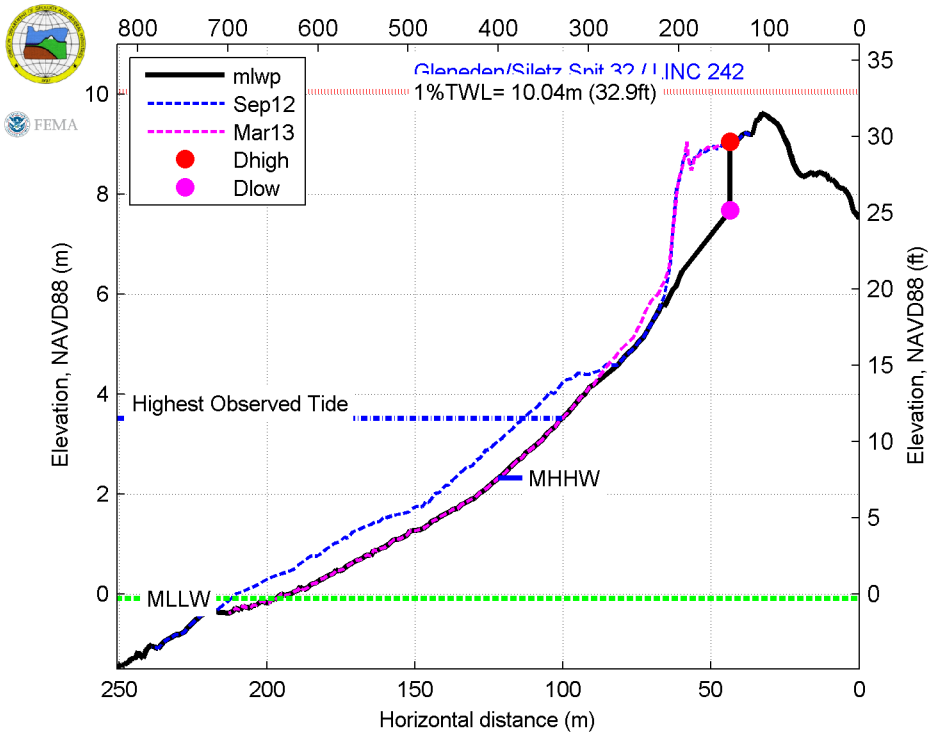

LINC 243

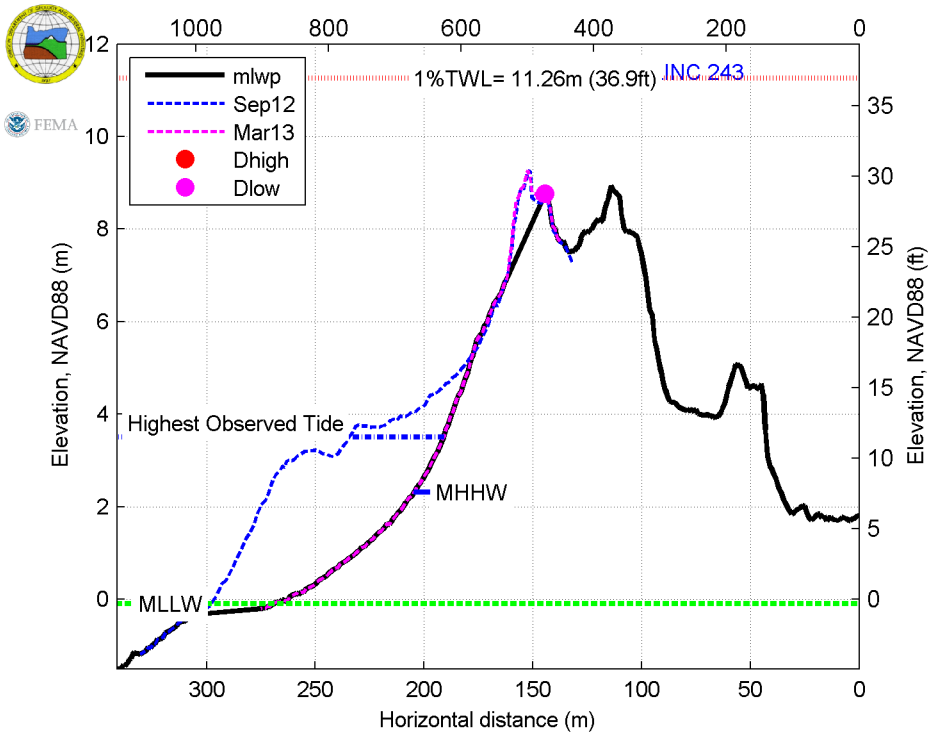

LINC 244

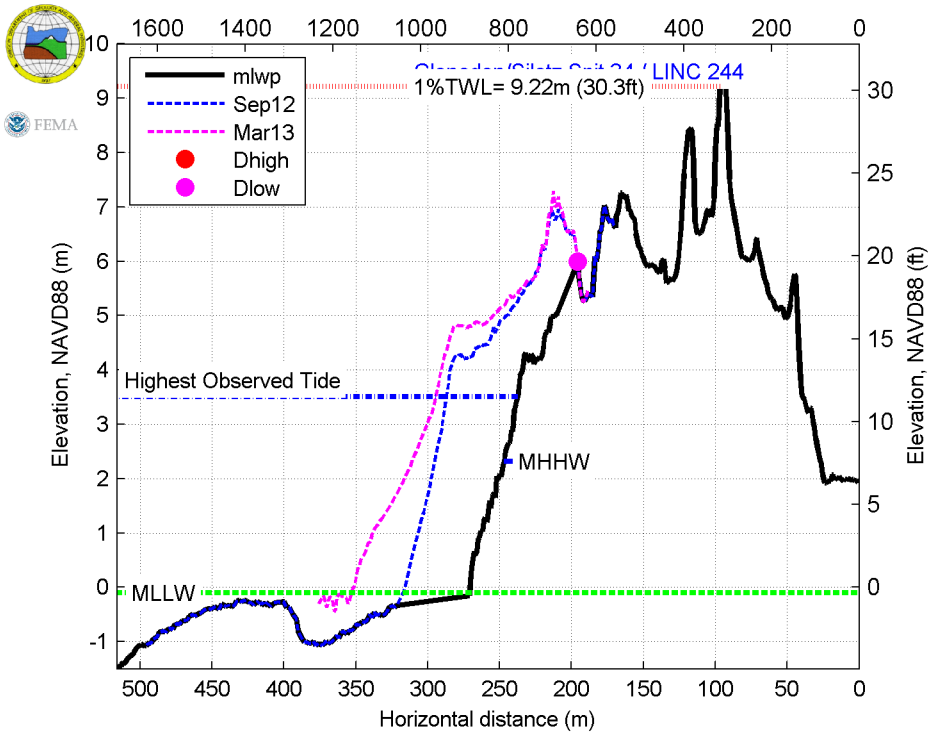

11.2.17 Lincoln City

LINC 245

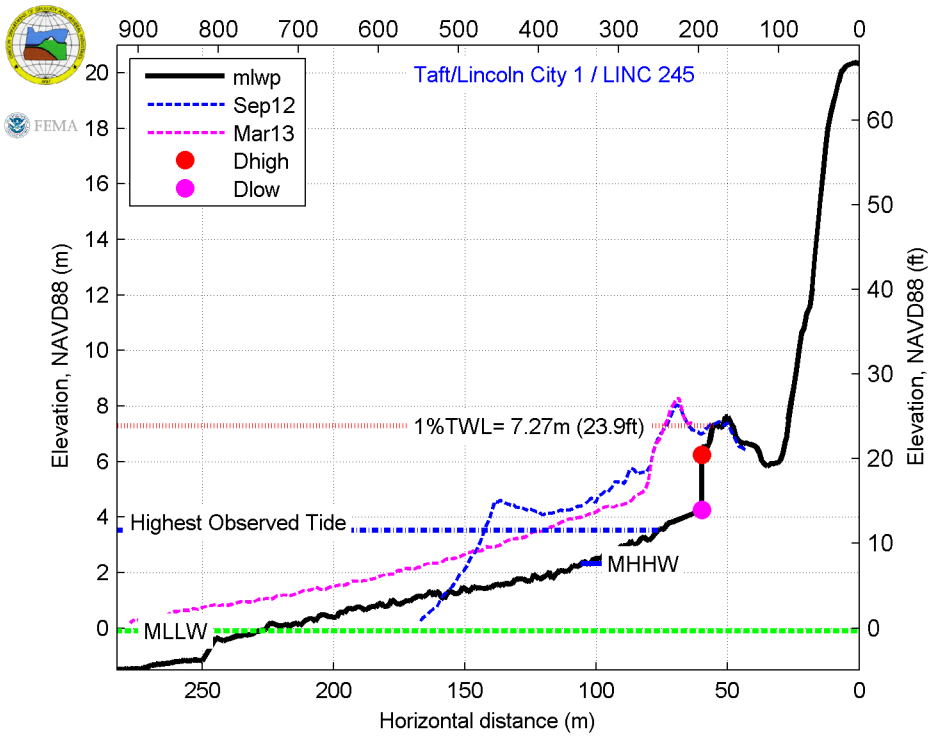

LINC 246

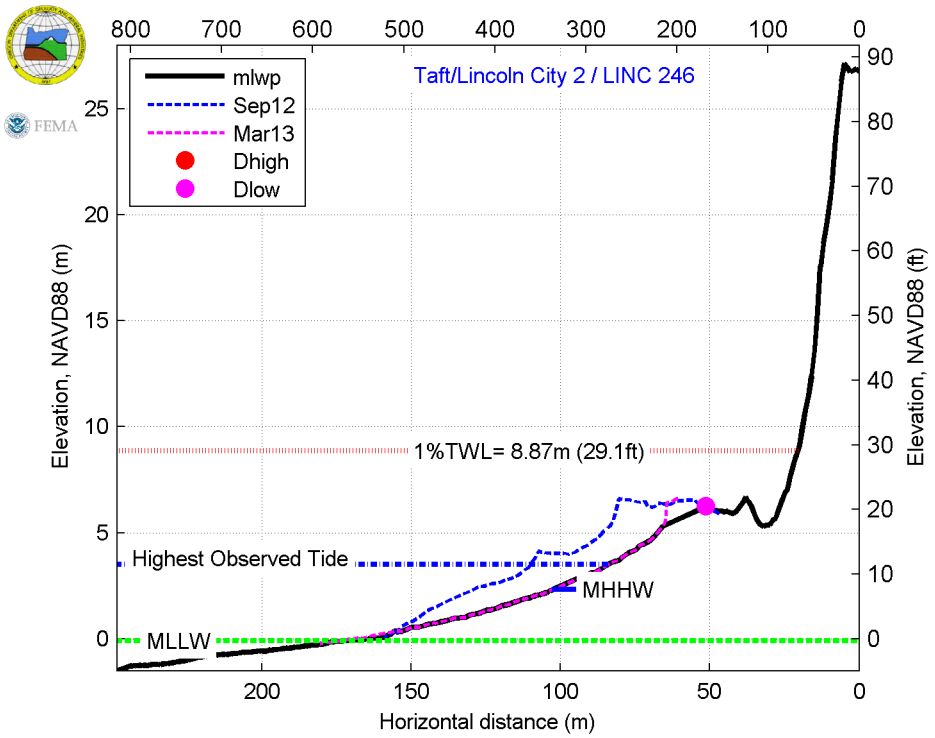

LINC 247

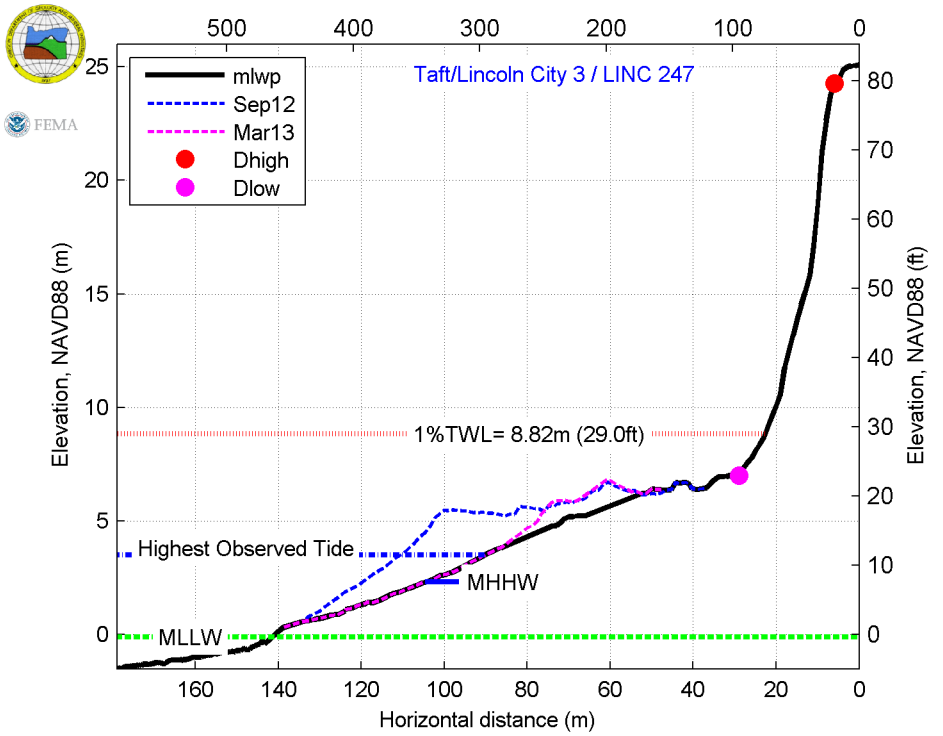

LINC 248

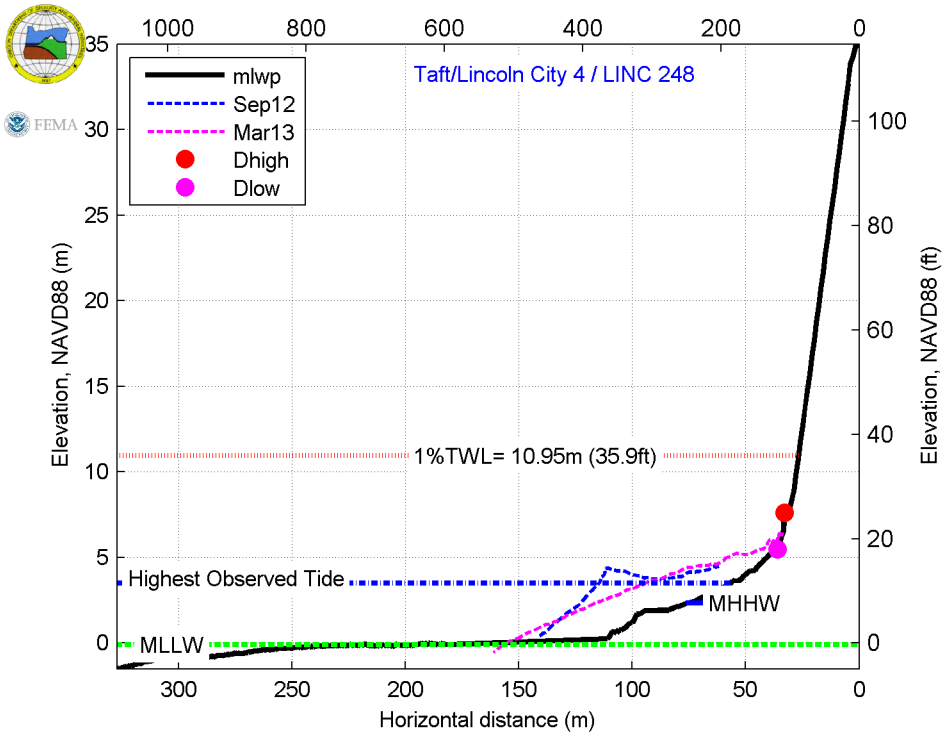

LINC 249

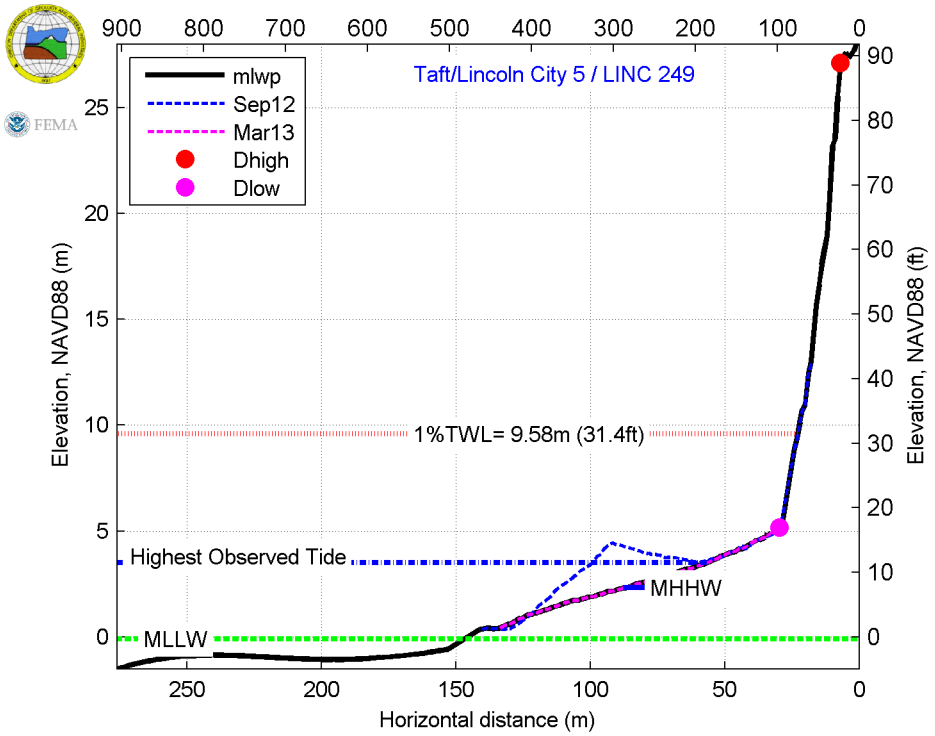

LINC 250

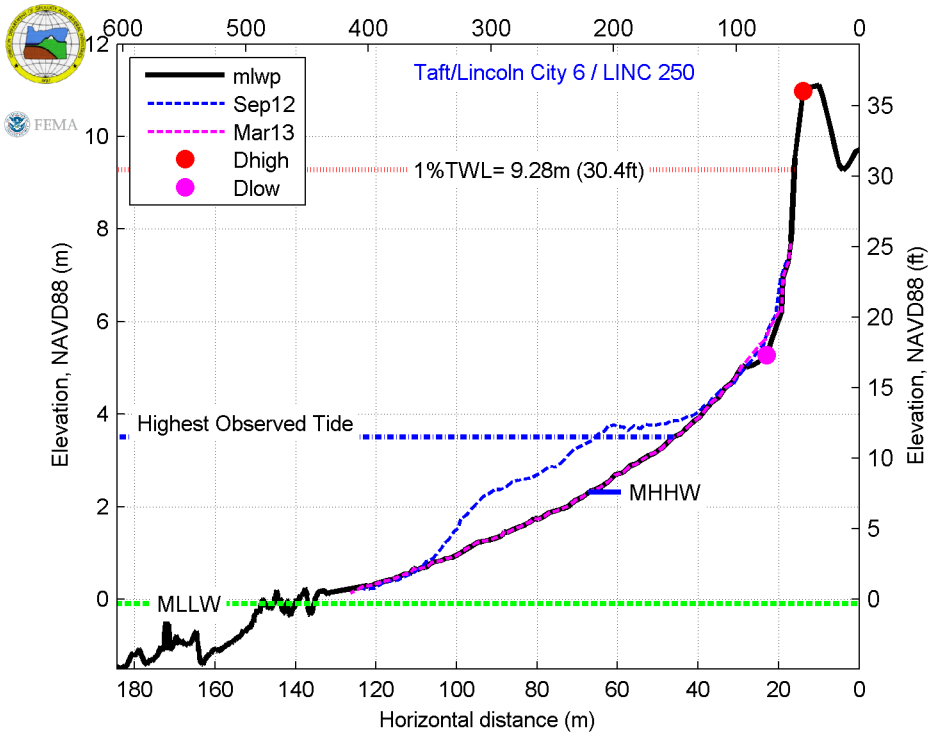

LINC 251

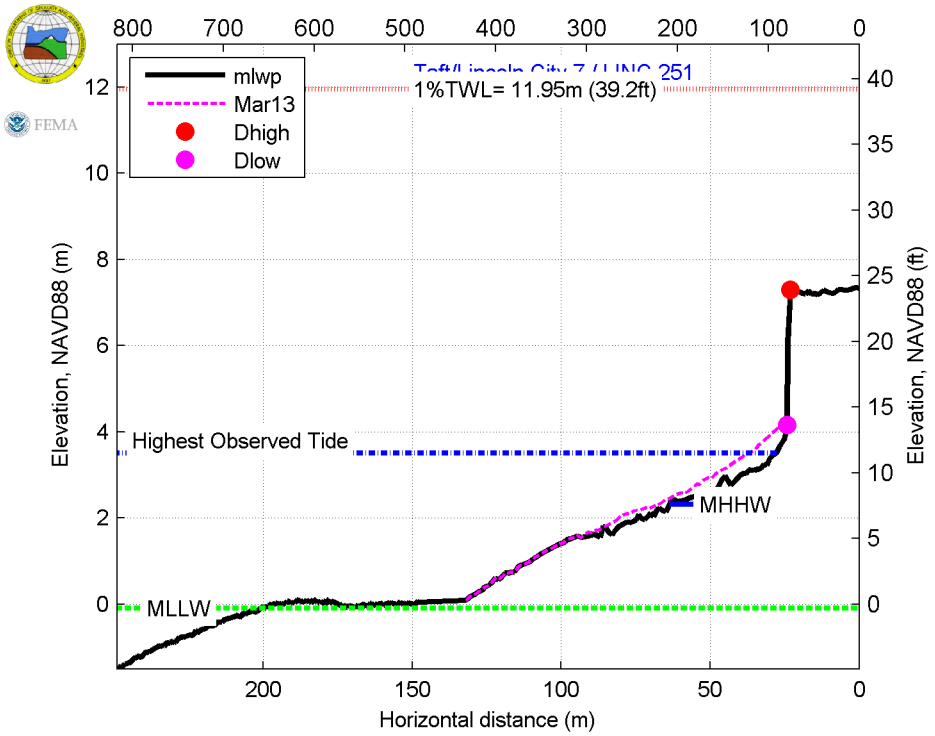

LINC 252

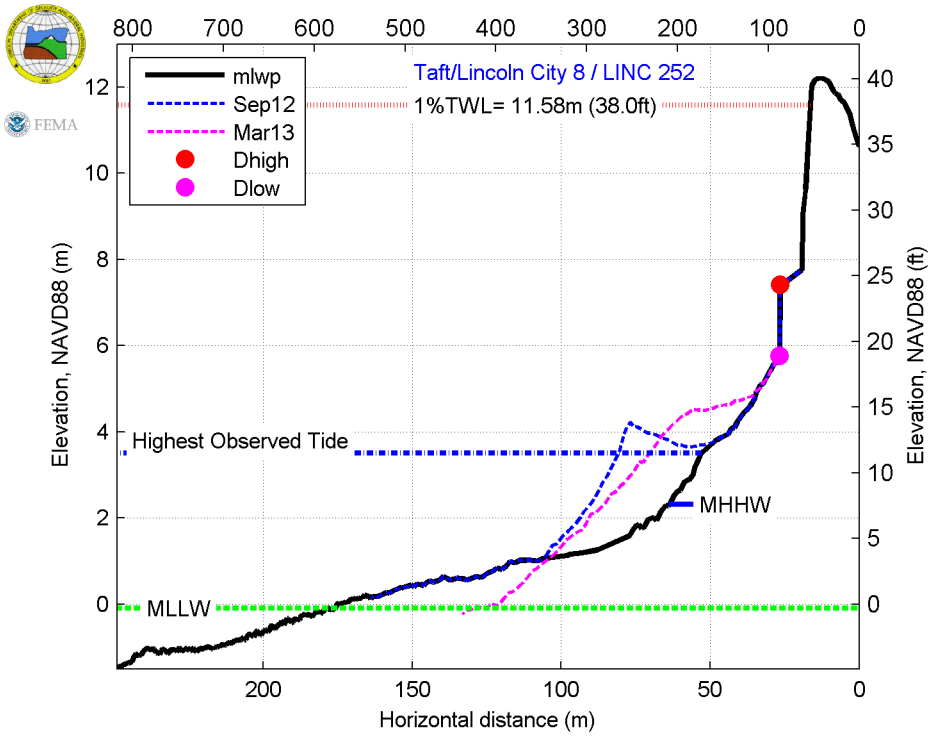

LINC 253

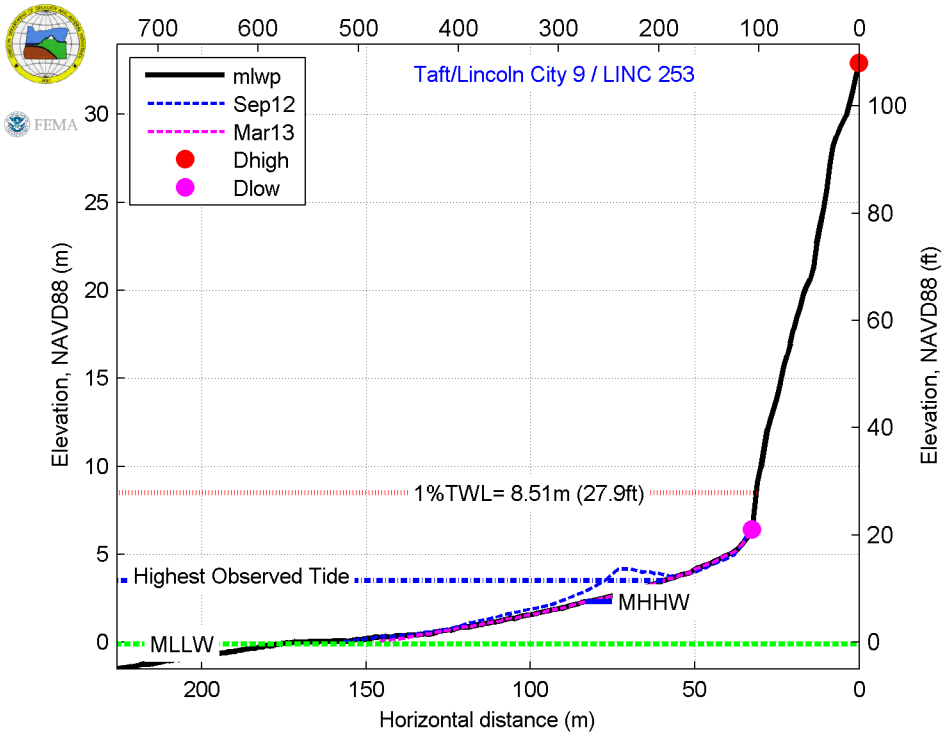

LINC 254

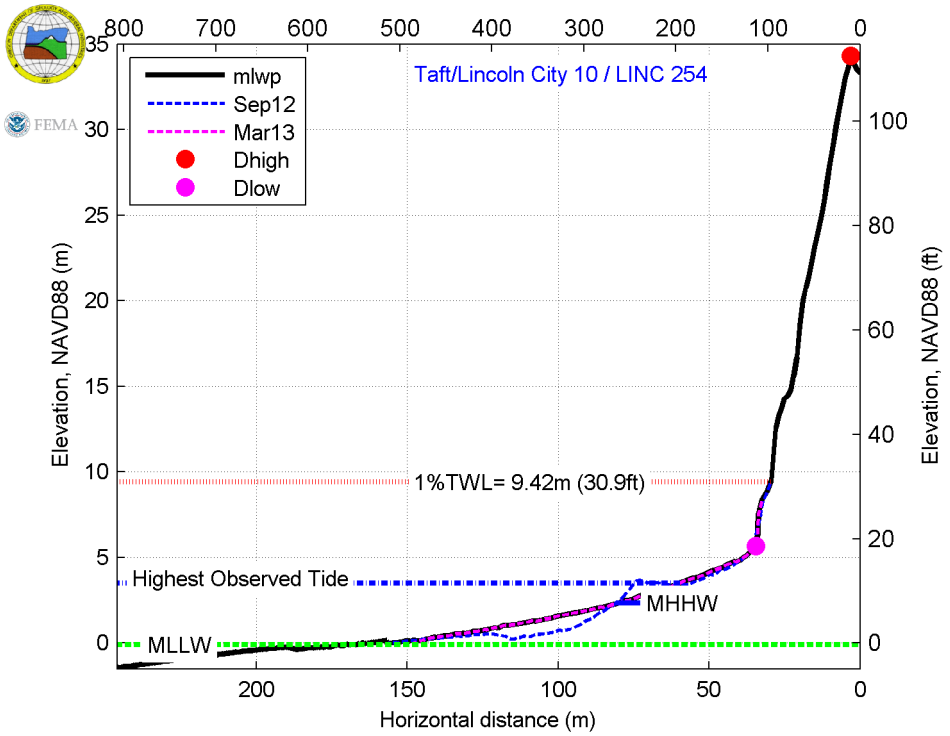

LINC 255

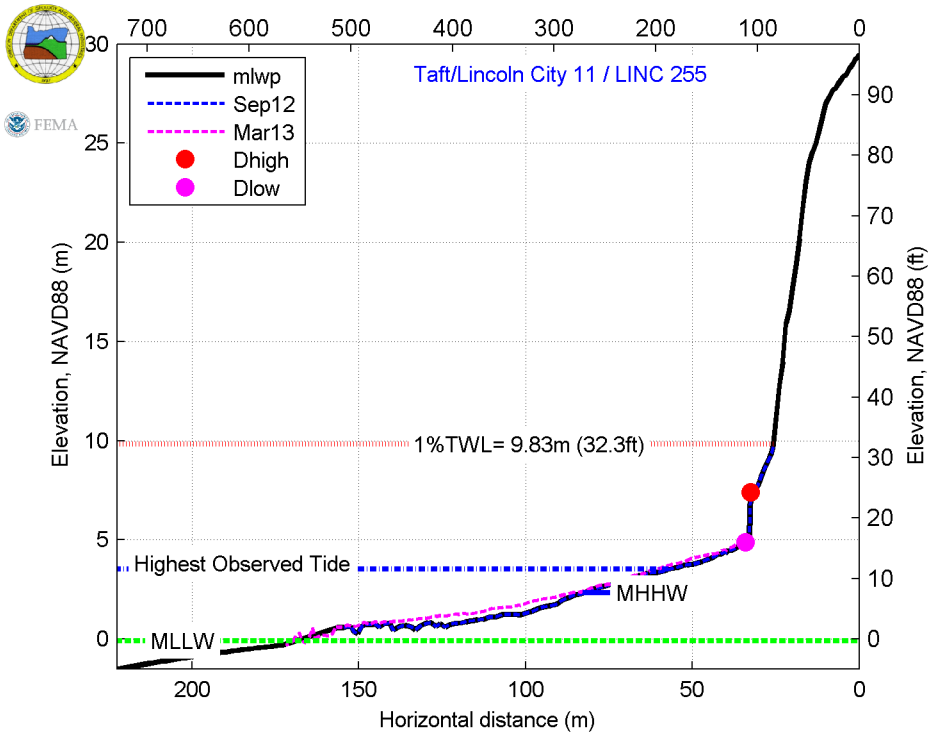

LINC 256

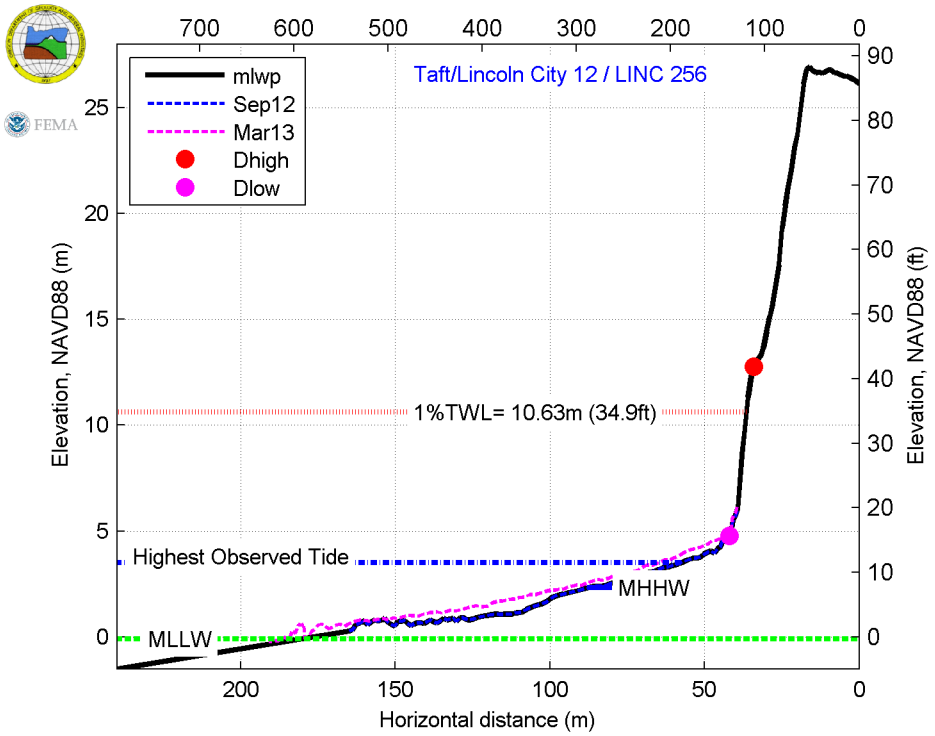

LINC 257

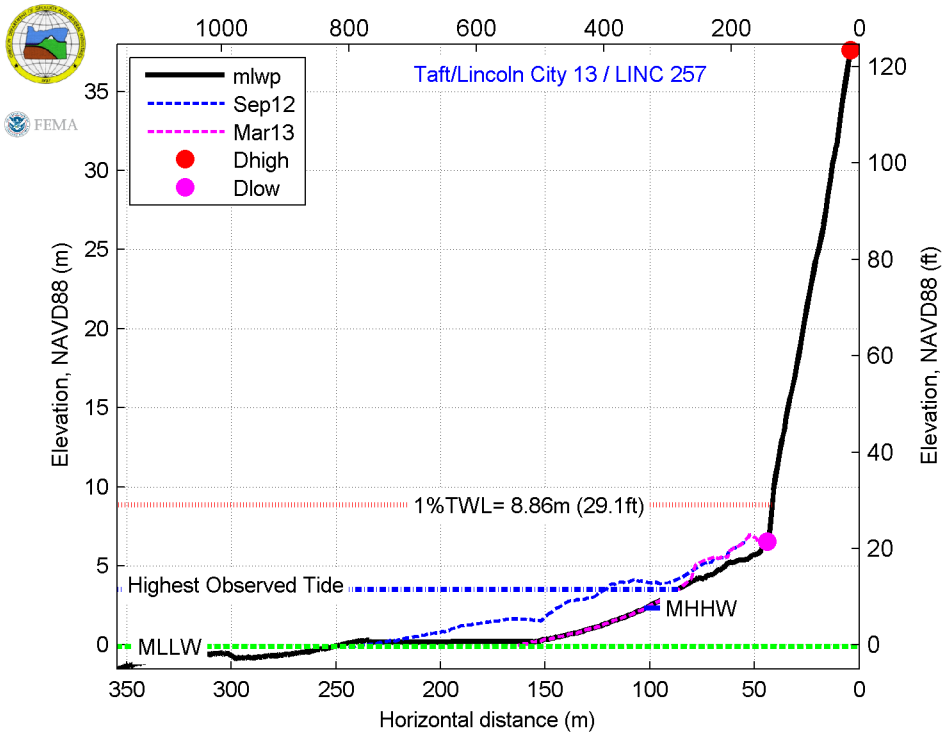

LINC 258

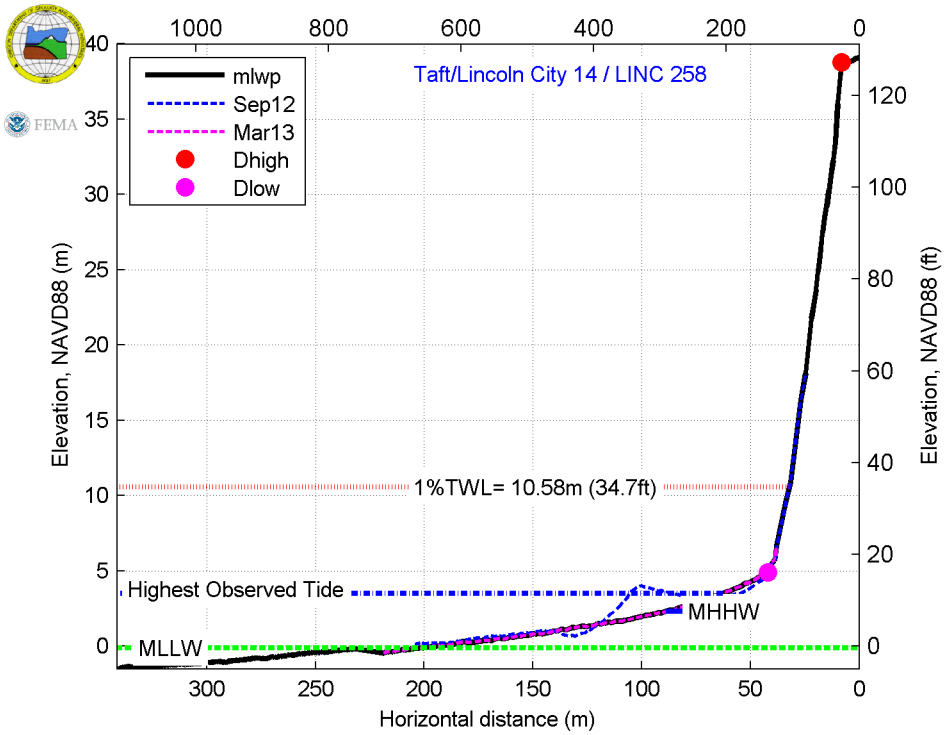

LINC 259

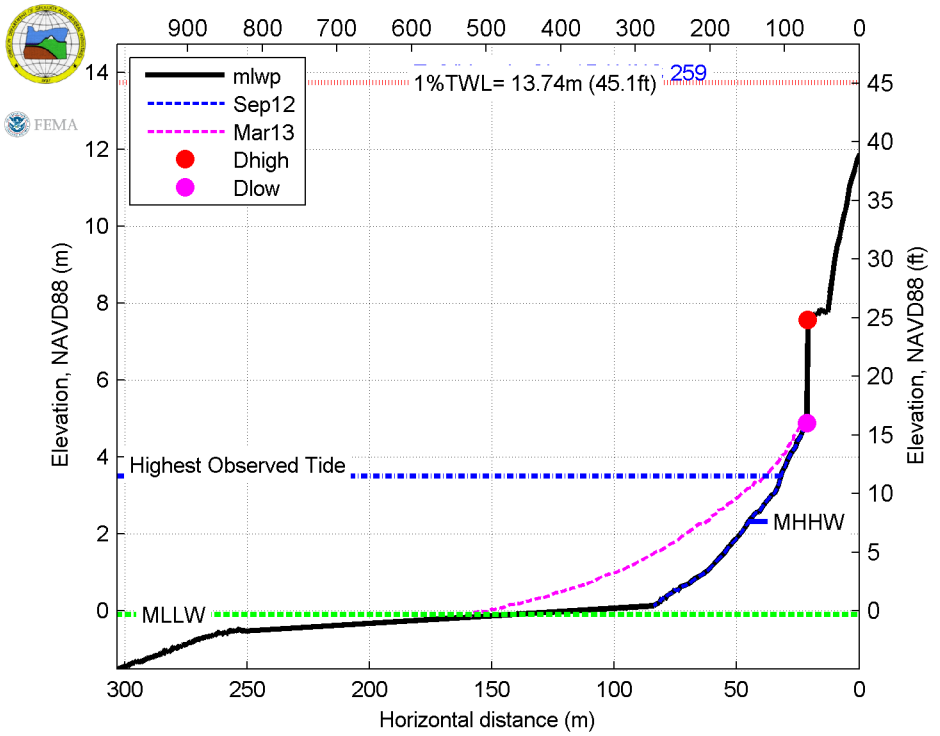

LINC 260

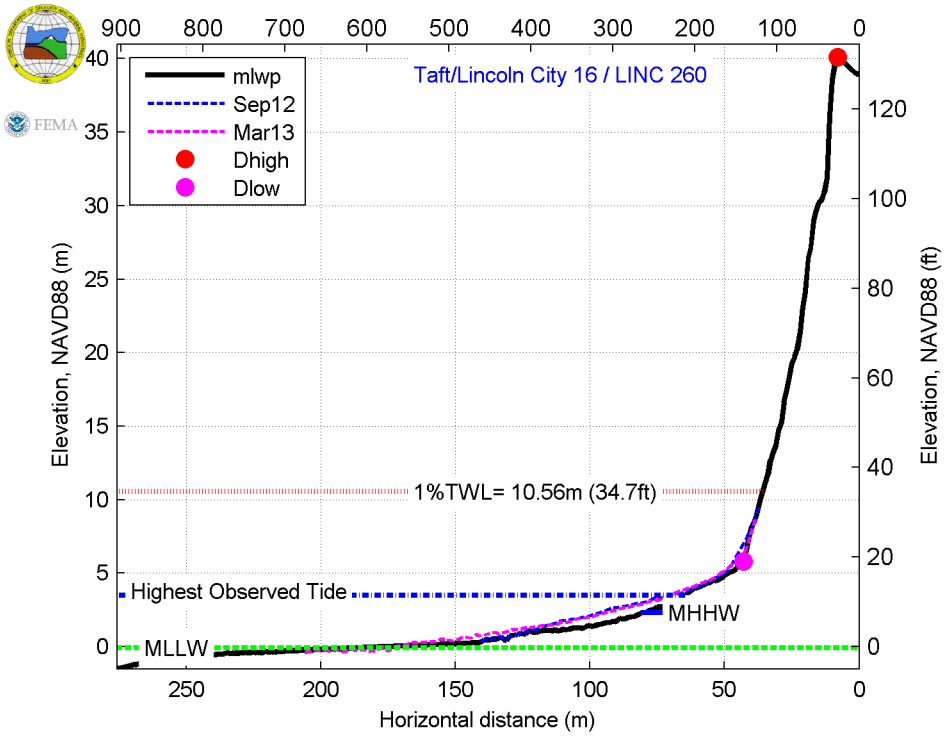

LINC 261

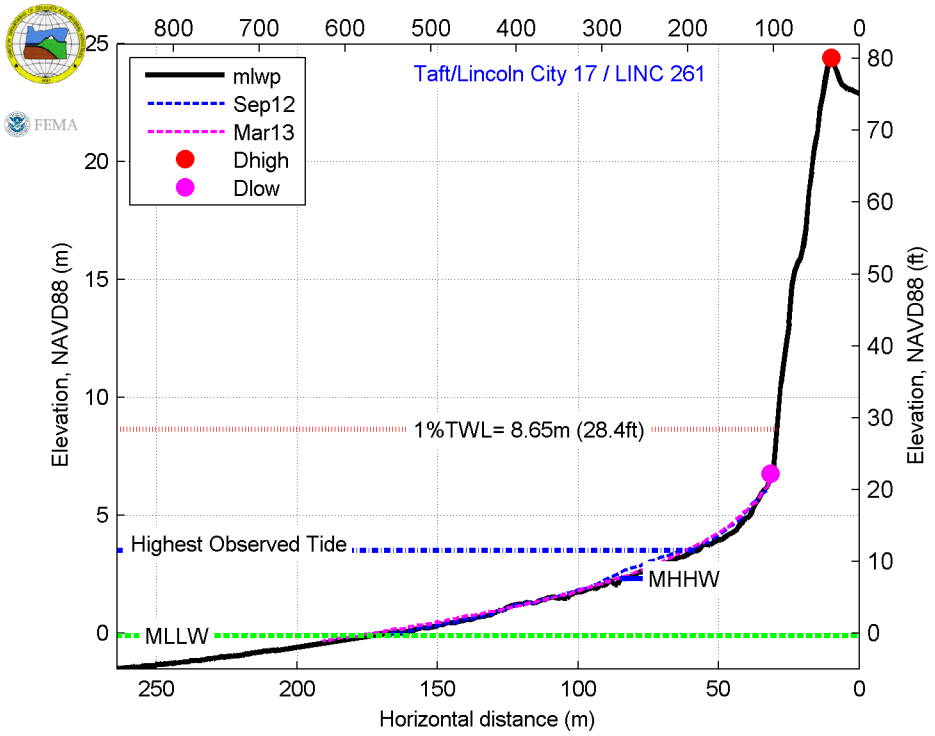

LINC 262

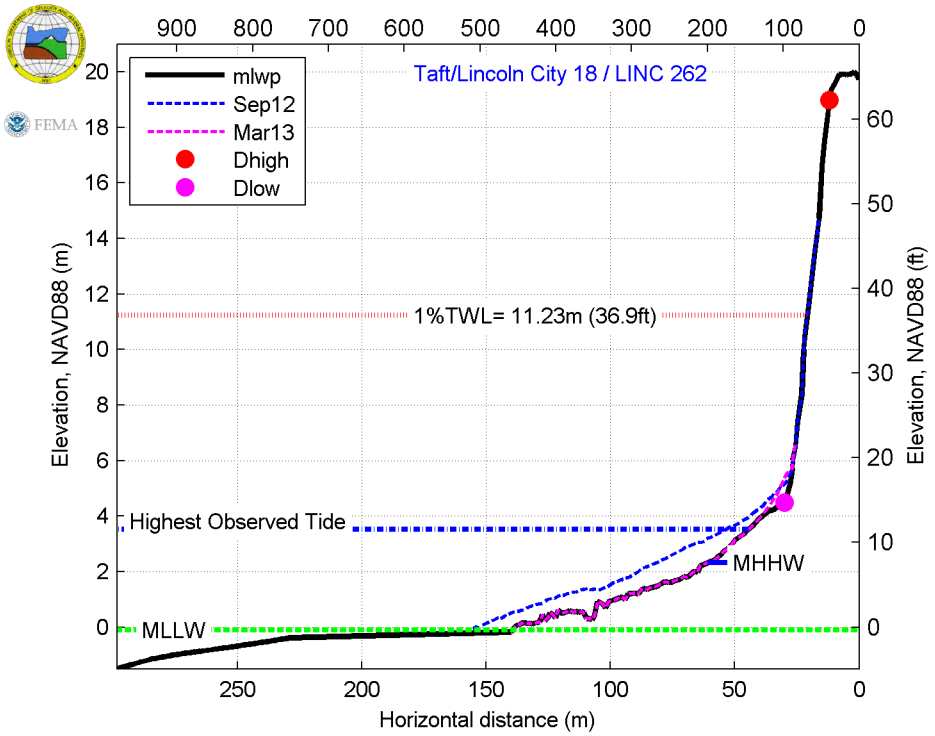

LINC 263

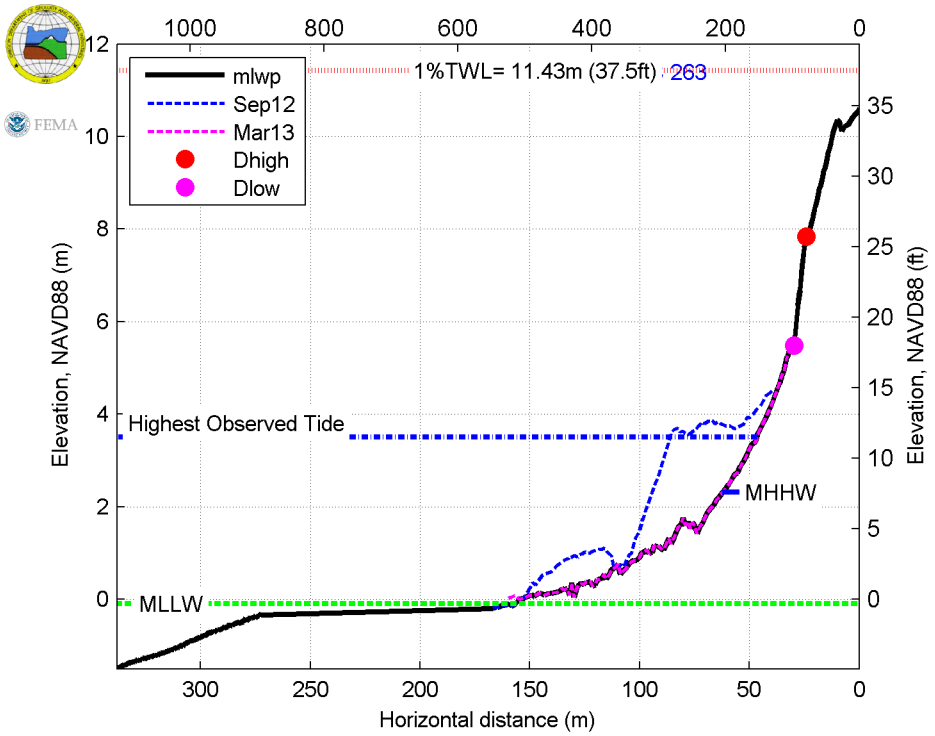

LINC 264

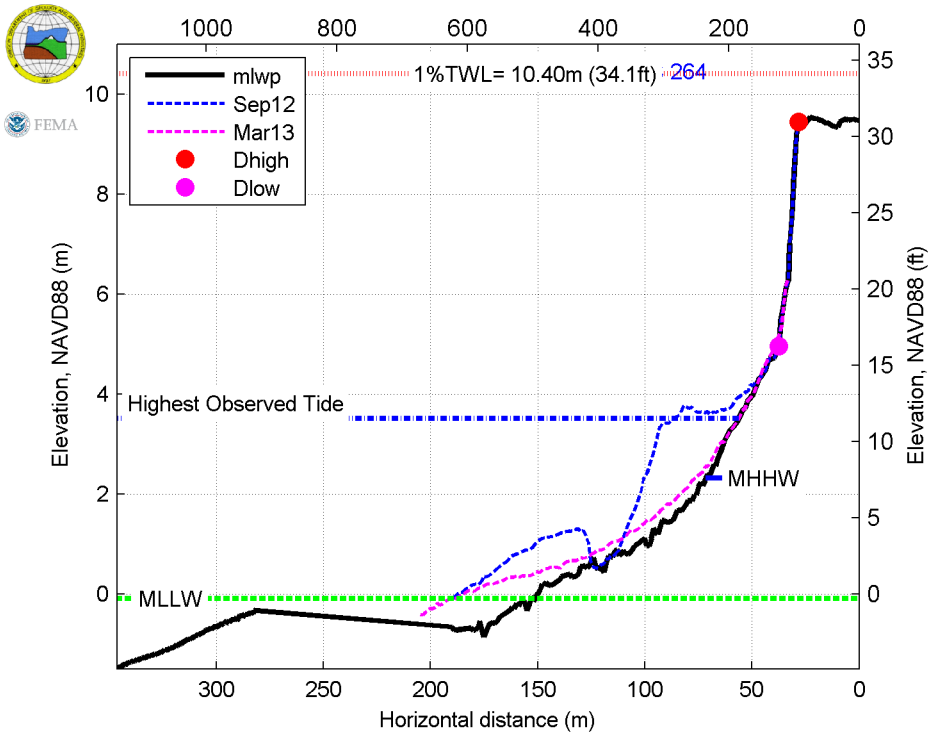

LINC 265

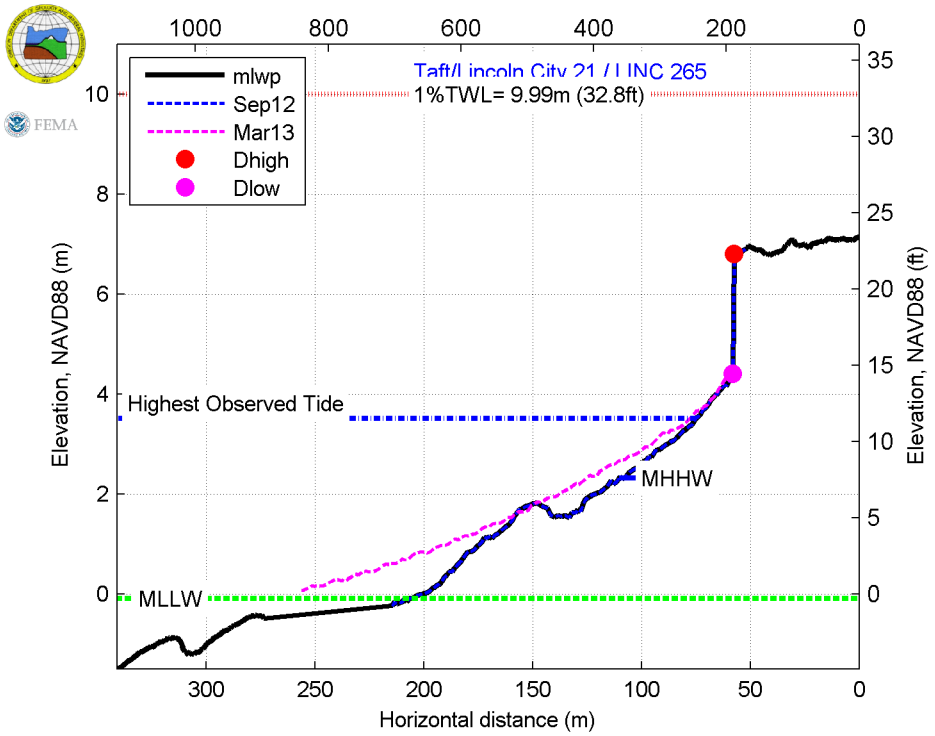

LINC 266

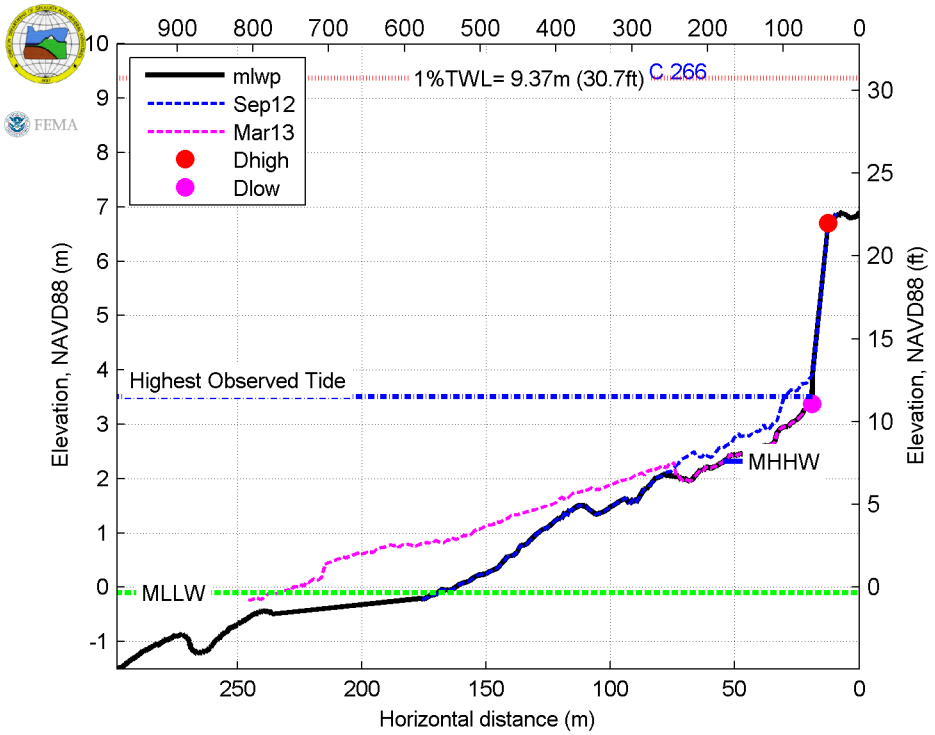

LINC 267

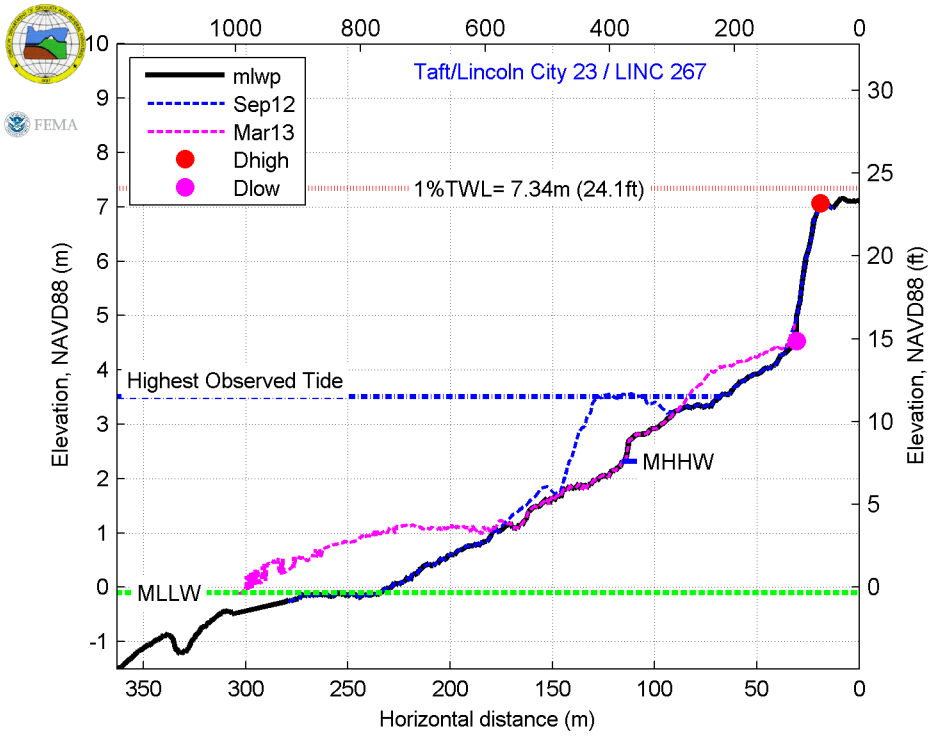

LINC 268

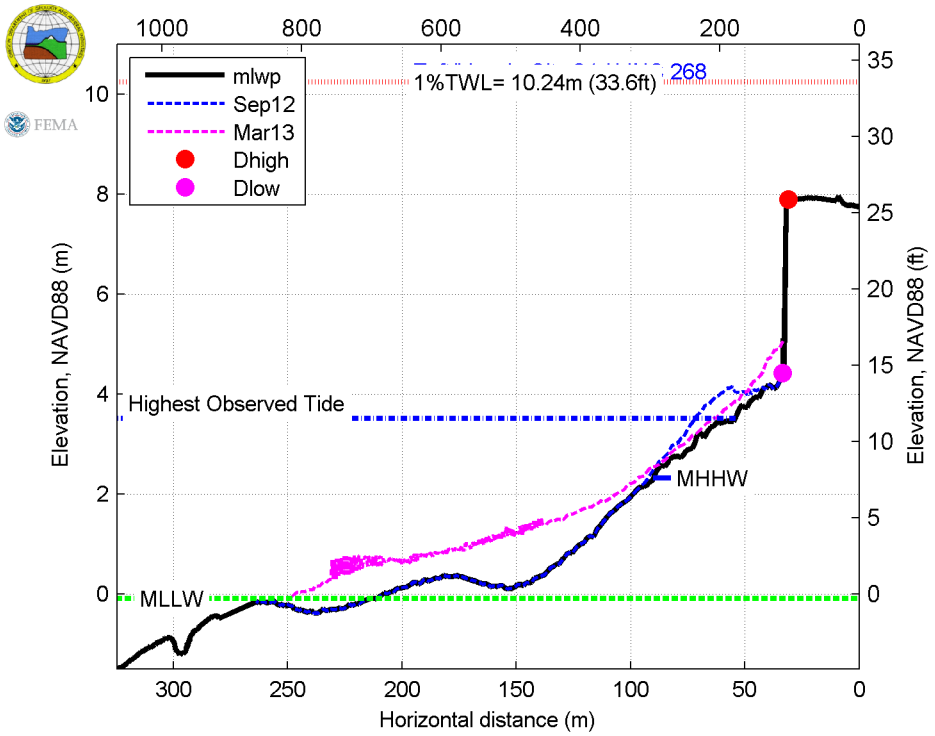

LINC 269

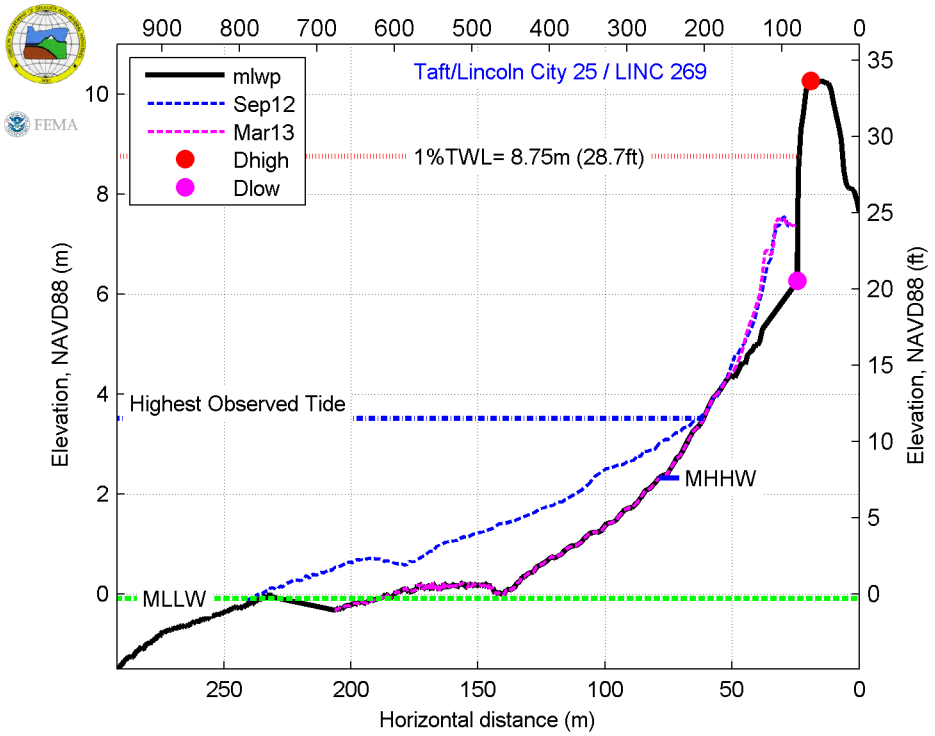

LINC 270

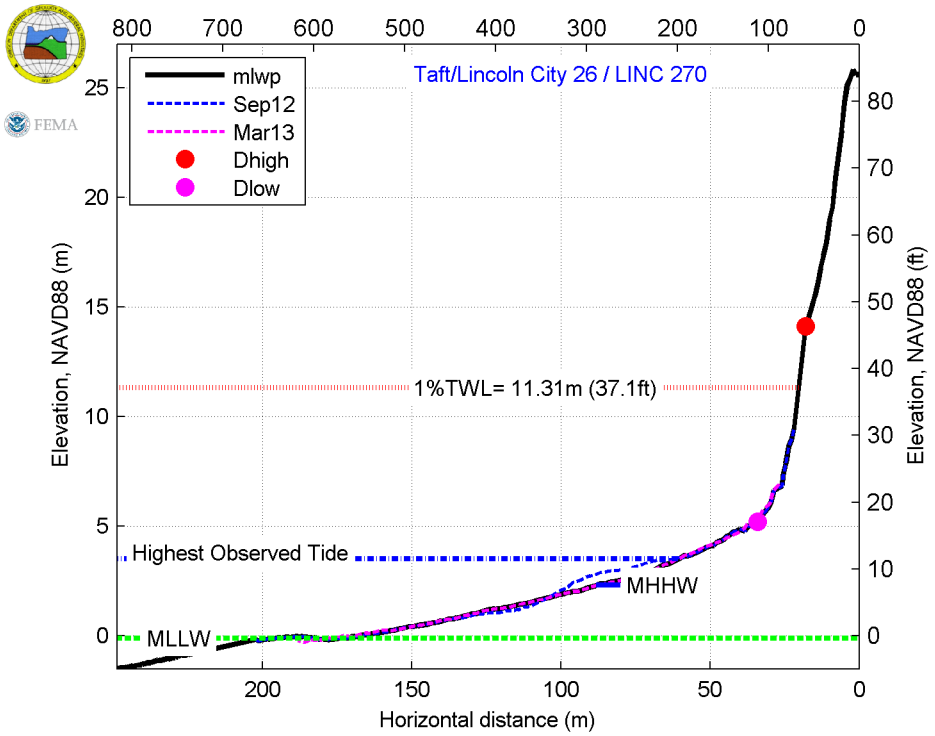

LINC 271

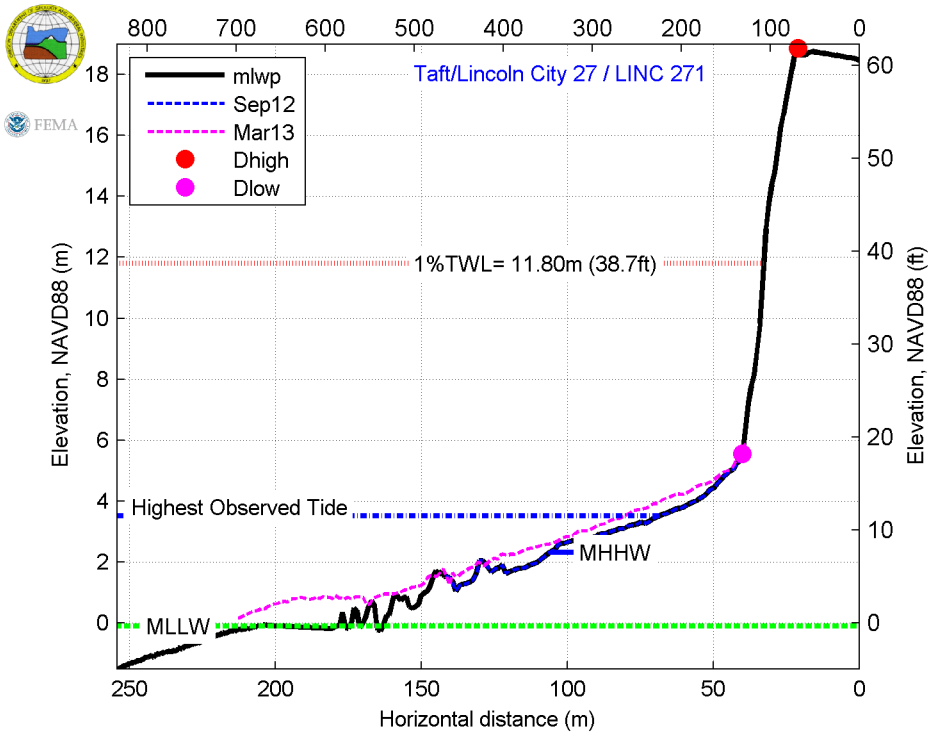

LINC 272

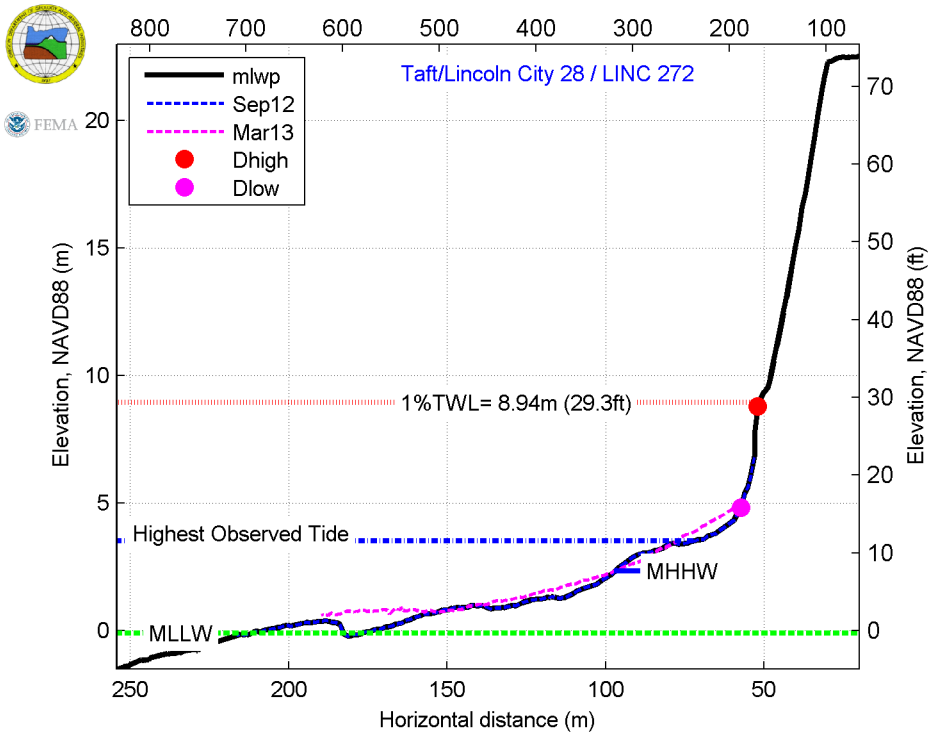

LINC 273

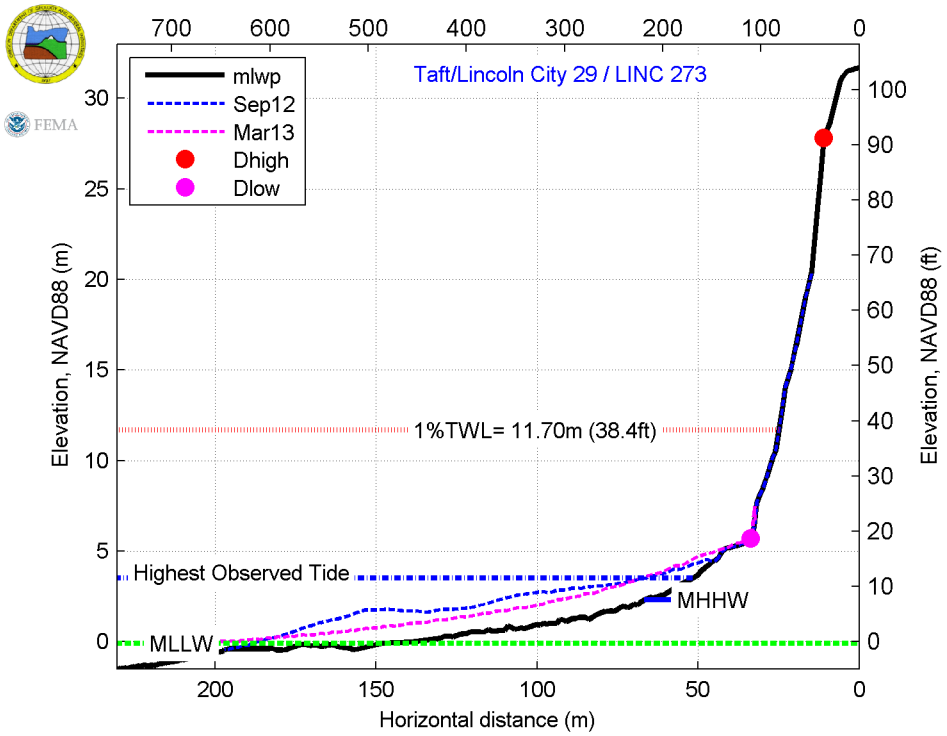

LINC 274

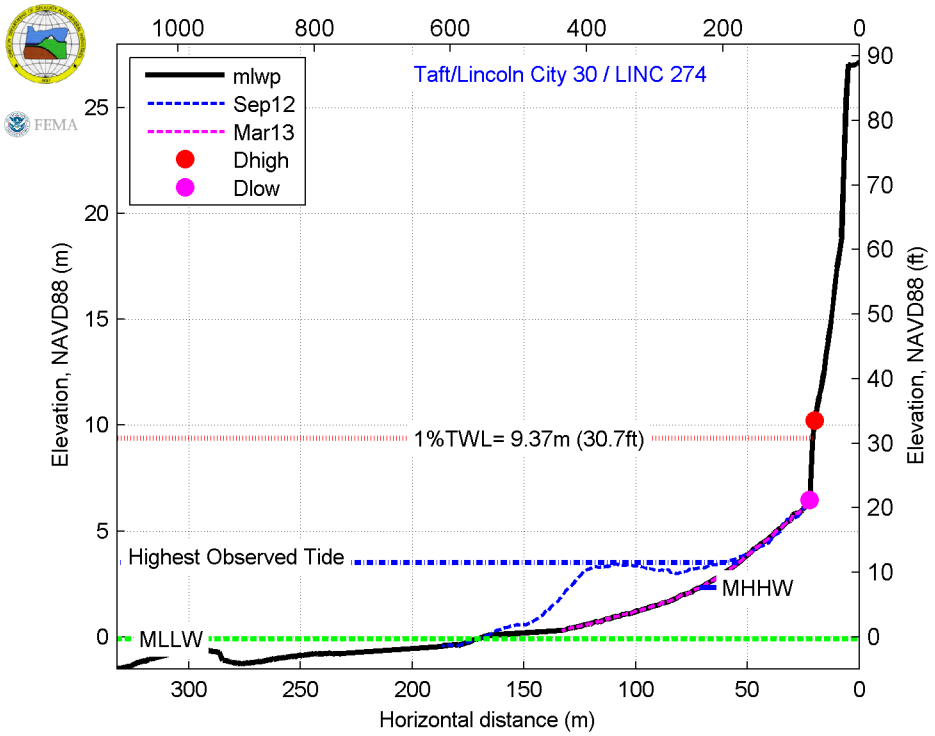

LINC 275

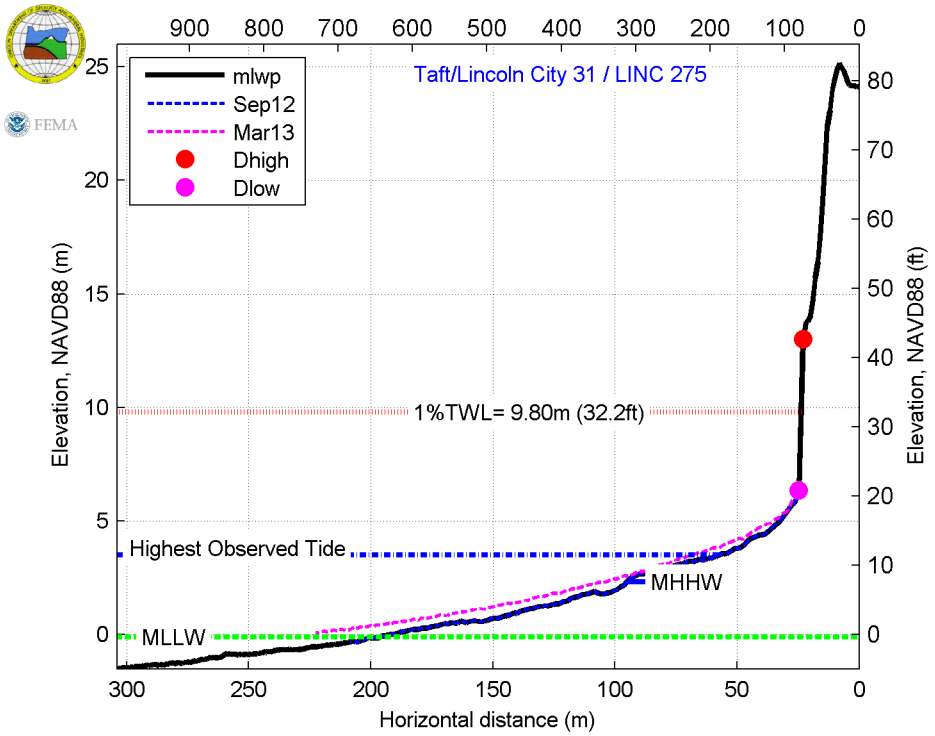

LINC 276

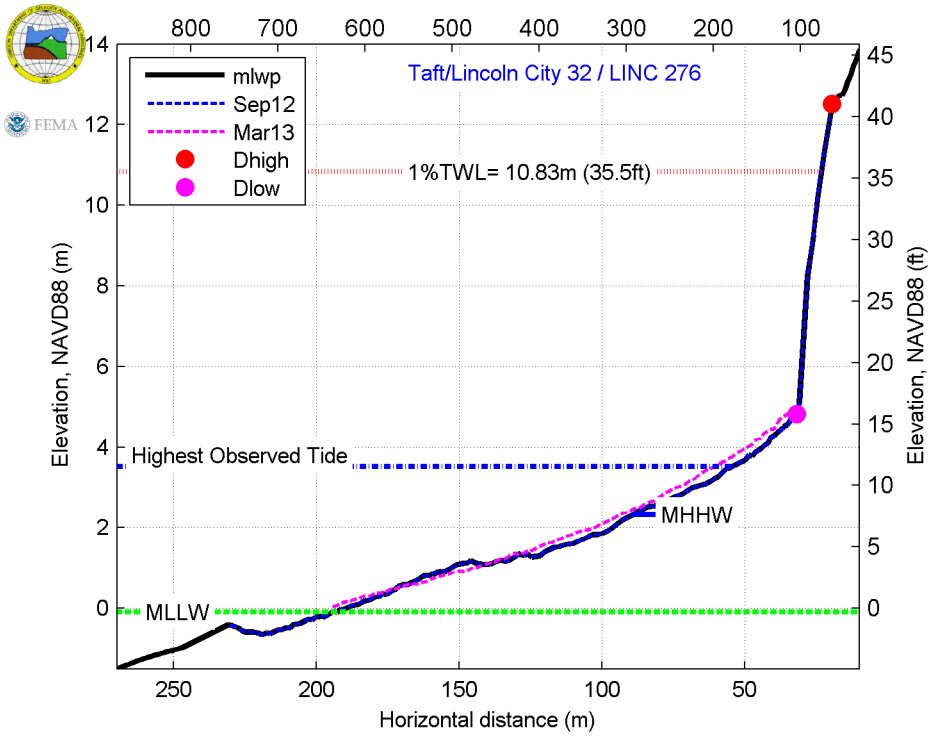

LINC 277

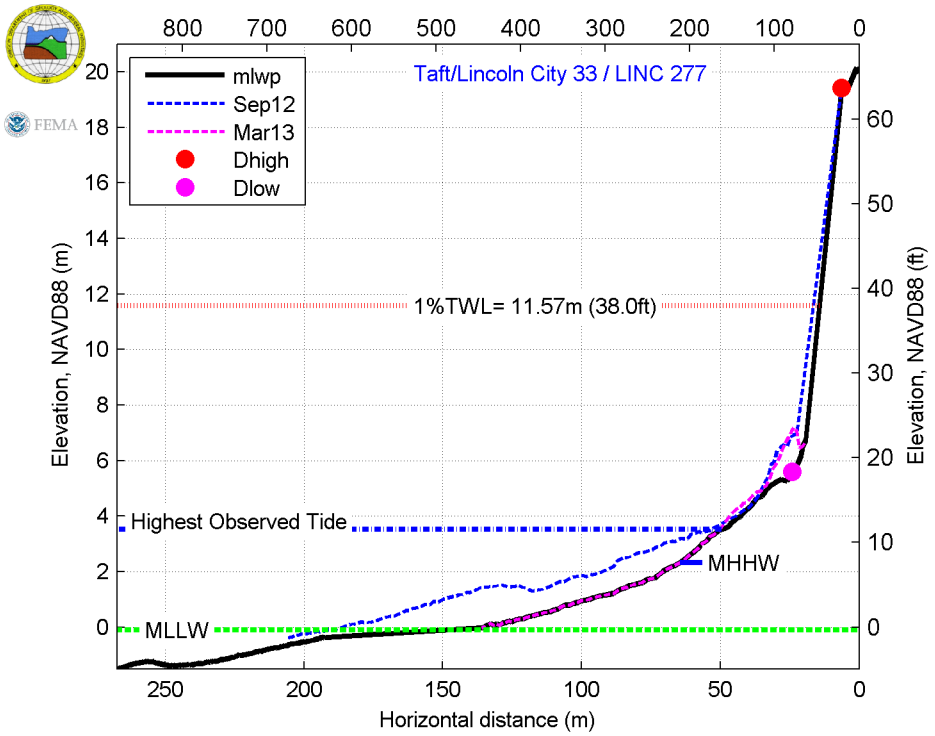

LINC 278

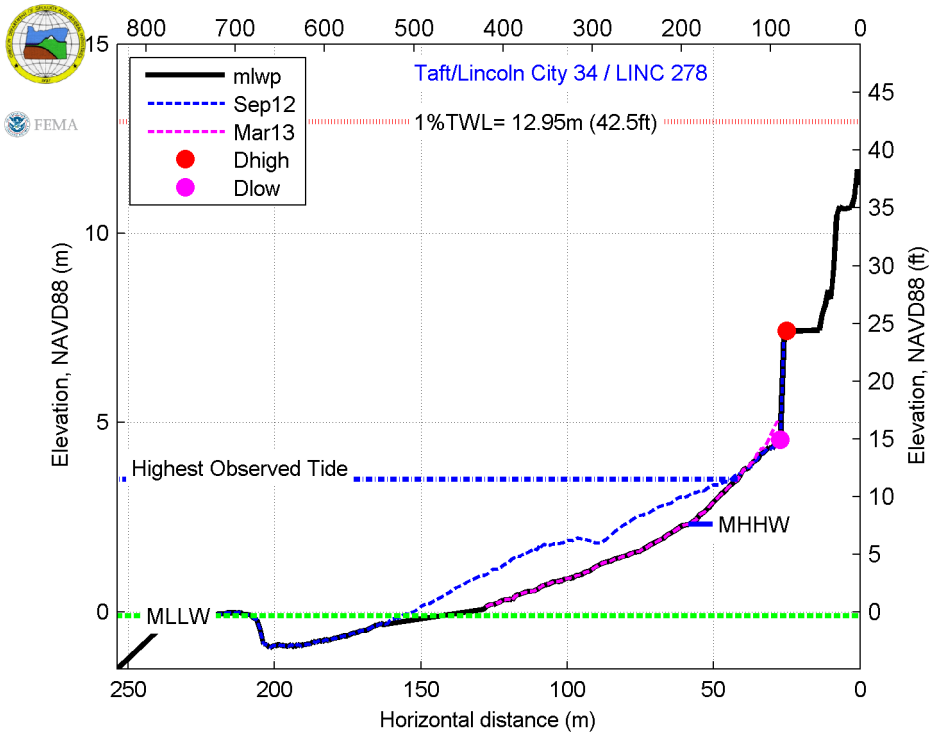

LINC 279

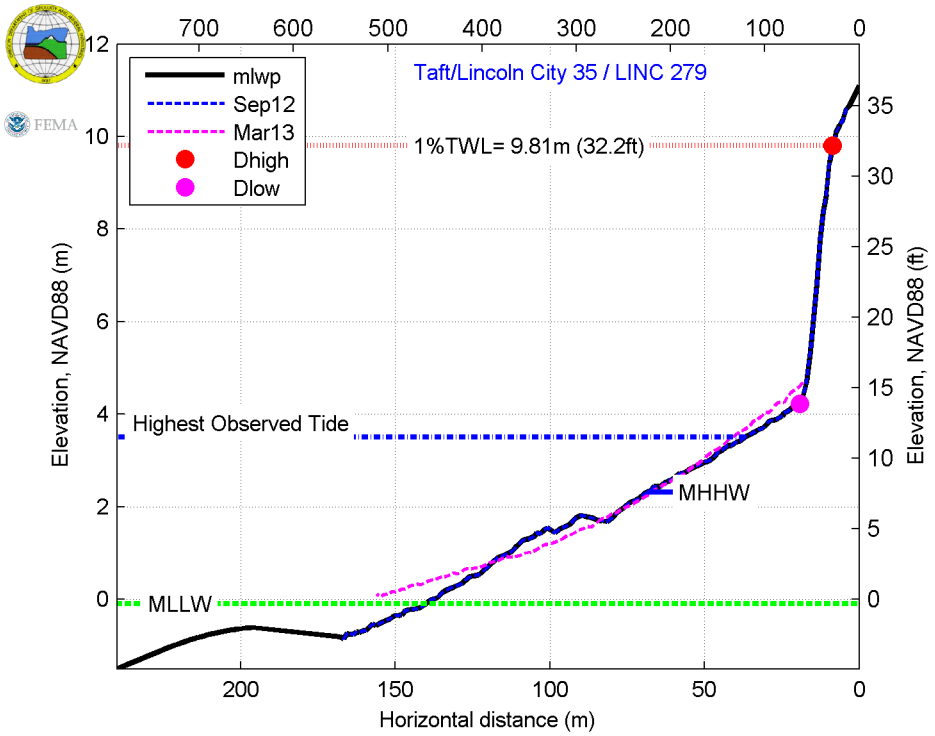

LINC 280

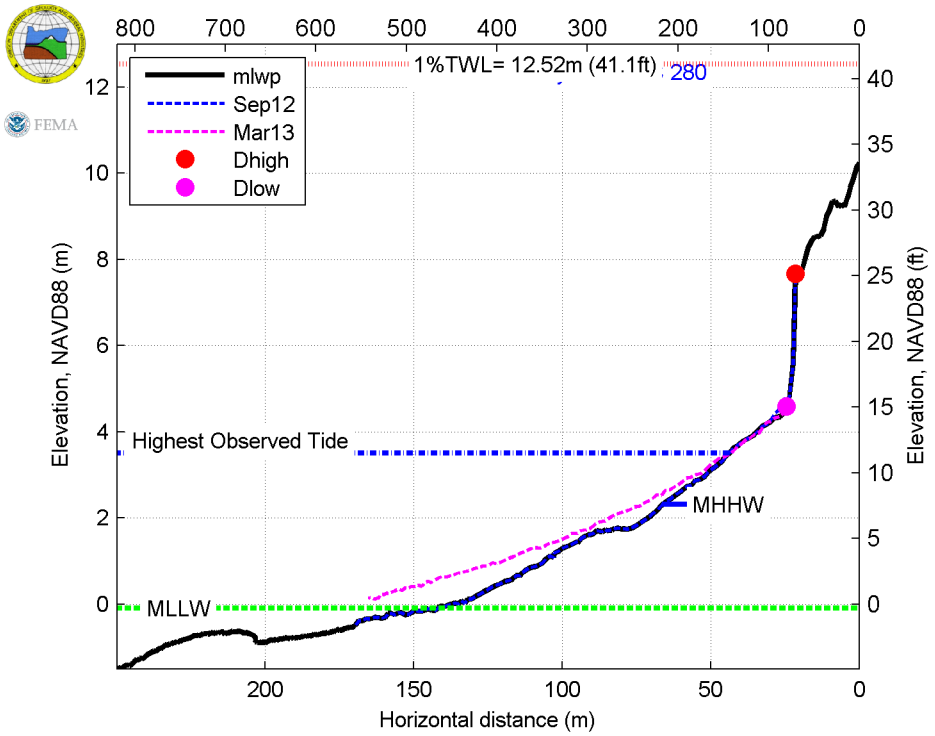

LINC 281

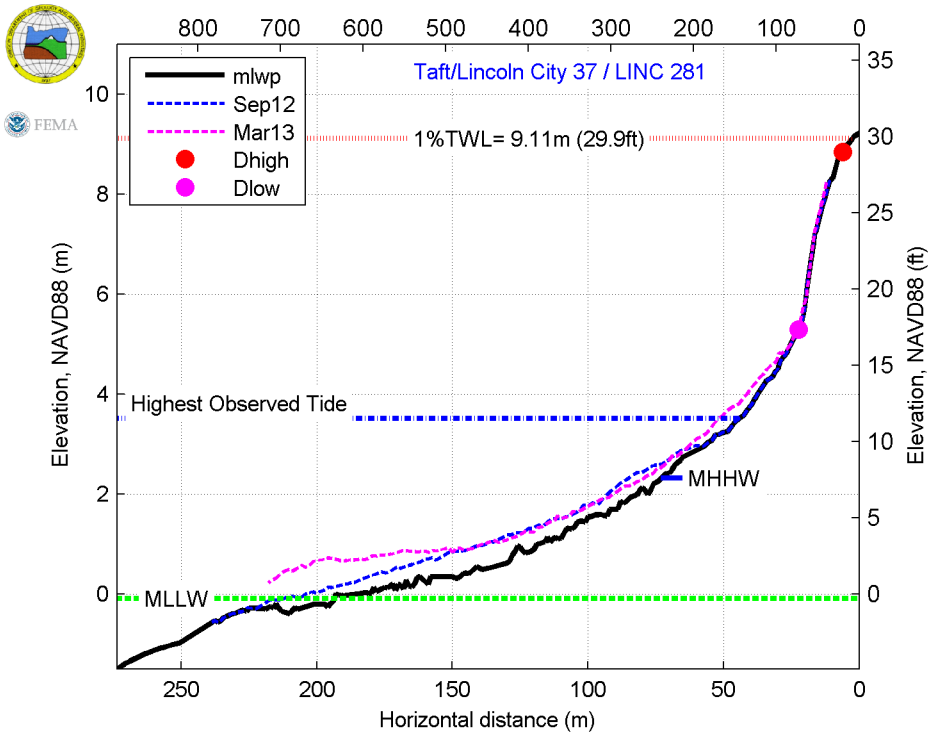

LINC 282

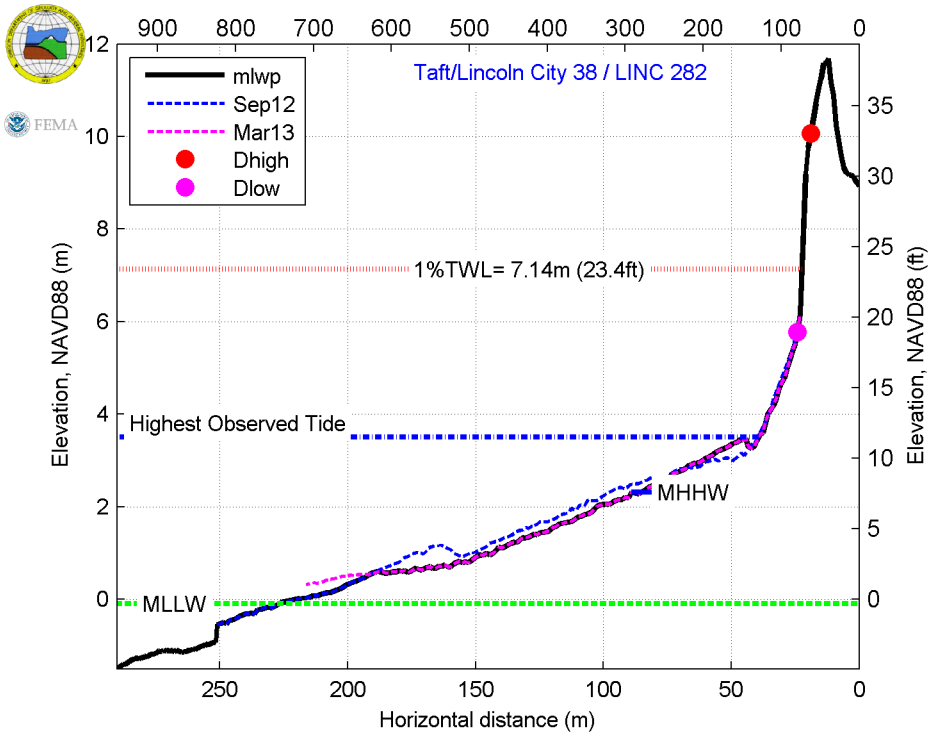

LINC 283

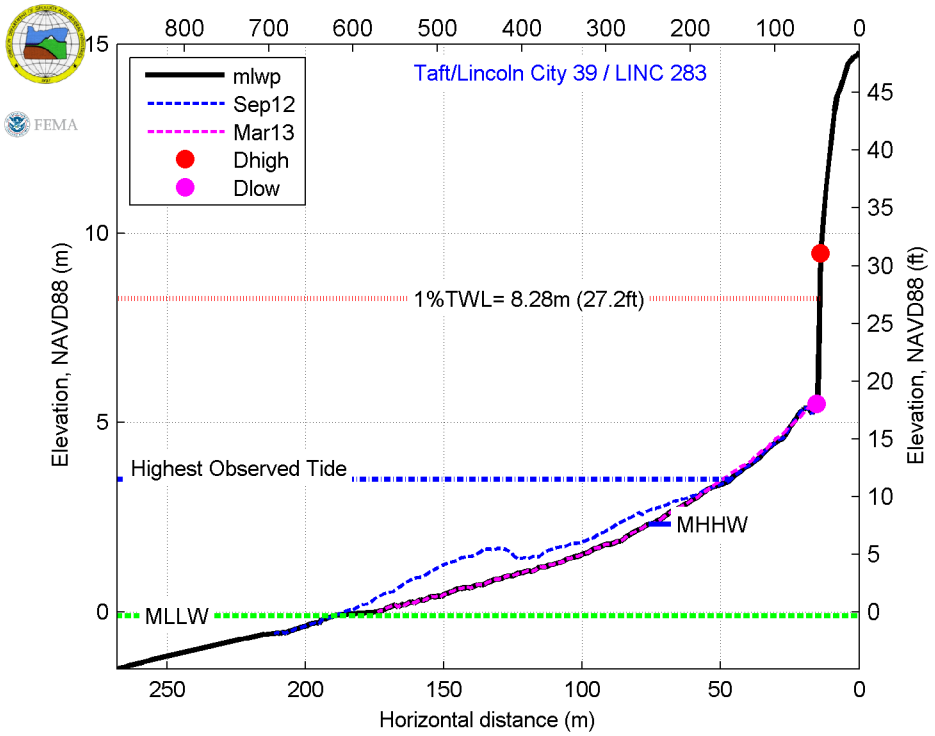

LINC 284

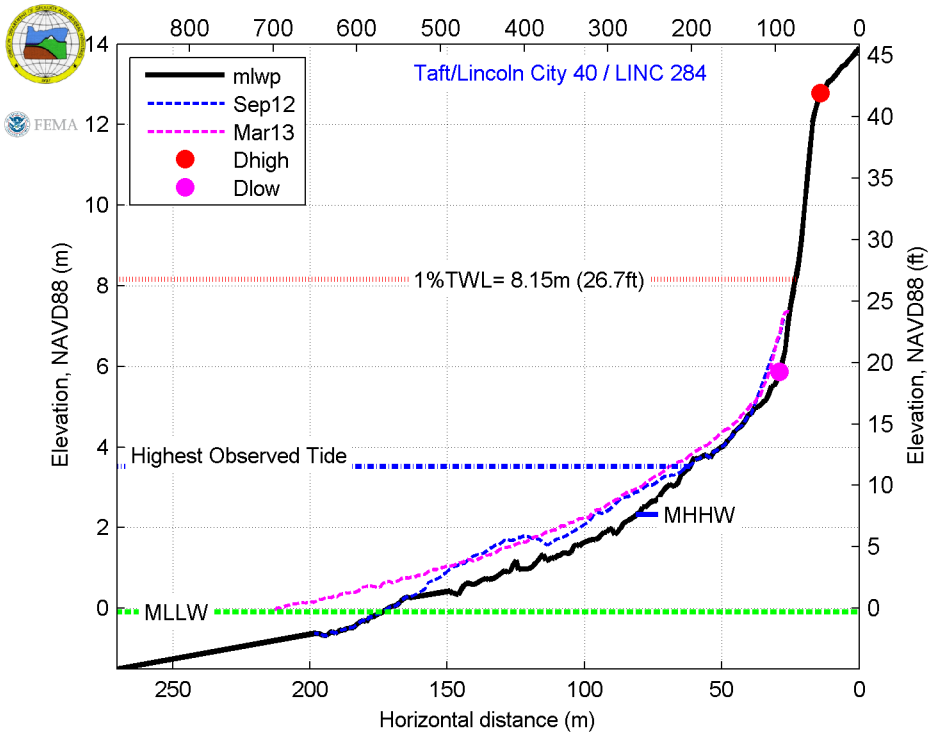

LINC 285

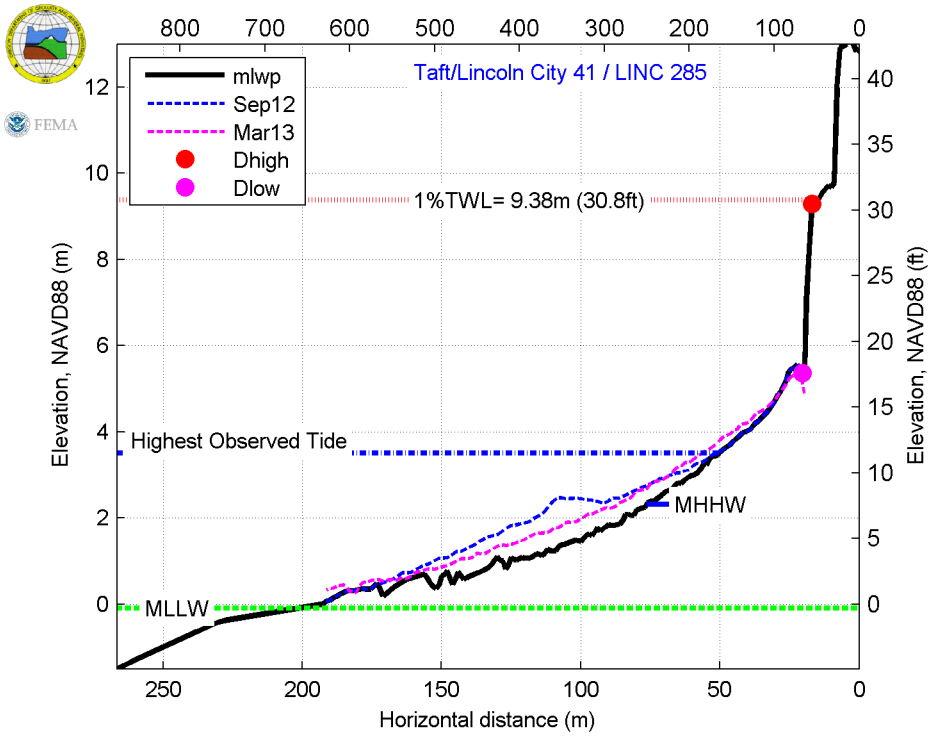

LINC 286

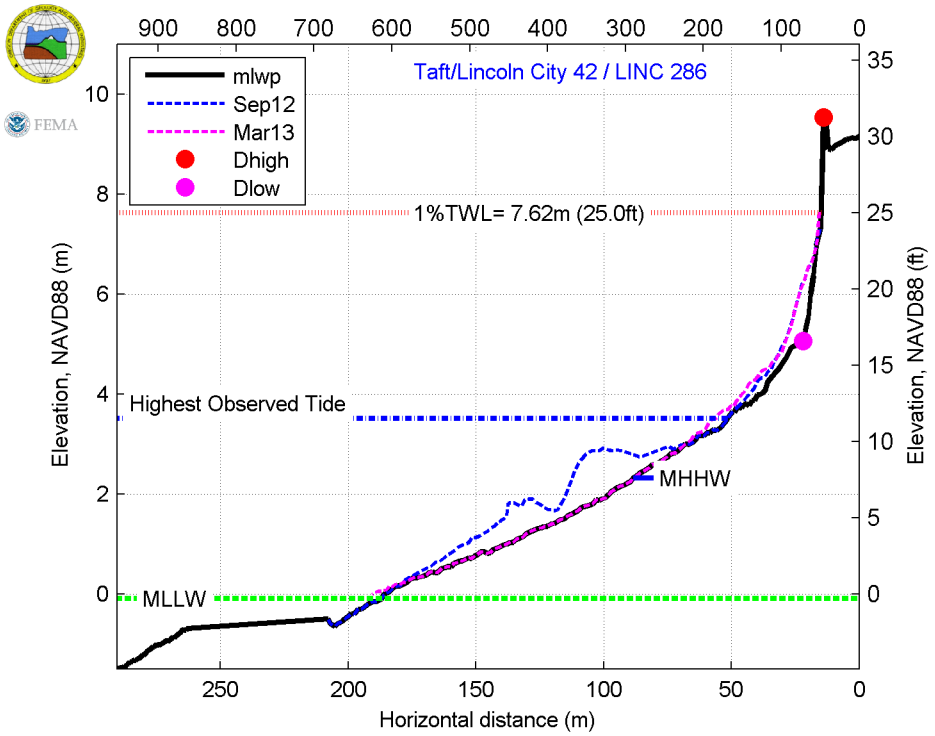

LINC 287

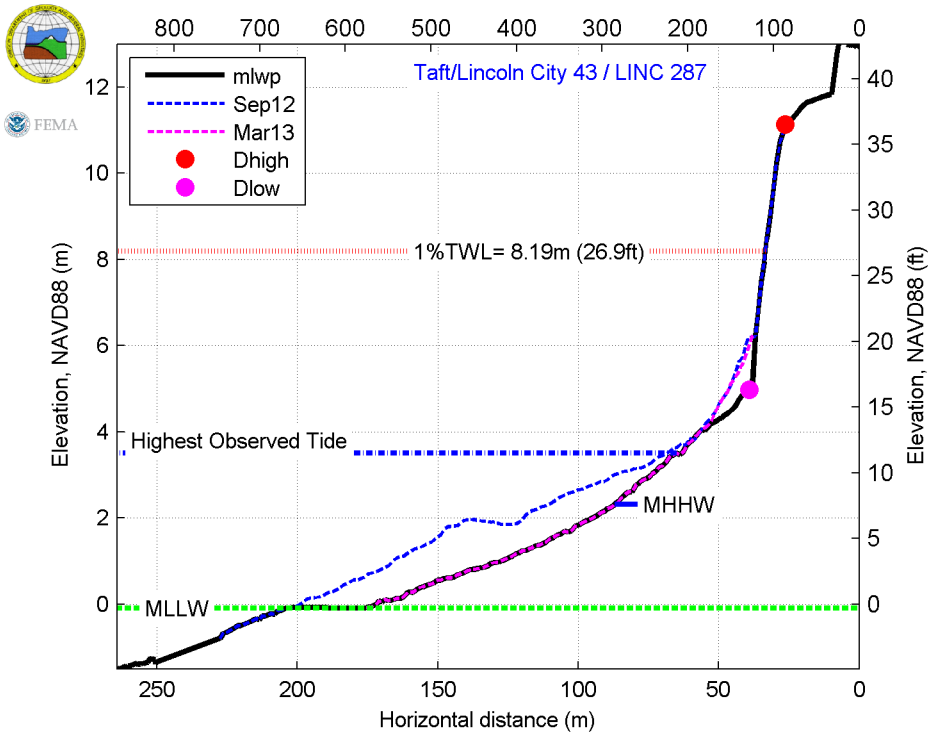

LINC 288

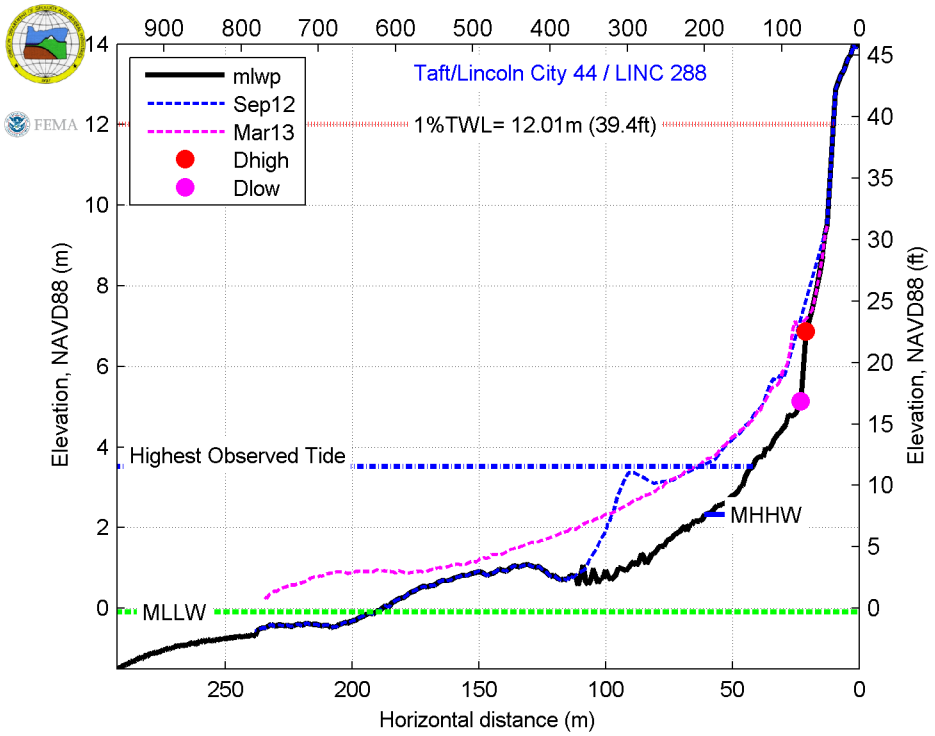

NC 289

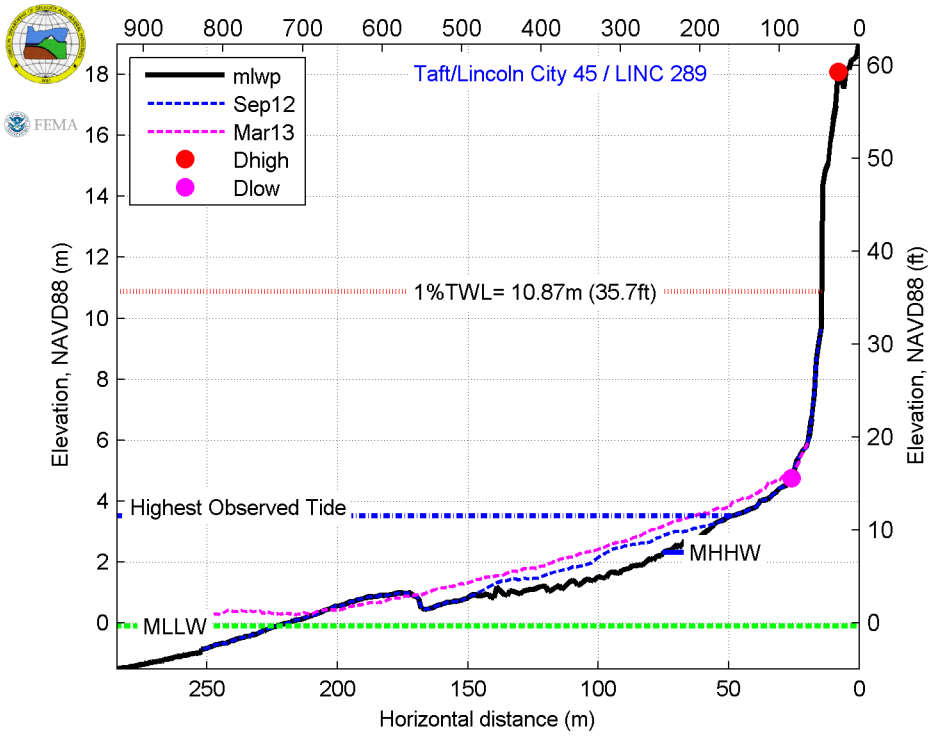

LINC 290

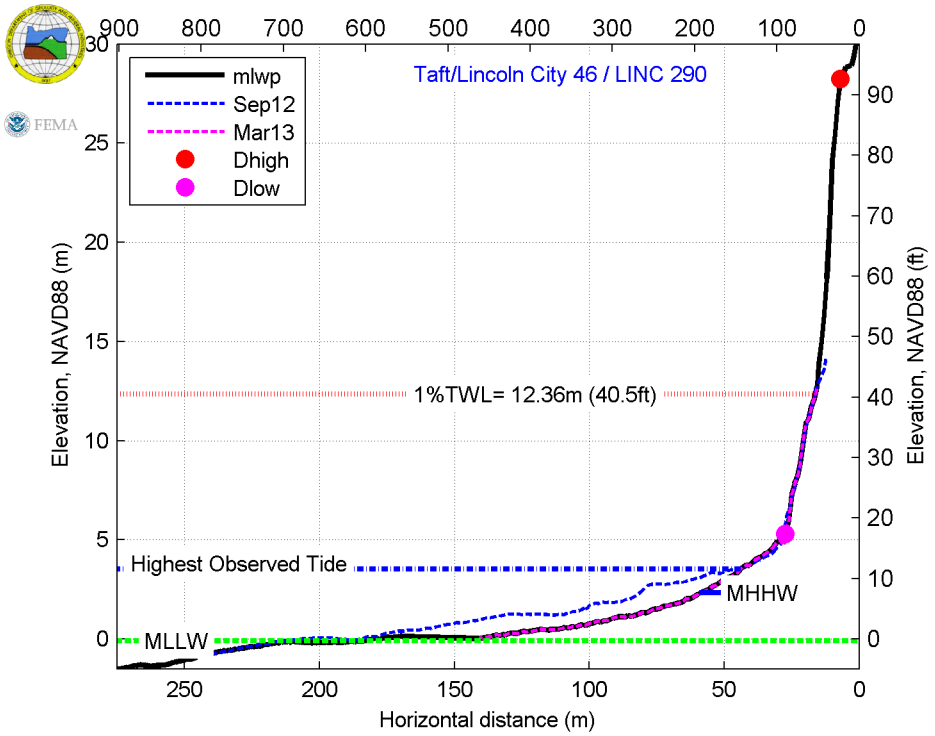

LINC 291

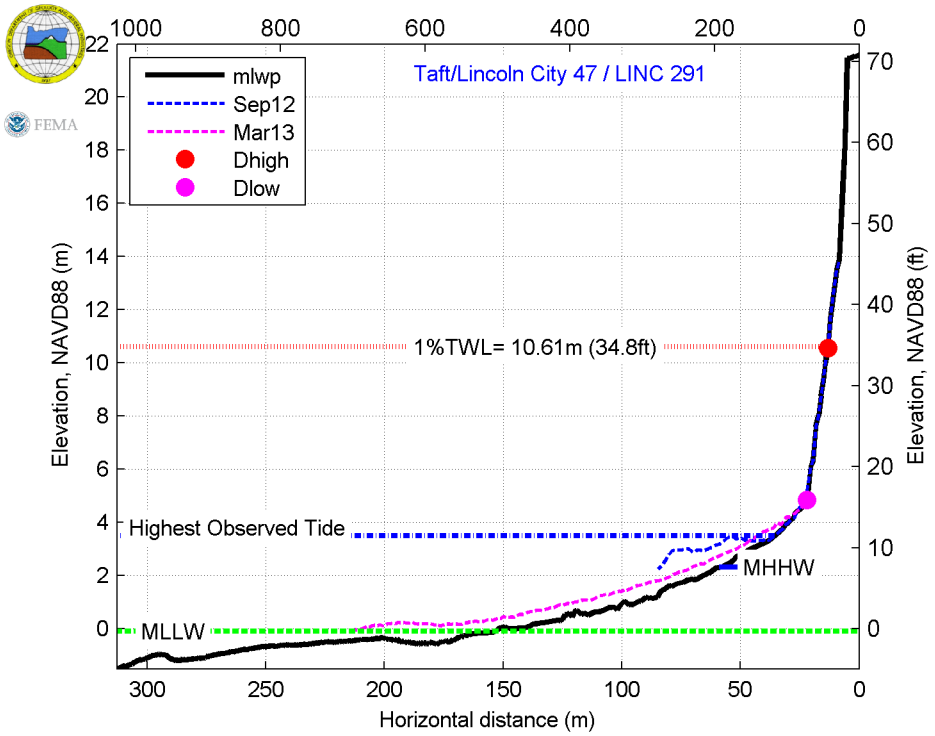

LINC 292

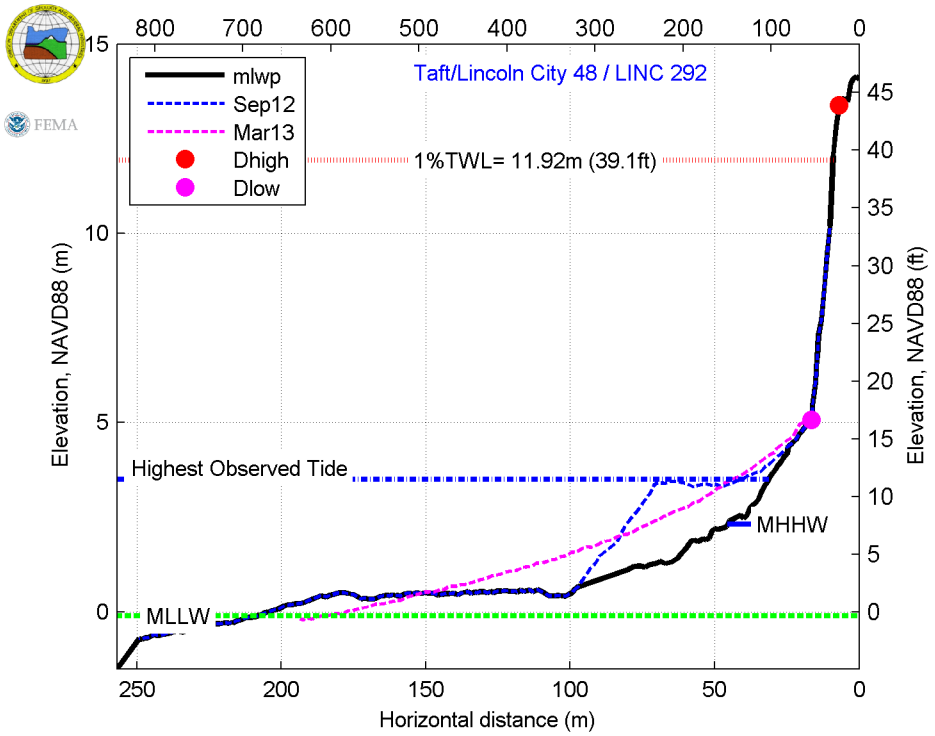

LINC 293

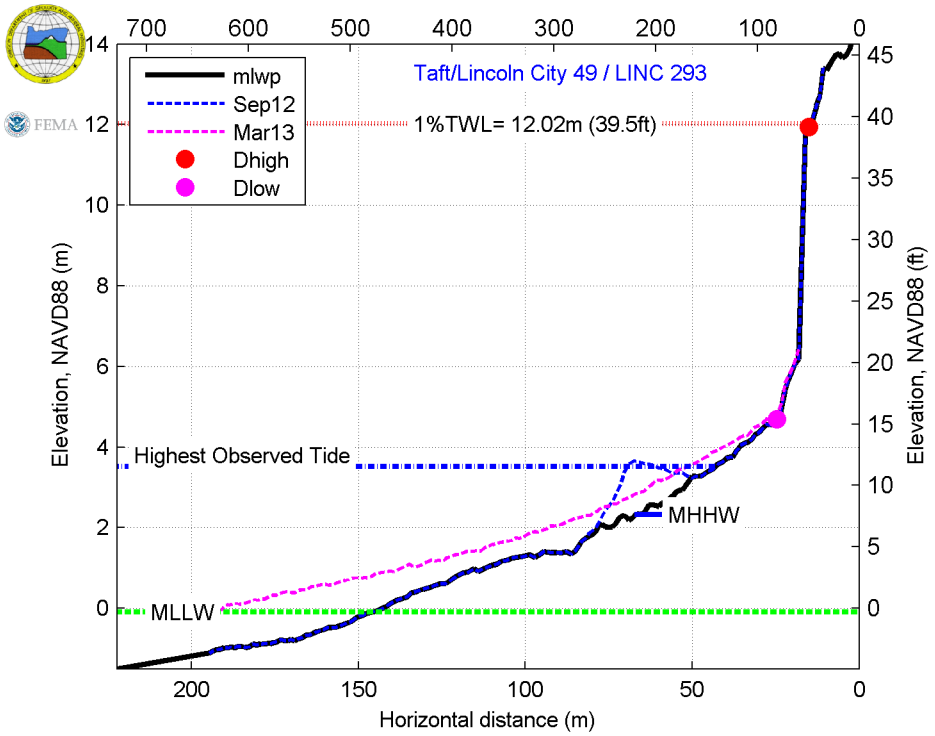

LINC 294

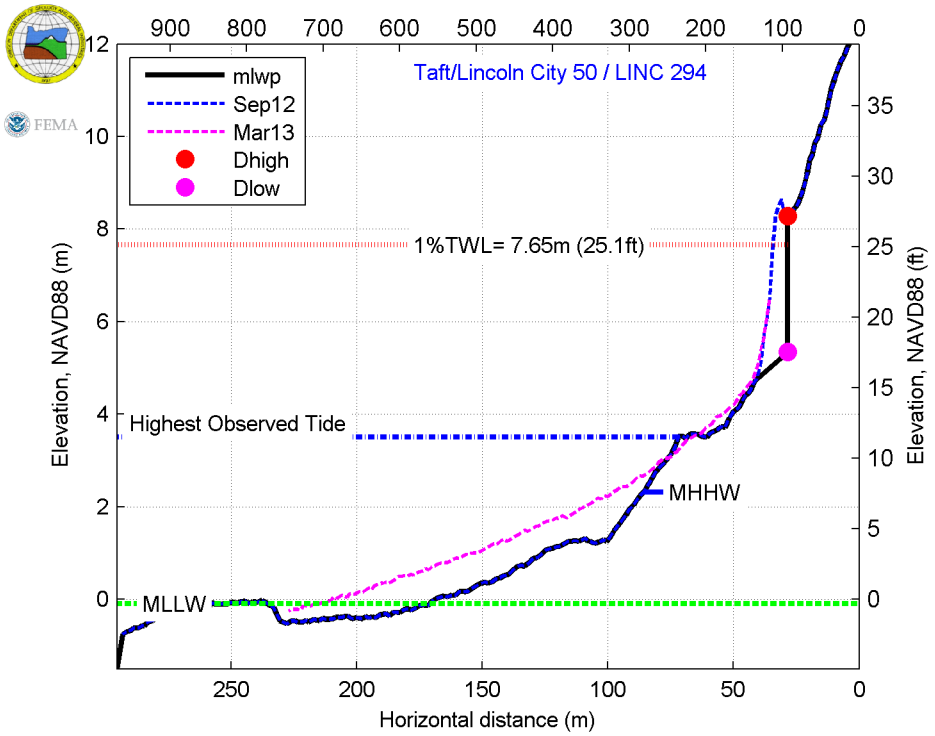

LINC 295

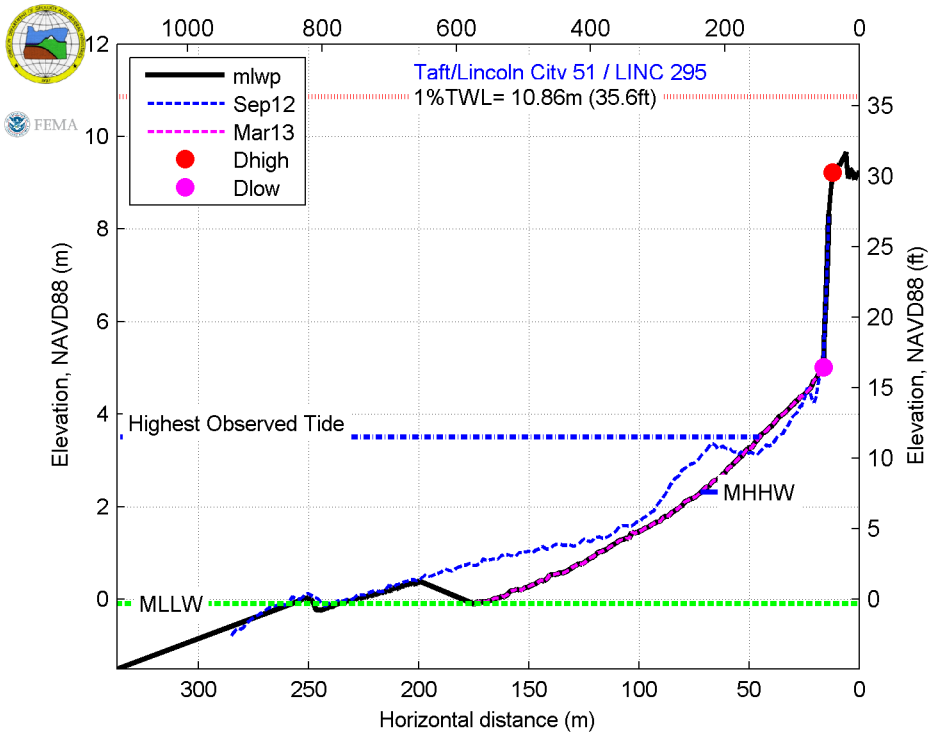

LINC 296

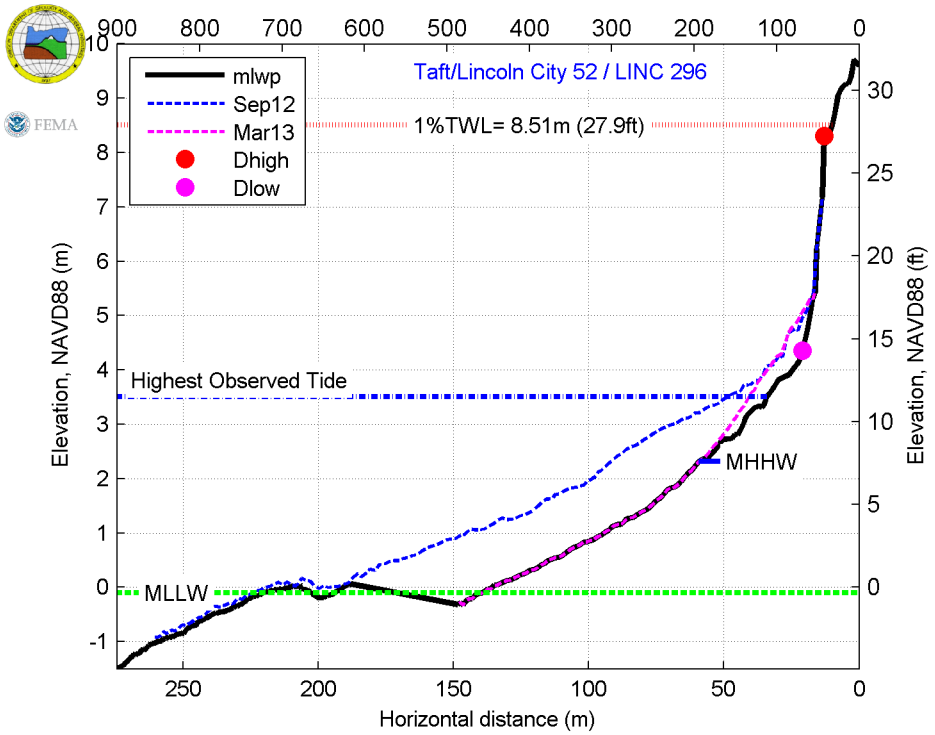

LINC 297

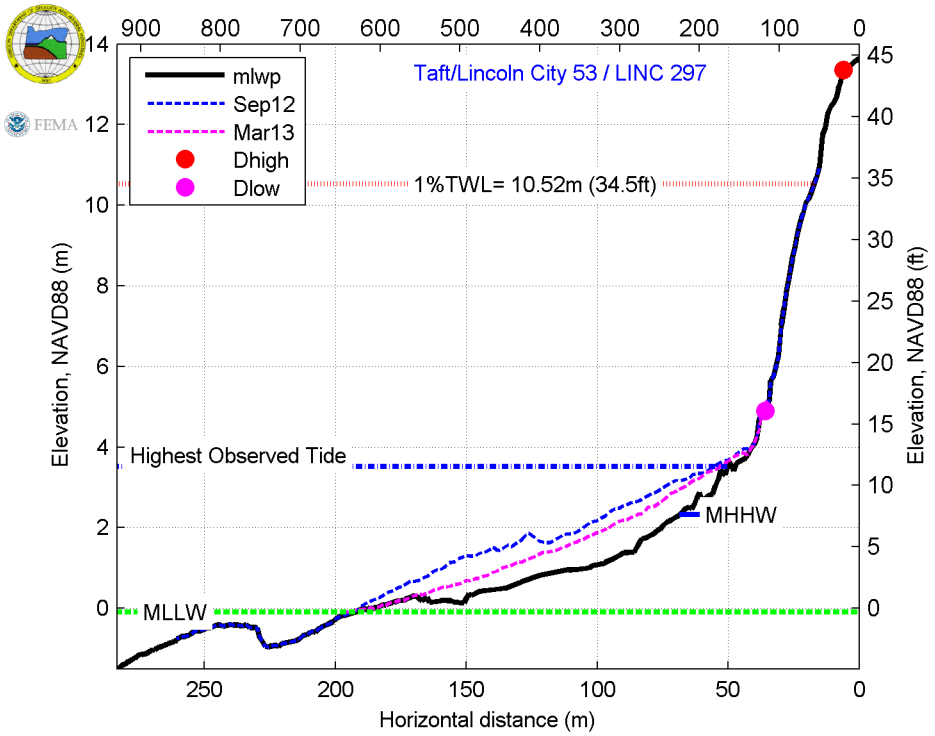

LINC 298

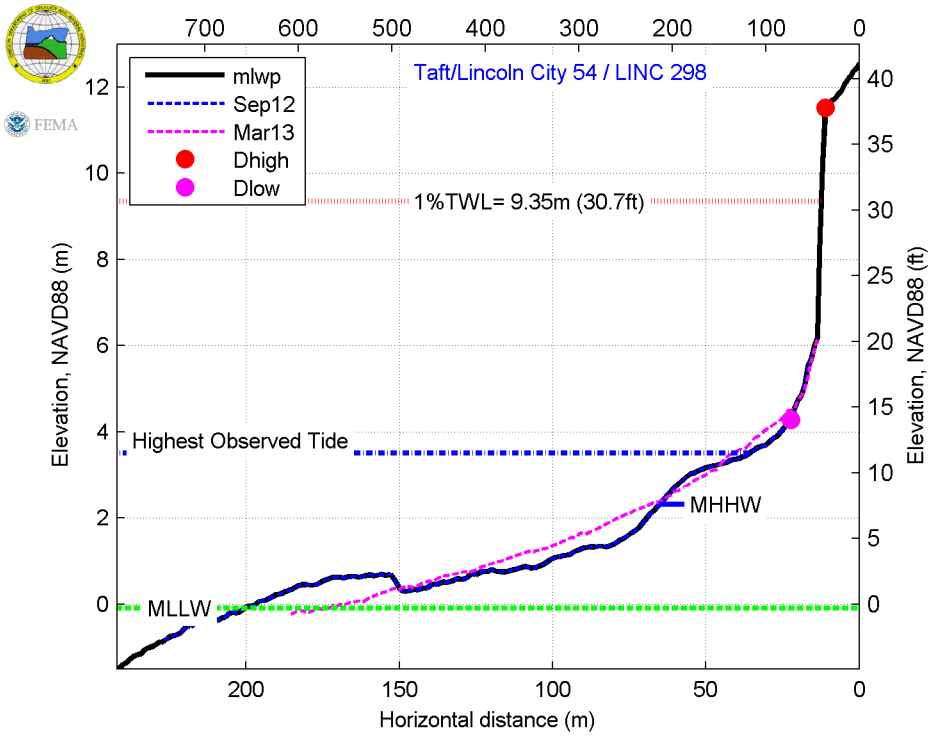

LINC 299

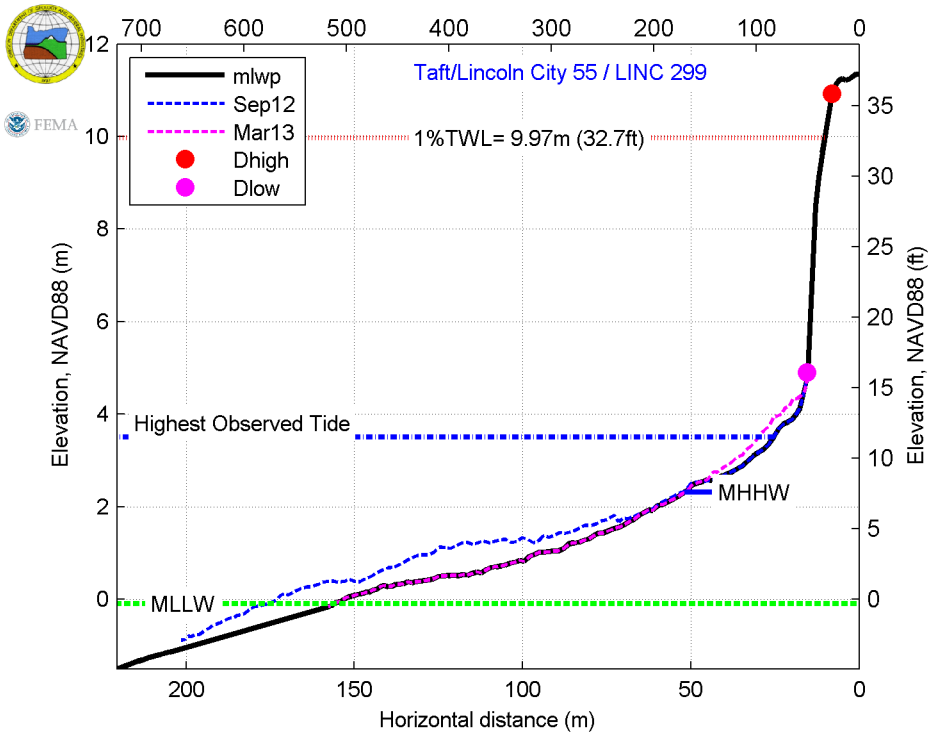

LINC 300

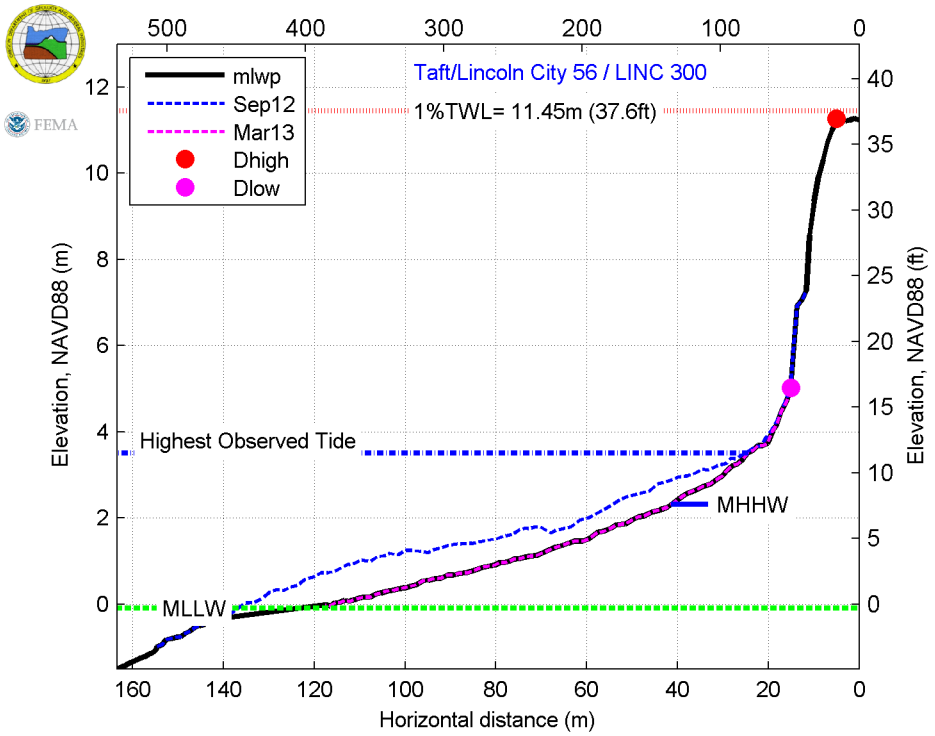

LINC 301

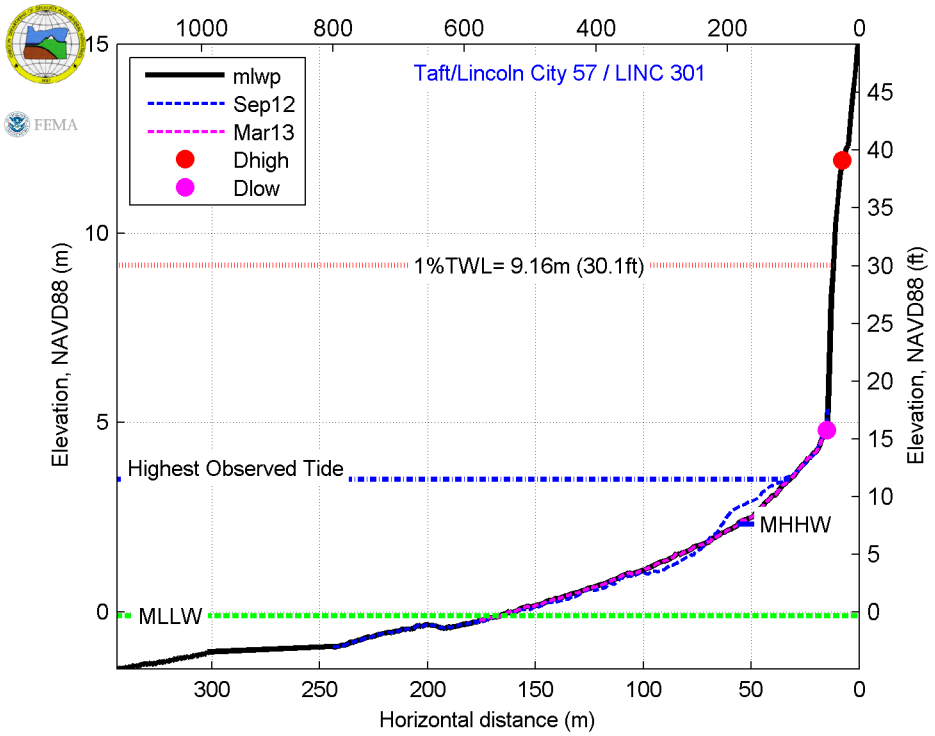

LINC 302

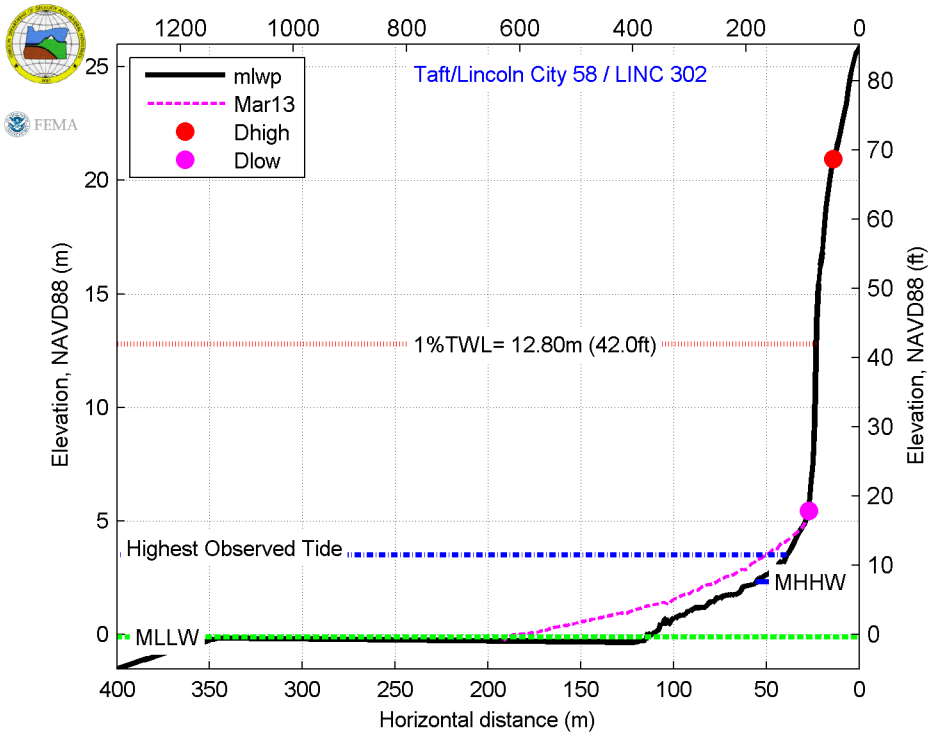

11.2.18 Salmon River

LINC 303

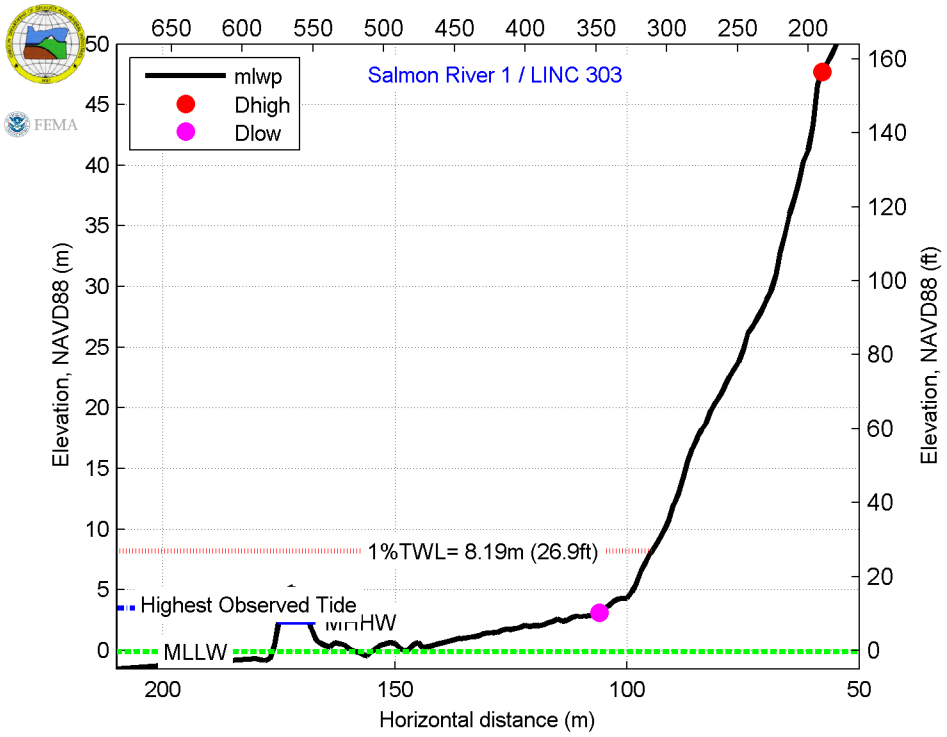

LINC 304

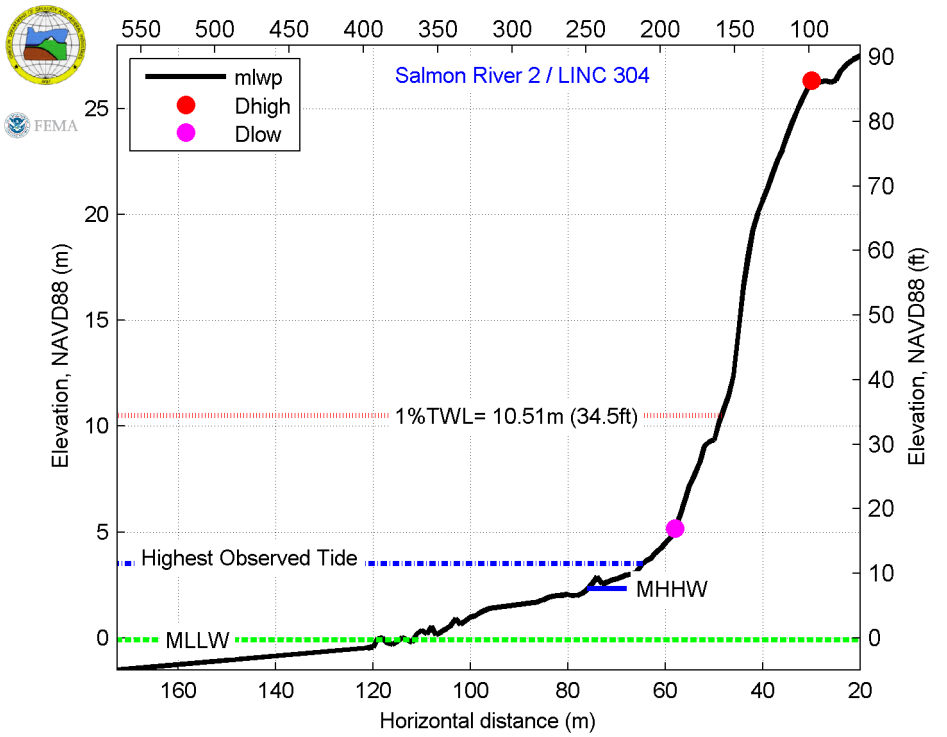

LINC 305

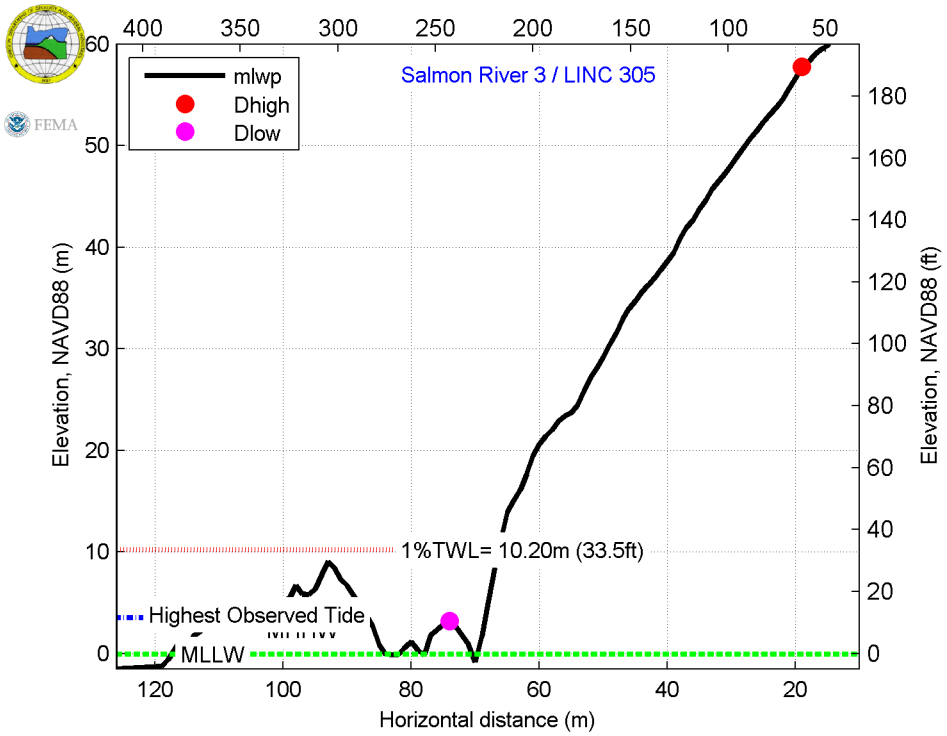

LINC 306

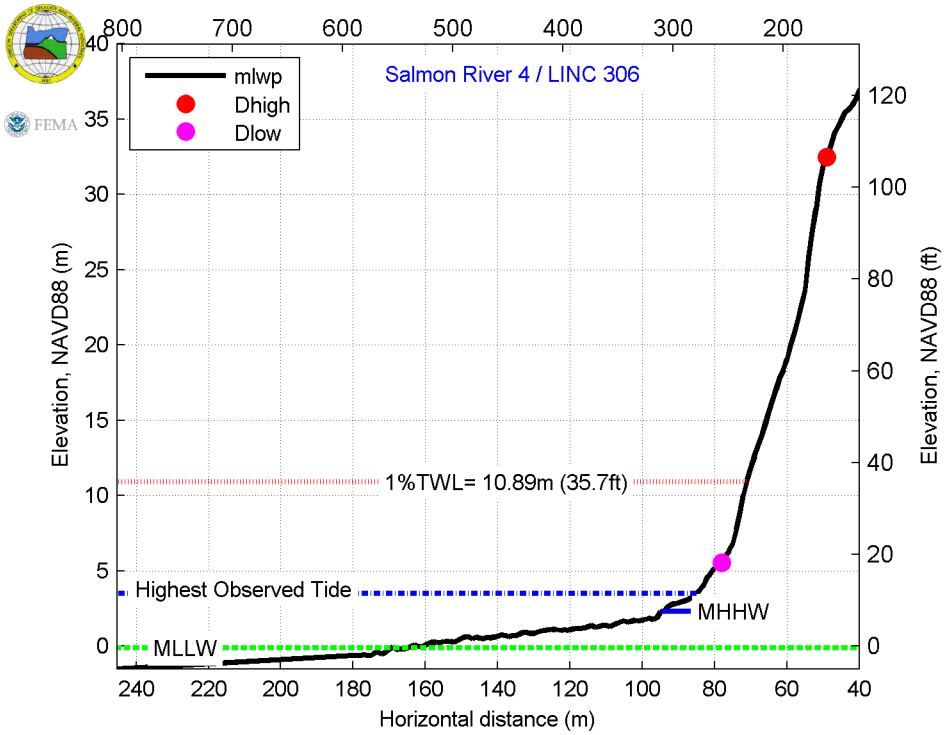

LINC 307

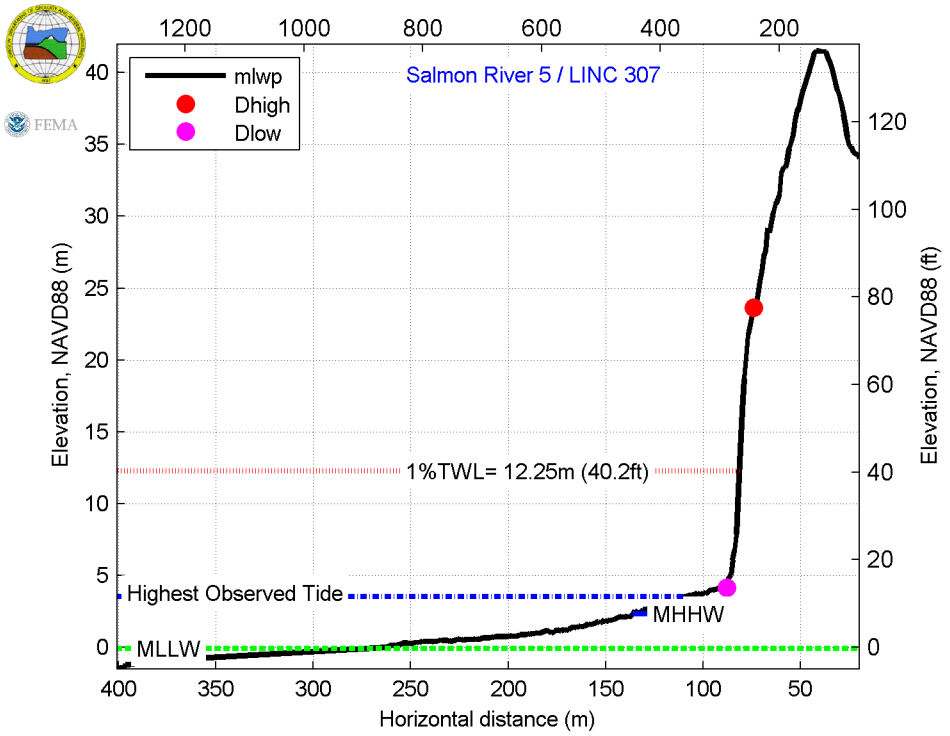

LINC 308

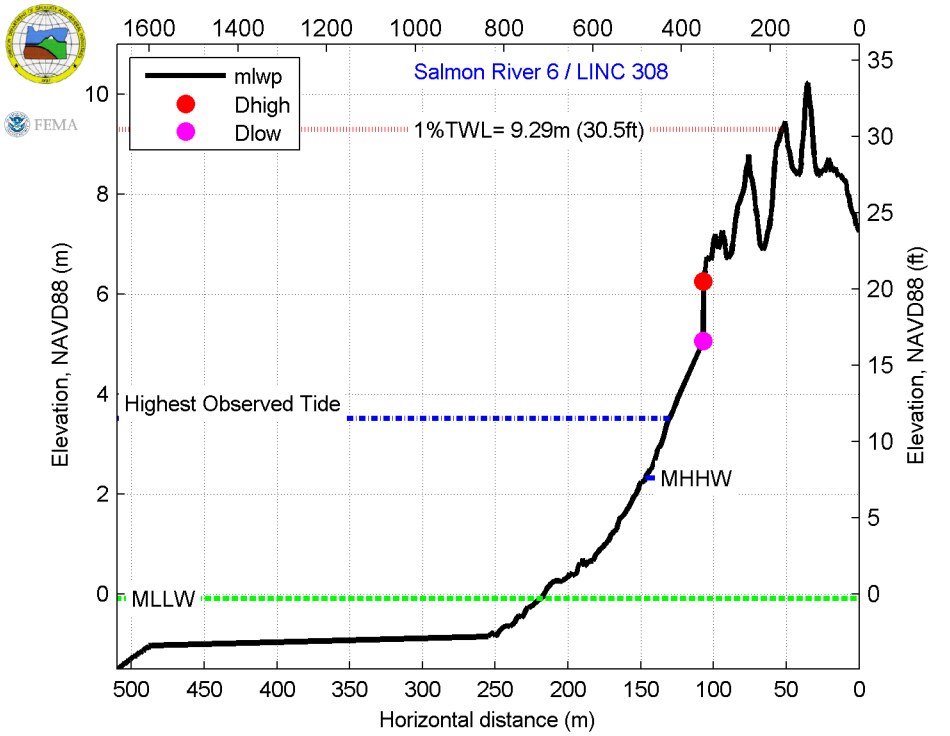

11.2.19 Cascade Head

LINC 309

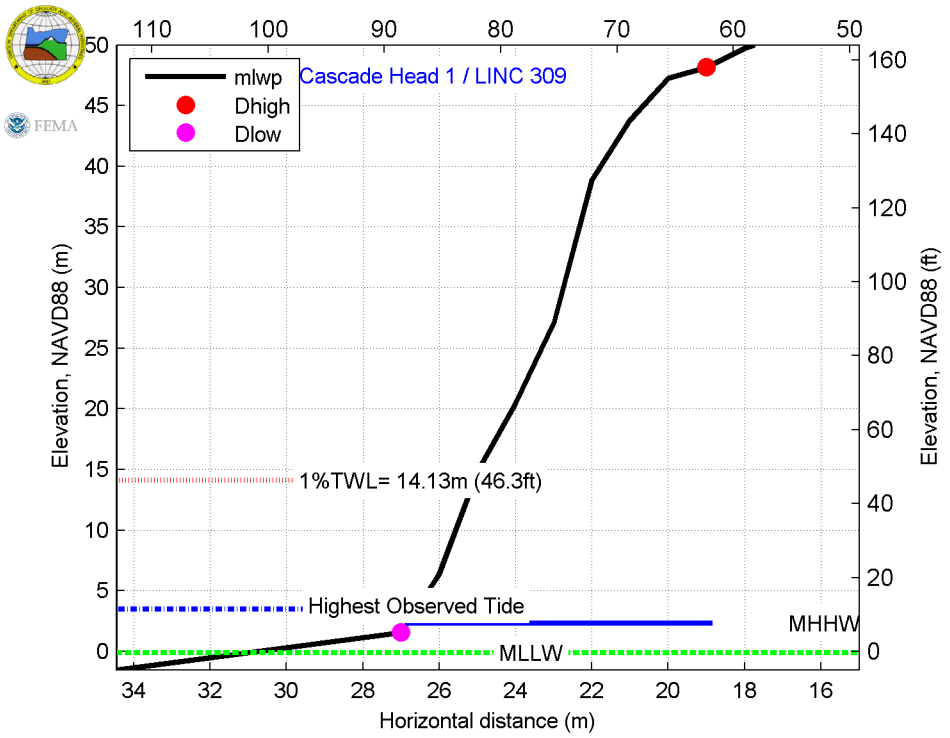

LINC 310

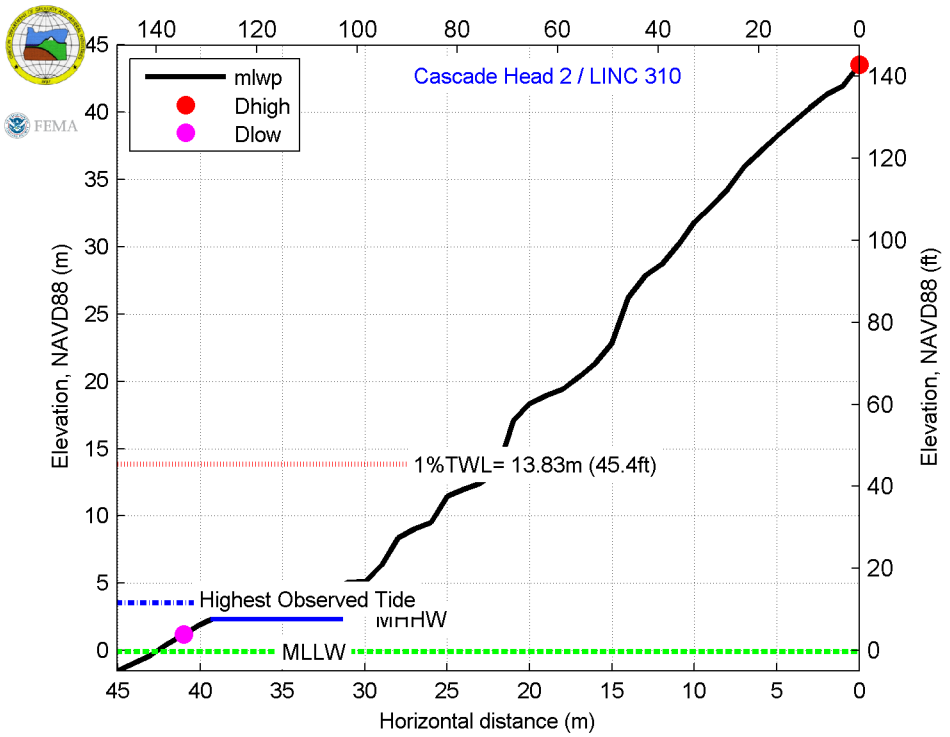

LINC 311

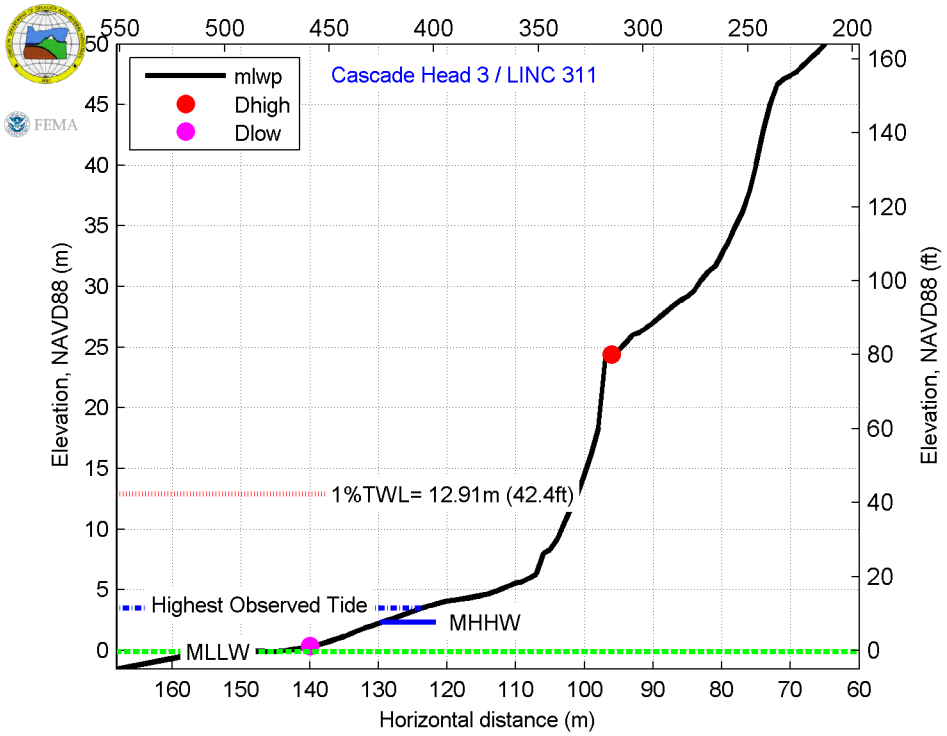

LINC 312

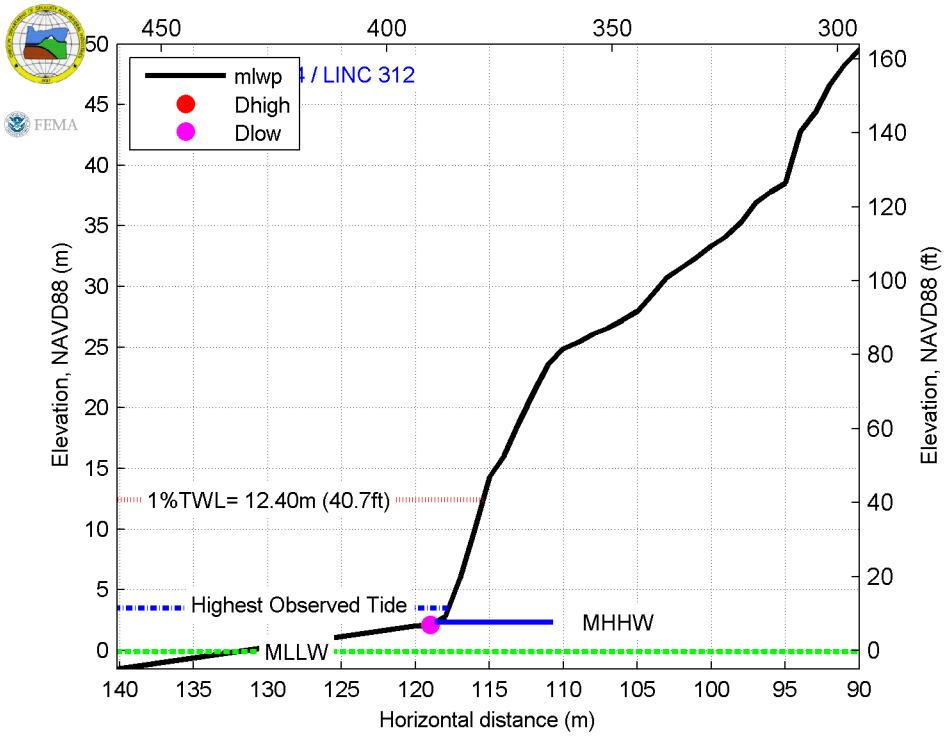

LINC 313

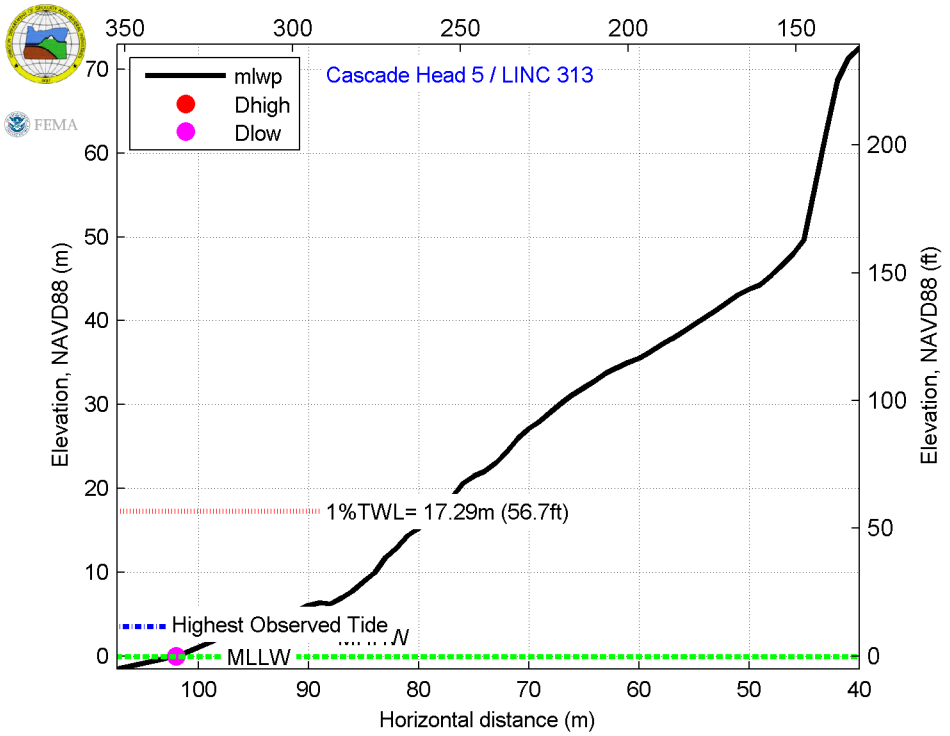
FEMA
mlwp
Dhigh
Dlow
Cascade Head 5 / LINC 313
1%TWL= 17.29m (56.7ft)
Highest Observed Tide
MLLW
Elevation, NAVD88 (m)
Elevation, NAVD88 (ft)
Horizontal distance (m)
350
300
250
200
150
100
90
80
70
60
50
40
0
10
20
30
40
50
60
70
0
50
100
150
200

11.2.20 Supplemental Transects

LINC_9_294

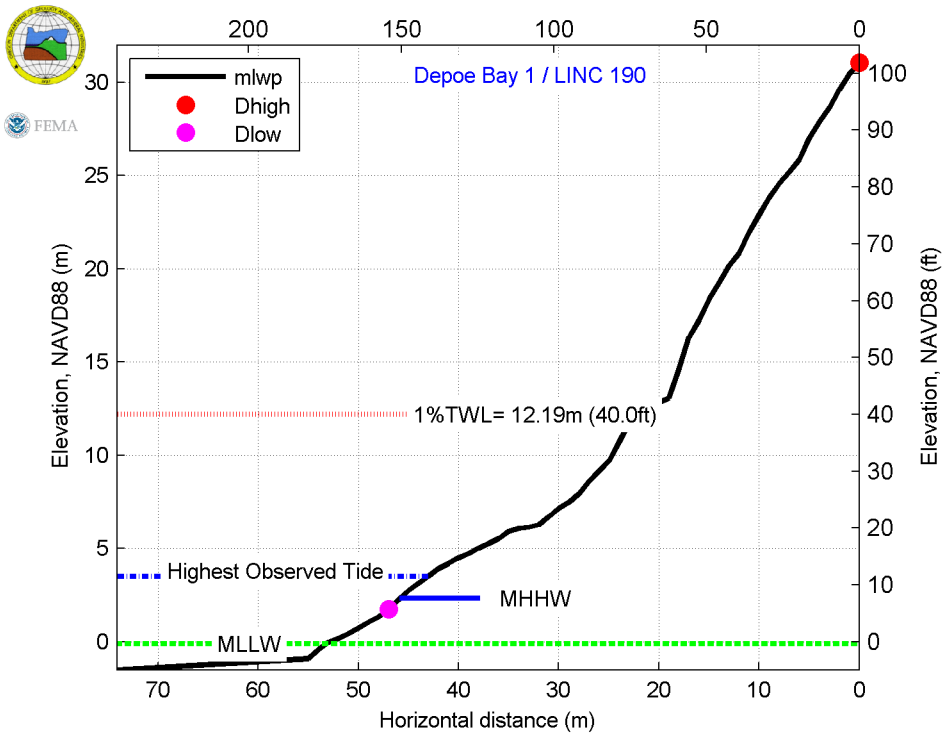

LINC_26_457

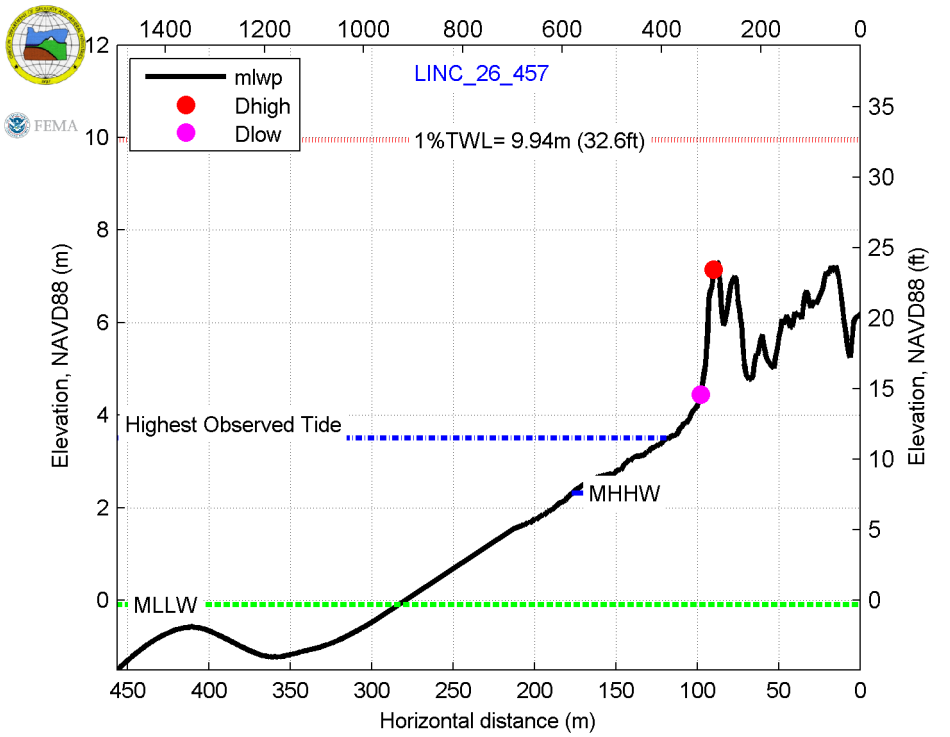

LINC_26_459

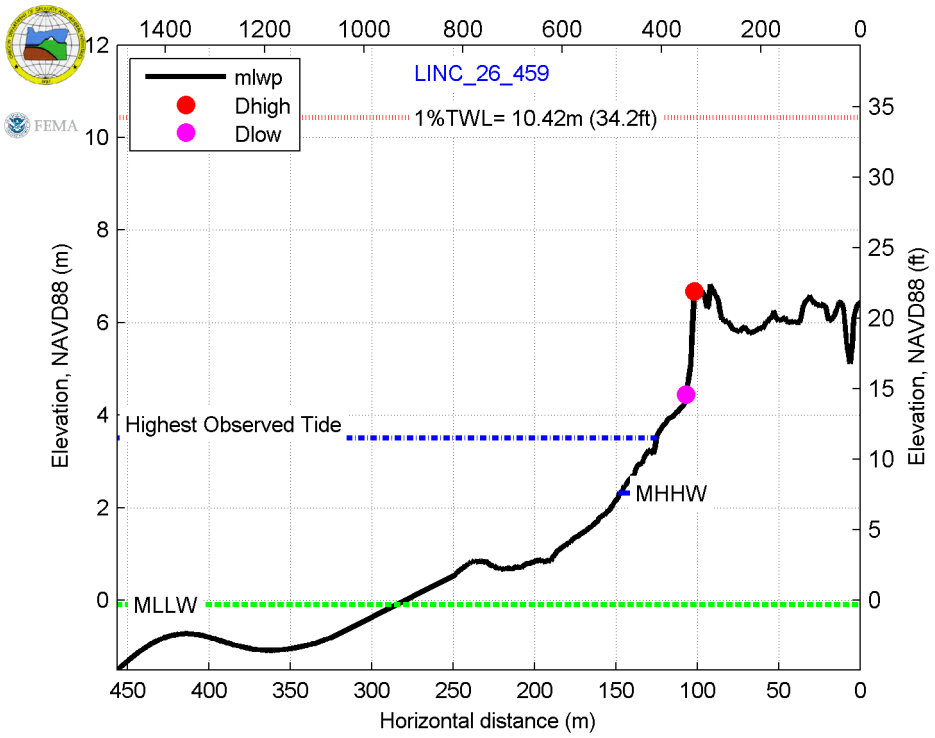

LINC_43_554

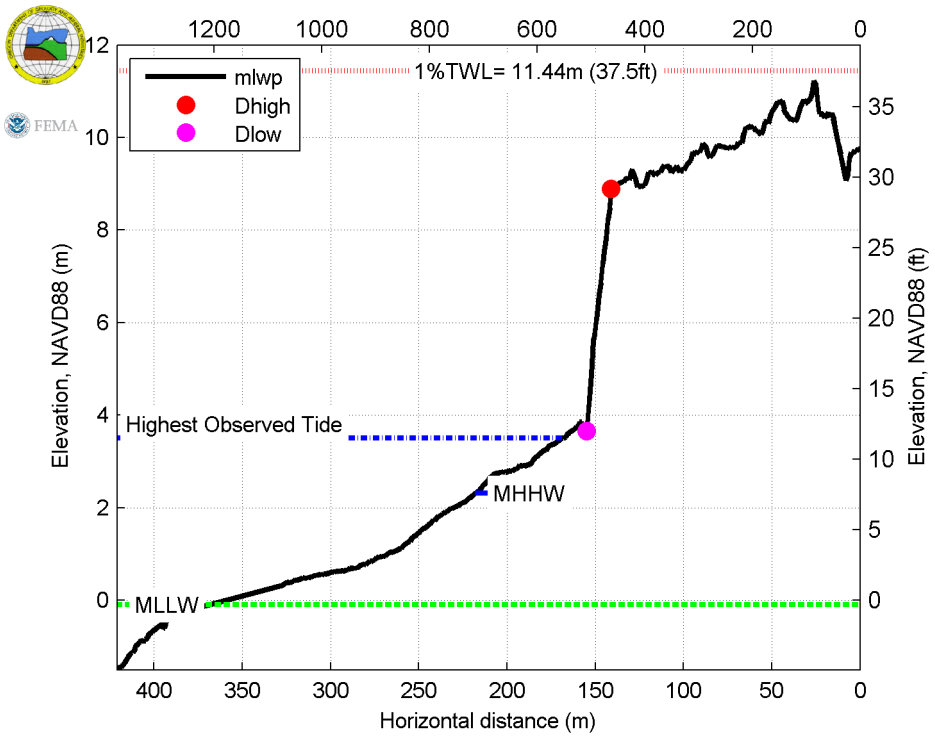

LINC_44_573

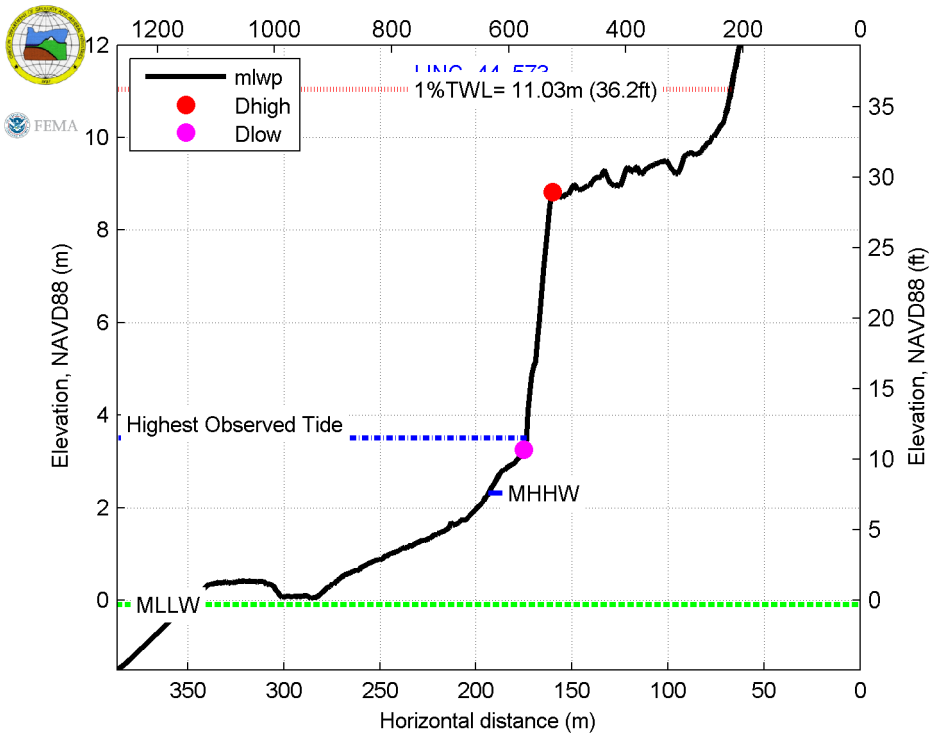

LINC_44_575

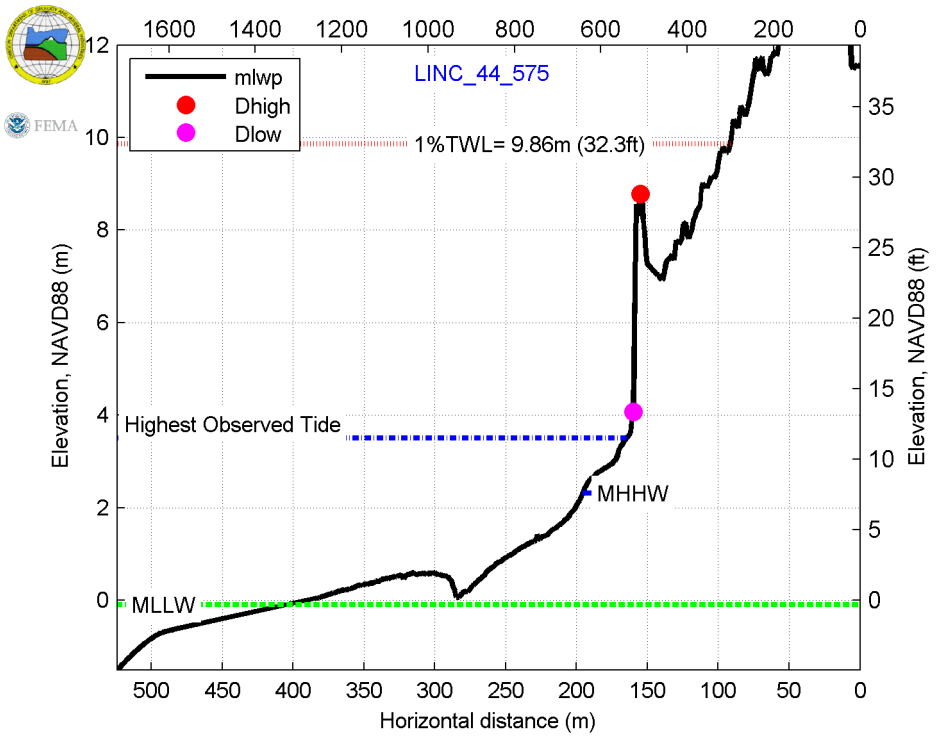

LINC_99_1257

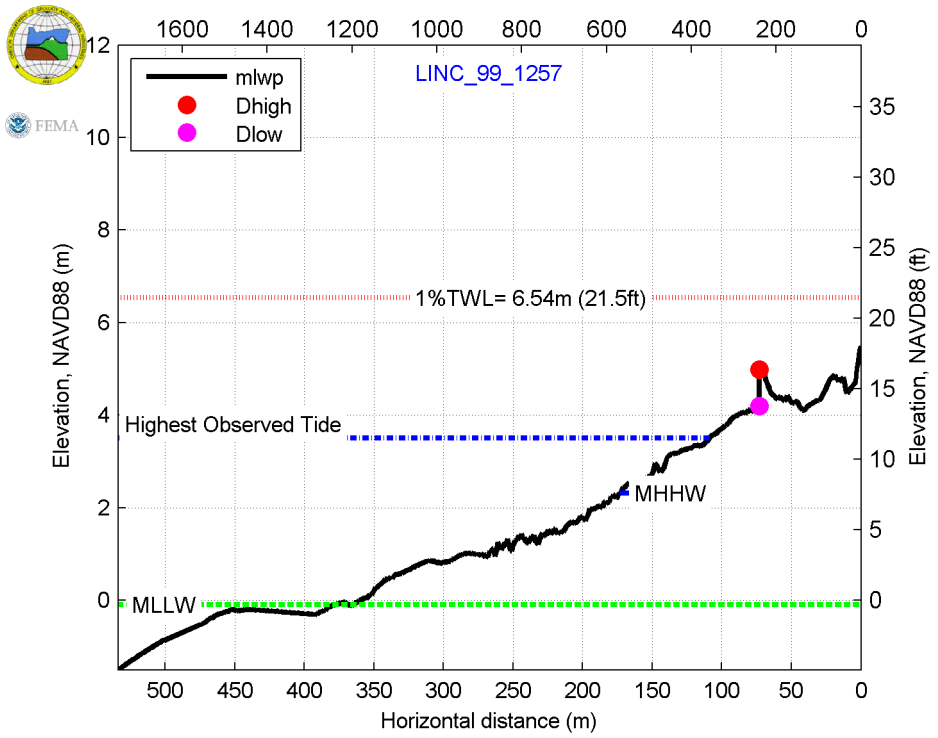

LINC_99_1274

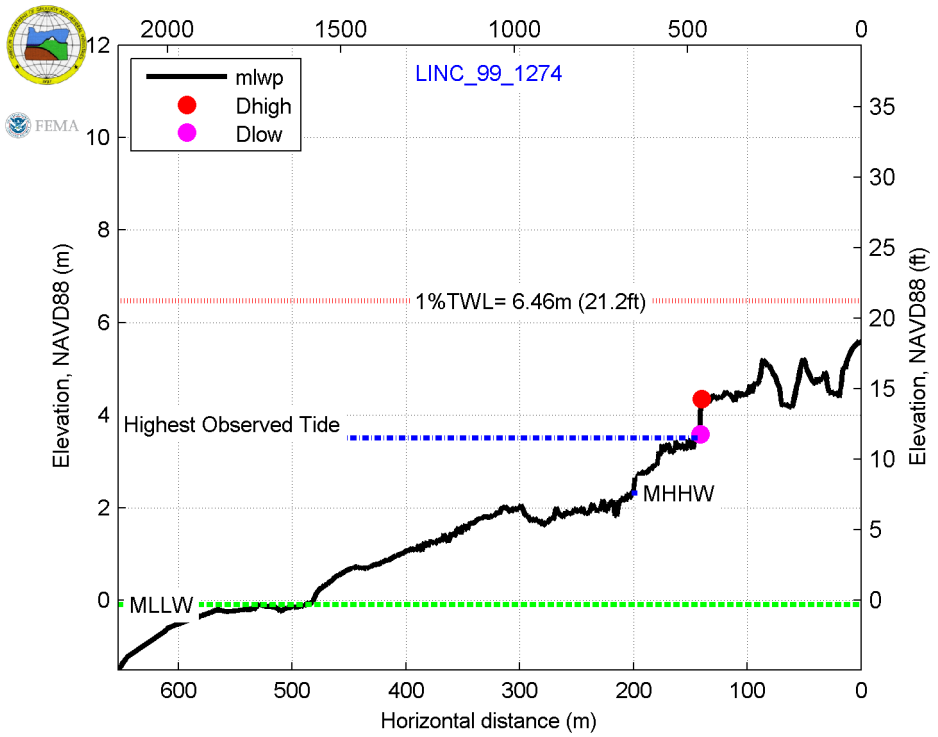

LINC_106_1340

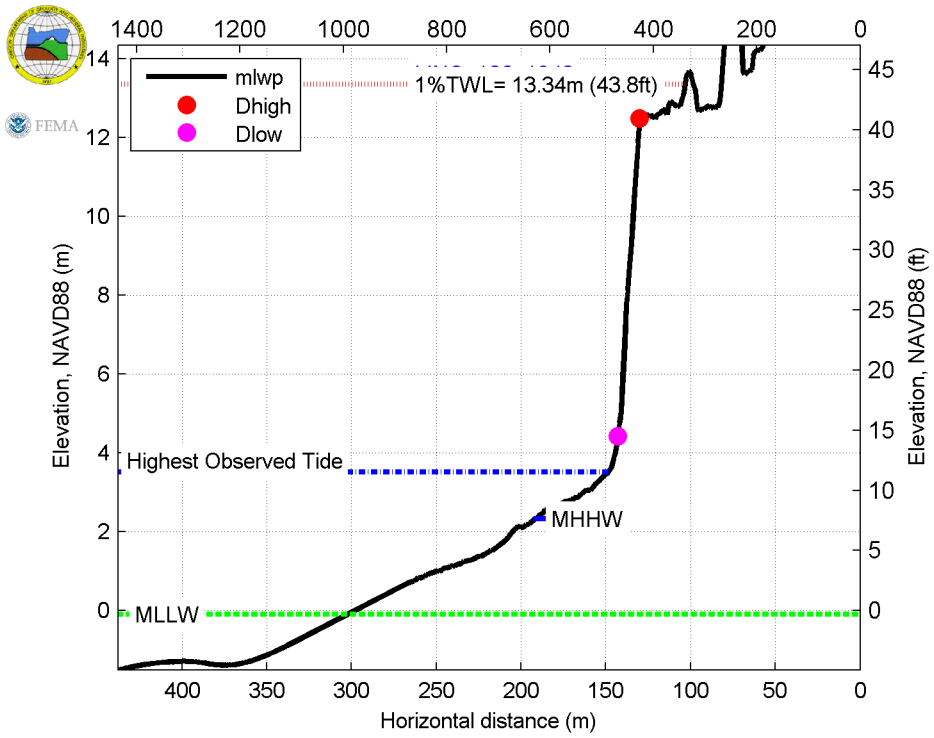

LINC_106_1343

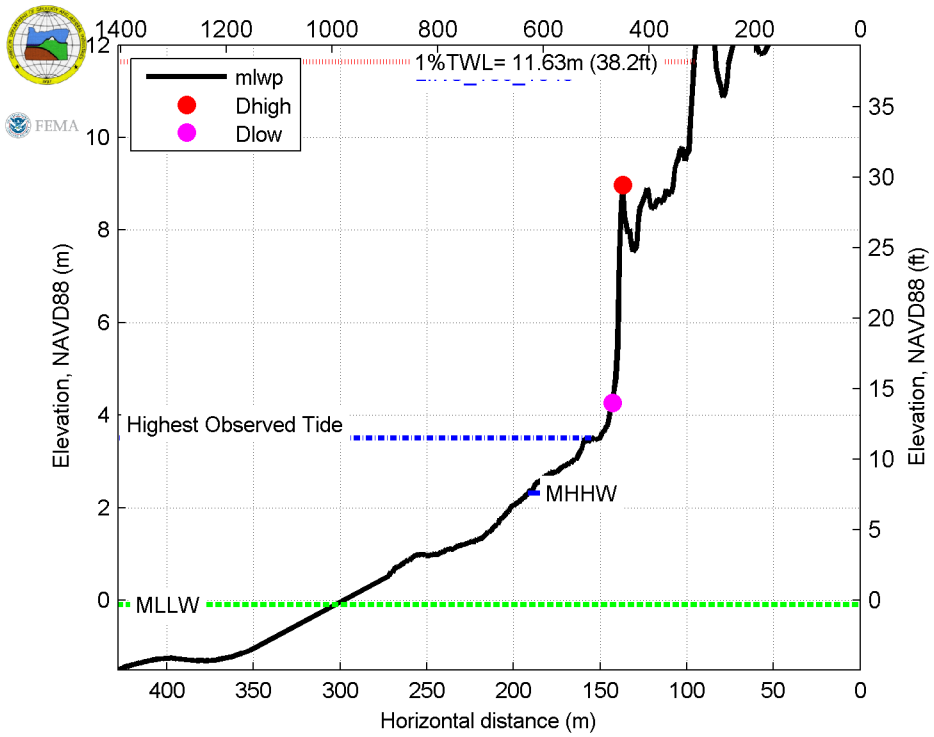

LINC_106_1345

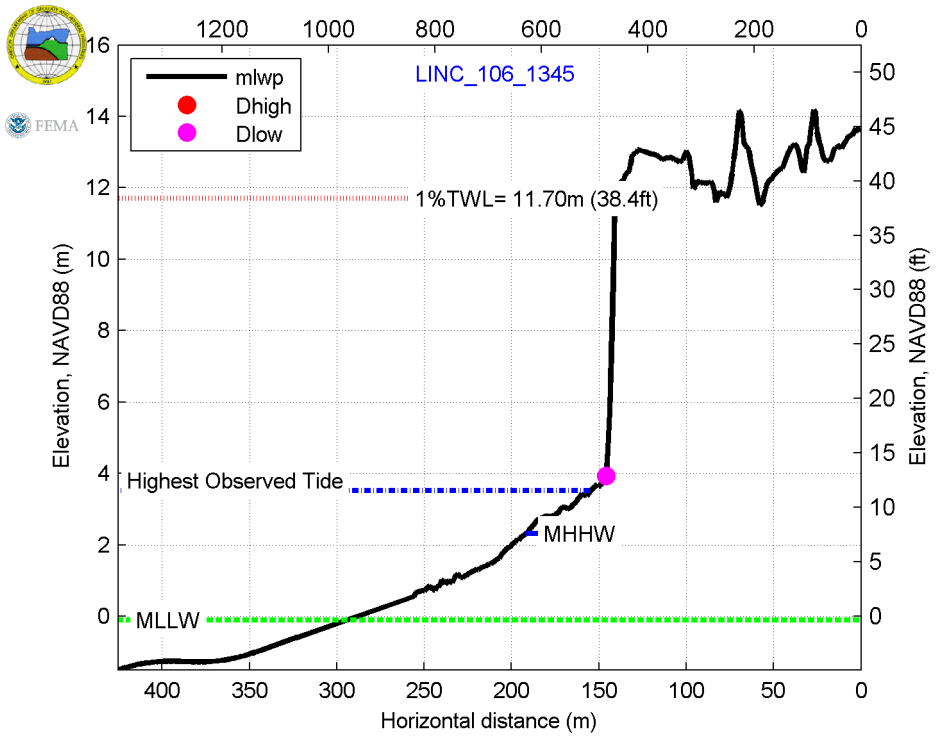

LINC_109_1366

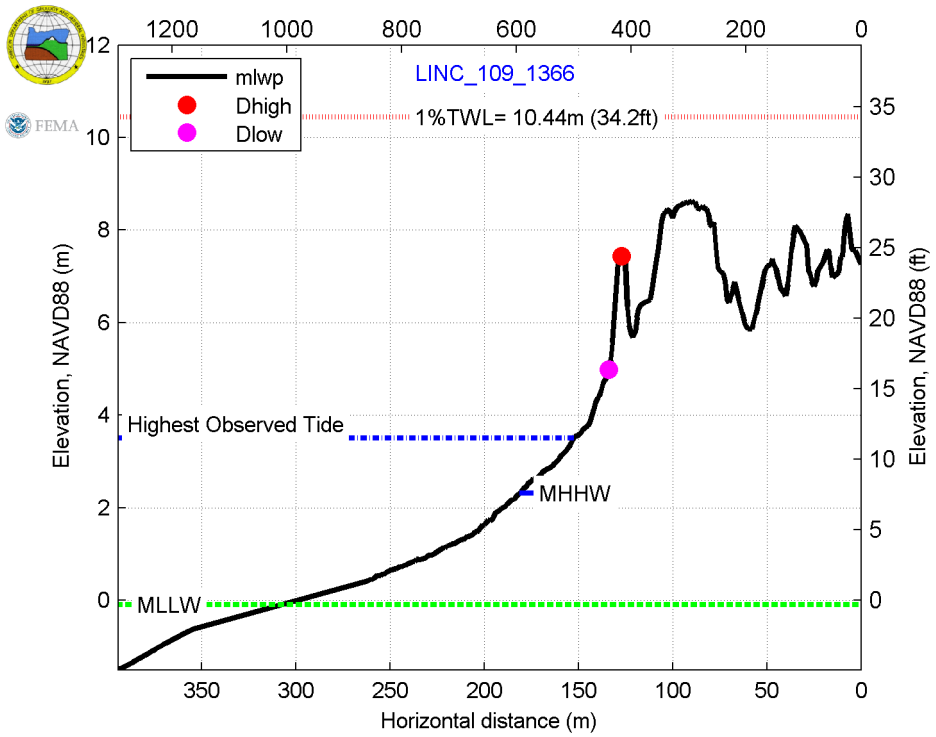

LINC_109_1367

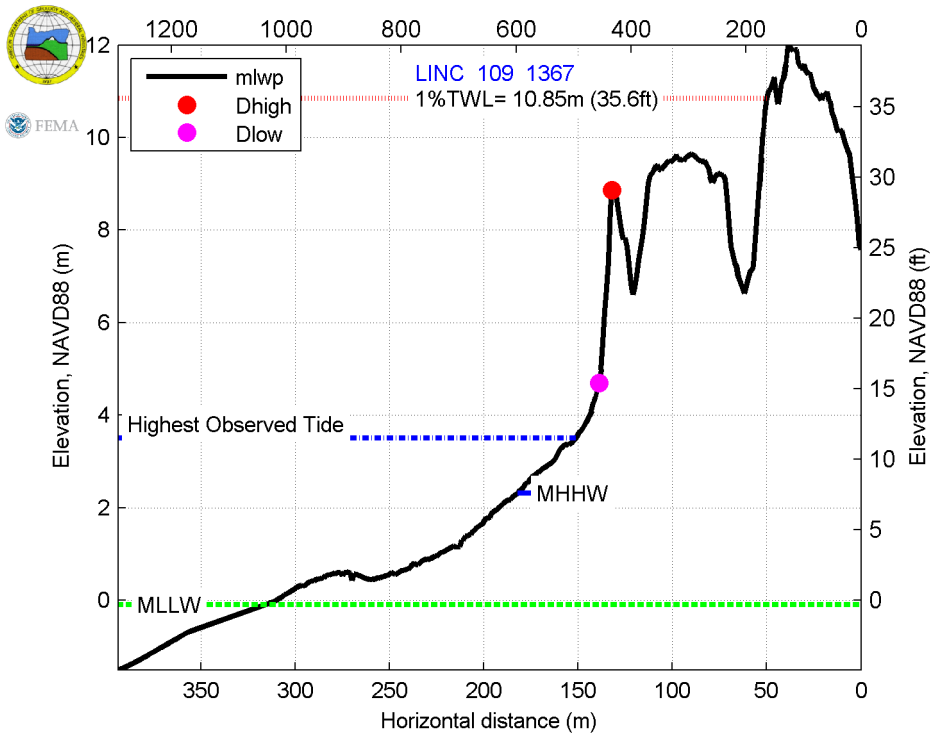

LINC_121_1528

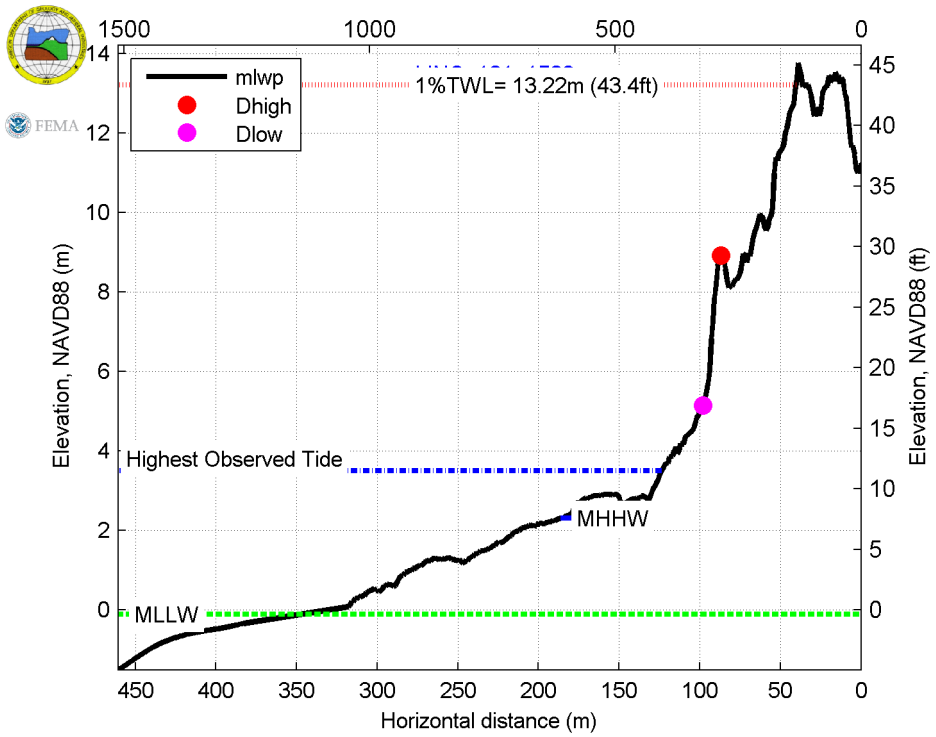

LINC_167_2257

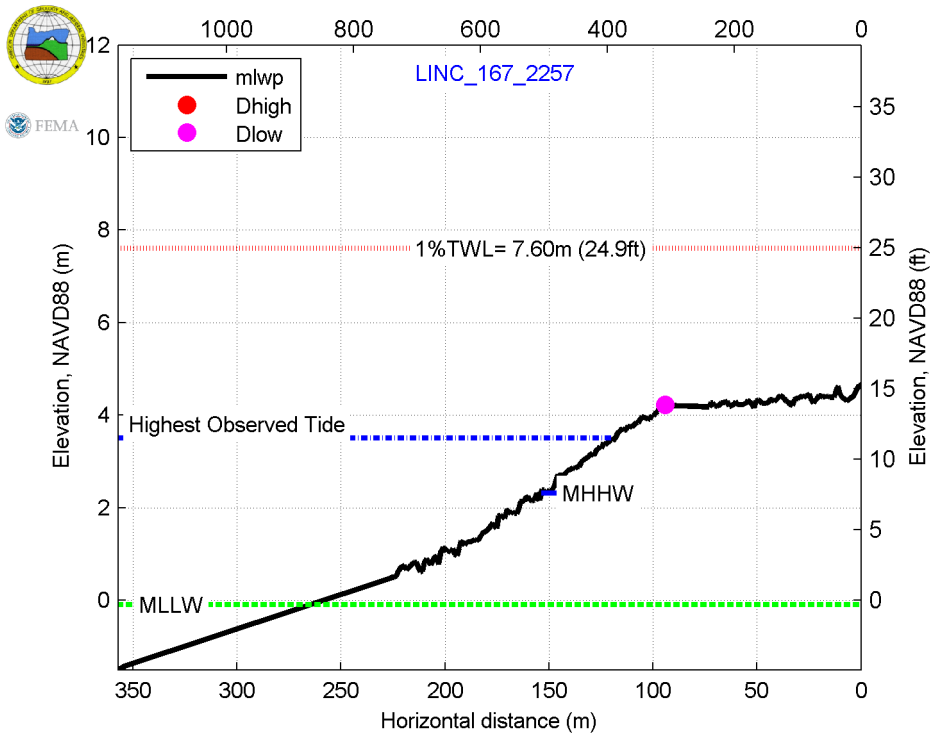

LINC_195_2790

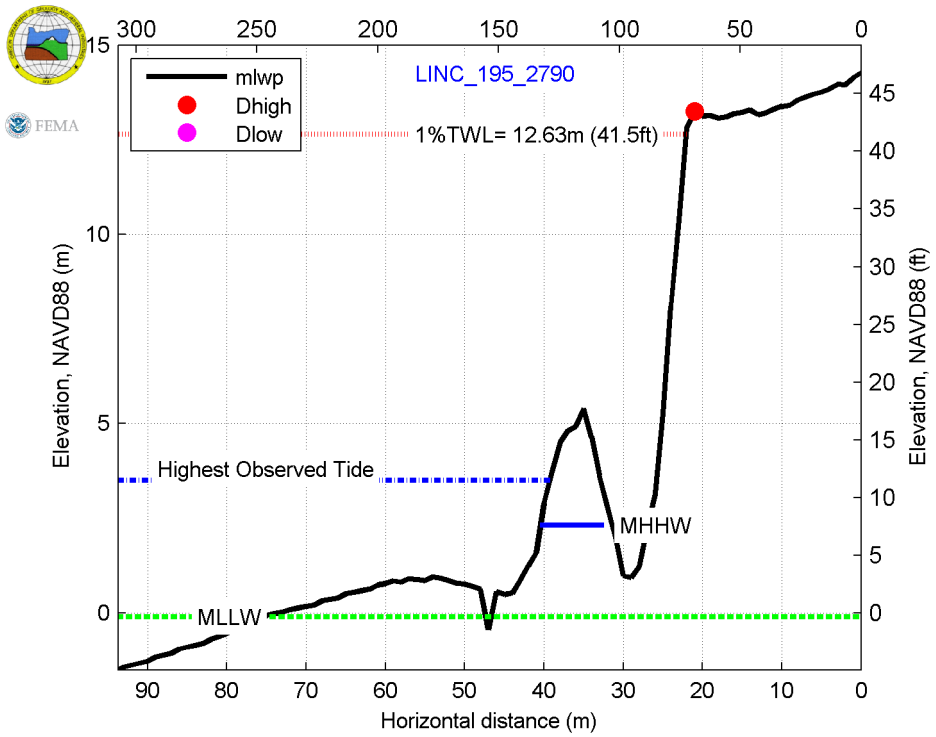

LINC_204_2928

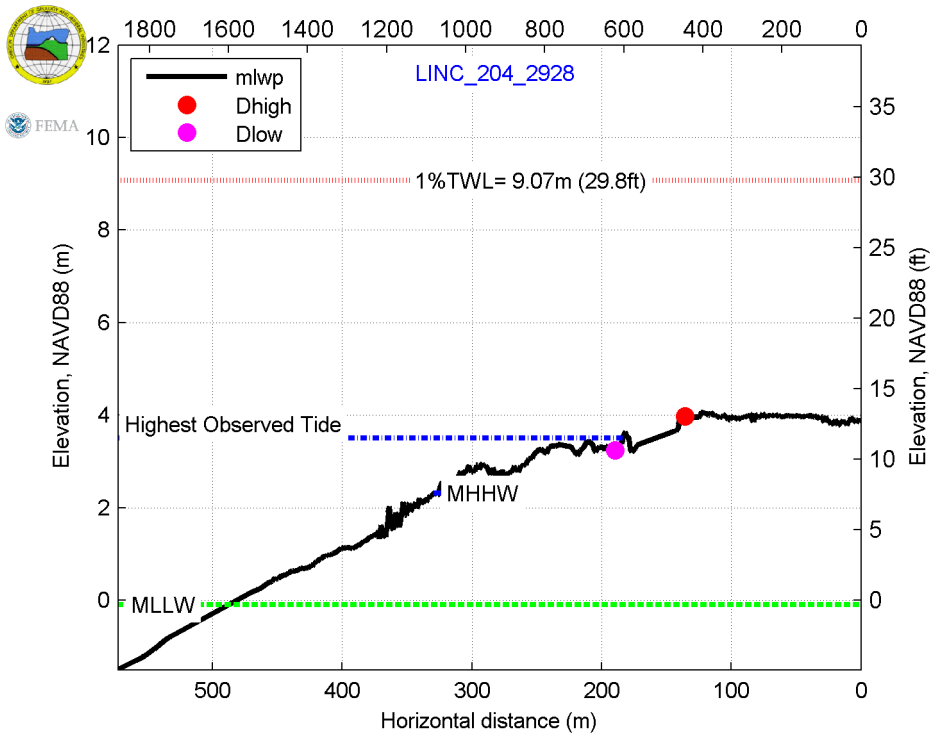

LINC_250_3385

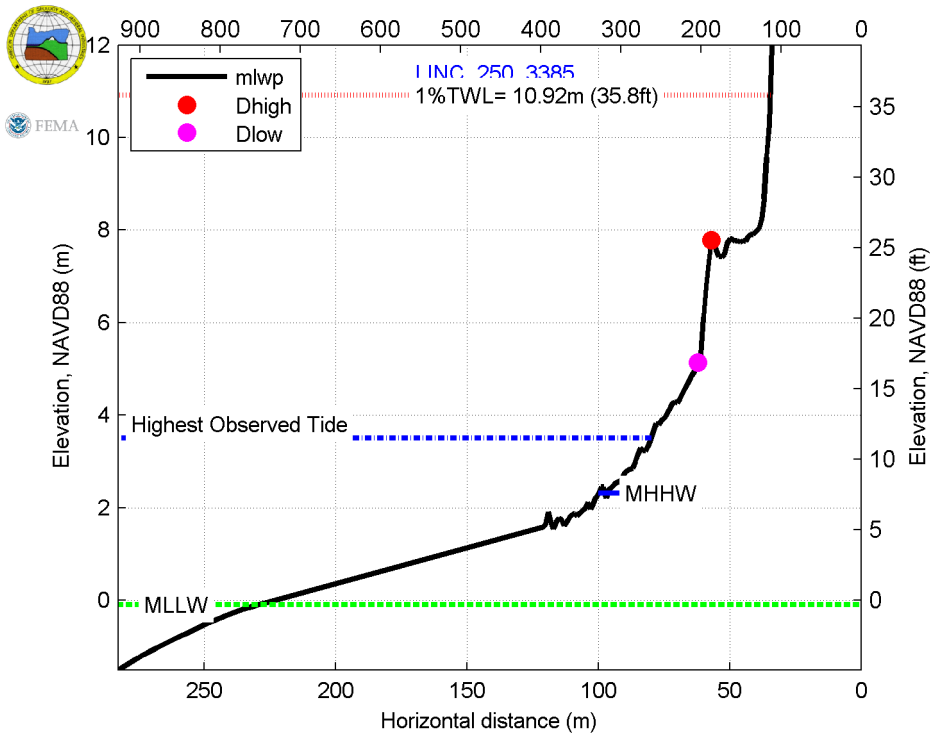

Oregon Department of Geology and Mineral Industries
Ian P. Madin, Interim Director
www.oregongeology.org

ERRATA SHEET for

DOGAMI Open-File Report O-15-06, Coastal Flood Hazard Study, Lincoln County, Oregon

Last update: 7/31/2015

This sheet identifies any errors identified after release of the publication. These errors have been corrected in the electronic version of the report available on the website.

#	Description	Location	Date Error Corrected
1	Coauthor Katherine Serafin was omitted from original author list; author list has been corrected.	page 1	7/31/12015